

**Effect of Improper Curing on Concrete Properties that may Affect
Concrete Durability**

Olusola Ige Idowu

Submitted in accordance with the requirements for the degree of
Doctor of Philosophy (PhD)

The University of Leeds

School of Civil Engineering

August, 2017

The candidate confirms that the work submitted is her own, except where work which has formed part of jointly-authored publications has been included. The contribution of the candidate and the other authors to this work has been explicitly indicated below. The candidate confirms that appropriate credit has been given within the thesis where reference has been made to the work of others.

Parts of the work in chapters 4,5 7 and 8 have appeared in the following publications:

Effects of Improper Curing on Concrete Performance, *34th Cement and Concrete Science Conference, 14-16th September 2014, Sheffield UK Reference 162. Poster Presentation*
Olusola Idowu and L.Black (parts 4,5 and 6)

Effect of Improper Curing on Durability, *35th Cement and Concrete Science Conference, 26-28th August 2015, Aberdeen, Scotland UK Reference Number 0032.* Olusola Idowu and L. Black (Parts of 6)

Effect of Improper Curing on Engineering Performance: A Microstructural Study, *36th Cement and Concrete Science Conference 5-6th September 2016, Cardiff Wales UK Reference Number 028.* Olusola Idowu and L.Black (parts of 4,5 and 6).

This copy has been supplied on the understanding that it is copyright material and that no quotation from the thesis may be published without proper acknowledgement.

The right of Olusola Ige Idowu to be identified as Author of this work has been asserted by her in accordance with the Copyright, Designs and Patents Act 1988.

© 2017 The University of Leeds and Olusola Ige Idowu

Acknowledgements

I want to appreciate God for seeing me through the programme.

My thanks goes to my supervisors Dr Leon Black, Professors Philip Purnell and John Forth for their ideas, suggestions, guidance and timely contributions towards the progress of this work.

I wish to express my profound gratitude to my sponsor Tertiary Education Trust Fund (TetFUND) Nigeria through Ekiti state University Ado Ekiti, Ekiti state for the scholarship provided to carry out this research.

Many thanks to all the technical staff at the university that put me through the laboratory work starting from Leslie Arkless, Peter Flatt Steve Holmes and Robert Clarke.

I also want to thank all the material group members Joseph, Ahmed who are still working on their research and those that have finished Julia, Roland, Sam, and Josh. I really appreciate our working together as a group.

My sincere appreciation goes to friends and family for support received from all, and lastly to my husband Olusegun Idowu and my lovely children Oluwaseunbabara and Opemipo for their support throughout the programme.

Abstract

The use of concrete is increasing annually due to its favourable properties and ready availability. Demand for concrete will continue to increase and it will remain the world's most important construction material for many years to come. However, the use of Portland cement concrete has an environmental burden, and so in a drive to reduce the carbon footprint of construction, there is widespread attention directed towards the utilisation of wastes and industrial by-products to minimise Portland cement (PC) consumption. The cement industry increasingly uses additions, such as fly ash.

The literature has established the use of fly ash as partial replacement of Portland cement to increase strength at later age and exhibit considerable enhancement in durability. However, such binders hydrate more slowly, so proper curing conditions become more important. Ideally, the durability of concrete should not be a concern. Some degree of weathering should be expected, but improper concreting procedures can cause the deterioration to be earlier than expected. Furthermore, since durability issues cannot be seen immediately, some assessment of the impact of improper concrete curing is needed.

The study has involved casting of concretes prepared with either CEM I or a CEM I blend with 30% replacement with fly ash to investigate the impact of improper curing. Performance was evaluated in terms of compressive strength, drying shrinkage, transport properties and resistance to carbonation. Paste samples were characterised by TGA, XRD and SEM to follow hydration and microstructural development. Also since the degree of saturation is known to affect the compressive strength of concrete, and curing under ambient conditions will lead to changes in the degree of concrete saturation, the work checked the impact of the degree of saturation on compressive strength; to enable an accurate understanding of the impact of improper curing.

Improper curing leads to reduced compressive strength development and increased drying shrinkage. Sorptivity and permeability values were increased. This is due to reduced levels of cement hydration, as water evaporates from the concrete surface. The effect of improper curing on resistance to carbonation revealed that samples improperly cured carbonated more than those ideally cured. This study has shown that the impact on sorptivity and permeability is far greater than the impact on compressive strength, with implications for the long-term durability of concrete.

Composite cements, containing 30% fly ash, showed comparable strengths to CEM I concretes and improved transport properties when ideally cured. Additions of fly ash reduced the drying shrinkage. Improper curing however led to reduced performance. Strength was compromised by improper curing to a greater degree than for equivalent CEM I mixes. However, it was sorptivity and permeability which were most severely affected. This was due to the reduced degree of cement hydration leading to preventing the pozzolanic reaction between the fly ash and portlandite. Also, higher carbonation depth was seen on fly ash samples that were not cured.

Low strength concrete, which already has an inherently higher porosity, is more greatly affected by improper curing than high strength concrete. This is presumed to be due to the ease with which water can evaporate from the surface of the more porous matrix. Also, concrete workability has been found to be a factor which can help to reduce the embodied carbon of concrete, with stiffer mixes having lower carbon footprints. However, this study

has shown that stiff concrete mixes may be less durable and more susceptible to improper curing. This may be explained by the lower overall water contents within the stiff mixes, and therefore the greater impact of surface water evaporation.

The effect of changes in the degree of saturation showed the deleterious effects of improper curing, with the saturated, ambient cured samples all exhibiting lower strengths than the equivalent ideally cured samples. The large capillary pores developed due to improper curing was seen with lower calcium hydroxide contents. The reduced hydration products obtained support the result that lower degree of hydration was produced due to improper curing since the hydration of cement cannot continue in the dry environment. This study confirms the need for good site practice, and shows that embodied carbon should not be the only factor when considering the environmental performance of concrete. Rather, durability and whole life performance should also be considered.

Table of Contents

Contents

Acknowledgements	ii
Abstract	iii
Table of Contents	v
List of Tables	x
List of Figures	xi
Chapter 1	1
1.1 Introduction.....	1
Chapter 2 Literature Review	4
2.1 Introduction.....	4
2.2 Concrete.....	4
2.2.1 Cement.....	5
2.2.2 Aggregates.....	5
2.2.3 Water.....	5
2.2.4 Admixture.....	6
2.2.5 Additions.....	6
2.3 Portland Cement.....	7
2.3.1 Hydration of Portland cement.....	8
2.3.2 Development of hydration product.....	9
2.3.3 Mechanism of hydration.....	10
2.4 Microstructure of cementitious materials.....	12
2.4.1 Pores in concretes.....	14
2.4.2 Water phases in concrete.....	15
2.5 Fly ash.....	15
2.5.1 General effect of fly ash in concrete.....	16
2.5.2 Workability.....	17
2.5.3 Effects of fly ash on the properties of hardened concrete.....	18
2.6 Effects of fly ash on the durability of concrete.....	18
2.6.1 Effects of fly ash on permeability of concrete.....	19
2.6.2 Effects of fly ash on carbonation.....	20
2.6.3 Effects of fly ash on sorptivity.....	20
2.7 Hydration of fly ash.....	21
2.7.1 The mechanism of fly ash reaction hydration.....	22

2.7.2	Microstructure of fly ash paste	24
2.8	Effect of conditioning on pore structure	27
2.8.1	Solvent replacement	27
2.8.2	Oven drying	28
2.8.3	Vacuum drying	28
2.8.4	Direct freeze-drying.....	29
2.9	Durability of the concrete	29
2.9.1	Durability tests	30
2.10	Improper curing.....	38
2.11	Effects of degree of saturation on compressive strength	39
2.12	Effects of drying on concrete.....	40
2.12.1	Effect of medium or low temperature on concrete.....	40
2.13	Shrinkage	41
2.13.1	Plastic shrinkage.....	42
2.13.2	Drying Shrinkage	42
2.13.3	Autogenous shrinkage.....	43
2.13.4	Chemical shrinkage	43
2.13.5	Carbonation shrinkage	43
2.13.6	Thermal Shrinkage	44
2.13.7	Mathematical modelling of drying shrinkage	44
2.13.8	Factors affecting shrinkage	47
2.14	Summary.....	53
Chapter 3 Materials and experimental methods.....		55
3.1	Materials.....	55
3.1.1	Portland cement (CEM I).....	55
3.1.2	Fly ash.....	58
3.1.3	Aggregates.....	58
3.1.4	Water.....	59
3.2	Mix design, curing and exposure conditions	60
3.3	Test Method	62
3.3.1	Slump Test.....	62
3.3.2	Absorption and Surface Moisture	62
3.3.3	Mixing, Casting and Curing.....	64
3.4	Unconfined Compressive Strength (UCS).....	64
3.5	Sorptivity	64

3.5.1	Sorptivity test	65
3.6	Permeability.....	66
3.6.1	Preconditioning of Samples before Measuring Permeability.	67
3.6.2	Permeability Experiment.....	67
3.7	Determination of Degree of Saturation	69
3.8	Carbonation.....	70
3.8.1	Carbonation experiment	70
3.9	Drying Shrinkage Test.....	71
3.10	Measuring the degree of hydration	71
3.10.1	Sample Preparation for XRD, TG and SEM	71
3.10.2	X-ray Diffraction (XRD)	73
3.10.3	XRD Measurement in this study.....	74
3.10.4	Thermogravimetric analysis (TGA).....	74
3.10.5	TGA measurement in this research.....	74
3.10.6	Bound water content	76
3.10.7	Scanning electron microscopy (SEM).....	76
3.10.8	SEM measurement in this project.....	76
3.10.9	Image analysis	77
Chapter 4 Effect of improper curing on strength development		79
4.1	Compressive strength of CEM I Concretes	81
4.2	Compressive strength of Fly ash Concretes	83
4.3	Compressive strength of 20 Fly ash stiff mix with minimum curing period (f_2/f_{28}).....	85
4.4	Compressive strength development of saturated CEM1 samples.....	85
4.5	Compressive strength of Fly ash immersed samples	90
4.6	Compressive strength of 20MPa Fly ash stiff mix with ambient cured immersed and f_2/f_{28} immersed.....	93
4.7	Compressive Strength at 28 days	94
4.8	Conclusion	96
Chapter 5 Effects of drying		98
5.1	Effect of drying in the present work.....	98
5.1.1	Effects of weight loss as a result of drying.....	98
5.2	Effects of drying on compressive strength.....	99
5.3	Compressive strength of concretes as the binder contents increases.....	100
5.4	Effect of drying on compressive strength of stiff mix and the wet mix	100

5.5	Effect of drying on Compressive strength of CEM1 and Fly ash concretes.....	101
5.6	Mass loss in ideal cured sample as a result of drying.....	102
5.7	Change in weight in ambient cured samples	104
5.8	Conclusion	106
Chapter 6 Results and Discussion of Shrinkage Following ideal and Ambient Curing		107
6.1	Effect of curing on drying shrinkage.....	107
6.2	Predicted and experimental shrinkage.....	108
6.3	Normalised Shrinkage.....	111
6.4	Effects of cement content on drying shrinkage.	111
6.5	Effects of water contents on shrinkage.....	112
6.6	Effects of Fly ash on drying shrinkage.	113
6.7	Conclusions.....	114
Chapter 7 Transport properties and Resistance to Carbonation		115
7.1	Sorptivity	115
7.2	Permeability.....	117
7.3	Carbonation	120
7.4	Summary.....	122
Chapter 8 Degree of hydration.....		124
8.1	Degree of cement hydration from SEM images	130
8.1.1	Image J.....	130
8.1.2	Image analysis	130
8.1.3	Image J procedure.....	131
8.1.4	Degree of hydration of ambient and ideal cured CEM1 and fly ash concretes.....	132
8.1.5	Effect of hydration on stiff and wet Mix	132
8.2	Porosity.....	133
8.3	Bound water content.....	136
8.3.1	Bound water content at 28 days.....	139
8.4	Thermogravimetry (TG) results	140
8.4.1	Portlandite content from thermogravimetric analysis at 28 days.....	143
8.5	XRD Analysis	145
8.6	Conclusion	148
Chapter 9 General discussion.....		150
9.1	Effect of improper curing compressive strength.....	150
9.2	The impact of improper curing on drying shrinkage	151

9.3	Effect of improper curing on permeability	152
9.4	The impact of improper curing on sorptivity	153
9.5	Impact of improper curing on carbonation resistance.....	153
9.6	Impact on degree of hydration.....	154
9.7	Practical implication of the study.....	157
Chapter 10 Conclusion and Suggestions for Further works.....		159
10.1	Conclusions.....	159
10.2	Suggestions for Further Works.....	160
References.....		161
Appendices		A1

List of Tables

Table 2-1 Shorthand Notations for the Oxides in Portland cement taken from (33)	8
Table 2-2 Four dominant phases of Portland cement and their typical features in hydrated cement pastes (33, 42-44).....	9
Table 2-3 Chemical and phase composition, and density of a typical fly ash (43)	17
Table 2-4 Temperature of the decomposition of cement pastes phases (43)	28
Table 2-5 Factors affecting shrinkage strain	47
Table 3-1 Composition of CEM 1 52.5N Manufactured at Ribblesdale	57
Table 3-2 Clinker compounds by Rietveld analysis.....	57
Table 3-3 Chemical composition of Drax Fly Ash.....	58
Table 3-4 Density and Fineness of the Binders.....	Error! Bookmark not defined.
Table 3-5 Particle size distribution of fine aggregate.....	59
Table 3-6 Particle size distribution of 10mm coarse aggregate	59
Table 3-7 Concrete mix designs used in this study	61
Table 3-8 Aggregates surface moisture content, Total moisture content and absorption	62
Table 3-9 Adjusted water used to cast the concrete and w/b ratio.....	63
Table 4-1 Nomenclature used in the graph with measured slump	80
Table 5-1 Drying age used in the experiment.....	98
Table 5-2 Mass loss in ideal cured concrete as a result of drying	102
Table 7-1 Effect of curing on sorptivity.....	115
Table 7-2 Ambient and Ideal Permeability coefficients	118
Table 8-1 CEM1 TG results	142
Table 8-2 Fly ash TG results	143
Table 9-1 Concrete compressive strengths at 28days of curing.....	151
Table 9-2 Permeability of ambient and ideal cured samples	152
Table 9-3 Carbonation depth and coefficient of sorptivity	154
Table 9-4 Degree of hydration of ambient and ideal samples.....	155

List of Figures

Figure 2-1 Rate of heat evolution during the hydration of Portland cement (33)	10
Figure 2-2 Alite heat evolution showing the effect of heat treatment and particle size distribution on the length of the induction period in alite hydration (54).....	11
Figure 2-3 BSE image of Portland cement mortar at 200 days (60)	13
Figure 2-4 BSE image of Portland cement paste at 28days taken from (61).....	13
Figure 2-5 Diagrammatic model of water associated with C-S-H (28, 34)	15
Figure 2-6 Semi-adiabatic calorimetry curves for FA and control pastes (99).	22
Figure 2-7 BSE image of fly ash blended cement paste at 28 days (109).....	25
Figure 2-8 Microstructure morphology of fractured surface paste of 20% fly ash at 7 days taken from (96)	25
Figure 2-9 Microstructure morphology of fractured surface paste of 20% fly ash at 28 days taken (96)	26
Figure 2-10 Microstructure morphology of fractured surface paste of 20% fly ash at 90 days taken from (96)	26
Figure 2-11 Resistivity / conductance testing of concrete samples	35
Figure 2-12 Schematic of rapid chloride permeability test	36
Figure 2-13 Effect of coarse aggregate content Taken from (227).....	48
Figure 2-14 Effect of cement content Taken from (227)	49
Figure 3-1 Schematic for each set of samples	56
Figure 3-2 Addition concrete cubes casted for minimum curing condition	57
Figure 3-3 Aggregate grading curves	59
Figure 3-4Schematic setup of sorptivity test.....	65
Figure 3-5 Linear fit for the determination of sorptivity coefficient for 20MPa CEM1 stiff mix ambient cured	66
Figure 3-6 Components of the Leeds cell (267)	69
Figure 3-7 Carbonation Experiment Set Up.....	70
Figure 3-8 8ml tube used for the paste samples	72
Figure 3-9 Ambient cured samples	72
Figure 3-10 Samples prepared to be cured in the bath.....	72
Figure 3-11 Paste samples after curing ready for cutting.....	73
Figure 3-12 SEM sample after cutting.....	73
Figure 3-13 Measuring the Portlandite and Calcium Carbonate using the tangent method, taken from (279)	75
Figure 3-14 Resin impregnated carbon coated samples for scanning electron microscope	77

Figure 3-15 Grey level histogram of a hydrated cement paste (279)	77
Figure 3-16 Grey level histogram of a fly ash blended cement paste from (109)	78
Figure 4-1 Various tests made with 100 x100 x100mm concrete cubes.....	79
Figure 4-2 Compressive strength of CEM1 stiff mix (slumps 10-30mm).....	82
Figure 4-3 Compressive strength of CEM1 wet mix (slumps 60-180mm).....	83
Figure 4-4 Compressive strength of fly ash stiff mix (slumps 10-30mm).....	84
Figure 4-5 Compressive strength of fly ash concrete wet mix (slumps 60-180mm).....	84
Figure 4-6 Compressive strength of 20MPa fly ash Concrete with f_2/f_{28}	85
Figure 4-7 Compressive strength of 20MPa CEM1 Stiff Mix and immersed	87
Figure 4-8 Compressive strength of 50MPa CEM1 Stiff Mix and Immersed	87
Figure 4-9 Compressive strength of 80MPa CEM1 Stiff Mix and Immersed	88
Figure 4-10 Compressive strength of 20MPa CEM1 Wet Mix and Immersed	88
Figure 4-11 Compressive strength of 50MPa CEM1 Wet Mix and Immersed	89
Figure 4-12 Compressive strength of 80MPa CEM1 Wet Mix and Immersed	89
Figure 4-13 Compressive strength 20MPa Fly ash Stiff Mix and Immersed.....	90
Figure 4-14 Compressive strength 50MPa PFA Stiff Mix and Immersed	91
Figure 4-15 Compressive strength 80MPa Fly ash Stiff Mix and Immersed.....	91
Figure 4-16 Compressive strength 20MPa Fly ash Wet Mix and Immersed	92
Figure 4-17 Compressive strength 50MPa Fly ash Wet Mix and Immersed	92
Figure 4-18 Compressive strength of 80MPa Fly ash Wet Mix and Immersed.....	93
Figure 4-19 Compressive strength of 20MPa Fly ash Stiff Mix and f_2/f_{28} Immersed	94
Figure 4-20 Figure showing the graphs mixes and the binders.....	94
Figure 4-21 Compressive strength of Ambient and Ideal cured concretes at 28 days.....	95
Figure 4-22 Compressive strength of CEM1 and Fly ash concretes	96
Figure 5-1 Change in mass for 20,50 and 80MPa CEM1 stiff mix	99
Figure 5-2 Percentage change in mass and compressive strength of CEM1 wet mix concrete	99
Figure 5-3 Compressive strength of 20, 50 and 80MPa CEM1 stiff mix	100
Figure 5-4 Compressive strength of Fly ash stiff and wet mix	101
Figure 5-5 Effect of drying on compressive strength of CEM1 and Fly ash Concrete	101
Figure 5-6 Percentage change in mass for CEM1 and fly ash concrete stiff mix	103
Figure 5-7 Percentage change in mass for CEM1 and fly ash concrete wet mix	103
Figure 5-8 Percentage increase in mass for CEM1 and fly ash concretes in stiff mix	105
Figure 5-9 Percentage increase in mass for CEM1 and fly ash concretes in wet mix	105
Figure 6-1 Ambient and Ideal Cured Shrinkage of CEM1 stiff mix	108

Figure 6-2 Predicted shrinkage and measured ambient and ideal Shrinkage for 20MPa CEM1 wet mix.....	109
Figure 6-3 Predicted and Experimental shrinkage of 50MPa CEM1 stiff mix.....	110
Figure 6-4 Predicted and experimental shrinkage of 80MPa CEM1 stiff mix.....	110
Figure 6-5 Normalised shrinkage with Model code 2010 for 20MPa CEM1	111
Figure 6-6 The effects of cement content on drying shrinkage	112
Figure 6-7 Shrinkage of Stiff mix and the Wet mix	113
Figure 6-8 Shrinkage of CEM1 concretes and Fly ash concretes	114
Figure 7-1 Effect of curing on sorptivity.....	116
Figure 7-2 Effect of stiff and wet mixes on sorptivity	117
Figure 7-3 Sorptivity coefficient of CEM1 and fly ash concretes.....	117
Figure 7-4 Ambient and ideal permeability of CEM1 and fly ash concretes	118
Figure 7-5 Effect of different mixes on permeability	119
Figure 7-6 Permeability of CEM1 and fly ash concretes	119
Figure 7-7 Carbonation depth of ambient and ideal cured samples at 28 days.....	120
Figure 7-8 Carbonation depth showing stiff and wet mix of ambient and ideal cured samples at 28 days.....	121
Figure 7-9 Carbonation depth of CEM1 and Fly ash concretes at 28 days.....	121
Figure 7-10 Selected Carbonated samples of 20MPa Stiff Mix.....	122
Figure 8-1 20MPa CEM1 Stiff mix Ambient cured.....	125
Figure 8-2 20MPa fly ash stiff mix Ambient cured.....	125
Figure 8-3 SEM images of CEM1 stiff and Wet mix.....	127
Figure 8-4 SEM images of Fly ash stiff and wet mix.....	129
Figure 8-5 Detailed Procedures for Calculations of anhydrous clinker	131
Figure 8-6 Degree of hydration of ambient and ideal cured samples measured from SEM images	132
Figure 8-7 Degree of hydration of stiff and wet mix.....	133
Figure 8-8 Degree of hydration of CEM1 and Fly ash concretes	133
Figure 8-9 Porosity of ambient and ideal cured samples at 28 days.....	135
Figure 8-10 Porosity of stiff and wet mixes.....	135
Figure 8-11 Porosity of CEM1 and fly ash concrete	136
Figure 8-12 Bound water content of CEM1 stiff mix.....	137
Figure 8-13 Bound water content of CEM1 wet mix.....	137
Figure 8-14 Bound water content of Fly ash stiff mix	138
Figure 8-15 Bound water content of Fly ash wet mix	138
Figure 8-16 Bound water content of ambient and ideal cured samples	139

Figure 8-17 Bound water content in stiff and wet mix	139
Figure 8-18 Bound content in CEM1 and Fly ash concrete	140
Figure 8-19 Measuring the calcium hydroxide and calcium carbonate by tangent method.....	141
Figure 8-20 CH contents in ambient and ideal cured samples.....	144
Figure 8-21 CH contents in stiff and wet mix	144
Figure 8-22 CH contents in CEM1 and Fly ash concretes	145
Figure 8-23 XRD of 20MPa CEM1 stiff mix from 1 day to 28 days of curing, plus the pattern from anhydrous CEM1	146
Figure 8-24 XRD of 20MPa CEM1 stiff mix from 1 day to 28 days of curing	146
Figure 8-25 XRD of 50MPa CEM1 wet mix from 1 day to 28days of curing	147
Figure 8-26 XRD of 20MPa Fly ash stiff mix from 1 day to 28days of curing.....	147
Figure 8-27 XRD of 50MPa Fly ash stiff mix from 1 day to 28days of curing.....	148

List of Abbreviations

Cement Nomenclature:

C = CaO

Si = SiO₂

A = Al₂O₃

M = MgO

F = Fe₂O₃

\bar{S} = SO₃

N = Na₂O

K = K₂O

H = H₂O

Techniques:

BSE Back Scattered Electron

CEM1 Portland cement

DOH Degree of Hydration

DOS Degree of Saturation

DTA Differential Thermal Analysis

EDX Energy Dispersive X-Ray Spectroscopy

GGBS Ground Granulated Blast Furnace Slag

PC Portland Cement

PFA Pulverised Fly Ash

RH Relative Humidity

SCM Supplementary Cementitious Material

SEM Scanning Electron Microscopy

STA Simultaneous Thermal Analysis

TEM Transmission Electron Microscope

TGA Thermogravimetric Analysis

UCS Unconfined Compressive Strength

W/B Water to Binder Ratio

W/C Water to Cement Ratio

XRD X-Ray Diffraction

Clinker and hydrated phases:

Alite (C₃S) 3CaO.SiO₂

Belite (C₂S) 2CaO.SiO₂

Tricalcium Aluminate (C₃A) 3CaO.Al₂O₃

Tetracalcium Aluminoferrite (C₄AF) 4CaO.Al₂O₃.Fe₂O₃

Gypsum CaSO₄.2H₂O

Portlandite (CH) Ca(OH)₂

Calcium Silicate Hydrate (C-S-H) CaO.SiO₂.H₂O

Ettringite (AF_t) 3CaO.Al₂O₃.3CaSO₄.32H₂O

Chapter 1

1.1 Introduction

Concrete is the most extensively used man-made construction material in the world (1-3). This is a result of the availability of plenty of raw materials for cement manufacture, its low relative cost and its flexibility in operations (4). Sabir *et al* (5) wrote that its consumption is second only to water as the most utilized man-made substance on the planet (6, 7). Global concrete production is approaching 20×10^{12} kg per annum (8), and increasing as vast developing nations upgrade and invest in their infrastructure.

The use of concrete however, is associated with environmental impacts both in terms of deterioration generated by the extraction of raw materials and CO₂ emissions during cement production. The cement industry alone is accountable for 5-10 % of the anthropogenic CO₂ (2, 9-11). Portland cement is the most commonly used binder in producing concrete. The global greenhouse gas emissions generated by production of cement has led to research into how these emissions can be reduced. One such approach is the increased use of Additions. Additions are finely divided inorganic materials used in concrete in order to improve certain properties or to achieve special properties according to EN 206:2013+A1:2016 (Concrete Specification, performance, production and conformity) (12). Nearly inert addition and pozzolanic or latent hydraulic addition designated as type I and II are the types of inorganic additions listed in EN 206:2013+A1:2016. These materials may be in their natural form, industrial wastes or by-products or those that necessitate only minimal further processing to produce. Fly ash, blast furnace slag, silica fume and metakaolin are common additions that can be used as partial replacements for Portland cement. These materials can enhance concrete durability, lessen the opportunity of thermal cracking in mass concrete and are of lower energy- and CO₂ concentration than cement (13, 14). Thomas (15) wrote that additions are often used in concrete mixes to cut down cement contents, improve workability, increase strength and enhance durability through hydraulic or pozzolanic activity. Utilization of these by-products in cement and concrete not only stops them from being land-filled but also enhances the properties of concrete in the fresh and hardened states.

Fly ash is an essential pozzolan, a by-product of coal combustion in the generation of electricity, or it can be better described as a finely segregated remnant trapped from the flue gas at coal-fired power plants. Most fly ash particles are spherical and amorphous, ranging in size between 10 and 100µm (3). Fly ash has a number of advantages compared with regular Portland cement. First, it is a suitable cement substitute for mass structures because the heat of hydration is lower. Probably the most significant advantage of fly ash is that, being a by-product of coal combustion, it has a lower carbon footprint than Portland cement. Also, improved strength and durability properties can be achieved from concrete produced by partial replacement of Portland cement with fly ash than concrete produce only with Portland cement. The availability of fly ash extensively anywhere coal is being burned is another advantage and finally, fly ash is usually cheaper than Portland cement (2).

Curing of concrete is one of the most essential requirements for optimal performance in any environment or application. It is important for strength development and durability of concrete (16). Neville (17) said that curing is the name given to steps to develop the hydration of cement, which involves regulations of temperature and moisture flow from and into the concrete. The need for curing is because hydration of cement can take place only in water-filled capillaries. This is why loss of water by evaporation from the capillaries must be prevented. The objective of curing is to put concrete in a saturated form or almost saturated, till the formerly water-filled space in the fresh cement paste has been replaced to desired extent by the products of cement hydration. Bentz and Stutzman (18) wrote that proper curing is equally emphasized to provide a source of external (or internal) water to replace that consumed by chemical shrinkage during the hydration of the cement. Curing is particularly important for concrete mixes where the water/cement ratio is below 0.42. This type of concrete is at greater risk of self-desiccation. Curing is vital also if the cement used to make the concrete has a high rate of strength development, and with the use of additions, which tend to hydrate more slowly than cement (19).

Durability of concrete is the capability of concrete to prevent weathering action, chemical attack, abrasion, or any process of deterioration according to ACI Committee 201 (Guide to Durable Concrete) (20) and this is highly affected by curing conditions. If the concrete is not properly cured, then the surface layer, about 30 to 50 mm (17, 21, 22), is most affected due to the potential for evaporation of water from the concrete surface. This means that regulation of moisture is not just for improving the compressive strength of structural element, rather it also reduces surface permeability and increases hardness, so as to improve the longevity of a structure, especially one exposed to harsh environments.

It has been established that fly ash may improve the long term strength of concrete with proper curing (19, 23-25). However, it is known that fly ash hydrates more slowly than Portland cement. Therefore, fly ash concretes would normally require prolonged curing. However, anecdotally, this does not appear to be common practice, and both concrete strength and durability could be compromised. Therefore studying the effect of improper curing on concrete durability is very important to correct known errors in practice and effective usage of fly ash.

Furthermore, the degree of saturation of concrete may affect its measured strength (26-28). Therefore, since changes in curing conditions will affect the degree of saturation of the resultant concrete, any study of improper curing must also consider the effects of changes in the degree of saturation (DOS).

This study investigates the effect of improper curing on concrete specimens. It will also look at the effect of improper curing on concrete properties that may affect concrete durability, in particular resistance to carbonation. The results will be interpreted with reference to the microstructures and phase assemblages of the ideally and improperly cured samples. In order to achieve this aim concrete samples were prepared, which covered a number of mix design variables. These were cured under ideal conditions, or under ambient conditions following demolding after one day.

Performance was assessed by measuring unconfined compressive strength and drying shrinkage. Transport properties (sorptivity and permeability) were determined according to methods developed in the published literature while durability was assessed by accelerated

carbonation studies. Information on the phase assemblages and microstructures was obtained by characterisation using SEM, TGA and XRD.

The research addressed the following objectives:

- To investigate the effect of improper curing on compressive strength, drying shrinkage, sorptivity and permeability
- To study whether these effects vary as a function of mix design parameters.
- To determine the effect of changes in the degree of saturation of concrete on its compressive strength, and see whether this is affected by various mix design variables.
- To understand changes in performance by understanding changes in the degree of hydration as measured by a suite of analytical techniques.
- To investigate the effect of improper curing on concrete durability, particularly resistance to carbonation.

The research work is explained under the following chapters outlined below:

- Chapter 2 comprises of an overview on the hydration and microstructure of Portland and fly ash blended cement systems, effects of fly ash on durability, durability of concretes, improper curing and shrinkage
- Chapter 3 explains in detail the materials and the experimental methods used in the study
- Chapter 4 reports the impact of improper curing on strength development and effect of degree of saturation on compressive strength.
- Chapter 5 describes the effect of drying on ideal cured concrete samples.
- Chapter 6 explains the effect of improper curing on drying shrinkage, predicted and experimental shrinkage were compared, also effect of using fly ash on drying shrinkage and different water binder ratio.
- Chapter 7 reports the impact of improper curing on sorptivity, permeability and resistance to carbonation.
- Chapter 8 follows the hydration mechanisms and developed microstructure of the ambient and ideal cured concretes.
- Chapter 9 presents general discussion on all the results
- Chapter 10 gives the conclusion and further works

Chapter 2 Literature Review

2.1 Introduction

Concrete as a construction material is durable and flexible in its use. It is strong and has excellent sound reduction and fire resistance properties. It is normally the cheapest and most readily available material on a construction project, which has resulted in its huge consumption throughout the world. It could be said that concrete underpins modern life. Cement is still an indispensable material in making concrete but cement's production is main source of environmental impacts of concrete structures (29, 30). This has brought about a trend towards lower clinker factors, hence the use of additions has greatly increased. However, these materials hydrate more slowly, so proper curing becomes more critical.

We know how to make good structures, but we are reminded every day that not all concrete structures are durable. Therefore, there is a need to improve concrete practice such that durability concerns are reduced. Curing is one concrete practice that is not new to civil engineers and construction workers but, is not always practised, the effects of which may not be seen for many years. Curing of concrete is essential for strength development and durability with the main objective of keeping concrete in a saturated state or approximately wet to help the hydration of cement. The curing process that follows placing and consolidation of the plastic concrete can determine the rate and degree of hydration, and the resulting strength of concrete and other properties. Basheer *et.al* (31) wrote that improper curing is one of the factors that have reduced the service life of many structures or resulted in mandatory comprehensive repairs, with great economic costs.

The effects of improper curing may not appear to demonstrably affect concrete quality immediately, and thus its impact on strength may not be an appropriate parameter with which to measure the durability of a structure. Cabrera *et.al* (32) commented that assessing curing methods based on the strength of the concrete does not adequately predict the performance of the concrete in a structure, since the durability of the concrete is controlled more by its porosity and permeability than its strength.

This chapter reviews the constituents of concrete, the hydration of Portland cement and the durability of concrete. Fly ash, one of the common additions and an important pozzolan, which has been in use for over 50 years will be reviewed also. The influence of fly ash on the properties and microstructure of concrete will be explained, together with the effects of improper curing on concrete durability.

2.2 Concrete

Concrete is a construction material, where aggregate is bound with a hydraulic cement and water. The properties of concretes depend on the characteristics of the constituent materials. Mindess (33) described concrete as a composite material produced by mixing cement, supplementary cementing materials, aggregates, water, and chemical admixtures in appropriate proportions and allowing the resulting mixture to set and harden over time. The aggregate does not take part in this reaction and ideally it remains inert.

Concrete can be a durable building material. It provides superior fire resistance, compared with wooden construction and can gain strength over time. Structures made of concrete can have a long service life. Concrete achieves high compressive strength but a relatively low tensile strength, it undergoes thermal movement and is vapour permeable.

Some constituents of concrete listed in EN 206:2013+A1:2016 are; cement, water, aggregates, admixtures and additions. These are discussed briefly in turn below.

2.2.1 Cement

Cement is a material which binds together solid bodies (aggregate) by hardening from a plastic state. Portland cement is by far the most important member of the family of hydraulic cements - that is, cements that harden through chemical interaction with water.

2.2.2 Aggregates

Aggregates are granular materials usually sand, gravel or crushed stone that, generally fill almost 60 to 75% of the volume of concrete. Aggregate properties certainly influence the workability of plastic concrete and also the durability, strength, thermal properties, and density of hardened concrete. Most aggregates have specific gravities in the range of 2.6 to 2.7 (17). The role of the aggregate is to provide much better dimensional stability and wear resistance. Aggregates make the production of concrete more economical because they are less expensive than Portland cement.

The aggregate may range in varying shapes and sizes from having angular shapes to rounded edges, in most common concretes the aggregate particle sizes vary from 0.15 to 37.5mm. Aggregates may then be divided into two specific types; fine and coarse. Fine aggregates usually exist as natural sand or crushed stone with most particles having a diameter less than 4.75mm, and passing through number four sieve. Coarse aggregates are any particles greater than 4.75mm and retained on a number four sieve (34). The grading of coarse aggregate is usually from 5 mm in particle size up to a maximum that should not exceed 40mm (35).

Generally, aggregates are much stronger than the cement paste, so their exact mechanical properties are not considered to be of much importance (except for very high-strength concretes). Similarly, they are also assumed to be completely inert in a cement matrix as they do not hydrate and do not undergo any dimensional changes. Additional physical and mineralogical properties of aggregate should be established before mixing concrete to obtain a desirable mixture. These properties include shape and texture, size gradation, moisture content, specific gravity, reactivity, soundness and bulk unit weight. These properties together with the water/cementitious material ratio determine the strength, workability, and durability of concrete. Also in a good concrete mix, aggregates should be clean, hard, strong particles free of absorbed chemicals or coatings of clay and other fine materials that could cause the deterioration of concrete.

2.2.3 Water

Water is an essential ingredient in production of concrete. Water reacts with cement to start the hydration process. Generally, any natural water that is drinkable can be used as mixing water for making concrete. The water needs to be free from contaminants such as silt, clay, acids, alkalis, organic matter and sewage and other impurities as they will have adverse effects on the concrete. Impurities in the water may not just affect the strength of

the concrete but it can also affect its appearance through staining, efflorescence and surface dampness.

2.2.4 Admixture

Admixtures are additives in concrete which are added to the mixture immediately before or during mixing. Admixtures have various functions to improve the behaviour of concrete and are of two types chemical and mineral. Kosmatka, *et al* (36) gave the following as the main reasons for using admixtures :

- To cut down the cost of concrete construction,
- To accomplish, achieve certain properties in concrete more efficiently than by other means,
- To control the quality of concrete during the stages of mixing, transporting, placing, and curing in adverse weather conditions,
- To overcome certain emergencies during concreting operations.

2.2.5 Additions

The use of additions in concrete is on increase as the industry is looking for ways to reduce its carbon footprint, and reducing the clinker content within cement in order to reduce the emission of CO₂ generated during the production of Portland cement. Fly ash, metakaolin, silica fume and ground granulated blast furnace slag (GGBS) are common additions used in blending Portland cement. These additions were type II according to EN 206:2013+A1:2016 (12) and may be Pozzolanic or latent hydraulic additions. In all cases, these additions are slightly depleted in calcium relative to Portland cement and usually react at slower rates.

2.2.5.1 Fly ash

Fly ash is generally grey in colour, abrasive, mostly alkaline, and refractory in nature. Fly ash are siliceous or siliceous and aluminous materials that when combine with water and calcium hydroxide produce cementitious products at ambient temperatures (37). Fly ash is a by-product of the combustion of pulverised coal in thermal power plants. The ash is composed of the fine particles that are driven out of the boiler with the flue gases, before being collected by electrostatic precipitators or other particle filtration equipment. The fly ash particles are formed upon the solidification of molten material suspended in the exhaust gases upon coal combustion. The rapid cooling of these particles lead to fly ashes generally being spherical, and also prevents crystallisation of mineral phases, resulting in fly ash comprising primarily of a glassy aluminosilicate matrix. The specific gravity of fly ash varies and is lower than that of Portland cement, ranging from 1.9 to 2.9. The composition of the incombustible components within the coal defines the composition of the fly ash and all fly ash possesses substantial amounts of silica (SiO₂), alumina (Al₂O₃) and lime (CaO). According to EN197-1:2011 (38) fly ash can replace Portland cement in proportions ranging from 6 to 55% by weight of the Portland cement.

2.2.5.2 Silica fume

Silica fume, also known as microsilica, is an extremely fine non-crystalline polymorph of silica, and is produced in electric arc furnaces as a by-product of silicon and ferrosilicon alloy production. It is captured from the oxidized vapour on top of the electric arc furnaces.

The particles are amorphous and ultra-fine in size, averaging from 0.1 to 0.5 μm (3). Silica fume is an efficient pozzolan and when use in concrete increases its compressive strength. The addition of silica fume to concrete has a minimal effect on both initial and final setting times at replacement levels of 5-10%, but leads to a slight increase in setting times at higher replacement levels. The fine nature of silica fume, and the resultant incredibly high specific surface area, can lead to a reduction in concrete workability.

2.2.5.3 Ground granulated blast-furnace slag (GGBFS)

GGBS is a latently hydraulic material, which can start to react hydraulically when water is added to it, but the reaction is very slow. The reaction may be accelerated by the addition of alkali. GGBFS is a fine powder grounded from the glassy, granular material that forms when molten iron blast furnace slag is air quenched with water or steam. The fineness and specific surface area of GGBFS is similar to cement particles and contains very limited amount of crystals. GGBFS is highly cementitious in nature and when 80% is partially replaced by cement a reduction in compressive strength is obtained at 28 days while the later-age strength increased with the slag replacement up to 60% (39). Utilization of GGBFS in concrete improved the pore structure of concrete and increased its chloride-binding capacity by forming more Friedel's salt which reduces the chloride diffusivity. GGBFS has a relative density of 2.85 to 2.95, with a bulk density of 1050 to 1375 kg/m^3 . GGBFS is a quite variable material due to the variability of its chemical composition (3, 40).

2.2.5.4 Metakaolin

Metakaolin is not an industrial by-product but a manufactured product, produced under carefully controlled conditions. It is produced by heating kaolin, a natural clay mineral, to temperatures typically between 650 and 750°C. At such temperatures, the kaolin is dehydroxylated; transforming from kaolin to metakaolin. A disordered structure and a highly reactive, amorphous, pozzolanic material is developed from this process. Metakaolin is often white in colour and greatly demand for specialist architectural applications. Though metakaolin is predominantly an aluminosilicate that is derived from natural minerals, there is slight variations in its chemical composition. The variation of the silica content is between 50 to 55%, while the alumina content variation is between 40 to 45%. Fe_2O_3 , TiO_2 , SO_3 , P_2O_5 , CaO , MgO , Na_2O and K_2O are the other phases that can be present in metakaolin. Metakaolin particles size are generally finer than cement but not as fine as silica fume (3). Consumption of Portlandite by metakaolin is through the pozzolanic reactivity and this produce more refined pore structure in concrete (41).

2.3 Portland Cement

Portland cement clinker is produced by heating a mixture of calcium carbonate (limestone or chalk) and an aluminosilicate (typically clay or shale) to about 1400°C, rapidly cooling the resultant clinker and grinding the product with approximately 5% gypsum to produce cement (42). Portland cement clinker is a complex mixture of silicates and aluminates with a composition primarily expressed in oxide equivalents. The principal oxides in the clinker are CaO , SiO_2 , Al_2O_3 , and Fe_2O_3 . Portland cement clinker comprises four dominant crystalline phases: tricalcium silicate (C_3S or alite); dicalcium silicate (belite or C_2S), tricalcium aluminate (aluminate or C_3A) and tetracalcium aluminoferrite (ferrite or C_4AF). Several more phases also present in small quantities (0-3% by weight) include free calcium

oxide (CaO), magnesium oxide (MgO) and alkalis (K₂O and Na₂O). Calcium sulphate (typically gypsum, CaSO₄·2H₂O (C \bar{S} H₂)) is added to regulate the rate of set and impacts the rate of strength development.

The chemical composition of Portland cement reported in terms of the oxides of the various elements that are present is shown in Table 2.1, while Table 2.2 summarises the four dominant phases of Portland cement and their typical features (33, 42-44).

Table 2-1 Shorthand Notations for the Oxides in Portland cement taken from (33)

Oxide	Shorthand Notation	Common Name	Typical Weight Percent in Ordinary Cement
CaO	C	Lime	63
SiO ₂	S	Silica	22
Al ₂ O ₃	A	Alumina	06
Fe ₂ O ₃	F	Ferric Oxide	2.5
MgO	M	Magnesia	2.5
K ₂ O	K	Alkalis	0.6
Na ₂ O	N	Alkalis	0.4
SO ₃	\bar{S}	Sulfur trioxide	2.0
CO ₂	\bar{C}	Carbon dioxide	-
H ₂ O	H	Water	-

2.3.1 Hydration of Portland cement

Hydration is the term used to describe the chemical reactions between the anhydrous cement and water, and hydration commences from the moment the cement and water are mixed (45, 46). The individual clinker minerals (alite, belite, tricalcium aluminate and calcium aluminoferrite), are involved in various reactions to form numerous hydration products. Calcium silicate hydrate (C-S-H) is the main hydrate, intermixed with portlandite (CH), ettringite and the AFm phases. Mindess and Eng (47) explained the fundamental characteristics of the hydration of Portland cement as follows:

- The cement paste will continue to be in fluid form if the respective cement grains continue to be separated from each other by water.
- Greater volume is being filled by the products of the hydration reactions than the one filled by the original cement grains.
- Setting follows when the hydration products start to develop.
- Continuation of hydration reactions result in additional bonds which are produced between the cement grains. Thus strengthening of the system is accomplished.

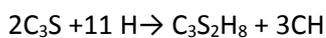
Table 2-2 Four dominant phases of Portland cement and their typical features in hydrated cement pastes (33, 42-44).

Shorthand notation	C ₃ S	C ₂ S	C ₃ A	C ₄ AF
Technical name	<u>Alite</u>	<u>Belite</u>	Aluminate phase	Ferrite Phase
Chemical Name	<u>Tricalcium silicate</u>	<u>Dicalcium silicate</u>	<u>Tricalcium aluminate</u>	<u>Tetracalcium aluminoferrite</u>
Chemical Formula	3CaO·SiO ₂	2CaO·SiO ₂	3CaO·Al ₂ O ₃	4CaO·Al ₂ O ₃
Weight Percent present in cement	40-80	0-30	3-15	4-15
Reaction rate	Moderate	Slow	Fast	Moderate
Possible impurities	Al ₂ O ₃ , Fe ₂ O ₃ , MgO	Al ₂ O ₃ , Fe ₂ O ₃ , K ₂ O, Na ₂ O, SO ₃	Fe ₂ O ₃ , MgO, K ₂ O, Na ₂ O	SiO ₂ , MgO, TiO ₂
Value of heat of hydration(J/g)	450-500	250	1340	420
Heat liberated	High	Low	Very high	Moderate
Contribution to strength	High at early ages	Initially low and high later	Low	Low

2.3.2 Development of hydration product

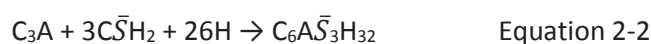
The chemical reactions of pure cement compounds have been described clearly by different authors (33, 42-44) and may be summarized as follows:

Calcium silicate hydrates are produced from the reaction between the two calcium silicates and water. These reactions are written as:



The calcium silicate hydrate, indicated by C₃S₂H₈ has a variable composition, and so is often represented as C-S-H. Tennis *et al* (48) explained that the first two equations are critical since they determine the amount of C-S-H produced.

The C₃A reacts with water causing early setting (within a few minutes) of the cement. This leads to flash set, where the cement stiffens without developing strength. To prevent this, cement clinker is ground with a source of sulphates, typically gypsum. Under such conditions, the C₃A reacts with the gypsum thus;

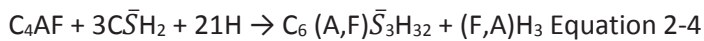


As the gypsum becomes depleted by this reaction, the ettringite and the C_3A react further to form calcium monosulfoaluminate:



The monosulfoaluminate is thus the stable phase in concrete. However, many modern cements, e.g. CEM I, contain small quantities of limestone. Under such conditions, ettringite forms, but instead of reacting to form monosulfoaluminate, the residual C_3A reacts to form calcium hemi or monocarboaluminate and the ettringite remains.

Meanwhile, the ferrite phase is much less reactive than the C_3A , so it reacts much more slowly. Its reaction may be written as:



2.3.3 Mechanism of hydration

Hydration begins as soon as the cement comes in contact with water. The reaction is exothermic and the initial heat output is high associated with rapid dissolution of the individual clinker phases and calcium sulphate which starts to develop hydrated products. The dissolution of C_3S results in the precipitation of a layer of a C-S-H phase at the surface of the cement grain. C_3A and C_4AF also dissolves and reacts with calcium sulphate to form ettringite, that is precipitated on the cement grain surface. The initial rapid reaction begins to slow down after a few minutes, resulting in a low heat output. After the slow reaction period, another period of accelerated hydration is noticed, which is influenced mainly by the nucleation and growth of the hydration products. The acceleration period is where the heat output reaches its maximum, after which it starts to decline due to a decrease in the hydration rate (49-55).

Figure 2.1 shows the development of the hydration of Portland cement, where the hydration procedure is characterized into five stages based on the amount of heat liberated.

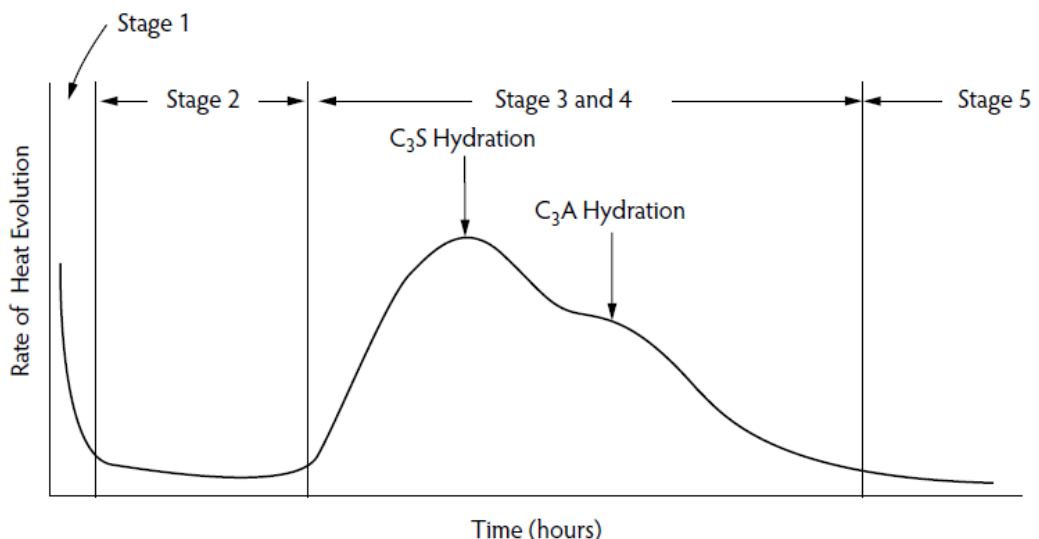


Figure 2-1 Rate of heat evolution during the hydration of Portland cement (33)

2.3.3.1 Pre-induction period

The primary stage starts as soon as the clinker comes into contact with water, there is a very quick evolution of heat (49) that stops within 15-20 minutes. Tricalcium silicate dissolves harmoniously and a layer of a C-S-H phase precipitates at the cement particle surface. Hydration in this phase is identified with an increase of the Ca^{2+} and OH^- concentration in the liquid phase. The fraction of C_3S hydrated in this phase stays low. Tricalcium aluminate breaks up and reacts with Ca^{2+} and SO_4^{2-} ions that exist in the liquid phase, producing ettringite (AFt) that also precipitates at the cement particle surface. This stage is called pre-induction period.

2.3.3.2 Dormant or induction period

Second stage is called dormant or induction period, the reaction rate is very slow and may last a few hours. It can be reduced by incorporating prehydrated C_3S while mixing with water, increasing particle fineness by prolonged grinding, and using higher w/c ratios; while it can be lengthened by cooling of the sample slowly, long lasting storage and doping with Al_2O_3 (56, 57). Here the hydration of all the clinker minerals develops very slowly. The concentrations of calcium and hydroxide ions in the liquid phase reaches a maximum. The sulphate concentration does not change, as that which is consumed to form AFt is replaced by the dissolution of additional amounts of calcium sulphate. At this stage the cement remains plastic and is workable.

In systems mostly in alite and C_3S , when retarders and heat treatment have not been used, the induction period is hardly noticed as shown in Figure 2.2 . In systems like this , the induction period is taken as the minimum in the hydration rate that is reached after the pre-induction period, and just before the start of the acceleration period (55).

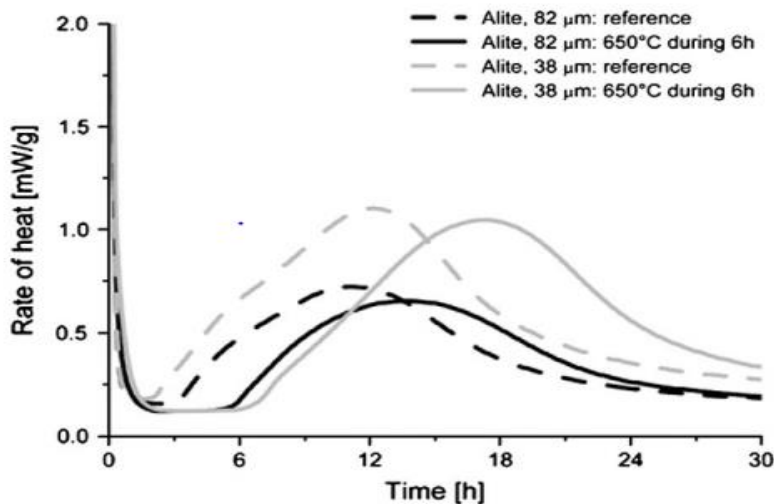


Figure 2-2 Alite heat evolution showing the effect of heat treatment and particle size distribution on the length of the induction period in alite hydration (54).

2.3.3.3 Acceleration stage

The acceleration stage is the third stage, which is about 3 to 12 hours after mixing. In this period hydration accelerates again and is regulated by the nucleation and growth of the

resultant hydration products (49, 54). The rate of C_3S hydration accelerates and the 'second-stage C-S-H' starts to be formed. Crystalline calcium hydroxide (portlandite) precipitates from the liquid phase, and so the concentration of Ca^{2+} in the liquid phase steadily drops. The maximum rate of hydration is attained at the end of this period. Initial set occurs at about the time when the rate of reaction becomes active. The final set also takes place before the end of this stage.

2.3.3.4 Post-acceleration period

The fourth stage, also called the post-acceleration period, is accompanied by continuous formation of hydration products but gradual slowing down of hydration rate. The C-S-H phase continues to grow as C_3S and β - C_2S continue to hydrate. The rate of additional calcium hydroxide formation falls as hydration of β - C_2S begins to make the largest contribution to hydration. When the calcium sulfate had been consumed, the SO_4^{2-} concentration in the liquid phase reduces. Therefore, the AFt phase which has been produced in the earlier stages of hydration begins to react with additional C_3A and C_4AF , producing monosulfate. When the initial water/cement ratio is high, hydration continues until all the original cement has reacted. But, residual larger cement particles may remain, even in mature pastes. At low water/cement ratios, the reaction may stop in the presence of meaningful quantity of non-reacted material, when there is insufficient water for hydration to progress.

2.3.3.5 Final stage

The final stage can be identified by slow formation of products and the reaction is diffusion controlled. Ageing of hydrated material occurs when the hydration process has been completed and the deposition of hydrates becomes constrained by lack of space. It is characterised by a further polycondensation of the SiO_4 tetrahedra which are present and an increase in the average SiO_4 chain length of the C-S-H phase formed (44). Hydration progresses slowly and some of the remaining anhydrous material reacts to develop more inner product C-S-H. The ferrite phase seems to remain unreacted. However, current investigations have shown that it can also be influenced by several factors including: lack of space, lack of water, and the effect of particle size distribution (54, 58, 59).

2.4 Microstructure of cementitious materials

A BSE image of a Portland cement mortar cured for 200 days is shown in Figure 2.3. Scrivener (60) explained that the microstructural development of cementitious materials is through hydration, which increases the solid volume of the system. The microstructure comprises unreacted materials, pores and hydrates. Hydrates are produced in the space initially filled with water (outer products) or within the space formerly occupied by the cement grains (inner product). The outer and inner products contain C-S-H, CH, AFt and AFm.

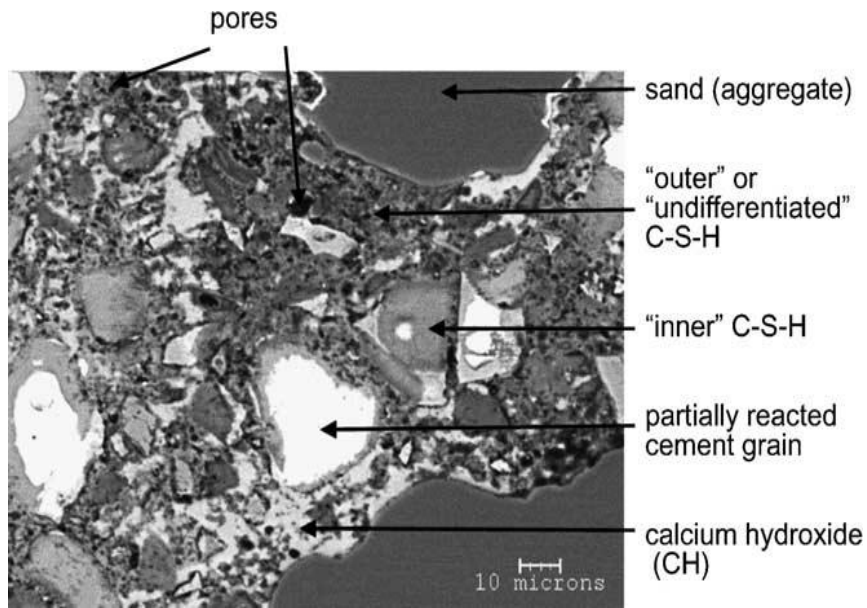


Figure 2-3 BSE image of Portland cement mortar at 200 days (60)

The microstructure of a Portland cement paste is shown in Figure 2.4. In Portland cement, the unhydrated cement grains appear bright; the calcium hydroxide phase shows light grey and the other hydration products (mainly C-S-H) look as various shades of darker grey. The pores appear uniformly black due to the low average atomic number of the epoxy that is filling the pores.

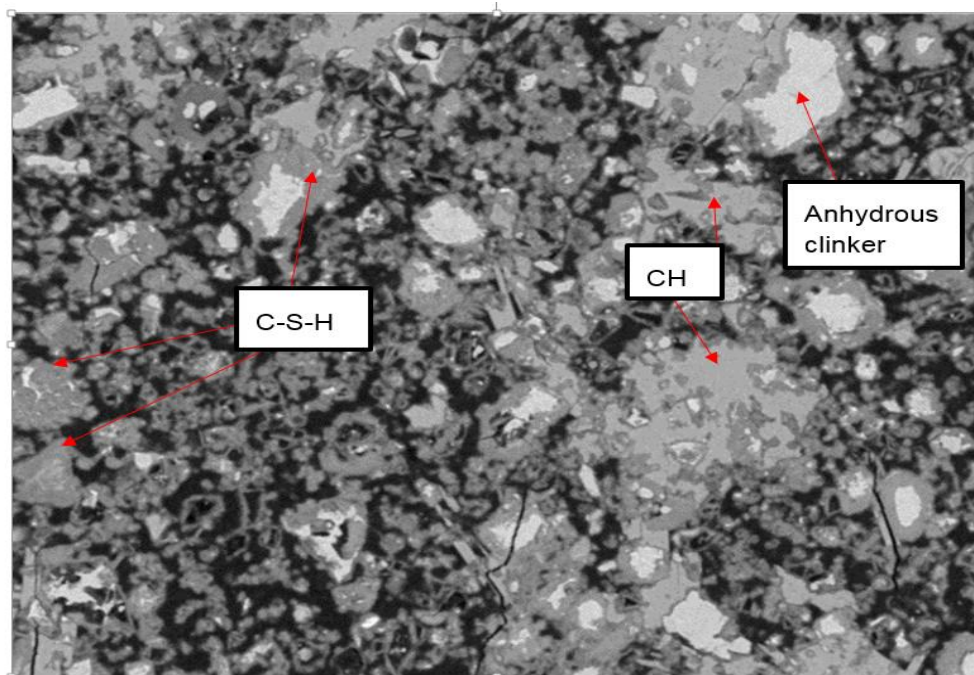


Figure 2-4 BSE image of Portland cement paste at 28 days taken from (61)

Thomas (33) wrote that in Portland cement paste, the hydration reaction is controlled by the reaction of the tricalcium silicate (C_3S) that generates calcium hydroxide (CH) and calcium silicate hydrate (C-S-H). The deposition of the two phases in the microstructure is very different. Calcium hydroxide precipitates in the water filled pores and calcium silicate

hydrate (C–S–H) deposits usually around the cement grains. The water-filled space in a freshly mixed cement paste represents space that is available for the formation of cement hydration products. As hydration proceeds, the volume of this space, which initially was determined by the water cement ratio (w/c) of the paste continually falls by the formation of the hydrated gel, which has a bulk volume larger than that of the original unhydrated cement. Part of the original water-filled space not occupied by the hydration products constitutes part of the pore system of the paste. The development of the pore structure causes the porous material (hardened cement paste) to be less permeable and more resistant to the infiltration of fluids and damaging agents.

2.4.1 Pores in concretes

Hardened cement paste is a porous material. The pore structure defines the properties of the cement paste as much as do the hydrates. Strength, durability, shrinkage, creep and permeability are all directly affected by the pore volume and pore size distribution. The hydration procedure develops an increase in the unhydrated cement bulk volume by 2.1 times (62). The pore structure, meanwhile, can be classified into two classes of pores: gel and capillary pores. The two classes are related, as both are a function of the hydration process and reliant on the moisture content.

2.4.1.1 Capillary pores

Capillary pores can be considered as space initially filled by water, where hydration of cement grains can progress in that particular space. The capillary pores range in size from 10nm to 10 μ m and greatly influence most of the mechanical and durability aspects in concrete (62). The capillary pores appear as black in Figure 2.4. Capillary pores are part of the gross volume that has not been filled by the products of hydration. Since these products fill more than twice the volume of the initial solid phase (i.e. cement) alone, the volume of the capillary system is reduced as hydration proceeds. Capillary pores depend on initial separation of cement particles and are regulated by the water-to-cement ratio (w/c), being larger for higher w/c. Large capillary pores affect strength and durability (permeability), with smaller pores impacting on shrinkage.

2.4.1.2 Gel pores

Gel pores (Interlayer hydration space) are typically within the primary hydration product C–S–H and form 30% of the total gel volume (63). While capillary porosity falls with increasing hydration, gel porosity increases. Gel pores are very small ranging from 0.5 to 4 nm, about an order of magnitude larger than the size of the water molecules. They have little effect on strength, permeability, or shrinkage.

2.4.1.3 Air void

Capillary pores have irregular shapes but air voids are usually spherical. Normally, small amount of air gets trapped in the cement paste when mixing concrete. Entrapped air voids may be as large as 3mm while entrained air voids usually range from 50 to 200 μ m (34). The entrapped and entrained air voids in the hydrated cement paste are much bigger than the capillary voids, and adversely affect strength.

2.4.2 Water phases in concrete

Water is fundamental for cement hydration. In concrete, the water is always present in three distinct forms, which are structural water, gel water, and capillary water. Figure 2.5 shows a diagrammatic model of the type of water associated with the calcium silicate hydrate.

2.4.2.1 Structural water

Structural water includes water of crystallization and chemically bound, non-evaporable water that can only be obtained by hydrate decomposition. It is an integral part of the structure of the different hydration products. This water may be removed at low relative humidity or at high temperatures.

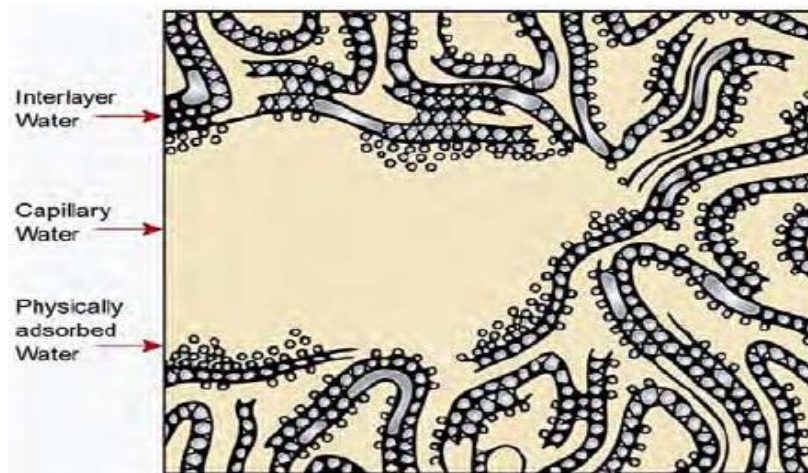


Figure 2-5 Diagrammatic model of water associated with C-S-H (28, 34)

2.4.2.2 Gel water

Gel water is held by capillary tension and strong hydrogen bonding on to the surface of the main cement hydration product, C-S-H gel. This water, which is in nanometer-scale pores, can be removed by evaporation at ambient or reduced pressure, at ambient or elevated temperature (64). The physically bonded water having about 15% by weight of the cement is water bonded to the solid material by adhesive forces. Gel water does not affect the strength but its removal may be the basis for creep and drying shrinkage.

2.4.2.3 Capillary water

Capillary water is the unbound water inside the pores that is usable for hydration. This free water is water that is beyond the range of solid surface forces and is considered to behave as bulk water.

2.5 Fly ash

Fly ash is a by-product of the combustion of pulverized coal in a thermal power plant. Fly ash is a fine particulate residue which is collected by a dust-collection system from combustion gases before they are discharged into the atmosphere. Fly ash is a fine-grained material consisting mostly of spherical, glassy particles. The size of particles varies

depending on the sources. Some ashes may be finer or coarser than Portland cement particles. The specific gravity ranges from a low value of 1.90 for a subbituminous ash to a high value of 2.96 for an iron-rich bituminous ash (3, 33, 37, 65).

The chemical composition of fly ash is determined by the types and relative amounts of incombustible matter in the coal. Most fly ashes comprise silicon, aluminium, iron, calcium, and magnesium elements. Commonly, fly ash from the combustion of subbituminous coals contains more calcium and less iron than fly ash from bituminous coal. Bituminous coals yield ashes with high glass contents, rich in SiO_2 , Al_2O_3 and Fe_2O_3 , and low in CaO. Meanwhile, fly ashes from subbituminous coals have very little unburned carbon, are higher in CaO and crystalline phases. Fly ashes used in Europe in composite cements mostly have CaO levels below 10% (43). Table 2.3 shows chemical and phase compositions, and density of such a typical fly ash. Fly-ash particles are mostly spherical with diameters from $<1\mu\text{m}$ to $150\mu\text{m}$. They show pozzolanic activity and have metastable aluminosilicates that will react with calcium ions, in the presence of moisture, to form calcium silicate hydrates.

2.5.1 General effect of fly ash in concrete.

The effect of fly ash on concrete has been described in three forms which are morphologic effect, pozzolanic effect, and micro aggregate effect (66, 67). These three effects influence each other but focus on different aspects of concrete performance.

The morphologic effect

The morphologic effect considers fly ash as comprising many microbeads, which work as “lubricating balls” when included in fresh concrete; hence fluidity is improved. This can be referred to as dilution effect experienced in blended system as a result of adding fly ash. The effective water/cement ratio is increased due to replacement of cement by fly ash.

The microaggregate effect

The microaggregate effect of fly ash assumes that the microbeads in fly ash can be distributed well in concrete and combine firmly with the gel formed during cement hydration, and hence density of concrete is improved.

The pozzolanic effect

The main effect of fly ash is the pozzolanic effect, which considers that the SiO_2 and Al_2O_3 in fly ash can be activated by portlandite, produced during cement hydration, and develop more hydrates. The gel formed by the pozzolanic reaction can occupy capillary pores, and so contributes to concrete strength. This is particularly true for high volume fly ash concretes where the long-term strength is often generated mainly from the pozzolanic effect (66).

Table 2-3 Chemical and phase composition, and density of a typical fly ash (43)

Chemical composition (%)	
Na ₂ O	1.5
MgO	1.6
Al ₂ O ₃	27.9
SiO ₂	48.7
P ₂ O ₅	0.2
SO ₃	1.2
K ₂ O	4.2
CaO	2.4
TiO ₂	0.9
Mn ₂ O ₃	Tr
Fe ₂ O ₃	9.5
C	1.5
H ₂ O	0.3
Total	99.9
Phase Composition (%)	
Quartz	2.8
Mullite	6.5
Hematite	1.6
Magnetite	1.9
Carbon	1.5
Glass	86
Density(kg m ⁻³)	2220

2.5.2 Workability

Workability is one of the most important properties of concrete, since concrete has to be placed and consolidated to achieve the hardened properties as designed. Also concretes that cannot be placed easily or be well consolidated will not have the expected durability, which can lead to early deterioration. A well-proportioned fly ash concrete mixture will improve workability compared to Portland cement concrete of the same slump (68-70). This implies that fly ash concrete flows and consolidates better than a Portland cement concrete vibrated at the same slump. Improved cohesiveness and a reduction in segregation was found when using fly ash. Also the spherical fly ash particles lubricate the mix making it easier to pump and lowering equipment wear. The use of fly ash in concrete is advantageous as far as workability and durability is concerned (71).

In the same way as other pozzolanic materials, fly ash, when added to concrete, enhances workability by making the blend more plastic and by reducing segregation and bleeding. It has been observed that workability is usually improved with finer fly ashes. However, grinding of fly ash increases the specific surface area which reduces the workability as a result of irregular particles from mechanical processing. In an older study (72), fly ash grinding produced a decreased workability at 0.4 and 0.5 water binder ratios for all fly ash binder ratios, with a more marked effect for prolonged grinding. However, workability improved greatly when the water binder ratio was increased to 0.6 and 0.7.

Fly ash replacement levels of 10%, 20%, and 30% by weight of the total cementitious materials in fly ash - kaolin blends showed that workability increased with the use of fly ash and maximum workability was achieved at 30% fly ash replacement (73).

2.5.3 Effects of fly ash on the properties of hardened concrete

2.5.3.1 Effects on compressive strength

While the aforementioned pozzolanic reaction should increase compressive strength, this reaction is slower than cement hydration. Therefore, the rate of strength development may be more gradual but it is sustained for longer periods than the rate of the strength increase of Portland cement concrete (74, 75). The compressive strength-developing behaviour of fly ash concrete may differ from that of Portland cement concrete due to the method and quantity of fly ash used (76). The properties of the fly ash, its chemical composition, particle size and reactivity, plus the temperature and other curing conditions are among the variables that influence the strength development of fly-ash concrete. Generally, it is found that the rate of strength development is lower for fly ash mixtures, at early ages, but strength gain in concretes with fly ash is significant between 28 and 180 days (77).

Kosior-Kazberuk *et al* (77) investigated the strength development of concrete with 20% fly ash addition and reported that, while early age strengths were compromised, fly ash had a positive influence on later age compressive strength in all cements tested. A 25 % higher strength was obtained for fly ash concretes after 180 days. Chindaprasirt *et al* (75) also concluded that blended cement pastes containing classified fly ash resulted in a paste with higher compressive strength. High strength concrete prepared with large volumes of low calcium fly ash was investigated by Poon *et al* (78). Testing the compressive strength of cubes containing 25% fly ash at ages of 3, 7, 28, and 90 days with w/b of 0.24 revealed lower compressive strengths after 3 and 7 days, but higher compressive strength after 28 and 90 days, compared with the mix without fly ash.

Hanehara *et al* (79) reported on the influence of grinding fly ash on strength development of fly ash/cement mortars cured at different temperatures. They found that increasing the curing temperature promotes pozzolanic activity and high compressive strengths are obtained at very early ages. Consequently, later increases in strength are limited, especially for the most reactive fly ashes. The performance of high-volume fly ash concrete was investigated by Siddique (14), who showed that the use of high volumes of fly ash as a partial replacement of cement in concrete reduced its 28-day compressive, splitting tensile and flexural strengths, modulus of elasticity, and abrasion resistance of the concrete. However, continuous and important development at the ages of 91 and 365 days were recorded for strength and abrasion resistance. This is a result of the pozzolanic reaction of fly ash. Shafiq & Nuruddin (45) studied the degree of hydration of OPC and OPC/FA pastes dried at different relative humidities. All samples were cured in a fog room for 28 days. They reported that the compressive strength of mortar containing fly ash was higher than a 100% OPC mortar.

2.6 Effects of fly ash on the durability of concrete

Durable concretes have the ability to withstand the destructive forces introduced by environmental pressure and do not require extra maintenance. Improvements in concrete durability is one among many reasons why fly ash is being used widely today, but an

understanding of its effect on concrete durability is essential for its correct and economical application (80).

2.6.1 Effects of fly ash on permeability of concrete

Concrete durability may be considered to be controlled by its permeability to a certain degree. Deterioration of concrete as a result of freezing and thawing, alkali-aggregate reaction, carbonation, etc. can all be reduced when there is a decrease in permeability. Pore refinement as a result of using fly ash and other mineral admixtures leads to reduced permeability. Naik (81) looked at the permeability of concrete containing large amounts of fly ash, and reported a significant improvement in concrete resistance to air permeability, notably after 28 days, ascribed to pozzolanic reactions of fly ash. The coefficient of variation values reported at 28 days were in the range of 18-46% while 19-27% was obtained at 91 days. Fly ash usage in concrete increased the average permeability values at both 14 and 28 days.

The permeability of fly ash concrete was studied by Thomas and Matthew (82) using oxygen permeability tests to investigate plain ordinary Portland cement and fly ash concrete at three nominal strength grades. The concretes were moist cured for 1,3,7 and 28 days before exposure to different curing conditions before testing. The results confirmed the significance of proper curing to obtain low permeability concrete, specifically at low ambient relative humidity. The benefits of using fly ash in concrete were clear, with concrete mixtures produced with 15, 30, and 50% fly ash replacement exhibiting reductions in permeability of 50, 60, and 86%, respectively, compared to concrete without fly ash. The following were the conclusions:

- Fly ash concretes moist cured for 28 days had lower permeabilities than the same grade of ordinary Portland cement concretes, with the difference increasing with fly ash content.
- Permeabilities were highest at the shortest curing times, particularly at low ambient relative humidities.
- When the ambient relative humidity increased during storage, lower permeabilities were obtained, making the effects of the duration of moist curing less important.
- Fly ash concretes cured and exposed at 20°C had lower permeabilities than the same grade of ordinary Portland cement concrete, even at poorest curing and storage conditions (one-day cure, low ambient relative humidity).
- 50% fly ash concretes cured and exposed at 5°C were more permeable than the same strength ordinary Portland cement concrete unless adequate curing was provided. 15 or 30% fly ash concretes stayed less permeable than the control concrete when cured for only one day and exposed to low ambient relative humidity.

Beglarigale *et al* (83) investigated the permeability of concrete incorporating fly ash. Replacement levels of 15% and 30 % were used and they concluded that the addition of fly ash reduced the air permeability of concrete, as well as reducing the measured capillary porosity and total water absorption. Elahi *et al* (84) studied the mechanical and durability properties of high performance concretes containing additions in both binary and ternary systems. They showed that partial replacement of Portland cement with fly ash at both 20% and 40% performed the best amongst all the other cement replacement materials in reducing the air permeability. Fly ash enhances the air permeability at 44 days.

2.6.2 Effects of fly ash on carbonation

Carbonation of concrete is one of the most destructive phenomena affecting the durability and serviceability of concrete structure. The mechanism of carbonation normally starts with the ingress of atmospheric CO₂ along with water, developing carbonic acid, which is very reactive with the hydrated cement paste, producing calcium carbonate (CaCO₃). The carbonic acid reacts with the hydrated Ca(OH)₂ and with other fundamental products, such as the C-S-H, and with the anhydrous phases tricalcium silicate (3CaO·SiO₂) and dicalcium silicate (2CaO·SiO₂), producing CaCO₃ (85-87). Carbonation of fly ash concrete was investigated by Atis (88) using an accelerated carbonation test in a controlled environment. Concrete mixtures of 0, 50 and 70% replacement of normal Portland cement with fly ash were produced with water/cement ratios ranging between 0.28 and 0.55. He reported that fly ash concrete produced with 70% replacement carbonated more than that of 50% replacement concrete and normal Portland cement concrete for moist and dry curing conditions. Fifty percent fly ash replacement concrete experienced lower or similar carbonation to normal Portland cement concrete under both curing conditions. The results also showed that longer initial curing periods before testing resulted in lower carbonation depth.

Khunthongkeaw *et al* (89) reported that the reduced water/binder ratio and reduced fly ash content generates a more excellent carbonation resistance. When comparing the same fly ash content, high CaO fly ash samples exhibited better carbonation resistance than low CaO fly ash samples. They also observed that under natural exposure environments, the carbonation rate was high for samples exposed in the city. Comparing carbonation of concrete and mortar samples showed that the same trends were observed for both. Papadakis (90) introduced fly ash as a fine aggregate replacement, and showed that the carbonation rate is reduced, while the carbonation rate increases when fly ash is used as a cement replacement.

The effects of curing on carbonation were also reported by Das and Pandey (91) where an extreme reduction in carbonation depth was obtained with an increase in curing time to 28 days. Their test results showed that the carbonation depth of concrete increased as fly ash replacement increased, and that the carbonation resistance of concrete increased notably with a prolonged curing time.

2.6.3 Effects of fly ash on sorptivity

Sorptivity is a property relating to the pore structure of concrete near the surface, and can be used to assess the quality of concrete. This property describes the 'rate' of water penetration due to capillary action. Concrete with low values of water sorptivity represents good quality concrete.

The effects of fly ash on the durability properties of high strength concrete was investigated by Nath and Sarker (92). Concrete mixtures having 30% and 40% fly ash of total binder were used for casting the test samples. The addition of fly ash led to lower sorptivity at early age with further reductions obtained after six months. Also sorptivity was reduced as the fly ash content increased. They concluded that, generally, use of fly ash as a partial replacement of cement enhanced concrete durability.

Tasdemir (93) examined the effect of mineral admixture and curing conditions on concrete sorptivity. Samples were cured under three conditions, one air cured at 65% RH and 20°C (±

3°C) for 28 days, while the second condition was an initial curing for 7 days under polyethylene sheet and wet burlap at 20°C ($\pm 3^\circ\text{C}$), with further 21 days air curing. The third curing condition was water curing for 28 days in a water tank saturated with lime at 20°C ($\pm 3^\circ\text{C}$). The result revealed that the sorptivity coefficient of concrete kept in the laboratory condition which is the air cured condition was extremely high.

2.7 Hydration of fly ash

Hydration of fly ash cements is different from pure Portland cement in four ways (94), namely:

- The rates at which the clinker phases hydrate
- The reduced amount of calcium hydroxide formed, as a result of the dilution of the clinker by fly ash and the pozzolanic reaction
- The composition of the clinker hydration products and
- Further hydration products from the reaction of fly ash.

The pozzolanic reaction between fly ash and calcium hydroxide produces calcium silicate hydrate. The consumption of $\text{Ca}(\text{OH})_2$ by the pozzolanic reaction reduces the alkalinity of the pore solution, which may affect the durability of concrete structure, such as the carbonation of concrete and corrosion of reinforcement (95). Conversely, there is also a reduction in permeability, which can increase the service life of a concrete structure as reported by Chindaprasirt *et al* (96).

Calorimetry can be utilized to examine the kinetics and mechanism of hydration in cementitious systems with various admixtures. A graph of the rate of heat evolution against time for fly ash mixtures is shown in Figure 2.6. The two peaks described in Figure 2.1, with the induction period between them, can be seen. Some cement blends also show a third peak (Figure 2.1). This is associated with the change in aluminat hydrated phase, and is normally a result of excess of tricalcium aluminate and substitution of tricalcium sulphoaluminate phase (AF_t) by monosulphoaluminate (AF_m) or renewed production of the former phase (43). The duration of the induction period and the height of peaks depend upon the action of the cementitious material and indicate the accelerating or retarding effects of solid admixtures or additives existing in solutions (97). Nocuñ-Wczelik and others (78, 97, 98) found that when the fly ash contents increased, heat evolution is generally slowed down. While Nocuñ-Wczelik said that this is as a result of the lower rate of pozzolanic reaction. Duran-Herrera *et al* (99) also reported that fly ash additions do not retard the hydration reactions of the cement but through dilution do significantly reduce the heat release-peak temperature at early ages under semi-adiabatic conditions.

The glassy, aluminosilicate phase is the main component of fly ash that converts to calcium silicate hydrate and ettringite on hydration, due to the pozzolanic reaction with calcium ions (43, 68). These calcium ions are discharged into solution from the calcium silicate clinker minerals. The pozzolanic reaction is slower with fly ashes than samples without admixtures, but the microstructure reveals a more compact microstructure and lower permeability, due to the presence of higher C–S–H with low calcium hydroxide volume. The hydrolysis of clinker minerals is accelerated by alkalis that always exist in fly ash.

Lower quantities of calcium hydroxide are present in hardened cement pastes when using fly ash, due to the pozzolanic reaction. The reaction of alite in the early stages are mostly retarded by fly ash and the middle stage reactions are accelerated (94). The accelerated reaction is traced to the presence of nucleation sites on fly ash grains. There is more rapid hydration of the aluminates and ferrite phases when fly ash is present, and there is also a change in the hydration rate of the belite phase up to 28 days. Thus, the action of fly ash depends on the ratio of the glass, aluminosilicate phase and crystalline phases. The higher the glass content, the greater the action of fly ash will be at the same chemical composition (100).

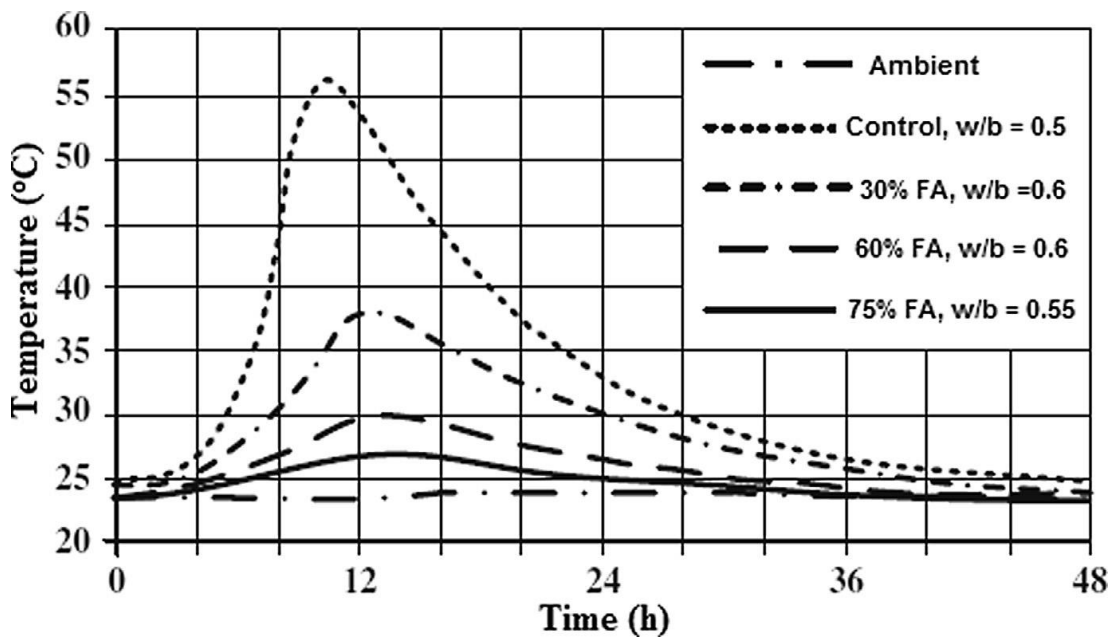
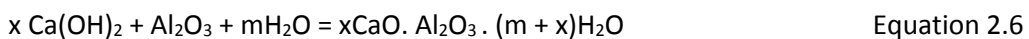
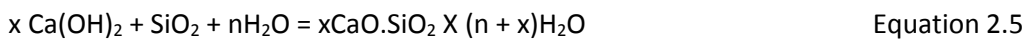


Figure 2-6 Semi-adiabatic calorimetry curves for FA and control pastes (99).

2.7.1 The mechanism of fly ash reaction hydration

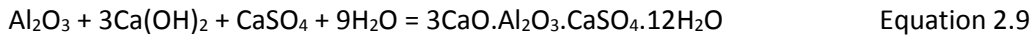
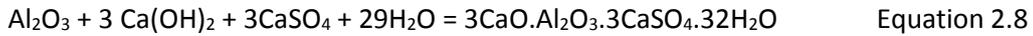
Hydration of fly ash starts with cement clinker hydrating first upon mixing with water. Calcium hydroxide is formed, thus creating the alkaline solution. Then the active compound of fly ash reacts with Ca(OH)_2 to produce calcium silicate hydrate and calcium aluminate hydrate, resulting in the calcium concentration in solution being reduced, and thus accelerating the hydration of cement clinker. The latter hydration reaction equation, as described by Fu et al (100) is shown as



In equations 2.5 and 2.6: $x \leq 3$,



When gypsum is present, the calcium aluminate hydrate reacts further, to produce Aft or AFm as shown in Eqs. (2.8) and (2.9)):



Fu *et al* (100), using X-ray diffraction, showed that the main hydration products of a fly ash blended cement were C-S-H gel, ettringite and a small amount of $\text{Ca}(\text{OH})_2$. They also showed that with increasing hydration, a large amount of fly ash begins to hydrate and more hydration products are produced. The result indicates that the amount of calcium hydroxide in the cement pastes is reduced as a result of adding fly ash to the cement. Production of ettringite was reported at the early age, and sulphate consumption due to production of ettringite was increased by adding fly ash. Ettringite was partially converted to monosulfate within the first 7 days of hydration in fly ash- Portland cement pastes, while the production of ettringite continued to form with hydration up to at least 28 days in pastes without fly ash. Analysis of the fly ash pastes displayed various amounts of calcium hydroxide and unreacted Portland cement, having minor quartz and lehleuite hydrate. The test shows that hydration reactions really take place in the fly ash cement pastes and to some extent on a particle-by-particle basis (101).

Sakai *et al* (102) clarified the influence of the glass content and glass phase basicity on the hydration of fly ash cement, with hydration characterized over long curing times. Two types of fly ash, with different glass contents i.e. 38.2% and 76.6%, were used, with replacement of 20, 40 and 60% by mass. They concluded that fly ash affected the hydration of clinker minerals in the fly ash cement. Hydration of alite was accelerated, while that of belite and C_4AF was retarded. Also, addition of fly ash resulted in a low CaO/SiO_2 ratio of C-S-H, with the CaO/SiO_2 ratios at 360 days of 1.54 for ordinary Portland cement and 1.39 for fly ash cement. Williams (103) discovered that in binary systems C-S-H developed by the pozzolanic reaction of fly ash had a lower Ca/Si ratio than the one produced in the hydration of Portland cement (95, 103, 104).

The degree of hydration and gel/space ratio of high-volume fly ash/cement systems was studied by Lam *et al* (105). Samples were prepared at different w/b ratios and fly ash replacement levels were 25% and 45% by weight. A small percentage of the fly ash reacted at 7 days. But, the degree of fly ash reaction depends on the amount of fly ash and the water-to binder ratio of the paste at different curing ages. Higher fly ash replacement levels showed lower degrees of fly ash reaction. Lam *et al* (105) also discovered that pastes having 45% to 55% fly ash more than 80% of the fly ash did not react even after 90 days of curing.

Narmluk and Nawa (106) investigated the effects of fly ash on the kinetics of Portland cement hydration at different curing temperatures. They reported that the effect of fly ash on the hydration kinetics of cement depends on fly ash replacement levels and curing temperatures. Fly ash retarded cement hydration at early ages but accelerated it in the later period.

The effect of initial water curing conditions on the hydration degree and compressive strengths of fly ash–cement pastes prepared with low water to binder ratios was studied by Termkhajornkit *et al* (107). Fly ash replacement levels were 25% and 50%. The hydration degree of belite is influenced by water curing conditions, more so than that of fly ash and alite. Hydration of fly ash still continues even without an additional, external supply of water. It was also observed that the strong dependence of fly ash–cement concrete on curing conditions does not come from the hydration degree of fly ash, but rather comes from the hydration degree of cement, especially belite. Also the degree of hydration of OPC and OPC/FA pastes dried at different relative humidities was examined. The study used ordinary Portland cement, plus 40 and 50% fly ash replacement pastes designated as OPC, FA40 and FA50. The samples were initially cured for 28 days at 100% RH and later dried at different relative humidities, at a constant temperature of 27°C. The degree of hydration was determined by measuring, using TG, the calcium hydroxide, content. They concluded that the addition of fly ash as partial replacement to cement slows down the rate of hydration, as all fly ash based samples displayed lower degrees of hydration compared to the respective OPC samples. Also drying conditions have significant effects on the degree of hydration of cement pastes, which affects other properties such as compressive strength (45).

Lothenbach *et al* (108) reported that fly ash hydration at ambient temperatures is slow and that portlandite is only consumed after hydration times typically longer than one week. They also wrote that more portlandite is produced initially when the hydration of the clinker is accelerated due to the filler effect. The initial hydrate assemblage in Portland cement–fly ash blends of C–S–H, portlandite, ettringite, and AFm phases like monocarbonate or monosulfate is similar to the pure Portland cement system, due to the slow reaction of the fly ash. Higher temperatures accelerate the reaction of fly ash, while higher replacement levels slow down the reaction.

2.7.2 Microstructure of fly ash paste

Figure 2.7 show the backscattered electron (BSE) images of a blended cement paste. Different phases can be distinguished on the basis of their grey level. In the fly ash paste, the major solid phases of hydration products are CH, C-S-H, C-A-H, C-A-S-H and unreacted phases, with the latter being either cement grains or unreacted fly ash particles. From the BSE image, it is not easy to differentiate C-A-H, C-A-S-H and C-S-H, but the unreacted fly ash shows a typical spherical appearance.

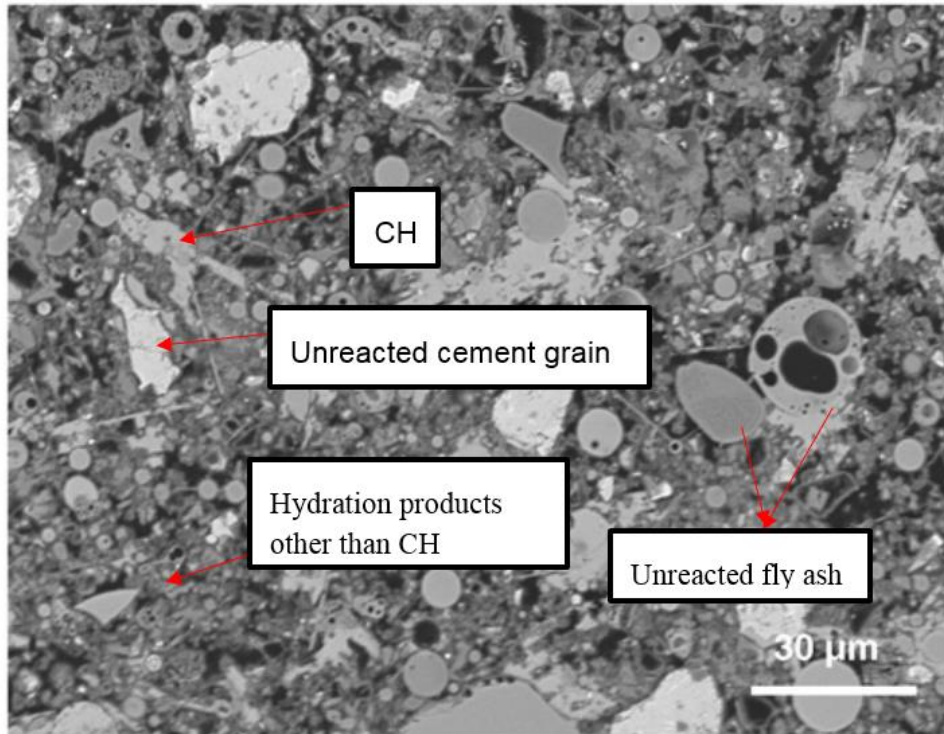


Figure 2-7 BSE image of fly ash blended cement paste at 28 days (109)

The microstructural analysis of fractured surface pastes at 7, 28 and 90 days was extensively discussed by Chindaprasirt *et al* (96). At 7 days, the microstructures of samples containing 20% fly ash were porous and possessed many voids as seen in Figure 2.8. The hydration products on the fly ash surface barely progressed, with the surface of the fly ash particles covered with layers of small quantity of hydration products. Some ettringite needles had developed in unoccupied space in the paste.

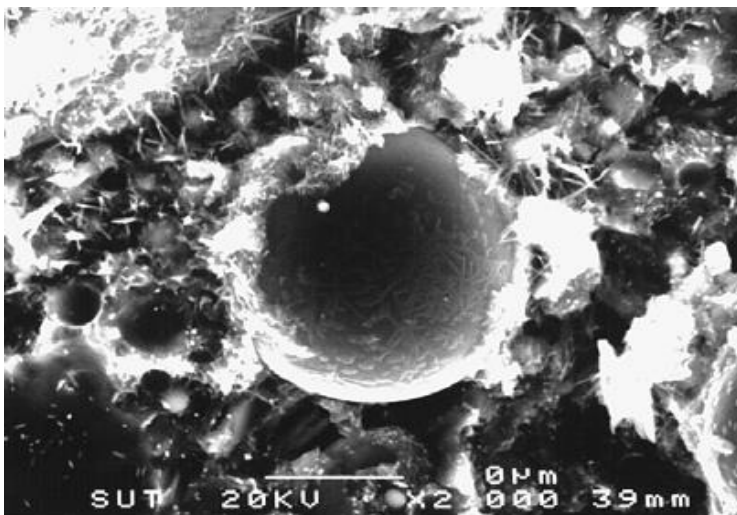


Figure 2-8 Microstructure morphology of fractured surface paste of 20% fly ash at 7 days taken from (96)

Figure 2.9 shows the morphology of fractured surface paste of 20% fly ash cured at 28 days. Fly ash particles at 28 days were noticed in three forms: particles with a dissolved surface,

smooth surface, and a covering of hydration product and pozzolanic reaction. In the first form, fly ash particles had traces of etching on their surface, revealing precipitation in the pozzolanic reaction. The smooth fly ash particles were unreacted or acted as an inert material with the ability to increase the packing effect and served as a precipitation nucleus for hydration compounds. Hydration and pozzolanic products around the fly ash particles were noticed in the third form.



Figure 2-9 Microstructure morphology of fractured surface paste of 20% fly ash at 28 days taken (96)

The fractured surface at 90 days is shown in Figure 2.10. At 90 days etched fly ash particles and evidence of fly ash hydration, with broken fly ash surfaces, was common. Hydrates had consumed a lot of fly ash particles. The pozzolanic reaction of fly ash accelerated at the later ages and production of C–S–H increased. The pozzolanic reaction between the fly ash and $\text{Ca}(\text{OH})_2$ covered the surface of fly ash particles with C–S–H (3, 75, 77). The hydration product layer thickened as the reaction progressed. The hydration products developing from the cement grains and fly ash particles were linked, although some particles still remained unreacted and served as a filling effect.

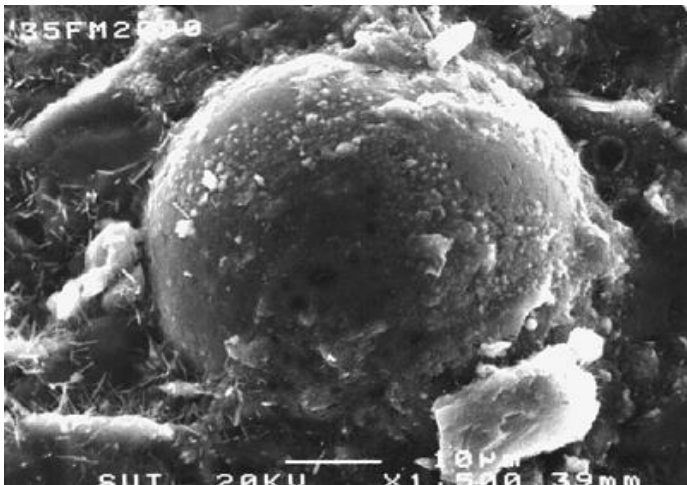


Figure 2-10 Microstructure morphology of fractured surface paste of 20% fly ash at 90 days taken from (96)

Xu *et al* (110) reported that fly ash has both enhancement and retardation effects on cement hydration and directly influences the pore system. Fly ash may also provide nucleation centres for the growth of hydration products such as CH.

Wang *et al* (95) studied the microstructures of hardened cement-fly ash pastes containing 50% fly ash, up to four years old. The microstructure of hardened cement-fly ash paste revealed a coarser pore size distribution than plain cement paste at early ages. Meanwhile, the pore size distribution of cement-fly ash paste was finer than that of cement paste after four years (68). Fly ash cement paste produces more hydration products from the age of 90 days to four years, resulting in a significant improvement in the pore structure. Most of the $\text{Ca}(\text{OH})_2$ formed by clinker hydration was consumed by the pozzolanic reaction, with only a small quantity of $\text{Ca}(\text{OH})_2$ present in the four year old hardened cement-fly ash paste. Fly ash particles that were small were found to be massively reacted while many of the large fly ash particles remained nearly unreacted.

2.8 Effect of conditioning on pore structure

Drying of cement paste, or conditioning, is necessary before analysing by XRD, TG and SEM. This is to remove the water and prevent further hydration reactions during storage. Drying methods influence the microstructures in different ways (111). Solvent exchange, oven drying, freeze drying and vacuum drying are the most common methods used. Some of the procedures involve the physical removal of water by using an oven or a vacuum, while others substitute the water with a liquid that has a lower surface tension, such as a hydrophilic organic liquid, before drying to reduce capillary forces. At times a mix of these methods is used. However, each of the methods may alter the delicate microstructure of the hardened cement paste, which might lead to structural and physical destruction of some of the cement hydrates, specifically ettringite (AFt), monosulphate (AFm) and C–S–H, as much water is connected with these phases. In hardened cement pastes having large quantities of AFt, like calcium sulphoaluminate cements, the dehydration of ettringite has been reported to be the basis of shrinkage cracks which are large enough to be observed by SEM (112).

2.8.1 Solvent replacement

This procedure involves substituting the bound/pore water in samples of hardened cement paste with organic liquids. Solvent exchange has been acknowledged to have a gentle effect on the microstructure of cement paste (64, 113, 114). Solvents are organic liquids that can mix with water but have a higher vapour pressure than water. Organic solvents possess physical properties that demonstrate various benefits for drying before pore structure characterization. For example having a lower surface tension reduces the pore structure damage during drying. The specific gravity of most organic solvents is also considerably lower than that of water; thus, organic solvents may easily substitute the pore solution in a hydrated cement paste by a simple counter-diffusion process. The solvents usually used for drying cement pastes are the alcohols methanol, ethanol and isopropanol. Other solvents that have been utilised to a lesser extent are acetone, benzene, toluene, xylene, and pentane (115). Konecny and Naqvi (113) reported that solvent replacement with isopropanol gave samples with fine pores that were least damaged, and that this method is the best to preserve the finest pores, compared to oven- or freeze-drying. The length and weight changes of particles in cement pastes immersed in isopropanol and methanol were examined by Feldman and Beaudoin (114). The test revealed that samples immersed in methanol or isopropanol showed the least microstructural stress. Feldman (116) concluded that there was no interaction between isopropanol and hydrated cement but that

methanol interacts with hydrated cement by penetrating the C–S–H. Beaudoin et al (117) also reported that methanol interacts with hardened cement paste and that the length of CH crystals increased when immersed in methanol, isopropanol or acetone. The advantages of using this method were that it was the least damaging to pore structures, it gave the finest pore size distribution, preserved the finest pores and applied the least stress. Isopropanol does not react with cement and is adequate for use with XRD (118).

2.8.2 Oven drying

Oven-drying at 105°C is one of the most convenient drying techniques. It is much quicker than most drying techniques and pore water removal is complete after 24 hours, with specimen being monitored regularly during the drying process. Although oven-drying is an effective way to remove evaporable water from a specimen, it has disadvantages, in that microcracking may be induced into the specimen as a result of differential thermal expansion and contraction of the constituent components during the drying cycle. This technique has been reported to be the method which can eliminate the “non-bound” water thoroughly and also destroyed the microstructure (111). Konecny and Naqvi (113) reported that pores of hardened cement paste were destroyed while Knapen et al (119) concluded that oven drying at 105°C is inappropriate because hydration was accelerated. Dehydration of some cement hydrates was observed and carbonation was favoured. Galle (120) wrote that ettringite and C–S–H lost a meaningful volume of non-evaporable water during oven drying at 105°C and even drying at 60°C did not protect the delicate microstructure of hardened cement paste. Collier *et al* (118) stated the following effects of oven drying: damages pores in cement, dehydrates C–S–H at 105°C, causes cracks in cement, crack damage increases as drying temperature increases, removes bound water from ettringite and does not preserve microstructure. A decomposition of some cement hydrated products with the increase of the temperature may also be observed at temperatures shown in Table 2.4.

Table 2-4 Temperature of the decomposition of cement pastes phases (43)

Compound	Temperature at which decomposition starts
Ettringite	60°C
Gypsum	80°C
C-S-H	<105°C

2.8.3 Vacuum drying

Vacuum drying involves putting the sample in a sealed container connected to a vacuum-generating mechanical pump where a vacuum is produced, pore water changes to vapour and is extracted from the cement paste. The technique is slow, and thus relevant for older specimens, i.e. from about 28 days. Vacuum-drying is also believed to induce some microcracking in the cement paste specimen. Knapen *et al* (119) reported that vacuum drying is an easy and fast technique to remove free water, especially when dealing with early-age hydrated cement. They explained further that reliable results were obtained by using vacuum drying method since no interaction were formed. Also the Ca(OH)₂ calculated by thermal analysis were good approximation of the real amount of Ca(OH)₂. Zhang and Glasser (64) however, revealed degradation of ettringite and monosulphate. They also

showed severe harm to the pore structure and pore volume. When comparing this method to oven drying at 105°C Diamond (121) reported that vacuum drying eliminated less water. Galle (120) reported that stresses and microcracks of samples were related to samples dried at 60° and 105°C. Collier et al (118) suggested the following disadvantages of oven drying (118) ettringite and monosulphate are degraded, the pore structure is critically damaged and the pore volume increased, stresses and microcracks are developed, and removal of less water than oven drying at 105°C.

2.8.4 Direct freeze-drying

Direct freeze-drying is a quick drying technique that causes little destruction to the microstructure of the cement paste. In this technique a specimen is immersed directly in liquid nitrogen (-196°C) for about 5 minutes, after which a vacuum is applied. Galle (120) concluded that freeze drying is a suitable drying technique prior to mercury intrusion porosimetry (MIP) and observed that the method produces significant harm in the C–S–H related to thermomechanical stress. A meaningful quantity of water may remain in the microstructure of the hardened cement paste (121). Konecny and Naqvi (113) noted that the pores of hardened cement pastes were destroyed by freeze drying technique while Taylor (43) was of the opinion that freeze drying produces better results in thermogravimetric analysis and scanning electron microscopy. Collier *et al* (118) concluded that freeze drying induced more microstructural cracking than other water removal techniques and states the following disadvantages: cement pores were destroyed, stresses in C–S–H were developed, and water was being left in cement. The method is suitable for use with TGA and SEM, yet adequate for use with MIP.

2.9 Durability of the concrete

The durability of Portland cement concrete is described as the competence of concrete to withstand weathering action, chemical attack, abrasion, or any other mechanism of deterioration for continuity of its original form, quality and serviceability especially when exposed to its proposed service environment (34). Gowripalan (21) wrote that the durability of a structure is widely affected by the ability of the concrete to prevent passage of different damaging substances from the environment. Durability in concrete covers a broad range of problems that could possibly reduce the service life of the structure. Durability issues commonly emerge as the materials deteriorate. Even though there may be no urgent safety issue for the material deteriorations, they will gradually lead to structural damage, that may endanger the structures (122). Alexander (123) wrote that corrosion and external chemical attack concerns are dominant, with these issues being responsible for the greatest costs on repair and rehabilitation.

Deterioration may be generated from the environment which the concrete is exposed or through internal causes within the concrete itself. The classification of causes of concrete deterioration can be grouped into three categories: physical, chemical, and mechanical. The external causes may be due to adverse effects of freezing and thawing, to abrasion and erosion, to attack by sulphates present in soil, groundwater and industrial liquids, to attack by soft water and of marine environments, to steel reinforcement corrosion due to carbonation and /or penetration of chlorides etc. The internal causes are corrosion of the steel reinforcement by the chloride present in the mix components in alkali-aggregate reaction and unsoundness of the aggregates (124). In most cases, the deterioration of a

concrete structure is a product of the combined effect of multi environmental factors and loading which the use of a single durability parameter cannot sufficiently define the quality of the concrete (122, 123).

All deterioration mechanisms are affected by transport systems within the pore structure of the concrete. The rate of the process primarily depends on the micro-environmental conditions on the concrete surface, the connections of the pore system with the micro-environment and the reactions of the penetrated substances with certain components of the matrix. The concrete composition, specifically the type of binder and the w/c-ratio, has a definite effect on resistance to deterioration in a particular environment. Thus, it can be established clearly that the main factor controlling all these parameters is the microstructure of concrete (123).

2.9.1 Durability tests

When assessing the durability of concrete, consideration may be given either to understanding the fundamental behaviour of concrete, or by performing ageing studies under accelerating conditions. These fundamental properties has been termed “durability indices” by some and it is these which are the focus of this section. However, some consideration is given later on in the section to accelerated ageing studies.

2.9.1.1 Durability indices

Durability indices are engineering parameters that are physically measurable. These describe or identify the concrete at early ages in the as-built structure and are sensitive to important material, processing, and environmental factors such as cement type, water: binder ratio, type and degree of curing, etc. The objective of material indexing is to provide a repeatable engineering measure of microstructure and properties relevant to concrete durability at a relatively early age (e.g. 28 days). It must be established, however, that durability index tests expressly point out parameters that control corrosion of rebars in concrete (123). Some of the additional common durability indicators as used in practice, or under development were discussed by Alexander and Thomas (125) and are listed as:

1. Physical parameters (physical microstructure of the material)

- Permeability to liquids and/or gases
- Water absorption and sorptivity
- Porosity; pore spacing parameters
- Mechanical parameters
- Abrasion resistance

2. Chemical, physio-chemical and electro-chemical parameters

- Calcium hydroxide content
- Diffusivity and conductivity
- Resistivity
- Electrical migration.

Some of the concrete durability indices used in this project will be discussed below.

2.9.1.1.1 Permeability of liquids and /or gases

Concrete is a porous material and fluids (liquids or gases) may flow through concrete under certain circumstances. The permeability of concrete to fluids is usually measured by applying a pressure gradient across a concrete sample and measuring the rate of fluid flow. As a general rule, Darcy's law is used for both water and gas permeability measurements.

The permeability of concrete to water, often termed the hydraulic conductivity, is often measured on a water-saturated cylindrical sample of concrete by sealing the curved surface of the sample, applying water under pressure to one flat face, and measuring the rate of water flowing out from the other face. The tests used to measure gas permeability can be divided into in-situ and laboratory tests. Nearly all the tests use a similar apparatus to a drained tri-axial test, where a pressure is applied to one side of the sample and the gas is measured at the escape boundary. Other tests use migration in a sealed environment to evaluate flow.

Permeability is the most essential property of concrete controlling its long-term durability and it's described as the flow of fluid through a porous medium under an applied pressure head (126). Concrete permeability relies upon its microstructure, moisture condition and the characteristics of the penetrating fluid; low permeability is obtained with dense microstructures possessing restricted pore interconnectivity. Water would be the ideal medium with which to study permeability since this is the medium in which much deterioration occurs. However, water permeability measurements are extremely slow and difficult, therefore recent approaches use gas permeability to define the concrete, with the parameter being used as a durability indicator (125). Cabrera et al (32) wrote that measuring the permeability of a concrete determines a suitable indication of the concrete's durability while Sanjuan and Munoz-Martialay (127) also report that air permeability coefficient can be used as an adequate tool to measure the potential durability of real concrete structures.

2.9.1.1.2 Water absorption and sorptivity

Water Absorption

Absorption testing involves the use of BS 1881-122:2011 (128) (Method for Determination of Water Absorption). The test requires a minimum of three concrete cores to be cut from the concrete to be tested or casting at least three cubes or cylinders prepared from fresh concrete in accordance with BS EN 12390-2 (129). This test gives an insight into the internal absorption qualities of the concrete. The duration of the test is 30 minutes once the samples have been prepared which makes the test to be quick and cheap. The test is also reliable. The measured absorption of each specimen is calculated as the increase in mass resulting from immersion and is expressed as a percentage of the mass of the dry specimen. Khatib (130) also reported that water absorption by shallow immersion is commonly determined by drying a specimen to constant mass, dipping it in water for a specific time and measuring its increase in mass as a percentage of the dry mass.

Sorptivity

Surface absorption is measured in accordance to BS 1881-208:1996 (131) (Recommendations for the determination of the initial surface absorption of concrete). This test procedure provides data for assessing the uniaxial water penetration characteristics of a concrete surface. The results may be considered to be related to the quality of finish and

to the durability of the surface under the effects of natural weathering. This is also known as the Capillary water absorption of concrete or in most cases sorptivity. It involves placing a sample with one surface just in contact with water and the mass or height of water absorbed by capillary action is measured at different time intervals. A lots of work (93, 130, 132-134) has been done on tests on water penetration by capillary action since this is more appropriate to define the quality of concrete. The fineness of the capillary pores in concrete causes absorption of water by capillary action, hence a measure of the rate of absorption provide a useful indication of the pore structure of concrete. If water is absorbed rapidly the capillaries will be large and if the absorption is slow then the capillaries will be small. Sorptivity test used in this study was determined using similar methods used by Tasdemir (93) and Güneyesi (134) .

Sorptivity has been identified as an important concrete durability index (135). It is a property related to capillary development, and is described as the gradient of a plot of the volume of water absorbed per unit area of section surface against the square root of the absorption time (136). Ho et al (137, 138) wrote that sorptivity is a property defining the rate of water penetration due to capillary action and is associated to the pore structure of concrete near the surface from which the quality of concrete can be determined. Alexander et al (123) reported that the lower the water sorptivity index, the better is the potential durability of the concrete. Sorptivity is particularly sensitive to the near-surface properties of concrete, and is thus a good indication of the nature and effectiveness of curing (125)

2.9.1.1.3 Porosity (Pore spacing parameters)

The pore volume includes all pores, both gel and capillary, but the interconnected porosity is normally determined in laboratory tests, commonly by oven drying a sample and then saturating it in water. Porosity affects most concrete properties, including strength, permeability, shrinkage, and creep. Concerning durability, porosity affects concrete transport properties and is thus a demanding parameter that can be used as a durability indicator. Pore spacing is also a demanding parameter, particularly with regard to freeze–thaw resistance of concrete, with specifications normally providing limits to the maximum pore spacing (125).

2.9.1.1.4 Mechanical parameters

Compressive strength

Compressive strength is generally used as the fundamental test of concrete quality, and thus it has to be accurately determined. BS EN 12390-3:2009 (139) which is Testing hardened concrete (Part 3: Compressive strength of test specimens) can be used as a simple and readily available test to evaluate the compressive strength of concrete cubes. This is extensively used and approved by industry. The load at which the cube fails is recorded and this is divided by the surface area of the cube in contact with the platens through which force is applied to the concrete cube. The units adopted are MPa or N/mm². Increase in strength is obtained through curing as hydration products develop within the water-filled capillary pores, water is consumed and more hydration products are formed which reduces the porosity of the concrete thereby increases the durability.

Modulus of elasticity

Modulus of elasticity of concrete is an essential determinant for estimating the deformation of structural elements, also is a basic factor for determining modular ratio, which is used for the design of structural members subjected to flexure. Based on the property of modulus of elasticity of concrete that it is proportional to the square root of compressive strength in the range of normal concrete strength. Lee *et al* (140) wrote that elastic modulus of concrete denoted by E_c is a basic fundamental parameter for calculating the static and dynamic performance of structural elements specifically, deflection, side sway of tall buildings, and vibration of concrete elements. Also, E_c is a great indicator of degree of concrete deterioration: lower E_c is as a result of more degradation. Thus, E_c is commonly used for quality evaluation of concrete structures such as building components, pavements, and bridge decks.

Elastic modulus of concrete is directly measured by the static uniaxial compressive test in accordance with ASTM C469 at 28 days, which is called static elastic modulus. In practice, elastic modulus of concrete is normally determined from compressive strength based on design codes rather than the direct measurement.

2.9.1.1.5 Abrasion resistance

Surface abrasion is one of the most common forms of deterioration imposed on concrete structures. It is a mechanical wearing that can be a catalyst for other forms of deterioration such as cracking and corrosion of reinforcing steel (141). Abrasion can also be a form of natural attacks on concrete. It mechanically generates friction and rubbing that cause serious damages on concrete surface. A complete wearing away of concrete from structural elements can occur in worst case.

ASTM described abrasion as the physical wear due to hard particles or protuberances forced against and moving along a solid interface. Thus, abrasion resistance can be defined as the ability of a surface to prevent being worn away by rubbing or friction. Horszczaruk (142) reported that the major factors affecting the abrasion resistance of concrete can be the environmental conditions and dosage of aggregate, the concrete strength, the mixture proportioning, the use of special cement, the use of additions such as: fly ash, the addition of fibre. Surface finishing and the curing conditions are two other important factors that can have effect on abrasion resistance. Also concrete's hardness, which is related to its strength determines how strong it will be to resist abrasion.

Four common areas which abrasion could be imposed on a concrete surface as stipulated by ACI are; wear on concrete floors due to human traffic, wear due to vehicular traffic with studded tires and snow tire chains, abrasive materials in water affecting hydraulic structures such as dam spillways, and high water velocities creating cavitation at the concrete surface.

Abrasion test

Multiple abrasion tests are available, but each varies in the type of wear pattern produced, and thus each may have varying purpose to the wear expected in service for the subject structure. Various ASTM methods which have been developed to determine the abrasion resistance of concrete are ASTM C418, ASTM C779, ASTM C944 and ASTM C1138 and explained by Bakke (143). Abrasion parameters are usually measured in standard tests

include mass loss and depth of wear, and these could be used as durability indicators for abrasion (125).

2.9.1.1.6 Calcium hydroxide content

Calcium hydroxide content is a measure of the 'alkalinity' of the concrete matrix. It is important in assessing the resistance of concrete to carbonation, and can be used as a measurable parameter in this respect. TG was used to measure the calcium hydroxide content in this research and it has been explained in the methodology and accelerated carbonation test was used to determine the carbonation depth of the concrete samples. Das et al (85) reported that carbonation of concrete is one of the most damaging phenomena that influence the durability and serviceability of concrete structures. Carbonation is usually a slow process under natural conditions, thus its being determined by accelerated carbonation. It involves in damaging the passivity of concrete owing to the drop in the alkaline environment surrounding the steel reinforcement and thus encouraging the corrosion of reinforcing steel. Carbonation is described as the procedure wherein the hydration products [particularly calcium hydroxide $\text{Ca}(\text{OH})_2$] of cement react with the dissolved carbon dioxide (CO_2), lowering the pH of the concrete pore solution from about 12.5 to less than 9 (86). The process of carbonation normally begins with the penetration of atmospheric CO_2 and, along with water, produces carbonic acid, which is very reactive with the hydrated cement paste to develop calcium carbonate (CaCO_3). It is reported that CO_2 obviously reacts with the hydrated $\text{Ca}(\text{OH})_2$ and with other essential products, such as the C-S-H, and with the non-hydrated products of tricalcium silicate and dicalcium silicate, to produce CaCO_3 (87).

2.9.1.1.7 Diffusivity and conductivity

These procedures attribute to the transport of ionic species through concrete, but also involve diffusion of liquids and gases. Diffusion is transport as a result of concentration difference while conduction at times called migration emanates from an electrical potential difference and is an electro-chemical parameter. Fick's first law for steady state diffusion and the Nernst–Planck equation are the governing equations, this give rise to material parameters in the form of diffusion coefficients and/or conductivity which can be used as durability indicators.

2.9.1.1.8 Resistivity

Resistivity is a very useful electro-chemical parameter of concrete and it is the inverse of conductivity. It is a geometry independent material property describing the electrical resistance and is fundamentally related to the penetrability of fluids and diffusivity of ions through porous materials. Though it is difficult to anticipate resistivity from idea of concrete's constituents and the environment, it is generally easy to measure and is often used as an indirect measure of the probability of corrosion initiation and corrosion rate in reinforced concrete.

Direct resistivity measurements that can be obtained from samples provide an indication of durability with regard to ion flow and water content. In order to avoid the capacitance effect an AC power supply should be selected. Example of resistivity / conductance testing of concrete samples is shown in Figure 2.11. A measurement free of polarisation effects

should be achieved if a signal generator is used to input a sine wave current (or voltage) at anywhere around 10 - 40 Hz and the resulting voltage (or current) is measured.

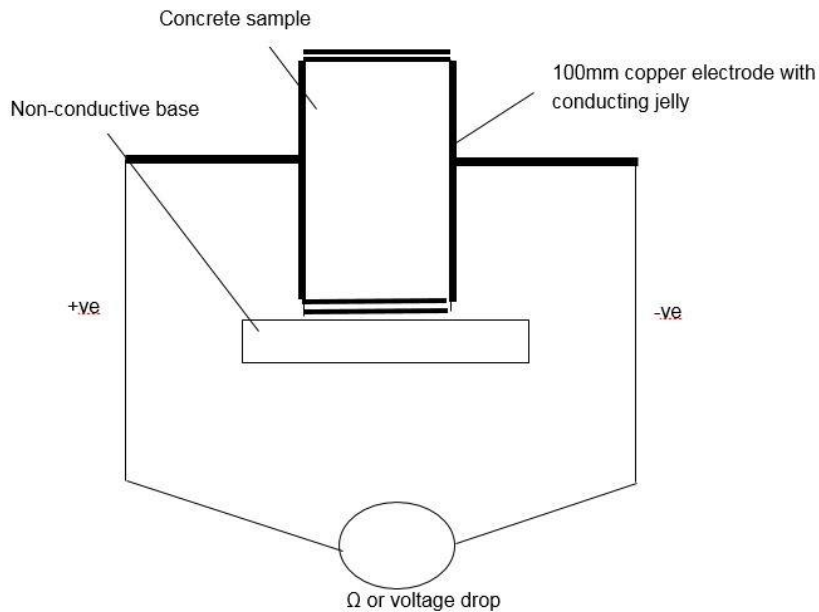


Figure 2-11 Resistivity / conductance testing of concrete samples

2.9.1.1.9 Electrical migration

Chloride migration coefficient is an example of a parameter measured in migration tests, acquired from the measured chloride penetration depth in a voltage-accelerated test also different method uses the rapid chloride permeability test.

Chloride-induced corrosion is presently considered to be the most important and most serious deterioration mechanism for concrete structures. chloride penetration is specified as an fundamental part of reinforcement corrosion. Chloride ions (originating from seawater or de-icing salt) may infiltrate through the pores to the interior of the concrete. Chloride invasion is as a result of either diffusion, taking place in totally or partially water-filled pores, or capillary suction of chloride containing water (144). Chloride-induced corrosion commences when the concentration of chloride at the steel bars attains a threshold value destroying the protective layer. The mechanisms by which corrosion influences the load carrying capacity of reinforced concrete structures are: loss of reinforcement section, loss of steel–concrete bond, concrete cracking and delamination (145). Chloride levels appropriate to initiate corrosion of steel range between 0.17 and 2.5 m/m of chloride atoms by mass of cement.

2.9.1.2 Accelerated Ageing Tests

2.9.1.2.1 Accelerated carbonation test

Carbonation is a slow process thus accelerated carbonation test is normally used to test for carbonation. Accelerated carbonation test main result is carbonated depth and this is normally achieved by exposing concrete samples to high CO_2 and relative humidity which the samples can be carbonated. This study used saturated NaBr solution having 65% RH. Rozière Emmanuel *et al* (146) reported that accelerated test can give reliable information

on potential durability in a short term. Therefore carbonated depth conducted may be used as an indicator to show equivalent performance. Also Khunthongkeaw *et al* (89) reported that since the rate of carbonation in the natural environment is usually slow due to low temperature and low CO₂ concentration level. Hence, the accelerated carbonation test is practical to assess the carbonation resistance of concrete within a reasonably short time. They further explained that estimating the carbonation depth in the natural environment based on the results of the accelerated test is a benefit obtained practically.

2.9.1.2.2 Rapid chloride permeability test (RCPT)

The rapid chloride permeability test is frequently used name for the Standard Test Method for Electrical Indication of Concrete's Ability to Resist Chloride Ion Penetration (ASTM C 1202- 12). This test method covers the determination of the electrical conductance of concrete to provide a rapid indication of its resistance to the penetration of chloride ions.

The method involves monitoring the amount of electrical current passed through 50-mm thick slices of 100-mm nominal diameter cores or cylinders during a six – hour period. A potential difference of 60 V dc is maintained across the ends of the specimen, one of which is immersed in a sodium chloride solution, the other in a sodium hydroxide solution as shown in Figure 2.12. The total charge passed, in coulombs, has been found to be related to the resistance of the specimen to chloride ion penetration. A high chloride permeability would be 4000 coulombs, whereas a low permeability would be 2000 coulombs. ASTM C1202 provides a measure of the electrical conductivity of the concrete but does not measures neither permeability nor chloride ion penetrability. However, despite a number of limitations the test does correlate reasonably well with other mass transport measurements and has the advantage of being relatively simple to conduct.

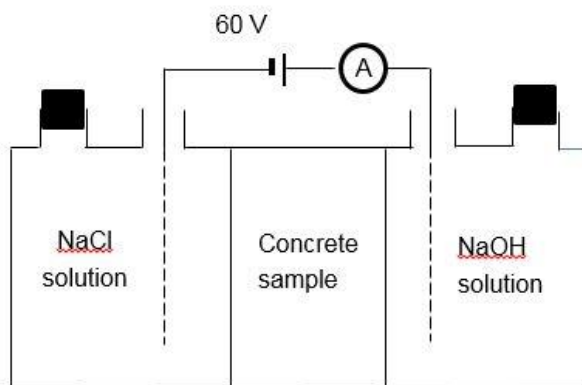


Figure 2-12 Schematic of rapid chloride permeability test

2.9.1.2.3 Freeze-thaw

Freezing and thawing have a substantial effect on weathering of all masonry and concrete materials. It has been reported to be one of the causes of concrete deterioration and failure. Durability loss through freezing and thawing action is common in concrete structural elements in many parts of the world especially in cold climates (147-150). Cracking and spalling of concrete are the dominant frequent damages by frost action, caused by gradual expansion of the cement paste matrix from repeated Freeze–thaw cycles. Freezing and thawing mechanical activity, when combined with the ingress of deleterious salts, can actually reduce the durability of concrete structural elements. Also

micro cracks are developed by wetting and drying of the concrete together with freezing - thawing thermal shock action which permits deep penetration of aggressive ions (149).

The freeze-thaw resistance of concrete depends on the freeze-thaw resistance of hardened cement paste because concrete degradation in aggressive mediums most commonly occurs in the binding of hardened cement paste. This occur because concrete is rich in alkali and thus it reacts strongly with acidic gasses and liquids and also by considering that aggregate usually have higher density and chemical resistance. Freeze-thaw resistance is one of the indicators that can be used to describe the durability of concrete (150). Kumara (151) wrote that freeze-thaw resistance of cement structures depends on the structure of the material, which are its porosity, the size of pores and capillaries, their distribution and type (open or closed pores). Penttala (152) also reported that freeze-thaw resistance of concrete depends on water-cement ratio, air content and curing time. The research further explained that there are two mechanisms of concrete destruction under freeze-thaw conditions which are surface damage and internal damage. The test results revealed that internal damage determines the need for air-entrainment in high-strength concretes while in normal or low strength concretes, surface scaling determines the need for higher air content compared to the internal damage freeze-thaw mechanism.

Liu and Hansen (153) wrote that freeze-thaw damage is a common materials-connected distress in concrete structural elements and it is extensively increased in the presence of deicers used for pavement or bridge maintenance in winter, which is known as salt frost deterioration. This degeneration reveals itself in two forms : (1) internal frost damage leading to most cracking and loss of integrity, (2) superficial scaling usually associating with gradual swelling and flaking of the mortar component.

Air-entrained can be used to protect concrete from freeze– thaw damage (154, 155). This can be achieved by adding air-entraining agent to the concrete mixture. The use of air-entraining agents can develop concrete that is highly resistant to severe frost action and cycles of wetting and drying or freezing and thawing and has a high degree of workability and durability.

Freeze-thaw tests

The damage by frost is mainly studied in a laboratory by accelerated freeze– thaw cycles. Rapid freezing and thawing test ASTM C 666 (156) are typical tests by which the internal damage of the concrete specimen can be assessed. Molero *et al* (157) reported that concrete resistance to freeze– thaw damage is commonly evaluated and classified depending on the type of damage, whether external or internal. They further explained that the standards used in some tests, evaluate external damage and scaling by the loss of mass of material, while internal damage is usually evaluated in some tests by the ultrasonic pulse transmission time and the fundamental transverse frequency measurements.

2.9.1.2.4 Sulphate

Sulphate attack comprises a set of chemical and physical interactions that develop between hardened cement paste and sulphates. Sulphates added during production of cement, usually as gypsum to prevent flash set may, depending on curing conditions, cause damage in the form of expansion and cracking in the form of delayed ettringite formation (158, 159). The formation of secondary sulphate-bearing phases from sulphate penetration at the

surface of the cementitious materials has been attributed to the loss of mechanical performance.

Ground water and sea water having sulphate chemicals which are transported through the pore spaces of adjacent concretes have been known to influence deterioration in concretes due to the formation of compounds such as ettringite, gypsum and thaumasite (160-162). Sulfate attack may be exhibited physically when dissolved salts diffuse through the concrete and precipitate in pores, causing damage (163-165).

The development of gypsum results in spalling and reduction of hydrated cement paste to cohesionless mass with exposed aggregate and loss of strength in mortars and concretes, due to decalcification of C-S-H in cement paste (166, 167). Ettringite formation in hydrated cement systems is also associated with expansion and cracking (166), specifically, delayed ettringite formation which is commonly due to heat curing can result in greater damage to cement based structures (168). Thaumasite form of sulphate attack results in loss of binding power of cement paste and consequently loss of strength in mortars and concrete (169).

Sulphate test

Expansion test is normally used to examine sulphate attack with sulphate solution concentration of about 50g/L (170) in order to accelerate the test process, but this is much higher than field conditions. Lower concentrations of about 3g/L has been used other researchers (171, 172) for proper reflection of field conditions. Expansion is affected by size of samples with deterioration being more rapid for smaller samples (172, 173).

2.10 Improper curing

Concrete is the most widely used construction material in the world because it can be durable. However, these fundamental properties can only be achieved if the correct procedures are maintained. Cement hydration requires water, therefore for concrete to achieve its full potential, samples must be cured properly. The objective of curing is to keep concrete saturated or as nearly wet to assist the hydration of cement. Hydration can only continue when the relative humidity within the concrete is greater than 80% (17). This is why loss of water by evaporation from the capillaries must be prevented (17).

Improper curing will have impact on the degree of hydration, so thus affect engineering performance (unconfined compressive strength, shrinkage) and also durability (carbonation, permeability, sorptivity). If concrete is permitted to dry without being cured, moisture from the surface will evaporate and result in insufficient water for cement hydration. Also, there will be moisture gradient across the section which will lead to development of uneven strength. Gowripalan et al (21) reported that inadequate curing can result in a very weak and porous material near the surface of the concrete that is exposed to ingress of various destructive substances from the environment. Also Basheer et al (31) wrote that inadequate curing is a factor that has shortened the service life of many structures and has forced extensive repairs, with a huge economic costs.

The following are the effects of improper curing as stated by Punmia et al (174):

- Appearance of minute cracks on the concrete surface.
- Development of internal cracks due to heat of hydration.

- Development of uneven strength across the section, with an overall strength reduction.
- Reduced resistance to abrasion at the exposed surface.
- Increased concrete permeability and subsequent decrease in durability.
- Reduced resistance to the action of frost and weathering.

The effects of improper curing will be more conspicuous in the parts of structures that are either directly exposed or those that have large surfaces compared to depth such as roads, canals, bridges, cooling towers, chimneys, etc.

2.11 Effects of degree of saturation on compressive strength

The degree of saturation is defined as the volume of voids filled with water divided by the total volume of voids, and expressed as a percentage (175). Jianhua Jiang (176) also wrote that the moisture content generally comprises water vapour and liquid water in the concrete's inner micro-environment due to the pore structure.

Concrete structures are exposed to continuous variations in temperature and moisture content, arising as the effects of climate load in a natural environment. Establishing the relationship between moisture content and compressive strength in concrete is of great importance in predicting the durability of concrete structures. Changes in moisture content affect the strength of porous solids. In most cases drying influences strengthening while the wetting produces a weakening of porous media. The moisture content of concrete however is also a significant factor affecting deterioration, specifically alkali–aggregate reaction, freeze–thaw damage, concrete carbonation, chloride ion diffusion and steel corrosion in concrete structures (177, 178).

It is known that the degree of saturation affects measured strength (27, 28). Meanwhile, samples cured under typical ideal, i.e. saturated, conditions will be fully saturated upon strength testing. Therefore, measuring strength at a constant degree of saturation is essential for accurately showing the effects of improper curing. Popovics (179) investigated changes in curing conditions and showed that the highest compressive strengths of concrete specimens were developed when samples were moist cured followed by a 3-day air curing before the strength test. While air cured samples followed by 3-day moist curing developed lower concrete strengths than samples that were cured continuously in air. The reduction in compressive strength obtained by soaking concrete samples in water before testing has been associated to the absorption of water by the gel pores (180). Soaking concrete specimens in benzene or paraffin, which cannot be absorbed into gel pores, does not have any effect on strength. However, under extremely dry conditions, a strength reduction can be observed (181).

Pihlajavaara (181) reported that moisture conditions or changes in moisture content have a critical effect on the strength, shrinkage and creep of mature concrete, and that strengths obtained from concretes that have been dried were about two thirds higher than the strengths from wet concrete samples.

Evaluation of the moisture effect on the strength of concrete specimens which had been cured completely was investigated by Chen et al (28). A relationship between the concrete properties and the moisture contents normally experienced in outside conditions was

developed. They concluded that the moisture content does have a significant effect on compressive strength, with specimens stronger at lower degrees of saturation. However, a surprising increase in compressive strength was obtained at an almost saturated condition.

Shoukry *et al* (27), worked on concrete mechanical properties to determine ideal air temperatures between 20 and 22 °C and relative humidity between 40 and 60% under laboratory condition. The development of concrete's mechanical properties when cured under different environmental conditions were also defined. Different tests were used to measure modulus of elasticity, compressive strength, and split tensile strength at varying temperatures and humidity conditions to study their effects on normal concrete. They concluded that temperature and moisture perform a large function in influencing the properties of concrete. Higher temperatures and moisture levels reduce concrete compressive and tensile strengths and corresponding elasticity moduli.

2.12 Effects of drying on concrete

Concrete structural members will experience a range of climatic conditions, both in terms of temperature and relative humidity. Also, in hot weather, where the temperature is sometimes over 35°C or more, direct sunlight can increase the temperature of concrete members up to 50°C (182). In these conditions, the properties of concrete may experience obvious changes. Generally, at increased temperature, concrete surfaces will lose moisture which could affect the hardened properties of concrete, by contributing to drying shrinkage cracking. Also, micro cracks might show up as a result of thermal stress and thus would affect the hardened properties of concrete.

This aspect of the study has investigated the effect of drying mature concrete at a constant temperature. The temperature of 40°C was chosen because at this temperature the concrete will dry and its microstructure will not be damaged. Literature available on effects of low or moderate temperatures on cured concrete were limited while there are lots on very high temperatures (183-192) in order to assess the strength of concrete in case of any accidental fire.

The effect of drying on fly ash concretes was considered in this study, there are few or no literature on the effect of medium or low temperature on fly ash concretes. Lots of research has been conducted on effects of high temperature (185, 193-197) on curing. All the studies revealed that fly ash concretes performed better than Portland cement at high temperature. They all reported an initial increase in concrete compressive strength with an increase in the temperature but with additional increase in the temperature there was a decrease in compressive strength.

2.12.1 Effect of medium or low temperature on concrete

Imane *et al* (198) worked to show the sensitivity of the concrete in different climatic environments, by studying concrete samples which had been cured for 28 days before being subjected to 24 hours of cold temperature (-15 and -10°C) or to high temperatures (40, 50 and 60 °C) with use of a thermal enclosure. The results were presented in three phases according to various temperatures observed in the experiment. Between -15°C to 0° C, there was an increase in the average compressive strength. A second phase, phase II, occurred when temperatures were between 0°C to 10°C, and 10°C to 40°C, here the concrete showed good resistance to temperature and temperature had limited influence

on concrete. Phase III was divided into two parts, the results from 40°C up to 50°C showed a gradual increase in strength for all concrete examined. The second part of phase III revealed decrease strength as the temperature increased from 50°C to 60°C. They concluded that temperatures perform a big function in affecting the properties of concrete and higher temperatures will produce lower concrete strength in compression.

The effects of medium temperature and industrial by-products on the key hardened properties of high performance concrete was studied by Safiuddin *et al* (182). Two industrial by-products, silica fume and Class F fly ash, were used separately and together with normal Portland cement to produce three concrete mixes in addition to the control mix. The concrete specimens were cured in water at 20°C for 3, 7, and 14 days before exposing the samples to medium temperature of 35°C or 50°C. The dried concrete samples were tested for compressive strength at the age of 28 and 91 days. Test results reveal that the temperature environment at 35°C generates higher compressive strength than the temperature environment at 50°C. They concluded that the compressive strength of concrete decreased as the temperature increased. Also the effects on the addition show that all types of concrete having additions revealed higher strength performance than normal Portland cement and that increase in temperature has little adverse effect in concretes with additions.

Janotka and Nurnbergerova (186) examined the effect of temperature on structural quality of cement paste and high-strength concrete with silica fume. The concrete samples used in the experiment were cured for 28 days before exposing to temperatures of 40, 60, 100, and 200°C. The result showed a slight increase in prism compressive strength up to 100°C while strength decrease was obtained at elevated temperatures. They report that the lower strengths measured explain that structural deterioration of concrete is distinctly influenced by increase in temperature and also elevated and prolonged heating will result in loss of weight and the growth of the air voids portion (186).

The effects of moisture and temperature on the mechanical properties of concrete were studied by Shoukry *et al* (27). The temperatures considered in their study were within the range -20°C to +50°C. The results showed that concrete specimens were stronger at lower temperatures and weaker at higher temperatures. Also there was a notable decrease in the compressive strength and tensile strength in all the tested samples as the temperature increased.

2.13 Shrinkage

Shrinkage of concrete is the principal cause for various kinds of cracks which affect the serviceability and durability of concrete. It is described as the reduction in volume of unloaded concrete at a constant temperature. The loss of water during the drying process and chemical reactions has been reported to be the primary cause of shrinkage. Shrinkage of concrete occurs at two specific phases which are early and later ages. The early stage is normally the first day when concrete is setting and beginning to harden (199, 200). Twenty four hours after casting and beyond is refer to as later ages or long term (199). As a result of low strength and strain capacity at early age, concrete is really susceptible to internal stresses. Shrinkage cracking occurs when tensile stresses due to restrained volume contraction exceed the tensile strength of concrete this leads to cracking (201). There are many types of shrinkage that affect concrete, namely plastic shrinkage, autogenous

shrinkage, chemical shrinkage, drying shrinkage, carbonation shrinkage and thermal shrinkage.

2.13.1 Plastic shrinkage

Plastic shrinkage is the shrinkage of freshly placed concrete that occurs when the concrete is still fluid. The duration is normally short, nearly one to two hours. It starts first after the water glaze disappears from the concrete surface and ends immediately thereafter, when the concrete sets (202). Plastic shrinkage in concrete is a complicated interaction of internal and external development which is controlled generally by the loss of water due to drying. It leads to production of water menisci that exert contraction forces within the microstructure (203). Also it can be as a result of a capillary pressure in the pore system of the material building up due to the loss of water. Plastic shrinkage is induced by evaporation of water and fully depends on the bleeding rate (204).

Plastic shrinkage cracking due to restrained shrinkage is a primary problem that often occurs in concrete structures with a relatively large surface area or thin concrete elements (having a high surface area to volume ratio) such as concrete walls, bridge decks, slabs, and overlays. Also concrete pavements, specifically those in road and airfield construction, are liable to plastic shrinkage due to their comparatively large, exposed, and occasionally unprotected surface. Early age cracks resulting from this capillary shrinkage may have an unfavourable effect on the durability of concrete pavements. High performance concretes, having low water to cement ratio, and combined with silica fume, due to the minuteness of pores formed and reduced bleeding rate, are also prone to plastic shrinkage cracking. Fresh concrete is sensitive to plastic shrinkage cracking especially during hot, windy, and dry weather environments when the evaporation rate is considerably higher than bleeding rate. Also plastic shrinkage cracks develop without any specific pattern with lengths varying from few centimetres to several metres, and widths that can reach values of 0.1 to 3mm (205).

2.13.2 Drying Shrinkage

Drying shrinkage occurs due to the loss of moisture from hardened concrete. This shrinkage is explained as the volume reduction that concrete experiences as a result of the movement of moisture when exposed to a lower relative humidity environment than the initial one in its own pore system (206). Also Neubauer *et al* (207) wrote that most of the drying shrinkage occurs in the C-S-H, while calcium hydroxide (CH), anhydrous cement and aggregate all restrain shrinkage. Aitcin (208) wrote that drying shrinkage develops when concrete dries in dry air and as concrete releases some of its internal water; menisci emerge within the coarse apparent capillaries which resulted into mass loss. Drying shrinkage of the hydrated cement paste starts at the surface of the concrete and advances further or less rapidly through the concrete, based on the relative humidity of the ambient air and the size of capillaries. Drying shrinkage in concrete is as a result of drying of water enclosed in the pore structures and the combined decrease in moisture content. It is a surface phenomenon the drying progress begins at the surface which is exposed to drying and slowly infiltrates into the concrete (209). The major cause of deterioration of concrete structures can be as a result of drying shrinkage (201).

2.13.3 Autogenous shrinkage

Autogenous shrinkage of concrete can be described as the macroscopic volume development that take place after the initial setting due to removal of moisture from capillary pores for continuity of cement hydration reactions (210). Also it's a macroscopic reduction in length under constant temperature without any movement of moisture to or from concrete (211). This is a change that occur at early ages when no moisture transfer is allowed with the environment. This volume reduction is connected to chemistry and internal structural developments. Autogenous shrinkage is generally a concern in high-strength or high-performance concrete where the strength is greater than 40 MPa, and where the water-to-cement (w/c) ratio is low (199). Holt also defined autogenous shrinkage of cement paste and concrete as the macroscopic volume development that exist when there is no moisture transported to the outside of the surrounding environment. It is an external volume change and a phenomenon in which cementitious materials shrink at a constant temperature without any change in weight. Autogenous shrinkage increases as the water-cement ratio decreases and the microstructure of cement becomes denser.

2.13.4 Chemical shrinkage

Chemical shrinkage, which is the reduction in the volume of hydration products compared with that of the reacting constituents. This has been considered as the main driving mechanism behind autogenous shrinkage. The chemical shrinkage is the outcome of the reactions between cement and water, which result to a volume reduction. Chemical shrinkage, starts immediately after mixing of water and cement and the rate is greatest during the first hours and days. Chemical shrinkage is considered as an internal volume reduction. The rate of chemical shrinkage rely on cement and concrete mixture specifications, like the cement fineness and the ability of cement dispersion (199, 210, 211).

2.13.5 Carbonation shrinkage

The surface zone of concrete experiences shrinkage due to carbonation as a result of drying. The reaction between carbon dioxide and the hardened cement paste results in carbonation shrinkage. The volume reduction caused by carbonation shrinkage is moderate (212, 213). Also carbonation shrinkage is possibly produced by the softening of crystals of $\text{Ca}(\text{OH})_2$ at the time under a compressive stress that is imposed by the drying shrinkage. This leads to depositing of CaCO_3 in spaces free from stress thereby temporarily increasing the compressibility of the hydrated cement paste. Carbonation shrinkage becomes gradually more obvious when concrete is constrained to alternating wetting and drying in air containing CO_2 (17).

Carbonation of concrete is a slow process and is one of the most destructive occurrences that affect the durability and serviceability of concrete structures. Carbonation is a process where the hydration products specifically calcium hydroxide ($\text{Ca}(\text{OH})_2$) of cement react with the dissolved carbon dioxide (CO_2), thus reducing the pH of the concrete pore solution from approximately 12 to less than 9 (86). The process of carbonation normally begins with the ingress of atmospheric CO_2 and, along with water, forms carbonic acid, which is very reactive with the hydrated cement paste, forming calcium carbonate (CaCO_3). Carbonation shrinkage is due to chemical reactions between hardened cement paste and carbon dioxide. When CO_2 reacts with calcium silicate hydrate (C-S-H), it induces a decrease in its calcium-silica (C/S) ratio which results to water loss. Carbonation shrinkage is a function of

relative humidity and is greatest around 50 per cent relative humidity. Carbonation shrinkage, although not very significant itself, can contribute to the effect of drying shrinkage and thereby lead to cracking. Its magnitude is usually negligible in comparison to the other types of shrinkage.

Carbonation reduces the permeability and pore volume of concrete. The reduction of permeability and porosity was found to be much more in concrete, which has low strength as a result of high water-to-cement (w/c) ratio. Also carbonation increases the density, strength, modulus of elasticity, and shrinkage of the concrete. The major factors that affect the carbonation shrinkage are permeability of concrete, moisture content, relative humidity, high w/c of the mixture, and rate of carbon dioxide in the air (214, 215).

2.13.6 Thermal Shrinkage

Solid materials such as concrete experience contraction on cooling and expansion on heating. Thermal expansion is generated by insufficient heat dissipation during the cement hydration and cooling of concrete. The liberated heat increases the concrete temperature causing thermal expansion when the cement hydrates at early age. As the hydration reactions attain their peak, the rate of heat liberation decreases and concrete starts to dissipate heat and cools down, causing contraction or thermal shrinkage. In massive concrete however, the variation in the rate of heat dissipation between the interior and exterior concrete can produce a thermal gradient, leading to thermal strains, and associated stresses which can influence cracking. This specifically develops in structural elements of greater thickness when the rate at which hydration heat released is larger than the rate of diffusion through conduction. Early-age thermal cracking takes place within a few days in thinner sections, but it may take longer to develop in thicker sections which cool more gradually. Thermal shrinkage is a concern with the concrete at early age when the tensile strength is low and in massive concrete structure where the heat of hydration produced is very high. Massive concrete structures such as bridge piers, dams and nuclear containments usually experience serious thermal expansion at times the maximum temperature may get to 70°C or more at early age especially during construction (216-219).

2.13.7 Mathematical modelling of drying shrinkage

Concrete shrinkage models are expected to determine an estimate of shrinkage strain. They take into account relative humidity, notional dimension, concrete compressive strength, and type of cement as parameters for predicting the shrinkage strain. The CEB-FIP 90 model is valid for concrete that has an average 28-day compressive strength in the range of 20 MPa to 90 MPa and an environmental relative humidity in the range of 40 to 100%, at a mean temperature of 5 to 30°C (220, 221).

The equations by CEB-FIP 1990 are only applicable for the longitudinal shrinkage deformation of plain or lightly reinforced normal weight concrete elements. The CEB-FIP 1990 model deals with dry curing conditions only. The model is appropriate to the experimental result in the early age, but it under predicts the drying shrinkage at a later age (221).

The total shrinkage or swelling strains $\varepsilon_{cs}(t, t_s)$ taken from (222) may be calculated from

$$\varepsilon_{cs}(t, t_s) = \varepsilon_{cs0} \beta_s (t - t_s) \text{ Equation 2.10}$$

Where:

ε_{CSO} Is the notional shrinkage coefficient

$$\varepsilon_{CSO} = \varepsilon_s (f_{cm}) \beta_{RH} \quad \text{Equation 2.11}$$

$$\varepsilon_s (f_{cm}) = [160 + 10 \beta_{sc} (9 - \frac{f_{cm}}{f_{cmo}})] \times 10^{-6} \quad \text{Equation 2.12}$$

f_{cm} is the mean compressive strength of concrete at the age of 28days (MPa).

$$f_{cmo} = 10$$

β_{sc} is a coefficient which depends on the type of cement:

$$\beta_{sc} = 4 \text{ for slowly hardening cements SL}$$

$$\beta_{sc} = 5 \text{ for normal or rapid hardening cements N and R,}$$

$$\beta_{sc} = 8 \text{ for rapid hardening high strength cements RS.}$$

$$\beta_{RH} = -1.55 \beta_{sRH} \text{ For } 40\% \leq RH < 99\% \text{ Equation 2.13}$$

$$\beta_{RH} = 0.25 \text{ for } RH \geq 99\% .$$

$$\beta_{sRH} = 1 - \left(\frac{RH}{RH_0} \right)^3 \quad \text{Equation 2.14}$$

RH is the relative humidity of the ambient atmosphere (%)

$$RH_0 = 100\%$$

β_s is the coefficient to describe the development of shrinkage with time.

The development of shrinkage with time is given by

$$\beta(t - t_s) = \left[\frac{(t - t_s)/t_1}{350(h/h_0)^2 + (t - t_s)/t_1} \right]^{0.5} \quad \text{Equation 2.15}$$

$$\text{Where } h = 2A_c / u \quad \text{Equation 2.16}$$

h is the notational size of member (mm), A_c is the cross section and u is the perimeter of member in contact with the atmosphere.

$$t_1 = 1 \text{ day}$$

$$h_0 = 100\text{mm}$$

t is the age of concrete (days)

t_s is the age of concrete (days) at the beginning of shrinkage or swelling.

This equation is potentially useful in terms of giving designers an indication of the magnitude of drying shrinkage and the likelihood of cracking.

Shrinkage model of *fib* Model Code 2010

Shrinkage model of *fib* Model Code 2010 is the latest version thus the research examined the shrinkage prediction using *fib* Model code 2010 and compare with the result with experimental data and the existing CEB-FIP 1990.

The drying shrinkage $\epsilon_{cds}(t)$ is calculated by means of the notional drying shrinkage coefficient $\epsilon_{cds0}(f_{cm})$, the coefficient $\beta_{RH}(RH)$, taking into account the effect of the ambient relative humidity and the function $\beta_{ds}(t-t_s)$ describing the time-development:

$$\epsilon_{cds0}(f_{cm}) = [(220 + 110 \cdot \alpha_{ds1}) \cdot \exp(-\alpha_{ds2} \cdot f_{cm})] \cdot 10^{-6}$$

According to the *fib* shrinkage model, the notional drying shrinkage coefficient depends on the mean compressive strength of the concrete at 28 days f_{cm} and on the coefficients α_{ds1} and α_{ds2} , both accounting for the cement type. The evolution of the drying shrinkage strain

$$\epsilon_{cds}(t-t_s) = \epsilon_{cds0}(f_{cm}) \cdot \beta_{RH}(RH) \cdot \beta_{ds}(t-t_s)$$

is given by multiplying the notional drying shrinkage coefficient $\epsilon_{cds0}(f_{cm})$ by the coefficient

$$\beta_{RH} = [-1.55 \cdot [1 - (\frac{RH}{100})^3]] \text{ for } 40 \leq RH < 99\% \cdot \beta_{s1}$$

$$\beta_{RH} = [0.25 \cdot [1 - (\frac{RH}{100})^3]] \text{ for } RH \geq 99\% \cdot \beta_{s1}$$

for taking into account the effect of ambient relative humidity RH (in %) and by the time-dependent function

$$\beta_{ds}(t-t_s) = \left(\frac{(t-t_s)}{0.035 \cdot h^2 + t-t_s} \right)^{0.5}$$

$$\beta_{s1} = \left(\frac{35}{f_{cm}} \right)^{0.1} \leq 1.0$$

Where

α_{ds1} and α_{ds2} are coefficients, dependent on the type of cement and was taken from table 5.1-13 in *fib* Model Code 2010.

The latter depends on the current age of the concrete t , the age of the concrete at the onset of drying t_s and on the notional size $h = 2 \cdot A_c/u$ of the member.

The shape and size effect is only considered in the time-dependent function $\beta_{ds}(t-t_s)$ by the notional size h in the *fib* shrinkage model

Neither the duration of moist curing nor the curing temperature are considered in the *fib* shrinkage model, which is intended for predicting shrinkage strains of concrete members moist-cured at normal temperatures for no longer than 14 days.

2.13.8 Factors affecting shrinkage

There are lots of factors that affect the shrinkage of concretes. The factors have been classified as internal and external factors. Internal factors affecting drying shrinkage of concrete are those related to its constituents and are fixed once and for all when the concrete is cast. Examples of such are: cements, aggregates, and admixtures; concrete mix design; water-cement ratio and water content; and aggregate properties and volume fraction. Also some are related to the construction of the concrete such as placing, compaction, and curing. The external factors affecting loss of moisture from concrete are ambient conditions and size and shape of the concrete member under consideration. Ambient conditions that affect drying shrinkage consist of relative humidity, wind velocity, and air temperature. The external factors are the factors which can vary after casting (206, 223). The factors affecting drying shrinkage are presented in Table 2.5.

Table 2-5 Factors affecting shrinkage strain

Category	Influencing Factors
Internal factor	Aggregate – volume and mechanical properties
	Cement types and content
	Water-cement ratio
	Concrete strength
	Member size
External factor	Curing condition
	Temperature and humidity
	Age when drying begins

2.13.8.1 Aggregate

Aggregates have a larger modulus of elasticity when compared with cement paste. Thus aggregate presence in concrete acts to internally restrain shrinkage (224). The volume and type of aggregates in the concrete mix is one of the factor that affect the shrinkage of concrete. Aggregates restrain the shrinkage of cement paste. Hence an increase in aggregate volume and the corresponding reduction in the volume of cement paste will lead to a reduction in shrinkage. Concrete shrinkage can be easily reduced by increasing the coarse aggregate content. Neville (225) wrote that the size and grading of aggregate do not influence the magnitude of shrinkage but a larger aggregate permits the use of a leaner mix and hence results in a lower shrinkage. Concrete of low workability contains more aggregate than a mix of high workability made with aggregate hence this results in lowering shrinkage.

An experimental study to explain the effect of various aggregate materials components on the drying shrinkage property in mortar and concrete specimens using fourteen kinds of

fine aggregate materials and three kinds of coarse aggregate materials was investigated by Zhang *et al* (226). The results obtained showed that the characteristics of fine and coarse aggregate materials perform an influential role in regulating the drying shrinkage property of mortar and concrete. They concluded that the drying shrinkage volume of concrete is usually smaller than the drying shrinkage of mortars at the same age, due to the effect of coarse aggregate on drying shrinkage and that the smaller the coarse aggregate shrinkage strain the less is the drying shrinkage strain of concrete, meaning that the coarse aggregate help in restraining the drying shrinkage of concrete, and also help in regard to the drying shrinkage development of concrete.

Mu and Forth (227) used different quantities of coarse aggregate in modelling by using 900kg/m^3 , 1050kg/m^3 and 1200kg/m^3 of coarse aggregates respectively. The result shows that the shrinkage decreases with the rise in the amount of aggregate. This is shown in Figure 2.11. Holts (199) performed tests on neat paste, mortar, and concrete to check effect of aggregates on shrinkage. The result shows that the neat paste had much greater shrinkage than the mortar due to the lack of aggregate to provide restraint. Also another two tests were done to compare the restraint provided by increasing the aggregate, both in size and volume to test concrete and mortar. Concrete samples shrink less than the mortar (199).

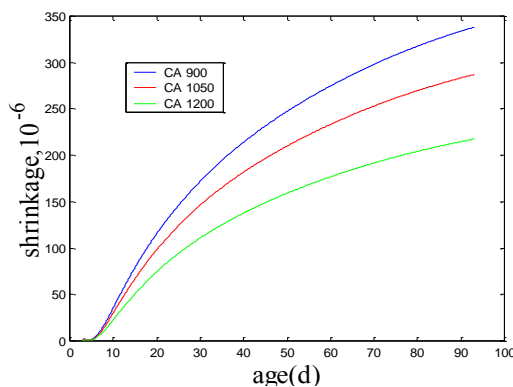


Figure 2-13 Effect of coarse aggregate content Taken from (227)

2.13.8.2 Cement types and content

Higher cement content increases the shrinkage and cracking tendency of concrete at a constant water/cement ratio. This is as a result of the larger volume of hydrated cement paste which is liable to shrinkage. Ray *et al* (228) result revealed that higher performance concrete having lower w/cement ratio had a higher shrinkage due to higher paste volume. Also Mu and Forth (227) in modelling kept the water to cement ratio and the amount of coarse aggregate in the three mixes constant with three different contents of cement to be 550kg/m^3 , 425kg/m^3 and 300kg/m^3 , as seen in Figure 2.12. The result revealed that shrinkage increases as the cement content increases. They concluded that the contraction of cement paste in concrete is the origin of shrinkage and the shrinkage of concrete is equivalent to the fraction of paste in the concrete.

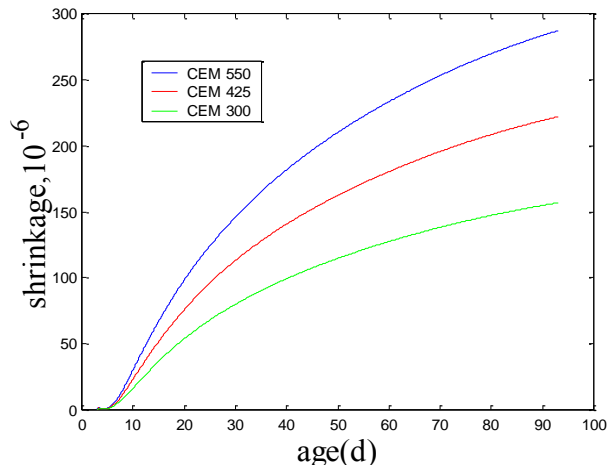


Figure 2-14 Effect of cement content Taken from (227)

2.13.8.3 Water Content

Water content of the concrete can be regarded as the fundamental factor that influences shrinkage. It has a main function during early-age shrinkage by regulating the amount of free water, and the development of the microstructure and pore system, which correspondingly change the capillary tension and meniscus development (autogenous shrinkage) (217). Also the more water that is available to evaporate from the concrete, the higher the tendency to shrink on drying (217). The result of 28-day-old samples of cement pastes cured at 20°C, with four different w/c ratios by Neubauer *et al* (207) shows that higher w/c ratios produce higher area and particle shrinkages. This is due to the fact that higher w/c values will make the samples to be more porous thus resulting in a more open microstructure. Thus shrinkage increased with high w/c ratios.

The shrinkage of concrete can be effectively reduced by keeping the water content of the paste (water/cement ratio) as low as possible, and the total aggregate content of the concrete (volume of restraining aggregates) as high as possible. This will result in a lower water content per unit volume of concrete and consequently lower shrinkage is obtained. Bissonnette *et al* (201) found that the influence of w/c ratio on the shrinkage of cementitious materials was relatively small. Bloom and Bentur (229) found that the higher w/c concrete exhibited the largest drying shrinkage. The test result from Zhang *et al* (226) showed that the drying shrinkage strain becomes larger when there is increase in total amount of water.

2.13.8.4 Age

Neubauer *et al* (207) showed the effect of age by presenting the area and particle shrinkage values of 7, 14 and 28 day old cement samples with w/c is 0.5 cured at 20°C. The area shrinkage and the particle shrinkage decrease with increasing age of the specimen. At intermediate humidities between 40 to 80% area shrinkage and particle shrinkage at early ages are relatively large but, at later ages, these values are significantly lower. This suggests that the stresses associated with capillary tension, which is the predominant mechanism at intermediate relative humidities have a decreasing effect on shrinkage at later ages. Thus young specimen has higher shrinkage.

2.13.8.5 Size

The size of concrete structural elements have an important effect over the rate of drying shrinkage. A larger ratio of surface area to volume will make the rate of evaporation of water from concrete faster which will result in faster rate of shrinkage (224). The shrinking of large concrete elements is slower than that of smaller specimens. The effect of specimen size on shrinking rate can be expressed by the volume/surface ratio. Higher shrinkage strain result was obtained in smaller size specimens (230, 231).

2.13.8.6 Effect of superplasticizers

Chemical admixtures, such as superplasticizers, water reducers, air-entraining agents, and shrinkage reducing admixtures, are often used with concrete. The effect of superplasticizers on the shrinkage of concrete cannot be ignored since superplasticizers help to reduce the water content of concrete, which is one of the important factors affecting shrinkage. A shrinkage-reducing admixture can decrease the surface tension of the capillary pore solution resulting in a reduction of the capillary tension. It was found to reduce both autogenous and drying shrinkage strains (199). Al-Saleh (230) found a moderate effect on shrinkage strain specimen with use of plasticizing admixture which is in contrast to what is in literature where an increase of about 20% was reported by Brooks (232).

2.13.8.7 Effect of fineness of cement

The fineness of the cement also influences the shrinkage of concrete. The rate of hydration of Portland cement relies upon the surface area of the clinker particles; finer cements develop strength more quickly. The finer pore structure of finer cements results in higher early age shrinkage in concrete. Also the fineness of cement influences the drying shrinkage of concrete when the water content is increased as a result of fineness, the drying shrinkage is increased (233).

2.13.8.8 Effect of Mineral Admixtures

Different mineral admixtures are often used in concrete to improve compressive strength and other mechanical properties. There are different conclusions on the effect of these materials on drying shrinkage and cracking. Three major types of mineral admixtures commonly utilized in concrete are fly ash, slag, and silica fume. The type, fineness, and percentage of cement replacement are the main parameters controlling the effect of pozzolanic materials on early-age shrinkage.

2.13.8.9 Effects of Silica fume on shrinkage

Silica fume (SF) is a by-product of the silicon and ferrosilicon industry. The reduction of high-purity quartz to silicon at temperatures up to 2000^o C produces SiO₂ vapours, which oxidize and condense in the low-temperature zone to tiny particles consisting of non-crystalline silica. More than 95% of silica fume particles are finer than 1µm. Silica fume has a very high content of amorphous silicon dioxide and consists of very fine spherical particles (234).

Silica fume was found to increase the autogenous shrinkage significantly due to refining the pore structure of concrete. Khatri *et al* (235) suggested that, although long-term shrinkage is reduced with the use of silica fume, the early age increase in shrinkage may lead to significant cracking because the tensile strength of concrete is low at early ages. Generally,

the inclusion and increase in the proportion of silica fume decreases drying shrinkage strain. Silica fume did not affect the total shrinkage; however, as the proportion of silica fume increased, the autogenous shrinkage of high-strength concrete increased and its drying shrinkage decreased. This pattern of behaviour is observed in the result of a study conducted by Mazloom *et al* (235, 236). The maximum plastic shrinkage strain was observed in silica fume cement concrete which was attributed to the un-densified nature of this silica fume and the lowest plastic shrinkage strain was noted in the plain cement concrete (237). The influence of silica fume on the plastic shrinkage of concrete exposed to hot-weather conditions (a wind velocity of 15 km/h, temperature of 45°C and RH of 35%) was studied by Al-Amoudi *et al* (238). The result shows that plastic shrinkage strain increased with increasing content of silica fume. This trend was observed in all the concrete specimens prepared with the selected silica fume cements.

Zhang *et al* (239) conducted an experimental study on the autogenous shrinkage of Portland cement concrete (OPC) and concrete incorporating silica fume. The result obtained revealed that both the w/c ratio and the addition of silica fume had significant effect on the autogenous shrinkage strain of the concrete. The autogenous shrinkage increased with decreasing w/c ratio and with increasing silica fume content.

2.13.8.10 Effects of Ground Granulated Blast Furnace Slag on shrinkage

Ground granulated blast-furnace slag (GGBFS) is a by-product of making iron and steel. It is a fine powder ground from the glassy, granular material that is produced when molten iron blast furnace slag is air quenched with water or steam. GGBFS has the same features in fineness and specific surface area to cement particles. It contains very limited amount of crystals and is highly cementitious in nature. GGBFS was found to considerably improve the pore structure of concrete (3, 40). Variety of results has been obtained in drying shrinkage with GGBFS concretes. Both increases and reductions in the shrinkage has been observed. The study on creep and shrinkage of high strength concrete conducted by Li and Yao (240) reported a reduction in the drying shrinkage of concrete having 30% replacement of ultrafine GGBS. The inclusion of GGBS helps to promote hydration of cement and increases the density of hardened cement paste. This strengthens the pore structure of concrete, thus producing concrete that is more resistant to deformation. Evaluation of autogenous shrinkage of concrete made with w/c ranging from 0.27 to 0.42 and Granulated blast-furnace slag (GGBS) replacement level of 0%, 30%, and 50% by Lee *et al* (241) present increases in shrinkage. The concrete made with GGBS exhibited higher autogenous shrinkage than ordinary concrete without any GGBS, and the higher the GGBS replacement level, the greater the autogenous shrinkage at the same w/c. This may be due to the greater chemical shrinkage and finer pore structure of the concrete with GGBS than pure Portland cement, and the particle shape of GGBS.

2.13.8.11 Effects of Fly ash on shrinkage

Incorporating fly ash considerably reduced autogenous shrinkage of high- performance concrete (HPC). The higher the fly ash content, the lower autogenous shrinkage. It is deliberated that the basic characteristics of fly ash, such as its spherical particle shape and delayed hydration, contribute to the reduction of autogenous shrinkage of HPC containing fly ash. This is the conclusion made by Lee *et al* (242) and similar result was obtained by Termkhajornkit *et al* (243, 244). Atis (208) reported that addition of high volumes of fly ash

in concrete with a low water-cementitious material ratio resulted in a reduction in the drying shrinkage values of up to 30% when compared to ordinary Portland cement (OPC).

Chindaprasirt *et al* (245) worked on mortar samples using fly ashes of different fineness reported that all of the fly ashes reduced the drying shrinkage of the mortars. Though the drying shrinkage is influenced by many factors, the results indicated that the water to cement ratio was the prime factor. Fly ash in concrete decreased drying shrinkage when the w/b ratio and the binder content were adjusted to achieve the same 28-day strength of the control concrete. Also concrete with 30% fly ash showed less shrinkage than that with 40% fly ash (92).

Bjegovic *et al* (246) worked on quaternary blended cement to produce concrete. The results presented by them concluded that the influence of fly ash has overcome the influence of slag and limestone on shrinkage since past research has shown that both the addition of slag, as binder, and limestone, as filler, to concrete causes an increase in shrinkage (247, 248). The inclusion of fly ash to concrete causes a decrease in shrinkage.

2.13.8.12 Effect of curing

Curing is one of the factors that affects drying shrinkage that is related to the construction of the concrete. When concrete surfaces are exposed to the atmosphere there is moisture loss which leads to shrinkage. The curing method, duration and temperature have a significant effect on early-age shrinkage. Proper curing can protect against moisture loss from fresh concrete. Huo and Wong (249) examined the early-age behaviour of high-performance concrete (HPC) under various curing methods. The results show that proper moisture-curing methods can effectively limit the development of shrinkage strains. Also curing concrete for longer period would produce lower shrinkage deformation and lower evaporation rate. Nassif *et al* (221) discovered that the shrinkage of the air cured concrete was highest, followed by the specimens coated with the curing compound, and then the burlap-wrapped specimens. They concluded that different curing methods have an effect on autogenous and drying shrinkage for HPC. They suggested that the HPC mixture needs to be cured with wet burlap immediately after finishing to prevent autogenous shrinkage since autogenous shrinkage occurs mainly in the first seven hours.

The effects of curing conditions on concrete shrinkage were studied by Alsayed and Amjad (250). Reinforced concrete slabs on grade were exposed to a hot, dry climate, and the effects of intermittent wet and dry curing were considered. The study concluded that intermittent wet curing reduces the ultimate shrinkage of concrete, and also increases the exposure time needed to develop it and wet curing produces concrete with less susceptibility to weather variations.

Six curing compounds were used by Nancy and Whitting (251) to examine the effectiveness of different types of curing compounds in retaining water for hydration, promoting concrete strength, and reducing permeability. Moisture loss was also considered. The result shows that all the curing compounds decreased the moisture loss and all performed better than the air-cured treatment, but none performed as well as water-cured specimens. Reduction in moisture loss from concrete was reported by Wang *et al* (252) when curing compounds were applied to concrete samples. Also the second peak in evaporation, which occurred in air-cured specimens, was eliminated in cured samples. In order to reduce the undesirable effects caused by excessive water evaporation from concrete surfaces, which

induce plastic shrinkage cracking and thereby reduce durability, Nabil *et al* (253) studied the effectiveness of curing procedures, namely plastic sheet, curing compound, cold water and polypropylene fibre on the properties of concrete. The effect of curing on plastic shrinkage cracks, evaporation rate, and strength was evaluated. They concluded that the most efficient way to minimize plastic shrinkage is to use a curing compound followed by the application of a plastic sheet cover; and the most efficient measure to decrease evaporation is the application of a plastic sheet cover.

Effect of curing methods on the properties of plain and blended cement concretes was investigated by Al-Gahtani (16), the efficiency of two curing compounds, namely water-based and acrylic-based, was evaluated. The results of that study indicated that the curing compounds were effective in moisture retention and decreased the plastic and drying shrinkage strain. A study conducted to assess the effect of curing on shrinkage by Maslehuddin *et al* (254) concluded that the application of curing compounds decreases the shrinkage strains and reinforcement corrosion, thereby enhancing the overall life of a structure. A field study was conducted to assess the effect of curing methods and specimen size on the plastic and drying shrinkage strain in plain and silica fume cement concretes by Al-Amoudi *et al* (231). The effect of specimen size and method of curing on plastic and drying shrinkage and some of the mechanical properties of silica fume and plain cement concrete specimens were evaluated. The result indicated that the shrinkage strains in both the plain and silica fume cement concrete specimens cured by continuous water-ponding were less than that in similar concrete specimens cured by covering them with wet burlap. Also good curing is suggested to avoid cracking of concrete due to plastic and drying shrinkage, particularly under hot weather conditions.

2.13.8.13 Effect of Environmental Conditions

Influence of environmental condition on concrete structures is an external factor which can vary after casting. Ali and Urgessa (206) wrote that ambient conditions, size and shape of the concrete member under consideration are the external factors that affect loss of moisture from concrete. Relative humidity, wind velocity, and air temperature has been highlighted as the ambient conditions which affect the loss of moisture from the concrete surface. Higher drying shrinkage will occur when there is decrease in relative humidity, rise in ambient temperature, increase in air movement around the concrete, and increase in the length of time for which concrete is subjected to drying conditions. The degree of early age drying shrinkage greatly depends on the surrounding environmental conditions. The degree of early age drying shrinkage increases when there is increase in evaporation of free water from the fresh concrete (255). Drying commences when the evaporation rate exceeds the bleeding rate, risk of drying depends on the environment and on the bleeding rate of the concrete (256). Drying shrinkage of the hydrated cement paste starts at the surface of the concrete and advances more or less very quickly through the concrete, depending on the relative humidity of the ambient air and the size of capillaries (208).

2.14 Summary

This chapter has reviewed the constituents of concrete, the hydration of Portland cement and the durability of concrete. The effects of fly ash on hydration, microstructure and transport properties of fly ash blended systems, drying shrinkage, factors that affect shrinkage and concrete shrinkage models which are expected to determine an estimate of

shrinkage strain were summarized. Although the scientific literature stresses that curing of concrete is essential for strength development and durability and that the main objective of curing is to keep concrete in a saturated state or nearly wet to help the hydration of cement, this does not appear to be common in practice, and the effects of improper curing have only infrequently been reported in the literature.

Furthermore, the literature has shown that the degree of saturation affects measured strength, and that strengths obtained from concretes that have been dried are about two thirds higher than the strengths of saturated concrete samples. Meanwhile, samples cured under typical ideal, i.e. saturated, conditions will be fully saturated upon strength testing. Therefore, since changes in curing conditions will affect the degree of saturation of the resultant concrete, this study on effect of improper curing also consider the effects of changes in the degree of saturation.

The durability of concrete may be highly affected by curing conditions. If the concrete is not properly cured, then the surface layer is most affected due to the potential for evaporation of water from the concrete surface. This means that regulation of moisture is not just for improving the compressive strength of structural element, rather it also reduces surface permeability and increases hardness, so as to improve the longevity of a structure, especially one exposed to harsh environments. Many studies show that fly ash improves the durability of concrete with proper curing. However, it has also been shown that fly ash hydrates more slowly than Portland cement. Therefore, the effect of improper curing becomes more critical when considering composite cement systems.

Thus the aim of this research is to compare the impact of improper curing on strength development to concrete properties which may affect durability that is permeability, sorptivity and resistance to carbonation. Then, so as to understand how improper curing brings about these changes in performance, the degree of hydration of various systems has also been determined using a suite of analytical techniques.

Chapter 3 Materials and experimental methods

This chapter presents the materials and experimental methods that were used for the study. The tests methods selected for the study have been grouped into three as shown below:

- Engineering performance which was evaluated in terms of compressive strength and drying shrinkage, transport properties (sorptivity and permeability) and resistance to carbonation. These were tested in different forms of concrete as shown in flow chart in Figure 3.1.
- Effects of drying were investigated on concrete cubes.
- Hydration and microstructural studies on cement paste samples using: thermogravimetric analysis (TGA), X-ray diffraction (XRD), and back-scattered electron image analysis with scanning electron microscopy (SEM).

The Schematic for each set of samples was shown in the experimental flow chart in Figure 3.1 (see Table 3.7 for composition).

3.1 Materials

The materials used in the research projects were:

- Portland cement, (CEM I)
- Fly ash (class F fly ash from Drax power station),
- Two types of oven dried aggregate
- Water.

3.1.1 Portland cement (CEM I)

High strength CEM I 52.5 N from Hanson Heidelberg Cement Group was used in all the experiments. All cement was taken from the same batch, and stored in sealed containers throughout the duration of the project. This cement has a clinker content of at least 95% and has high one day strength development. This complies with BS EN 197 -1 – 2011 (38) . Chemical composition, as determined by XRF and provided by the manufacturers, is shown in Table 3.1, and the mineralogy, as determined by XRD Rietveld analysis (also performed by the manufacturer) is presented in Table 3.2.

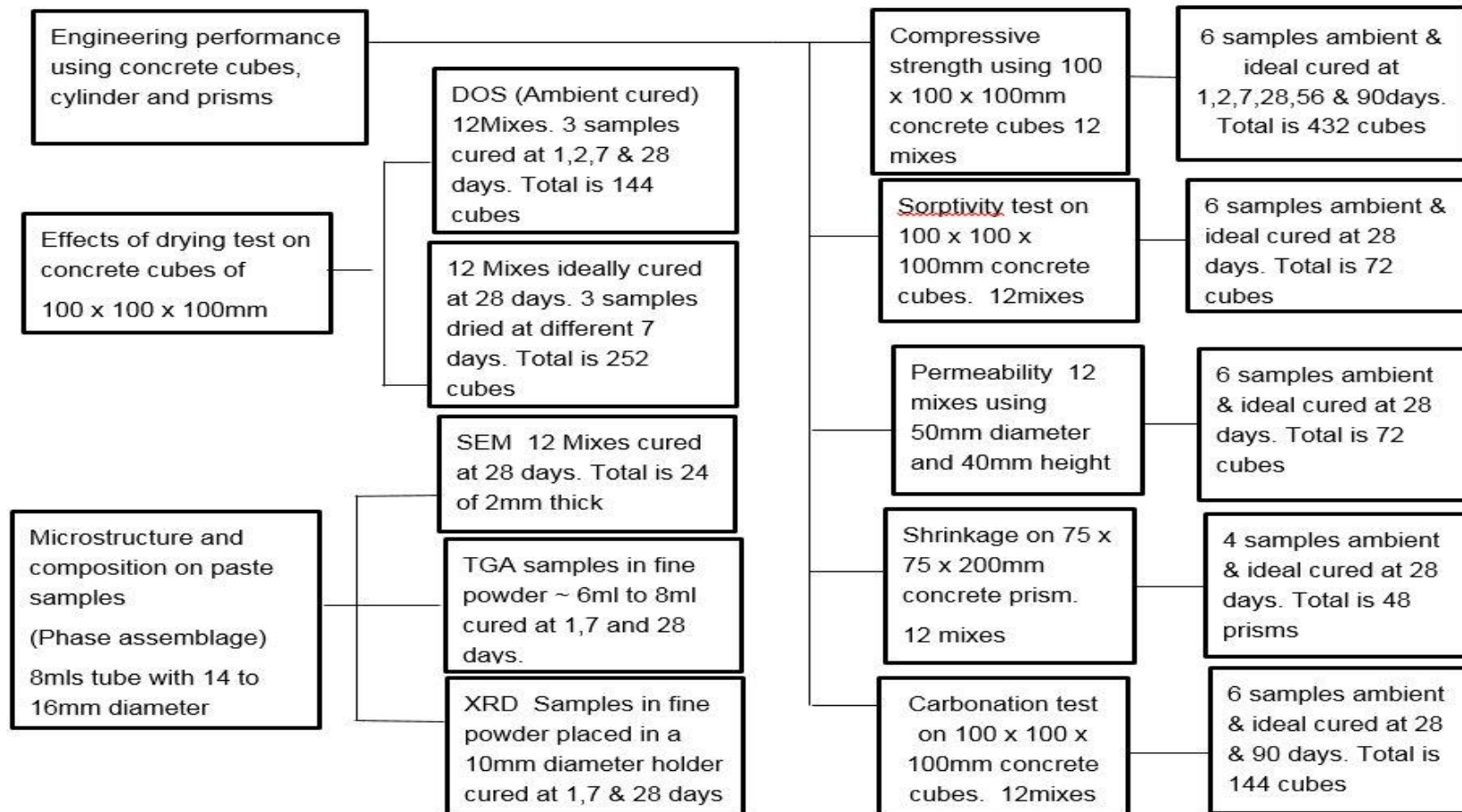


Figure 3-1 Schematic for each set of samples

Table 3-1Composition of CEM 1 52.5N
Manufactured at Ribblesdale

Compound	(% wt)
SiO ₂	19.85
Al ₂ O ₃	4.93
Fe ₂ O ₃	2.14
CaO	63.95
MgO	2.01
SO ₃	3.13
K ₂ O	0.58
Na ₂ O	0.37
Cl	0.07
Loss on Ignition	2.60
Not Detected	0.37
Total	100

Table 3-2Clinker compounds by Rietveld
analysis

Clinker compounds by Rietveld analysis	
C ₃ S	58.8
C ₂ S	17.8
C ₃ A	5.1
C ₄ AF	5.3

Curing Conditions

Two curing conditions were used in the study for most of the mixes. Ideal curing condition is curing at 20 ± 1⁰ C temperature and 99% relative humidity (RH) while ambient curing condition is curing at temperature of 20 ± 1⁰ C and 42 ± 5% RH. Third curing condition applied the minimum curing condition as specified in BS EN 13670:2009 based on the ratio of the mean compressive strengths at 2 and 28 days followed by continued curing under ambient condition (f_2 / f_{28} + ambient). If the value of f_2 / f_{28} is less than 0.5 then the third curing condition will be applied. The mean compressive strengths at 2 and 28 days (f_2 / f_{28}) of 20MPa fly ash concrete calculated was 0.46 thus this mix used the third curing conditions. Additional concrete cubes of 100 x 100 x 100mm were casted for further investigation and this is presented in the flow chart in Figure 3.2.

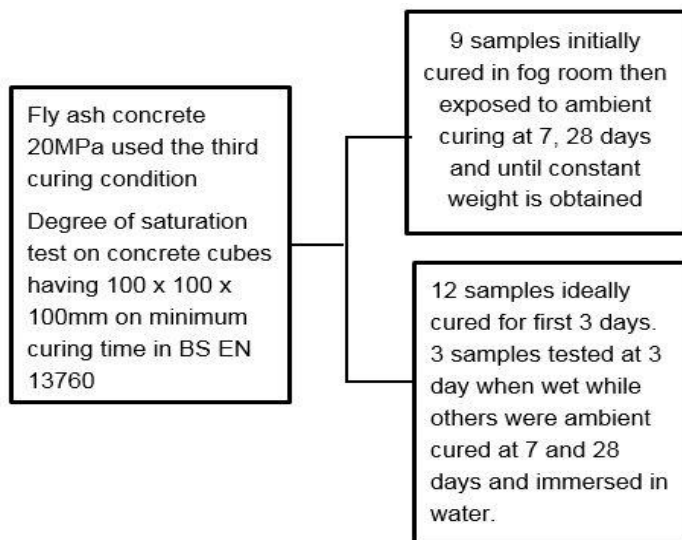


Figure 3-2 Addition concrete cubes casted for minimum curing condition

3.1.2 Fly ash

Drax power station supplied all the fly ash used in the research; this complies with BS EN 450-1:2012 (257). Enough fly ash was obtained at the start of the study for all the tests, to avoid changes in the composition of the material. The fly ash density calculated is 2.3194g/cm. The fly ash chemical composition, as obtained by XRF is shown in Table 3.3, while density and fineness of the binders obtained were presented in Table 3.4

Table 3-3 Chemical composition of Drax Fly Ash **Table 3-4 Density and Fineness of the Binders**

Compound	DRAX FLY ASH (% wt)
SiO ₂	50.73
Al ₂ O ₃	25.49
Fe ₂ O ₃	10.05
CaO	2.28
MgO	1.63
SO ₃	0.41
K ₂ O	3.46
Na ₂ O	0.90
P ₂ O ₅	0.20
TiO ₂	1.04
V ₂ O ₅	0.05
Cr ₂ O ₃	0.02
Mn ₃ O ₄	0.10
ZnO	0.03
SrO	0.04
Y ₂ O ₃	0.09
ZrO ₂	0.09
BaO	0.11

Binder	Cement	Fly ash
Density (gm/cm ³)	3.3047	2.31
Fineness (cm ² /gm)	3125	3013

3.1.3 Aggregates

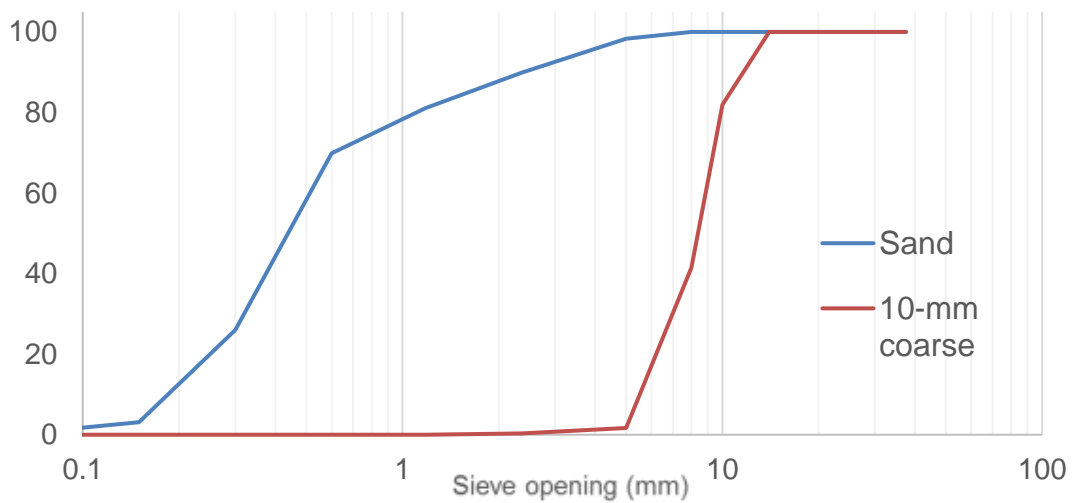
All of the aggregates used in this study met the requirements for particle size distribution as set out in BS EN 12620:2002 + A: 2008 (258). The coarse aggregate was uncrushed 10mm quartzite aggregate. The fine aggregate was sand whose particle diameters ranged from 150 µm to 5mm. The fine and coarse aggregates were oven dried in-situ before use. The particle size distribution of fine aggregate is shown in Table 3.5 while Table 3.6 shows the particle size distribution of 10mm coarse aggregate. The aggregate grading curve is shown in Figure 3.3.

Table 3-5 Particle size distribution of fine aggregate

Sieve size (mm)	Percentage cumulative passing (%)	BS 882: 1992 Requirement
10	100	100
5	98.3	89-100
2.3	89.9	60-100
1.18	81.1	30-100
600 μm	69.9	15-100
300 μm	26	5-70
150 μm	3.1	0-15
75 μm	0.8	-

Table 3-6 Particle size distribution of 10mm coarse aggregate

Sieve size (mm)	Percentage cumulative passing (%)	BS 882: 1992 Requirement
14	100	100
10	92.175	85-100
5	3.18	0-25
2.36	0.188	0-5

**Figure 3-3 Aggregate grading curves**

3.1.4 Water

Potable mains water, as permitted by BS EN 196-1: 2005(259) was used for all casting.

3.2 Mix design, curing and exposure conditions

Three curing conditions were used throughout this study, namely:

1. According to EN 196-1:2005 (259), 99% relative humidity at a temperature of $(20, 0 \pm 1, 0)$ °C
2. Demoulding after 24 hours then leaving the samples under ambient conditions, typically 20.0 ± 1.0 °C $42 \pm 5\%$ relative humidity.
3. Moist curing first for a time as defined in Euro code 2 BS EN 13670:2009 (260), followed by curing under ambient conditions.

Two concrete mixes were investigated, a stiff mix having 10 to 30mm slump and a wet mix with a slump of 60 to 180mm. The reason for using two mixes was to investigate how water content impacts upon curing under non-ideal conditions. Most research uses high slumps and according to Teychenne *et al* (261), low slump concrete is more suitable than one with high slump in road construction. However, low workability concretes have lower ECO_2 (8) and so if low carbon construction is to be achieved then these systems' resilience to improper curing needs to be investigated.

Two binders were employed; CEM I and CEM I with 30% replacement by fly ash. Three target strengths, 20, 50 and 80MPa were investigated. Samples were tested in triplicate for unconfined compressive strength (UCS) at 1, 2, 7, 28, 56 and 90 days. The binder type, slumps, target strength, curing conditions and the curing duration for the experiment are shown in Table 3.7

The mixes were worked out using a spread sheet created by Professor Phil Purnell of Leeds University based upon the tables, graphs and figures from the BRE mix design method (261). Moisture content and absorption tests were carried out on the aggregates to determine potential water uptake by the oven dried materials, the adjusted water calculated serve as guide to know the actual water to add in order not to exceed the required slumps for the mix. The result of moisture content and absorption tests were presented in Table 3.8.

Trial mixes were made up and a slump test was carried out on 20 and 60MPa targeted strengths mixes to check that the concrete had the desired workability. The targeted strength of 60MPa was chosen to represent the high strength concretes. Materials for 21 concrete cubes with dimensions of 100 x 100 x 100mm were measured, to cast 18 cubes of concretes. This measurement of 21 cubes provided enough material for 3 cubes to be tested after 1,2,7,28,56 and 90 days curing. Three extra cubes worth of material were added due to the inevitable loss of materials on the mixing equipment and through any spillages.

The water to binder ratio of the cements was found using the Equation 3.1. The fly ash content was multiplied by a reduction factor of 0.3 since fly ash is not an efficient binder as cement.

$$\frac{\text{water}}{\text{binder}} \text{ ratio} = \frac{\text{water}}{\text{cement content} + 0.3 \text{ fly ash content}} \text{ Equation 3.1}$$

Table 3-7 Concrete mix designs used in this study

Mix NO	Binder Type	Target Strength (MPa)	Slump (mm)	W/b ratio	Water (kg/m ³)	Cement (kg/m ³)	Fly ash Content (kg/m ³)	Fine Aggregate (kg/m ³)	Coarse Aggregate (kg/m ³)
1	CEM1	20	10 to 30	0.66	180	275	0	849	1033
2		50		0.36	180	499	0	650	1007
3		80		0.19	180	930	0	440	786
4	CEM1	20	60 to 180	0.66	225	343	0	911	805
5		50		0.36	225	624	0	675	760
6		80		0.19	225	1162	0	391	506
7	30% Fly ash	20	10 to 30	0.66	165	223	96	844	1026
8		50		0.36	165	405	174	631	978
9		80		0.19	165	755	324	398	712
10	30% Fly ash	20	60 to 180	0.66	205	277	119	906	801
11		50		0.36	205	504	216	651	732
12		80		0.19	205	938	402	332	429

3.3 Test Method

3.3.1 Slump Test

The slump test is used to determine the workability of fresh concrete. It is an indirect measurement of concrete consistency or stiffness. The standard used in the slump test according to BS EN 12350-2 (262) is that when fresh concrete is compacted into a mould in the shape of a frustum of a cone and when the cone is withdrawn upwards, the distance the concrete has slumped provides a measure of the consistency of the concrete. The slump test was carried out on all the mixes before casting to be sure that the mixes have the required slumps of 10 to 30 mm for the stiff mix and 60 to 180 mm for the wet mix.

3.3.2 Absorption and Surface Moisture

The absorption and surface moisture of aggregates were determined according to BS EN 1097-6 (263) so that the total water content of the concrete could be controlled and correct batch weights determined. Adjustments to water content depend on both the absorption and moisture content of the aggregate thus water content adjustments for moisture content of aggregates were carried out to calculate the water adjustment.

According to report of Suchorski *et al* (264) Surface moisture content can be obtained by subtracting absorption from the moisture content that is

Surface moisture content = Moisture content – Absorption

They reported also that if an aggregate is in air-dry state that is when the aggregate surface is dry but the pores are partially filled with water, the total moisture content is less than the absorption and the surface moisture content will have a negative value. This process will lead to the aggregate absorbing water when mixed in concrete. Thus for aggregates having extremely high absorption and are batched in an unusually dry state, the amount of water absorbed should be added to keep the intended water cement ratio and consistency.

All the calculations involved to generate the data shown in Table 3.8 were presented in Appendix A with the table showing the water content adjustments for moisture content of aggregates used to prepare the concrete mixes.

Table 3-8 Aggregates surface moisture content, Total moisture content and absorption

	Fine aggregate	Coarse aggregate
Surface moisture content	-2.63%	-1.02%
Total moisture content	0.42%	0.25%
Absorption	3.05%	1.27%

The new water binder ratio calculated due to the adjusted water obtained from the aggregates is presented in Table 3.9

Table 3-9 Adjusted water used to cast the concrete and w/b ratio.

Binder type	Target strength(MPa)	Slump (mm)	Adjusted water (kg/m ³)	Cement (kg/m ³)	Fly ash (kg/m ³)	Fine Agg (kg/m ³)	Coarse Agg (kg/m ³)	w/b
CEM1	20	10 to 30	212.87	275	0	849	1033	0.77
	50		207.37	499	0	650	1007	0.42
	80		199.59	930	0	440	786	0.21
CEM1	20	60 to 180	257.17	343	0	911	805	0.75
	50		250.50	624	0	675	760	0.40
	80		240.44	1162	0	391	506	0.21
30% fly ash	20	10 to 30	197.66	223	96	844	1026	0.78
	50		191.57	405	174	631	978	0.42
	80		182.73	755	324	398	712	0.21
30% fly ash	20	60 to 180	237.00	277	119	906	801	0.76
	50		229.59	504	216	651	732	0.40
	80		218.11	983	402	332	429	0.20

3.3.3 Mixing, Casting and Curing

Mixing started after weighing out all of the mix ingredients in the correct proportions and making sure that all the metal instruments and tools were moist (mixing drum, trowels, mixing trays, and rods). This ensured that the moisture content was not drastically reduced by the properties of the metallic instruments. The coarse aggregate was placed into the mixing drum followed by fine aggregate. The mixer was turned on and allowed to mix for one minute. Portland cement was added after stopping the mixer, this also was allowed to mix with the aggregates in the mixer before adding water to the mix. Half of the water was first added to the mix and the remaining water was gradually added. Mixing continued for another few minutes. The mixer was stopped and some of the contents were poured into slump cone to measure the slump. After the slump test was completed, the mixer was turned on again to mix the contents together before pouring into 100 mm x 100 mm x 100 mm steel moulds. The moulds were oiled and placed on a levelled surface vibrating table to be filled with the concrete mixture and compacted. The filling of the moulds was done in two layers. The cast concrete cubes were put on a flat table and left for 24 hours to cure in a controlled environment. After 24 hours, the specimens were stripped from their respective moulds and placed in the fog room to cure at a constant temperature of 20 °C and 99%RH or put in the casting shop at a constant temperature of 20°C and 43 %RH.

3.4 Unconfined Compressive Strength (UCS)

Compressive strength is the competence of a material or structure to resist compressive loads. It is the most frequent measure used by engineers in designing buildings and other structures.

The unconfined compressive strength test was measured using a Retrofit Tonipact Concrete and Transverse Beam Machine according to BS EN 12390-3 (139). The concrete cubes were placed into the machine in such a way that they sat on and were loaded upon sides which had been 'machined' finished as these were the flattest and had the least imperfections. The compression load was applied to the cubes until the concrete cubes failed. An average compressive strength for the three samples tested for each mix cured under each condition. The ideally-cured samples were tested immediately after removal from the water, the cubes just being made surface dry with a towel before testing.

3.5 Sorptivity

Sorptivity is a property related with capillary effects, which is described as the slope of the volume of water absorbed per unit area of section surface and the square root of the absorption time (136). Ho et al (137, 138) also reported that sorptivity is a property associating to the pore structure of concrete near the surface which can determine quality of concrete and as a property illustrating the amount of water infiltration due to capillary force.

Dias (135) while working on reduction of concrete sorptivity with age through carbonation wrote that sorptivity, is an indicator of moisture transport into unsaturated specimens, which has been identified as crucial indicator of concrete durability, due to following reasons:

(i) The test method used for its investigation follows the way water and other damaging agents will pass through most concretes and

(ii) It is an excellent measure of the quality of the near surface concrete, which governs durability associated to reinforcement corrosion (135).

3.5.1 Sorptivity test

Sorptivity method applied in this work was similar to methods used by Tasdemir (93), and Güneysi (134). Sorptivity tests were carried out on 100 x 100 x 100 mm concrete cubes. The schematic set up was shown in Figure 3.4 and the test was conducted on three triplicate samples. Six concrete cubes were cast for each mix; half of the samples were cured in the fog room designated as ideal condition at 20⁰ C and 99% RH while the other half were cured in the laboratory under ambient condition at 20⁰ C and 42% RH for a period of 28 days. Subsequent to curing, the samples were dried in an oven at 40°C to constant mass which is up to 100 days. After drying, the samples were allowed to cool to ambient temperature. With the trowelled area facing upward, the lower areas on the sides of the specimens were coated with petroleum jelly so as to ensure unidirectional flow. The coated samples were then weighed before being placed in a trough of water, with the water level kept at about 5mm from the base of the specimens. The specimens were removed from the trough, surface water removed with a dampened tissue, and weighed at different time intervals up to one hour to evaluate mass gain. At each of these times, the mass of water absorbed by each specimen was calculated by subtracting the initial mass from the recorded mass, and from this the sorptivity coefficient (k) was calculated using the following expression:

$$K = \frac{Q}{A\sqrt{t}} \text{ Equation 3.1}$$

Where:

Q is the amount of water absorbed in m³, which was calculated by dividing the mass of the water absorbed in kg, by the density of water (1000 kg/m³)

t is the time in seconds,

A cross-sectional area of the specimen that was in contact with the water in m²

K sorptivity coefficient in m³/m²s^{1/2}

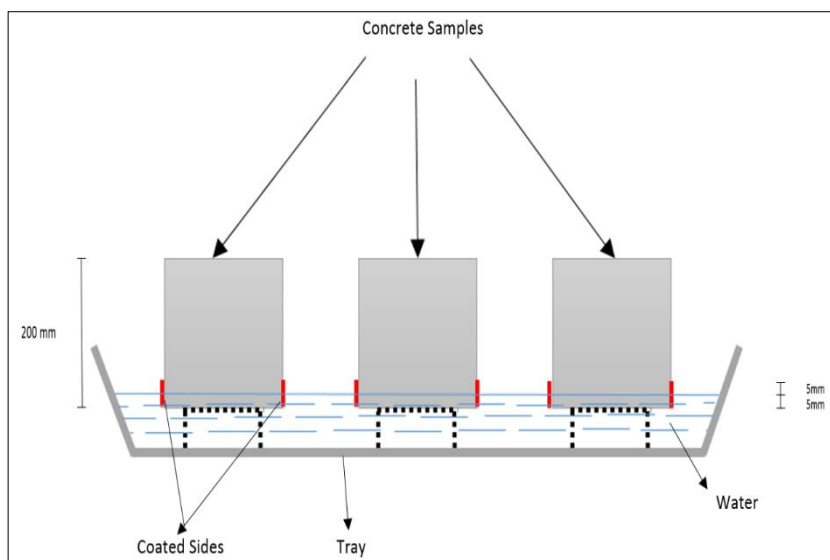


Figure 3-4 Schematic setup of sorptivity test

In determining k , values of Q/A were plotted against \sqrt{t} , and k was taken as the slope of the straight line as shown below in Figure 3.5

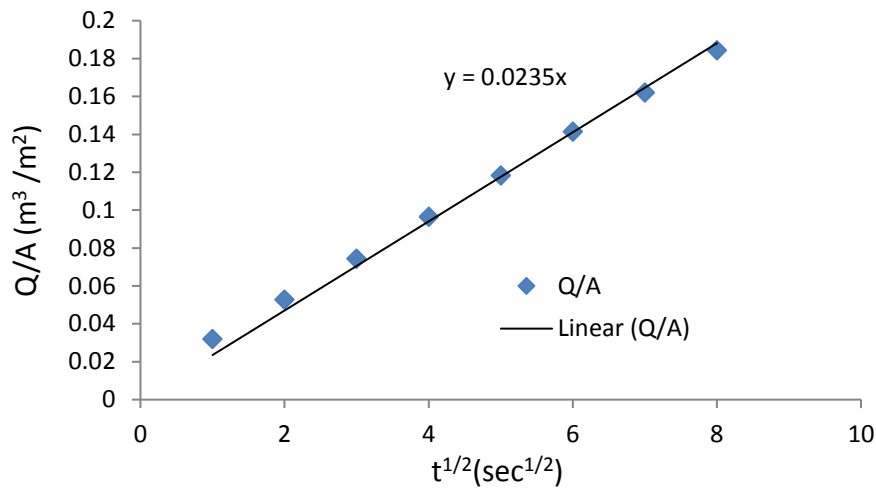


Figure 3-5 Linear fit for the determination of sorptivity coefficient for 20MPa CEM1 stiff mix ambient cured

3.6 Permeability

Permeability is one of the main essential criteria controlling the durability of concrete. Permeability of concrete regulates the ease with which liquids, gases and diffused harmful materials like chloride or sulphate ions or carbon dioxide, can permeate concrete. It is also associated to the deterioration generated by freezing and thawing since it restrains the ease with which concrete can be filled with water. All the detrimental effects on durability engage the transport of fluids through the concrete except mechanical deterioration (17). Bhargava and Banthia (126) described permeability as migration of fluid along a porous medium under an applied pressure and reported that permeability is the most influential characteristic of concrete controlling its long-term durability. Cabrera et al (32) stated that estimation of any curing method based on the strength of the concrete does not sufficiently predict the performance of the concrete in a structure, as the durability of the concrete is more controlled by its porosity and permeability than its strength. They further explained that measuring permeability of a concrete grants a sufficient explanation of the concrete durability. Sanjuan and Munoz- Martialay (127) also said that permeability and compressive strength are separate properties of concrete therefore air permeability value can be used as a sufficient tool to measure the potential durability of concrete structures and not the mechanical strength.

Permeability is determined in the laboratory by measuring the flow rate of a fluid of known viscosity through a sample of known dimensions. This is followed by determining the intrinsic permeability of the sample using D'arcy's law:

$$K = \frac{u\eta L}{a\Delta p} \text{ Equation 3.2}$$

K is the intrinsic permeability (m²)

u is the flow rate in m^3/s

a is the cross sectional area in m^2

Δp is the change in fluid pressure in Pa

η is fluid viscosity in PaS

L is the length of specimen in m

3.6.1 Preconditioning of Samples before Measuring Permeability.

The air permeability of concrete is greatly affected by its moisture content (17, 225). The presence of liquid in sample pores prevents gas flowing through the sample. Drying of samples is very important before measuring gas permeability. Researchers have used several methods to dry samples before measuring gas permeability, but methods used should be carefully selected as pore structures can be damaged in the process.

Air permeability of concrete is on the increase due to preconditioning temperature when the degree of saturation of concrete is low by Sanjuan and Munoz- Martialay (127). They found out that increase in the preconditioning temperature encourages increase in air permeability coefficient due to clear impact of the degree of saturation on this parameter when they worked on oven-drying as a preconditioning method for air permeability test on concrete. The preconditioning process may change the microstructure of the concrete, thereby creating micro cracks and damaging the C-S-H gel . Some methods of drying have been recommended to avoid extreme drying. The preconditioning process generates gradients of moisture in mass concrete and may develop microstructural alteration.

Gallie (120) reported that oven-drying greatly damages the material's microstructure in the capillary porosity area and proposed freeze-drying as good enough process to investigate cement based materials pore structure with MIP. Overestimation of total porosity during oven-drying at $105^{\circ}C$ was also reported as hydrates like ettringite and C-S-H lost an important amount of non-evaporable water. However, water porosity obtained by oven-drying at $60^{\circ}C$ and vacuum-drying were in close agreement and more realistic.

Dhir (265) noted also that the moisture condition of concrete can highly change the results obtained, while Parrott (266) concluded that air permeability and water absorption rate were susceptible to the moisture content of the concrete.

3.6.2 Permeability Experiment

Permeability testing was carried out at room temperature using the Leeds cell constructed by Cabrera and Lynsdale (267). Input pressures were varied between 0.5 and 2.5 bar with atmospheric outlet pressure. A bubble flow rate meter was used to measure the flow rates. The samples for the permeability test were cast in a PVC cylinder. The length of the cylinder was 40mm and diameter was 50mm. The samples were cured for 28 days under either standard or ambient conditions, after which the samples were put in the oven to dry at $40^{\circ}C \pm 1^{\circ}C$ until constant weight; this temperature was selected as it was deemed high enough to allow for pore water to be driven off in a reasonable time and not so high as to result in decomposition of the C-S-H or the ettringite. Also Neville (225) reported that conditioning a specimen in air at a constant relative humidity as long as 28 days does not necessarily result in a uniform moisture condition within the concrete. Thus the samples were in the oven to dry for 60 days.

In this research nitrogen was used for permeability testing, as opposed to oxygen (as was the case in the work of Cabrera and Lynsdale (267)). The equation for calculating permeability proposed by Grube and Lawrence (268) was altered slightly to take account of the change in gas as shown in equation below. The difference between this testing and that of Cabrera and Lynsdale (267) is the temperature at which the samples were dried, as explained above.

Grube and Lawrence (268) reported that when a compressible fluid, such as nitrogen is used, a modified D'Arcy's equation should be applied, thus equation below was used as suggested by Grube and Lawrence:

$$\mathbf{k} = \frac{2P_2 \times uL1.78 \times 10^{-6}}{A(P_1^2 - P_2^2)} \text{ Equation 3.3}$$

Where:

P_1 is the absolute applied pressure (bar)

P_2 is pressure at which the flow rate is measured in bar and is 1.01325 bar.

u is measured in cm^3/s

L and a measured in m

1.78×10^{-6} = dynamic viscosity of nitrogen at 20°C (g/cm/s).

The dried concrete samples were sanded at their ends to expose the pore structure and remove any potential coatings from oils used in the moulds.

The experimental set-up is shown in Figure 3.6. Concrete samples (S) weight and the height were measured before being put into the rubber cylinder (A) which was placed into the plastic ring cylinder (B). This was placed into the Leeds cell and the metal O ring (C) was put in place before the cell cap (D) was positioned. A force was applied vertically downward in order to form a seal to ensure that all nitrogen passing through the system would go directly through the sample.

Nitrogen gas was forced through the sample at a defined pressure after which the flow was allowed to normalise to a steady flow (generally 10-15 minutes). The time for a known volume of nitrogen to pass through the sample was recorded by using a bubble flow meter. This was repeated three times to provide an average and standard deviation and to ensure that the flow had fully normalised.

This procedure was repeated for each sample at a different applied pressures; 0.5, 1, 1.5, 2 and 2.5 bar (above atmospheric). Ten millimetres (10mm) flowmeter tube was used for more permeable samples, and five millimetres (5mm) for less permeable samples. All mixes were tested in triplicate at 28 days following curing under standard and ambient conditions.

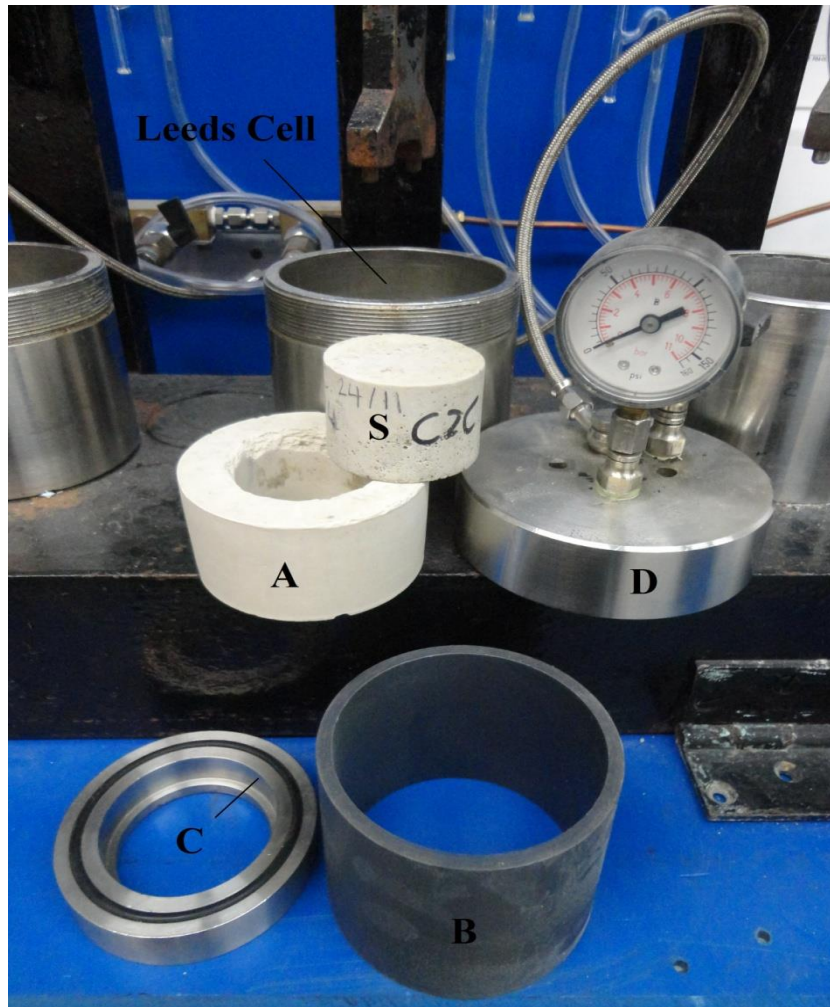


Figure 3-6 Components of the Leeds cell (267)

3.7 Determination of Degree of Saturation

The degree of saturation was measured by weighing concrete samples which had been cured in the fog room at 20°C and 99% RH for 28 days (defined as 100% DOS). Excess water was removed from the sample surface and the samples weighed. All the specimens were put in the oven to dry at 40°C to constant weight. The temperature 40°C was chosen to avoid damage to the concrete cubes from microcracking. The specimens were dried for three months in order to remove any liquid water in the pores of the specimens and to stop the curing process of all the specimens at the same time. All the samples were weighed until a constant mass was obtained which predicts that the DOS of the samples were close to zero. The UCS was also measured at this point.

DOS for the samples cured at 20°C and 42%RH was measured by weighing the samples which had been cured also at 28 days. The compressive strength at 28 days was measured and six samples were immersed in water for three hours. Three of the samples were removed from water after three hours, the weight was recorded to get the mass and UCS was determined after. The remaining three samples were put in oven for several days until a constant mass is obtained followed by measuring the UCS.

3.8 Carbonation

Carbonation is the reaction between concrete and atmospheric CO₂. The process starts at the exposed surface and proceeds in a diffusion controlled manner. The pore structure of the concrete plays an important role in defining the carbonation behaviour of concrete.

Therefore, improper curing may be assumed to have a deleterious effect on carbonation resistance. Also Carbonation is a measure of concrete durability.

3.8.1 Carbonation experiment

Carbonation of concrete is a long-term process in natural environment as a result of the low concentration of carbon dioxide in the environment which is only about 0.03–0.04% by volume (269). Therefore, an accelerated carbonation testing system was used to carbonate the concrete in the short time available.

Carbonation experiments were performed on 100x100x100mm concrete cubes cured under ideal or ambient conditions for 28 and 90 days. After curing, samples were allowed to dry under an ambient environment for two weeks in order to stabilize the internal relative humidity of the concretes. This helped to reduce the variation in the internal relative humidity between the concrete samples before subjecting them to accelerated carbonation tests; and so will minimize the effect on the carbonation depth results by making the pores not to be saturated, so carbonation can proceed more readily. Thereafter concrete samples were taken to a carbonation chamber where dried CO₂ was introduced initially to accelerate the initial intake of the CO₂. The experimental set up is shown in Figure 3.7.

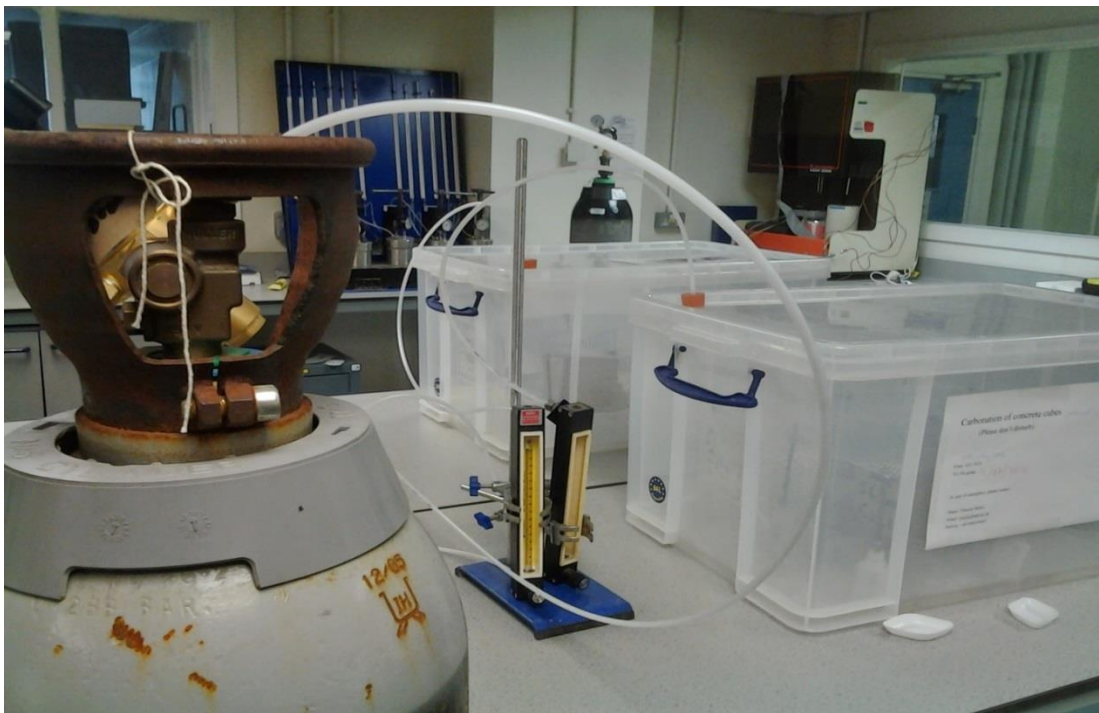


Figure 3-7 Carbonation Experiment Set Up.

Hundred per cent of (100%) CO₂ was introduced to the carbonation box at the flow rate of 0.8m³/s. Saturated sodium bromide solution was used to control the relative humidity (RH) of the chamber at 65%. This RH value was chosen since it has been established that carbonation

of concrete is fastest at this humidity range as reported by Ho (270) and conforms with the recommendations by RILEM ("Measurement" 1987) (271).

The concrete samples were in the carbonation box for two weeks, after which, the samples were removed from the box for cutting. The freshly cut samples were sprayed with a 1% phenolphthalein solution of 70% ethyl alcohol (271). Carbonation depth was measured from the edge of the specimen to the beginning of the purple zone and these depths were recorded as the average of the three samples in mm. The depths of the trowel side of the cubes were not considered as part of the carbonation depth.

3.9 Drying Shrinkage Test

Drying shrinkage experiments were carried out by using samples cast in 75 x75x 200mm steel moulds. The specimens were removed from their mould 24 hours after casting and demec points were fixed on the concrete samples at the measured points (50mm horizontal and 37.5mm vertical from both ends). The initial length was recorded, before putting the samples in either the fog room or in the control room respectively.

The drying shrinkage strain was measured every day for the first 28 days, excluding weekends and bank holidays when there was no access to the laboratory. The measurement continued in the control room after curing for 28 days for samples cured under standard conditions. The test was carried out according to BS ISO 1920-8:2009 (272). Drying shrinkage measurements continued up to six months after casting.

3.10 Measuring the degree of hydration

Degree of hydration is the percentage of cement which has already reacted in any mix. Ideally the ultimate degree of hydration is 100%, but practically this final condition will never occur (273). Measuring the heat of hydration, the non-evaporable water content and calculating the amount of calcium hydroxide reacted in the mix are some of the experimental techniques used to measure the degree of hydration of Portland cement. The techniques mentioned above used comparison of the measured values with predicted or measured values of fully hydrated paste (274). In this work three analytical techniques will be used to measure the degree of hydration which are XRD, TG and SEM.

3.10.1 Sample Preparation for XRD, TG and SEM

The XRD, TGA and SEM experiments were performed on paste samples. Paste samples were used for the three tests, as the presence of quartz in concrete samples can affect the accuracy of the tests or swamp the data of interest. Samples were prepared by using the same water / binder ratio as in concrete mixes presented in Table 3.9. The fresh prepared pastes were poured into 8 ml plastic tubes having a diameter of 14 – 16 mm and a thickness of 2 mm with tight lids shown in Figure 3.8. The prepared pastes were sealed in order to prevent moisture loss and placed in tube rotator at ten rph overnight to minimize the effects of settlement and bleeding. The samples were removed from the rotator after 24 hours, whereupon the ideally cured samples were sealed as shown in Figure 3.10 and cured in a water bath at 23°C, while the plastic tubes for the ambient-cured samples were left open at both ends, and left to cure in the casting shop. The ambient cured samples were shown in Figure 3.9. The samples were cured for 1, 7 and 28 days.



Figure 3-8 8ml tube used for the paste samples



Figure 3-9 Ambient cured samples



Figure 3-10 Samples prepared to be cured in the bath

The samples were removed from the plastic tubes at the desired age, after which an isomet slow speed saw was used to slice the samples. A thin layer of one millimetre was removed first, followed by cutting of three two millimetre thick samples for each of the experiments. The samples that were ready to be cut and showing the cut ends were shown in Figure 3.11 and the samples cut for hydration stoppage were shown in Figure 3.12.

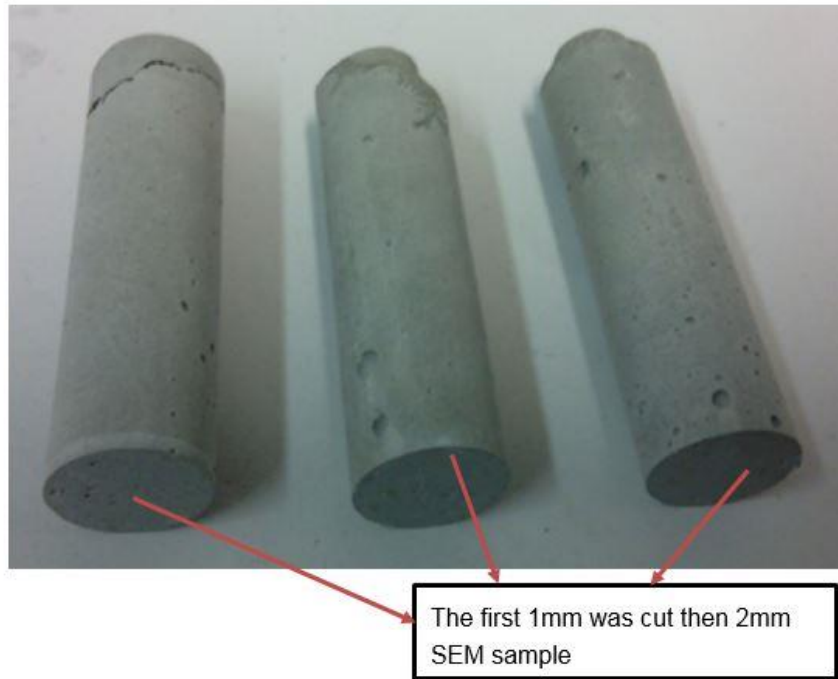


Figure 3-11 Paste samples after curing ready for cutting



Figure 3-12 SEM sample after cutting

3.10.2 X-ray Diffraction (XRD)

XRD is a technique used to determine crystalline phases in samples. The technique involves the use of direct X-rays at the samples. Ramachandran and Beaudoin (275) defined XRD as the elastic scattering of x-ray photons by atoms in a periodic lattice. An intensity peak of diffracted x-rays develops when the distance travelled by rays diffracting from consecutive atomic planes differs by an integral number of wavelengths of the x-ray, causing constructive interference. This happens when atoms are periodically distributed throughout the sample i.e. the material is crystalline. In hydrated cements it can be used to identify crystalline phases such as calcium hydroxide (Portlandite) and ettringite. Various application of XRD analysis in concretes include measurement of glass content in pozzolanic materials, degree of hydration and to predict the strength of slag cements.

Each crystalline material has a unique XRD pattern where the peak positions are defined by the spacing of crystallographic planes according to Bragg's law:

$$n\lambda = 2d\sin\theta \text{ Equation 3.4}$$

Where:

n = an integer corresponding to the order of the diffraction peak

λ = wavelength of the radiation used

d = characteristic spacing between crystal planes

θ = the angle of the diffraction peak

Bye (276) reported that identifying phases present in clinker by XRD has been a supplement to microscopy, particularly when identifying polymorphs which may be difficult to distinguish if several are present. XRD can be qualitative or quantitative. In this study the data had been considered qualitatively, i.e. identifying the phases which are present in the pastes.

3.10.3 XRD Measurement in this study

Paste samples were hydration stopped by immersing in isopropanol prior to analysis. Samples were ground to a fine powder with pestle and mortar before being placed in a 10mm diameter holder using the back loading method. In order to minimise the effect of preferred orientation, samples were prepared carefully and minimal pressure was applied when back loading the samples onto the sample holders (277, 278). A Bruker D2 Phaser with a Cu X-ray source (wavelength 0.154184nm) working at 300W (30KV at 10mA) was used. The scan step size was 0.02θ , the collection time 1s, and patterns were collected over the range 7° to $70^\circ 2\theta$ with effective total time of 3403 s. The divergence slit, air scatter, filter and Soller slits were set to 1, 1, 0.5 and 2.5 respectively.

3.10.4 Thermogravimetric analysis (TGA)

Thermogravimetric analysis techniques are widely used to measure the rate of hydration of cement /blended cement. These techniques are easy to use and yield important results within a short time. In TGA changes in weight of samples are followed as a function of temperature with decomposition temperatures characteristic of specific phases. Unreacted gypsum can be identified by endothermic peaks in the temperature range 140–170°C, the C-S-H gel at temperatures below 150°C, ettringite at temperatures 120–130°C, calcium hydroxide by an endotherm in the range 450–550°C, and calcium carbonate at 750–850°C (275). Furthermore, mass loss over the range 50–550°C can be used as a measure of the bound water content, and thus as a proxy for the degree of hydration.

3.10.5 TGA measurement in this research

TGA technique was used in this research to measure the degree of hydration of samples by using the tangent method to evaluate the Portlandite (CH) content and the equivalent (CH)_{eq} from the calcium carbonate (CaCO₃) content. The sum of the CH and (CH)_{eq} contents were used to assess the degree of hydration of each sample.

A Stanton Redcroft Thermal Gravimetric Analyser TG 760 was used under a nitrogen atmosphere. Samples of $\approx 6-8\text{mg}$ were loaded in a clean crucible and heated from 20° to 1000° at a constant rate of $20^\circ\text{C}/\text{min}$. The mass loss due to portlandite composition, and hence the portlandite content, was determined at the midpoint between the inception and end of the mass loss event using the tangent method, as sketched in Figure 3.13. The same method was used over the temperature range $600-800^\circ\text{C}$ to determine the calcium carbonate content, as shown in red in Figure 3.13.

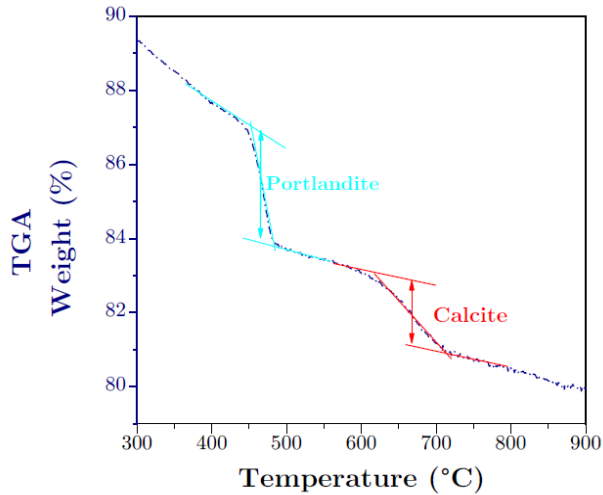


Figure 3-13 Measuring the Portlandite and Calcium Carbonate using the tangent method, taken from (279)

$$\% \text{Ca(OH)}_2 = \left(ML_{CH} \times \frac{M_{CH}}{M_{H_2O}} \right) \div \text{Residue} \quad \text{Equation 3.5}$$

$$\text{CaCO}_3 = \left(ML_{\text{CaCO}_3} \times \frac{M_{\text{CaCO}_3}}{M_{\text{CO}_2}} \right) \div \text{Residue} \quad \text{Equation 3.6}$$

$$[\text{Ca(OH)}_2]_{\text{eq}} = \left(ML_{\text{CaCO}_3} \times \frac{M_{\text{Ca(OH)}_2}}{M_{\text{CO}_2}} \right) \quad \text{Equation 3.7}$$

Where:

ML_{CH} mass loss due to dehydroxylation of CH

ML_{CaCO_3} mass loss due to decarbonation of CaCO_3

M_{CH} molar mass of CH, taken as 74g/mol

$M_{\text{H}_2\text{O}}$ molar mass of water, taken as 18g/mol

M_{CaCO_3} molar mass of CaCO_3 . $M_{\text{CaCO}_3} = 100\text{g/mol}$

M_{CO_2} molar mass of $\text{CO}_2 = 44\text{g/mol}$

$$\text{Total CH} = \% \text{Ca(OH)}_2 + [\text{Ca(OH)}_2]_{\text{eq}} \quad \text{Equation 3.8}$$

3.10.6 Bound water content

The bound water content (W_n) was taken as the difference between the mass loss at 50 and 550°C, at which point it was assumed that all the phases containing water had fully decomposed. W_n , normalised to the total mass loss at 550°C was calculated using equation 3.9

$$W_n = \left(\frac{W_{50} - W_{550}}{W_{550}} \right) \times 100 \quad \text{Equation 3.9}$$

Where:

W_{550} = mass loss at 550°C

W_{50} = mass loss at 50°C

3.10.7 Scanning electron microscopy (SEM)

SEM is a technique used to study microstructure of materials and has been broadly used in exploring microstructure of cementitious materials. This technique has also been applied to study the degree of hydration of cement or blended cement at different ages by different researchers (18, 60, 108, 274, 280, 281) both quantitatively and qualitatively. SEM image is produced when a beam of electrons is focussed over the sample surface and scattered electrons are collected by detectors and this is used to construct an image. The common characteristics of SEM are enhanced resolution, high magnification and large depth of field which results in a three dimensional appearance of texture surfaces (275).

The production of secondary electrons, backscattered electrons (BSE) or X-rays will normally depend on the way the electrons interact with the sample (282). Secondary electrons are low-energy electrons and they give information relating to the topography of the sample. BSE are high-energy electrons (>50 eV) (282) from the primary incident beam that are ejected back out from the sample. These BSE are used to produce a different kind of image. Such an image uses contrast to give information about the average atomic number of the sample. As the atomic number of a feature increases, more electrons are reflected and appear brighter. Features having low atomic numbers appear dark grey or black. As a result, different phases can be identified according to greyscale and this can be used for the characterisation and quantification of the various phases present in the sample. Repeatable contrast that makes BSE images a useful techniques are the flat polished surfaces and paired detectors on either sides of the beam which adequately remove topographic contrast (60). This study involved the use of BSE imaging.

3.10.8 SEM measurement in this project.

Preparation of sample is very important phase of the SEM technique. When using BSE to determine the degree of hydration of hydrated cement paste samples, flat polished samples is better in other to reduce edge effects (283). The thick discs (2 mm) described in section 3.10.1 were used for SEM analysis. The first two layer of 2 mm disc, after a thin 1mm layer had been removed, was examined for each sample. The disc was hydration stopped by immersion in iso propanol for 24 hours before drying in vacuum desiccator. The samples were resin impregnated using an epoxy based resin and a hardener. The resin impregnated samples were further polished by using silicon carbide paper and then diamond paste to obtain flat surfaces.

Figure 3.14 shows the resin impregnated sample that had been coated with carbon ready for the scanning electron microscope for image capturing.



Figure 3-14 Resin impregnated carbon coated samples for scanning electron microscope

A Jeol 5900 LV scanning electron microscope with accelerating voltage of 15KeV was used for imaging. Electron images were collected at a magnification of x400 and a working distance of 10 -10.5 mm, and were analysed to determine the degree of hydration.

3.10.9 Image analysis

Image analysis was carried out on BSE–SEM images to determine the degree of hydration. The analysis used the assumption that the volume fraction in a three dimensional surface is equal to the area fraction of a two dimensional surface. The assumption is based on the principle of stereology, which uses two dimensional sections to interpret three dimensional structures (18, 284).

A consistent analysis technique was applied to all the images by using a grey level histogram as shown in Figure 3.15. The histogram was obtained for each image. Four components of the hydrated paste microstructure: capillary porosity, calcium hydroxide (CH), calcium silicate hydrate gel along with other hydration products, and unhydrated cement will be displayed by the histogram. The histogram also indicates the number of pixels in the image having each possible brightness value (between 0 and 255). Pores in the microstructure appear as dark spots on the electron images and can be easily distinguished from the hydrated phases (C-S-H and CH), C-S-H are dark grey, but the grey level varies depending on the C/S ratio, temperature, water content and micro porosity (60, 281, 285). Other phases (Ht, AF_t, AF_m) cannot be easily established based on grey level alone as a result of mingling with the C-S-H phase (60, 275). The CH phase is brighter than the C-S-H phase and appears as light grey while unhydrated cement is the brightest.

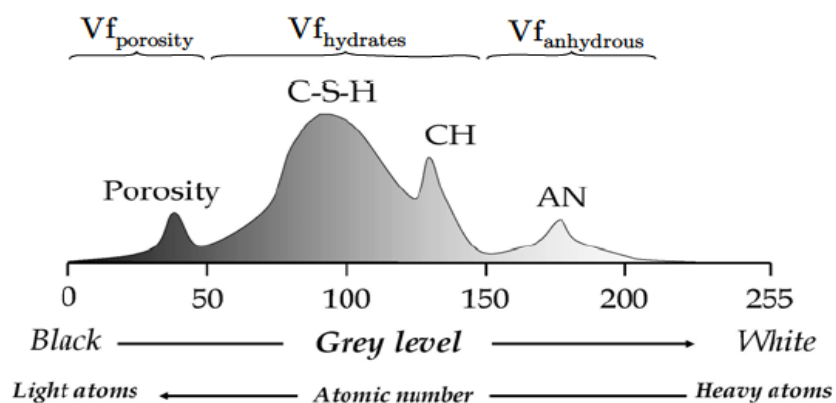


Figure 3-15 Grey level histogram of a hydrated cement paste (279)

For a fly ash blended cement paste, it is often difficult to distinguish between the unreacted fly ash grain and the CH phase as they have similar grey levels. The grey value of the remaining fly ash overlapped with that of CH and C-S-H gel, which prevented the discrimination of the remaining fly ash on the basis of grey level segmentation as shown in Figure 3.16. In quantitative analysis, different approach had been developed and used for the segmentation of the unreacted FA particles and additions (104, 109, 286, 287). This study used the qualitative approach to determine the degree of hydration using the grey level segmentation.

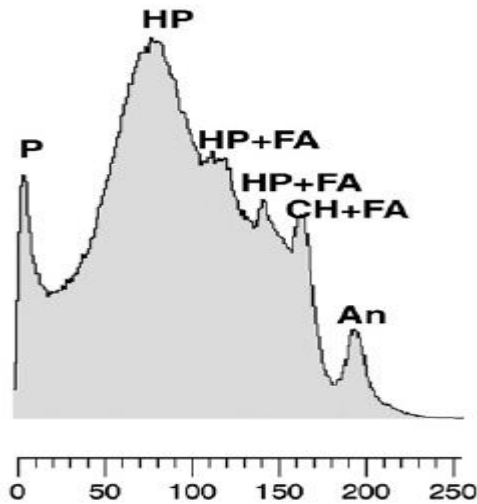


Figure 3-16 Grey level histogram of a fly ash blended cement paste from (109)

(P: porosity, HP: hydration products other than Portlandite, CH: Portlandite, An: unreacted clinker particle, FA: fly ash)

Degree of hydration

The degree of hydration was determined for 28 day old samples using the expressions below for the cement and fly ash blended systems.

$$DH_{SEM}^{cem}(t) = 1 - \frac{V_{(t)cem}}{V_{(o)cem}} \quad \text{Equation 3.10}$$

$$DR_{SEM}^{SCM}(t) = 1 - \frac{V_{(t)SCM}}{V_{(o)SCM}} \quad \text{Equation 3.11}$$

Where:

$V_{(o)cem}$ is the volume fraction of cement before hydration

$V_{(o)SCM}$ is the volume fraction of unreacted SCM before hydration

$V_{(t)cem}$ is the volume fraction of unhydrated cement at hydration time t, and

$V_{(t)SCM}$ is the volume fraction of unreacted SCM at hydration time t.

Chapter 4 Effect of improper curing on strength development

Impact of improper curing was examined on compressive strength by testing 100 x100 x100mm concrete cubes. The composition of the materials used has been explained in chapter three. Figure 4.1 shows the various experiments where the concrete cubes were used.

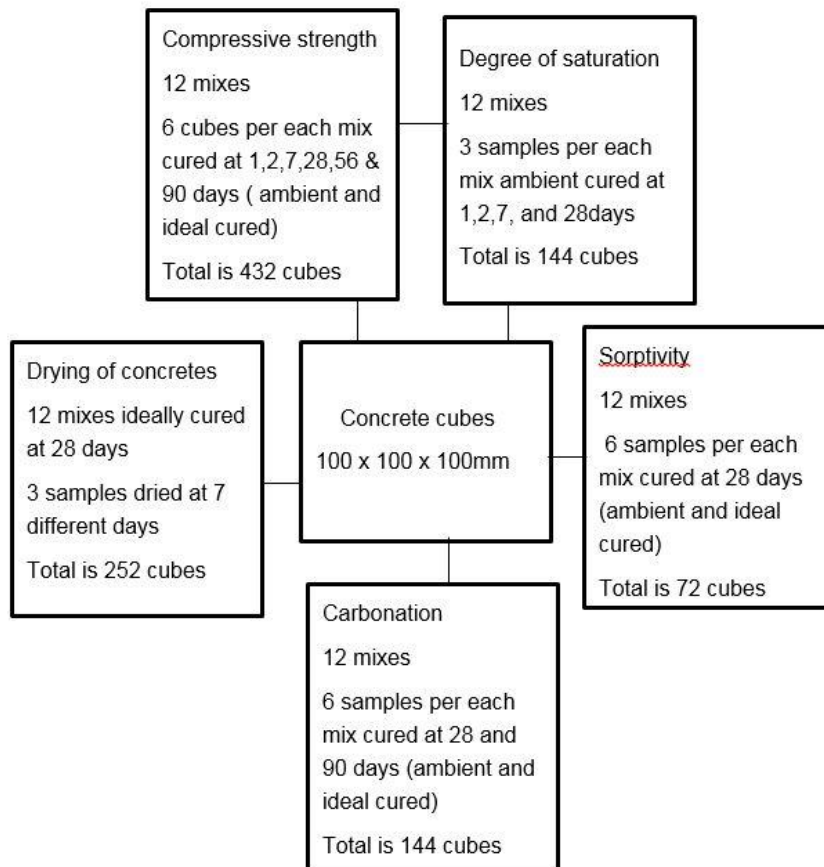


Figure 4-1 Various tests made with 100 x100 x100mm concrete cubes

Table 4.1 presents the binder type, targeted strength, slumps, nomenclature used in the figures, measured slump during casting, numbered of cubes casted and the water binder ratio.

The study used twelve mixes with three strength of 20,50 and 80MPa with 52.5 N CEM1 ordinary Portland cements and 30% fly ash replacement to prepare the concrete cubes for compressive strength experiment. Some properties of the cement and fly ash are given in Tables 3.1 to 3.4. The water/cement ratio used in the each of the mix were obtained using the aggregates absorption, surface moisture content and total moisture content given in Table 3.8. These values were used to calculate the additional water added to the mix since the aggregates were dried. 10 mm diameter uncrushed coarse aggregate and quartz sand of diameter 150 μ m to 5mm was used with the particle size distribution of the aggregates presented in Tables 3.5 and 3.6 while the mix proportions used are given in Table 3.9.

Table 4-1 Nomenclature used in the graph with measured slump

Binder type	Target strength (MPa)	Slump (mm)	Nomenclature	Measured slump (mm)	Number of cubes	w/b
CEM1	20	10 to 30	20 S-C	25	21	0.77
	50		50 S-C	20	42	0.42
	80		80 S-C	10	42	0.21
CEM1	20	60 to 180	20 W-C	110	42	0.75
	50		50 W-C	95	37	0.40
	80		80 W-C	100	42	0.21
30% fly ash	20	10 to 30	20 S-FA	18	21	0.78
	50		50 S-FA	25	21	0.42
	80		80 S-FA	30	21	0.21
30% fly ash	20	60 to 180	20 W-FA	60	21	0.76
	50		50 W-FA	100	21	0.40
	80		80 W-FA	110	21	0.20

The total of 432 cubes of 100 x100 x 100mm concrete cubes were casted in 24 batches, all the samples in each batch were either ideally or ambiently cured until the testing date. Each batch is made up of 18 cubes testing three cubes for 1,2,7,28,56 and 90 days.

The unconfined compressive strength was measured using a Retrofit Tonipact Concrete and Transverse Beam Machine according to BS EN 12390-3 The ideally-cured samples were tested immediately after removal from the fog room, the cubes just being made surface dry with a towel before testing while the ambient cured samples were tested straight away.

Degree of saturation was measured by using 100 X 100 X 100 mm concrete cubes. Ambient cure condition was use and the samples were cured for 1,2,7 and 28 days. The compressive strength for degree of saturation was determined in triplicate by immersing the samples in water for three hours prior to testing. This was to remove any influence of the degree of sample saturation on the measured strength. The water cement ratio and the mix proportions were the same with the samples prepared for strength development. 144 concrete cubes were casted for all the 12 mixes.

The variables considered in this experiments were listed as follows:

- the two curing conditions which are ideal and ambient,
- the two slumps of 10 to 30 and 60 to 180mm,
- the two binders CEM1 and 30% fly ash and
- the three targeted strengths of 20,50 and 80MPa.

Compressive strength under different curing conditions will be examined with varying degrees of saturation (0% DOS and 100%DOS), the effect on normal and blended concrete will be investigated. This will enable us to study improper curing on strength then understanding impact of degree of hydration, then work further to understand impact on the concrete properties that may affect concrete durability.

Investigation were carried out to determine the following:

- Compressive strength development
- Degree of hydration
- Degree of saturation
- Transport Properties and resistance to carbonation.

The compressive strength and transport properties will give an indication of the engineering performance, which can then be related to the degree of hydration.

4.1 Compressive strength of CEM I Concretes

In all the Figures presented the ambient cured samples were designated with letter A and the ideal cured samples used letter I. Also slumps having 10 to 30mm which were stiff mix were abbreviated to S and the wet mix with slumps 60 to 180 mm used letter W. Other abbreviations used for better understanding of the figures can be seen in Table 4.1.

An increase in the compressive strength with age was noted in all the concrete samples, irrespective of the curing methods used. In all mixes with target strengths of 20MPa achieved compressive strengths greater than 30MPa, while mixes with 50MPa actual strengths was

approximately 60MPa. However, mixes with 80MPa target strength failed to achieve this, with most having compressive strengths of between 50 and 60 MPa.

Figure 4.2 shows the compressive strength of CEM1 stiff mix cured in ambient and in fog room. In all the three target strengths considered, there was no significant difference in compressive strength as a function of curing regime. This was unexpected, since theoretically, concrete cured under ideal conditions should have a higher strength. When concrete is exposed to ambient conditions, evaporation of water takes place and loss of moisture will result in the incomplete hydration of the cement and hence lower compressive strength of the concrete follows.

The situation where the ambient cured samples were showing higher strengths than ideally-cured samples has been attributed to the increase in the secondary forces between the surfaces of the cement gel (179, 288) and also the reduction in the disjoining pressure due to the drying. Few researchers (288, 289) reported similar result in their work.

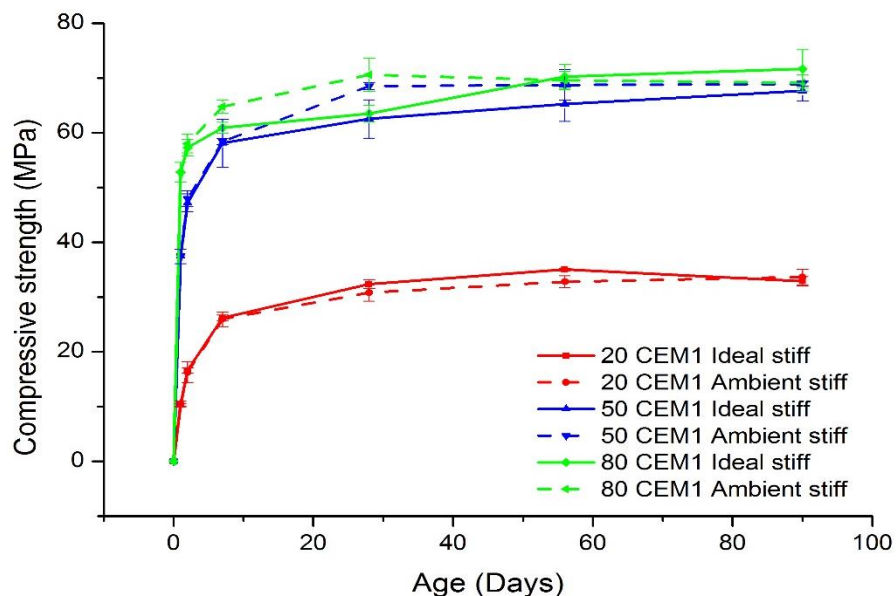


Figure 4-2 Compressive strength of CEM1 stiff mix (slumps 10-30mm)

As shown in Figure 4.3 also over the first 28 days, curing conditions did not have an apparent effect on strength development when considering wet mix. However, beyond this, differences were apparent. Unlike for the dry mixes, there did appear to be a slight decrease in performance when the samples were cured under ambient conditions. The extent of this difference in performance diminished ever so slightly with increasing target strength.

This implies that loss of water from the samples cured under ambient conditions led to a reduction in the degree of cement hydration, with a consequent negative impact on compressive strength. Comparing these results with those from the dry mixes, the observations are somewhat counterintuitive. The wet mixes had a greater water content than the dry mixes, yet it was the wet mixes which seemed more affected by desiccation during curing under ambient conditions. One possible explanation is that the wet mixes had a greater paste content and so a greater surface area from which water could evaporate (assuming that water would not evaporate from the aggregate). Another reason is that there is more water in the wet mixes which will make the concretes to evaporates more than the stiff mix.

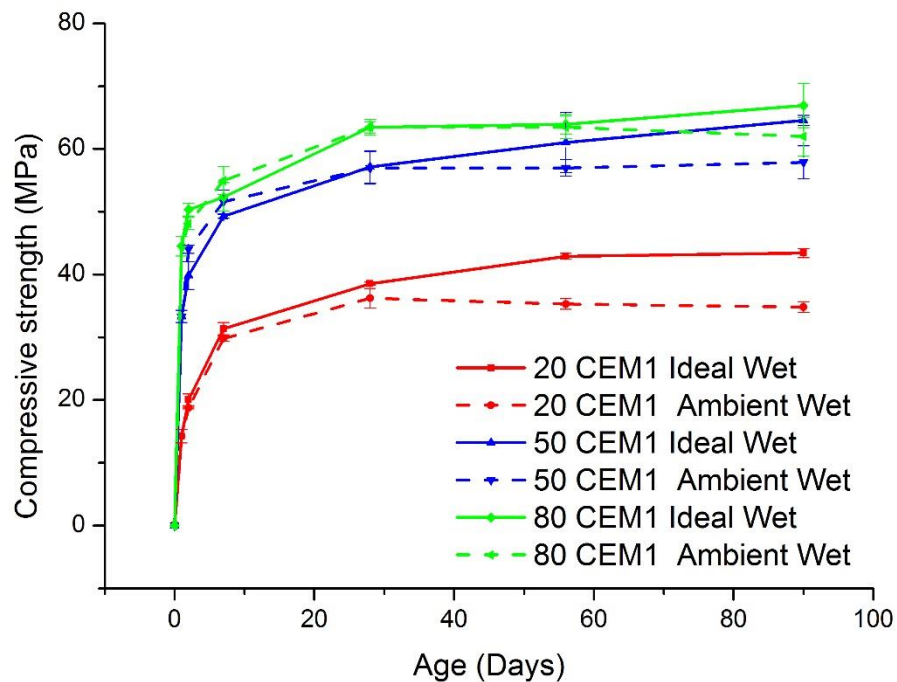


Figure 4-3 Compressive strength of CEM1 wet mix (slumps 60-180mm)

4.2 Compressive strength of Fly ash Concretes

Figures 4.4 show the compressive strength development of stiff and wet mixes prepared with 30% fly ash. Unlike for the CEM I mixes, the Figures show that Fly ash ideally-cured samples were stronger than the ambient cured samples from beyond about 7 days. This result clearly shows that poor curing affects the hydration, and hence strength development of fly ash concretes more adversely than CEM I concretes, in agreement with other researcher (19, 66, 289-295). This had been explained in the literature when considering the effect of fly ash on the properties of hardened concrete specifically on effects on compressive strength. Similar to wet CEM I mixes, the effect of non-ideal curing diminished with increasing target strength. Furthermore, the diminished performance under non-ideal curing conditions became evident at earlier ages as the target strength dropped. Thus, the 20 MPa mix started to show diminished performance when cured under non-ideal conditions after 7 days, while this diminished performance was seen after 28 days for the 50 MPa mix and only at 90 days for the 80 MPa mix. This suggests that the higher w/b ratio facilitates loss of water more readily, presumably due to the increased porosity of the mix. Meanwhile, lower w/b ratios lead to lower porosity and smaller capillary pores. This impedes evaporation from the concrete and thus the effects of improper curing are not seen until later for the higher strength mixes.

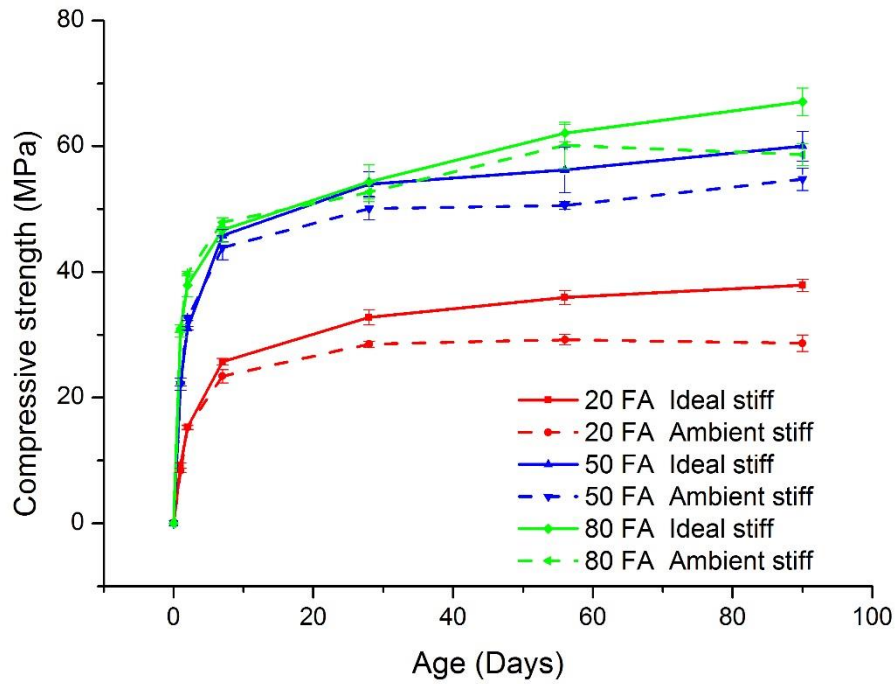


Figure 4-4 Compressive strength of fly ash stiff mix (slumps 10-30mm)

As for the stiff fly ash-bearing mixes, the wet mixes were adversely affected by improper curing conditions (Figure 4.5), with all ambient cured mixes having lower compressive strengths than the ideally cured samples. Again, the difference diminished with increasing target strength, but the deviation in strength was not seen until later ages when compared to the stiff mixes. This suggests that the higher water contents of the wet mixes led to less desiccation of the fine pore-structured hydrated cement-fly ash blend.

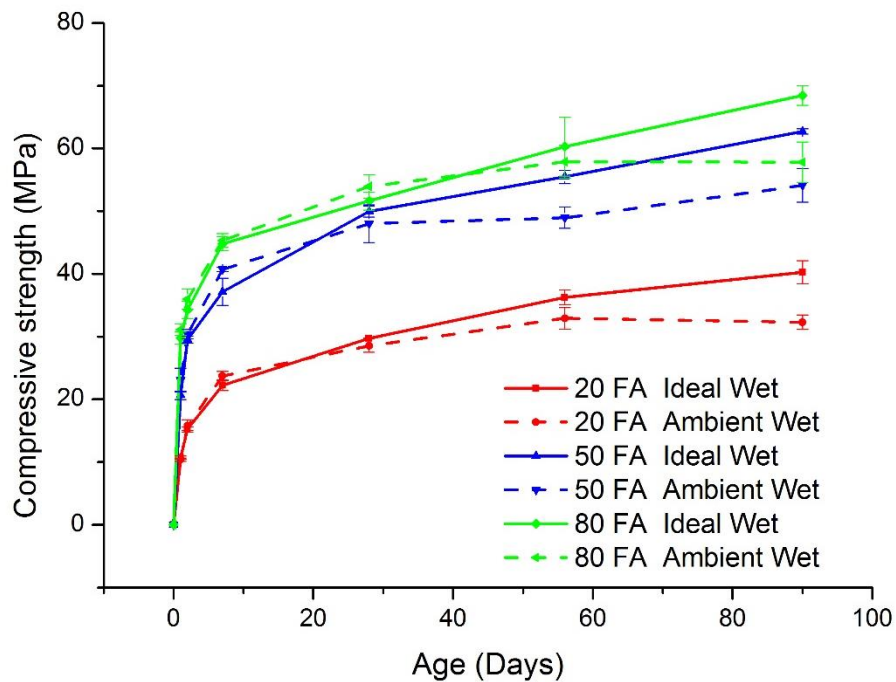


Figure 4-5 Compressive strength of fly ash concrete wet mix (slumps 60-180mm)

4.3 Compressive strength of 20 Fly ash stiff mix with minimum curing period (f_2/f_{28})

The minimum curing period was defined in Table F.1 in BS EN 13670:2009 (260) for curing class 2 (corresponding to a surface concrete strength equal to 35 % of the specified characteristic strength). The table assesses the performance of concrete by considering the ratio of the mean compressive strengths after 2 and 28 days (f_2/f_{28}), determined from initial tests or based on known performance of concrete of comparable composition. In all the CEM I concretes, the value of f_{cm2}/f_{cm28} was greater than 0.5, hence the third curing regime mentioned in section 3.2 was not required. The f_{cm2}/f_{cm28} values for the fly ash containing concretes were calculated, and only the 20 MPa stiff mix concrete necessitated prolonged moist curing, with an f_{cm2}/f_{cm28} value of 0.46. Using Table F.1 for a temperature of less than 25°C, the minimum curing time is 2.5 days. Since curing for half days was impractical, this was approximated to 3 days. The cubes were cured in the fog room for 3 days after casting, before being transferred to the laboratory at 20°C and 42% relative humidity for the remaining time.

The compressive strength development of the 20 MPa, fly ash concrete stiff mix cured under all 3 conditions is shown in Figure 4.6. The figure shows the effect of three days moist curing in the fog room before exposing to ambient conditions. While curing under ambient conditions from 1 day had a detrimental effect on strength from 7 days onwards, there was no such drop off in strength development for the sample moist cured for 3 days. The result agrees with other findings (107, 179) .

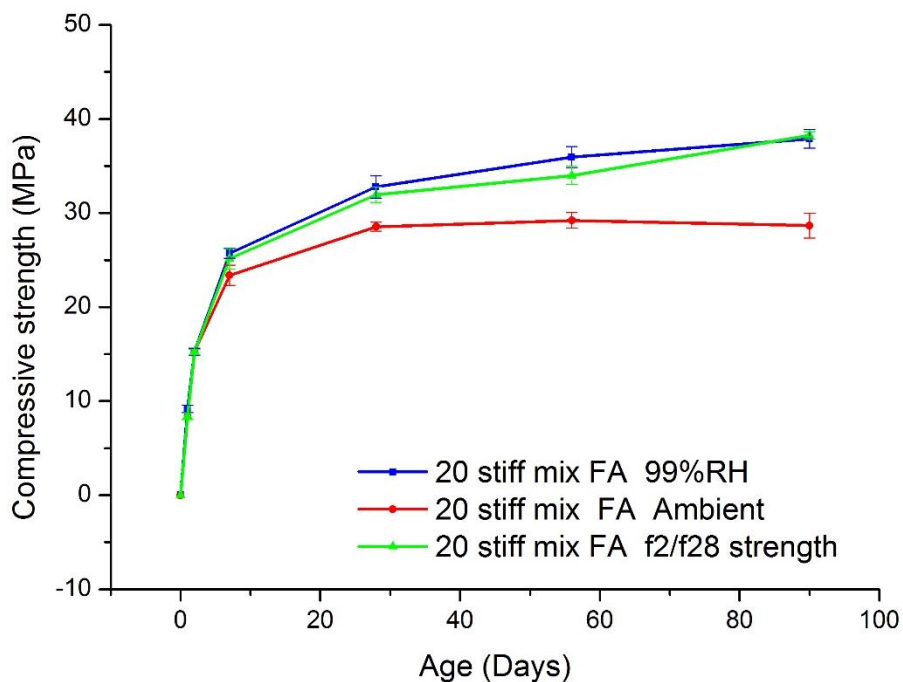


Figure 4-6 Compressive strength of 20MPa fly ash Concrete with f_2/f_{28}

4.4 Compressive strength development of saturated CEM1 samples.

The compressive strength of concrete falls as the degree of concrete saturation rises. Bartlett and MacGregor (180) explained that the reduction in strength as a result of immersing concrete compression test specimens in water has been associated with the absorption of

water by the gel pores since immersing the specimens in benzine or paraffin, which cement gel cannot absorb, has no effect on strength. The same principle is likely responsible for the increase in strength that happens when specimens are left in air to dry. They further explained the differences between uniform and non-uniform moisture changes throughout the volume of the specimen, and their respective effects on the specimen strength.

One of the explanations given for the effect of uniform moisture change on strength is based on the Griffiths fracture theory. When water is absorbed into the gel, forcing the gel surfaces further apart, Van der Waals forces between gel particles are reduced. These adhesive forces are proportional to the specific surface energy; the critical stress for a given crack size is therefore reduced when the intermolecular distances are increased.

Bartlett and MacGregor (180) concluded that the compressive strength of a concrete specimen is influenced both by moisture content changes that are uniform throughout the specimen volume and moisture content gradients between the surface of the specimen and interior.

Popovics (179) checked the effect of a moisture gradient on the specimen when studying the effect of curing method and final moisture condition on the compressive strength of concrete. Swelling at the surface of the core is obtained where the moisture content is increased as a result of soaking while the surface layer shrinks due to air-drying. The material at the centre of the core is restrained by these volume changes that does not gain or lose moisture. A set of residual strains and corresponding self-equilibrated residual stresses are created by the restraint.

Consequently, concrete samples which had been cured under non-ideal, ambient conditions would have exhibited a variation in moisture content from the dry surface to the saturated bulk. This would have meant that direct comparisons between ideally-cured and ambient cured samples, as just discussed in the preceding section, may not be appropriate. An accurate comparison can only be made when the samples cured under different regimes had the same degree of saturation upon testing. Therefore, a fresh set of ambient-cured samples was prepared, where the samples were cured as before but immersed in water for three hours immediately prior to strength testing at 2, 7 and 28 days. Figures 4.7 to 4.12 shows the compressive strength development of the various mixes cured under ideal conditions, ambient conditions and ambient conditions yet saturated following immersion.

The figures clearly show the deleterious effects of improper curing, with the saturated, ambient cured samples all exhibiting lower strengths than the equivalent ideally cured samples. These results agree with other findings (27, 28, 179-181).

Figures 4.7 to 4.9 show the results from the CEM I stiff mixes. These Figures will be compared with one another since putting them together will be too clumps and difficult to understand. The diminished strength development was evident from 7 days onwards for the 20 and 50 MPa mixes, but from only 2 days for the 80 MPa mix. The 80 MPa mix was affected by improper curing from an earlier age. This was likely due to the very low water/cement ratio, which meant that any evaporation of water from the surface reduced the amount of water available for hydration. This was evident later when determining the degree of cement hydration upon improper curing for the various mixes.

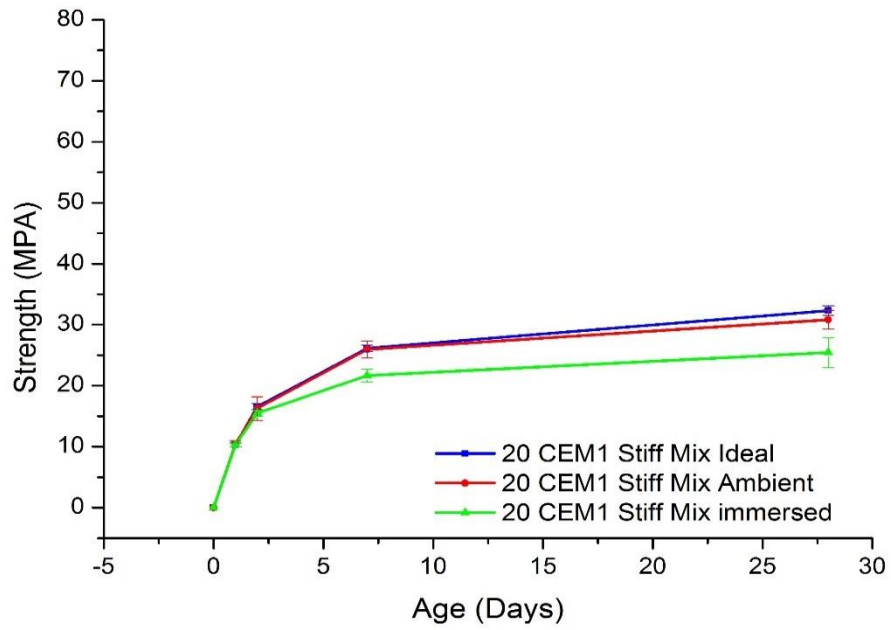


Figure 4-7 Compressive strength of 20MPa CEM1 Stiff Mix and immersed

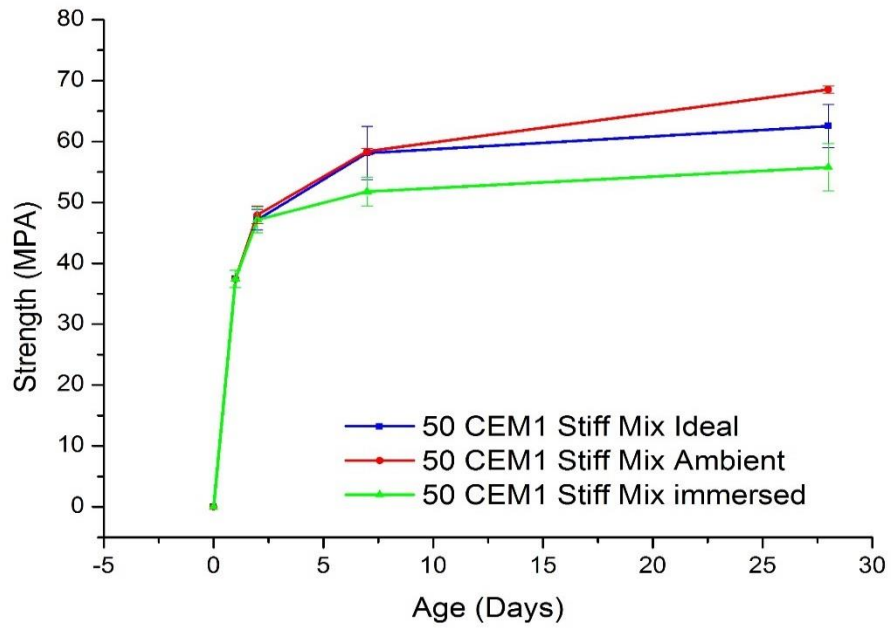


Figure 4-8 Compressive strength of 50MPa CEM1 Stiff Mix and Immersed

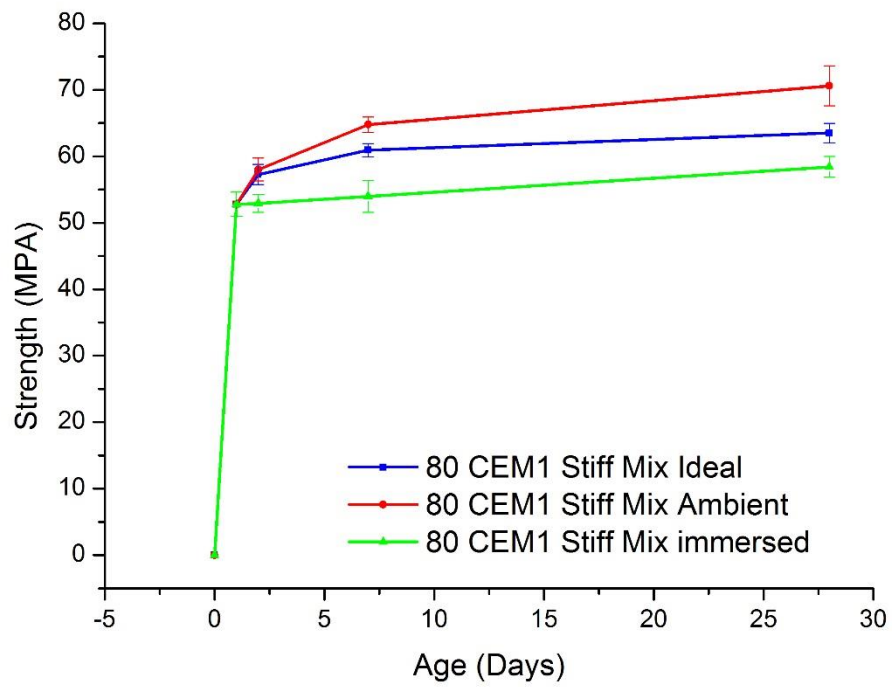


Figure 4-9 Compressive strength of 80MPa CEM1 Stiff Mix and Immersed

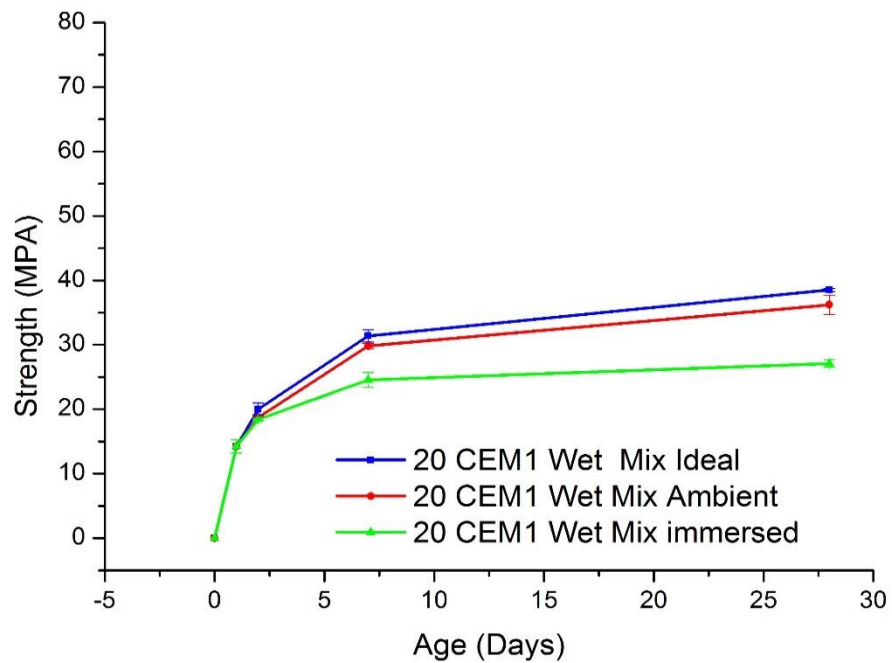


Figure 4-10 Compressive strength of 20MPa CEM1 Wet Mix and Immersed

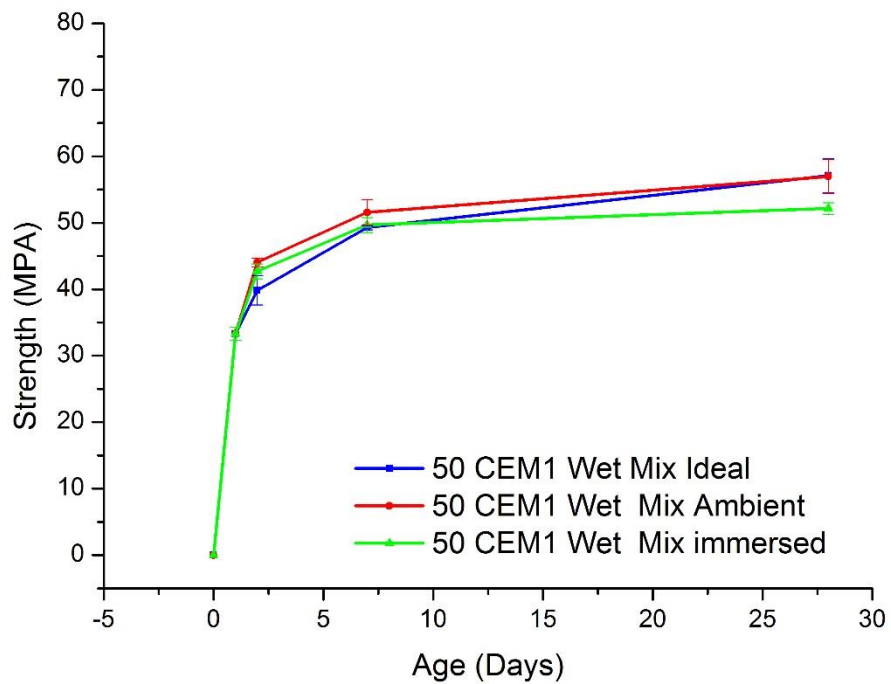


Figure 4-11 Compressive strength of 50MPa CEM1 Wet Mix and Immersed

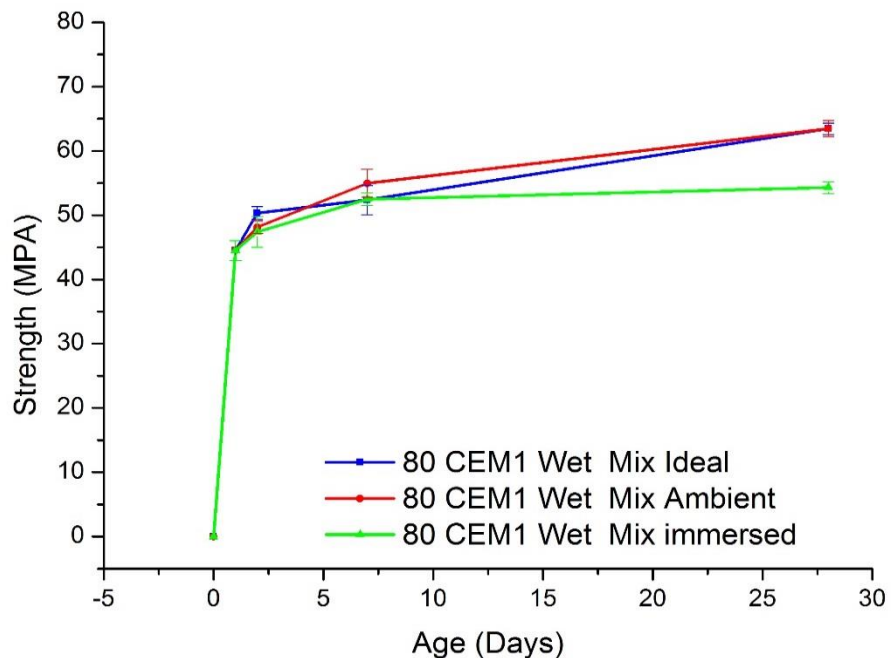


Figure 4-12 Compressive strength of 80MPa CEM1 Wet Mix and Immersed

Figures 4.10 to 4.12 show the compressive strength of CEM1 wet mixes cured under the three conditions which will be compared to one another to avoid too much graphs in one position. Diminished performance was seen with improper curing from 7 days and beyond for the 20 MPa mix. However, it was not seen until later for the 50 and 80 MPa mixes. In this instance,

unlike for the dry mixes, there appeared to be sufficient water present in the mix to delay the effects of improper curing. The 20 MPa mix was affected at an earlier age because its more open pore structure allowed more rapid water loss (as seen when following the drying of the various mixes in Chapter five).

4.5 Compressive strength of Fly ash immersed samples

Figures 4.13 to 4.15 show the compressive strength development of the stiff fly ash mixes under the three testing conditions. As explained earlier, in order to prevent the figures being too cluttered, these three sets of data will be displayed separately. The results were similar to those obtained from the CEM I mixes, with diminished strength observed for samples cured under non-ideal conditions from 7 days onwards and a diminishing effect with increasing strength.

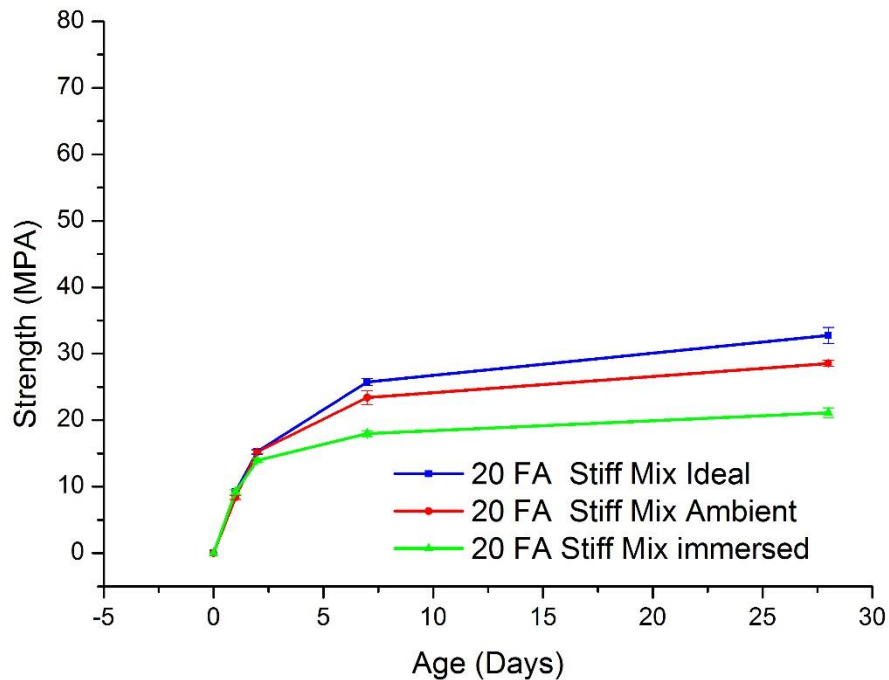


Figure 4-13 Compressive strength 20MPa Fly ash Stiff Mix and Immersed

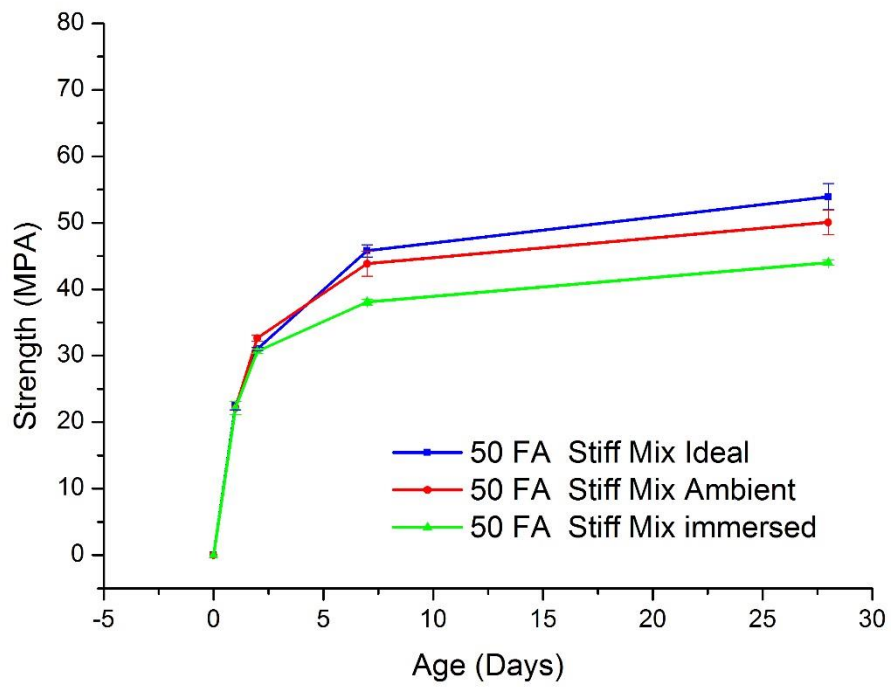


Figure 4-14 Compressive strength 50MPa PFA Stiff Mix and Immersed

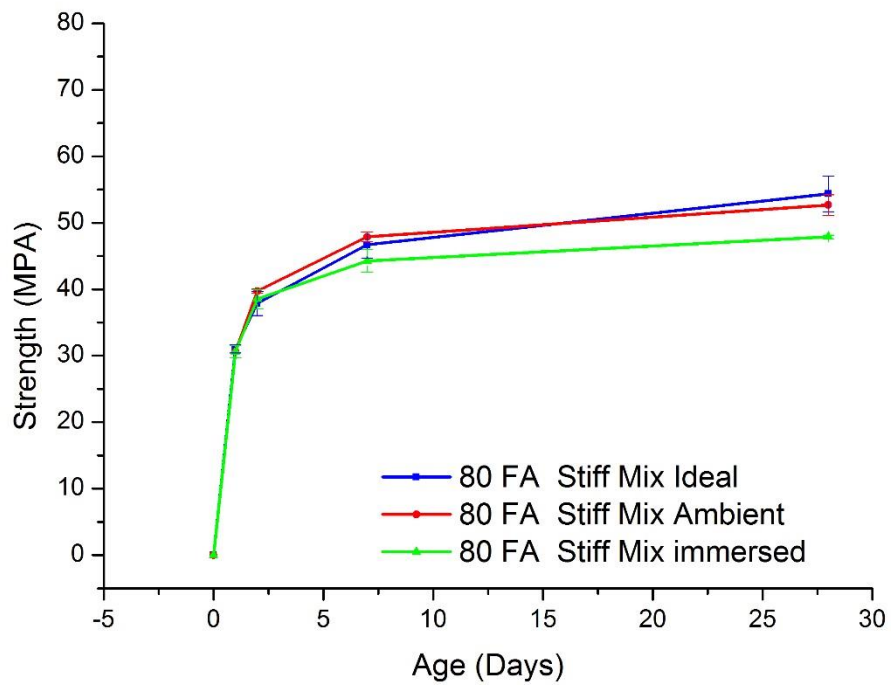


Figure 4-15 Compressive strength 80MPa Fly ash Stiff Mix and Immersed

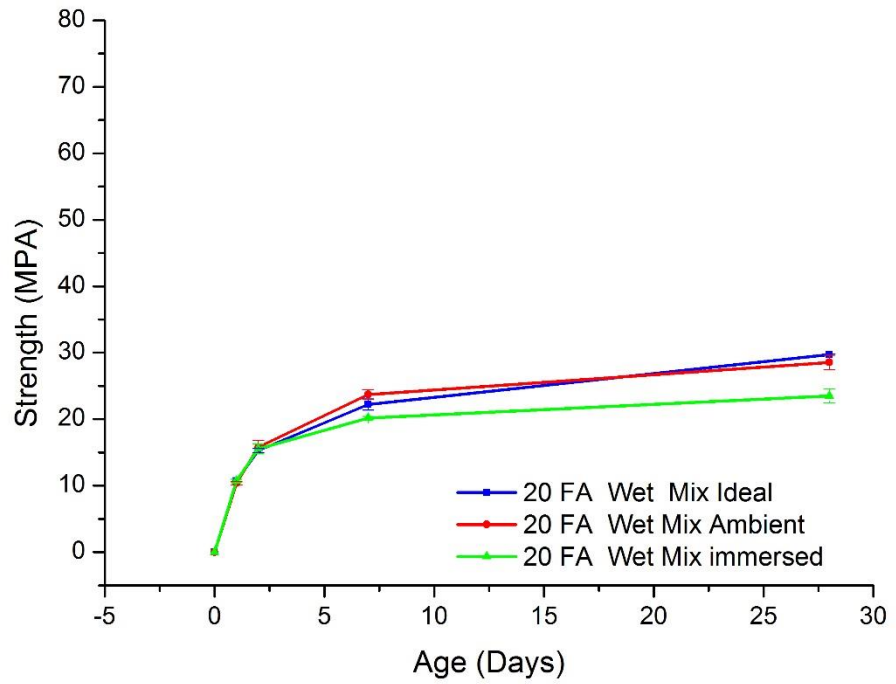


Figure 4-16 Compressive strength 20MPa Fly ash Wet Mix and Immersed

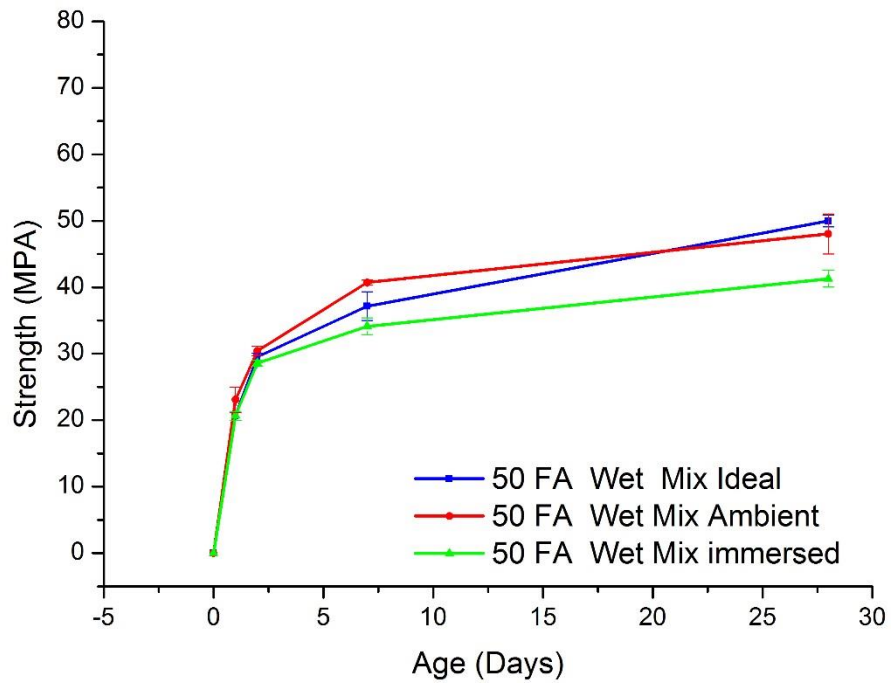


Figure 4-17 Compressive strength 50MPa Fly ash Wet Mix and Immersed

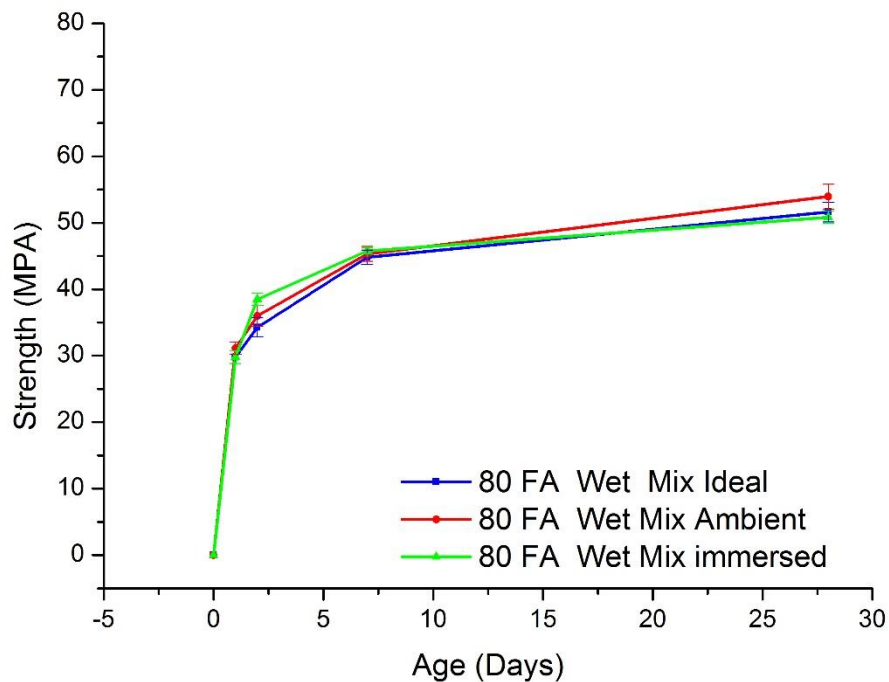


Figure 4-18 Compressive strength of 80MPa Fly ash Wet Mix and Immersed

Figures 4.16 to 4.18 show the compressive strength development for the wet fly ash mixes under the three testing conditions. The loss of strength due to improper curing diminished with increasing target compressive strength, such that the 80 MPa concrete did not show any loss of performance when cured under non-ideal conditions. It was somewhat surprising that the fly ash mixes did not show reduced performance.

4.6 Compressive strength of 20MPa Fly ash stiff mix with ambient cured immersed and f_2/f_{28} immersed

Figure 4.19 shows the compressive strength development of the stiff 20MPa fly ash mix. The figure shows four curves, the ideally-cured samples, the samples cured and tested under ambient conditions, the saturated ambient-cured sample and finally the sample moist cured for three days, in line with BS EN 13670:2009, and tested in the saturated state. The latter case follows the minimum curing time specified in Table F1 of BS EN 13670:2009 based on the f_2/f_{28} compressive strengths. The prolonged curing certainly improved performance compared to the sample moist-cured for only one day, but there was still diminished performance compared to the samples moist cured for 28 days.

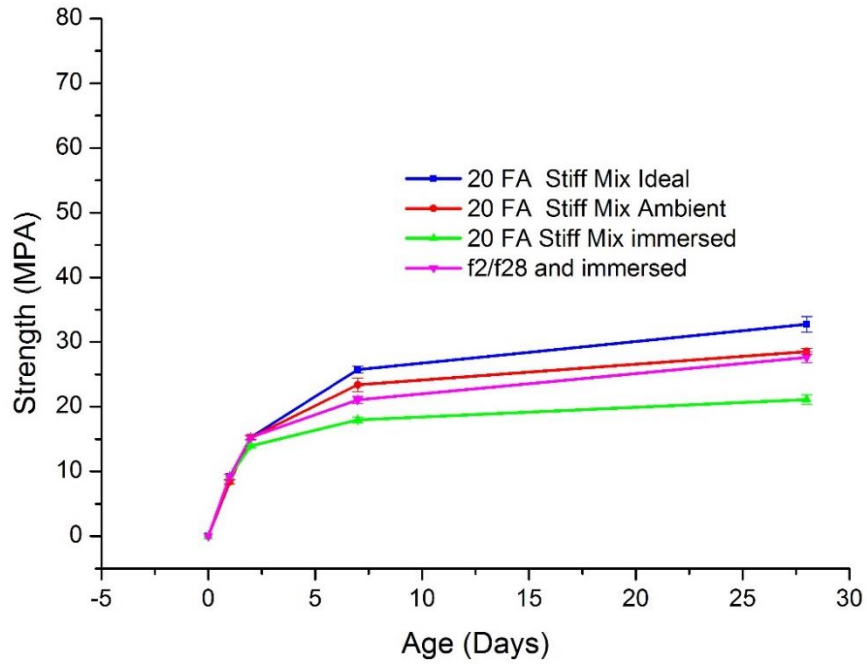


Figure 4-19 Compressive strength of 20MPa Fly ash Stiff Mix and f_2/f_{28} Immersed

4.7 Compressive Strength at 28 days

The strength development for ideally cured and ambient cured samples then immersed at 28 days was shown in Figure 4.20. The reason for this is to compare the compressive strengths at 28 days with other experiments that were conducted at only 28 days. Figure 4.20 shows that the pattern that will be used to present the results at 28 days especially when comparing the ideal and ambient cured samples. The pattern starting from left will show CEM1 stiff mixes of 20,50 and 80MPa followed by CEM1 wet mixes of 20, 50 and 80MPa. The fly ash stiff and wet mixes of 20,50 and 80MPa follows respectively. Other abbreviation used can be found on Table 4. 1.

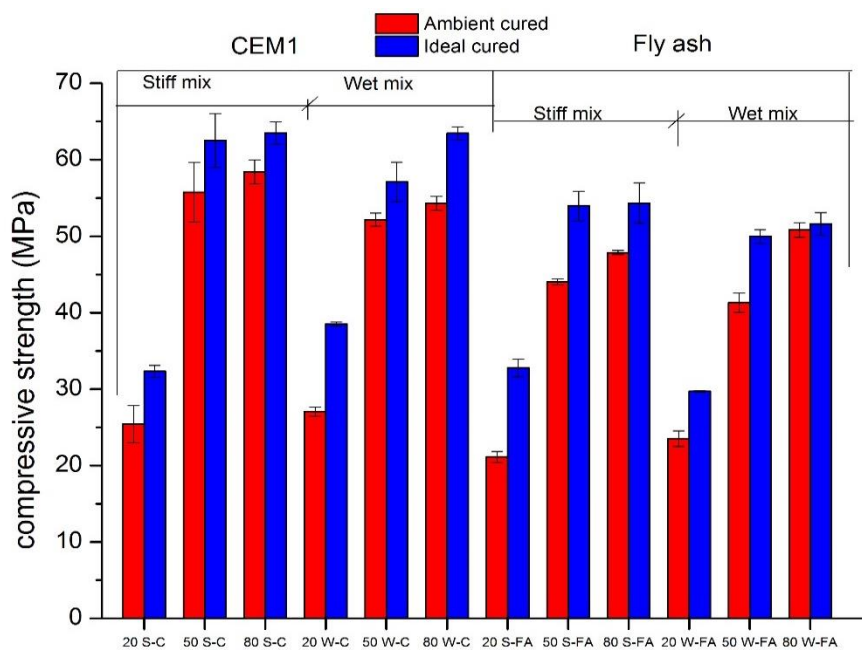


Figure 4-20 Figure showing the graphs mixes and the binders

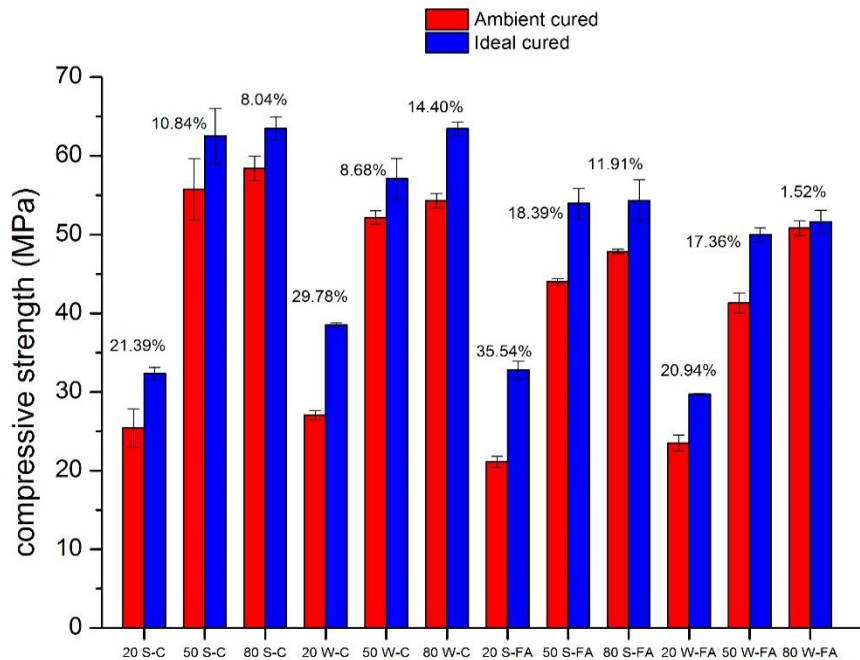


Figure 4-21 Compressive strength of Ambient and Ideal cured concretes at 28 days

Figure 4.21 shows the compressive strength of ambient and ideal cured concretes of CEM1 and fly ash at 28 days. The figures show that ideal cured samples had higher strengths than ambient-cured samples. The effect is more pronounced at lower strengths, higher percentage loss due to ambient curing of 21.39%, 29.78%, 35.54% and 20.94% were obtained in 20 MPa concretes for stiff and wet mixes of CEM1 and fly ash samples. The percentage loss due to ambient curing reduces as the strength increases that is 80 MPa had the lowest percentage between ideal and ambient cured samples followed by 50 MPa. There is slight difference in CEM1 wet mix where the 50 MPa percentage is higher than the 80 MPa. Ambient cured samples having lower strength is as a result of early drying of concrete which stops the cement hydration before the pores are blocked by hydration products hence developments of a more continuous pore structures. Also the ideal samples were in the environment where the hydration of cement can occur. This result agrees with other findings (233, 251, 288, 289, 296).

In Figure 4.21 comparing the stiff mix with the wet mix, there is no huge effect for CEM I, but the fly ash blends the compressive strength was higher for the stiff mixes than the wet, but ambient curing had a greater effect, such that ambient-cured stiff mixes performed worse than ambient cured wet mixes. This shows that the lower water content meant that the dry mixes were more susceptible to improper curing for the slower-hydrating fly ash blends. Also the difference that can be seen is that ideal cured samples seemed to be slightly weaker when they were wet mixes.

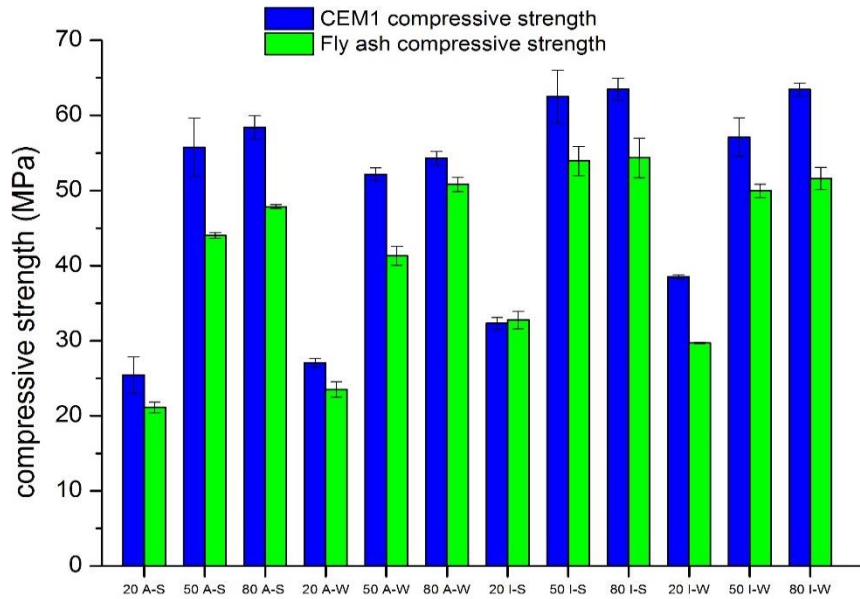


Figure 4-22 Compressive strength of CEM1 and Fly ash concretes

Figure 4. 22 shows the effect of improper curing on compressive strength of CEM1 and fly ash concrete. In the figure 20,50 and 80 denotes the targeted strength while letter A is for ambient, letter S for stiff, I for ideal and W for wet mix. From the figure samples containing fly ash showed lower strengths, irrespective of curing conditions. Improper curing affected fly ash mixes more than CEM I mixes and the effect is more on stiff mixes. This result agrees with other findings (296, 297).

4.8 Conclusion

This chapter has looked at the effect of improper curing on strength development of CEM1 and fly ash concretes. The strength development were observed on samples were cured for 1,2,7,28,56 and 90 days. Ambient and ideal cure compressive strengths of stiff and wet mixes were checked, while the ambient and ideal compressive strengths of CEM1 and fly ash concretes were compared. An increase in the compressive strength with age was noted in all the concrete samples, irrespective of the curing methods used.

There was no significant difference in compressive strength as a function of curing regime for CEM1 stiff mix cured in ambient and ideal conditions for all the three targeted strength. Over the first 28 days, curing conditions did not have an apparent effect on strength development when considering wet mix in CEM1 however, beyond this, differences were apparent. The extent of this difference in performance diminished ever so slightly with increasing target strength. Thus loss of water from the samples cured under ambient conditions led to a reduction in the degree of cement hydration, with a consequent negative impact on compressive strength.

Fly ash stiff mix samples show similar result to wet CEM1 mixes, the effect of non-ideal curing diminished with increasing target strength. The wet mixes were adversely affected by improper curing conditions, with all ambient cured mixes having lower compressive strengths than the ideally cured samples. Also, the difference diminished with increasing target strength, but the deviation in strength was not seen until later ages when compared to the stiff mixes.

Samples that were moist cured for three days in the fog room before exposing to ambient conditions compressive strengths were stronger like samples cured for 28 days in the fog room.

All the ambient cured samples and immersed in water for three hours before testing show the deleterious effects of improper curing, all exhibiting lower strengths than the equivalent ideally cured samples.

The strength development for ideally cured and ambient cured samples then immersed at 28 days shows that ideal cured samples had higher strengths than ambient-cured samples. The effect is more pronounced at lower strengths and the percentage loss due to ambient curing reduces as the strength increases. Also samples containing fly ash showed lower strengths, irrespective of curing conditions. Improper curing affected fly ash mixes more than CEM I mixes and the effect is more on stiff mixes.

Chapter 5 Effects of drying

5.1 Effect of drying in the present work

While it is known that the degree of saturation of concrete can affect its strength, it is not immediately clear to what extent this occurs and whether various mix design variables affect the degree of strength gain. Therefore, the effect of drying on concrete was investigated by drying concrete samples to constant weight at 40°C with regular strength testing. Concrete cubes were cast and cured for 28 days at 99% RH at 20°C. Samples were removed from the fog room and all the samples were weighed and recorded before being put in the oven. Samples at 28 days were weighed before testing for compressive strength and recorded as time 0, subsequent samples were removed from oven weighed and tested. Table 5.1 shows the system of age adopted in the research for the drying experiments. Mass changes were reported as percentages.

Table 5-1 Drying age used in the experiment.

Age(days)	Drying age (day)
28days	28
28days +2	30
28days + 5	35
28days+7	42
28days + 14	56
28days +21	77
28 days + until constant weight (120)	197

5.1.1 Effects of weight loss as a result of drying

Figure 5.1 shows the continuous weight loss for a selection of concretes. This pattern was observed in all the mixes i.e. stiff and wet mix, in CEM1 and fly ash concretes. Other Figures were presented in the appendix. The 20MPa samples lost more moisture initially which is higher than the 50 and 80MPa concretes. This is due to the fact that the low strength mixes do have a higher water/cement ratio and so a greater porosity. 80 MPa concretes moisture lost were next to 20MPa, this might be as a result of more water in the mix than 50MPa concretes which is added during the processing to make it more workable because of high content of binder in the mix.

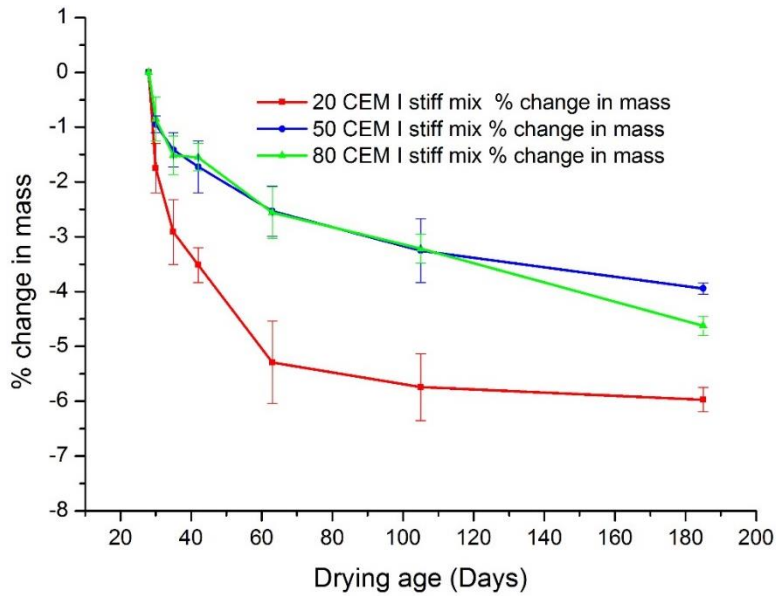


Figure 5-1 Change in mass for 20,50 and 80MPa CEM1 stiff mix

5.2 Effects of drying on compressive strength

The effect of drying on the compressive strength as the concretes loses moisture in the oven is checked also at various drying age indicated in Table 5.1. The moisture lost is recorded first and the result is presented in Table 5.2 before testing the compressive strength as the concrete dries out.

The percentage change in mass and compressive strength of 20,50 and 80MPa concrete CEM1 wet mix is shown in Figure 5.2. The Figure show that as the concrete lost moisture there were increase in compressive strength. This was observed in all the mixes either stiff or wet CEM1 and fly ash concretes. Other results were shown in the appendix.

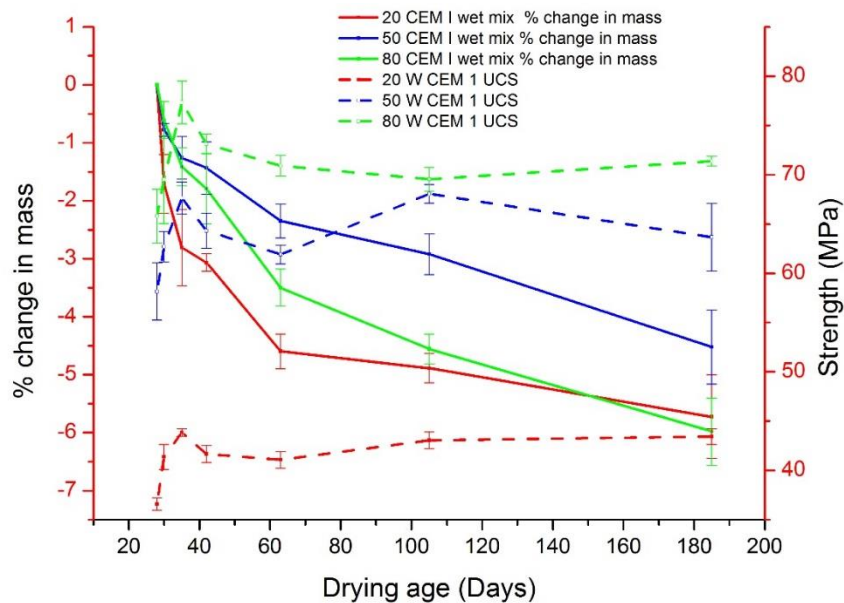


Figure 5-2 Percentage change in mass and compressive strength of CEM1 wet mix concrete

5.3 Compressive strength of concretes as the binder contents increases

The targeted strength used in the study were 20, 50 and 80MPa and the composition of the binder had been presented in Table 3.9. The higher the targeted strength the more binder in the mix. The effect of water binder ratio can be seen also as the binder content in the mix increases. As the binder contents increases the water binder ratio reduces and this produces more strength as shown in Figure 5.3. The binder water of 20,50 and 80MPa were 0.77, 0.42 and 0.21 respectively.

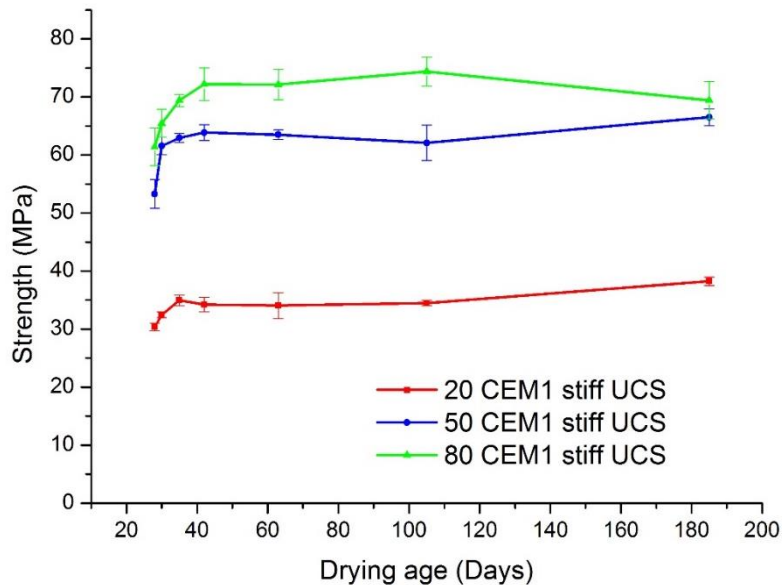


Figure 5-3 Compressive strength of 20, 50 and 80MPa CEM1 stiff mix

Also Figure 5.3 shows the compressive strength of the three targeted strength used in the experiment as the concrete is drying. This figure clearly shows the strength development as the concrete lost moisture as a result of drying. The result is the same with wet mix, and the two mixes of fly ash concretes. The result shows increase in compressive strength for all the samples. The increase in strength revealed the importance of curing, as effective curing reduces the loss of water and increases the hydration of the cement, and hence reduces the total porosity and increases the probability of the pores being either blocked or narrowed down by continued formation of hydration products (298).

5.4 Effect of drying on compressive strength of stiff mix and the wet mix

Figure 5.4 show the effect of drying on stiff and wet mixes. In all the targeted strength wet mix is greater than stiff mix. The difference seen in 20MPa between the stiff and wet mix is greater than the one observed in the higher strength concretes especially when the drying age is 185 days. This result support or confirm the result obtained by Ait-Aide et al (299) that under severe conditions in a hot climate, the introduction of supplementing quantity of water, or the increase in the w/c ratio, until a certain limit, has no marked influence on the strength of concrete since under standard conditions, an increase in w/c ratio would inevitably lead to a decreased strength of concrete.

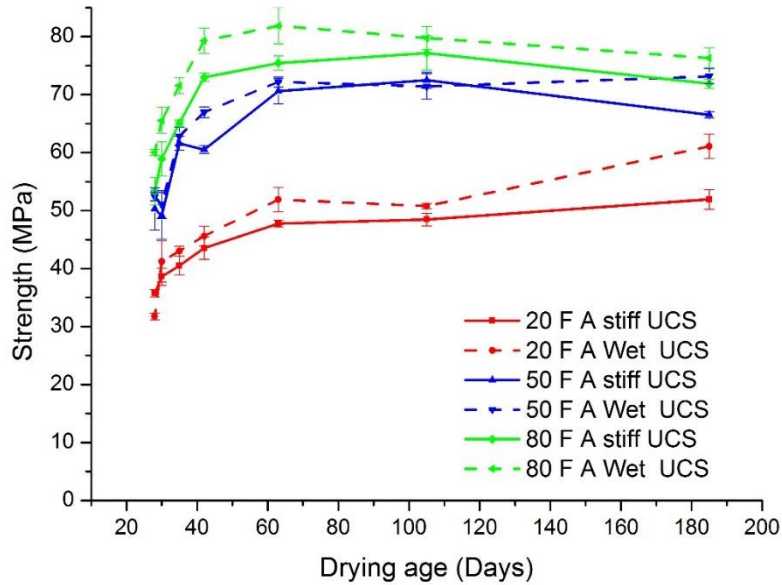


Figure 5-4 Compressive strength of Fly ash stiff and wet mix

5.5 Effect of drying on Compressive strength of CEM1 and Fly ash concretes

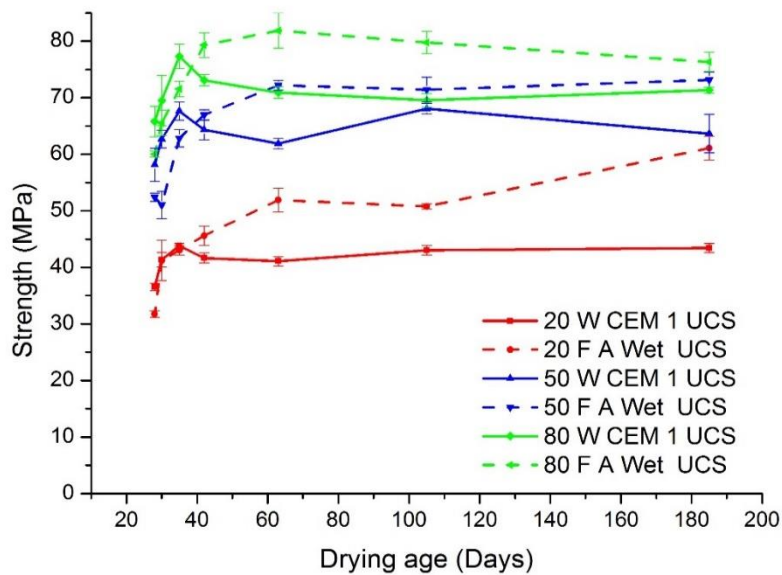


Figure 5-5 Effect of drying on compressive strength of CEM1 and Fly ash Concrete

The compressive strength of wet mix CEM1 and fly ash concretes is shown in Figure 5.5. The compressive strength of fly ash concretes was higher than that of CEM1 concretes as the concretes lost moisture. The same result is found in 20MPa stiff mix while 50 and 80 MPa were almost the same and slightly higher. This result explain the importance of curing before drying and effect of using fly ash in concrete mixes and effect of exposing concretes to prolonged drying. The result shows an increase in compressive strength as the concrete dries and as the age increases. Fly ash concretes exhibit higher strength than CEM1 concretes at later age. This result confirms increase in strength at later age especially with the use of fly ash as partial replacement (75, 77). In the experiment the targeted strength of 80MPa was reached when the concretes dries out. This result agrees with similar findings by Safiuddin et

al (182). Even the result of fly ash concretes when exposed to elevated temperature confirms an initial increase in compressive strength with an increase in the temperature up to 100°C (193). Also other researchers (185, 194-197) confirms that fly ash concretes prevent the decrease of concrete strength against high temperature.

5.6 Mass loss in ideal cured sample as a result of drying

The effect of drying was studied on ideally cured concretes. The concrete samples used for this experiments were cured in the fog room for 28 days. At 28 days all the samples were removed from fog room the surface were wiped with towel to remove any residue water, the samples were weighed and put in the oven at 40°C. The samples were dried at seven different times as shown in Table 5.1, at the designated time of testing the samples weight were measured before testing the compressive strength. The amount of water lost as a result of drying were recorded and presented in Table 5.2 while Figures 5.6 and 5.7 shows the same result but in graphical form for better understanding of the result. In Figures 5.6 and 5.7 all the fly ash concretes were represented in broken lines and CEM1 samples in solid lines. Figure 5.6 shows the percentage change in mass for CEM1 and fly ash concrete stiff mix. In the Figure, 20MPa CEM1 samples lost more water than the fly ash samples. Also in the Figure high strength concretes fly ash samples lost more water than the CEM1 samples this is more noticeable as the drying age increases.

Table 5-2 Mass loss in ideal cured concrete as a result of drying

Age(Days)	20MPa CEM1	50MPa CEM1	80MPa CEM1	20MPa PFA	50MPa PFA	80MPa PFA
Stiff mix						
1	-1.75	-0.95	-0.85	-1.74	-0.88	-1.19
5	-2.91	-1.41	-1.51	-2.20	-1.62	-2.03
7	-3.51	-1.72	-1.55	-2.64	-1.91	-2.10
21	-5.29	-2.53	-2.56	-3.48	-2.75	-2.84
42	-5.74	-3.25	-3.21	-4.08	-3.20	-3.64
70	-5.97	-3.94	-4.63	-5.17	-4.38	-5.40
Wet mix						
1	-1.71	-0.78	-0.61	-2.63	-1.11	-1.55
5	-2.81	-1.26	-1.41	-2.76	-1.79	-2.39
7	-3.07	-1.43	-1.79	-2.92	-2.04	-2.67
21	-4.60	-2.35	-3.50	-3.91	-2.95	-3.86
42	-4.89	-2.92	-4.56	-4.86	-3.48	-5.20
70	-5.72	-4.52	-5.98	-5.76	-4.98	-7.02

The pattern seen in Figure 5.6 shows that lower strength concretes loses more water than the higher strength concretes, and when considering higher strength concretes 80MPa lost more

water than the 50MPa. The results revealed that 20MPa CEM1 concretes were more porous followed by 20 and 80MPa fly ash, 80MPa CEM1, 50MPa fly ash and 50MPa CEM1 concretes.

Figure 5.7 presents the percentage change in mass for CEM1 and fly ash concrete wet mix . Figure 5.7 shows similar pattern to the Figure 5.6 but with slight different. The wet mix especially at the early drying age percentage change in mass is the same with the stiff mix but at the later drying age 20MPa CEM1 and fly ash samples were having the same value and the 80MPa fly ash lost more water than the lower strength concretes as shown in Figure 5.7.

The Figures shows that in drying process concretes with larger pores evaporates more water.

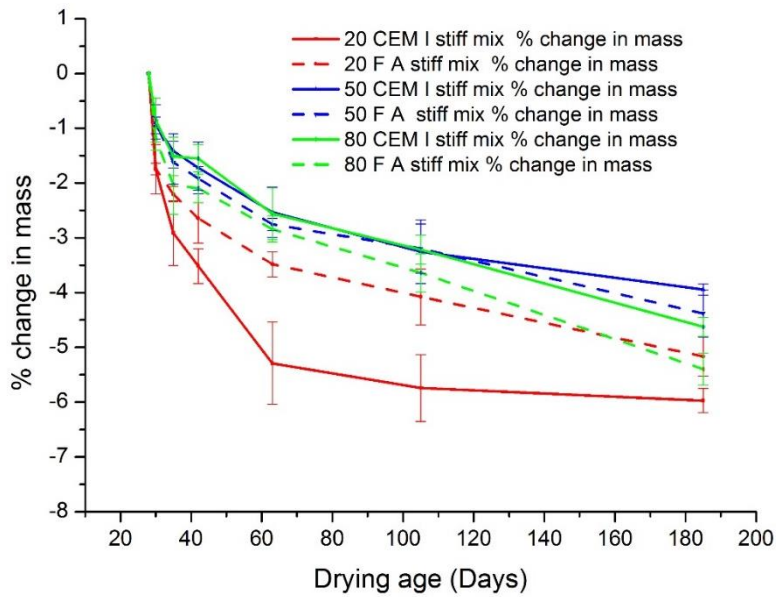


Figure 5-6 Percentage change in mass for CEM1 and fly ash concrete stiff mix

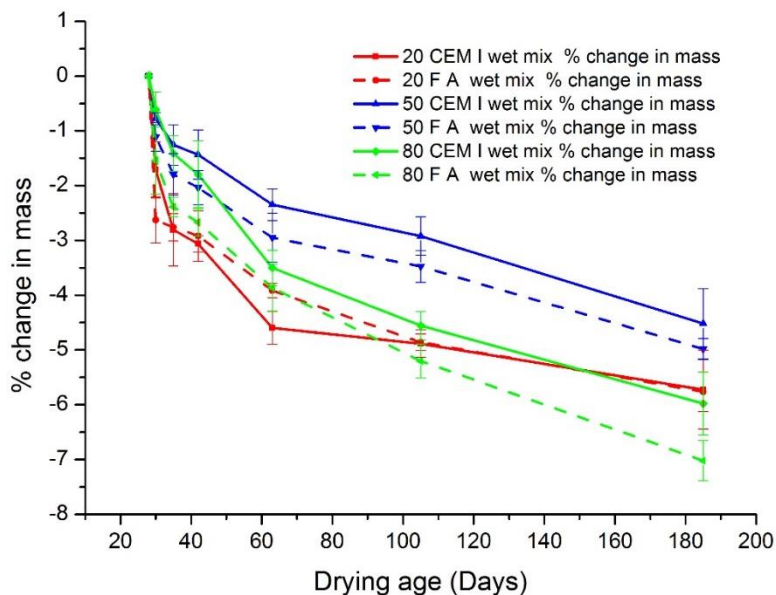


Figure 5-7 Percentage change in mass for CEM1 and fly ash concrete wet mix

5.7 Change in weight in ambient cured samples

The impact of degree of saturation on compressive strength was examined by immersing the ambient cured samples in water for three hours. The concrete samples were weighed before and after immersion before testing the compressive strength. Table 5.3 shows the percentage of water absorbed in three hours for CEM1 and fly ash concretes. Figure 5.8 and 5.9 shows the rate of water absorbed by the stiff and wet mix concrete samples. CEM1 concretes were presented in solid lines and fly ash concretes were shown in broken lines.

The rate of water absorption in stiff mix concretes presented in Figure 5.8 shows that 20MPa fly ash concretes absorbed more water than CEM1 concretes. When considering the high strength concretes 80 and 50MPa fly ash absorbed more water than CEM1 concretes. Also at 28 days 50 and 80MPa CEM1 concretes were having the same absorption rate.

Table 5-3 Change in weight in ambient cured samples

Age(Days)	20MPa CEM1	50MPa CEM1	80MPa CEM1	20MPa PFA	50MPa PFA	80MPa PFA
Stiff mix						
1	0.98	0.98	0.98	0.98	0.98	0.98
2	1.12	1.05	1.01	1.97	1.17	1.17
7	2.48	1.25	1.04	2.54	1.47	1.55
28	2.61	1.49	1.52	3.13	1.83	2.10
Wet mix						
1	0.98	0.98	0.98	0.98	0.98	0.98
2	1.61	0.95	1.12	2.05	1.38	1.28
7	2.23	1.23	1.40	2.64	1.80	1.76
28	3.09	1.84	1.97	3.26	2.32	2.49

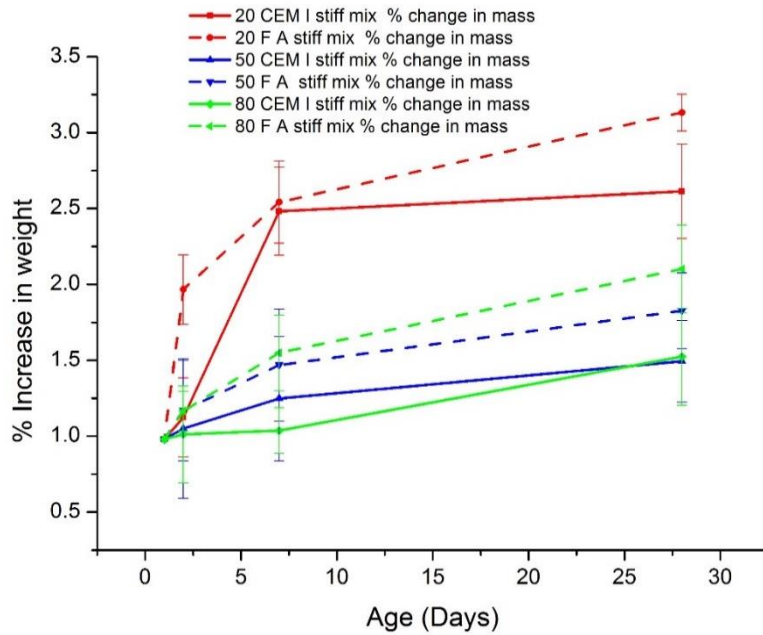


Figure 5-8 Percentage increase in mass for CEM1 and fly ash concretes in stiff mix

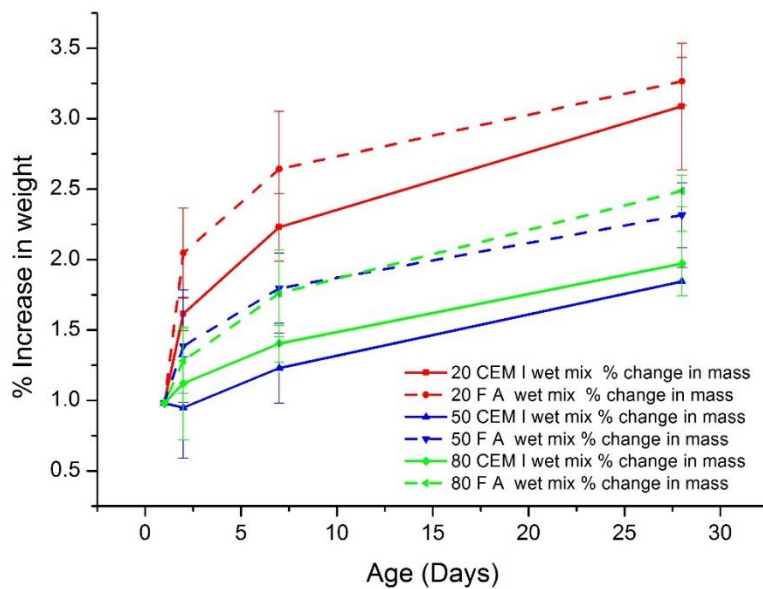


Figure 5-9 Percentage increase in mass for CEM1 and fly ash concretes in wet mix

The percentage increase in mass for CEM1 and fly ash wet mix concretes is presented in Figure 5.9. The Figure shows that fly ash concretes absorbed more water than CEM1 concretes in lower strength samples which is the similar to the result shown in Figure 5.8. The gap between the CEM1 and fly ash samples seen in wet mix is not as wide as the one shown in stiff mix. In high strength concretes the result is the same as the stiff mix concretes 80MPa fly ash absorbed more water than the 50MPa fly ash concretes. Also the difference between the 80 and 50MPa fly ash in wet mix is not as wide as the one seen in the stiff mix. The slight difference seen in 80 and 50MPa CEM1 wet mix is that 80MPa absorbed more water than the 50MPa from the early age up to the 28 days while in stiff mix 50MPa absorbed more water at

the early days and were having almost the value at the 28 days. Figures 5.8 and 5.9 shows that concretes with larger pores permits larger water absorption.

5.8 Conclusion

Effect of drying has been considered in this chapter, the result revealed that lower strength samples lost more moisture than the high strength concretes. This is due to the fact that the low strength mixes do have a higher water/cement ratio and so a greater porosity.

The effect of drying on the compressive strength as the concretes loses moisture in the oven is checked at various drying age, increase in compressive strength is obtained as the concrete lost moisture.

Since the age of the concrete is up to 190 days, fly ash concretes exhibit higher strength than CEM1 concretes at later age. This result confirms increase in strength at later age especially with the use of fly ash as partial replacement.

The mass loss as the concretes dries out shows that in drying process concretes with larger pores evaporates more water thus 20MPa concretes lost more water hence they are more porous. Also when the ambient cured samples were immersed in water, fly ash concretes absorbed more water than CEM1 concretes this revealed that fly ash concretes were more affected by improper curing and were more porous as samples with larger pores permits larger water absorption.

Chapter 6 Results and Discussion of Shrinkage Following ideal and Ambient Curing

This chapter presents the results of the study into shrinkage following curing under ideal and ambient conditions. Drying shrinkage is one of the significant factors that contributes to development of cracks which have extensive effect on failure, durability, serviceability and reliability of the structure. Thus, shrinkage of concrete is a very important property of concrete to be examined and also it is very essential to use an accurate prediction model to predict shrinkage.

Concrete prism of 75 x75x 200mm were used for the test. Twelve mixes were used also and each mix have the same water binder ratio with compressive strength samples. Two prisms were used for each curing condition. The ambient and ideal cured samples were casted at the same time with six concrete cubes of 100 x100 x100mm used for sorptivity test. Forty eight concrete prisms having the same variables with the compressive strength were casted. The test procedure has been explained in section 3.9 and the purpose of the test is to know the effect of improper curing on engineering performance.

The drying shrinkage result is presented with discussion of the results in this chapter. In analysing the data, according to BS EN 1992-1-1:2004+A1:2014: (300) it is assumed that the variations in the results that are within approximately $\pm 20\%$ are accurate and in agreement with theoretical predictions, as they can be connected to experimental tolerances.

The average ambient temperature and the relative humidity in the laboratory during the test period were $20^0 \pm 2^0\text{C}$ and $36 \pm 5\%$ respectively. Concrete samples were cast and demoulded after 24 hours. DEMECS were mounted on the two sides of the samples, ambient samples were stored in the control room having the temperature of $20^0 \pm 2^0\text{C}$ and relative humidity (RH) of $36 \pm 5\%$. The ideal cured samples were put in the fog room to cure for 28 days at the temperature of 20^0C and 99% RH. After curing the ideal samples were removed from fog room and kept in the same environment with the ambient samples. The drying shrinkage measurement of the samples were taken every week till the next six months. Ambient sample measurement is from day one in the control room while the ideal cured samples were taken after 28 days. Table 3.9 shows the parameters used in casting the concrete, i.e. the binders, targeted strengths, slumps, the calculated and the adjusted water content used to cast the cubes.

6.1 Effect of curing on drying shrinkage

The effect of curing on drying shrinkage is presented in Figure 6.1. The Figure shows the shrinkage of concretes measured when the samples were ambient and ideally cured. The result shows that the ambient cured samples have the highest shrinkage value than the ideal cured samples for lower (20MPa) and high targeted strengths (50 and 80 MPa), which were cured in the fog room before putting in the control room. The shrinkage obtained is the same for CEM 1 wet mix and fly ash concretes both stiff and wet mix and this is presented in the appendix. The result obtained is attributed to fact that the well cured concretes reduces drying shrinkage by protecting against moisture loss from fresh mixes (233). Curing is essential from the fact that hydration of cement can take place only in water-filled capillaries so in order to obtain a good concrete, the placing of an appropriate mix must be followed by curing in a suitable environment during the early stages of hardening and a loss of water by evaporation from capillaries must be prevented (17, 301). The most adequate method of

curing is to keep the exposed concrete surfaces moist continuously by ponding or spraying with water. This method keeps the concrete fully saturated during the curing period, and is ideal condition for strength development and hydration of cement (16). Curing helps concrete to develop enough tensile strength to resist contraction stresses. The continuous development of strength reduces shrinkage. This result agrees with similar findings (16, 221, 230, 231, 249-251, 254) .

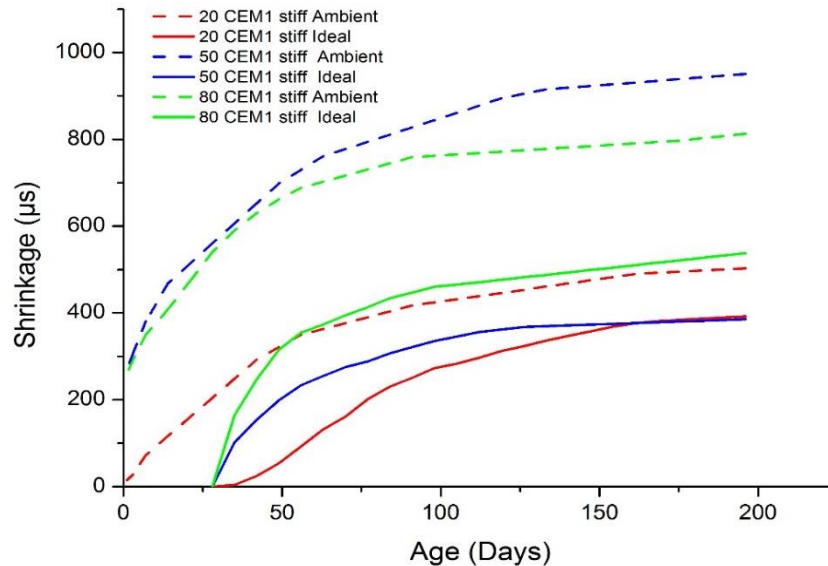


Figure 6-1 Ambient and Ideal Cured Shrinkage of CEM1 stiff mix

6.2 Predicted and experimental shrinkage

CEB-FIP Model code 90 and fib model code 2010 was used to predict the drying shrinkage based on the data that were used in the experiment. Such data were the compressive strength of the cubes to calculate f_{cm} [which is the mean compressive strength of concrete at the age of 28 days (MPa)]. This was converted to cylinder strength by multiplying the cube compressive strength by 0.85. The notational size of member calculated was based on the dimension used to cast the concrete samples for the drying shrinkage. Also the relative humidity of the control room at the time of the experiment which is $36 \pm 5\%$ was used to calculate the shrinkage. Figure 6.2 shows the development of shrinkage with time as calculated by using CEB-FIP Model code 90 and fib Model code 2010. The result of the predicted shrinkage from the model codes shows the uniform shrinkage distribution with time. The shape is the same in all the mixes for all the targeted strength and binders. The experimental results are compared with the shrinkage models discussed earlier.

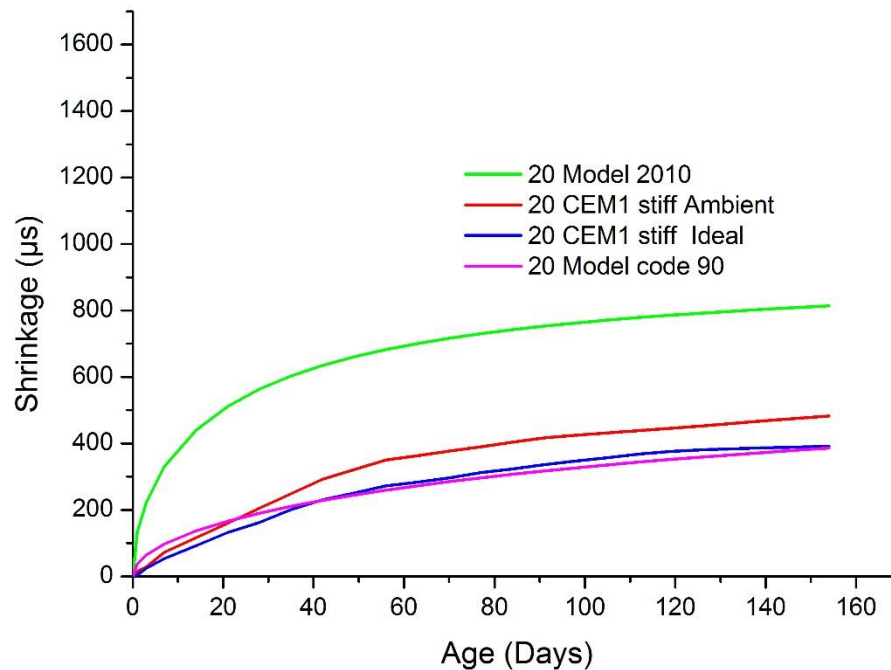


Figure 6-2 Predicted shrinkage and measured ambient and ideal Shrinkage for 20MPa CEM1 wet mix.

Measured ambient, ideal and predicted shrinkage strains of normal concrete having targeted strength of 20MPa are shown in Figure 6.2. The result shows that CEB-FIP model code 90 overestimate the shrinkage at the early age and under estimate at later age for ambient cured samples. The predicted value is almost the same for ideal cured samples. The Figure also shows that fib Model 2010 overestimate the shrinkage values both at early and later age. The result is similar to other findings (221).

Figure 6.3 shows the predicted shrinkage and the experimental shrinkage of high strength concretes. The predicted shrinkage value from model code 90 is very low to either ideal cured samples or ambient cured samples for 50MPa and 80MPa concretes. The same result is obtained for either stiff or wet mix concretes. This value agrees with other findings that the CEB-FIP 90 model underestimates the shrinkage strain for high strength concretes i.e. samples with compressive strength above 40 MPa (220, 228). In the CEB-FIP Model Code 1990, the concrete characteristic cylinder strength is specified up to 80N/mm². However, Clause 2.1.1.1 comments state that constitutive relations for concrete characteristic cylinder strength higher than 50N/mm² should be used with caution and appropriate judgement because available information on behaviour of concrete with characteristic cylinder strength higher than 50N/mm² is limited (222). Also in Figure 6.3, model code 2010 overestimate the ideal cured sample but underestimate the ambient cured sample but Figure 6.4 shows a slight different when considering the shrinkage of 80MPa. Model code 2010 underestimate ideal cured sample at early age but a little overestimate at later age while ambient cured samples were under estimated.

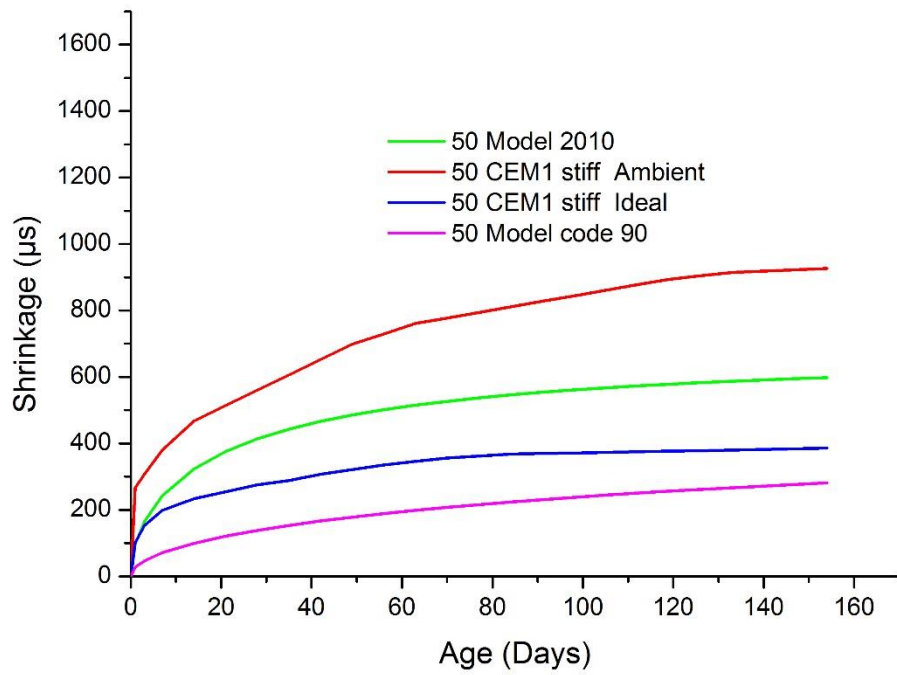


Figure 6-3 Predicted and Experimental shrinkage of 50MPa CEM1 stiff mix

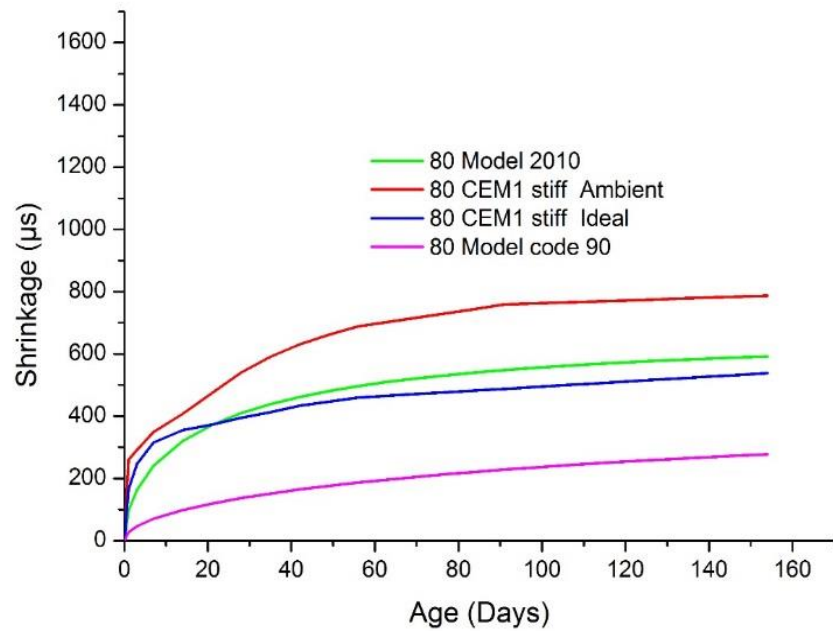


Figure 6-4 Predicted and experimental shrinkage of 80MPa CEM1 stiff mix

The rest of the result were shown in appendix for CEM1 wet mix and fly ash stiff and wet mix showing the same result with slight differences.

6.3 Normalised Shrinkage

Normalising the shrinkage of ambient cured samples at one day to shrinkage of ideal cured sample at 28 days is just to remove or eliminate the effect of moisture loss between the day one and the 28 days. This is achieved by subtracting the shrinkage values at 28 days of ambient cured sample from the rest of the ambient shrinkage values. The normalised shrinkage is necessary in order to compare the ideal shrinkage at 28 days with the ambient values. Figure 6.5 shows the normalised shrinkage value compared with the predicted and the ideal shrinkage. The result shows that the normalised ambient shrinkage has lower shrinkage than the ideal cured sample. This is the result obtained for the stiff and wet mixes CEM1 and fly ash samples presented in appendix.

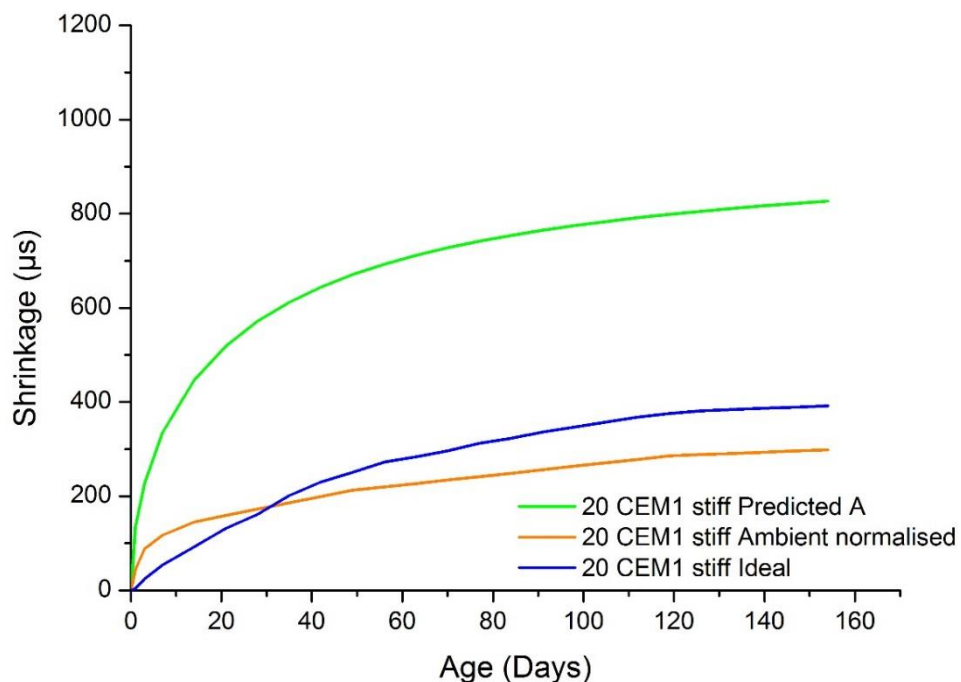


Figure 6-5 Normalised shrinkage with Model code 2010 for 20MPa CEM1

Incorporating the predicted value into normalised drying shrinkage also revealed that model code 2010 over predicted the drying shrinkage at early and later age for 20 and 50MPa. The predicted value it's almost the same with the ideal cured samples at 80MPa while the normalised shrinkage and ideal shrinkage were having the same value for 50MPa. The result of ambient normalised shrinkage with model code 2010 and all ideal drying shrinkage were the same with the predicted shrinkage which had been explained in the section 6. 2.

6.4 Effects of cement content on drying shrinkage.

The experiment involved three targeted strengths which were 20, 50 and 80MPa. The shrinkage of the three targeted strength were compared for two different binders and mixes. The cement content in 20MPa is the least among the three followed by 50MPa and 80MPa. The mixes with highest cement contents is 80MPa and has the highest shrinkage. The effects of drying shrinkage on cement content is shown in Figure 6.6.

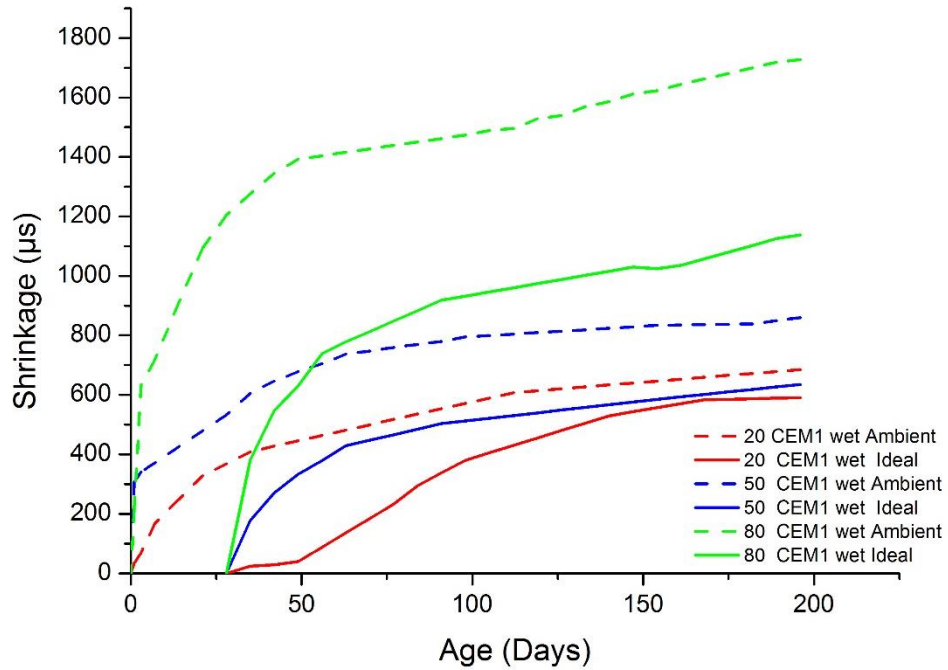


Figure 6-6 The effects of cement content on drying shrinkage

The result shows that higher cement content displayed higher shrinkage followed by 50 and 20MPa. The low strength concrete 20MPa has the least shrinkage either in ambient cured or ideal cured samples. Similar result is also obtained in fly ash concretes. The result obtained is similar to other findings where the higher cement contents in high strength concretes shrinks more. Bissonnette et al concluded that the effect of paste volume on shrinkage was significant, with drying shrinkage directly proportional to the paste volume content (201, 228). The only difference to this result is in stiff mix ambient cured samples where the 50MPa shrinks more than the 80MPa concretes, Also in stiff mix ideal cured samples 20MPa and 50MPa were having almost the same value.

6.5 Effects of water contents on shrinkage.

The effects of water content on drying shrinkage is examined by working on two different mixes. The stiff mix having the slumps between 10 to 30mm and the wet mix with slumps between 60 to 180mm. Figure 6.7 shows the shrinkage of stiff mix and the wet mix. In the figure all the wet mixes were designated with broken lines and stiff mixes with solid lines.

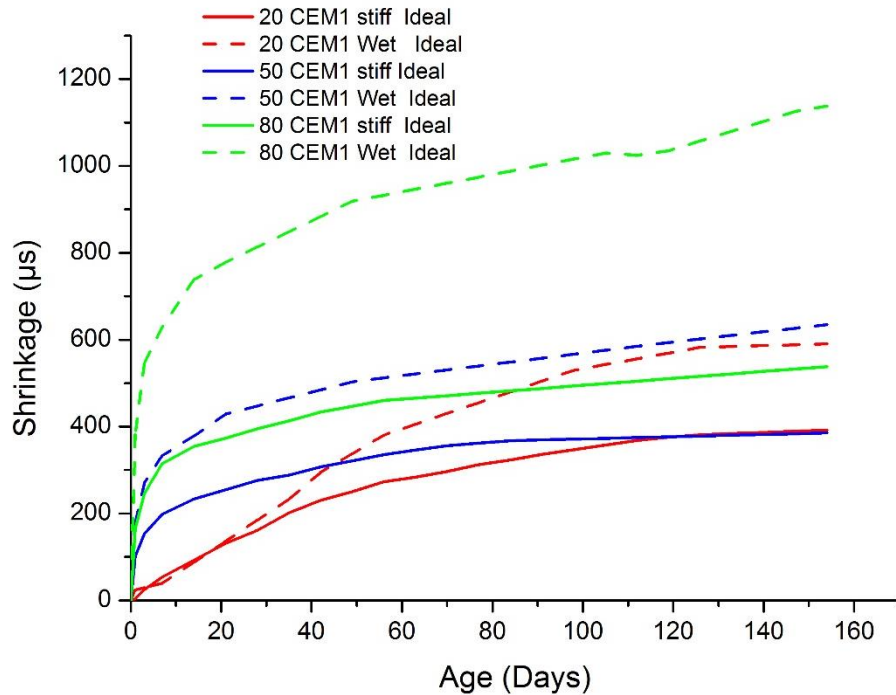


Figure 6-7 Shrinkage of Stiff mix and the Wet mix

The result from figure 6.7 shows that wet mix has the higher shrinkage value than the stiff mix. The same result is seen in the fly ash concretes either ambient cured or ideal cured. This is a proof that concretes with more paste content and water experience more shrinkage since these mixes have more paste and higher water content values which will make the concrete to be more porous hence resulting in a more open microstructure (207). Also increasing the unit water content can result in the increase of capillary water amount which will lead to more shrinkage strain (226). In 50MPa CEM1 ambient cured samples shows a different result where the stiff mix sample has higher shrinkage than the wet sample.

6.6 Effects of Fly ash on drying shrinkage.

The experiment used 30% fly ash as a replacement in all the mixes. The effect of shrinkage on fly ash is shown in Figure 6.8. In this Figure shrinkage of CEM1 concrete was compared with fly ash concretes and the result revealed that fly ash concretes have lower shrinkage values than the CEM1 concretes in all the wet mix for three targeted strengths. This is due to the fact that fly ash replacement will improve the pore structure of concrete by pozzolanic reaction which will lead to lower drying shrinkage of the fly ash concretes (244, 302). The result obtained is the same with other findings (92, 208, 245, 246).

The rest of the result is shown in the shrinkage appendix and the same result is seen for 20MPa stiff mix ambient and ideal cured samples, 50MPa stiff mix ambient cured samples while a slight different result is obtained for 50MPa stiff ideal cured sample, 80MPa stiff ambient cured sample and ideal cured sample. Here the CEM1 has a lower shrinkage than fly ash concretes. At 80MPa stiff ideal cured samples the fly ash shrinkage is lower initially but increased and it's slightly higher than CEM1 concretes.

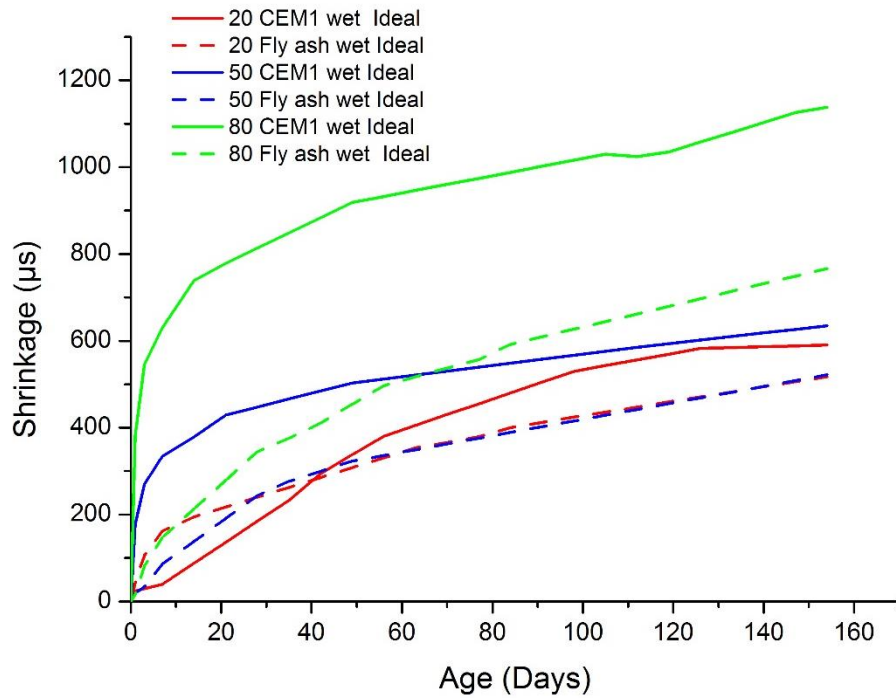


Figure 6-8 Shrinkage of CEM1 concretes and Fly ash concretes

6.7 Conclusions

Shrinkage of concrete is the principal cause for various kinds of cracks which affect the serviceability and durability of concrete. Thus the impact of improper curing on drying shrinkage was examined on CEM1 and fly ash concretes. Concretes that were not properly cured have the highest shrinkage value than the ideal cured samples. The result obtained is attributed to fact that the well cured concretes reduces drying shrinkage by protecting against moisture loss from fresh mixes.

The effect of drying shrinkage on volume of paste examined showed that the higher the cement contents in the mix the more the shrinkage.

When comparing the drying shrinkage of stiff and wet mix of CEM1 and fly ash concretes, wet mix has the higher shrinkage value than the stiff mix.

In all the mixes when comparing the drying shrinkage of fly ash concretes with CEM1, fly ash concretes has lower shrinkage values than the CEM1 concretes in all the wet mix for three targeted strength. This is due to the fact that fly ash replacement will improve the pore structure of concrete by pozzolanic reaction which will lead to lower drying shrinkage of the fly ash concretes.

CEB-FIP 90 model underestimates the shrinkage strain for high strength concretes while model code 2010 works better with high strength concretes.

Chapter 7 Transport properties and Resistance to Carbonation

7.1 Sorptivity

Having demonstrated the impact of improper curing on compressive strength development, and therefore by inference, on the degree of hydration (which is discussed in Chapter 8), this chapter presents the results concerning the impact of improper curing on transport properties and subsequently on the resistance to carbonation.

Sorptivity is an occurrence where by water is absorbed into concrete by capillary action. The process involves putting a sample with one surface just in contact with water and the mass of water absorbed by capillary action is measured at different time intervals. Absorption of water by capillary action is caused by the fineness of the capillary pores in the concrete. Thus measuring the rate of absorption provided a useful indication of the pore structure of concrete. Large capillaries will cause rapid absorption of water while in small capillaries absorption will be slow.

Concrete cubes of 100 x 100 x 100mm were used in the test. The samples were ambient and ideally cured for 28 days and dried in the oven at 40°C to constant mass for 100 days. The test was conducted on three triplicate samples and 72 concrete cubes were casted for the mixes.

Table 7.1 shows the sorptivity of CEM1 and fly ash concretes cured at 28 days. From the table it can be seen that the ambient cured samples has higher sorptivity value than the ideal cured samples. The effect on the workability is also considered and the result shows that the mixes having higher workability have higher sorptivity especially the ideal cured samples. Thus higher water content leads to higher sorptivity. The result also show that addition of fly ash produces lower sorptivity values.

Table 7-1 Effect of curing on sorptivity

	CEM1 Sorptivity, $k (m^3/m^2s^{1/2}) \times 10^{-8}$		30% fly ash Sorptivity, $k (m^3/m^2s^{1/2}) \times 10^{-8}$	
	Stiff	Wet	Stiff	Wet
20 Ideal	0.74	0.97	0.72	0.95
20 Ambient	2.35	2.44	2.52	2.44
50 Ideal	0.67	1.22	0.88	0.89
50 Ambient	1.22	1.76	1.52	1.88
80 Ideal	1.54	2.44	1.18	1.6
80 Ambient	2.56	3.95	1.88	2.77

The effect of curing on sorptivity is presented in Figure 7.1. The Figures show that the sorptivity coefficients of ambient cured concretes are higher than the ideal cured samples. This agree with other findings (93, 296). The Figure also shows that 80MPa wet mix ambient cured sample has the highest sorptivity value followed by 20MPa mixes. The effect of curing condition on the sorptivity coefficient of concrete appears to be higher in low-strength concretes. However, an increase in sorptivity was expected with decreasing compressive strength, but this was not observed. In every instance, the 20 MPa mixes showed higher

sorptivities than the corresponding 50 MPa mixes, but the 80 MPa mixes showed the greatest sorptivities of all. This was most likely due to the problems encountered in preparing the 80 MPa mixes, which were all difficult to mix. Similarly, there were no clear relationships between sorptivity and mass loss upon drying (as reported in Chapter 5), but the relationships were better when the 80 MPa mixes were ignored. In this case, the 20 MPa mixes, which showed higher sorptivities, also showed the greatest mass loss upon drying.

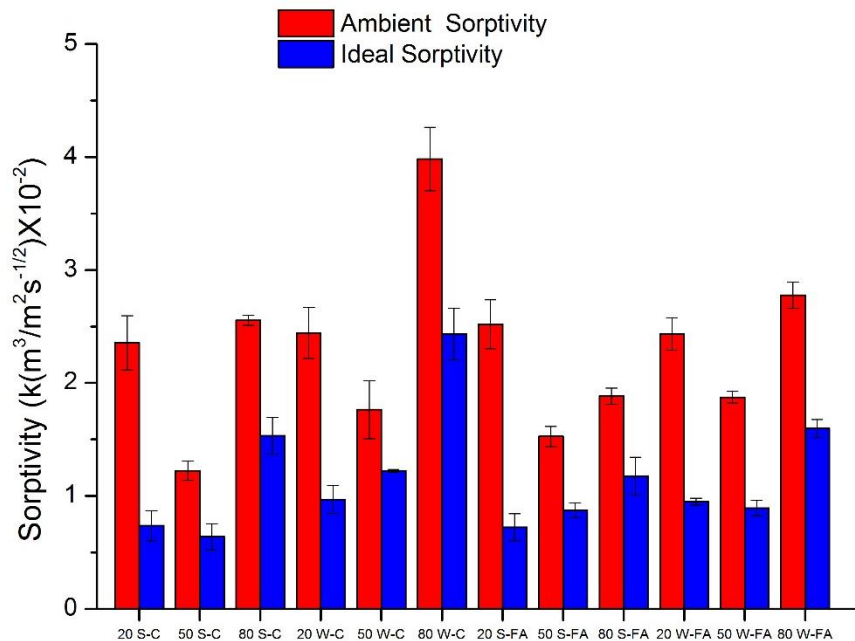


Figure 7-1 Effect of curing on sorptivity

The effects of stiff and wet mixes were checked on the sorptivity as shown in Figure 7.2. The Figure shows that the wet mixes showed higher sorptivities than stiff mixes. This is more noticed in the ideal cured samples.

Relating the sorptivity result with the weight loss due to drying in section 5. 2 was difficult. The wet mixes (Figure 5.7) generally lost slightly more mass upon drying than did the stiff mixes (Figure 5.6). However, these differences were not too clear-cut.

There is no clear relationship between mass loss and sorptivity value. The ability to discern any trends was complicated by the data from the 80 MPa mixes. Ignoring these, the trends could be understood a little more clearly, but it is difficult to make firm conclusions based on pairs of data. Further problems will have arisen due to continued hydration during sample drying, thus affecting the results, with porosity changing over time (reduced progressively).

The sorptivity of CEM1 and fly ash concrete is shown in Figure 7.3. It can be seen from the Figure that fly ash concretes were having lower sorptivity value than CEM1 concretes. Addition of fly ash produced lower sorptivity values than CEM1 particularly the ideal cured samples. This agree with other findings (71, 92, 133, 296, 297, 303) .

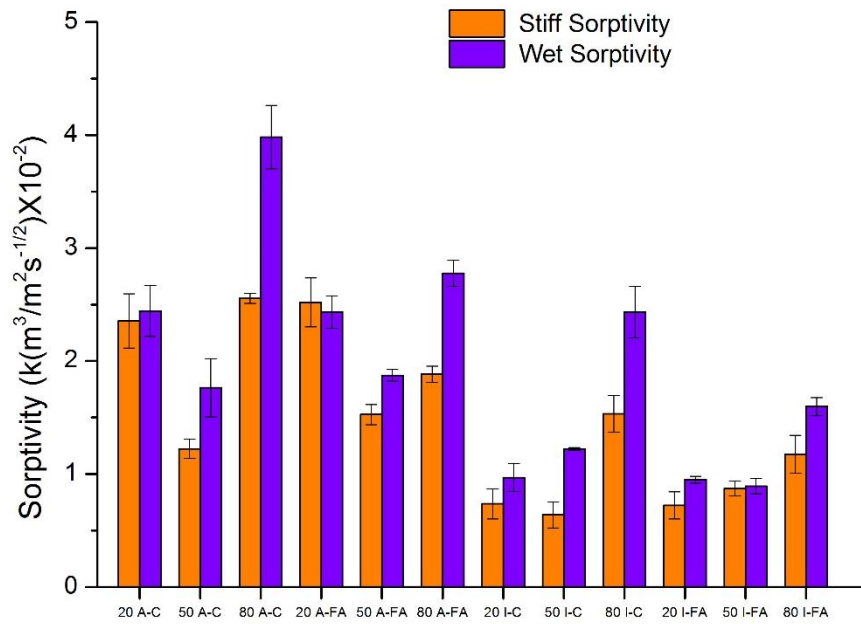


Figure 7-2 Effect of stiff and wet mixes on sorptivity

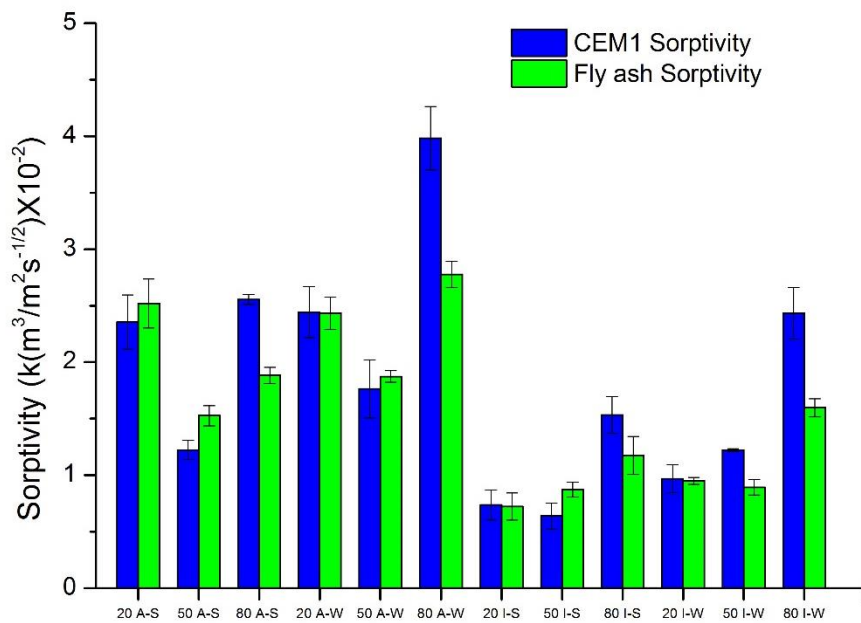


Figure 7-3 Sorptivity coefficient of CEM1 and fly ash concretes

7.2 Permeability

Permeability of concrete is a characteristic that measures the flow of fluid through concrete under a pressure gradient. This makes it different from capillary water absorption and is significant in water retaining structures.

Concrete samples of 50mm diameter and 40mm height were casted using PVC pipe and cured for 28 days. Following curing, the samples were placed in an oven to dry to constant weight at 40± 2°C for 60 days. This drying temperature was selected as being high enough to allow for pore water to be driven off in a reasonable time and not so high as to result in decomposition

of the C-S-H or the ettringite. All mixes were tested in triplicate following curing under ideal and ambient conditions.

Table 7-2 Ambient and Ideal Permeability coefficients

	Ambient Permeability (10 ⁻¹⁶ m ²)	Ideal Permeability (10 ⁻¹⁶ m ²)	Percentage increase upon ambient curing
20MPa Stiff mix CEM 1	6.26	0.29	2160
50MPa Stiff mix CEM 1	1.65	0.14	1180
80MPa Stiff mix CEM 1	2.74	0.66	313
20MPa Wet mix CEM 1	7.00	0.61	1150
50MPa Wet mix CEM 1	2.01	0.23	870
80MPa Wet mix CEM 1	3.34	0.83	301
20MPa Stiff mix fly ash	6.38	0.45	1420
50MPa Stiff mix fly ash	1.64	0.16	1030
80MPa Stiff mix fly ash	3.81	0.39	880
20MPa Wet mix fly ash	5.60	0.30	1870
50MPa Wet Mix fly ash	2.57	0.21	1220
80MPa Wet mix fly ash	5.04	0.52	872

The permeability results of ambient and ideal cured samples of CEM1 and fly ash concretes from the various samples are presented Table 7.2. From the table the permeability of ambient cured samples are higher than the ideal cured samples. The impact of improper curing on all samples was immediately clear, there being at least a ten-fold increase in permeability for almost all ambient-cured samples compared to their ideal-cured equivalents. The key factor in determining the effect of improper curing on permeability was the compressive strength, with the 20 MPa samples exhibiting an average increase in permeability about 50% greater than the 50 MPa samples.

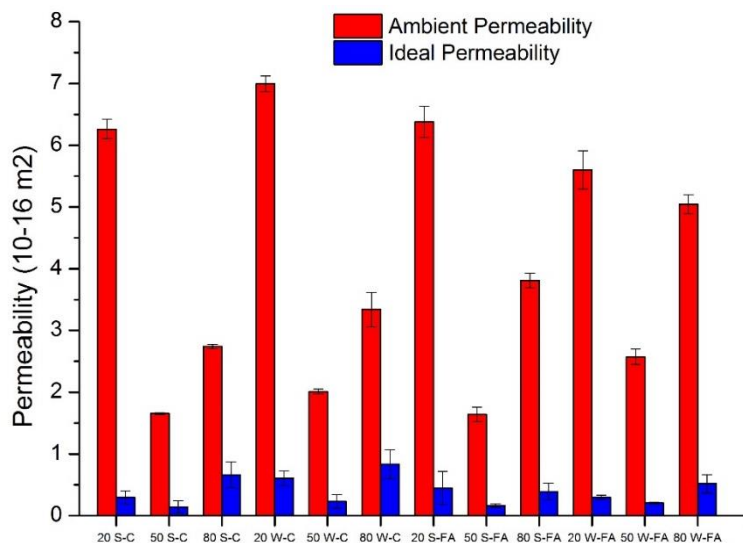


Figure 7-4 Ambient and ideal permeability of CEM1 and fly ash concretes

Also Figure 7.4 shows the impact of curing on permeability. The Figure show the huge difference between the ambient cured and the ideal cured samples. Low strength ambient cured concretes were more affected with higher permeability followed by 80MPa and 50MPa were having the least values. The pattern is the same for stiff and wet mix CEM 1 and fly ash concretes. The Figure also show that in all ideal cured samples 50MPa concretes were having the least permeability value in stiff and wet mix ,CEM1 and fly ash samples.

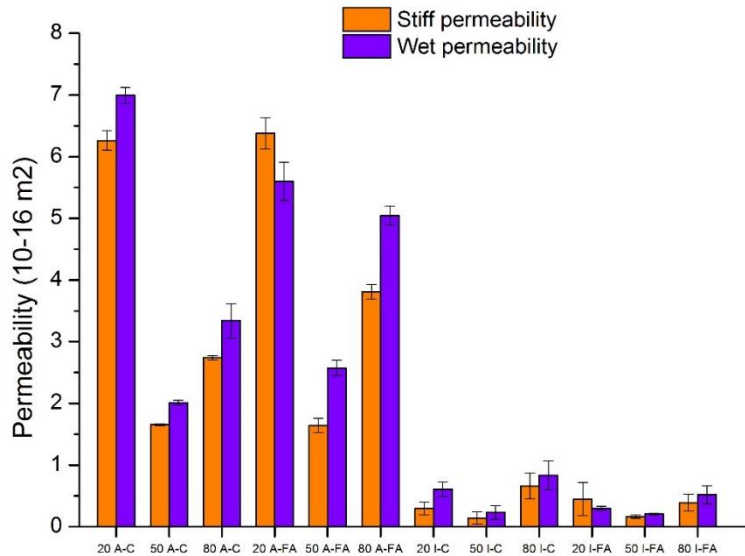


Figure 7-5 Effect of different mixes on permeability

The effect of stiff and wet mixes on permeability is shown in Figure 7.5. The Figure shows that wet mixes generally showed higher permeabilities than their equivalent stiff mixes, both following ideal and ambient curing.

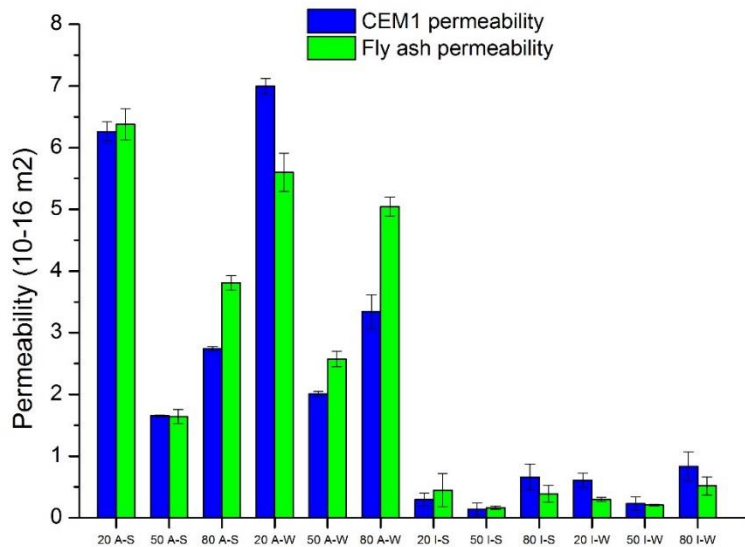


Figure 7-6 Permeability of CEM1 and fly ash concretes

The permeability of CEM1 and fly ash concretes is shown in figure 7.6. The Figure shows that in all ideal cured wet mix fly ash concretes and 80MPa stiff mix ideal cured samples, CEM1 has higher permeability than fly ash concretes. In all ideal cured stiff mix fly ash concretes, the fly ash has higher permeability than CEM1. The effect is more pronounced on the fly ash ambient cured samples. This agrees with other findings (83, 265, 297, 304). The effect of binder type

was less clear-cut. Stiff fly ash-containing concretes had higher permeabilities than their CEM1 equivalents, but wet fly ash containing mixes showed lower permeabilities.

7.3 Carbonation

The depth of carbonation was determined on 100 x 100 x 100mm concrete cubes cured for 28 and 90 days. After curing, samples were allowed to dry in an ambient environment for two weeks. This step is necessary to stabilize the internal relative humidity of the concretes, and reduce the variation in the internal relative humidity between the concrete samples before subjecting them to accelerated carbonation tests.

Carbonation depths were determined by spraying a freshly broken surface with alcoholic 1% phenolphthalein solution. The average depths of carbonation were measured at two points perpendicular to three faces of the broken concrete cubes. The depths of penetration of the trowelled face were ignored due to the influence of trowelling.

The carbonation depth of 20MPa CEM1 and fly ash concretes is presented in Figures 7.7 to 7.9. Test were performed on the three targeted strengths 20,50 and 80MPa but all the higher strength concretes (50 and 80MPa) did not carbonated either ambient or ideal cured. The results of 90 days cured samples for CEM1 and fly ash concretes were presented in appendix.

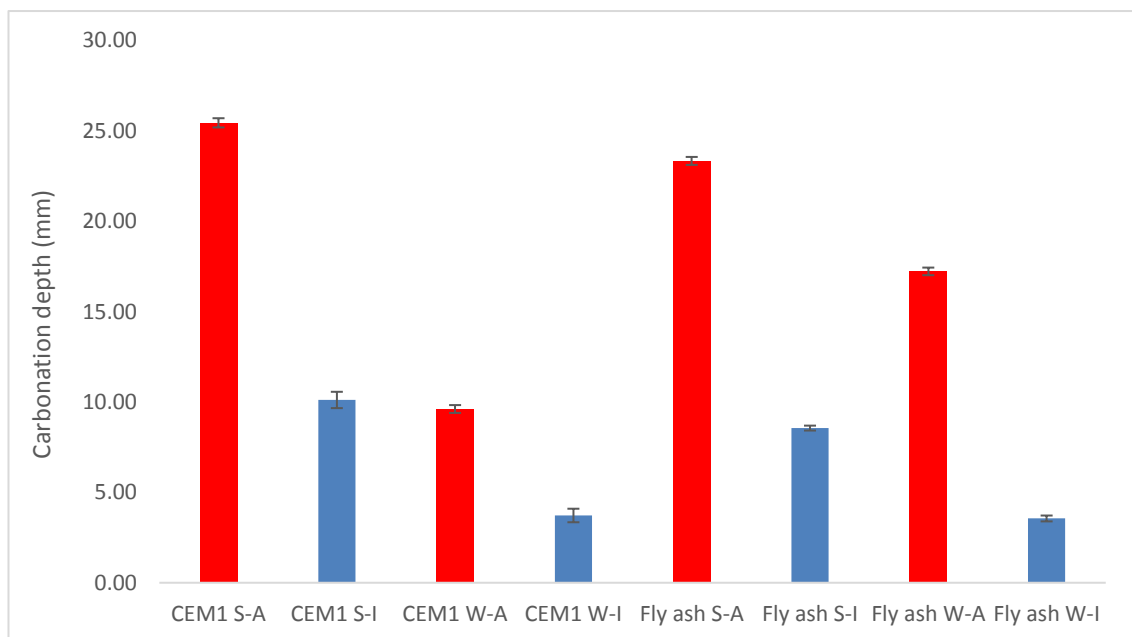


Figure 7-7 Carbonation depth of ambient and ideal cured samples at 28 days

Figure 7.7 shows the carbonation depth of ambient and ideal cured samples of CEM1 and fly ash concretes. From the Figure it can be seen that ambient samples have higher carbonation depth than the ideal cured samples. This can be associated to the fact that curing helped to increase the degree of hydration, thereby reducing the porosity and, thus, the permeability of concrete. This results agree with other findings (88, 146, 305-307). Ambient curing had a detrimental effect on carbonation resistance.

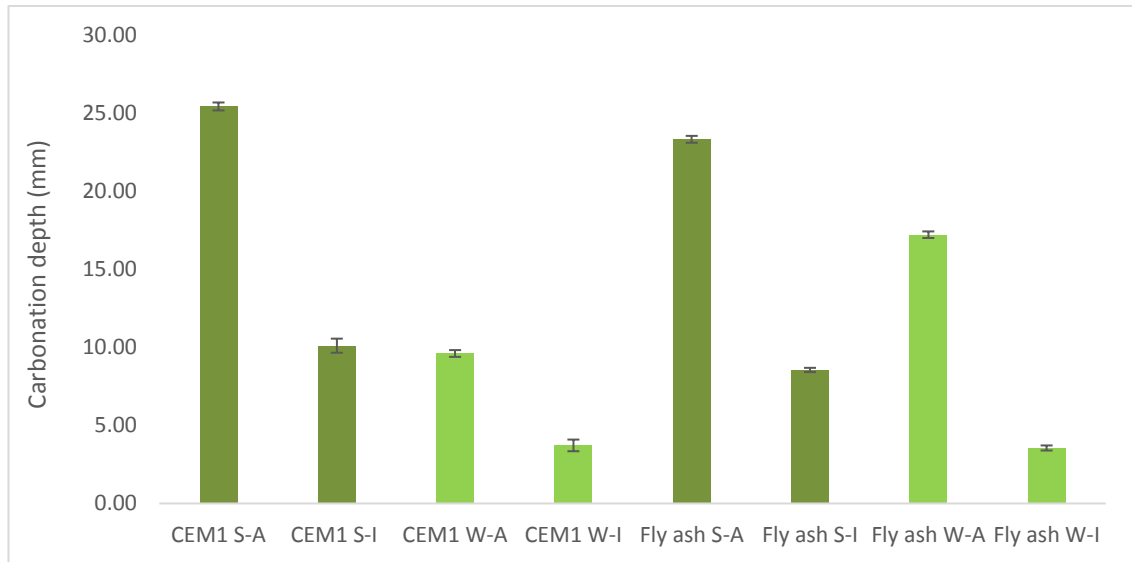


Figure 7-8 Carbonation depth showing stiff and wet mix of ambient and ideal cured samples at 28 days

The carbonation depth showing stiff and wet mix of ambient and ideal cured samples is shown in Figure 7.8. From the Figure stiff mixes concretes carbonated to a greater depth than the wet mixes. Stiff mixes showed slightly higher carbonation rates than wet mixes, but the impact of improper curing was not related to concrete workability. The slightly improved carbonation resistance may be due to the higher degree of hydration in the stiff mixes (Chapter 8) and also the slightly lower sorptivity (Section 7.1).

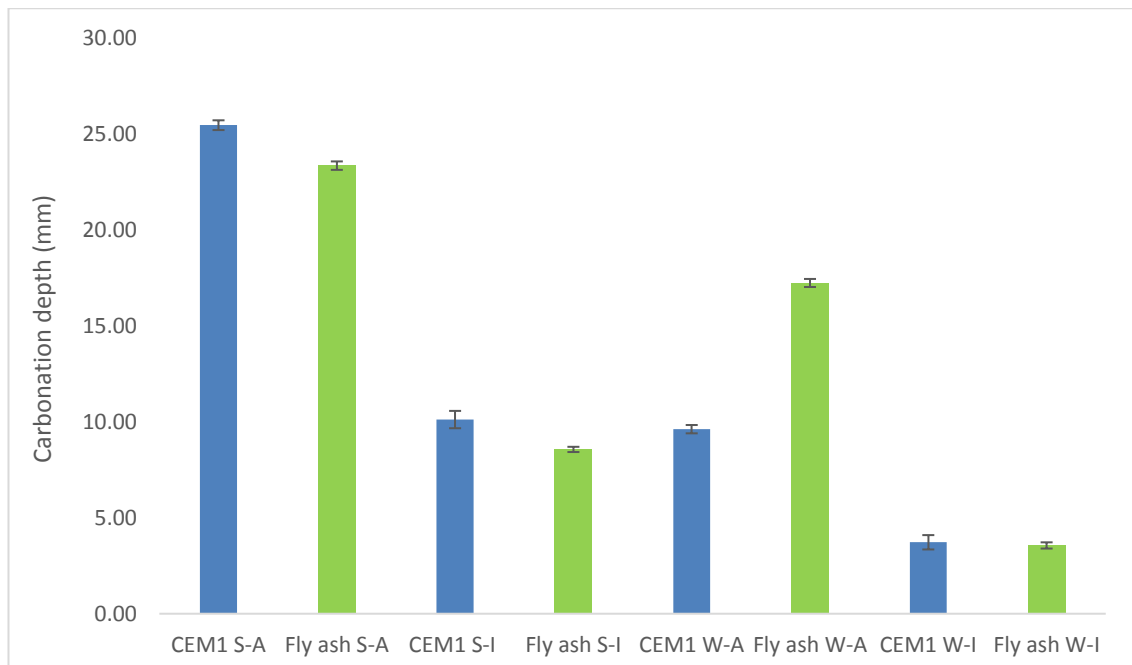


Figure 7-9 Carbonation depth of CEM1 and Fly ash concretes at 28 days

The carbonation depth of CEM1 and fly ash samples is presented in Figure 7.9, the Figure shows that ideally cured fly ash blends performed better than the equivalent CEM1 mixes. Also the composite wet mix samples cured under ambient conditions behaved considerably

worse than the CEM1 equivalents. This result agrees with other findings (85, 88). Figure 7.10 shows the carbonated samples of stiff mix ambient and ideal cured of CEM1 and fly ash concretes.

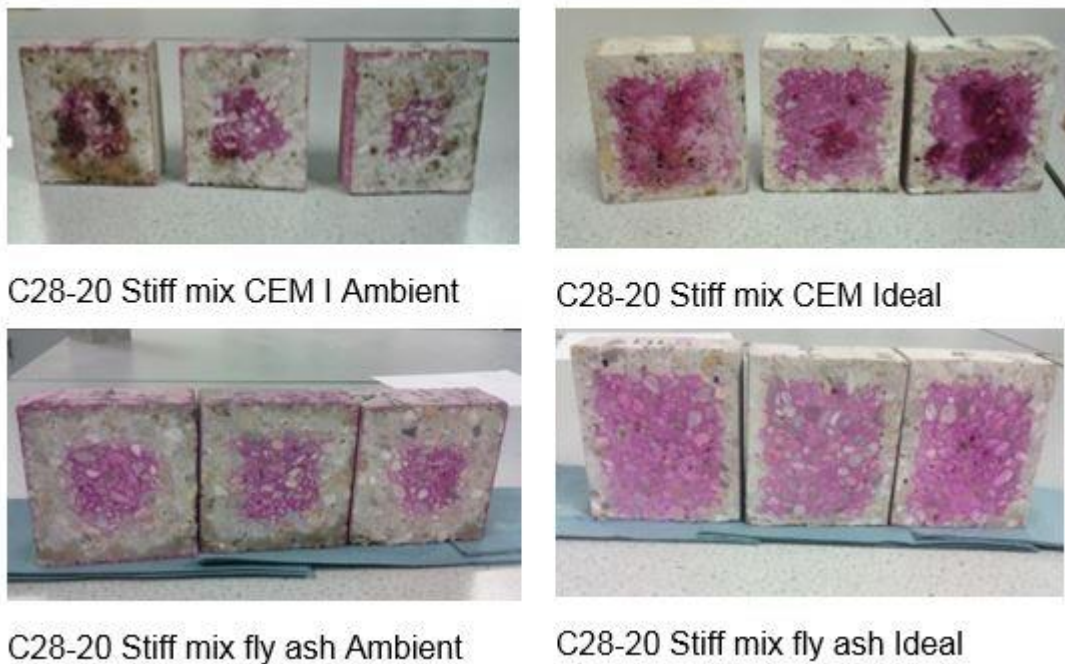


Figure 7-10 Selected Carbonated samples of 20MPa Stiff Mix

7.4 Summary

The effect of improper curing on transport property and resistance to carbonation in this chapter. The following were the conclusions made on sorptivity

- the sorptivity coefficients of ambient cured concretes are higher than the ideal cured samples and the effect of curing condition on the sorptivity coefficient of concrete appears to be higher in low-strength concretes. This result support the result obtained in mass loss due to drying where the more porous samples lost more water.
- the wet mixes were susceptible to higher sorptivity than the stiff mix which is more noticed in all the ideal cured samples.
- Addition of fly ash produced lower sorptivity values than CEM1 particularly in the ideal cured samples.

The impact of improper curing on Permeability also concludes that:

- ambient cured samples were having higher permeability than the ideal cured samples. There is about ten-fold increase in permeability for almost all ambient-cured samples compared to their ideal-cured equivalents. Also as seen in sorptivity low strength ambient cured concretes were more affected with higher permeability.
- wet mixes generally showed higher permeabilities than their equivalent stiff mixes, both following ideal and ambient curing.
- The effect of binder type was less clear-cut. Stiff fly ash-containing concretes had higher permeabilities than their CEM1 equivalents, but wet fly ash containing mixes showed lower permeabilities.

The effect of improper curing on resistance to carbonation showed that:

- ambient samples have higher carbonation depth than the ideal cured samples. This can be associated to the fact that curing helped to increase the degree of hydration, thereby reducing the porosity and, thus, the permeability of concrete.
- stiff mixes concretes carbonated to a greater depth than the wet mixes.
- concerning binder type, there were no clear, consistent trends in the data but ideally cured fly ash blends performed better than the equivalent CEM1 mixes.

Chapter 8 Degree of hydration

Conclusions from the previous sections has demonstrated that non-ideal curing affected strength development and transport properties. The loss of water from the hydrating cement had impaired performance. As discussed, the presence of water is essential for continued hydration. Therefore, paste samples were prepared with matching water/binder ratios to equivalent concrete samples and cured under ideal or non-ideal conditions. These paste samples were then characterised to determine the degree of cement hydration.

Figures 8.1 and 8.2 shows selected SEM images of ambient and ideal cured samples of CEM1 and fly ash concrete having the scale of 100 μ m. The field of view in each image is 326 x 244 μ m. Also Figures 8.3 and 8.4 compare the ambient and ideal images of CEM1 and fly ash Concretes. The Figures revealed the capillary structure of the ambient cured and ideal cured samples. The ambient cured samples were more porous than the ideal cured samples. The images also shows the porosity of wet mixes.

The ideally cured samples show a mixture of hydrated cement paste, residual anhydrous material and coarse porosity (with the smallest feature being ca. 2x2 microns). The wet mixes were more porous than the dry mixes. This is in line with the intrinsic permeability measurements presented earlier in section 6.4 .

Changing the binder from CEM I to 30% fly ash blend did not appear to have a significant effect on the microstructure just the initial view but this will be quantified later.

Ambient curing led to reduced degrees of hydration, evidenced by the increased presence of anhydrous clinker. The ambient cured samples also showed considerably higher coarse porosities. However, under ambient curing, it seems that wet mixes show higher degrees of hydration, but even then it's not conclusive.

20MPa CEM1 stiff mix ambient

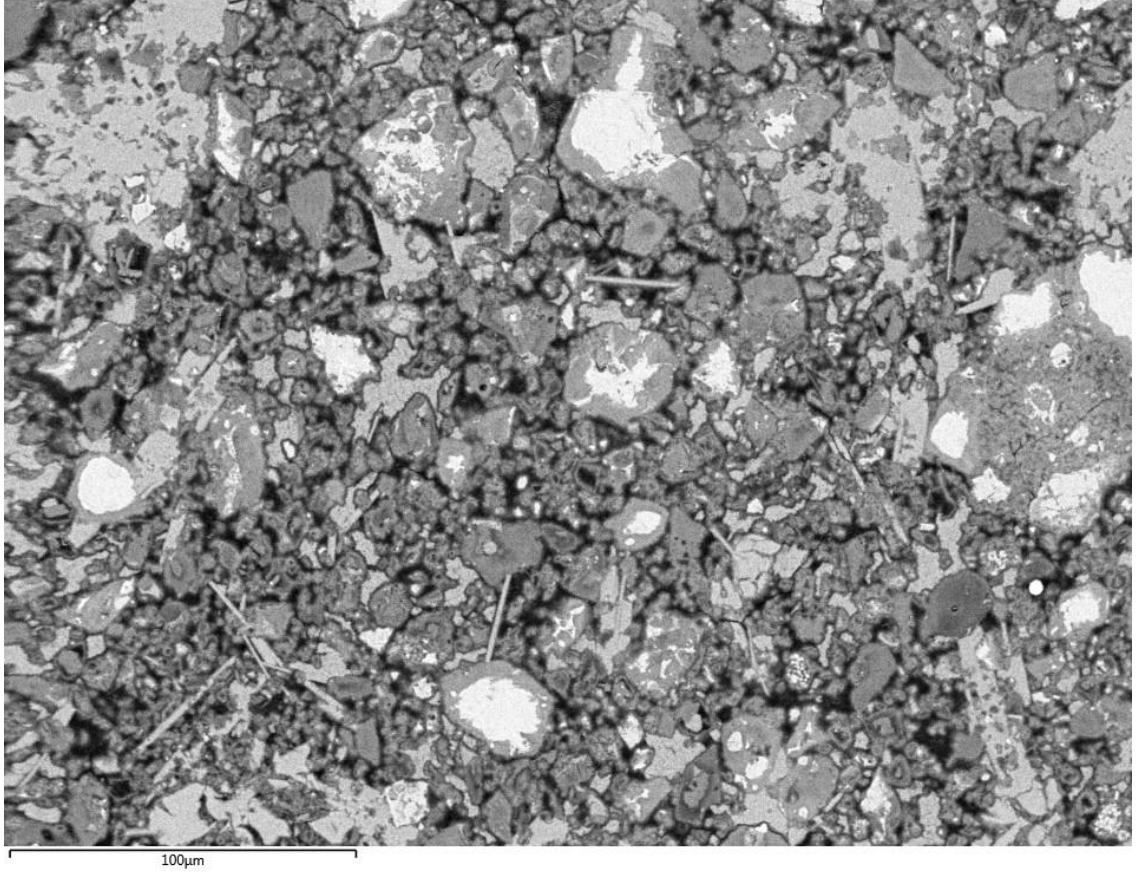


Figure 8-1 20MPa CEM1 Stiff mix Ambient cured

20MPa fly ash stiff ambient

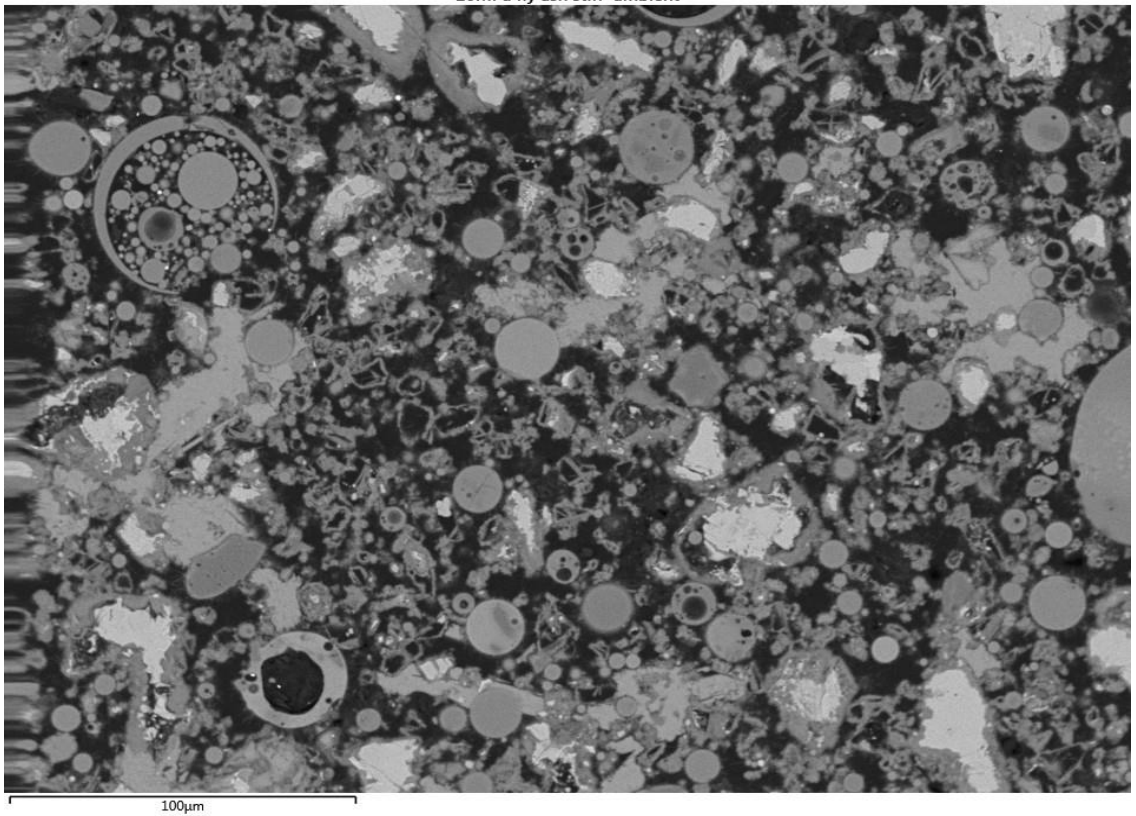
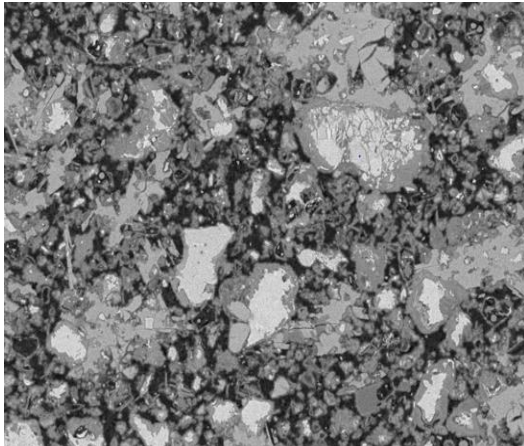
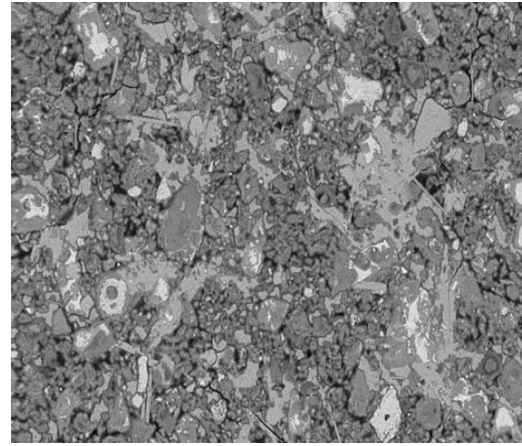


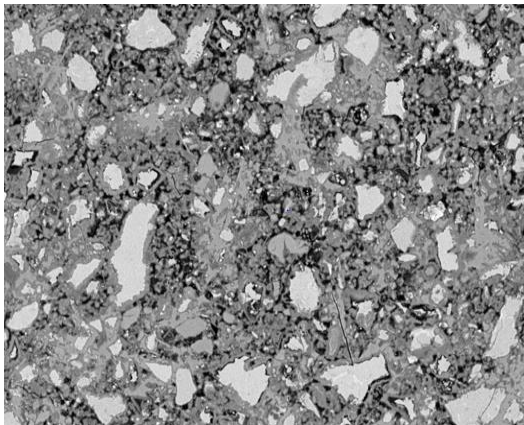
Figure 8-2 20MPa fly ash stiff mix Ambient cured



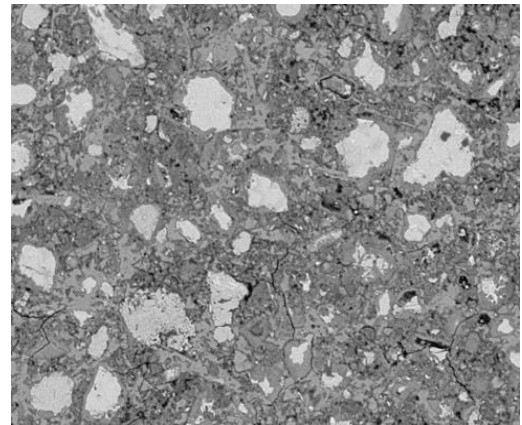
20MPa Stiff mix Ambient cured



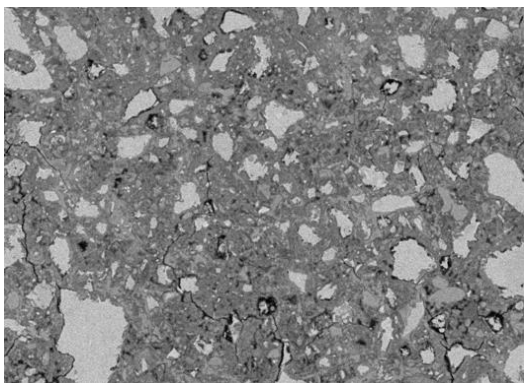
20MPa Stiff mix Ideal cured



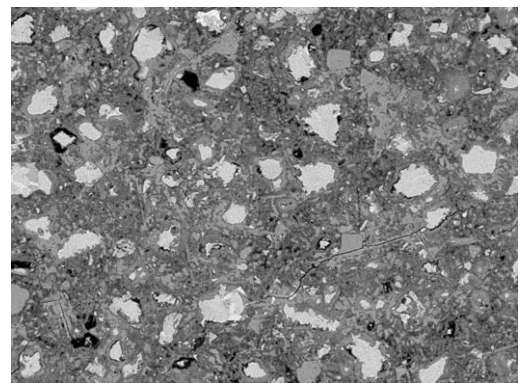
50MPa Stiff mix Ambient cured



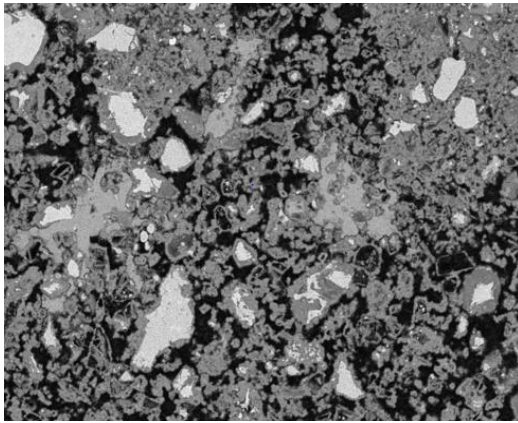
50MPa Stiff mix Ideal



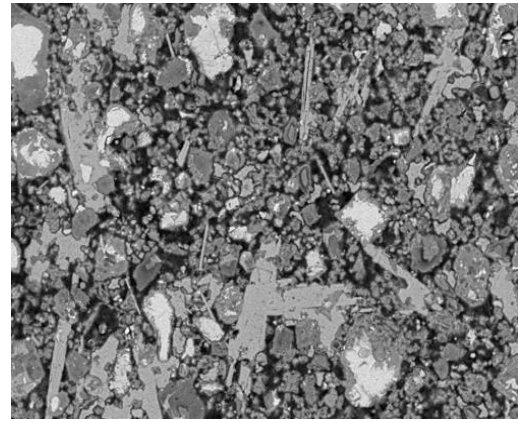
80MPa Stiff mix Ambient cured



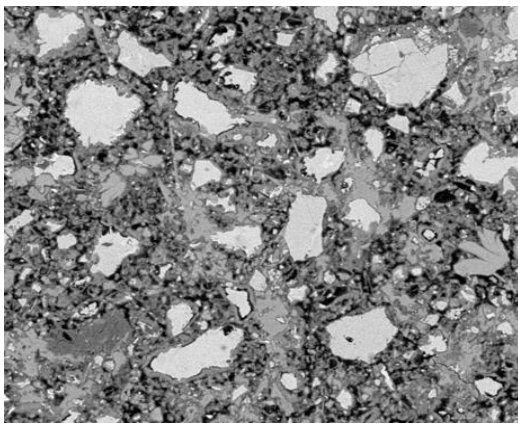
80MPa Stiff mix Ideal cured



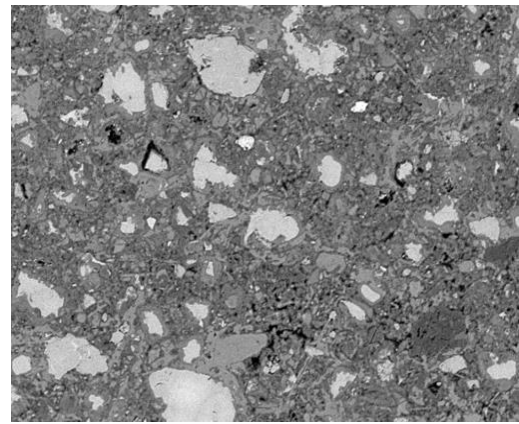
20MPa Wet mix Ambient



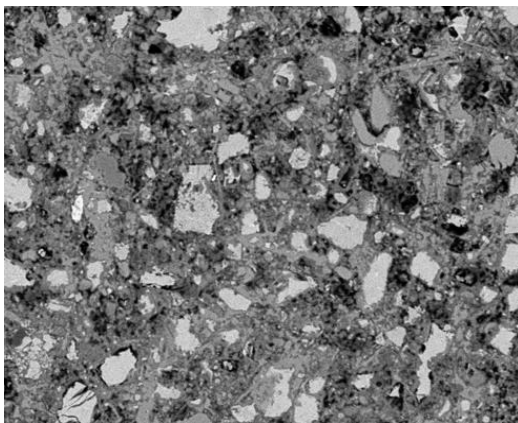
20MPa Wet mix ideal cured



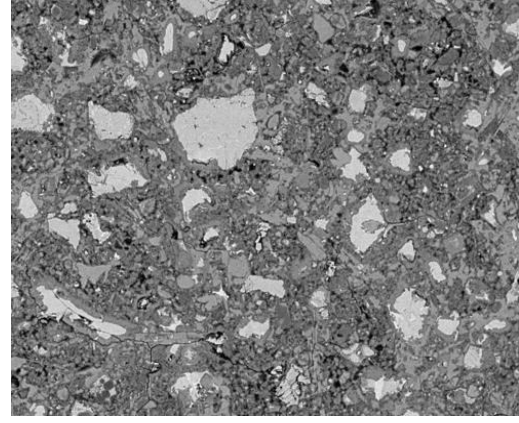
50MPa Wet mix Ambient cured



50MPa Wet mix Ideal cured

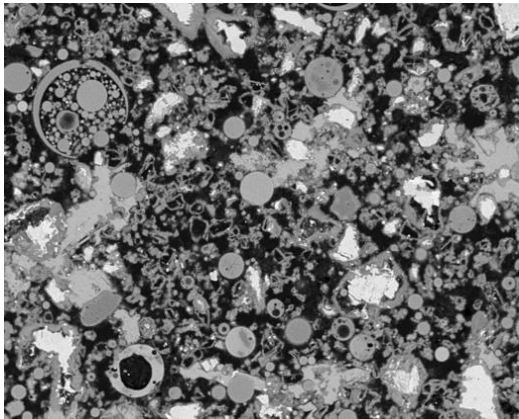


80MPa Wet mix Ambient cured

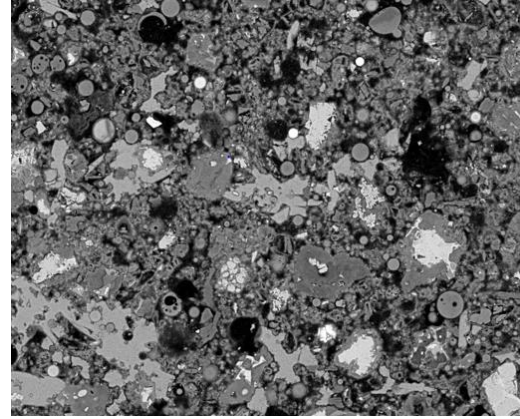


80MPa Wet mix Ideal cured

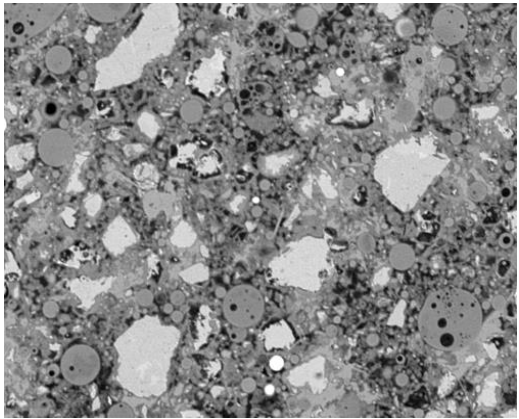
Figure 8-3 SEM images of CEM1 stiff and Wet mix



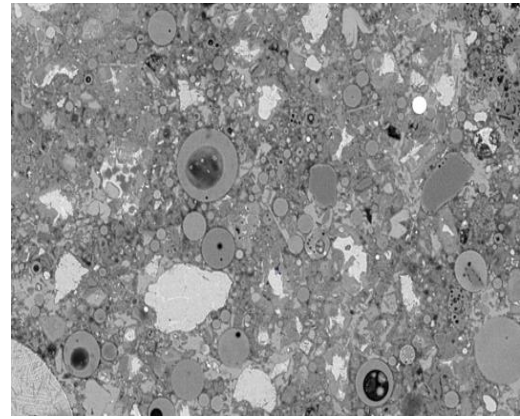
20MPa Stiff mix Ambient



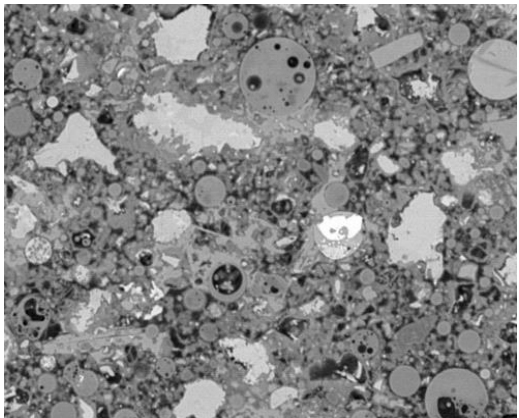
20MPa Stiff mix Ideal



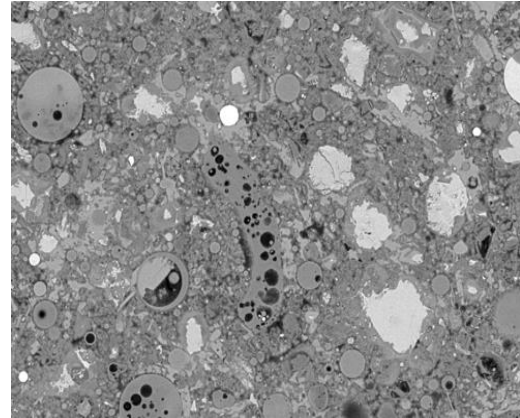
50MPa Stiff mix Ambient



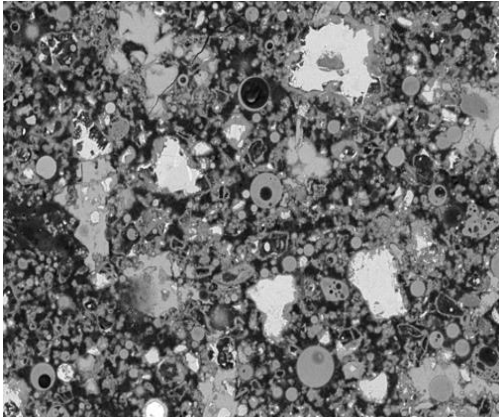
50MPa Stiff mix Ideal



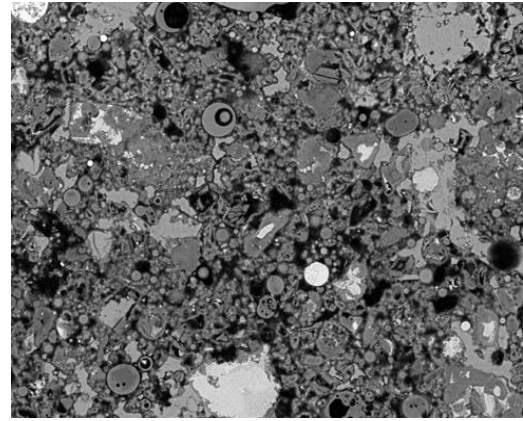
80MPa Stiff mix Ambient



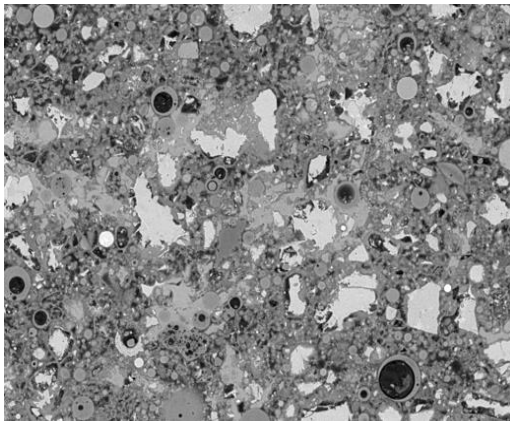
80MPa Stiff mix Ideal



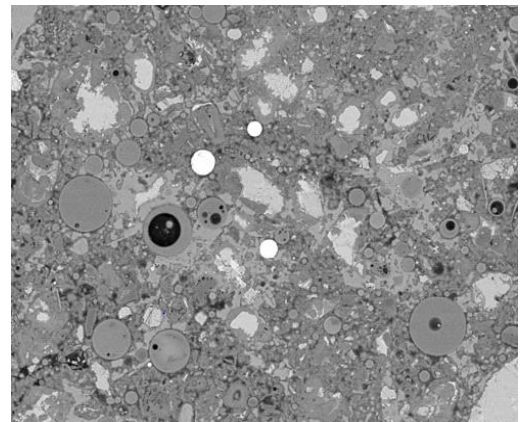
20MPa Wet mix Ambient



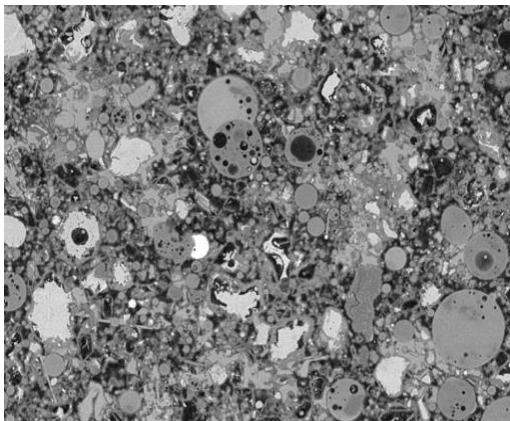
20MPa Wet mix Ideal



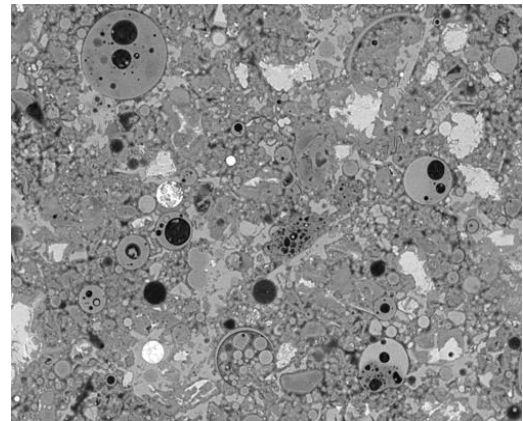
50MPa Wet mix Ambient



50MPa Wet mix Ideal



80MPa Wet mix Ambient



80MPa Wet mix Ideal

Figure 8-4 SEM images of Fly ash stiff and wet mix

8.1 Degree of cement hydration from SEM images

The degree of hydration was measured on 30 images obtained at 400X magnification using the method described by Whittaker, Kocaba, Haha (109, 279, 280). Scrivener (60) suggested a minimum of 10 images with 400X magnification while work within our laboratory though not published has found that the accuracy is about $\pm 3\%$. Fifty images at 800X were used but a further increase in the number of images result to standard error reduction without changing the mean. The degree of hydration from SEM images were calculated by using image j.

8.1.1 Image J

Image J as explained by Ferreira and Rasband (308) is a general field of Java image processing and program analysis that runs, either as an online applet or as a downloadable application, on any computer with a Java 1.5 or later virtual machine. Downloadable circulations are accessible for Windows, Mac OS X and Linux. It can display, edit, analyse, process, save and print 8-bit, 16-bit and 32-bit images. Many image formats including TIFF, GIF, JPEG, BMP, DICOM and FITS can be read by image J.

Area and pixel value statistics selected by the user can be calculated by image J. It measures distances and angles, creates density histograms and line profile plots. Image J supports standard image processing functions such as contrast manipulation, sharpening, smoothing, edge detection and median filtering.

The analysis started by opening each image by clicking the file on the image J main window. ImageJ's main window have only a menu bar having all the Menu Commands, a Toolbar, a Status bar and a Progress bar. Images, histograms, profiles, widgets, etc. are presented in additional windows. Measurement results are shown in the Results Table. Image J converts 8-bit to 8-bit grayscale with the minimum to maximum value ranging from 0–255. The steps involved in using image j were outlined in the flow chart as Figure 8.5 but all the pictures of image j were shown in SEM appendix.

8.1.2 Image analysis

Image analysis was carried out on BSE–SEM images to determine the degree of hydration. All the 30 images used to calculate the degree of hydration for each mix were presented in SEM appendix. A consistent analysis technique was applied to all the images by using a grey level histogram which has been outlined in Figure 8.5. The histogram was obtained for each image. Four components of the hydrated paste microstructure: capillary porosity, calcium hydroxide (CH), calcium silicate hydrate gel along with other hydration products, and unhydrated cement will be displayed by the histogram. The histogram also indicates the number of pixels in the image having each possible brightness value (between 0 and 225). Pores in the microstructure appear as dark spots on the electron images and can be easily distinguished from the hydrated phases (C-S-H and CH), C-S-H are dark grey.

The Java applet Image J was used to calculate the amount of unreacted cement, from which the equation below was used to calculate the degree of hydration for cement and fly ash blends.

$$DH_{SEM}^{cem}(t) = 1 - \frac{V_{(t)cem}}{V_{(o)cem}}$$

$$DR \frac{SCM}{SEM} (t) = 1 - \frac{V_{(t)SCM}}{V_{(o)SCM}}$$

Where:

$V_{(o)cem}$ is the volume fraction of cement before hydration

$V_{(o)SCM}$ is the volume fraction of unreacted SCM before hydration

$V_{(t)cem}$ is the volume fraction of unhydrated cement at hydration time t, and

$V_{(t)SCM}$ is the volume fraction of unreacted SCM at hydration time t.

8.1.3 Image J procedure

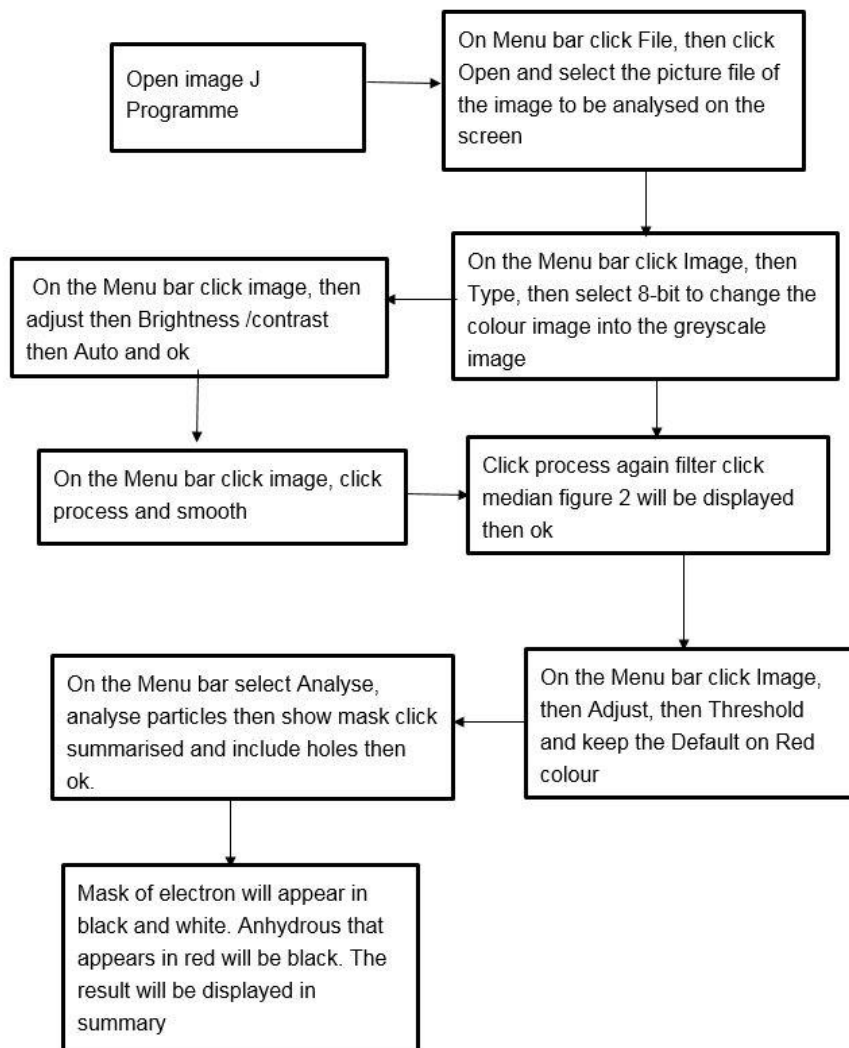


Figure 8-5 Detailed Procedures for Calculations of anhydrous clinker

8.1.4 Degree of hydration of ambient and ideal cured CEM1 and fly ash concretes

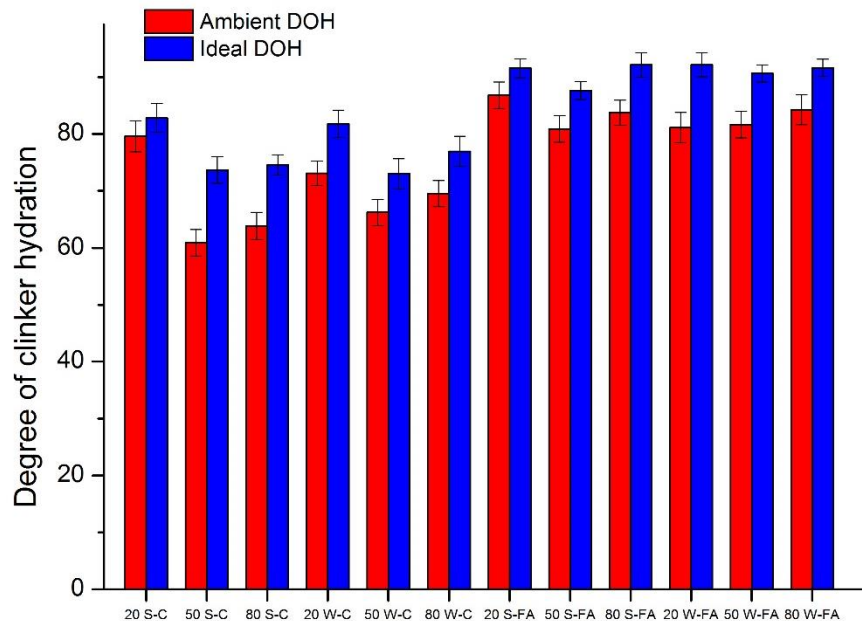


Figure 8-6 Degree of hydration of ambient and ideal cured samples measured from SEM images

Degree of hydration of ambient and ideal cured samples were shown in Figure 8.6. The figure shows that ideal cured samples were having higher degree of hydration than the ambient cured samples. Thus degree of hydration depends on curing and this agrees with other findings (309, 310). Drying affects hydration and leads to higher porosity and coarser pore structure compared to concrete with longer curing (311).

8.1.5 Effect of hydration on stiff and wet Mix

The effect of different mixes on degree of hydration was displayed in Figure 8.7. The Figure shows that DOH of wet mix are higher than that of stiff mix in high strength ambient cured concretes. Also 20 and 50 MPa CEM1, and 80MPa fly ash, Ideal cured samples DOH of stiff mix is higher than wet mix while 80MPa CEM1, 20 and 50MPa fly ash have wet mix higher than stiff mix.

The degree of hydration of CEM1 and fly ash concrete is shown in Figure 8.8. In the Figure fly ash increases the degree of hydration because of the filler effect. The degree of clinker hydration is higher, but this doesn't necessarily relate to overall degree of hydration because the fly ash will only have reacted to a small degree. Figure 8.9 also shows that degree of hydration of 20MPa is very small in stiff, and ambient samples compared to others.

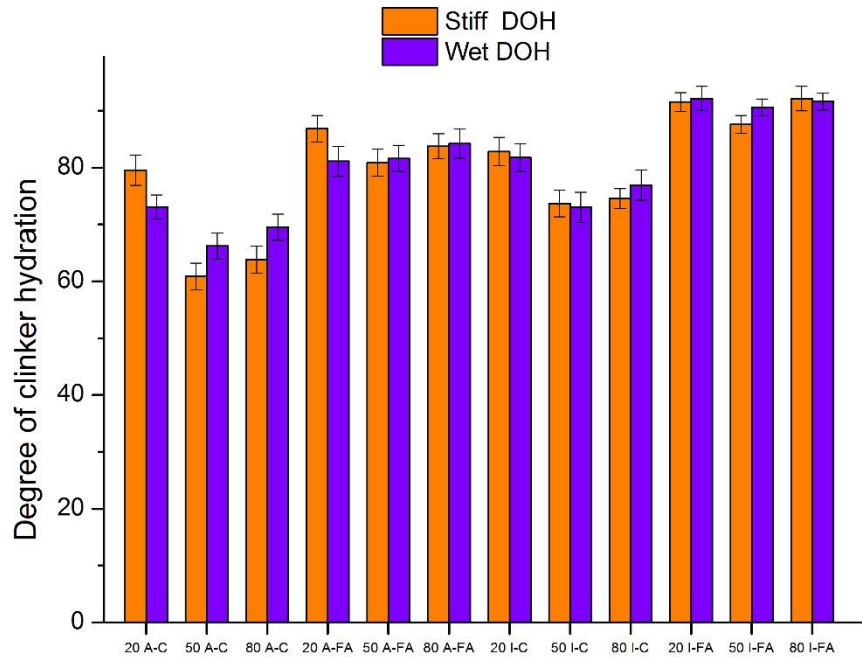


Figure 8-7 Degree of hydration of stiff and wet mix

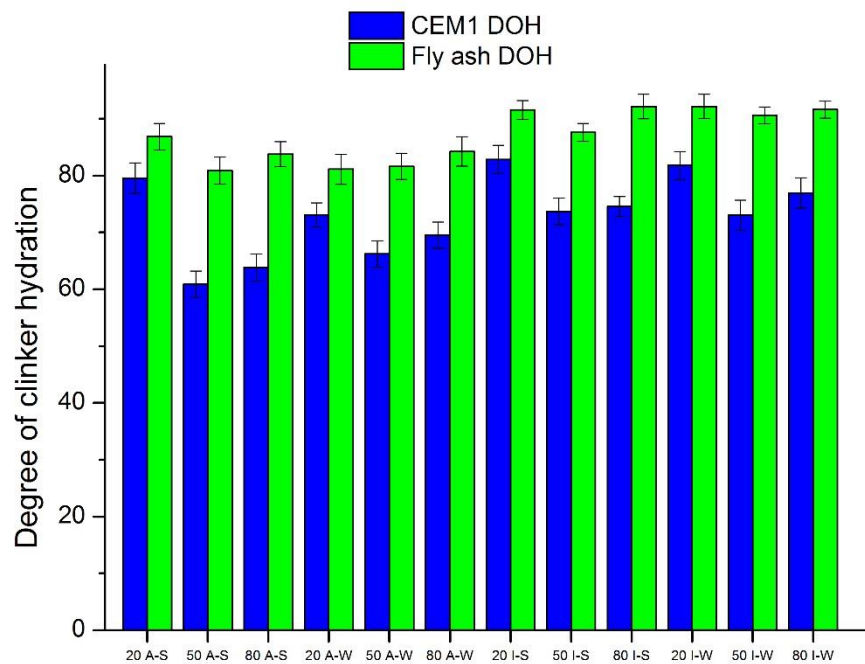


Figure 8-8 Degree of hydration of CEM1 and Fly ash concretes

8.2 Porosity

The strength and durability of cement based materials are usually influenced by the microstructure (284). The microstructure of cement based material is made up of hardened cement based products such as calcium silicate hydrate, calcium hydroxide, ettringite and monosulphate with residual pore system (18, 60). The pore system consists of porosity and pore sizes. The pore size characteristics of the porous material are represented by pore size

distribution (PSD) either in the form of cumulative pore size distribution or differential pore size distribution (312). The porosity and pore size distribution are signifying quality of concrete as they regulate the ease with which fluid can pass through the concrete (313).

The porosity and pore size distribution of cement based materials have a dominant impact on their mechanical and durability properties. Mechanical and durability properties consist of strength, ingress of harmful substances and the attack on the actual material. This ingress is identified with the volume of pores present as well as the size and distribution of such pores (314). Gel pores are enclosed in the hydrates while the spaces originally occupied by water but are not filled with hydrates form the capillary pores. Berodier and Scrivener(315) recently shows that water filled capillary pores influences the hydration of supplementary cementitious materials (SCM).

Das and Kondraivendhan (312) reported that different methods and techniques which had been used to measure the porosity and pore size distribution of concrete and other cement based materials were fluid displacement method, helium pycnometer, capillary condensation and adsorption desorption isotherm, small angle X-ray scattering (SAXS) method, scanning electron microscope (SEM), nuclear magnetic resonance (NMR), AC impedance spectroscopy, mercury intrusion porosimetry (MIP) and back scattered electron images (BSE). Another method to determine the porosity and characteristics of coarse capillary pore structures is the quantitative SEM-BSE image analysis (280, 316). Pores as one of constituent phases in an original BSE image can be quantitatively calculated by the procedures of image analysis. Based on the simple stereological principles, area fractions obtained for a 2D cross-section are equal to volume fractions for the 3D real structure when materials have a completely random and isotropic nature. The microstructure of cement paste can be considered to satisfy those stereological conditions. Thus, the imaging technique for BSE images is a method for quantitatively evaluating the actual 3D microstructure by analysing information on 2D cross-sections (18, 284) .

The degree of capillary porosity was determined for 28 day old samples using the same images which had been used to determine the degree of hydration. Capillary porosity was taken as the area fraction corresponding to the pores present in an electron image. A total of 30 electron images were collected at random and analysed using image j and the average was taken as the degree of porosity. Pores are identified by the black pixels of the images and at 400 magnification each pixel is equivalent to approximately 100 μm with the field of view in each image to be 326 x 244 μm . The steps involved in the analysis were similar to the one which had been outlined in Figure 8.5 .The little additions to the steps used with figures is presented in Appendix.

The porosity of ambient and ideal cured samples at 28 days was presented in Figure 8.9 . The Figure shows higher porosity in all the ambient cured sample either stiff or wet mix for CEM1 and fly ash concretes. The lower strength concretes having higher water binder ratios displayed higher porosity.

The porosity of stiff and wet mixes were presented in Figure 8.10. In all the lower strength concrete that is in 20MPa samples either ambient or ideal cured for CEM1 and fly ash concretes, wet mixes were more porous than the stiff mix. In ambient cured samples for high strength concretes (50 and 80MPa) stiff mixes are more porous than the wet mixes. The result obtained in ideal cured high strength concretes were similar to the ambient cured samples expect that there is a slight increase in wet mix in 80MPa CEM1.

Porosity of CEM1 and fly ash concrete is presented in Figure 8.11. The fly ash concretes were more porous than CEM concretes and this is as a result of empty spaces (black pixels) in the interior of the fly ash particles which overestimate the volume of pores measured by SEM.

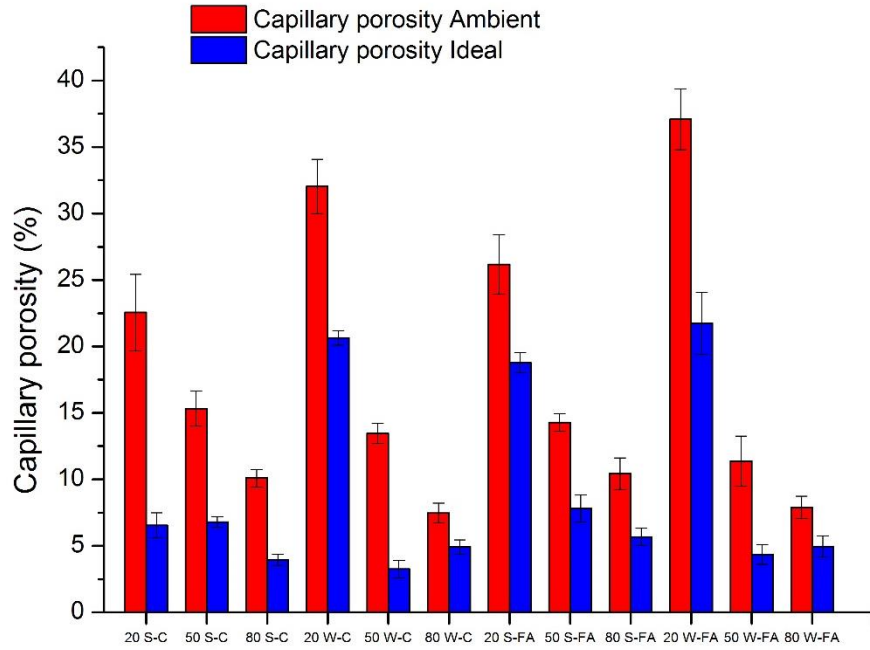


Figure 8-9 Porosity of ambient and ideal cured samples at 28 days

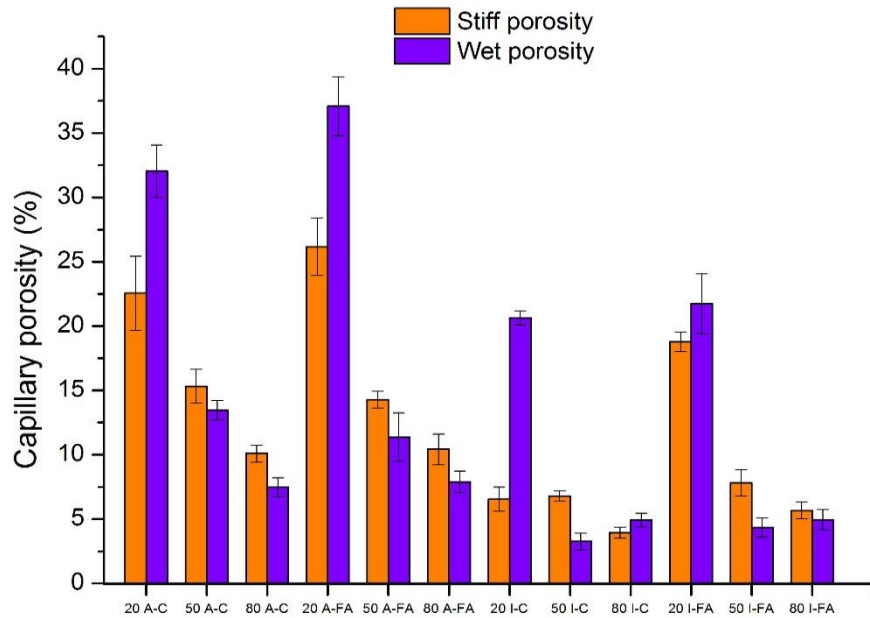


Figure 8-10 Porosity of stiff and wet mixes

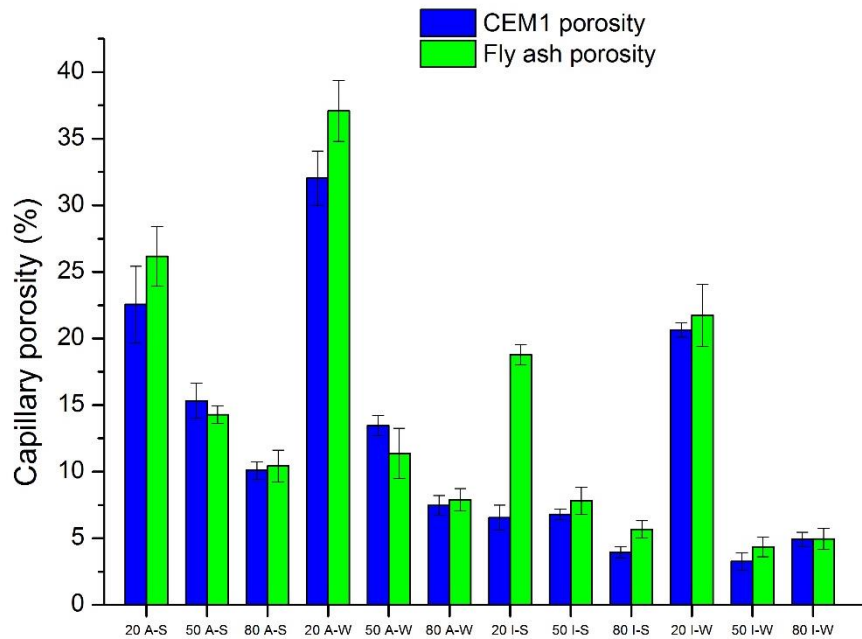


Figure 8-11 Porosity of CEM1 and fly ash concrete

8.3 Bound water content

The bound water content (W_n) was taken as the difference between the mass loss at 50 and 550°C, at which point it was assumed that all the water bearing phases had fully decomposed. W_n , normalised to the total mass loss at 550°C was calculated using Equation below.

$$W_n = \left(\frac{W_{50} - W_{550}}{W_{550}} \right) \times 100$$

Where

W_n = Bound water content

W_{50} is the mass loss at 50°C

W_{550} is the mass loss at 550°C

The hydration of cementitious materials can be examined by the bound water content. Bound water content cannot be directly related to the overall degree of hydration but gives an indication of the progress of hydration (280, 317). Figures 8.13 to 8.16 shows the bound water calculated for CEM1 and fly ash concretes at 1,7 and 28 days and bound water content increases over time, with the difference between ideal and ambient cured samples also increasing over time. The ambient and ideal cured samples bound water content was presented in the Figures. In all the tested samples the effects of ambient cured samples has started to show at 7 days by having a lower bound water content. At 28 days there is a large gap between them.

Figure 8.12 shows the bound water content of CEM1 stiff mix. The figures shows that the 20MPa concretes were more affected, there is a decrease in the bound water content and its flat. The Figure also shows that as the water-cement ratio decreases, the wide difference is

getting smaller. This result shows that the mixes with higher w/c ratio are more porous as they lose water more quickly than the mixes with low w/c ratio.

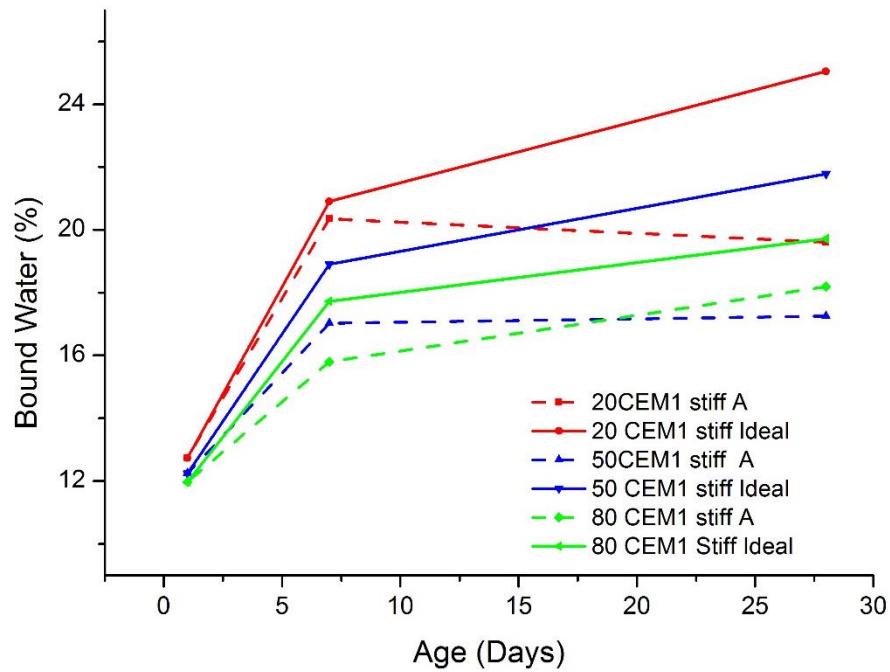


Figure 8-12 Bound water content of CEM1 stiff mix

The ambient and ideal cured CEM1 wet mix is shown in Figure 8.13. The Figure shows that the bound water content of 50 and 80MPa were almost the same, this result agrees with the compressive strength result shown in Figure 4.3 where the two targeted strength were having the same value at 28 days. Here also it can be seen that the difference between the ambient and ideal cure were almost the same for all the mixes.

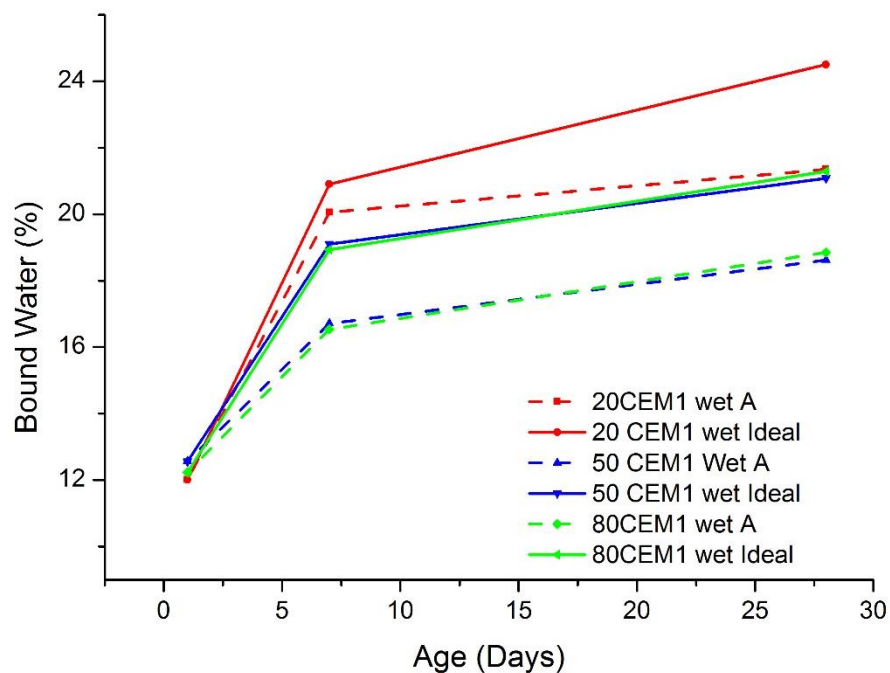


Figure 8-13 Bound water content of CEM1 wet mix

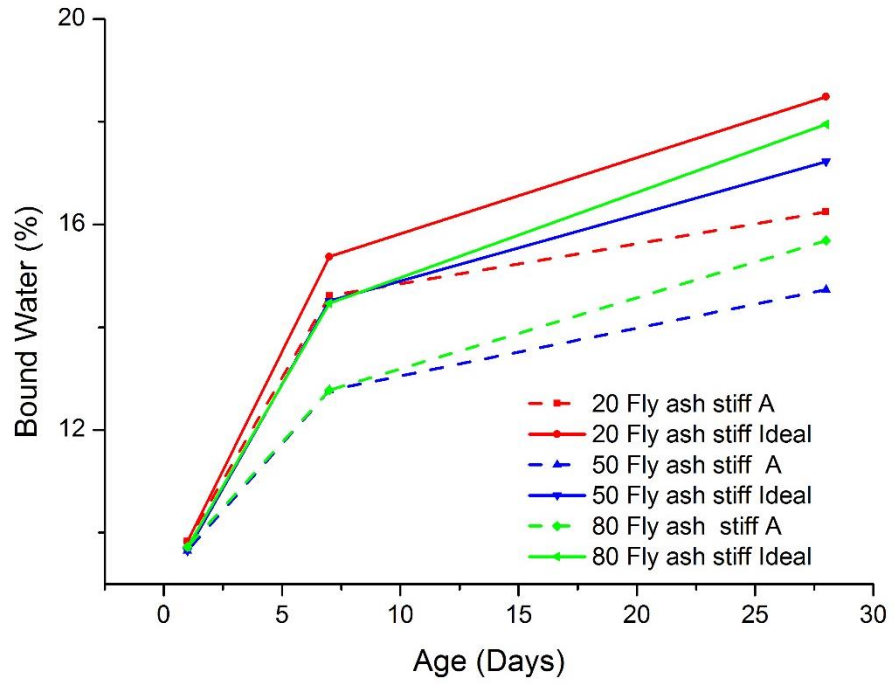


Figure 8-14 Bound water content of Fly ash stiff mix

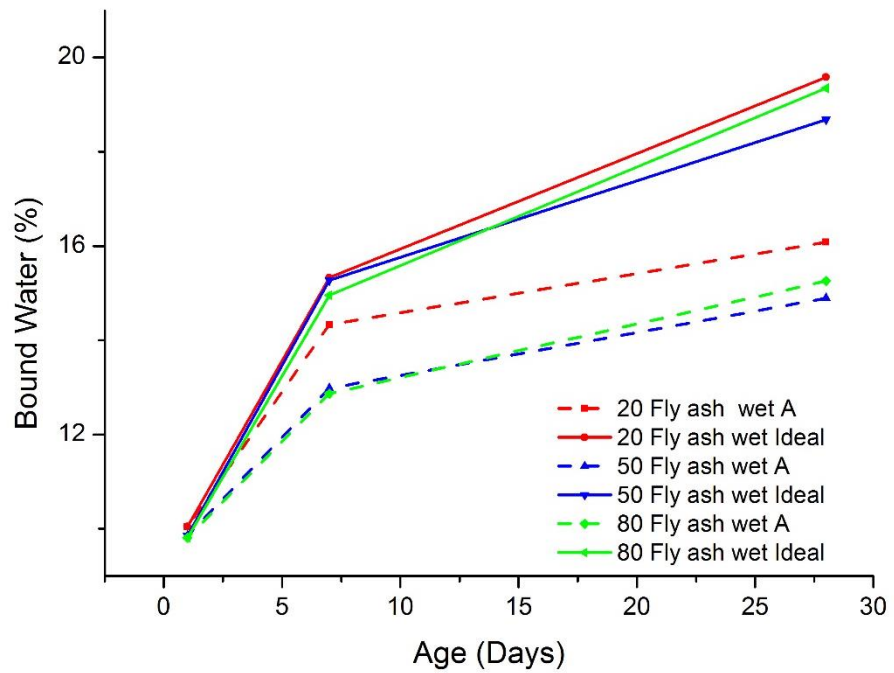


Figure 8-15 Bound water content of Fly ash wet mix

Figure 8.14 shows the bound water content of fly ash stiff mix. The figure shows that as the w/c binder is reducing the difference between the ambient and ideal cured samples were almost the same. This support the value obtained in Figure 4.4 where the 50 and 80MPa were having the same compressive strength at 28 days. Figure 8.15 shows the bound water for fly ash wet mix ,here the bound water were almost the same for all the ideal cured samples at 7 days and slight difference at 28days. The figure shows that as the binder water reduces there is wider difference between the ideal and the ambient cured samples with 80MPa having the highest.

8.3.1 Bound water content at 28 days

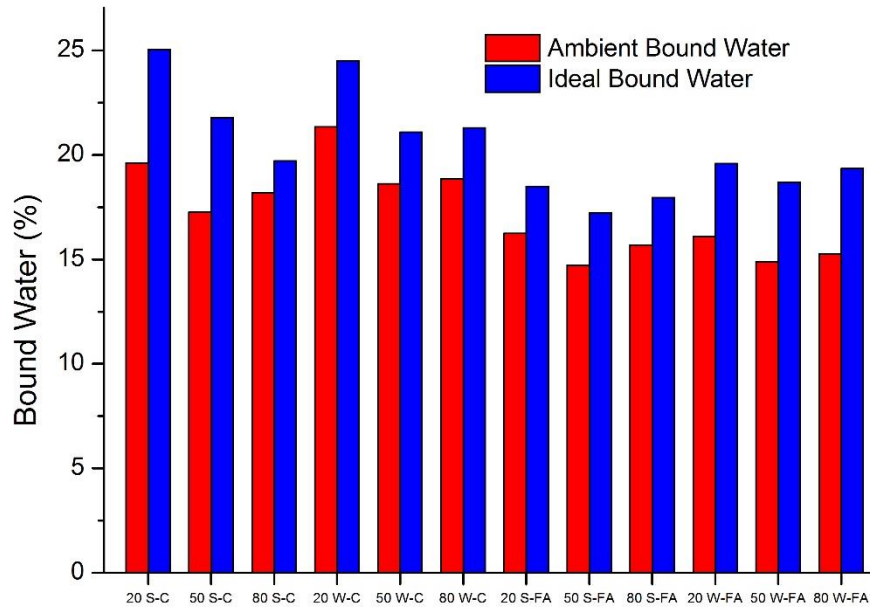


Figure 8-16 Bound water content of ambient and ideal cured samples

Figure 8.16 shows the bound water content in ambient and ideal cured samples at 28 days. The Figure shows that the bound water content in all the ideal cured samples are higher than that of ambient cured samples as the higher bound water content signifies higher degree of hydration.

The bound water calculated result support the degree of hydration calculated in SEM where all the ideal cured samples degree of hydration is higher than the ambient cured sample. Also the result shows that the compressive strength result obtained is as a result of the degree of hydration of the cement clinker in the mix.

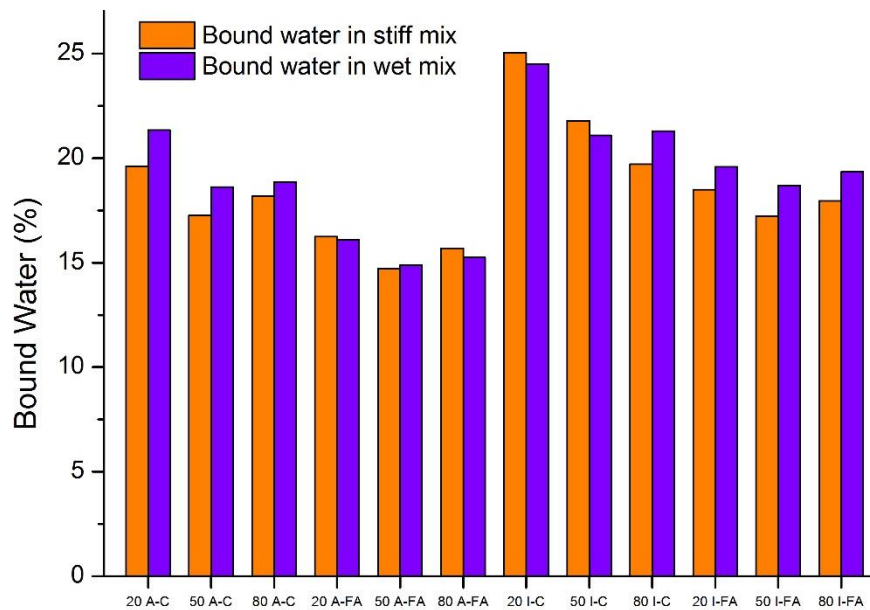


Figure 8-17 Bound water content in stiff and wet mix

The bound water content in stiff and wet mix is shown in Figure 8.17. Figure 8.17 shows higher bound water contents in CEM1 ambient cured and fly ash Ideal cured samples. In this Figure workability doesn't appear to have a strong effect on the DOH but does affect the susceptibility to improper curing.

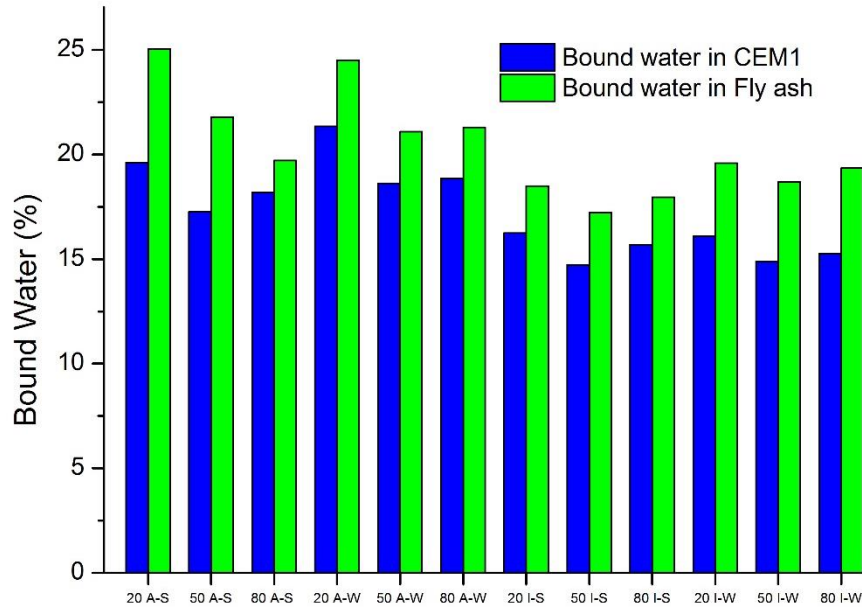


Figure 8-18 Bound content in CEM1 and Fly ash concrete

Figure 8.18 shows the bound water content obtained in CEM1 and fly ash concretes. The fly ash result here has been normalised to the cement content by dividing the fly ash value by 0.7 since the mix contain 70% CEM1 and 30% fly ash. The result show that the fly ash concretes shows a higher DOH . The result is in the same order with the DOH calculated by using SEM images.

8.4 Thermogravimetry (TG) results

Thermogravimetry is measuring the change in mass of a material over a temperature range using a predetermined heating rate. It involves heating a small amount of sample during which the hydrated cements, phases decompose releasing water (from hydrates) or carbon dioxide (CO₂) (from calcite).

In a typical thermogravimetric curve (TGA) for a cement sample with its corresponding differential curve (DTA) the following decomposition occurs as the sample is heated as reported by Ramachandran and Kocaba (279, 318)

- the unreacted gypsum (calcium sulphate) decomposes at temperatures between 140 and 170°C
- ettringite at temperatures of 120 – 130°C,
- C-S-H gel decomposes at temperatures below 150°C .
- Portlandite (CH) decomposes to CaO between 420 and 550°C, releasing water in the process.
- calcium carbonate decomposes to CaO, releasing CO₂ at higher temperatures of 650 to 800°C

The calcium hydroxide content was measured using the tangent method shown in Figure 8.19. Tangents were drawn on the TGA curve at the points where inflection occurred on the DTA curve. A line was then drawn along the slope of the TGA curve between the inflection points. The mass loss due to the water bound to CH (n), is taken as the length of the vertical line drawn through the midpoint of this line connecting the tangent lines. The CH content was then calculated using Equation 2 . Also this process is repeated at the last inflection point in the Figure 8.19 to determine the value of m and this is needed to correct the CH content for carbonation, thus Equation 4 becomes modified to Equation 6. The total Portlandite (CH_{Total}) is the addition of $Ca(OH)_2$ and $Ca(OH)_2_{eq}$. Equation 1 to 7 was used to calculate the values in Table 1 and 2 using the results presented in appendix to calculate the CH content.

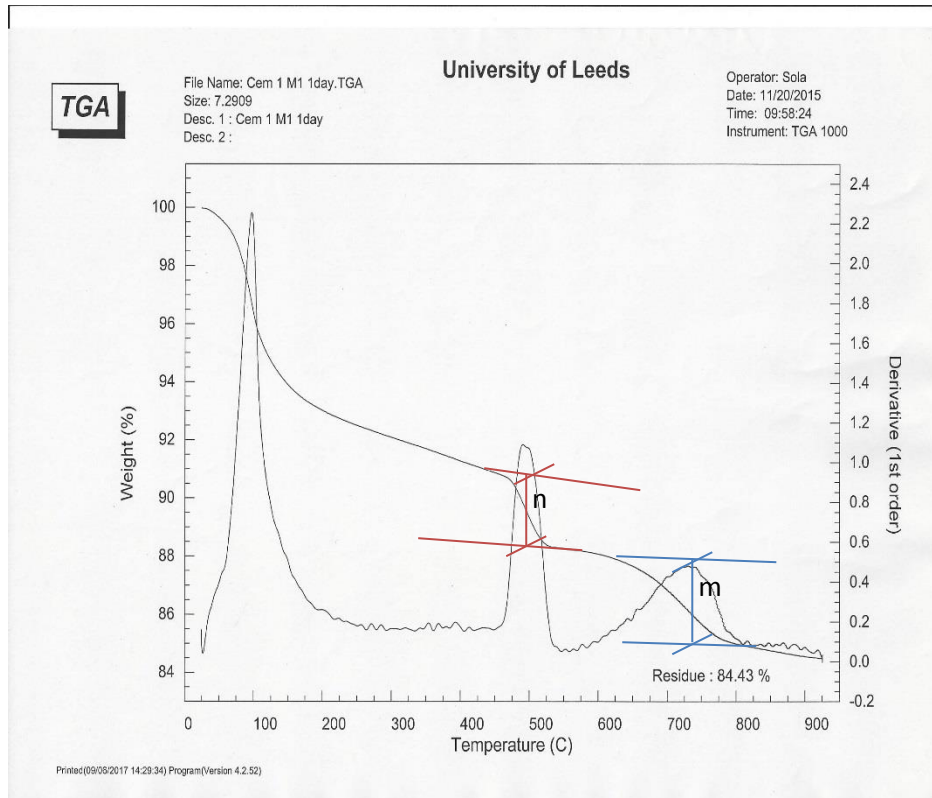
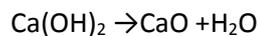


Figure 8-19 Measuring the calcium hydroxide and calcium carbonate by tangent method

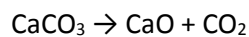


equation 1

Molar mass 74 56 18

$$[Ca(OH)_2] = \left[n \times \frac{74}{18} \right] \div \text{Residue}$$

equation 2

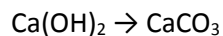


equation 3

Molar mass 100 56 44

$$[CaCO_3] = \left[m \times \frac{100}{44} \right] \div \text{Residue}$$

equation 4



equation 5

Molar mass 74 100

$$[Ca(OH)_2_{eq}] = [CaCO_3] \times \frac{74}{100}$$

equation 6

$$[\text{Ca(OH)}_2 \text{ eq}] = m \times \frac{100}{44} \times \frac{74}{100}$$

$$[\text{Ca(OH)}_2 \text{ eq}] = m \times \frac{74}{44}$$

Total calcium hydroxide content is the CH_{Total}

$$\text{CH}_{\text{Total}} = \text{Ca(OH)}_2 + \text{Ca(OH)}_2 \text{ eq} \quad \text{equation 7}$$

Table 8.1 and 8.2 shows the CH content calculated from thermogravimetric analysis (TGA) for all the samples. The steps explained in Equation 1 to 7 was used to calculate the values in columns 3 to 6 in the Tables and has been explained in section 3.10.5. CH is a hydration product of cement therefore the CH content of the fly ash blends had been normalised to Portland cement content in order to compare the results with the CEM1 results.

Table 8-1 CEM1 TG results

Mix	Age	Ca(OH) ₂	CaCO ₃	Ca(OH) _{2 eq}	CH _{Total}
20MPa Dry mix	1	7.30	3.77	2.35	9.66
20MPa Dry mix	28 A	6.52	5.41	3.03	9.55
20MPa Dry mix	28 Ideal	9.74	0.90	0.50	10.24
50MPa Dry mix	1	7.26	3.75	2.35	9.62
50MPa Dry mix	28 A	6.91	2.26	1.35	8.26
50MPa Dry mix	28 Ideal	8.42	0.00	0.00	8.42
80MPa Dry Mix	1	7.26	4.82	3.03	10.29
80MPa Dry Mix	28 A	7.14	1.97	1.18	8.32
80MPa Dry Mix	28 Ideal	8.09	2.02	1.18	9.26
20MPa Wet Mix	1	8.64	3.19	2.02	10.66
20MPa Wet Mix	28 A	7.51	3.56	2.02	9.53
20MPa Wet Mix	28 Ideal	10.37	2.72	1.51	11.89
50MPa Wet Mix	1	7.73	2.94	1.85	9.58
50MPa Wet mix	28 A	7.29	2.59	1.51	8.80
50MPa Wet Mix	28 Ideal	7.37	1.02	0.59	7.96
80MPa Wet mix	1	8.20	3.20	2.02	10.22
80MPa Wet mix	28 A	7.76	2.00	1.18	8.93
80MPa Wet	28 ideal	8.15	0.00	0.00	8.15

Table 8-2 Fly ash TG results

Mix	Age	Ca(OH) ₂	CaCO ₃	Ca(OH) _{2 eq}	CH _{Total}
20MPa Dry mix	1	7.58	6.55	4.20	11.78
20MPa Dry mix	28 A	8.06	2.51	1.51	9.57
20MPa Dry mix	28 Ideal	8.21	1.98	1.18	9.38
50MPa Dry mix	1	6.63	6.80	4.37	11.00
50MPa Dry mix	28 A	7.43	5.21	3.20	10.63
50MPa Dry mix	28 Ideal	7.05	1.95	1.18	8.23
80MPa Dry Mix	1	6.62	6.27	4.04	10.65
80MPa Dry Mix	28 A	7.49	3.45	2.10	9.59
80MPa Dry Mix	28 Ideal	7.63	1.97	1.18	8.80
20MPa Wet Mix	1	7.54	2.87	1.85	9.39
20MPa Wet Mix	28 A	6.04	4.73	2.86	8.90
20MPa Wet Mix	28 Ideal	8.04	1.86	1.09	9.14
50MPa Wet Mix	1	7.08	7.57	4.88	11.96
50MPa Wet Mix	28 A	6.43	4.10	2.52	8.96
50MPa Wet Mix	28 Ideal	7.18	1.84	1.09	8.28
80MPa Wet mix	1	7.05	5.72	3.70	10.75
80MPa Wet mix	28 A	6.96	2.75	1.68	8.64
80MPa Wet mix	28 Ideal	7.74	1.43	0.84	8.58

8.4.1 Portlandite content from thermogravimetric analysis at 28 days

Figures 8.20 to 8.22 shows the CH content calculated from thermogravimetric analysis (TGA) of CEM1 and fly ash samples cured at 28 days. Figure 8.20 shows the CH contents in ambient and ideal cured samples. The Figures show higher CH contents in ambient stiff mix CEM1 and 20MPa Fly ash wet mix while in others the result is not conclusive the CH values were almost the same or slightly greater.

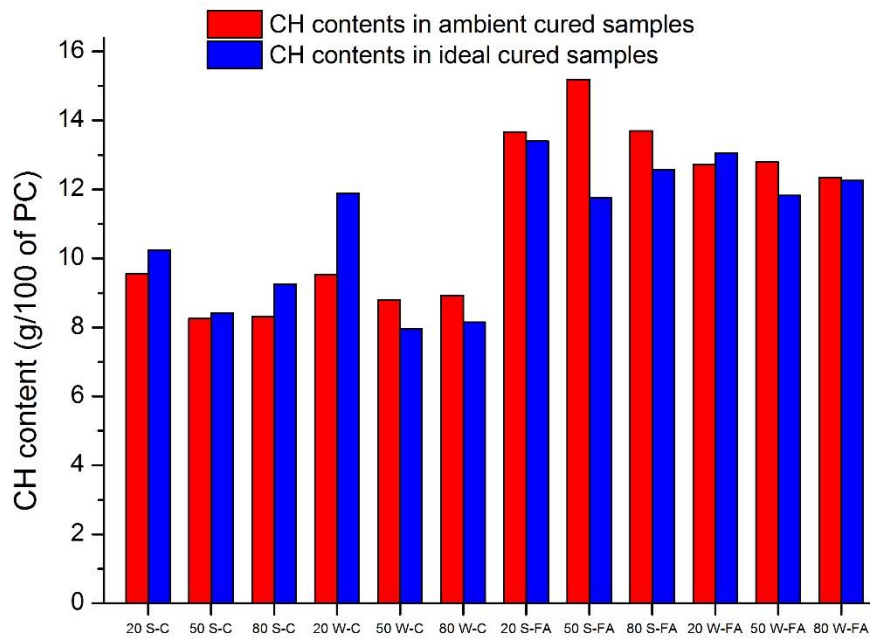


Figure 8-20 CH contents in ambient and ideal cured samples

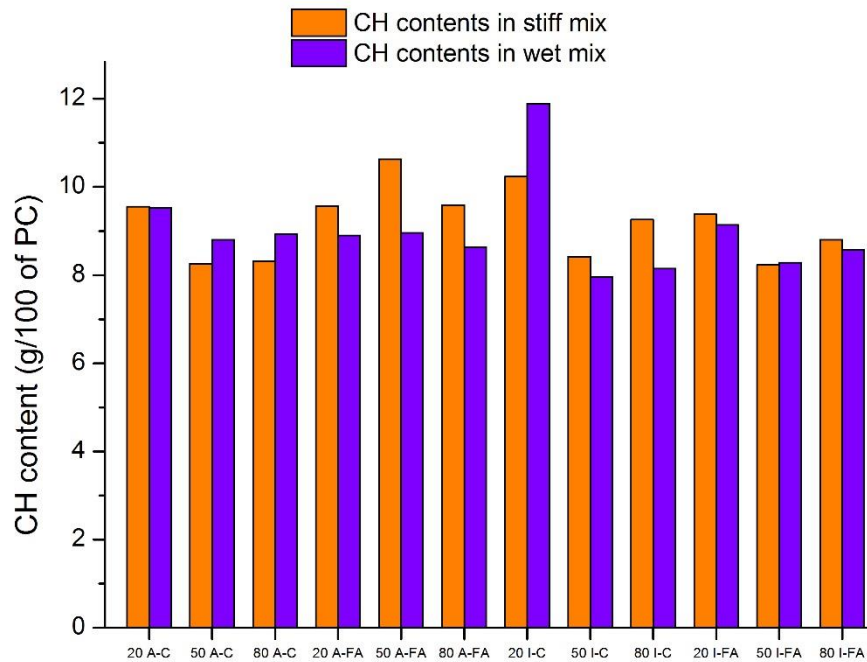


Figure 8-21 CH contents in stiff and wet mix

The CH contents in stiff and wet mix is displayed in Figure 8.21 from the Figure all the ambient cured CEM1 and fly ash samples stiff mix had higher CH contents while most ideal cured CEM1 and fly ash samples wet mix CH contents were higher.

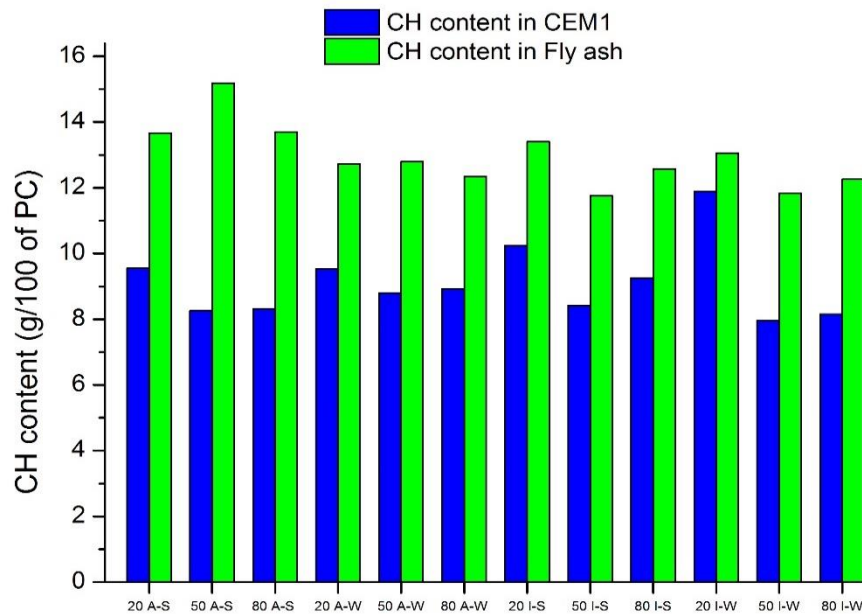


Figure 8-22 CH contents in CEM1 and Fly ash concretes

Figure 8.22 shows the CH contents in CEM1 and fly ash concretes. The Figure shows that the CH contents in fly ash samples were higher than CEM1 samples in all the mixes irrespective of the curing conditions.

8.5 XRD Analysis

XRD analysis was carried out to examine the effect of curing on the hydration of the clinker phases present in the mixes. Figure 8.23 to Figure 8.27 shows the XRD patterns obtained for 1, 7 and 28 day old CEM1 and fly ash concretes in stiff and ideal mix. Calcium hydroxide content has normally been considered as a good indicator of the evolution of hydration reactions (319, 320). The effect of different curing methods can be seen on the content of CH. At 2θ of 18° , 34° and 47° the XRD diffraction intensity of CH is different. CH contents had been used also to analyse cement samples (321, 322). In ideal cured samples the CH content increased showing higher degree of hydration while in ambient cured samples there is reduction in CH content.

The diffraction peaks of Alite and Belite were also used as seen near $2\theta = 29.50$, this suggest that some unhydrated cement clinkers were still in the samples. Checking the effect of this peak on the samples revealed that the intensity of diffraction peak of Alite and Belite decreased with the increase in the age with the ideal cured samples. Ambient cured samples showed the greatest intensity of diffraction of Alite and Belite, which shows that ambient cured samples had lower degree of hydration than the ideal cured samples. In the Figures 8.25 to 8.27 * stands for Alite and Belite and CH stands for $\text{Ca}(\text{OH})_2$,

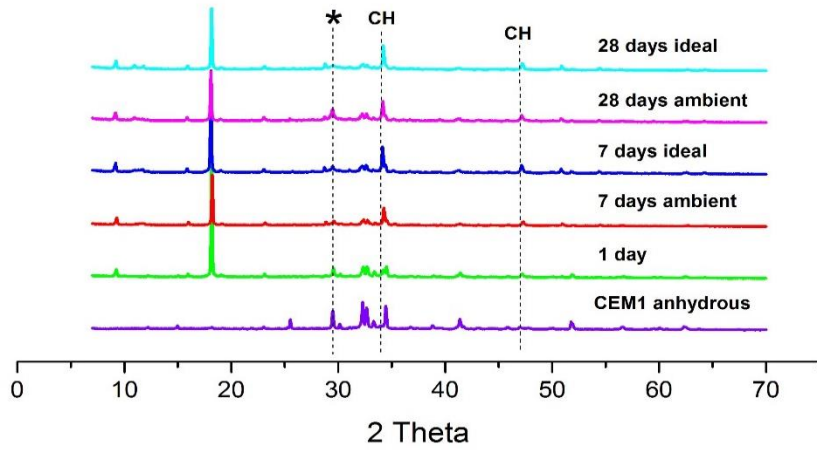


Figure 8-23 XRD of 20MPa CEM1 stiff mix from 1 day to 28 days of curing, plus the pattern from anhydrous CEM1

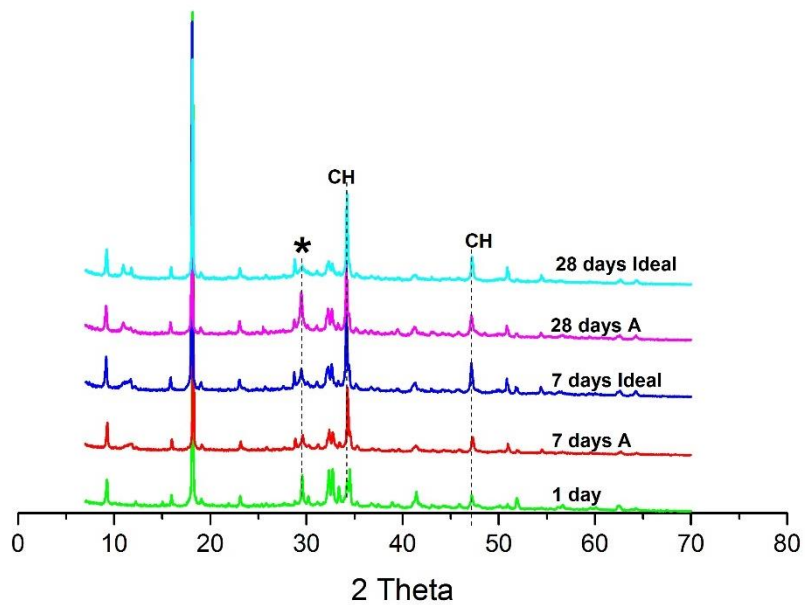


Figure 8-24 XRD of 20MPa CEM1 stiff mix from 1 day to 28 days of curing

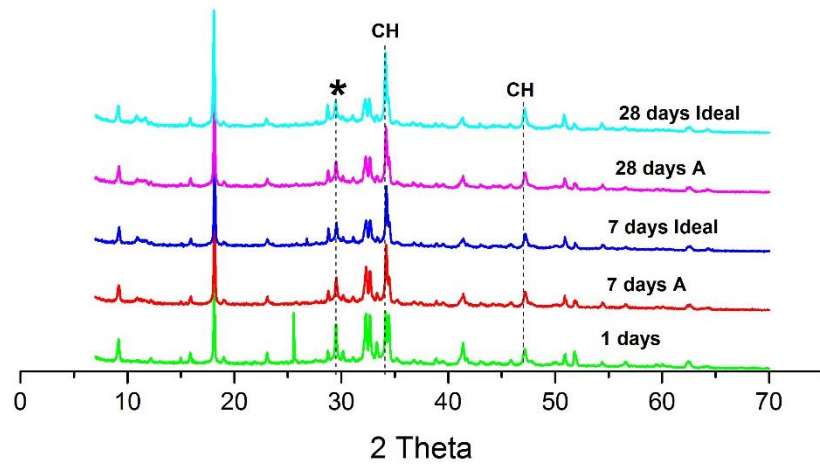


Figure 8-25 XRD of 50MPa CEM1 wet mix from 1 day to 28days of curing

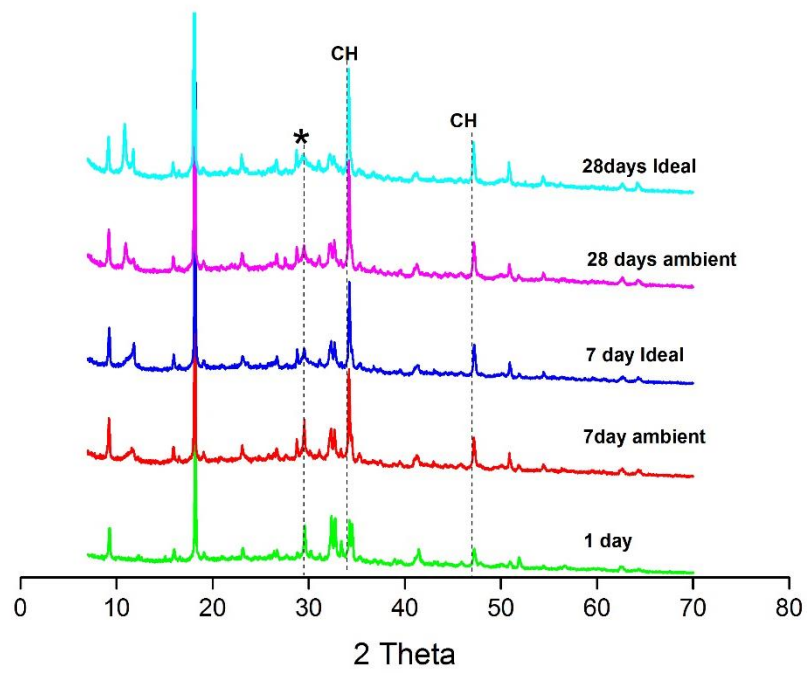


Figure 8-26 XRD of 20MPa Fly ash stiff mix from 1 day to 28days of curing

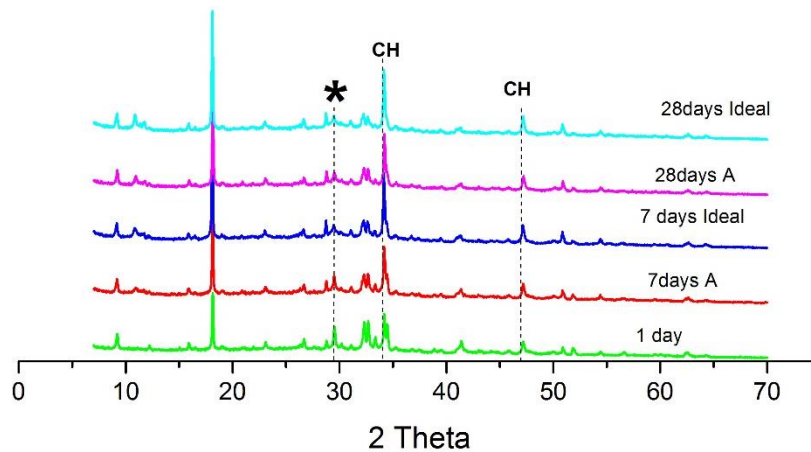


Figure 8-27 XRD of 50MPa Fly ash stiff mix from 1 day to 28days of curing

8.6 Conclusion

Paste samples were characterised by TGA, XRD and SEM to follow hydration and microstructural development to investigate the impact of improper curing the following were the conclusion made based on all the technical analysis used:

- The result from SEM to determine the degree of hydration result showed that ideal cured samples were having higher degree of hydration than the ambient cured samples. Thus degree of hydration depends on curing as drying affects hydration and leads to higher porosity and coarser pore structure compared to concrete with longer curing.
- The degree of clinker hydration is higher, but this doesn't necessarily relate to overall degree of hydration because the fly ash will only have reacted to a small degree
- Higher porosity in all the ambient cured sample either stiff or wet mix for CEM1 and fly ash concretes were obtained. The lower strength concretes having higher water binder ratios displayed higher porosity. The result confirms the sorptivity, permeability, change in mass as a result of drying obtained in the study.
- Also in lower strength concretes wet mixes were more porous than the stiff mixes.
- In porosity calculation fly ash concretes were more porous than CEM1 concretes and this is as a result of empty spaces (black pixels) in the interior of the fly ash particles which overestimate the volume of pores measured by SEM.

The hydration of cementitious materials can be examined by the bound water content. Bound water content cannot be directly related to the overall degree of hydration but gives an indication of the progress of hydration. The bound water calculated result support the degree of hydration calculated in SEM where all the ideal cured samples degree of hydration is higher than the ambient cured sample. Also the result shows that the compressive strength result obtained is as a result of the degree of hydration of the cement clinker in the mix.

As expected, the bound water contents of the ideal cured samples were higher than those of the ambient cured samples. This is a reflection of the higher degree of hydration, as evidenced by the SEM data and supporting the improved engineering performance.

Calcium hydroxide (CH) is one of the major phases in the hardened Portland cement paste and the amount of CH in the paste can be determined by TGA. The TG result showed that for the

CEM I systems, the portlandite contents were always higher when the samples were cured under ideal conditions, i.e. hydration had been allowed to proceed, so had led to the formation of portlandite from the hydration of alite and belite. However, the situation for fly ash- containing samples was different. In these samples, the ideally cured specimens invariably had lower portlandite contents. This is due to the consumption of portlandite during the pozzolanic reaction.

Qualitative XRD analysis was carried out to examine the effect of curing on the hydration of the clinker phases present in the mixes. The reflections for portlandite (at 18° , 34° and $47^\circ 2\theta$) can be considered as a good indicator of the evolution of hydration reactions. Ideal curing led to increased portlandite contents in the CEM I samples, while the portlandite contents in the ambient-cured samples did not increase so dramatically. Similarly, the decrease in the intensity of the peaks due to alite and belite, (near $29.5^\circ 2\theta$) was more profound under ideal curing conditions.

Chapter 9 General discussion

The effect of improper curing on concrete properties that may affect concrete durability has been thoroughly examined. The effects on mechanical performance have been considered, i.e. on compressive strength and drying shrinkage. The impact on transport properties had been considered through research into sorptivity, permeability and resistance to carbonation. Finally, this work has attempted to understand the impact of improper curing on the aforementioned properties by considering the microstructural changes induced by improper curing. With this aim, the work has investigated the effect of improper curing on the degree of hydration using SEM, XRD and TGA.

All of the above-mentioned tests were performed on various concrete mixes. These mixes had been chosen so as to span a range of mix designs, specifically focussing on those factors which had been shown to have an impact on the embodied carbon of concrete, i.e. binder type (CEM I or CEM I with 30% replacement by fly ash), workability (workable or stiff) and compressive strength (20, 50 or 80 MPa characteristic compressive strength). This section will discuss all the various factors and relates the factors to one another to check the effect on improper curing.

9.1 Effect of improper curing compressive strength

In the framework of structural design, concrete strength has been considered as the fundamental property controlling the totality of performance. Like all performance properties, strength is a function of the mixture proportions, primarily the water-cement ratio, and the degree of hydration of the cementitious materials. The mix proportions are inherent within the design, while curing conditions will define the latter.

Table 9.1 shows the compressive strength of concretes at 28 days under the two curing conditions considered in this research with the percentage decrease obtained as a result of ambient curing. As expected (289, 322, 323), improper curing always led to a decrease in compressive strength. This was ultimately related to reduced degrees of hydration (Chapter 8).

There were no consistent trends relating the loss of strength with the target characteristic strength, but the percentage reduction in strength was generally greater with decreasing target strength. The results in Chapter 4 showed that the mass loss upon drying was greater for lower strength concretes, implying that the greater inherent porosity enabled greater evaporation of water during curing under ambient conditions. This was supported by lower inherent permeabilities of higher strength samples cured under ideal conditions, as reported in chapter 7.

When checking the effect of improper curing on CEM1 and fly ash blends, the result revealed that ambient curing had a more detrimental effect on the composite cement mixes. This is perhaps as expected, since drying of the samples under ambient conditions is not immediate, thus the CEM I concretes will have hydrated to a greater degree than the blended cement systems, binding water and thus not allowing it to evaporate. Running counter to this, however, the increased rate of early-age clinker hydration when fly ash was present due to

the filler effect and higher effective water/cement ratio, may have made the loss of performance less than may have been expected.

Table 9-1 Concrete compressive strengths at 28days of curing

	Saturated Ambient UCS (MPa)	Ideal UCS (MPa)	Percentage decrease upon ambient curing
20MPa stiff mix CEM 1	25.43	32.35	-21.39
50MPa stiff mix CEM 1	55.75	62.53	-10.84
80MPa stiff mix CEM 1	58.41	63.51	-8.03
20MPa Wet mix CEM 1	27.06	38.54	-29.79
50MPa Wet mix CEM 1	52.16	57.12	-8.68
80MPa Wet mix CEM 1	54.31	63.45	-14.41
20MPa stiff mix fly ash	21.13	32.77	-35.52
50MPa Stiff mix fly ash	44.02	53.94	-18.39
80MPa stiff mix fly ash	47.87	54.35	-11.92
20MPa Wet mix fly ash	23.5	29.72	-20.93
50MPa Wet Mix fly ash	41.29	49.97	-17.37
80MPa Wet mix fly ash	50.83	51.62	-1.53

9.2 The impact of improper curing on drying shrinkage

Shrinkage of concrete is the principal cause for various kinds of cracks which affect the serviceability and durability of concrete. Shrinkage cracking occurs when tensile stresses due to restrained volume contraction exceed the tensile strength of concrete this leads to cracking. Thus, shrinkage of concrete is a very important property of concrete to be examined. Shrinkage cracking in concrete can later lead to premature failure of the concrete elements. Increased corrosion rate of steel reinforcement in the concrete can also occur as a result of cracking in concrete. The rate at which corrosion occurs and the time to initiate corrosion is essentially influenced by the cracks in the concrete, which increase the permeability of the concrete. For marine concrete or concrete structures close to the coastal region, the penetration of aggressive ions through cracks into the interior of concrete is a very critical factor in causing the corrosion of steel reinforcement.

Improper curing was found to lead to greater shrinkage than for samples cured under ideal conditions, with shrinkage increasing with increasing strength. These two observations may not be related. The greater shrinkage with increasing strength occurred for both curing conditions, and is related to the binder content; with more binder leading to greater shrinkage. Improper curing however may have led to much greater shrinkage because of the greater surface porosity (Chapter 7) leading to increased drying.

Furthermore, shrinkage was also found to be greater for the workable (wet) mixes. This suggests that concretes containing more water will experience more shrinkage as higher water content will make the concrete to be more porous hence resulting in a more open

microstructure. Comparing this result with the porosity result calculated from SEM images confirms that wet mixes were more porous than the stiff mix. Also the permeability results also show that dry mixes were (again) less permeable than wet mixes when improperly cured.

Addition of fly ash to the concrete mix showed that fly ash concretes has lower drying shrinkage values than the CEM1 concretes in all the wet mix for the three-targeted strength.

9.3 Effect of improper curing on permeability

Concrete is a porous material and fluids (liquids or gases) may flow through concrete under certain conditions. The permeability of concrete to fluids is commonly measured by applying a pressure gradient across a concrete sample and measuring the rate of fluid flow. Permeability has an essential action on the durability of concrete, and is one of the suite of durability indices mentioned in Chapter 2.

The permeability results from the various samples are presented in Table 9.2. It was anticipated that permeability would decrease with increasing strength. However, this was not always the case. The 80 MPa mixes tended to show much higher than anticipated permeabilities. This may be due to the problems encountered when trying to cast these samples. Therefore, the subsequent discussion will focus on a comparison between the 20 and 50 MPa mixes.

For the ideally cured samples, permeability decreased with increasing strength. Workability also influenced permeability, with stiff mixes generally having lower permeabilities than their corresponding wet mixes. The effect of binder type was less clear-cut. Stiff fly ash-containing concretes had higher permeabilities than their CEM1 equivalents, but wet fly ash –containing mixes show lower permeabilities.

Table 9-2 Permeability of ambient and ideal cured samples

	Ambient Permeability (10^{-16} m^2)	Ideal Permeability (10^{-16} m^2)	Percentage increase upon ambient curing
20MPa Stiff mix CEM 1	6.26	0.29	2160
50MPa Stiff mix CEM 1	1.65	0.14	1180
80MPa Stiff mix CEM 1	2.74	0.66	313
20MPa Wet mix CEM 1	7.00	0.61	1150
50MPa Wet mix CEM 1	2.01	0.23	870
80MPa Wet mix CEM 1	3.34	0.83	301
20MPa Stiff mix fly ash	6.38	0.45	1420
50MPa Stiff mix fly ash	1.64	0.16	1030
80MPa Stiff mix fly ash	3.81	0.39	880
20MPa Wet mix fly ash	5.60	0.30	1870
50MPa Wet Mix fly ash	2.57	0.21	1220
80MPa Wet mix fly ash	5.04	0.52	872

The impact of improper curing on all samples was immediately clear, there being at least a ten-fold increase in permeability for almost all ambient-cured samples compared to their

ideal-cured equivalents. The key factor in determining the effect of improper curing on permeability was the compressive strength, with the 20 MPa samples exhibiting an average increase in permeability about 50% greater than the 50 MPa samples. This was much greater than the difference observed in compressive strengths, but may be related to the increased mass loss seen upon drying (Chapter 4). The loss of water from the already stiffened concrete paste will leave a greater residual porosity, thus dramatically increasing permeability.

While wet mixes generally showed higher permeabilities than their equivalent stiff mixes, both following ideal and ambient curing, concrete workability did not appear to influence the extent of the increase in permeability upon ambient curing. Somewhat surprisingly, binder type did not appear to have a clear effect on permeability but addition of fly ash reduces the permeability which can be seen in the Table that permeability of ideal cured fly ash sample having lower permeability than CEM1 samples and this agrees with other researchers (83, 265, 297).

9.4 The impact of improper curing on sorptivity

Sorptivity is an index of moisture transport into unsaturated specimens under capillary action. It has been identified as an essential index of concrete durability as the method used for the test follows the way water and other damaging agents will penetrate concrete. Also it is a good measure of the quality of the near surface concrete, that controls durability associated to reinforcement corrosion according to Dias (135). Also as the extent of curing has been studied to be a main influence on the quality of cover zone concrete, and sorptivity is very sensitive to the type and duration of curing.

Improper curing led to higher sorptivity values for all mixes. Mixes with higher workabilities had higher sorptivities when ideally cured. Thus higher water content produces higher sorptivity and the use of fly ash in the mix produces lower sorptivity. This result agrees with other findings (92, 133). The sorptivity coefficient obtained was compared with the carbonation depth as shown in Table 9.3. The Table reveals that sorptivity decreased with increasing compressive strength, and that non-ideal curing had a greater effect on the lower strength mixes, as was seen for permeability and also for the loss in mass upon drying.

Wet mixes often showed higher sorptivities than the corresponding stiff mixes, and non-ideal curing also seemed to have a slightly greater effect on the wet mixes than the corresponding stiff mixes, but the effect was not too clear cut. The increased paste volume in the wet mixes may be the cause of this slightly elevated permeability.

Finally, the importance of ideal curing conditions for composite cements is clear in Figure 7.3. For the ideally cured samples, the fly ash blends normally had lower sorptivities than their corresponding CEM I blends.

However, under ambient curing conditions, the situation was reversed and the fly ash blends all showed worse performance than the equivalent CEM I concrete.

9.5 Impact of improper curing on carbonation resistance.

Carbonation is a chemical reaction between the calcium hydroxide in the concrete due to the hydration of the cement and the carbon dioxide of the surrounding atmosphere. The CO_2 reacts with calcium hydroxide in the concrete to form calcium carbonate which reduces the pH and thus accelerates the corrosion of reinforcing steel. Carbonation itself does not usually

cause any damage to concrete, but the reduction of the pH value may cause corrosion of the reinforcement. The alkalinity of concrete, characterised by the high pH value of the pore water in the concrete, provides a very adequate protection to the reinforcement against corrosion through the passivation of the steel. Carbonation can reduce the alkalinity of the concrete which may cause depassivation of the embedded steel and trigger corrosion eventually leading to damage to the concrete. Corrosion damage due to carbonation in concrete elements has been attributed to a combination of poor quality concrete, inadequate curing, and insufficient concrete cover.

All the ideally cured samples carbonated less, hence curing reduces the carbonation. The improvement in carbonation resistance with improved curing conditions has been shown previously (85, 88, 146, 305-307, 324, 325). Conversely, ambient curing had a detrimental effect on carbonation resistance. The ambient cured samples desiccated as a result of improper curing and hydration was stopped. This was observed in Chapter 7 where the degree of hydration was measured. The reduced degree of hydration led to lower quantities of portlandite being produced, plus increased permeability. Stiff mixes showed slightly higher carbonation depths than wet mixes, but the impact of improper curing was not related to concrete workability. Similar conclusions could be made concerning binder type, where there were no clear, consistent trends in the data but ideally cured fly ash blends performed better than the equivalent CEM I mixes (85, 88, 91). This is in line with the permeability data.

Table 9.3 shows the result of carbonation depth and the sorptivity value. The carbonation data available is small since all the high strength tested did not carbonated, thus the comparison will be between 20MPa samples. Table 9.3 clearly showed that with high sorptivity values high greater carbonation depth were obtainable. All the ideal cured samples showed lower sorptivity value as well as lower carbonation depths. Also when considering the water content in the mix the result revealed that lower sorptivity and less carbonation is obtained with higher workability. The impact of fly ash in the mix is variable.

Table 9-3 Carbonation depth and coefficient of sorptivity

28 days cured samples	Carbonation depth(mm)	Sorptivity value k ($m^3/m^2s^{1/2}$) $\times 10^{-8}$
20 CEM1 stiff ambient	25.44	2.35
20 CEM1 stiff ideal	10.11	0.74
20 CEM1 wet ambient	9.61	2.44
20 CEM1wet ideal	3.72	0.97
20 fly ash stiff ambient	23.33	2.52
20 fly ash stiff ideal	8.56	0.72
20 fly ash wet ambient	17.22	2.44
20 fly ash wet ideal	3.56	0.95

9.6 Impact on degree of hydration

Hydration starts when cement mixes with water, it involves the different compounds in cement to start to react with some part of mixing water thus the cement starts to hydrate and that part of water becomes chemically bound. Calcium silicate hydrate (C-S-H) which is the main hydrate, intermixed with portlandite (CH), ettringite and the AFm phases are some of numerous hydration products formed.

The degree of hydration which has been specified as the ratio of the hydrated cement and the original cement content can be determined by using various parameters such as the amount

of calcium hydroxide, $\text{Ca}(\text{OH})_2$ in the paste, quantity of the chemically bound water, specific gravity of the paste, fraction of un-hydrated cement, liberated heat of hydration and strength of the hydrated cement. Degree of hydration of cement paste controls many properties of hardened concrete and/or mortar such as compressive strength. As explained, in order for hydration to continue the presence of water is important. Thus, paste samples having the same water/binder ratio with the concrete samples were prepared and cured under ideal or non-ideal conditions. These paste samples were then characterised using SEM image analysis, TGA and XRD to determine the degree of cement hydration, which could then be related to the engineering performance measures detailed above.

Table 9-4 Degree of hydration of ambient and ideal samples

	Ambient DOH	Ideal DOH
20MPa Stiff mix CEM 1	79.58	82.81
50MPa Stiff mix CEM 1	60.9	73.68
80MPa Stiff mix CEM 1	63.85	74.54
20MPa Wet mix CEM 1	73.08	81.76
50MPa Wet mix CEM 1	66.22	73.02
80MPa Wet mix CEM 1	69.53	76.95
20MPa Stiff mix fly ash	86.83	91.55
50MPa Stiff mix fly ash	80.87	87.62
80MPa Stiff mix fly ash	83.74	92.13
20MPa Wet mix fly ash	81.13	92.15
50MPa Wet Mix fly ash	81.63	90.61
80MPa Wet mix fly ash	84.25	91.62

These results could be understood by examining the degree of binder hydration in the different mixes. The degree of clinker hydration as determined by SEM image analysis, TGA and XRD revealed that the degree of clinker hydration was greater in the ideally-cured samples. This led to the higher compressive strengths and lower permeabilities. The effects of improper curing were more pronounced in the higher strength samples, with the 50 and 80 MPa concretes showing considerably lower degrees of hydration than the 20 MPa mixes.

Similarly, the degree of clinker hydration was greater in the composite cements than in the CEM I systems, but the presence of fly ash did not appear to have a significant effect on the degree of hydration under non-ideal curing conditions. Meanwhile, the degree of clinker hydration fell with increasing target compressive strength. This is presumed to be due to the lower availability of water within the mixes.

In conclusion, improper curing led to a decrease in the degree of clinker hydration, which in turn had a deleterious effect on permeability. However, compressive strengths were not affected to the same degree. Therefore, a reliance on compressive strength for quality control purposes might not be appropriate if durability is a key performance criterion.

Figures 8.3 and 8.4 in chapter 8 show how, as expected, capillary porosity was greater for the lower strength samples. The wet mixes were more porous than the equivalent dry mixes. This is in line with the intrinsic permeability measurements presented earlier.

Meanwhile, changing the binder from CEM I to a fly ash blend did not appear to have a significant effect on the microstructure.

Most clearly, ambient-cured samples exhibited reduced degrees of hydration, evidenced by the increased presence of anhydrous clinker (appearing as bright angular features), and much higher capillary porosities than their ideal-cured counterparts. The figures are a clear indication of how ideal curing can improve the pore structure of concrete, as has been reported by others previously (24, 84, 326-328).

Using the approach developed elsewhere (279, 280) and as described in section 3.10.9, it was then possible to determine the degree of clinker hydration in each of the samples. Table 9.4 show the degree of clinker hydration for each of the samples. In all cases, the ideal cured samples showed a higher degree of hydration than their corresponding ambient cured ones, confirming that prolonged moist hydration increases the degree of hydration (309, 310). Allowing the samples to dry under ambient curing conditions affected hydration, in turn leading to higher porosity and coarser pore structure compared to ideal-cured concrete (311).

Workability had no distinct effect on the degree of hydration. This is despite higher water/cement ratios being known to lead to increased early-age hydration (79, 105, 310, 315). However, it appeared that by 28 days any effect was insignificant.

Figure 8.8 also shows that the degree of clinker hydration was consistently higher for the fly ash-containing blends than their corresponding CEM I samples, irrespective of curing conditions. This may be ascribed to the filler effect and increased effective water/cement ratio at early ages (79, 102, 105, 317, 329). Note also that, while the degree of clinker hydration is higher, this doesn't necessarily relate to the overall degree of binder hydration because the fly ash will only have reacted to a small degree (78, 105, 330).

The hydration of cementitious materials can be examined by the bound water content. Bound water content cannot be directly related to the overall degree of hydration but gives an indication of the progress of hydration (280, 317). Figure 8.20 shows the bound water content calculated for each sample at 28 days. As expected, the bound water contents of the ideal cured samples were higher than those of the ambient cured samples. This is a reflection of the higher degree of hydration, as evidenced by the SEM data and supporting the improved engineering performance.

As with many of the other measures, the workability of the sample did not appear to have an effect on the bound water content. The binder type, however, did affect the bound water content. All of the fly ash samples showed lower bound water contents than the corresponding CEM I mixes. This is due to the low reactivity of the fly ash compared to the cement clinker and explains why, despite the higher degree of clinker hydration (as determined by SEM-BSE analysis) the engineering performance of the fly ash containing samples concretes was not significantly better than that of the corresponding CEM I concretes. Furthermore, comparing the difference in bound water content for ideal and ambient cured samples according to binder type, the presence of the fly ash in the concrete did not appear to affect the susceptibility to improper curing.

Calcium hydroxide is a hydration product of cement and can be calculated from thermogravimetric analysis (TGA). The CH content of the fly ash blends had been normalised to cement content (by dividing the obtained data by 0.7) in order to compare the results with the CEM I results.

For the CEM I systems, the portlandite contents were always higher when the samples were cured under ideal conditions, i.e. hydration had been allowed to proceed, so had led to the formation of portlandite from the hydration of alite and belite. However, the situation for fly ash- containing samples was different. In these samples, the ideally cured specimens invariably had lower portlandite contents. This is due to the consumption of portlandite during the pozzolanic reaction.

Qualitative XRD analysis was carried out to examine the effect of curing on the hydration of the clinker phases present in the mixes. The typical XRD patterns obtained from CEM I and fly ash- containing pastes obtained after hydration for 1, 7 and 28 days. The reflections for portlandite (at 18° , 34° and $47^\circ 2\theta$) can be considered as a good indicator of the evolution of hydration reactions (319, 320). Ideal curing led to increased portlandite contents in the CEM I samples, while the portlandite contents in the ambient-cured samples did not increase so dramatically. Similarly, the decrease in the intensity of the peaks due to alite and belite, (near $29.5^\circ 2\theta$) was more profound under ideal curing conditions.

As with the thermogravimetric data, the production of portlandite under ideal curing conditions was not so pronounced in the fly ash –containing mixes. The pozzolanic reaction led to portlandite consumption when the samples were cured under ideal conditions. However, the aforementioned consumption of alite and belite could be observed.

9.7 Practical implication of the study

The result of the study clearly shows that measuring the quality of concrete by strength development alone is not appropriate. Proper curing ensures strength development and durability, with the effects being greater on the latter than the former. This can be seen on the compressive strength result in Figure 4.21 that the non-ideal cured samples were having higher strength which is almost the same value with the ideal cured samples. The impact of improper curing was glaring on the permeability as seen in Figure 7.4 as all the ambient samples were having higher permeability. The higher compressive strength of ambient cured samples is also accompanied with higher sorptivity values as displayed in Figure 7.1.

The importance of the proper curing cannot be over emphasized especially with the use of fly ash in the concrete mix. The impact of improper curing was more pronounced on non-ideal cured fly ash samples, while in ideal cured samples fly ash performs better than CEM1 concretes though all the fly ash concretes produces low strength at the early age. Exposing fly ash concrete to the environment without proper curing will cause early deterioration.

The study shows that improper curing is detrimental to the performance of concrete. Improper curing leads to reduced compressive strength development and increased sorptivity and permeability. This is due to reduced levels of cement hydration as water evaporates from the concrete surface. This study has shown that the impact on the durability indices sorptivity and permeability is far greater than the impact on compressive strength, with implications for the long-term durability of concrete.

The extent of the impact of improper curing depends on the properties of the concrete. Low strength concrete, which has a slightly higher water content and also an inherently higher porosity, is more greatly affected by improper curing than high strength concrete. This is presumed to be due to the ease with which water can evaporate from the surface of the more porous cement paste.

The research confirms the need for good site practice, and also shows that embodied carbon should not be the only factor when considering the environmental performance of concrete. Rather, durability and whole life performance should also be considered.

Chapter 10 Conclusion and Suggestions for Further works

10.1 Conclusions

This work has examined the effect of improper curing on concrete properties that may affect concrete durability with the effect on fly ash concretes. In conclusion the following points were highlighted in relation to the objective of the study.

- The effect of improper curing on compressive strength, drying shrinkage, sorptivity and permeability*

The study shows that improper curing has adverse effect on concrete performance. Improper curing leads to reduced compressive strength development and increased the drying shrinkage. Sorptivity and permeability values were having higher values. This is due to reduced levels of cement hydration as water evaporates from the concrete surface. This study has shown that the impact on sorptivity and permeability is far greater than the impact on compressive strength, with implications for the long-term durability of concrete.

Composite cements, containing 30% fly ash, showed comparable strengths to CEM I concretes and improved transport properties when ideally cured. Additions of fly ash reduced the drying shrinkage. Improper curing however led to reduced performance. Strength was compromised by improper curing to a greater degree than for equivalent CEM I mixes. However, it was sorptivity and permeability which were most severely affected. This was due to the reduced degree of cement hydration leading preventing the pozzolanic reaction between the fly ash and portlandite.
- Impact of improper curing as a function of mix design parameters.*

The extent of the impact of improper curing depends on the properties of the concrete. Low strength concrete, which already has an inherently higher porosity, is more greatly affected by improper curing than high strength concrete. This is presumed to be due to the ease with which water can evaporate from the surface of the more porous cement paste.

Concrete workability has been found to be a factor which can help to reduce the embodied carbon of concrete, with stiffer mixes having lower carbon footprints. This study has shown that while stiff concrete mixes may show improved transport properties, their lower paste volumes leave them more susceptible to carbonation. Also the study shows that stiff concrete mixes may be less durable and more susceptible to improper curing. This may be explained by the lower overall water contents within the stiff mixes, and therefore the greater impact of surface water evaporation.
- The effect of changes in the degree of saturation on concrete compressive strength*

The effect of changes in the degree of saturation showed the deleterious effects of improper curing, with the saturated, ambient cured samples all exhibiting lower strengths than the equivalent ideally cured samples.
- Performance as a result of changes in the degree of hydration as measured by a suite of analytical techniques.*

The large capillary pores developed due to improper curing was seen with lower CH contents. The reduced hydration products obtained support the result that lower

degree of hydration was produced due to improper curing since the hydration of cement cannot continue in the dry environment.

- *The effect of improper curing on concrete durability, particularly resistance to carbonation.*

The effect of improper curing on resistance to carbonation reveals that samples that were not cured carbonated more than the ideal cured samples. Also higher carbonation depth were seen on fly ash samples that were not cured. The initial 28 days curing is sufficient to resist carbonation as the result of 90 days curing does not have much difference on the carbonation depth.

Concrete workability has been found to be a factor which can help to reduce the embodied carbon of concrete [Purnell and Black 2012] with stiffer mixes having lower carbon footprints. This study has shown that while stiff concrete mixes may show improved transport properties, their lower paste volumes leave them more susceptible to carbonation.

This study confirms the need for good site practice, and also shows that embodied carbon should not be the only factor when considering the environmental performance of concrete. Rather, durability and whole life performance should also be considered.

10.2 Suggestions for Further Works

The impact of improper curing on concrete properties that may affect concrete durability has been examined in this study with the degree of hydration mostly at 28 days. Further research should examine the degree of hydration qualitatively. The samples can be ambient and ideally cured for 28 days but examination days can be extended to 90 days and 180 days to really know the impact of improper curing at longer days.

The SEM images should be further examined on the sliced specimen cut horizontally to study the rate of hydration from the surface to the core of the concrete.

The method of exposing ambient cured paste samples should be changed for further study. Ambient samples should be exposed completely just like stripping concrete samples from the mould after 24 hours of casting. This can be achieved by using high early rise cement (CEM1 52.5R) in order to get high early strength for low strength concrete.

The samples for carbonation experiments should be put in the oven at 40°C after curing for two weeks before putting them in the carbonation chamber. This is important particularly for the high targeted concretes (50 and 80MPa) for enough water to dry from the samples.

This study has examined the impact of improper curing on resistance to carbonation, further works should involve other durability problems such as resistance to the ingress of chloride ions, sulphate attack, freeze thaw.

References

1. Aïtcin, P.-C. Cements of yesterday and today: concrete of tomorrow. *Cement and Concrete Research*. 2000, **30**(9), pp.1349-1359.
2. Meyer, C. The greening of the concrete industry. *Cement and Concrete Composites*. 2009, **31**(8), pp.601-605.
3. Shi, X. ,Xie, N. ,Fortune, K. and Gong, J. Durability of steel reinforced concrete in chloride environments: An overview. *Construction and Building Materials*. 2012, **30**, pp.125-138.
4. Mindess, S. ,Young, J. and Darwin, D. *Concrete*. 2nd ed. New Jersey: Prentice Hall, 2003.
5. Sabir, B. ,Wild, S. and Bai, J. Metakaolin and calcined clays as pozzolans for concrete: a review. *Cement and Concrete Composites*. 2001, **23**(6), pp.441-454.
6. Meyer, C. Concrete as a green building material. In: *Construction Materials Mindess Symposium*, 2005.
7. Gaimster, R. and Munn, C. The Role of Concrete in Sustainable Development. *Nueva Zelanda*. 2007.
8. Purnell, P. and Black, L. Embodied carbon dioxide in concrete: Variation with common mix design parameters. *Cement and Concrete Research*. 2012, **42**(6), pp.874-877.
9. Chandler David L. Paving the way to greenhouse gas reductions. [Online]. 2011, [Accessed 8/2013]. Available from: <http://web.mit.edu/newsoffice/2011/concrete-pavements-0829.html>.
10. Damtoft, J. ,Lukasik, J. ,Herfort, D. ,Sorrentino, D. and Gartner, E. Sustainable development and climate change initiatives. *Cement and Concrete Research*. 2008, **38**(2), pp.115-127.
11. Mehta, P.K. Reducing the environmental impact of concrete. *Concrete International*. 2001, **23**(10), pp.61-66.
12. British Standards Institution. 9780580907463;0580907465;. *BS EN 206:2013+A1:2016: Concrete. Specification, performance, production and conformity*. British Standards Institute, 2013.
13. Berndt, M. Properties of sustainable concrete containing fly ash, slag and recycled concrete aggregate. *Construction and Building Materials*. 2009, **23**(7), pp.2606-2613.
14. Siddique, R. Performance characteristics of high-volume Class F fly ash concrete. *Cement and Concrete Research*. 2004, **34**(3), pp.487-493.
15. Thomas, M.D.A. *Supplementary cementing materials in concrete*. Boca Raton, FL: CRC Press, 2013.
16. Al-Gahtani, A. Effect of curing methods on the properties of plain and blended cement concretes. *Construction and Building Materials*. 2010, **24**(3), pp.308-314.
17. Neville, A.M. *Properties of concrete*. 5th ed. Harlow: Prentice Hall, 2011.
18. Bentz, D.P. and Stutzman, P.E. Curing, hydration, and microstructure of cement paste. *ACI materials journal*. 2006, **103**(5), p.348.
19. Ramezaniapour, A. and Malhotra, V. Effect of curing on the compressive strength, resistance to chloride-ion penetration and porosity of concretes incorporating slag, fly ash or silica fume. *Cement and Concrete Composites*. 1995, **17**(2), pp.125-133.
20. Butler, W.B. ,Janssen, D.J. ,Schell, H.C. ,Cabrera, J.G. ,Keck, R.H. ,Schmitt, J.W. ,Carrasquillo, R.L. ,Khan, M.S. ,Scholer, C.F. and Ellis Jr, W.E. *Guide to Durable Concrete*. 2001.
21. Gowripalan, N. ,Cabrera, J. ,Cusens, A. and Wainwright, P. Effect of curing on durability. *Concrete International*. 1990, **12**(2), pp.47-54.
22. Taylor, P.C. *Curing concrete*. CRC Press, 2013.
23. Haque, M. Some concretes need 7 days initial curing. *Concrete International*. 1990, **12**(2), pp.42-46.

24. Toutanji, H. ,Delatte, N. ,Aggoun, S. ,Duval, R. and Danson, A. Effect of supplementary cementitious materials on the compressive strength and durability of short-term cured concrete. *Cement and Concrete Research*. 2004, **34**(2), pp.311-319.
25. Thomas, M.D. ,Matthews, J. and Haynes, C. Effect of curing on the strength and permeability of PFA concrete. *Special Publication*. 1989, **114**, pp.191-218.
26. Visser, J. and Van Mier, J. Dry and hydraulic extensile fracturing of porous impermeable materials. *HERON*, **41** (4), 1996. 1996.
27. Shoukry, S.N. ,William, G.W. ,Downie, B. and Riad, M.Y. Effect of moisture and temperature on the mechanical properties of concrete. *Construction and Building Materials*. 2011, **25**(2), pp.688-696.
28. Chen, X. ,Huang, W. and Zhou, J. Effect of moisture content on compressive and split tensile strength of concrete. *Indian Journal of Engineering & Materials Sciences*. 2012, **19**(6), pp.427-435.
29. Flower, D.J. and Sanjayan, J.G. Green house gas emissions due to concrete manufacture. *The international Journal of life cycle assessment*. 2007, **12**(5), pp.282-288.
30. Collins, F. Inclusion of carbonation during the life cycle of built and recycled concrete: influence on their carbon footprint. *The international Journal of life cycle assessment*. 2010, **15**(6), pp.549-556.
31. Basheer, L. ,Kropp, J. and Cleland, D.J. Assessment of the durability of concrete from its permeation properties: a review. *Construction and Building Materials*. 2001, **15**(2), pp.93-103.
32. Cabrera, J. ,Gowripalan, N. and Wainwright, P. An assessment of concrete curing efficiency using gas permeability. *Magazine of Concrete Research*. 1989, **41**(149), pp.193-198.
33. Nawy, E.G. *Concrete construction engineering handbook*. CRC press, 2008.
34. Mehta, P.K. and Monteiro, P. *Concrete: microstructure, properties, and materials*. New York;London;: McGraw-Hill, 2006.
35. Eglinton, M.S. *Concrete and its chemical behaviour*. London: Thomas Telford, 1987.
36. Kosmatka, S.H. ,Panarese, W.C. ,Allen, G.E. and Cumming, S. *Design and control of concrete mixtures*. Portland Cement Association Skokie, IL, 2002.
37. Ahmaruzzaman, M. A review on the utilization of fly ash. *Progress in Energy and Combustion Science*. 2010, **36**(3), pp.327-363.
38. British Standards Institution. *BS EN 197-1 Cement Part 1: Composition, specifications and conformity criteria for common cements*. 2011.
39. Khatib, J. and Hibbert, J. Selected engineering properties of concrete incorporating slag and metakaolin. *Construction and Building Materials*. 2005, **19**(6), pp.460-472.
40. Hadj-sadok, A. ,Kenai, S. ,Courard, L. and Darimont, A. Microstructure and durability of mortars modified with medium active blast furnace slag. *Construction and Building Materials*. 2011, **25**(2), pp.1018-1025.
41. Justice, J. and Kurtis, K. Influence of metakaolin surface area on properties of cement-based materials. *Journal of Materials in Civil Engineering*. 2007, **19**(9), pp.762-771.
42. Bye, G.C. ,Livesey, P. ,Struble, L.J. and Institution of Civil, E. *Portland cement*. London: ICE Pub, 2011.
43. Taylor, H.F.W. *Cement chemistry*. London: Thomas Telford, 1997.
44. Hewlett, P.C. *Lea's chemistry of cement and concrete*. Oxford: Elsevier Butterworth-Heinemann, 2004.
45. Shafiq, N. and Nuruddin, M.F. Degree of hydration of OPC and OPC/FA pastes dried in different relative humidity. *Concrete Research Letters*. 2010, **1**(3), pp.81-89.
46. Xiao, L. and Li, Z. New understanding of cement hydration mechanism through electrical resistivity measurement and microstructure investigations. *Journal of Materials in Civil Engineering*. 2009, **21**(8), pp.368-373.

47. Mindess, S. and Eng, P. Concrete Constituent Materials. *Concrete construction engineering handbook*. 1997.
48. Tennis, P.D. and Jennings, H.M. A model for two types of calcium silicate hydrate in the microstructure of Portland cement pastes. *Cement and Concrete Research*. 2000, **30**(6), pp.855-863.
49. Odler, I. Hydration, setting and hardening of Portland cement. *Lea's chemistry of cement and concrete*. 2003, **4**, pp.241-297.
50. Gartner, E.M. and Gaidis, J.M. Hydration mechanisms: I. *Materials Science of Concrete III, I, 1 pp*. 1989, **95**.
51. Gaidis, J. and Gartner, E. Hydration mechanisms: II. *Materials Science of Concrete II*. 1991, pp.9-39.
52. Chen, Y. and Odler, I. On the origin of Portland cement setting. *Cement and Concrete Research*. 1992, **22**(6), pp.1130-1140.
53. Ylmén, R. ,Jäglid, U. ,Steenari, B.-M. and Panas, I. Early hydration and setting of Portland cement monitored by IR, SEM and Vicat techniques. *Cement and Concrete Research*. 2009, **39**(5), pp.433-439.
54. Bullard, J.W. ,Jennings, H.M. ,Livingston, R.A. ,Nonat, A. ,Scherer, G.W. ,Schweitzer, J.S. ,Scrivener, K.L. and Thomas, J.J. Mechanisms of cement hydration. *Cement and Concrete Research*. 2011, **41**(12), pp.1208-1223.
55. Gartner, E.M. ,Young , J.F. ,Damidot, D.A. and Jawed, I. Hydration of portland cement.In: *Structure and performance of cements*. 2002, (Book, Whole), pp.57-113.
56. Odler, I. and Schüppstuhl, J. Early hydration of tricalcium silicate III. Control of the induction period. *Cement and Concrete Research*. 1981, **11**(5), pp.765-774.
57. Brown, P.W. ,Franz, E. ,Frohsdorff, G. and Taylor, H. Analyses of the aqueous phase during early C 3 S hydration. *Cement and Concrete Research*. 1984, **14**(2), pp.257-262.
58. Costoya Fernández, M.M. Effect of particle size on the hydration kinetics and microstructural development of tricalcium silicate. 2008.
59. Bishnoi, S. and Scrivener, K.L. Studying nucleation and growth kinetics of alite hydration using μ c. *Cement and Concrete Research*. 2009, **39**(10), pp.849-860.
60. Scrivener, K.L. Backscattered electron imaging of cementitious microstructures: understanding and quantification. *Cement and Concrete Composites*. 2004, **26**(8), pp.935-945.
61. Idowu, O. and Black, L. Effects of improper concrete curing on engineering performance: a microstructural study In: *Cement and Concrete Science Conference, 5th and 6th September Cardiff*. 2016.
62. Yaman, I. ,Hearn, N. and Aktan, H. Active and non-active porosity in concrete part I: experimental evidence. *Materials and structures*. 2002, **35**(2), pp.102-109.
63. Bapat, J.D. *Mineral admixtures in cement and concrete*. Boca Raton: CRC Press, Taylor & Francis Group, 2013.
64. Zhang, J. and Scherer, G.W. Comparison of methods for arresting hydration of cement. *Cement and Concrete Research*. 2011, **41**(10), pp.1024-1036.
65. Siddique, R. and Khan, M.I. *Supplementary cementing materials*. Springer, 2011.
66. Cao, C. ,Sun, W. and Qin, H. The analysis on strength and fly ash effect of roller-compacted concrete with high volume fly ash. *Cement and Concrete Research*. 2000, **30**(1), pp.71-75.
67. Uysal, M. and Akyuncu, V. Durability performance of concrete incorporating Class F and Class C fly ashes. *Construction and Building Materials*. 2012, **34**, pp.170-178.
68. Thomas, M. *Supplementary cementing materials in concrete*. CRC Press, 2013.
69. Dhir, R. ,Hubbard, F. ,Munday, J. ,Jones, M. and Duerden, S. Contribution of PFA to concrete workability and strength development. *Cement and Concrete Research*. 1988, **18**(2), pp.277-289.

70. Bai, J. ,Wild, S. ,Sabir, B.B. and Kinuthia, J.M. Workability of concrete incorporating pulverized fuel ash and metakaolin. *Magazine of Concrete Research*. 1999, **51**(3), pp.207-216.
71. Camões, A. ,Aguiar, J. and Jalali, S. Durability of low cost high performance fly ash concrete. 2003.
72. Megat Johari, M.A. ,Brooks, J.J. ,Kabir, S. and Rivard, P. Influence of supplementary cementitious materials on engineering properties of high strength concrete. *Construction and Building Materials*. 2011, **25**(5), pp.2639-2648.
73. Tahir, M.A. THE WORKABILITY AND STRENGTH DEVELOPMENT OF GROUND FLY ASH-CONCRETES. 2006.
74. Hwang, K. ,Noguchi, T. and Tomosawa, F. Prediction model of compressive strength development of fly-ash concrete. *Cement and Concrete Research*. 2004, **34**(12), pp.2269-2276.
75. Chindapasirt, P. ,Jaturapitakkul, C. and Sinsiri, T. Effect of fly ash fineness on compressive strength and pore size of blended cement paste. *Cement and Concrete Composites*. 2005, **27**(4), pp.425-428.
76. Oner, A. ,Akyuz, S. and Yildiz, R. An experimental study on strength development of concrete containing fly ash and optimum usage of fly ash in concrete. *Cement and Concrete Research*. 2005, **35**(6), pp.1165-1171.
77. Kosior-Kazberuk, M. and Lelusz, M. Strength development of concrete with fly ash addition. *Journal of Civil Engineering and Management*. 2007, **13**(2), pp.115-122.
78. Poon, C. ,Lam, L. and Wong, Y. A study on high strength concrete prepared with large volumes of low calcium fly ash. *Cement and Concrete Research*. 2000, **30**(3), pp.447-455.
79. Hanehara, S. ,Tomosawa, F. ,Kobayakawa, M. and Hwang, K. Effects of water/powder ratio, mixing ratio of fly ash, and curing temperature on pozzolanic reaction of fly ash in cement paste. *Cement and Concrete Research*. 2001, **31**(1), pp.31-39.
80. Bijen, J. Benefits of slag and fly ash. *Construction and Building Materials*. 1996, **10**(5), pp.309-314.
81. Naik, T.R. ,Singh, S.S. and Hossain, M.M. Permeability of concrete containing large amounts of fly ash. *Cement and Concrete Research*. 1994, **24**(5), pp.913-922.
82. Thomas, M. and Matthews, J. The permeability of fly ash concrete. *Materials and structures*. 1992, **25**(7), pp.388-396.
83. Beglarigale, A. ,Ghajeri, F. ,Yiğiter, H. and Yazıcı, H. Permeability Characterization of Concrete Incorporating Fly Ash. 2014.
84. Elahi, A. ,Basheer, P.A.M. ,Nanukuttan, S.V. and Khan, Q.U.Z. Mechanical and durability properties of high performance concretes containing supplementary cementitious materials. *Construction and Building Materials*. 2010, **24**(3), pp.292-299.
85. Das, B. ,Singh, D. and Pandey, S. Rapid Chloride Ion Permeability of OPC-and PPC-Based Carbonated Concrete. *Journal of Materials in Civil Engineering*. 2011, **24**(5), pp.606-611.
86. Chi, J.M. ,Huang, R. and Yang, C. Effects of carbonation on mechanical properties and durability of concrete using accelerated testing method. *Journal of marine science and technology*. 2002, **10**(1), pp.14-20.
87. Sulapha, P. ,Wong, S. ,Wee, T. and Swaddiwudhipong, S. Carbonation of concrete containing mineral admixtures. *Journal of Materials in Civil Engineering*. 2003, **15**(2), pp.134-143.
88. Atiş, C.D. Accelerated carbonation and testing of concrete made with fly ash. *Construction and Building Materials*. 2003, **17**(3), pp.147-152.
89. Khunthongkeaw, J. ,Tangtermsirikul, S. and Leelawat, T. A study on carbonation depth prediction for fly ash concrete. *Construction and Building Materials*. 2006, **20**(9), pp.744-753.

90. Papadakis, V.G. Effect of supplementary cementing materials on concrete resistance against carbonation and chloride ingress. *Cement and Concrete Research*. 2000, **30**(2), pp.291-299.
91. Das, B.B. and Pandey, S.P. Influence of Fineness of Fly Ash on the Carbonation and Electrical Conductivity of Concrete. *Journal of Materials in Civil Engineering*. 2011, **23**(9), pp.1365-1368.
92. Nath, P. and Sarker, P. Effect of fly ash on the durability properties of high strength concrete. *Procedia Engineering*. 2011, **14**, pp.1149-1156.
93. Tasdemir, C. Combined effects of mineral admixtures and curing conditions on the sorptivity coefficient of concrete. *Cement and Concrete Research*. 2003, **33**(10), pp.1637-1642.
94. Ramachandran, V.S. *Handbook of thermal analysis of construction materials*. Norwich, N.Y: Noyes Publications, 2002.
95. Wang, Q. ,Feng, J. and Yan, P. The microstructure of 4-year-old hardened cement-fly ash paste. *Construction and Building Materials*. 2012, **29**, pp.114-119.
96. Chindapasirt, P. ,Jaturapitakkul, C. and Sinsiri, T. Effect of fly ash fineness on microstructure of blended cement paste. *Construction and Building Materials*. 2007, **21**(7), pp.1534-1541.
97. Nocuń-Wczelik, W. Heat evolution in hydrated cementitious systems admixed with fly ash. *Journal of thermal analysis and calorimetry*. 2001, **65**(2), pp.613-619.
98. Li, G. Properties of high-volume fly ash concrete incorporating nano-SiO₂. *Cement and Concrete Research*. 2004, **34**(6), pp.1043-1049.
99. Duran-Herrera, A. ,Juarez, C. ,Valdez, P. and Bentz, D. Evaluation of sustainable high-volume fly ash concretes. *Cement and Concrete Composites*. 2011, **33**(1), pp.39-45.
100. Fu, X. ,Wang, Z. ,Tao, W. ,Yang, C. ,Hou, W. ,Dong, Y. and Wu, X. Studies on blended cement with a large amount of fly ash. *Cement and Concrete Research*. 2002, **32**(7), pp.1153-1159.
101. Jun-Yuan, H. ,Scheetz, B.E. and Roy, D.M. Hydration of fly ash-portland cements. *Cement and Concrete Research*. 1984, **14**(4), pp.505-512.
102. Sakai, E. ,Miyahara, S. ,Ohsawa, S. ,Lee, S.-H. and Daimon, M. Hydration of fly ash cement. *Cement and Concrete Research*. 2005, **35**(6), pp.1135-1140.
103. Williams, P.J. ,Biernacki, J.J. ,Walker, L.R. ,Meyer, H.M. ,Rawn, C.J. and Bai, J. Microanalysis of alkali-activated fly ash-CH pastes. *Cement and Concrete Research*. 2002, **32**(6), pp.963-972.
104. Hu, C. Microstructure and mechanical properties of fly ash blended cement pastes. *Construction and Building Materials*. 2014, **73**, pp.618-625.
105. Lam, L. ,Wong, Y. and Poon, C. Degree of hydration and gel/space ratio of high-volume fly ash/cement systems. *Cement and Concrete Research*. 2000, **30**(5), pp.747-756.
106. Narmluk, M. and Nawa, T. Effect of fly ash on the kinetics of Portland cement hydration at different curing temperatures. *Cement and Concrete Research*. 2011, **41**(6), pp.579-589.
107. Termkhajornkit, P. ,Nawa, T. and Kurumisawa, K. Effect of water curing conditions on the hydration degree and compressive strengths of fly ash-cement paste. *Cement and Concrete Composites*. 2006, **28**(9), pp.781-789.
108. Lothenbach, B. ,Scrivener, K. and Hooton, R. Supplementary cementitious materials. *Cement and Concrete Research*. 2011, **41**(12), pp.1244-1256.
109. Haha, M.B. ,De Weerd, K. and Lothenbach, B. Quantification of the degree of reaction of fly ash. *Cement and Concrete Research*. 2010, **40**(11), pp.1620-1629.
110. Xu, A. ,Sarkar, S. and Nilsson, L. Effect of fly ash on the microstructure of cement mortar. *Materials and structures*. 1993, **26**(7), pp.414-424.
111. Korpa, A. and Trettin, R. The influence of different drying methods on cement paste microstructures as reflected by gas adsorption: comparison between freeze-drying (F-

- drying), D-drying, P-drying and oven-drying methods. *Cement and Concrete Research*. 2006, **36**(4), pp.634-649.
112. Zhang, L. and Glasser, F. Critical examination of drying damage to cement pastes. *Advances in cement research*. 2000, **12**(2), pp.79-88.
113. Konecny, L. and Naqvi, S. The effect of different drying techniques on the pore size distribution of blended cement mortars. *Cement and Concrete Research*. 1993, **23**(5), pp.1223-1228.
114. Feldman, R.F. and Beaudoin, J.J. Pretreatment of hardened hydrated cement pastes for mercury intrusion measurements. *Cement and Concrete Research*. 1991, **21**(2-3), pp.297-308.
115. Kalliopi, K. Pore structure of cement-based materials. *Testing, interpretation and requirements. Modern concrete technology series*. 2006, **12**, pp.1-33.
116. Feldman, R.F. Diffusion measurements in cement paste by water replacement using propan-2-ol. *Cement and Concrete Research*. 1987, **17**(4), pp.602-612.
117. Beaudoin, J.J. ,Gu, P. ,Marchand, J. ,Tamtsia, B. ,Myers, R.E. and Liu, Z. Solvent replacement studies of hydrated Portland cement systems: the role of calcium hydroxide. *Advanced Cement Based Materials*. 1998, **8**(2), pp.56-65.
118. Collier, N. ,Sharp, J. ,Milestone, N. ,Hill, J. and Godfrey, I. The influence of water removal techniques on the composition and microstructure of hardened cement pastes. *Cement and Concrete Research*. 2008, **38**(6), pp.737-744.
119. Knapen, E. ,Cizer, O. ,Van Balen, K. and Van Gemert, D. Effect of free water removal from early-age hydrated cement pastes on thermal analysis. *Construction and Building Materials*. 2009, **23**(11), pp.3431-3438.
120. Gallé, C. Effect of drying on cement-based materials pore structure as identified by mercury intrusion porosimetry: a comparative study between oven-, vacuum-, and freeze-drying. *Cement and Concrete Research*. 2001, **31**(10), pp.1467-1477.
121. Diamond, S. A discussion of the paper "Effect of drying on cement-based materials pore structure as identified by mercury porosimetry—a comparative study between oven-, vacuum-, and freeze-drying" by C. Gallé. *Cement and Concrete Research*. 2003, **33**(1), pp.169-170.
122. Tang, S.W. ,Yao, Y. ,Andrade, C. and Li, Z. Recent durability studies on concrete structure. *Cement and Concrete Research*. 2015, **78**, pp.143-154.
123. Alexander, M.G. ,Santhanam, M. and Ballim, Y. Durability design and specification for concrete structures—the way forward. *International Journal of Advances in Engineering Sciences and Applied Mathematics*. 2010, **2**(3), pp.95-105.
124. Frigione, G. and Zenone, F. *Quality control of concrete*. 1991.
125. Alexander, M. and Thomas, M. Service life prediction and performance testing—Current developments and practical applications. *Cement and Concrete Research*. 2015, **78**, pp.155-164.
126. Bhargava, A. and Banthia, N. Measurement of concrete permeability under stress. *Experimental Techniques*. 2006, **30**(5), pp.28-31.
127. Sanjuan, M. and Munoz-Martialay, R. Oven-drying as a preconditioning method for air permeability test on concrete. *Materials Letters*. 1996, **27**(4), pp.263-268.
128. British Standards Institution. *BS 1881-122:2011 Testing concrete Part 122: Method for determination of water absorption*. 2011.
129. British Standards Institution. *BS EN 12390-2:2009: Testing hardened concrete. Making and curing specimens for strength tests*. British Standards Institute, 2009.
130. Khatib, J. Effect of initial curing on absorption and pore size distribution of paste and concrete containing slag. *KSCE Journal of Civil Engineering*. 2014, **18**(1), p.264.
131. British Standards Institution. 9780580262012;0580262014;. *BS 1881-208:1996: Testing concrete. Recommendations for the determination of the initial surface absorption of concrete*. British Standards Institute, 1996.

132. Hall, C. Water movement in porous building materials—IV. The initial surface absorption and the sorptivity. *Building and environment*. 1981, **16**(3), pp.201-207.
133. Gopalan, M. Sorptivity of fly ash concretes. *Cement and Concrete Research*. 1996, **26**(8), pp.1189-1197.
134. Güneyisi, E. and Gesoğlu, M. A study on durability properties of high-performance concretes incorporating high replacement levels of slag. *Materials and structures*. 2008, **41**(3), pp.479-493.
135. Dias, W. Reduction of concrete sorptivity with age through carbonation. *Cement and Concrete Research*. 2000, **30**(8), pp.1255-1261.
136. Chidiac, S. ,Maadani, O. ,Razaqpur, A. and Mailvaganam, N. Correlation of rheological properties to durability and strength of hardened concrete. *Journal of Materials in Civil Engineering*. 2003, **15**(4), pp.391-399.
137. Ho, D. ,Cui, Q. and Ritchie, D. The influence of humidity and curing time on the quality of concrete. *Cement and Concrete Research*. 1989, **19**(3), pp.457-464.
138. Ho, D. and Chirgwin, G.J. A performance specification for durable concrete. *Construction and Building Materials*. 1996, **10**(5), pp.375-379.
139. British Standards Institution. *BS EN 12390-3 Testing hardened concrete Part 3: Compressive strength of test specimens*. 2009.
140. Lee, B.J. ,Kee, S.-H. ,Oh, T. and Kim, Y.-Y. Effect of cylinder size on the modulus of elasticity and compressive strength of concrete from static and dynamic tests. *Advances in Materials Science and Engineering*. 2015, **2015**.
141. Safiuddin, M. and Scott, B. Abrasion Resistance of Concrete—Design, Construction and Case Study. *Concrete Research Letters*. 2015, **6**(3), pp.136-148.
142. Horszczaruk, E. Abrasion resistance of high-strength concrete in hydraulic structures. *Wear*. 2005, **259**(1), pp.62-69.
143. Bakke, K.J. *Abrasion Resistance, Significance of Tests and Properties of Concrete and Concrete-Making Materials*. ASTM STP 169D, Bridgeport, 2006.
144. Jason, C.Y. ,Yu, C. and Bull, J.W. *Durability of Materials and Structures in Building and Civil Engineering*. Whittles, 2006.
145. Bastidas-Arteaga, E. ,Chateauneuf, A. ,Sánchez-Silva, M. ,Bressolette, P. and Schoefs, F. A comprehensive probabilistic model of chloride ingress in unsaturated concrete. *Engineering Structures*. 2011, **33**(3), pp.720-730.
146. Roziere, E. ,Loukili, A. and Cussigh, F. A performance based approach for durability of concrete exposed to carbonation. *Construction and Building Materials*. 2009, **23**(1), pp.190-199.
147. Shang, H.S. and Song, Y. Experimental study of strength and deformation of plain concrete under biaxial compression after freezing and thawing cycles. *Cement and Concrete Research*. 2006, **36**(10), pp.1857-1864.
148. Yun, H.-D. ,Kim, S.-W. ,Lee, Y.-O. and Rokugo, K. Tensile behavior of synthetic fiber-reinforced strain-hardening cement-based composite (SHCC) after freezing and thawing exposure. *Cold Regions Science and Technology*. 2011, **67**(1), pp.49-57.
149. Hamze, Y. Concrete durability in harsh environmental conditions exposed to freeze thaw cycles. *Physics Procedia*. 2014, **55**, pp.265-270.
150. Skripkiūnas, G. ,Nagrockienė, D. ,Girskas, G. ,Vaičienė, M. and Baranauskaitė, E. The cement type effect on freeze–thaw and deicing salt resistance of concrete. *Procedia Engineering*. 2013, **57**, pp.1045-1051.
151. Kumar, R. and Bhattacharjee, B. Porosity, pore size distribution and in situ strength of concrete. *Cement and Concrete Research*. 2003, **33**(1), pp.155-164.
152. Penttala, V. Surface and internal deterioration of concrete due to saline and non-saline freeze–thaw loads. *Cement and Concrete Research*. 2006, **36**(5), pp.921-928.
153. Liu, Z. and Hansen, W. Effect of hydrophobic surface treatment on freeze-thaw durability of concrete. *Cement and Concrete Composites*. 2016, **69**, pp.49-60.

154. Zalocha, D. and Kasperkiewicz, J. Estimation of the structure of air entrained concrete using a flatbed scanner. *Cement and Concrete Research*. 2005, **35**(10), pp.2041-2046.
155. Zhang, Z. and Ansari, F. Fracture mechanics of air-entrained concrete subjected to compression. *Engineering fracture mechanics*. 2006, **73**(13), pp.1913-1924.
156. Concrete, A.I.C.C.o. and Aggregates, C. *Standard Test Method for Resistance of Concrete to Rapid Freezing and Thawing*. ASTM International, 2008.
157. Molero, M. ,Aparicio, S. ,Al-Assadi, G. ,Casati, M. ,Hernández, M. and Anaya, J. Evaluation of freeze–thaw damage in concrete by ultrasonic imaging. *NDT & E International*. 2012, **52**, pp.86-94.
158. Taylor, H. ,Famy, C. and Scrivener, K. Delayed ettringite formation. *Cement and Concrete Research*. 2001, **31**(5), pp.683-693.
159. Collepardi, M. A state-of-the-art review on delayed ettringite attack on concrete. *Cement and Concrete Composites*. 2003, **25**(4), pp.401-407.
160. Brown, P. and Badger, S. The distributions of bound sulfates and chlorides in concrete subjected to mixed NaCl, MgSO₄, Na₂SO₄ attack. *Cement and Concrete Research*. 2000, **30**(10), pp.1535-1542.
161. Brown, P. and Doerr, A. Chemical changes in concrete due to the ingress of aggressive species. *Cement and Concrete Research*. 2000, **30**(3), pp.411-418.
162. Bellmann, F. ,Möser, B. and Stark, J. Influence of sulfate solution concentration on the formation of gypsum in sulfate resistance test specimen. *Cement and Concrete Research*. 2006, **36**(2), pp.358-363.
163. Scherer, G.W. Stress from crystallization of salt. *Cement and Concrete Research*. 2004, **34**(9), pp.1613-1624.
164. Thaulow, N. and Sahu, S. Mechanism of concrete deterioration due to salt crystallization. *Materials Characterization*. 2004, **53**(2), pp.123-127.
165. Rodriguez-Navarro, C. ,Doehne, E. and Sebastian, E. How does sodium sulfate crystallize? Implications for the decay and testing of building materials. *Cement and Concrete Research*. 2000, **30**(10), pp.1527-1534.
166. Al-Amoudi, O.S.B. Sulfate attack and reinforcement corrosion in plain and blended cements exposed to sulfate environments. *Building and environment*. 1998, **33**(1), pp.53-61.
167. Chen, J.-k. and Jiang, M.-q. Long-term evolution of delayed ettringite and gypsum in Portland cement mortars under sulfate erosion. *Construction and Building Materials*. 2009, **23**(2), pp.812-816.
168. Lawrence, C. Mortar expansions due to delayed ettringite formation. Effects of curing period and temperature. *Cement and Concrete Research*. 1995, **25**(4), pp.903-914.
169. Rahman, M. and Bassuoni, M. Thaumasite sulfate attack on concrete: Mechanisms, influential factors and mitigation. *Construction and Building Materials*. 2014, **73**, pp.652-662.
170. ASTM, C. 1012-95a, "Standard Test Method for Length Change of Hydraulic Cement Mortars Exposed to a Sulfate Solution". *American Society for Testing and Materials, Committee C-1, Subcommittee C*. 1995, **1**, p.29.
171. El-Hachem, R. ,Rozière, E. ,Grondin, F. and Loukili, A. New procedure to investigate external sulphate attack on cementitious materials. *Cement and Concrete Composites*. 2012, **34**(3), pp.357-364.
172. Whittaker, M.J. *The impact of slag composition on the microstructure of composite slag cements exposed to sulfate attack*. thesis, University of Leeds, 2014.
173. Bonakdar, A. and Mobasher, B. Multi-parameter study of external sulfate attack in blended cement materials. *Construction and Building Materials*. 2010, **24**(1), pp.61-70.
174. Punmia, B. ,Jain, A.K. and Jain, A.K. *Basic Civil Engineering*. Firewall Media, 2003.
175. Abbas, A. ,Carcasses, M. and Ollivier, J.-P. Gas permeability of concrete in relation to its degree of saturation. *Materials and structures*. 1999, **32**(1), pp.3-8.

176. Jiang, J. and Yuan, Y. Relationship of moisture content with temperature and relative humidity in concrete. *Magazine of Concrete Research*. 2013, **65**(11), pp.685-692.
177. Andrade, C. ,Sarría, J. and Alonso, C. Relative humidity in the interior of concrete exposed to natural and artificial weathering. *Cement and Concrete Research*. 1999, **29**(8), pp.1249-1259.
178. Rucker-Gramm, P. and Beddoe, R.E. Effect of moisture content of concrete on water uptake. *Cement and Concrete Research*. 2010, **40**(1), pp.102-108.
179. Popovics, S. Effect of curing method and final moisture condition on compressive strength of concrete. In: *Journal Proceedings*, 1986, pp.650-657.
180. Bartlett, F.M. and MacGregor, J.G. Effect of moisture condition on concrete core strengths. *ACI materials journal*. 1994, **91**(3).
181. Pihlajavaara, S. A review of some of the main results of a research on the ageing phenomena of concrete: Effect of moisture conditions on strength, shrinkage and creep of mature concrete. *Cement and Concrete Research*. 1974, **4**(5), pp.761-771.
182. Safiuddin, M. ,Raman, S.N. and Zain, M.F.M. Effects of medium temperature and industrial by-products on the key hardened properties of high performance concrete. *Materials*. 2015, **8**(12), pp.8608-8623.
183. Arioz, O. Effects of elevated temperatures on properties of concrete. *Fire Safety Journal*. 2007, **42**(8), pp.516-522.
184. Zhang, B. Effects of moisture evaporation (weight loss) on fracture properties of high performance concrete subjected to high temperatures. *Fire Safety Journal*. 2011, **46**(8), pp.543-549.
185. Chen, B. ,Li, C. and Chen, L. Experimental study of mechanical properties of normal-strength concrete exposed to high temperatures at an early age. *Fire Safety Journal*. 2009, **44**(7), pp.997-1002.
186. Janotka, I. and Nürnbergerová, T. Effect of temperature on structural quality of the cement paste and high-strength concrete with silica fume. *Nuclear Engineering and Design*. 2005, **235**(17), pp.2019-2032.
187. Sarker, P.K. ,Kelly, S. and Yao, Z. Effect of fire exposure on cracking, spalling and residual strength of fly ash geopolymer concrete. *Materials & Design*. 2014, **63**, pp.584-592.
188. Sakr, K. and El-Hakim, E. Effect of high temperature or fire on heavy weight concrete properties. *Cement and Concrete Research*. 2005, **35**(3), pp.590-596.
189. Georgali, B. and Tsakiridis, P. Microstructure of fire-damaged concrete. A case study. *Cement and Concrete Composites*. 2005, **27**(2), pp.255-259.
190. Handoo, S. ,Agarwal, S. and Agarwal, S. Physicochemical, mineralogical, and morphological characteristics of concrete exposed to elevated temperatures. *Cement and Concrete Research*. 2002, **32**(7), pp.1009-1018.
191. Bastami, M. ,Chaboki-Khiabani, A. ,Baghbadrani, M. and Kordi, M. Performance of high strength concretes at elevated temperatures. *Scientia Iranica*. 2011, **18**(5), pp.1028-1036.
192. Ma, Q. ,Guo, R. ,Zhao, Z. ,Lin, Z. and He, K. Mechanical properties of concrete at high temperature—a review. *Construction and Building Materials*. 2015, **93**, pp.371-383.
193. Khan, M. ,Prasad, J. and Abbas, H. Effect of high temperature on high-volume fly ash concrete. *Arabian Journal for Science and Engineering*. 2013, **38**(6), pp.1369-1378.
194. Tanyildizi, H. and Coskun, A. The effect of high temperature on compressive strength and splitting tensile strength of structural lightweight concrete containing fly ash. *Construction and Building Materials*. 2008, **22**(11), pp.2269-2275.
195. Xu, Y. ,Wong, Y. ,Poon, C. and Anson, M. Impact of high temperature on PFA concrete. *Cement and Concrete Research*. 2001, **31**(7), pp.1065-1073.
196. Xu, Y. ,Wong, Y. ,Poon, C. and Anson, M. Influence of PFA on cracking of concrete and cement paste after exposure to high temperatures. *Cement and Concrete Research*. 2003, **33**(12), pp.2009-2016.

197. Poon, C.-S. ,Azhar, S. ,Anson, M. and Wong, Y.-L. Comparison of the strength and durability performance of normal-and high-strength pozzolanic concretes at elevated temperatures. *Cement and Concrete Research*. 2001, **31**(9), pp.1291-1300.
198. Imane, B. ,M'Hammed, M. ,Boudjemaa, L. and Abdelmadjid, H. Contribution to the Experimental Study of the Concrete Behavior in Its Climatic Environment. *Energy Procedia*. 2013, **36**, pp.1320-1327.
199. Holt, E. Contribution of mixture design to chemical and autogenous shrinkage of concrete at early ages. *Cement and Concrete Research*. 2005, **35**(3), pp.464-472.
200. Wongtanakitcharoen, T. and Naaman, A.E. Unrestrained early age shrinkage of concrete with polypropylene, PVA, and carbon fibers. *Materials and structures*. 2007, **40**(3), pp.289-300.
201. Bissonnette, B.t. ,Pierre, P. and Pigeon, M. Influence of key parameters on drying shrinkage of cementitious materials. *Cement and Concrete Research*. 1999, **29**(10), pp.1655-1662.
202. Cohen, M.D. ,Olek, J. and Dolch, W.L. Mechanism of plastic shrinkage cracking in portland cement and portland cement-silica fume paste and mortar. *Cement and Concrete Research*. 1990, **20**(1), pp.103-119.
203. Mora-Ruacho, J. ,Gettu, R. and Aguado, A. Influence of shrinkage-reducing admixtures on the reduction of plastic shrinkage cracking in concrete. *Cement and Concrete Research*. 2009, **39**(3), pp.141-146.
204. Schmidt, M. and Slowik, V. Capillary Pressure Controlled Concrete Curing in Pavement Construction. In: *Airfield and Highway Pavement 2013: Sustainable and Efficient Pavements*: ASCE, 2013, pp.295-306.
205. Sivakumar, A. and Santhanam, M. A quantitative study on the plastic shrinkage cracking in high strength hybrid fibre reinforced concrete. *Cement and Concrete Composites*. 2007, **29**(7), pp.575-581.
206. Ali, W. and Urgessa, G. Computational Model for Internal Relative Humidity Distributions in Concrete. *Journal of Computational Engineering*. 2014, **2014**.
207. Neubauer, C. ,Bergstrom, T. ,Sujata, K. ,Xi, Y. ,Garboczi, E. and Jennings, H. Drying shrinkage of cement paste as measured in an environmental scanning electron microscope and comparison with microstructural models. *Journal of materials science*. 1997, **32**(24), pp.6415-6427.
208. Aitcin, P. The durability characteristics of high performance concrete: a review. *Cement and Concrete Composites*. 2003, **25**(4), pp.409-420.
209. Abbasnia, R. ,Kanzadi, M. ,Zadeh, M.S. and Ahmadi, J. Prediction of free shrinkage strain related to internal moisture loss. *International Journal of Civil Engineering*. 2009, **7**(2), pp.92-98.
210. Mihashi, H. and Leite, J.P.d.B. State-of-the-art report on control of cracking in early age concrete. *Journal of Advanced Concrete Technology*. 2004, **2**(2), pp.141-154.
211. Tazawa, E.-i. ,Miyazawa, S. and Kasai, T. Chemical shrinkage and autogenous shrinkage of hydrating cement paste. *Cement and Concrete Research*. 1995, **25**(2), pp.288-292.
212. Theiner, Y. and Hofstetter, G. Evaluation of the effects of drying shrinkage on the behavior of concrete structures strengthened by overlays. *Cement and Concrete Research*. 2012, **42**(9), pp.1286-1297.
213. Gribniak, V. ,Kaklauskas, G. ,Kliukas, R. and Jakubovskis, R. Shrinkage effect on short-term deformation behavior of reinforced concrete—when it should not be neglected. *Materials & Design*. 2013, **51**, pp.1060-1070.
214. Jerga, J. Physico-mechanical properties of carbonated concrete. *Construction and Building Materials*. 2004, **18**(9), pp.645-652.
215. Claisse, P.A. ,Elsayad, H.I. and Shaaban, I.G. Absorption and sorptivity of cover concrete. *Journal of Materials in Civil Engineering*. 1997, **9**(3), pp.105-110.
216. Acker, P. and Ulm, F.-J. Creep and shrinkage of concrete: physical origins and practical measurements. *Nuclear Engineering and Design*. 2001, **203**(2), pp.143-158.

217. Nehdi, M. and Soliman, A.M. Early-age properties of concrete: overview of fundamental concepts and state-of-the-art research. *Proceedings of the Institution of Civil Engineers-Construction Materials*. 2011, **164**(2), pp.57-77.
218. Azenha, M. and Faria, R. Temperatures and stresses due to cement hydration on the R/C foundation of a wind tower—A case study. *Engineering Structures*. 2008, **30**(9), pp.2392-2400.
219. Shi, N. ,Ouyang, J. ,Zhang, R. and Huang, D. Experimental study on early-age crack of mass concrete under the controlled temperature history. *Advances in Materials Science and Engineering*. 2014, **2014**.
220. Pan, Z. ,Li, B. and Lu, Z. Re-evaluation of CEB-FIP 90 prediction models for creep and shrinkage with experimental database. *Construction and Building Materials*. 2013, **38**, pp.1022-1030.
221. Nassif, H. ,Suksawang, N. and Mohammed, M. Effect of curing methods on early-age and drying shrinkage of high-performance concrete. *Transportation Research Record: Journal of the Transportation Research Board*. 2003, (1834), pp.48-58.
222. Comité euro-international du, b. and Fédération internationale de la, p. *CEB-FIP model code 1990: design code*. London: Thomas Telford, 1993.
223. Rao, G.A. Long-term drying shrinkage of mortar—influence of silica fume and size of fine aggregate. *Cement and Concrete Research*. 2001, **31**(2), pp.171-175.
224. Dyer, T. *Concrete Durability*. Hoboken: CRC Press, 2014.
225. A.M., N. *Properties of concrete*. 5th Edition ed. England: Pearson Education Limited, 2011.
226. Zhang, W. ,Zakaria, M. and Hama, Y. Influence of aggregate materials characteristics on the drying shrinkage properties of mortar and concrete. *Construction and Building Materials*. 2013, **49**, pp.500-510.
227. Mu, R. and J.P, F. Modelling the shrinkage of early age concrete due to drying diffusion. 2009, **Internal report school of Civil Engineering**.
228. Ray, I. ,Gong, Z. ,Davalos, J.F. and Kar, A. Shrinkage and cracking studies of high performance concrete for bridge decks. *Construction and Building Materials*. 2012, **28**(1), pp.244-254.
229. Bloom, R. and Bentur, A. Free and restrained shrinkage of normal and high-strength concretes. *Materials Journal*. 1995, **92**(2), pp.211-217.
230. Al-Saleh, S.A. and Al-Zaid, R.Z. Effects of drying conditions, admixtures and specimen size on shrinkage strains. *Cement and Concrete Research*. 2006, **36**(10), pp.1985-1991.
231. Al-Amoudi, O. ,Maslehuddin, M. ,Shameem, M. and Ibrahim, M. Shrinkage of plain and silica fume cement concrete under hot weather. *Cement and Concrete Composites*. 2007, **29**(9), pp.690-699.
232. Brooks, J. Influence of mix proportions, plasticizers and superplasticizers on creep and drying shrinkage of concrete. *Magazine of Concrete Research*. 1989, **41**(148), pp.145-153.
233. Sajedi, F. and Razak, H.A. Effects of curing regimes and cement fineness on the compressive strength of ordinary Portland cement mortars. *Construction and Building Materials*. 2011, **25**(4), pp.2036-2045.
234. Siddique, R. Utilization of silica fume in concrete: Review of hardened properties. *Resources, Conservation and Recycling*. 2011, **55**(11), pp.923-932.
235. Khatri, R. ,Sirivivatnanon, V. and Gross, W. Effect of different supplementary cementitious materials on mechanical properties of high performance concrete. *Cement and Concrete Research*. 1995, **25**(1), pp.209-220.
236. Mazloom, M. ,Ramezaniapour, A. and Brooks, J. Effect of silica fume on mechanical properties of high-strength concrete. *Cement and Concrete Composites*. 2004, **26**(4), pp.347-357.

237. Al-Amoudi, O.S.B. ,Abiola, T.O. and Maslehuddin, M. Effect of superplasticizer on plastic shrinkage of plain and silica fume cement concretes. *Construction and Building Materials*. 2006, **20**(9), pp.642-647.
238. Al-Amoudi, O.S.B. ,Maslehuddin, M. and Abiola, T.O. Effect of type and dosage of silica fume on plastic shrinkage in concrete exposed to hot weather. *Construction and Building Materials*. 2004, **18**(10), pp.737-743.
239. Zhang, M. ,Tam, C. and Leow, M. Effect of water-to-cementitious materials ratio and silica fume on the autogenous shrinkage of concrete. *Cement and Concrete Research*. 2003, **33**(10), pp.1687-1694.
240. Li, J. and Yao, Y. A study on creep and drying shrinkage of high performance concrete. *Cement and Concrete Research*. 2001, **31**(8), pp.1203-1206.
241. Lee, K. ,Lee, H. ,Lee, S. and Kim, G. Autogenous shrinkage of concrete containing granulated blast-furnace slag. *Cement and Concrete Research*. 2006, **36**(7), pp.1279-1285.
242. Lee, H. ,Lee, K. and Kim, B. Autogenous shrinkage of high-performance concrete containing fly ash. *Magazine of Concrete Research*. 2003, **55**(6), pp.507-515.
243. Termkhajornkit, P. ,Nawa, T. ,Nakai, M. and Saito, T. Effect of fly ash on autogenous shrinkage. *Cement and Concrete Research*. 2005, **35**(3), pp.473-482.
244. Tongaroonsri, S. and Tangtermsirikul, S. Effect of mineral admixtures and curing periods on shrinkage and cracking age under restrained condition. *Construction and Building Materials*. 2009, **23**(2), pp.1050-1056.
245. Chindapasirt, P. ,Homwuttiwong, S. and Sirivivatnanon, V. Influence of fly ash fineness on strength, drying shrinkage and sulfate resistance of blended cement mortar. *Cement and Concrete Research*. 2004, **34**(7), pp.1087-1092.
246. Bjegovic, D. ,Stirmer, N. and Serdar, M. Durability properties of concrete with blended cements. *Materials and Corrosion*. 2012, **63**(12), pp.1087-1096.
247. Kanna, V. ,Olson, R. and Jennings, H. Effect of shrinkage and moisture content on the physical characteristics of blended cement mortars. *Cement and Concrete Research*. 1998, **28**(10), pp.1467-1477.
248. Chi, M.-c. ,Chang, J.-j. and Huang, R. Strength and drying shrinkage of alkali-activated slag paste and mortar. *Advances in Civil Engineering*. 2012, **2012**.
249. Huo, X.S. and Wong, L.U. Experimental study of early-age behavior of high performance concrete deck slabs under different curing methods. *Construction and Building Materials*. 2006, **20**(10), pp.1049-1056.
250. Alsayed, S. and Amjad, M. Effect of curing conditions on strength, porosity, absorptivity, and shrinkage of concrete in hot and dry climate. *Cement and Concrete Research*. 1994, **24**(7), pp.1390-1398.
251. Whiting, N. and Snyder, M. Effectiveness of Portland cement concrete curing compounds. *Transportation Research Record: Journal of the Transportation Research Board*. 2003, (1834), pp.59-68.
252. Wang, J. ,Dhir, R. and Levitt, M. Membrane curing of concrete: moisture loss. *Cement and Concrete Research*. 1994, **24**(8), pp.1463-1474.
253. Nabil, B. ,Aissa, A. and Aguida, B.I. Use of a new approach (design of experiments method) to study different procedures to avoid plastic shrinkage cracking of concrete in hot climates. *Journal of Advanced Concrete Technology*. 2011, **9**(2), pp.149-157.
254. Maslehuddin, M. ,Ibrahim, M. ,Shameem, M. ,Ali, M. and Al-Mehthel, M. Effect of curing methods on shrinkage and corrosion resistance of concrete. *Construction and Building Materials*. 2013, **41**, pp.634-641.
255. Kockal, N.U. and Turker, F. Effect of environmental conditions on the properties of concretes with different cement types. *Construction and Building Materials*. 2007, **21**(3), pp.634-645.
256. Al-Fadhala, M. and Hover, K.C. Rapid evaporation from freshly cast concrete and the Gulf environment. *Construction and Building Materials*. 2001, **15**(1), pp.1-7.

257. British Standards Institution. *BS EN 450-1 Fly ash for concrete Part 1: Definition, specifications and conformity criteria*. 2012.
258. British Standards Institution. 9780580633270;0580633276;. *BS EN 12620:2002+A1:2008: Aggregates for concrete*. British Standards Institute, 2002.
259. British Standards Institution. *BS EN 196-1 Methods of testing cement — Part 1: Determination of strength*. 2005.
260. British Standards Institution. *BS EN 13670 Execution of concrete structures*. 2009.
261. Teychenné, D.C. ,Franklin, R.E. ,Erntroy, H.C. ,Nicholls, J. ,Hobbs, D. and MARSH, D. *Design of normal concrete mixes*. 1997.
262. British Standards Institution. *BS EN 12350-2 Testing fresh concrete Part 2: Slump-test*. 2009.
263. British Standards Institution. *BS EN 1097-6 Tests for mechanical and physical properties of aggregates Part 6: Determination of particle density and water absorption*. 2013.
264. Suchorski, D.M. *AGGREGATES FOR CONCRETE, ACI Education Bulletin E1-07, ACI commite E-701, Materials for Concrete Construction*. ISBN 978-0-87031-248-9, August, 2007.
265. Dhir, R. ,Hewlett, P. and Chan, Y. Near-surface characteristics of concrete: assessment and development of in situ test methods. *Magazine of Concrete Research*. 1987, **39**(141), pp.183-195.
266. Parrott, L.J. ,Geiker, M. ,Gutteridge, W.A. and Killoh, D. Monitoring Portland cement hydration: comparison of methods. *Cement and Concrete Research*. 1990, **20**(6), pp.919-926.
267. Cabrera, J. and Lynsdale, C. A new gas permeameter for measuring the permeability of mortar and concrete. *Magazine of Concrete Research*. 1988, **40**(144), pp.177-182.
268. Grube, H. and Lawrence, C.D. 'Permeability of Concrete to Oxygen', in Proceedings of RILEM seminar on Durability of Concrete Structures under Normal Outdoor Exposure, University of Hanover Germany. 1984, pp.68--79
269. Sisomphon, K. and Franke, L. Carbonation rates of concretes containing high volume of pozzolanic materials. *Cement and Concrete Research*. 2007, **37**(12), pp.1647-1653.
270. Ho, D. Durability of Concrete. *Edited by: Wf Chen, Jy Richard Liew, The Civil Engineering Handbook, 2nd ed. CRC Press LLC*. 2003.
271. Recommendations, R. and DE LA RILEM, R. CPC-18 Measurement of hardened concrete carbonation depth. *Mater. Struct.* 1988, **21**(6), pp.453-455.
272. British Standards Institution. *BS ISO 1920-8:2009 Testing of concrete Part 8:Determination of drying shrinkage of concrete for samples prepared in the field or in the laboratory*. 2009.
273. De Schutter, G. Finite element simulation of thermal cracking in massive hardening concrete elements using degree of hydration based material laws. *Computers & Structures*. 2002, **80**(27), pp.2035-2042.
274. Feng, X. ,Garboczi, E. ,Bentz, D. ,Stutzman, P. and Mason, T.O. Estimation of the degree of hydration of blended cement pastes by a scanning electron microscope point-counting procedure. *Cement and Concrete Research*. 2004, **34**(10), pp.1787-1793.
275. Ramachandran, V.S. and Beaudoin, J.J. *Handbook of analytical techniques in concrete science and technology: principles, techniques and applications*. Elsevier, 2000.
276. Bye, G.C. *Portland Cement* LONDON: Thomas Telford Limited, 1999, 1999.
277. Aranda, M.A. ,Ángeles, G. and León-Reina, L. Rietveld quantitative phase analysis of OPC clinkers, cements and hydration products. *Reviews in Mineralogy and Geochemistry*. 2012, **74**(1), pp.169-209.
278. McCusker, L. ,Von Dreele, R. ,Cox, D. ,Louer, D. and Scardi, P. Rietveld refinement guidelines. *Journal of Applied Crystallography*. 1999, **32**(1), pp.36-50.

279. Kocaba, V. Development and evaluation of methods to follow microstructural development of cementitious systems including slags. 2009.
280. Whittaker, M. ,Zajac, M. ,Haha, M.B. ,Bullerjahn, F. and Black, L. The role of the alumina content of slag, plus the presence of additional sulfate on the hydration and microstructure of Portland cement-slag blends. *Cement and Concrete Research*. 2014, **66**, pp.91-101.
281. Famy, C. ,Scrivener, K. and Crumbie, A. What causes differences of CSH gel grey levels in backscattered electron images? *Cement and Concrete Research*. 2002, **32**(9), pp.1465-1471.
282. Stutzman, P. Scanning electron microscopy imaging of hydraulic cement microstructure. *Cement and Concrete Composites*. 2004, **26**(8), pp.957-966.
283. Kjellsen, K. ,Monsøy, A. ,Isachsen, K. and Detwiler, R. Preparation of flat-polished specimens for SEM-backscattered electron imaging and X-ray microanalysis—importance of epoxy impregnation. *Cement and Concrete Research*. 2003, **33**(4), pp.611-616.
284. Aligizaki, K.K. *Pore structure of cement-based materials: testing, interpretation and requirements*. CRC Press, 2005.
285. Gallucci, E. ,Zhang, X. and Scrivener, K. Effect of temperature on the microstructure of calcium silicate hydrate (CSH). *Cement and Concrete Research*. 2013, **53**, pp.185-195.
286. Haha, M.B. ,Gallucci, E. ,Guidoum, A. and Scrivener, K.L. Relation of expansion due to alkali silica reaction to the degree of reaction measured by SEM image analysis. *Cement and Concrete Research*. 2007, **37**(8), pp.1206-1214.
287. Yang, R. and Buenfeld, N. Binary segmentation of aggregate in SEM image analysis of concrete. *Cement and Concrete Research*. 2001, **31**(3), pp.437-441.
288. Tan, K. and Gjørsv, O.E. Performance of concrete under different curing conditions. *Cement and Concrete Research*. 1996, **26**(3), pp.355-361.
289. Ozer, B. and Ozkul, M.H. The influence of initial water curing on the strength development of ordinary Portland and pozzolanic cement concretes. *Cement and Concrete Research*. 2004, **34**(1), pp.13-18.
290. Nassif, H. and Suksawang, N. Effect of curing methods on durability of high-performance concrete. *Transportation Research Record: Journal of the Transportation Research Board*. 2002, **1798**(1), pp.31-38.
291. Güneýisi, E. ,Özturan, T. and Gesođlu, M. A study on reinforcement corrosion and related properties of plain and blended cement concretes under different curing conditions. *Cement and Concrete Composites*. 2005, **27**(4), pp.449-461.
292. Aprianti, E. ,Shafigh, P. ,Zawawi, R. and Hassan, Z.F.A. Introducing an effective curing method for mortar containing high volume cementitious materials. *Construction and Building Materials*. 2016, **107**, pp.365-377.
293. Atiř, C.D. Strength properties of high-volume fly ash roller compacted and workable concrete, and influence of curing condition. *Cement and Concrete Research*. 2005, **35**(6), pp.1112-1121.
294. Khan, M.S. and Ayers, M.E. Curing requirements of silica fume and fly ash mortars. *Cement and Concrete Research*. 1993, **23**(6), pp.1480-1490.
295. Haque, M. ,Goplan, M. ,Joshi, R. and Ward, M. Strength development of inadequately cured high fly ash content and structural concretes. *Cement and Concrete Research*. 1986, **16**(3), pp.363-372.
296. Bai, J. ,Wild, S. and Sabir, B. Sorptivity and strength of air-cured and water-cured PC–PFA–MK concrete and the influence of binder composition on carbonation depth. *Cement and Concrete Research*. 2002, **32**(11), pp.1813-1821.
297. Khan, M. and Lynsdale, C. Strength, permeability, and carbonation of high-performance concrete. *Cement and Concrete Research*. 2002, **32**(1), pp.123-131.

298. Bushlaibi, A.H. and Alshamsi, A.M. Efficiency of curing on partially exposed high-strength concrete in hot climate. *Cement and Concrete Research*. 2002, **32**(6), pp.949-953.
299. Ait-Aider, H. ,Hannachi, N. and Mouret, M. Importance of W/C ratio on compressive strength of concrete in hot climate conditions. *Building and environment*. 2007, **42**(6), pp.2461-2465.
300. British Standards Institution. 0580837262;9780580837265;. *BS EN 1992-1-1:2004+A1:2014: Eurocode 2: Design of concrete structures. General rules and rules for buildings*. British Standards Institute, 2004.
301. Çakır, Ö. and Aköz, F. Effect of curing conditions on the mortars with and without GGBFS. *Construction and Building Materials*. 2008, **22**(3), pp.308-314.
302. Li, G. ,Otsuki, N. and Yuan, Y.-s. Effects of the initial water curing time on the corrosion behavior of steel bar corrosion in fly ash concrete. *Procedia Earth and Planetary Science*. 2009, **1**(1), pp.742-749.
303. Kelham, S. A water absorption test for concrete. *Magazine of Concrete Research*. 1988, **40**(143), pp.106-110.
304. Matthews, J. and Building Research Establishment , W. *Pulverised-fuel Ash-Its Use in Concrete: Part 2; Influences on Durability*. Building Research Establishment (BRE), 1987.
305. Ewertson, C. and Petersson, P. The influence of curing conditions on the permeability and durability of concrete. Results from a field exposure test. *Cement and Concrete Research*. 1993, **23**(3), pp.683-692.
306. Lo, Y. and Lee, H. Curing effects on carbonation of concrete using a phenolphthalein indicator and Fourier-transform infrared spectroscopy. *Building and environment*. 2002, **37**(5), pp.507-514.
307. Balayssac, J. ,Détriché, C.H. and Grandet, J. Effects of curing upon carbonation of concrete. *Construction and Building Materials*. 1995, **9**(2), pp.91-95.
308. Ferreira, T. and Rasband, W. ImageJ user guide. *ImageJ/Fiji*. 2012, **1**.
309. Bentz, D.P. ,Snyder, K.A. and Stutzman, P.E. Hydration of Portland cement: The effects of curing conditions. In: *Proceedings of the 10th International Congress on the Chemistry of Cement*, 1997.
310. Chen, X. and Wu, S. Influence of water-to-cement ratio and curing period on pore structure of cement mortar. *Construction and Building Materials*. 2013, **38**, pp.804-812.
311. Patel, R. ,Killoh, D. ,Parrott, L. and Gutteridge, W. Influence of curing at different relative humidities upon compound reactions and porosity in Portland cement paste. *Materials and structures*. 1988, **21**(3), pp.192-197.
312. Das, B. and Kondraivendhan, B. Implication of pore size distribution parameters on compressive strength, permeability and hydraulic diffusivity of concrete. *Construction and Building Materials*. 2012, **28**(1), pp.382-386.
313. Khatib, J. and Mangat, P. Absorption characteristics of concrete as a function of location relative to casting position. *Cement and Concrete Research*. 1995, **25**(5), pp.999-1010.
314. Khatib, J.M. ,Wright, L. and Mangat, P.S. Effect of desulphurised waste on long-term porosity and pore structure of blended cement pastes. *Sustainable Environment Research*. 2016, **26**(5), pp.230-234.
315. Berodier, E. and Scrivener, K. Evolution of pore structure in blended systems. *Cement and Concrete Research*. 2015, **73**, pp.25-35.
316. Igarashi, S.-i. ,Kawamura, M. and Watanabe, A. Analysis of cement pastes and mortars by a combination of backscatter-based SEM image analysis and calculations based on the Powers model. *Cement and Concrete Composites*. 2004, **26**(8), pp.977-985.

317. Pane, I. and Hansen, W. Investigation of blended cement hydration by isothermal calorimetry and thermal analysis. *Cement and Concrete Research*. 2005, **35**(6), pp.1155-1164.
318. Beaudoin, J.J. and Ramachandran, V.S. *Building Materials: Handbook of Analytical Techniques in Concrete Science and Technology : Principles, Techniques and Applications*. Elsevier Science, 2001.
319. Mounanga, P. ,Khelidj, A. ,Loukili, A. and Baroghel-Bouny, V. Predicting Ca (OH) 2 content and chemical shrinkage of hydrating cement pastes using analytical approach. *Cement and Concrete Research*. 2004, **34**(2), pp.255-265.
320. WANG, P.-m. ,FENG, S.-x. and LIU, X.-p. Research Approaches of Cement Hydration Degree and Their Development [J]. *Journal of Building Materials*. 2005, **6**, pp.1-10.
321. Liu, J. ,Xing, F. ,Dong, B. ,Ma, H. and Pan, D. Study on surface permeability of concrete under immersion. *Materials*. 2014, **7**(2), pp.876-886.
322. Xue, B. ,Pei, J. ,Sheng, Y. and Li, R. Effect of curing compounds on the properties and microstructure of cement concretes. *Construction and Building Materials*. 2015, **101**, pp.410-416.
323. Nahata, Y. ,Kholia, N. and Tank, T. Effect of Curing Methods on Efficiency of Curing of Cement Mortar. *APCBEE Procedia*. 2014, **9**, pp.222-229.
324. Fattuhi, N. Concrete carbonation as influenced by curing regime. *Cement and Concrete Research*. 1988, **18**(3), pp.426-430.
325. Younsi, A. ,Turcry, P. ,Aït-Mokhtar, A. and Staquet, S. Accelerated carbonation of concrete with high content of mineral additions: effect of interactions between hydration and drying. *Cement and Concrete Research*. 2013, **43**, pp.25-33.
326. Mangat, P. and El-Khatib, J. Influence of initial curing on sulphate resistance of blended cement concrete. *Cement and Concrete Research*. 1992, **22**(6), pp.1089-1100.
327. Khatib, J. and Mangat, P. Influence of superplasticizer and curing on porosity and pore structure of cement paste. *Cement and Concrete Composites*. 1999, **21**(5), pp.431-437.
328. El-Sakhawy, N. ,El-Dien, H. ,Ahmed, M. and Bendary, K. Influence of curing on durability performance of concrete. *Magazine of Concrete Research*. 1999, **51**(5), pp.309-315.
329. Lawrence, P. ,Cyr, M. and Ringot, E. Mineral admixtures in mortars: effect of inert materials on short-term hydration. *Cement and Concrete Research*. 2003, **33**(12), pp.1939-1947.
330. Li, D. ,Chen, Y. ,Shen, J. ,Su, J. and Wu, X. The influence of alkalinity on activation and microstructure of fly ash. *Cement and Concrete Research*. 2000, **30**(6), pp.881-886.

Appendices

Appendix A Absorption and Moisture Content Test Results

Absorption and Moisture content Test

$$\text{Absorption (\%)} = [W_{SSD} - W_{OD}] / [W_{OD}] * 100$$

Where

W_{SSD} is the weight of saturated surface dry aggregates

W_{OD} is the weight of oven dry aggregate

Moisture content

$$\text{Moisture content (\%)} = [W - W_{OD}] / [W_{OD}] * 100$$

Where

W is the mass of the original sample

W_{OD} is the weight of oven dry aggregate

Absorption and moisture content are percentages of oven dry masses.

Surface moisture content

Surface or free moisture content of an aggregate can be determined by subtracting the absorption from the total moisture content.

Fine aggregate

Weight of container = 1233g

Dry sample + container = 2265.3g

Wet sample + container = 2292.4g

Fully saturated sample = 2479g

Oven dry sample = 2261g

$$\text{Absorption} = [2292.4 - 2261] / [2261 - 1233] = 31.4/1028 = 0.0305$$

$$= 3.05\%$$

$$\text{Moisture content} = [2265.3 - 2261] / [2261 - 1233] = 4.3/1028 = 0.0042$$

$$= 0.42\%$$

Surface moisture content = Moisture content – Absorption

$$\text{Surface moisture content} = 0.0042 - 0.0305 = -0.0263 = -2.63\%$$

Coarse aggregate

Weight of container = 1265g

Dry sample + container = 2271.4g

Wet sample + container = 2281.6g

Fully saturated sample = 2311.8g

Oven dry sample = 2268.9g

Absorption = $[2281.6 - 2268.9] / [2268.9 - 1265] = 12.7/1003.9 = 0.0127$

= 1.27%

Moisture content = $[2271.4 - 2268.9] / [2268.9 - 1265] = 2.5 / 1003.9 = 0.0025$

= 2.5%

Surface moisture content = $0.0025 - 0.0127 = -0.0102 = -1.02\%$

Surface moisture content = Moisture content – Absorption

If an aggregate is air-dry (surface is dry but pores are partially filled with water), the total moisture content is less than the absorption and the surface moisture content has a negative value. This means that the aggregate will absorb water when mixed in concrete. For aggregates with unusually high absorption that are batched in an unusually dry state, water equal to the amount absorbed should be added to maintain the intended water cement ratio and consistency.

Comments

Adjustments to water content are much more significant than aggregate adjustments, and water content adjustments for moisture content of aggregate must always be carried out.

Adjustments to water content depend on both the absorption and moisture content of the aggregate, while adjustments to aggregate contents depend only on moisture content

Fine aggregate

Surface moisture content -2.63%

Total moisture content 0.42%

Absorption 3.05%

Coarse aggregate

Surface moisture content -1.02%

Total moisture content 0.25%

Absorption 1.27%

The Table A1 was calculated using the surface moisture content, total moisture content and absorption of fine and coarse aggregates to calculate the adjusted water since the aggregates were oven dried.

Surface moisture content (SMC)

Table A 1 Adjusted water calculated from surface moisture content of aggregates

Mixes	Water (kg/m ³)	Cement (kg/m ³)	FA (kg/m ³)	0.3 FA (kg/m ³)	Fine Agg(kg/m ³)	Coarse Agg (kg/m ³)	SMC x fine agg	SMC x coarse agg	Additions of the aggregates (kg/m ³)	Adjusted water(kg/m ³)	Binder (kg/m ³)	w/b
M1	180	275	0	0	849	1033	22.33	10.54	32.87	212.87	275.00	0.77
M2	180	499	0	0	650	1007	17.10	10.27	27.37	207.37	499.00	0.42
M3	180	930	0	0	440	786	11.57	8.02	19.59	199.59	930.00	0.21
M4	225	343	0	0	911	805	23.96	8.21	32.17	257.17	343.00	0.75
M5	225	624	0	0	675	760	17.75	7.75	25.50	250.50	624.00	0.40
M6	225	1162	0	0	391	506	10.28	5.16	15.44	240.44	1162.00	0.21
M7	165	223	96	28.8	844	1026	22.20	10.47	32.66	197.66	251.80	0.78
M8	165	405	174	52.2	631	978	16.60	9.98	26.57	191.57	457.20	0.42
M9	165	755	324	97.2	398	712	10.47	7.26	17.73	182.73	852.20	0.21
M10	205	277	119	35.7	906	801	23.83	8.17	32.00	237.00	312.70	0.76
M11	205	504	216	64.8	651	732	17.12	7.47	24.59	229.59	568.80	0.40
M12	205	983	402	120.6	332	429	8.73	4.38	13.11	218.11	1103.60	0.20

Appendix B Compressive strength of concretes

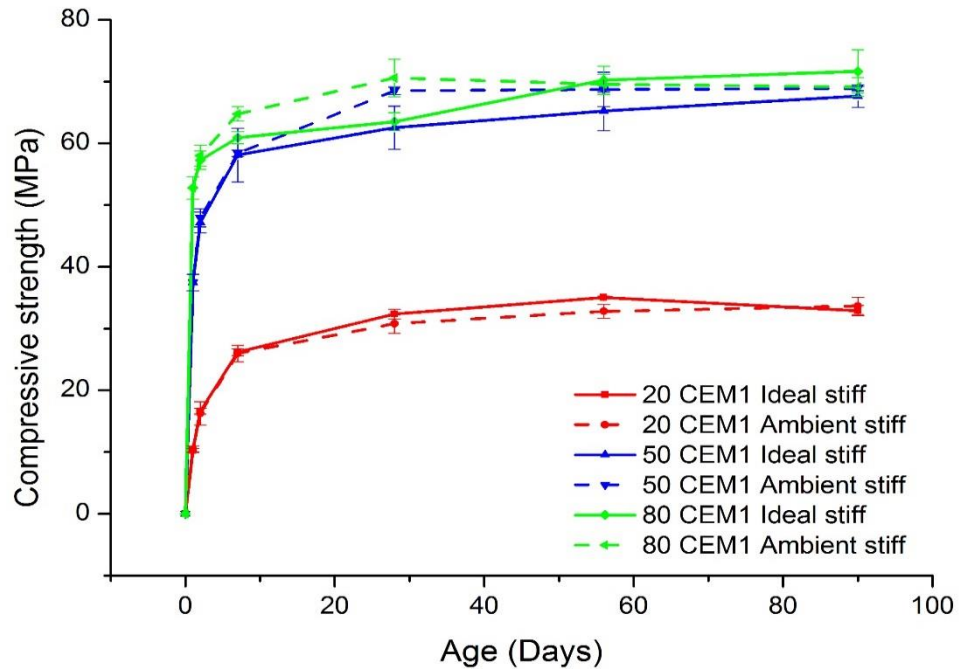


Figure A 1 Compressive strength of CEM1 stiff mix (slumps 10-30mm)

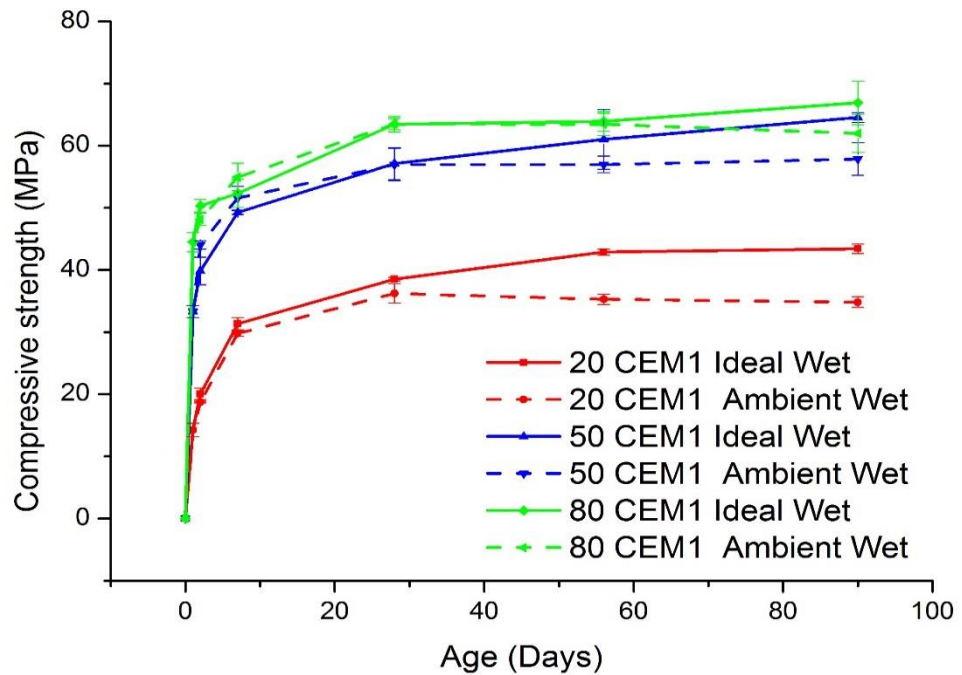


Figure A 2 Compressive strength of CEM1 wet mix (slumps 60-180mm)

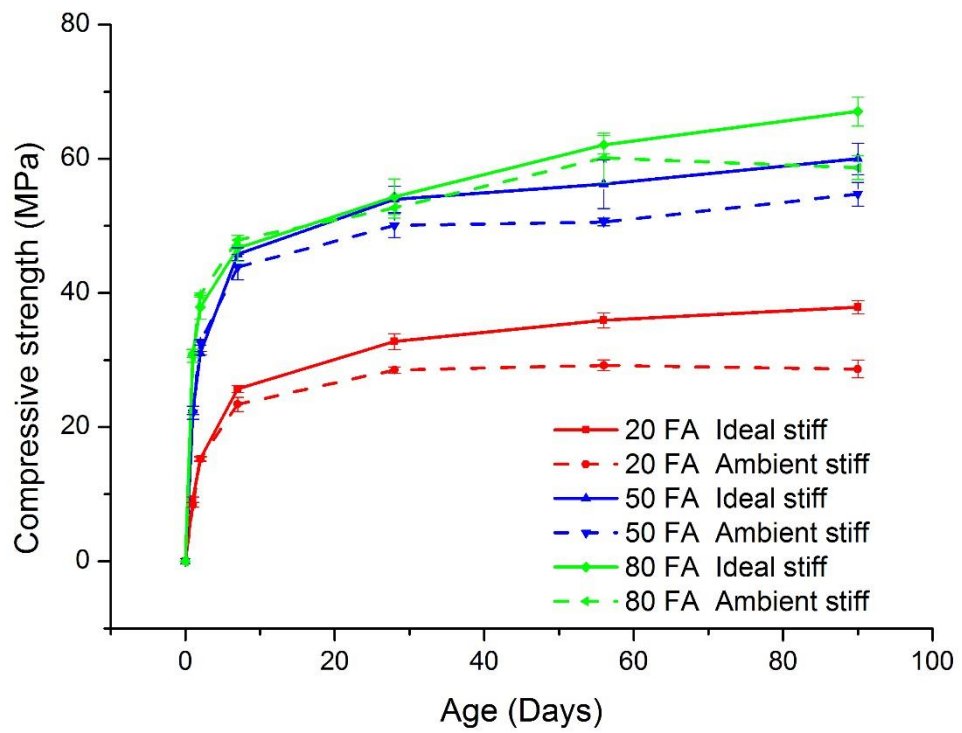


Figure A 3 Compressive strength of Fly ash stiff mix (slumps 10-30mm)

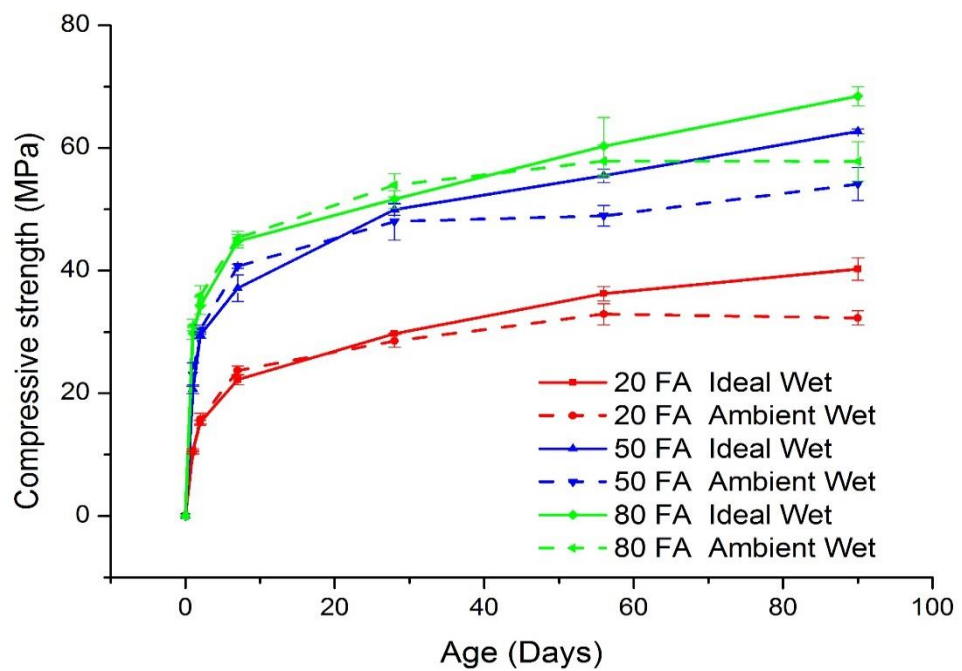


Figure A 4 Compressive strength of fly ash wet mix (slumps 60-180mm)

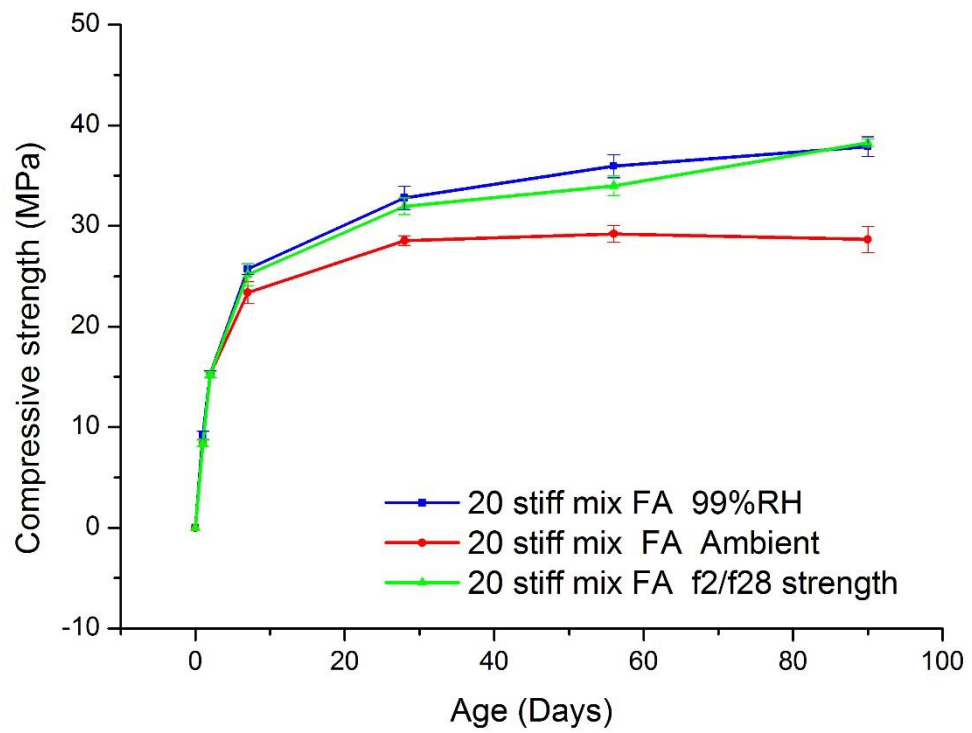


Figure A 5 Compressive strength of 20MPa Fly ash stiff mix (slumps 10-30mm) with minimum curing condition (f_2/f_{28})

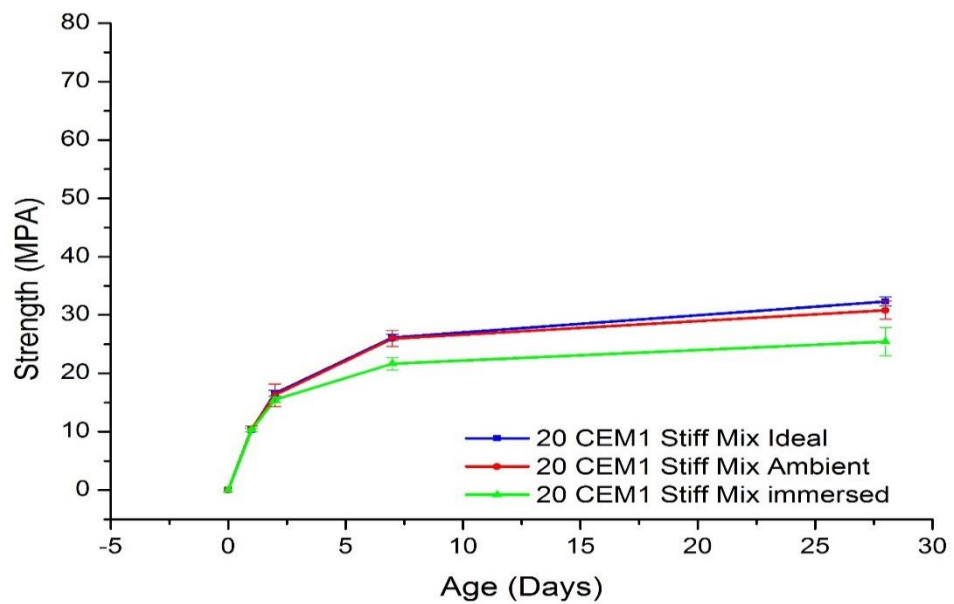


Figure A 6 Compressive strength of 20 MPa CEM1 stiff mix (slumps 10-30mm) and immersed

A7

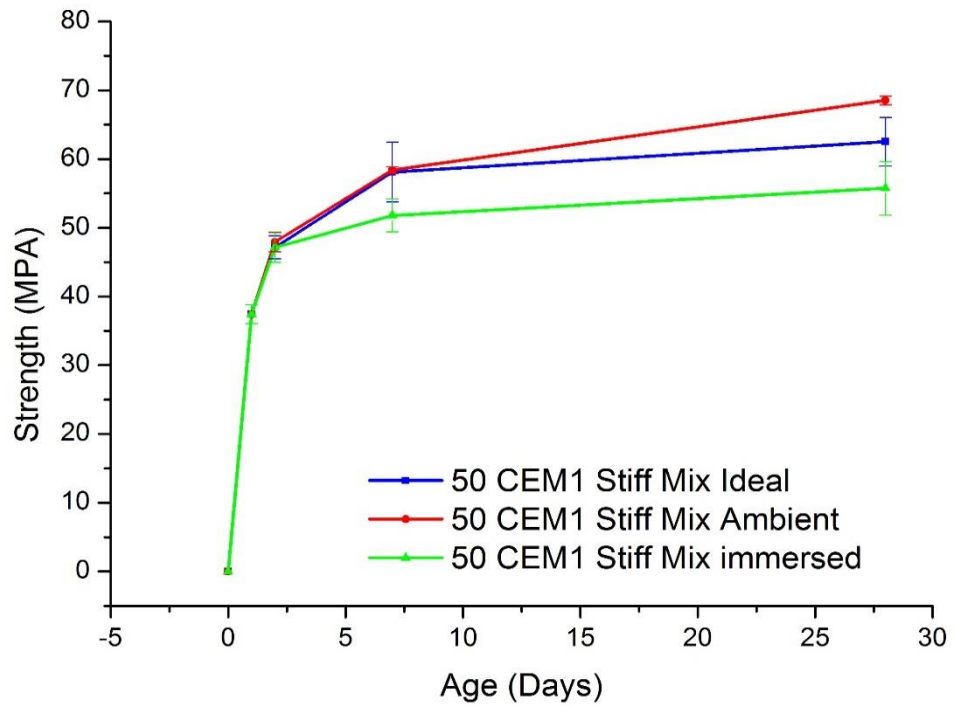


Figure A 7 Compressive strength of 50 MPa CEM1 stiff mix (slumps 10-30mm) and immersed

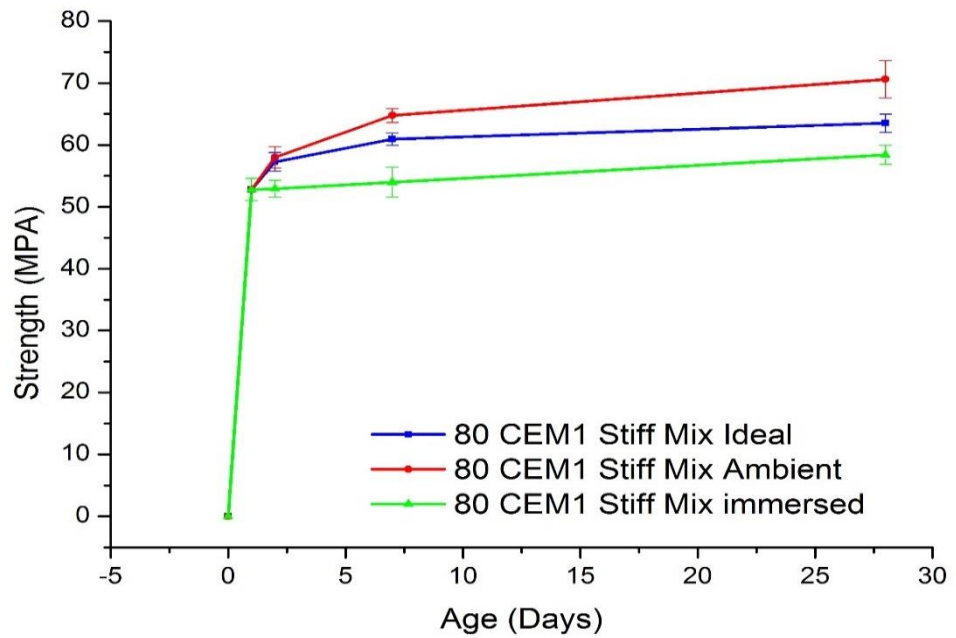


Figure A 8 Compressive strength of 80 MPa CEM1 stiff mix (slumps 10-30mm) and immersed

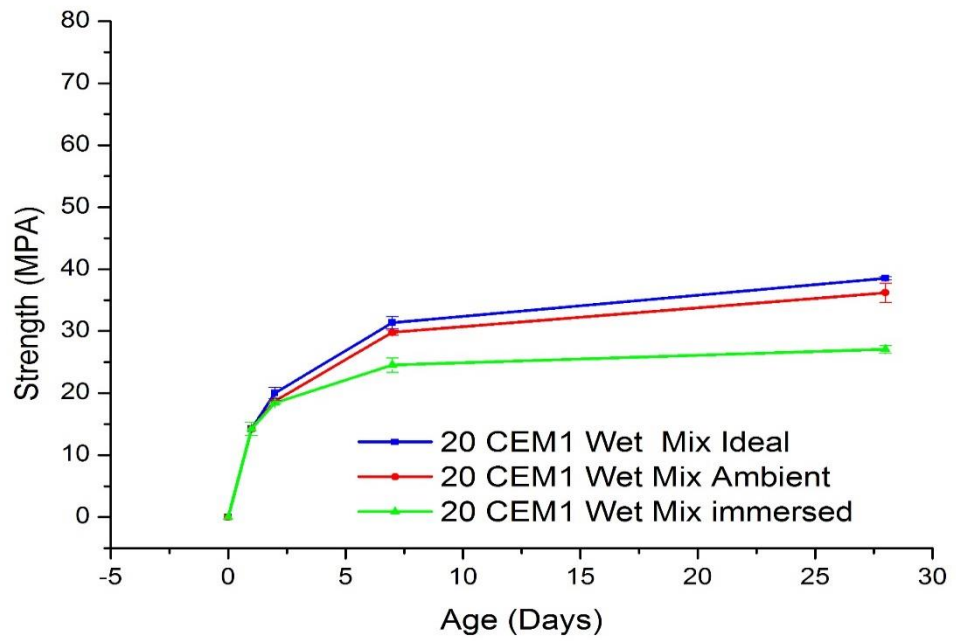


Figure A 9 Compressive strength of 20MPa CEM1 wet mix (slumps 60-180mm) and immersed

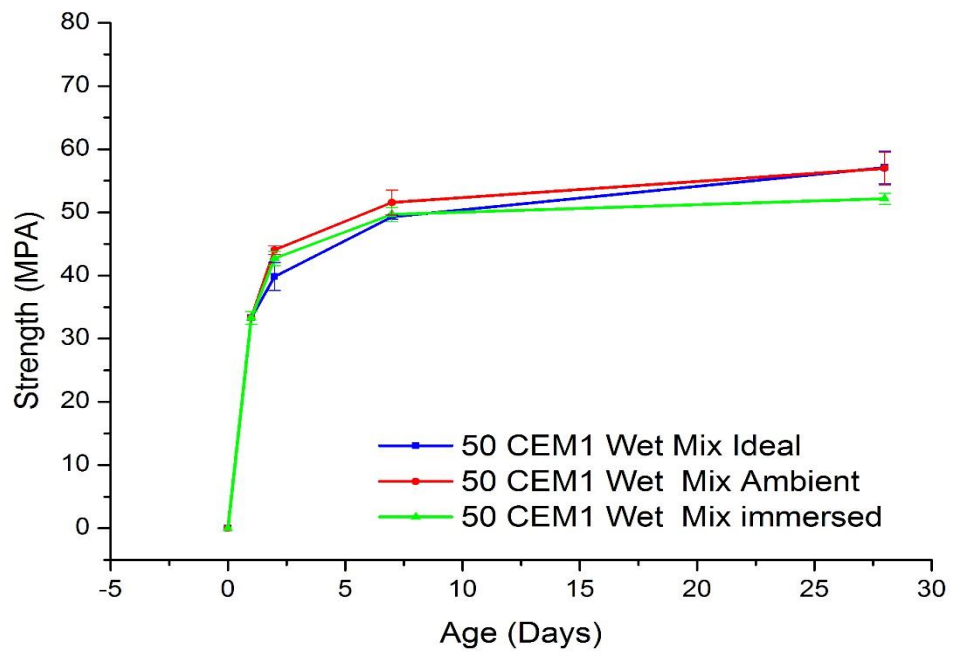


Figure A 10 Compressive strength of 50MPa CEM1 wet mix (slumps 60-180mm) and immersed

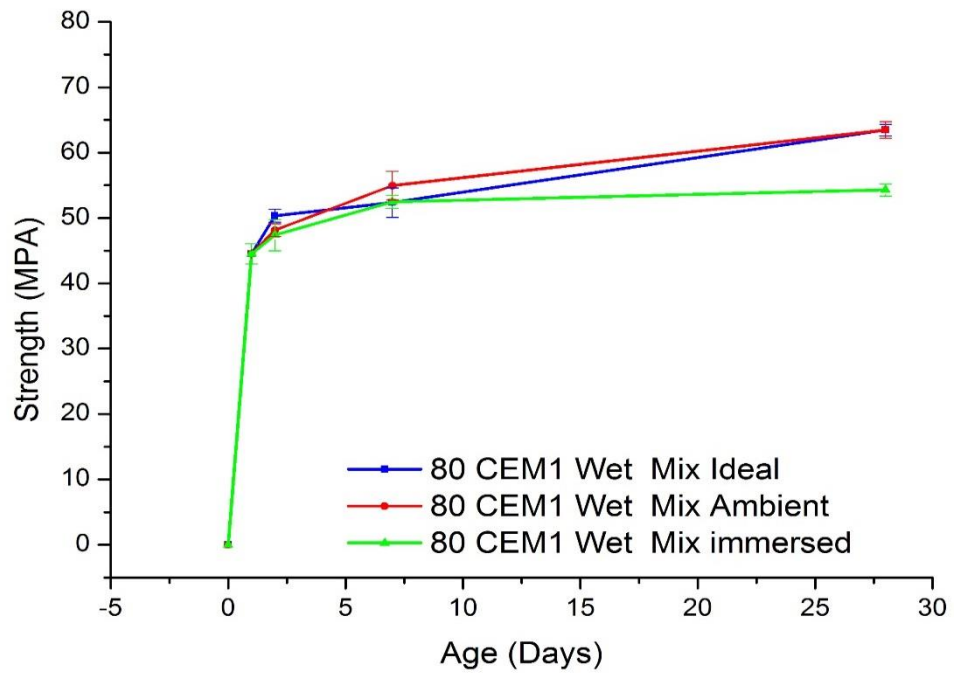


Figure A 11 Compressive strength of 80MPa CEM1 wet mix (slumps 60-180mm) and immersed

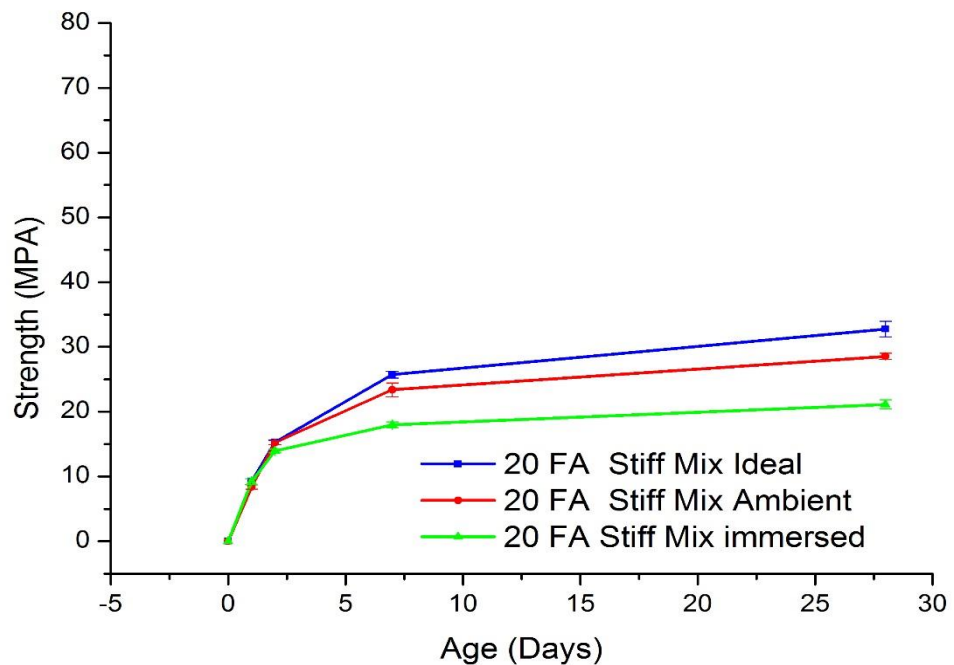


Figure A 12 Compressive strength of 20MPa Fly ash stiff mix (slumps 10-30mm) and immersed

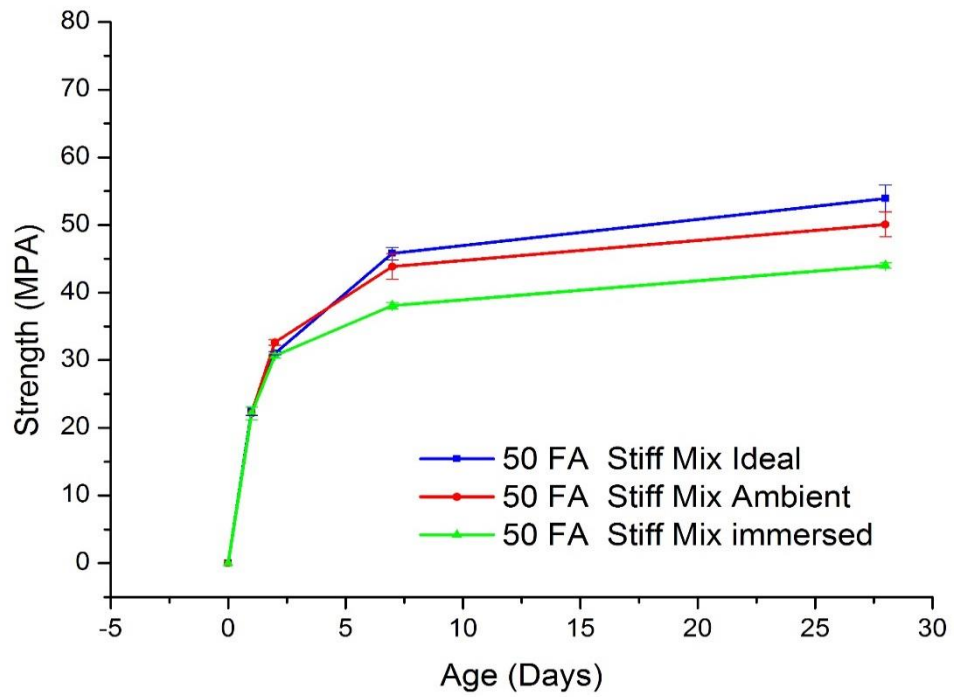


Figure A 13 Compressive strength of 50MPa Fly ash stiff mix (slumps 10-30mm) and immersed

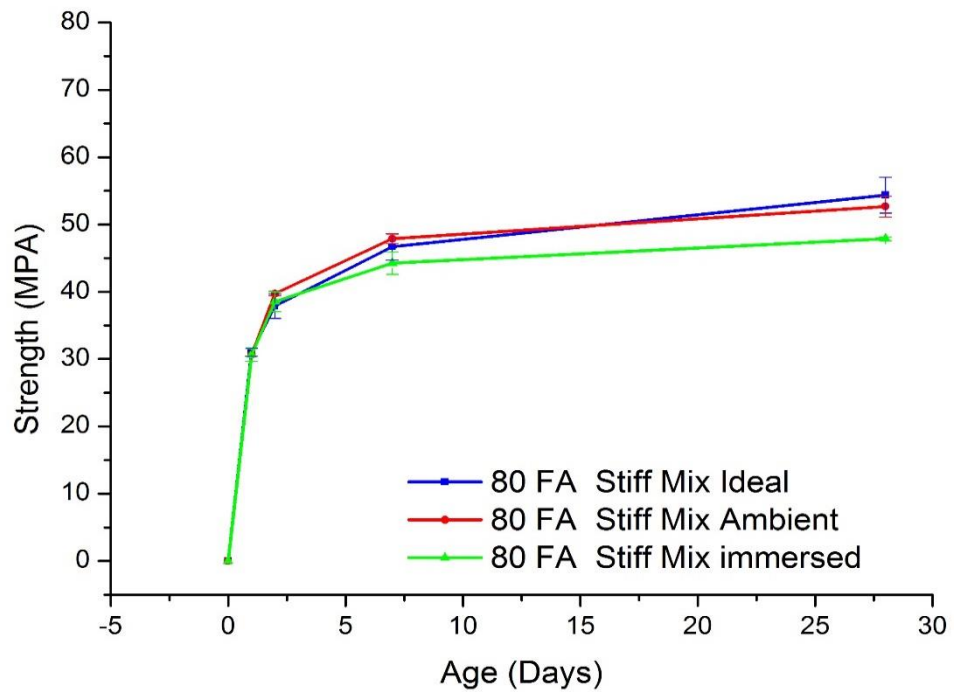


Figure A 14 Compressive strength of 80MPa Fly ash stiff mix (slumps 10-30mm) and immersed

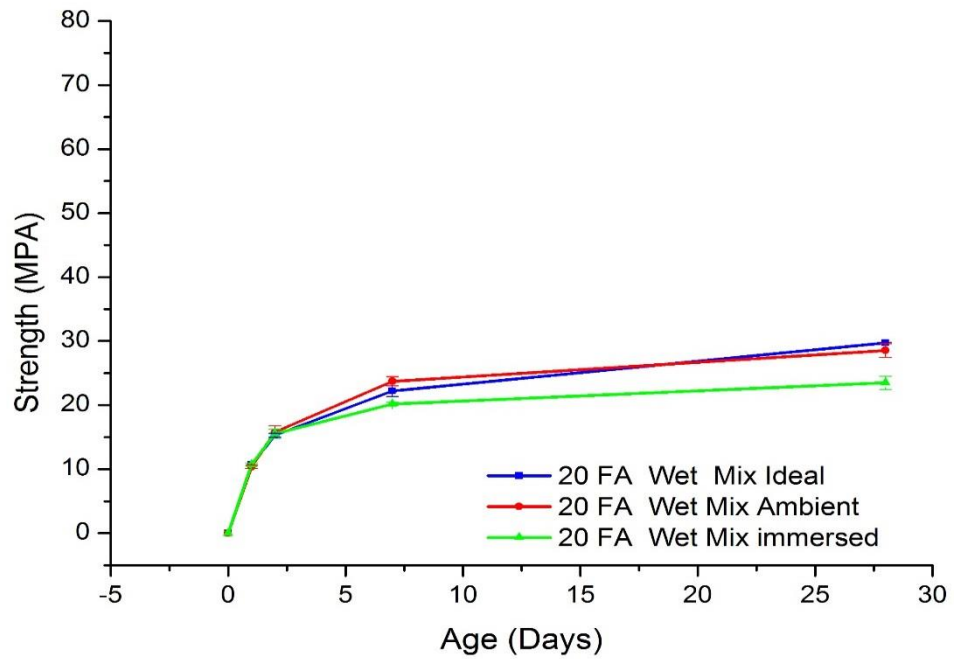


Figure A 15 Compressive strength of fly ash 20MPa wet mix (slumps 60-180mm) and immersed

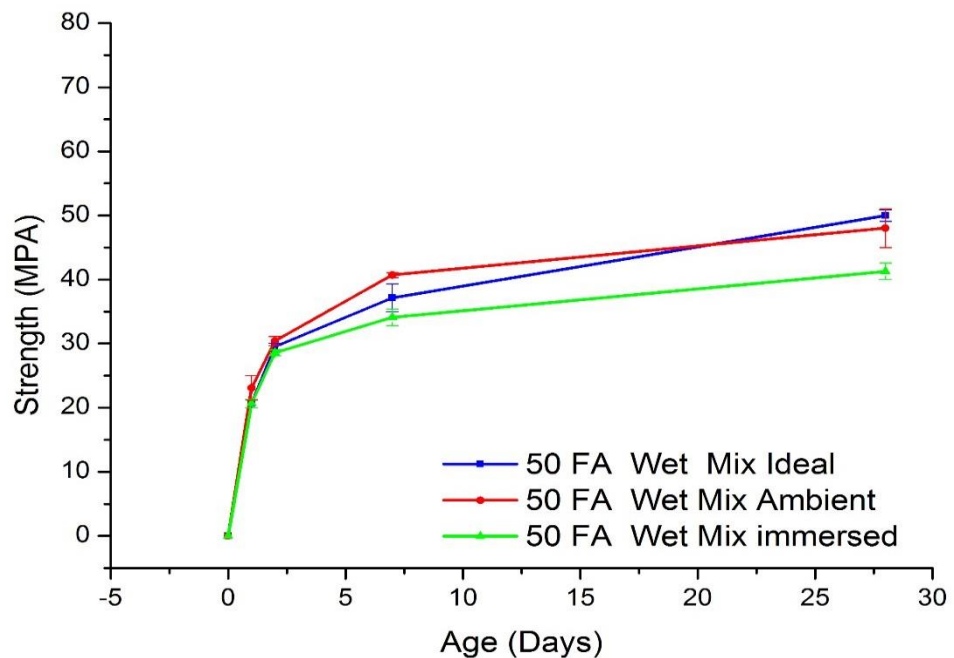


Figure A 16 Compressive strength of fly ash 50MPa wet mix (slumps 60-180mm) and immersed

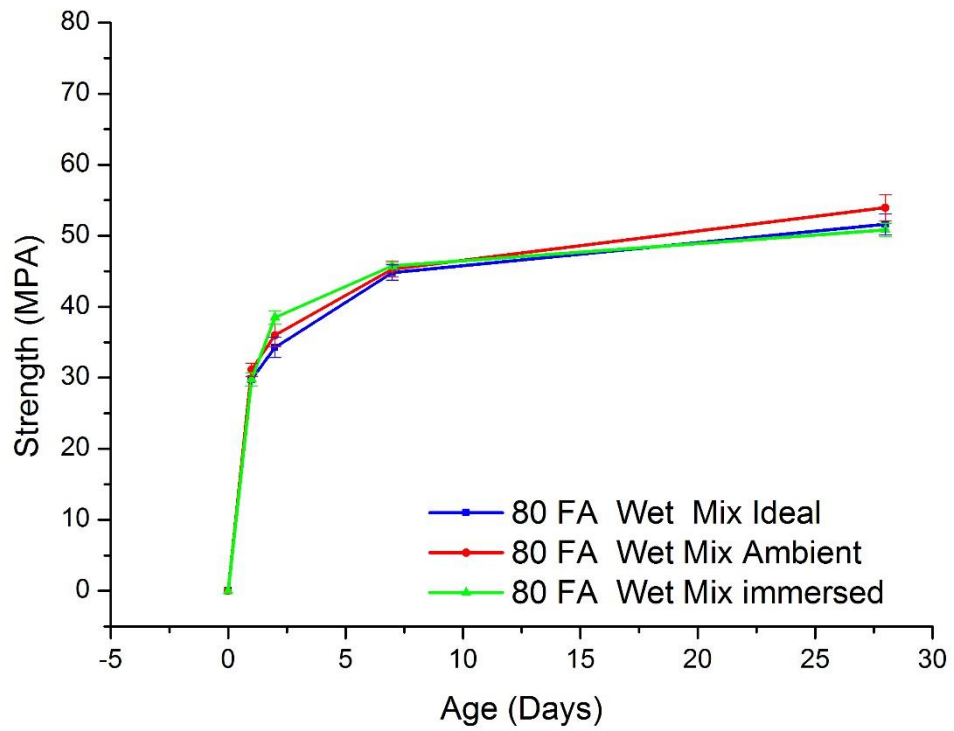


Figure A 17 Compressive strength of fly ash 80MPa wet mix (slumps 60-180mm) and immersed

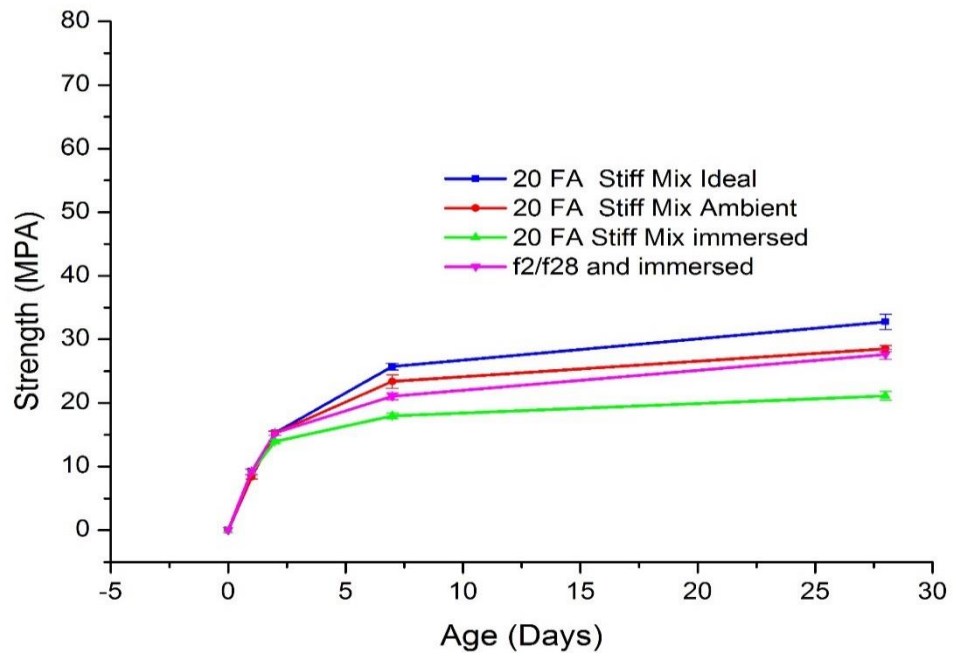


Figure A 18 Compressive strength of 20MPa Fly ash stiff mix (slumps 10-30mm) with minimum curing condition (f2/f28) and immersed

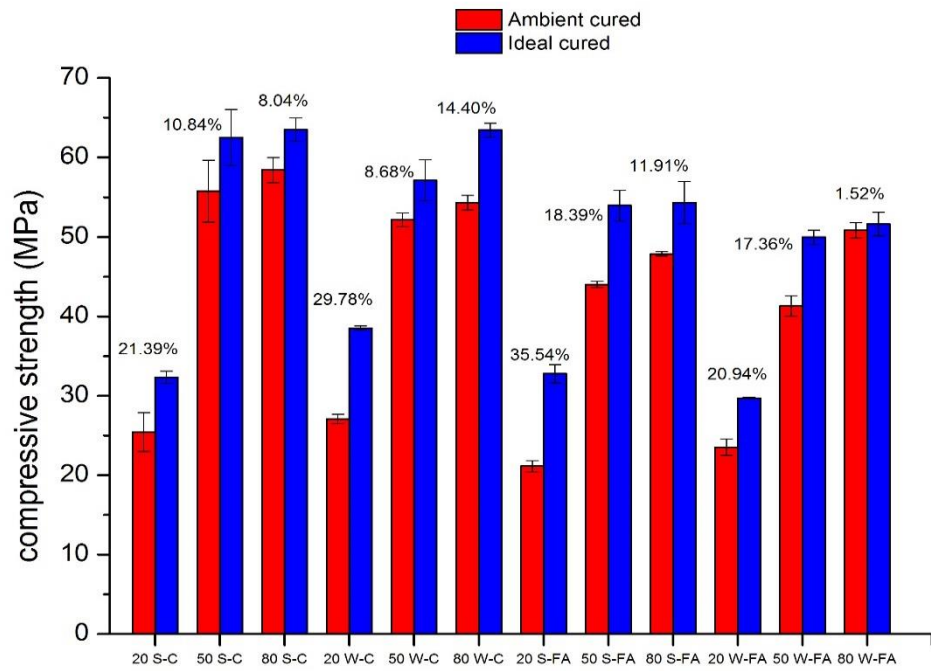


Figure A 19 Compressive strength of Ambient and Ideal cured concretes at 28 days

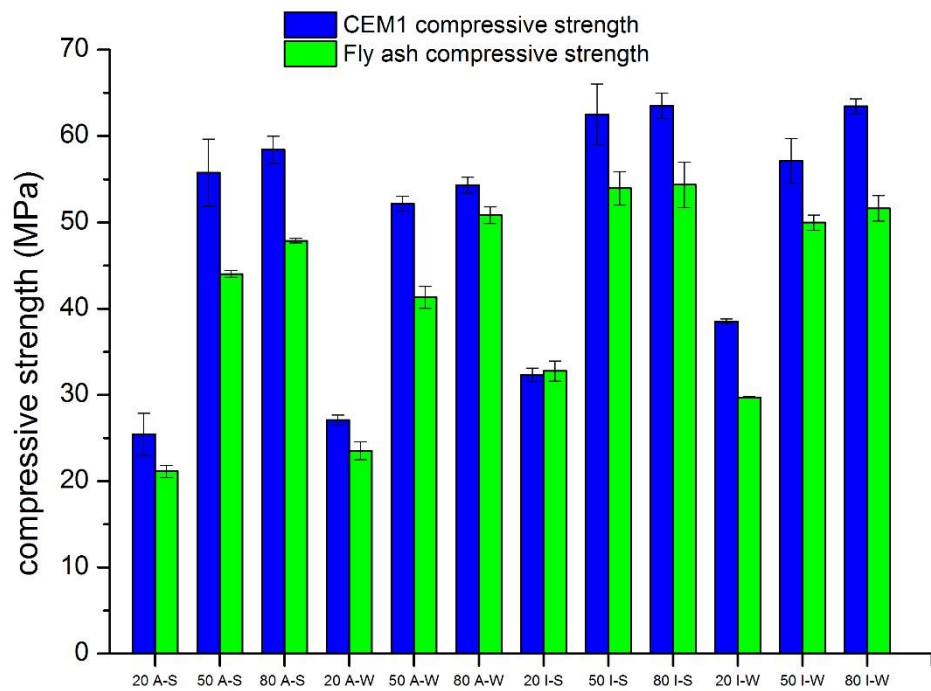


Figure A 20 Compressive strength of CEM1 and Fly ash concretes

Appendix C Effect of drying

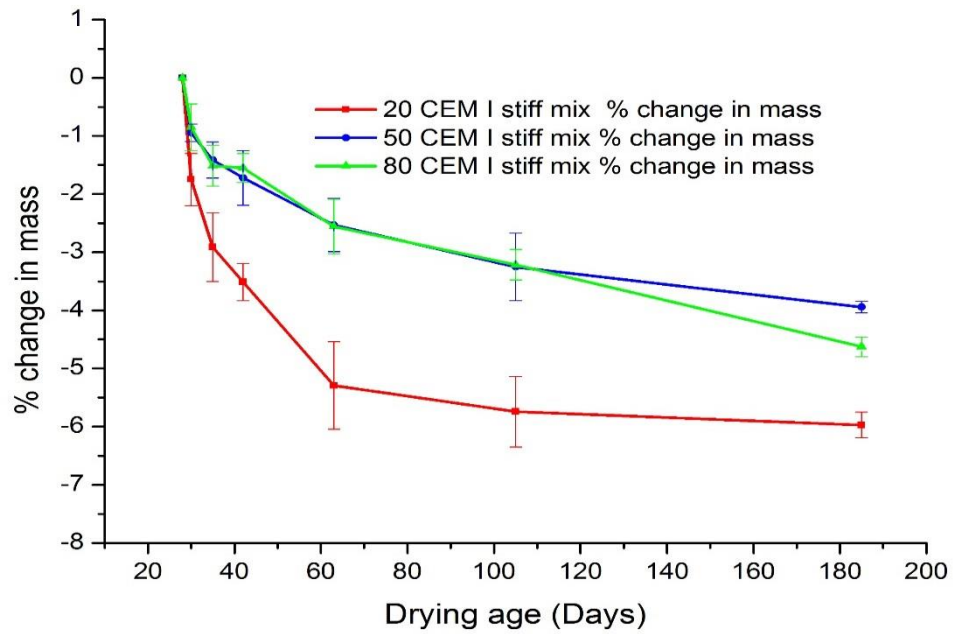


Figure A 21 Percentage change in mass for 20,50 and 80MPa CEM1 stiff mix

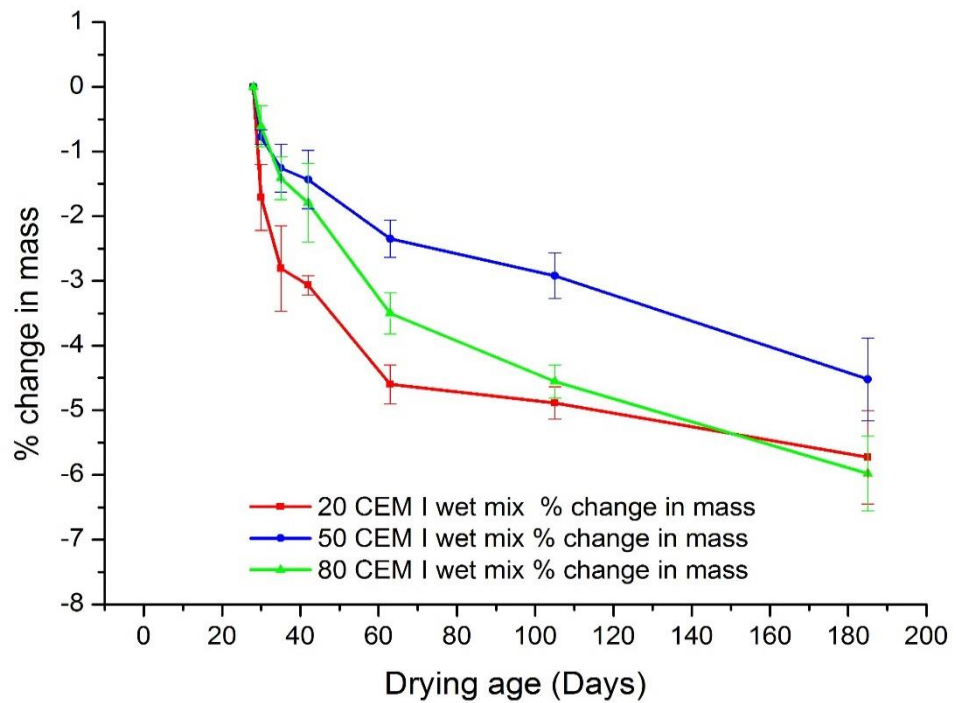


Figure A 22 Percentage change in mass for 20,50 and 80MPa CEM1 wet mix

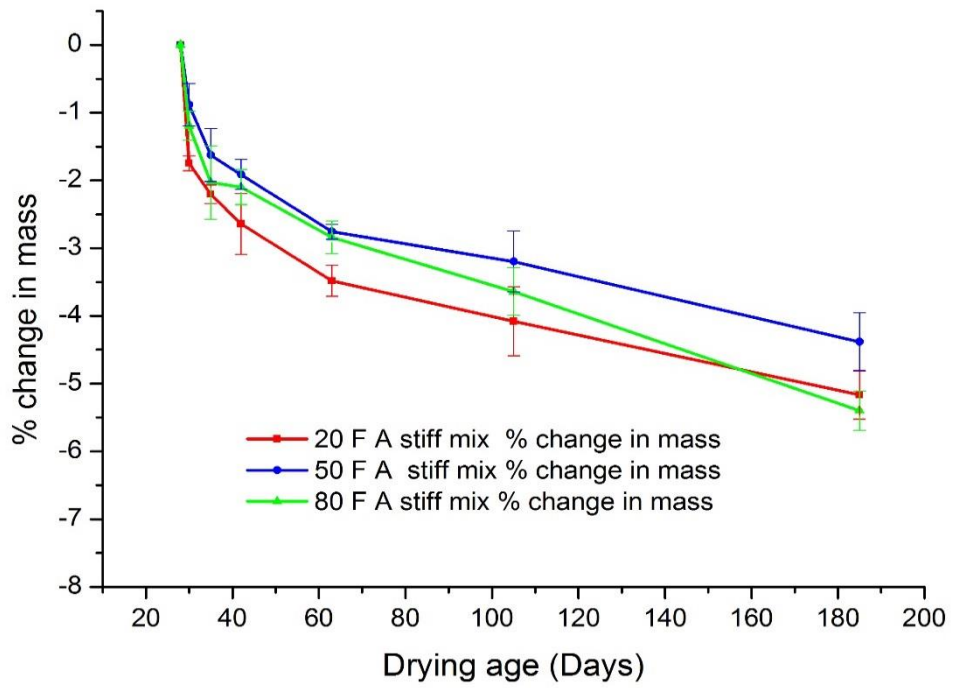


Figure A 23 Percentage change in mass for 20,50 and 80MPa fly ash stiff mix

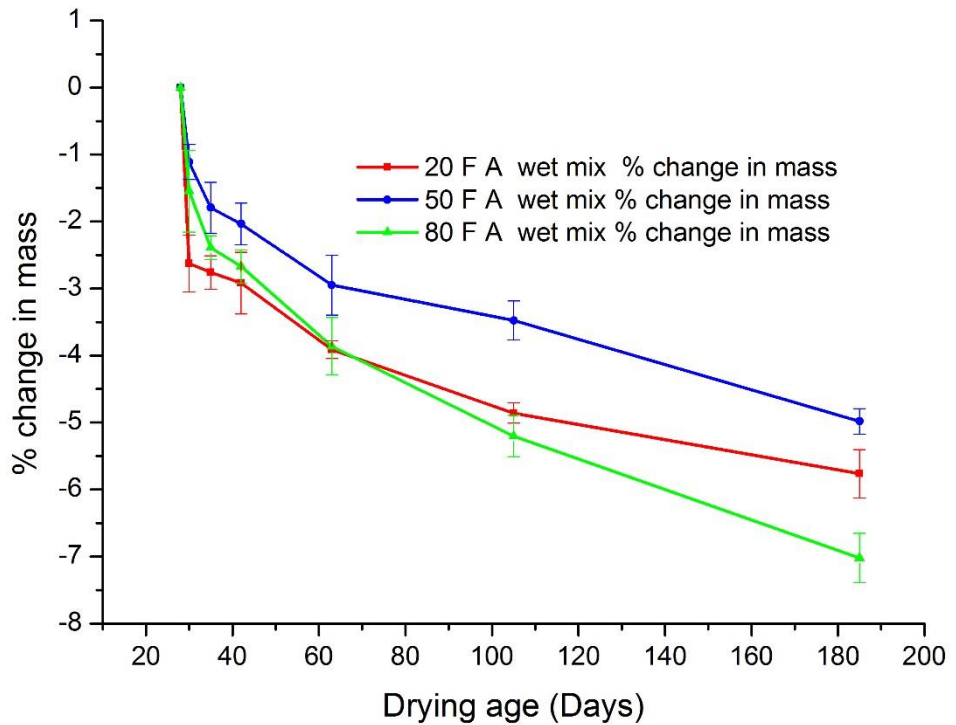


Figure A 24 Percentage change in mass for 20,50 and 80MPa fly ash wet mix

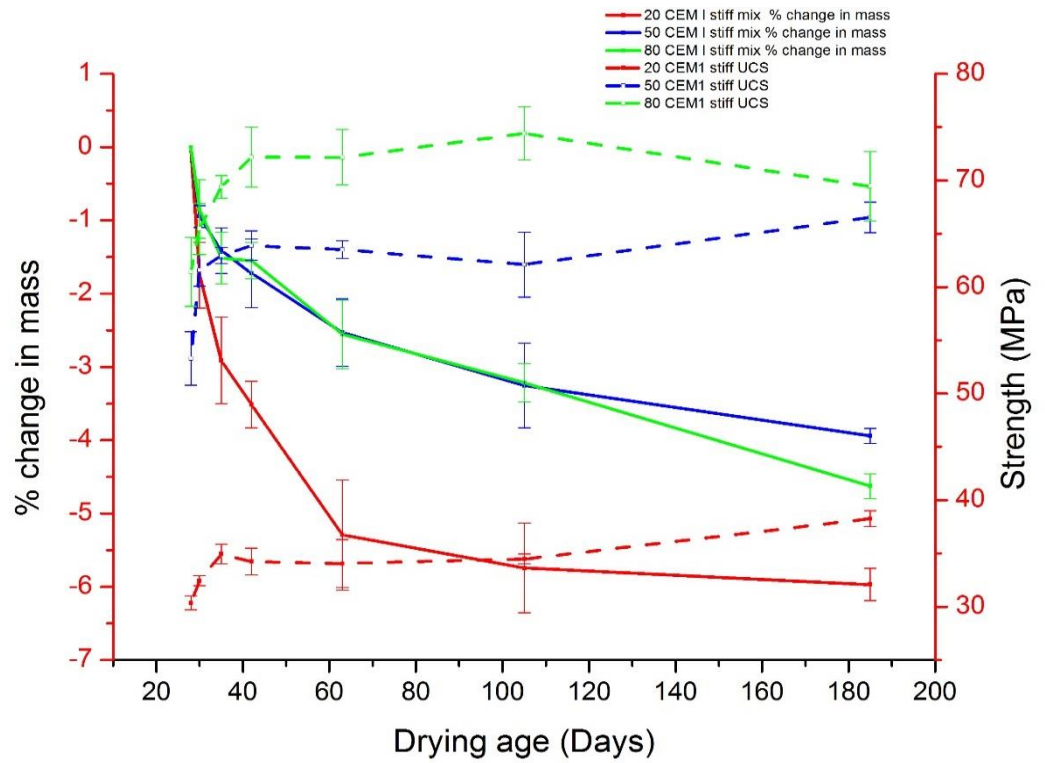


Figure A 25 Percentage change in mass and compressive strength of CEM1 stiff mix concrete

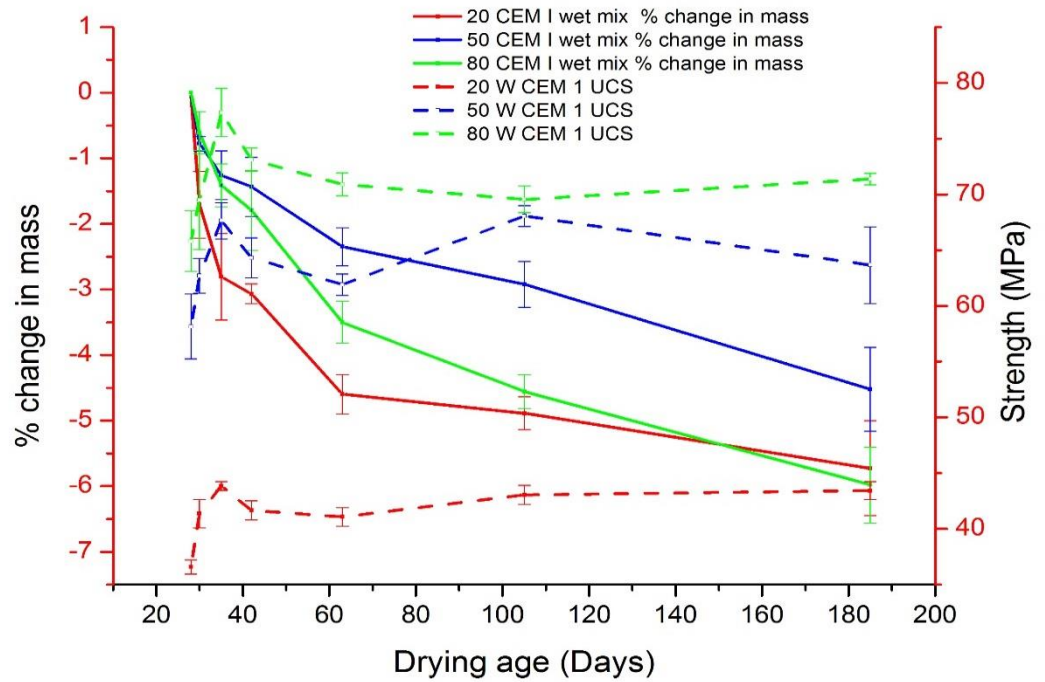


Figure A 26 Percentage change in mass and compressive strength of CEM1 wet mix concrete

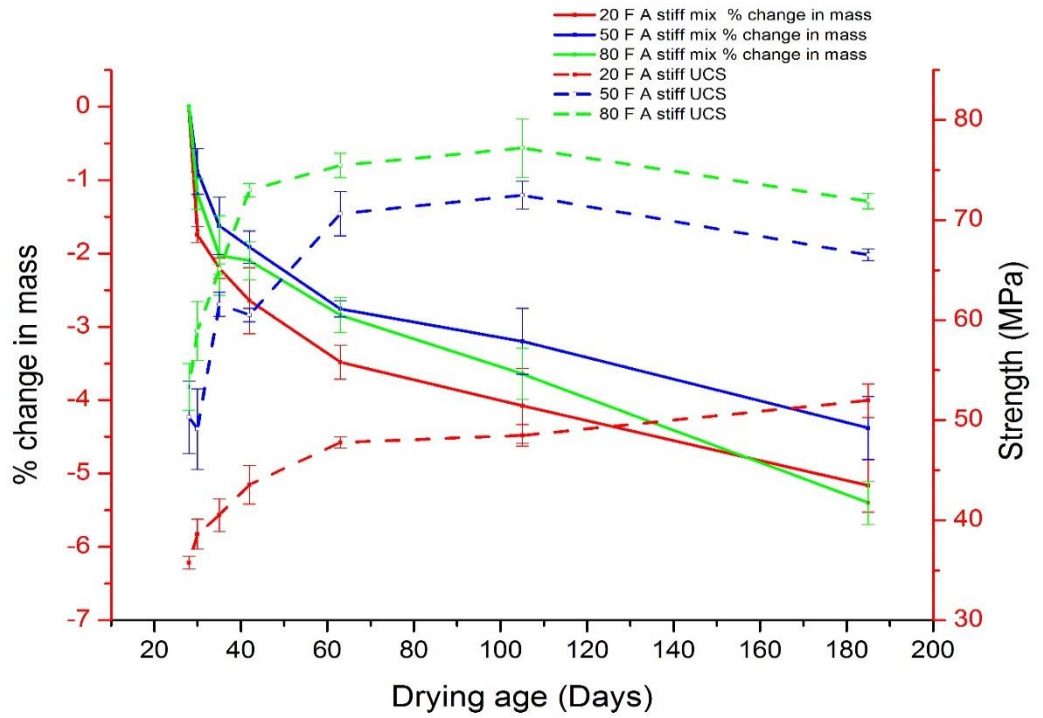


Figure A 27 Percentage change in mass and compressive strength of fly ash stiff mix concrete

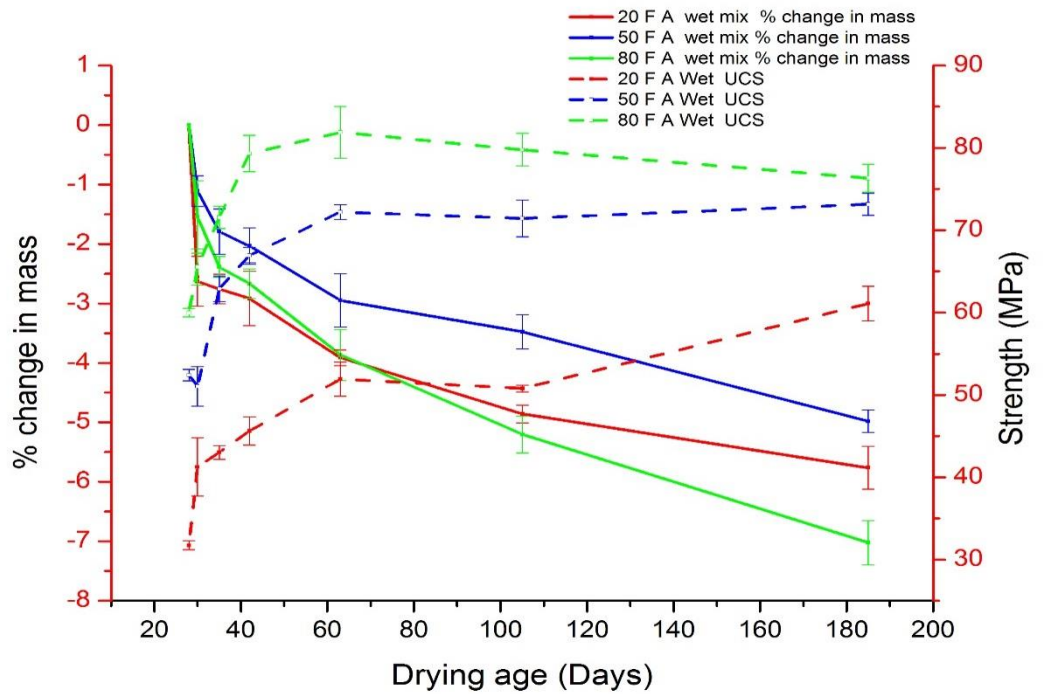


Figure A 28 Percentage change in mass and compressive strength of fly ash wet mix concrete

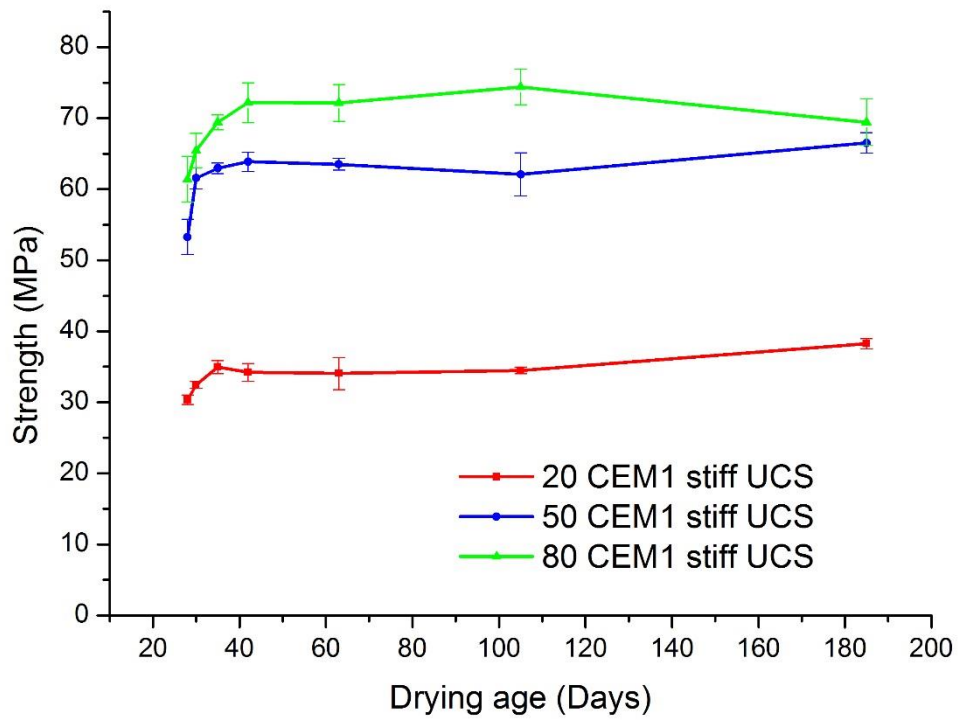


Figure A 29 Compressive strength of 20, 50 and 80MPa CEM1 stiff mix

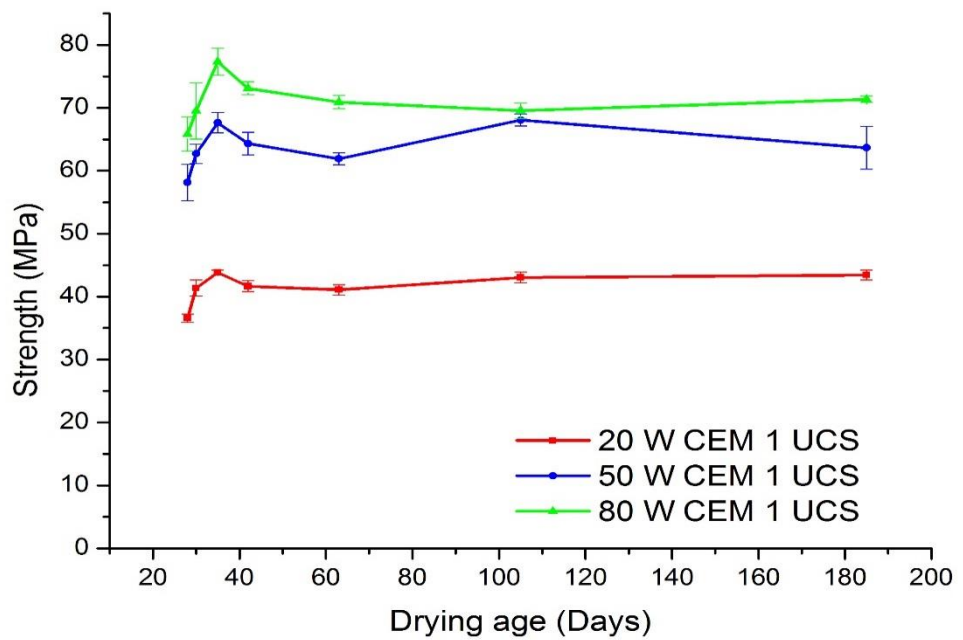


Figure A 30 Compressive strength of 20, 50 and 80MPa CEM1 wet mix

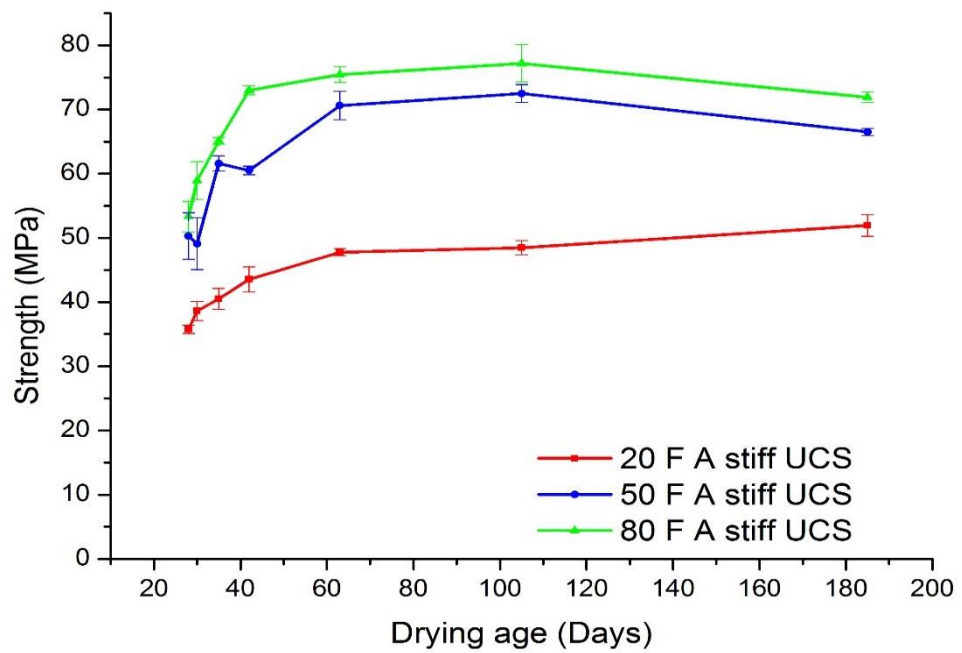


Figure A 31 Compressive strength of 20, 50 and 80MPa fly ash stiff mix

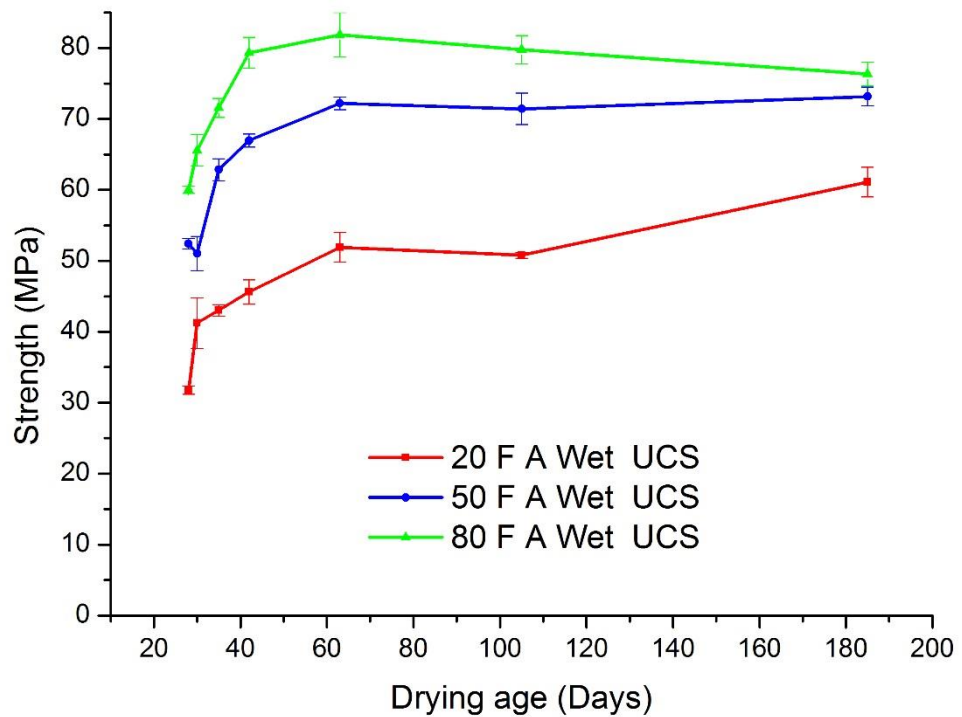


Figure A 32 Compressive strength of 20, 50 and 80MPa fly ash wet mix

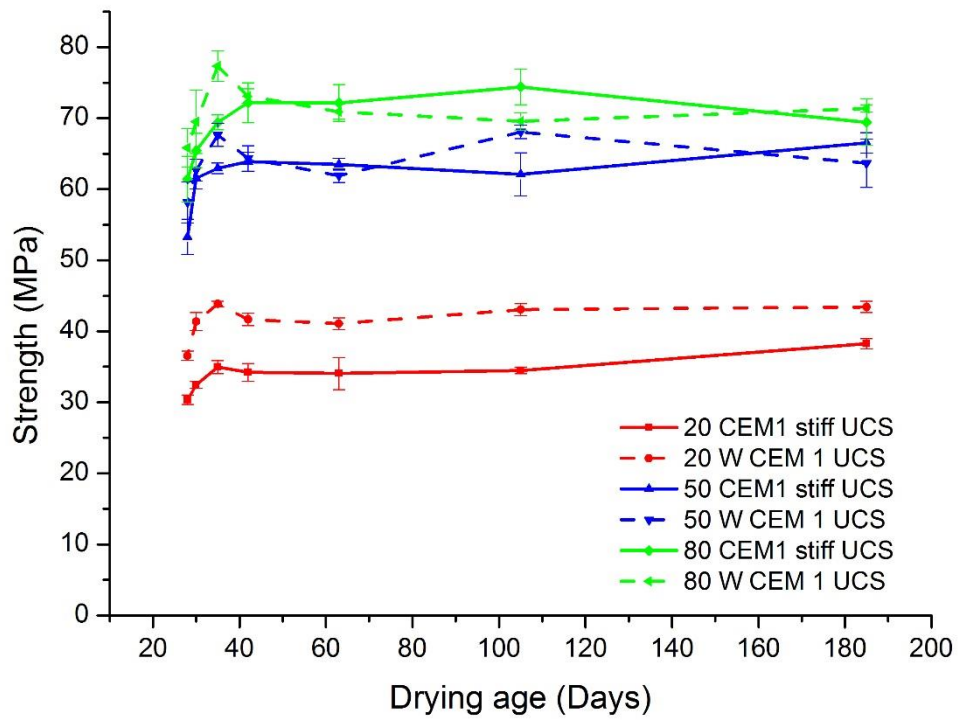


Figure A 33 Compressive strength of CEM1 stiff and wet mix

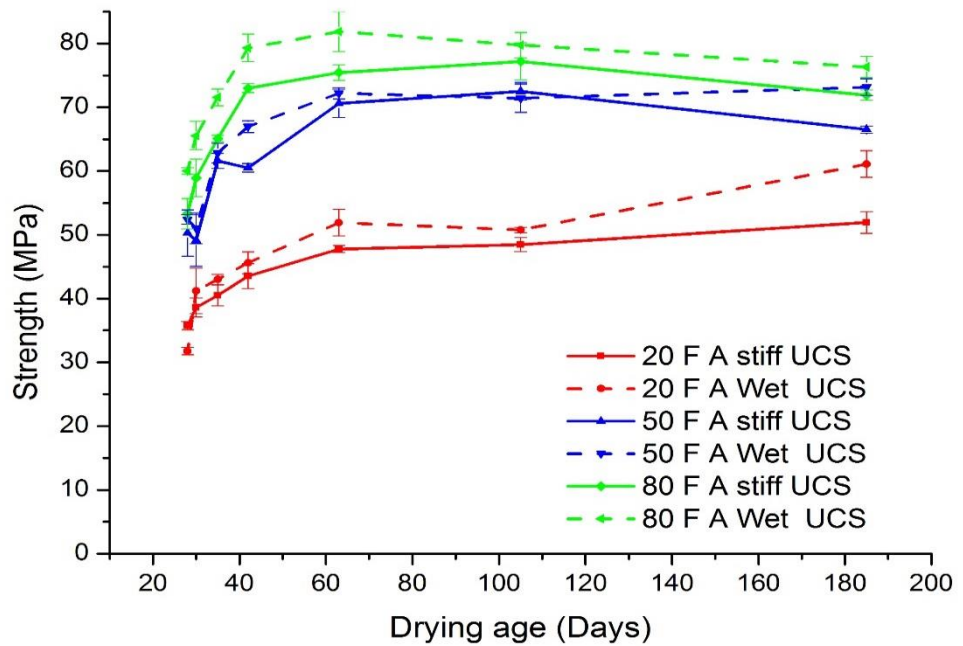


Figure A 34 Compressive strength of Fly ash stiff and wet mix

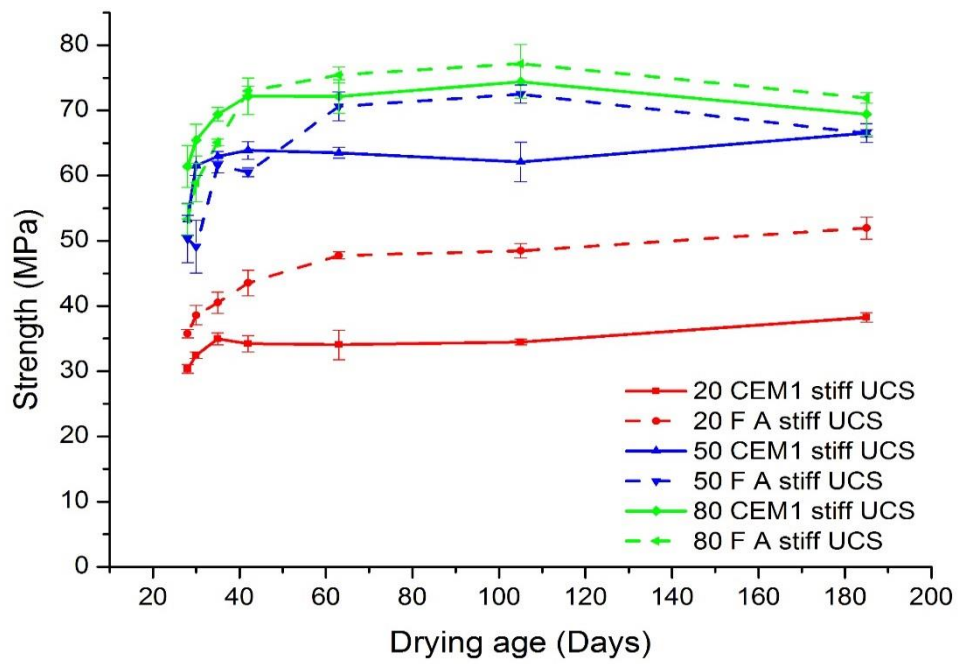


Figure A 35 Effect of drying on compressive strength of CEM1 and Fly ash stiff mix concrete

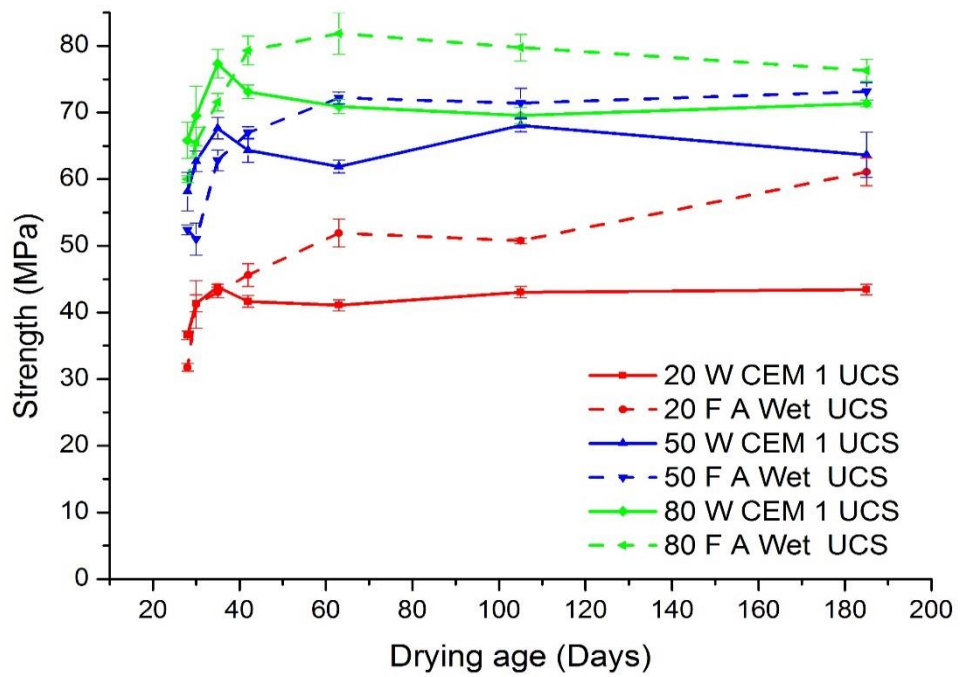


Figure A 36 Effect of drying on compressive strength of CEM1 and Fly ash wet mix concrete

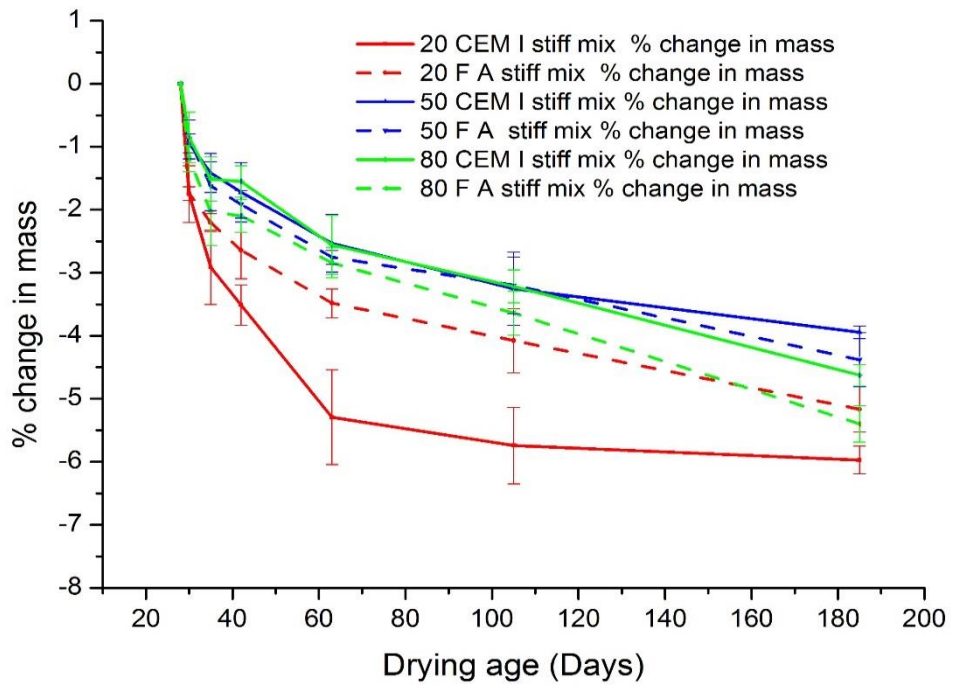


Figure A 37 Percentage change in mass for CEM1 and fly ash concrete stiff mix

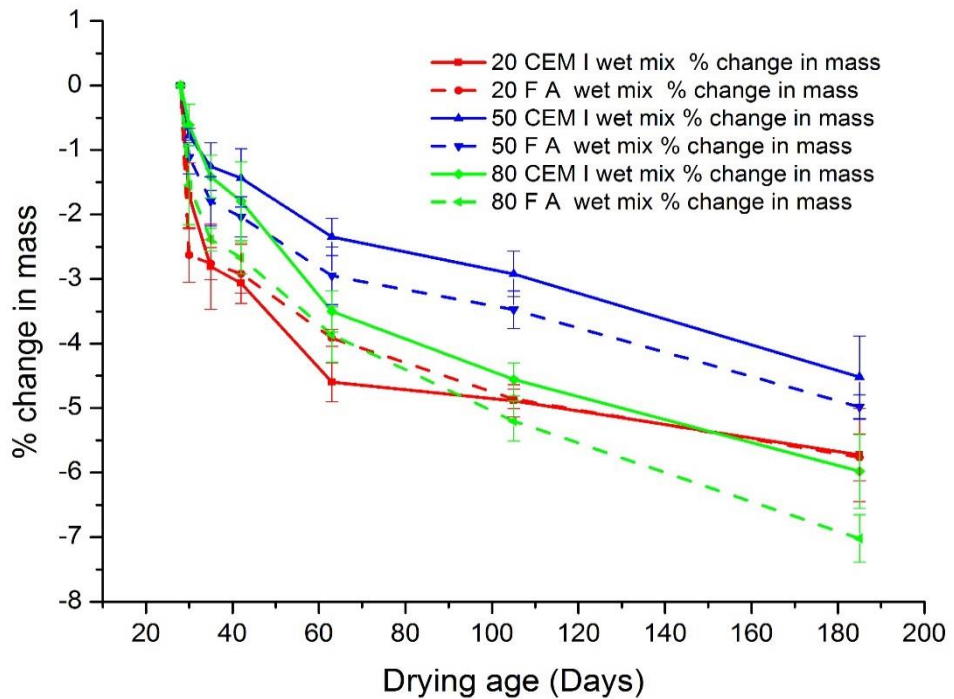


Figure A 38 Percentage change in mass for CEM1 and fly ash concrete wet mix

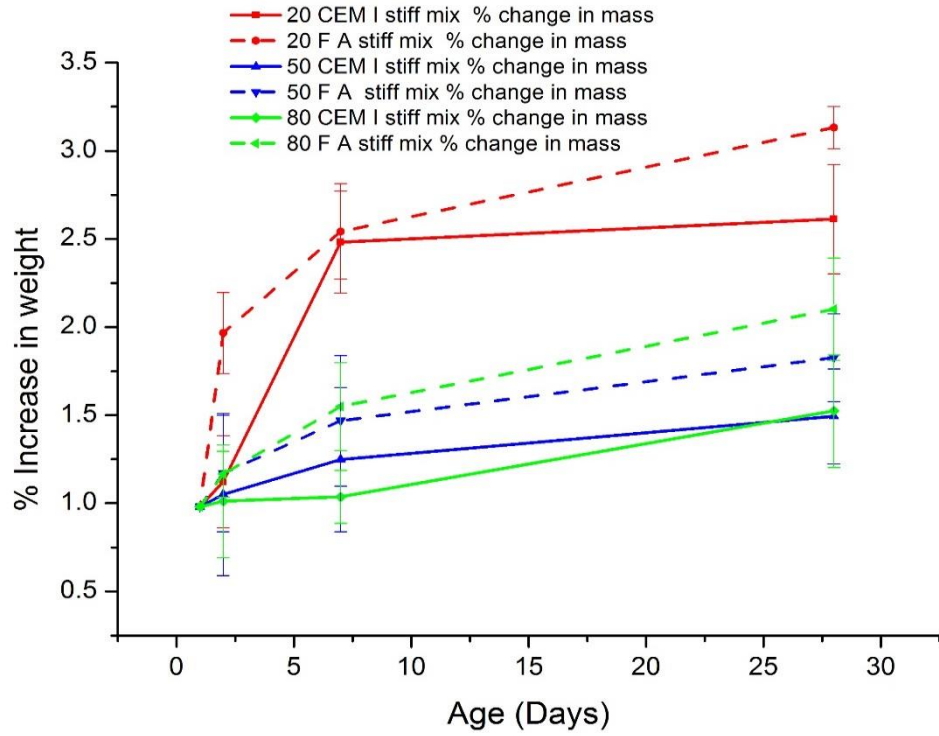


Figure A 39 Percentage increase in mass for CEM1 and fly ash concretes in stiff mix

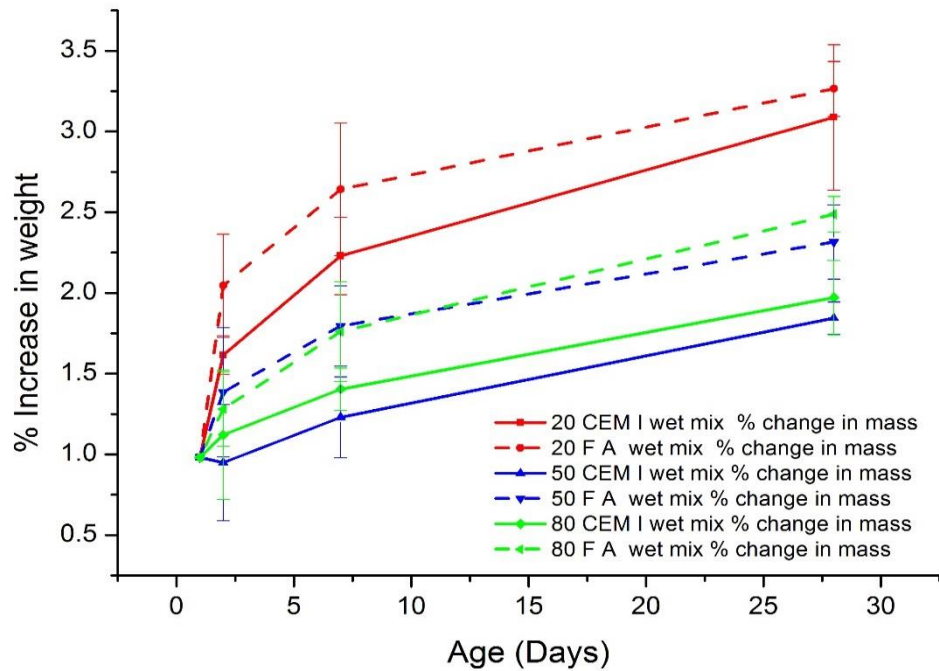


Figure A 40 Percentage increase in mass for CEM1 and fly ash concretes in wet mix

Appendix D Drying Shrinkage

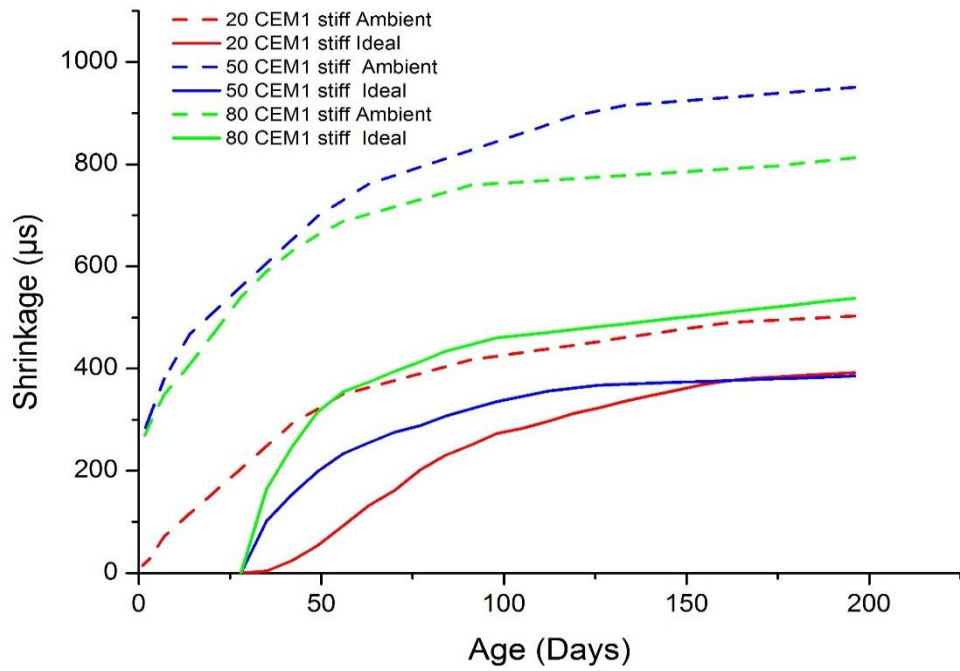


Figure A 41 Ambient and Ideal Cured Shrinkage of CEM1 stiff mix

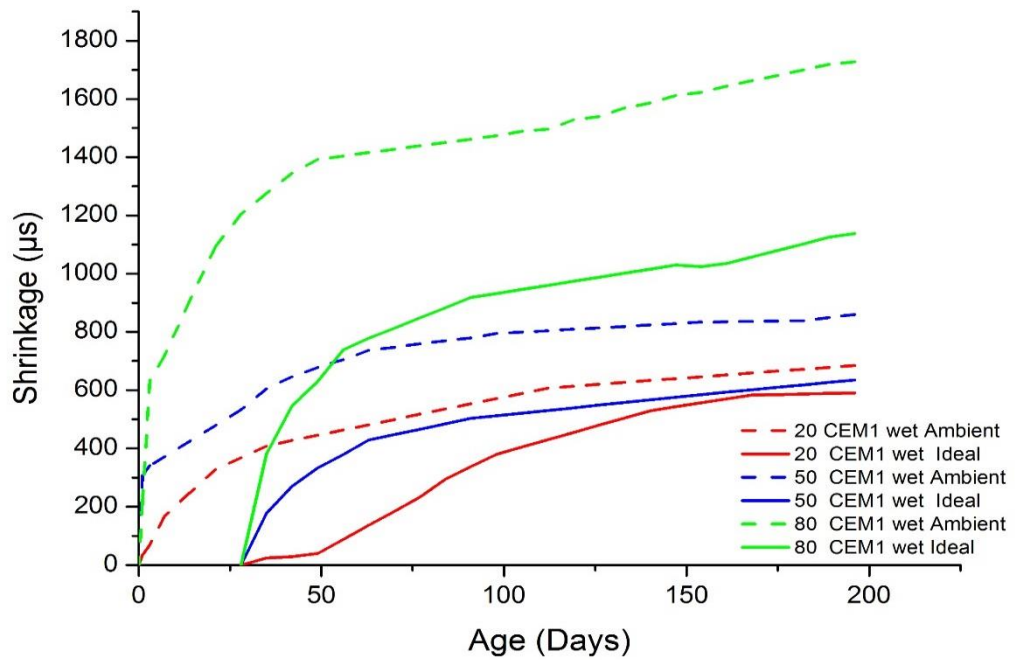


Figure A 42 Ambient and Ideal Cured Shrinkage of CEM1 wet mix

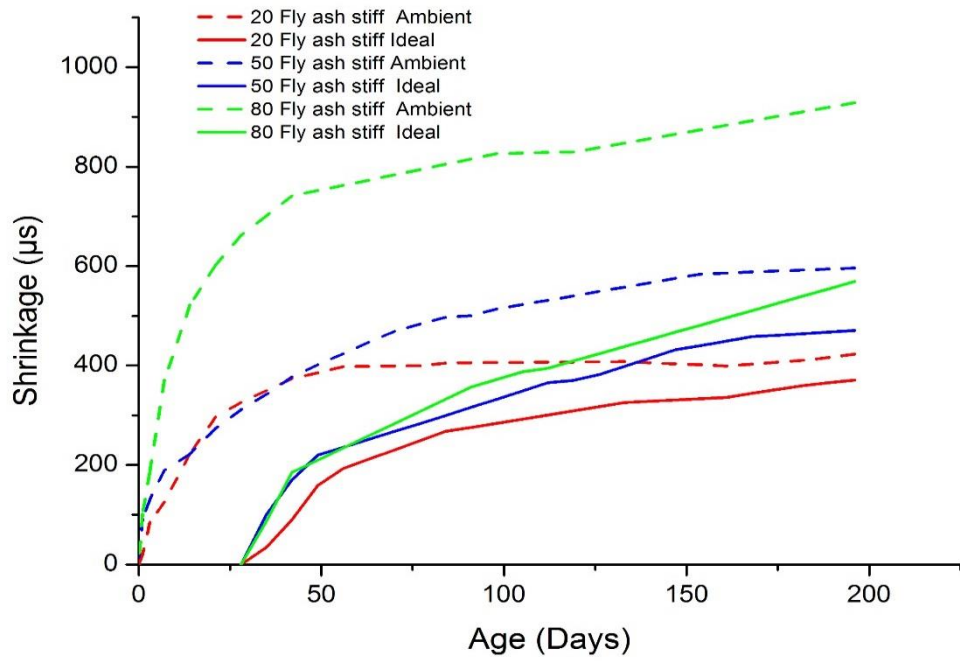


Figure A 43 Ambient and Ideal Cured Shrinkage of fly ash stiff mix

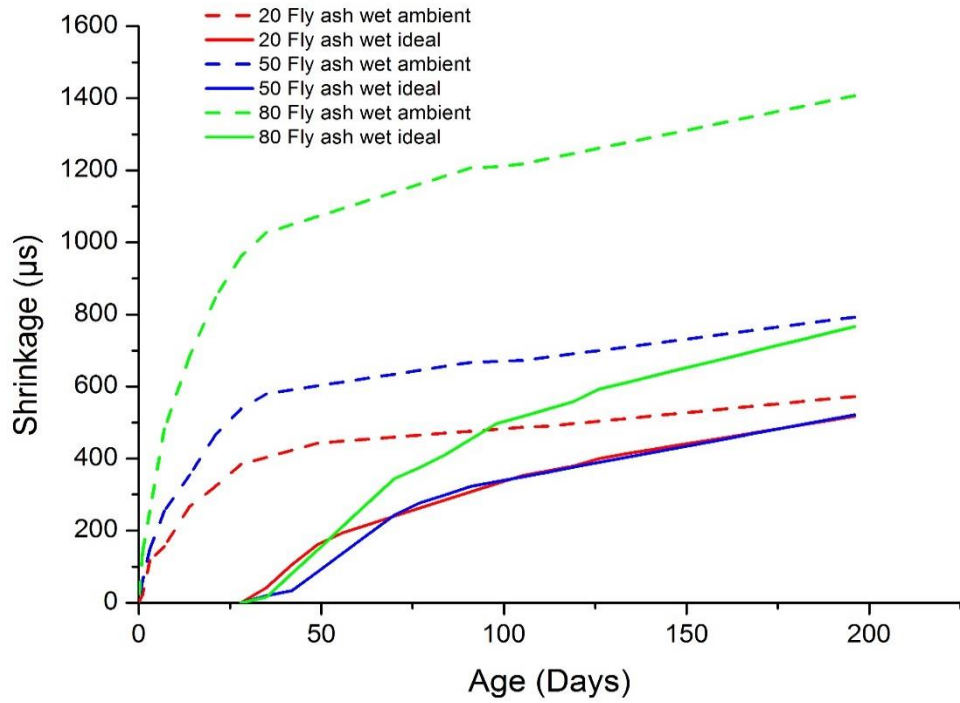


Figure A 44 Ambient and Ideal Cured Shrinkage of fly ash wet mix

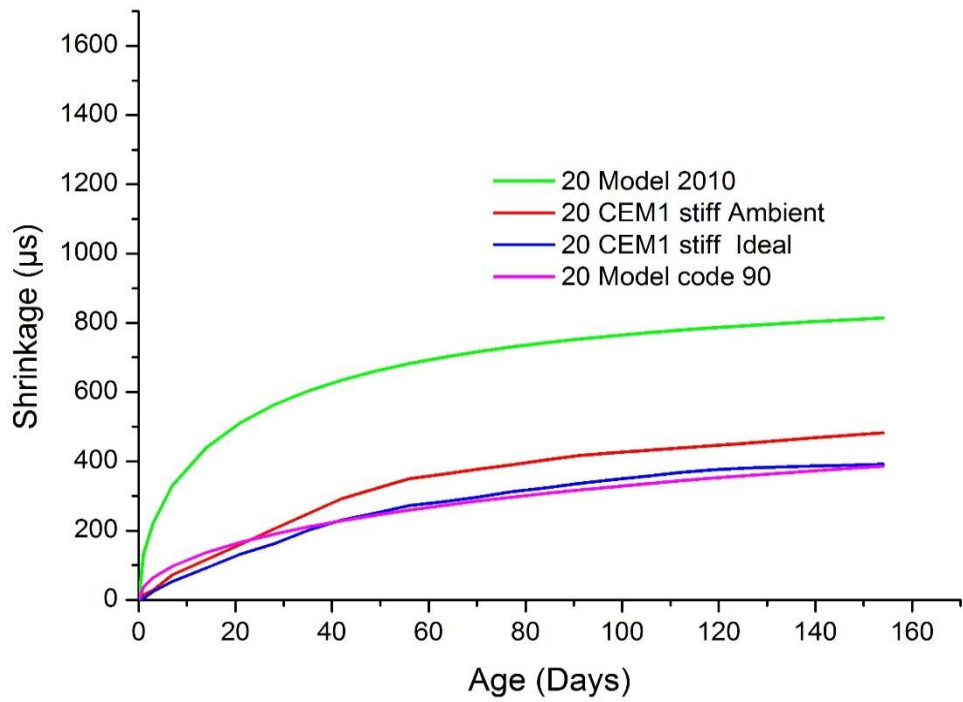


Figure A 45 Predicted shrinkage and measured ambient and ideal shrinkage for 20MPa CEM1 stiff mix

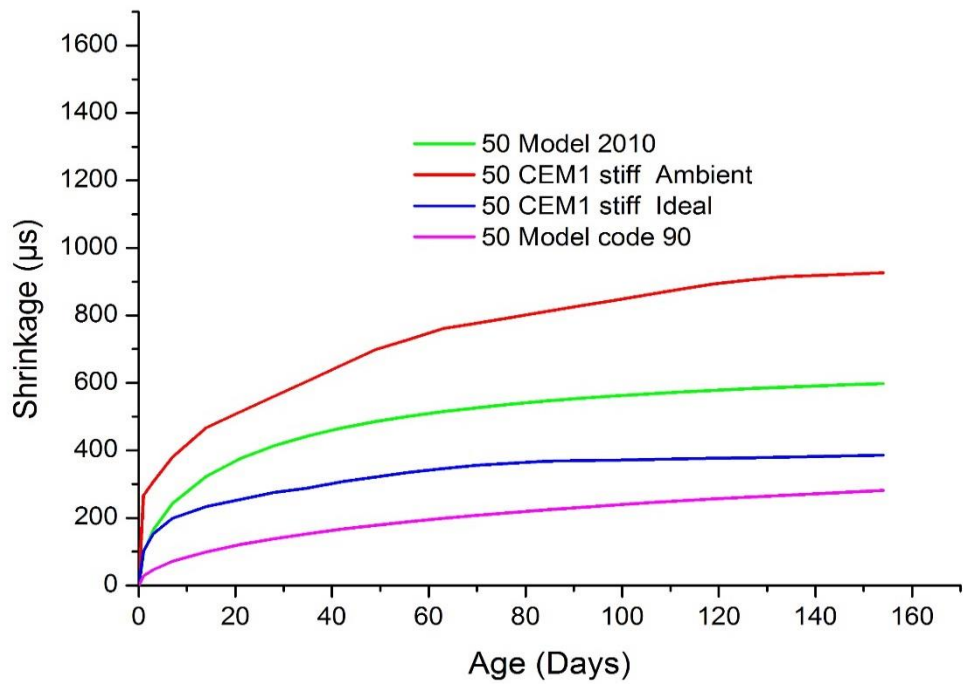


Figure A 46 Predicted shrinkage and measured ambient and ideal shrinkage for 50MPa CEM1 stiff mix

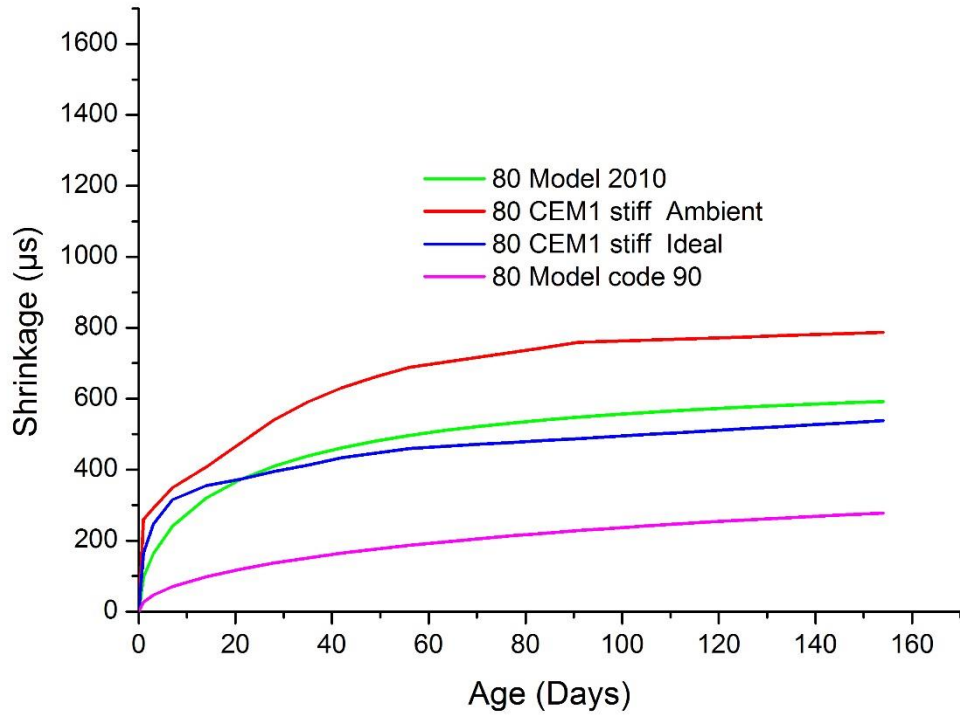


Figure A 47 Predicted shrinkage and measured ambient and ideal shrinkage for 80MPa CEM1 stiff mix

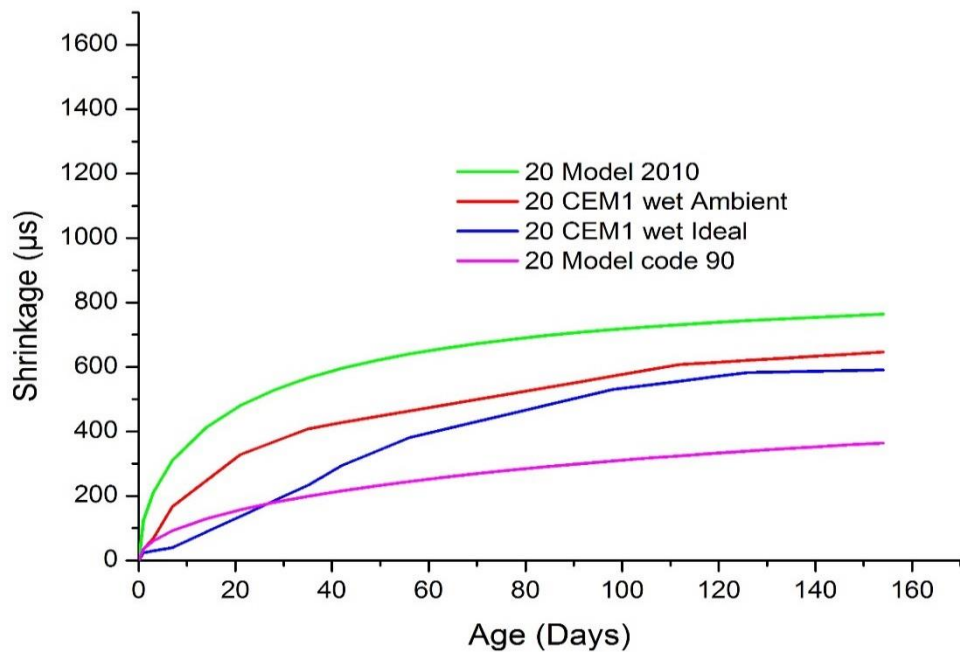


Figure A 48 Predicted shrinkage and measured ambient and ideal shrinkage for 20MPa CEM1 wet mix

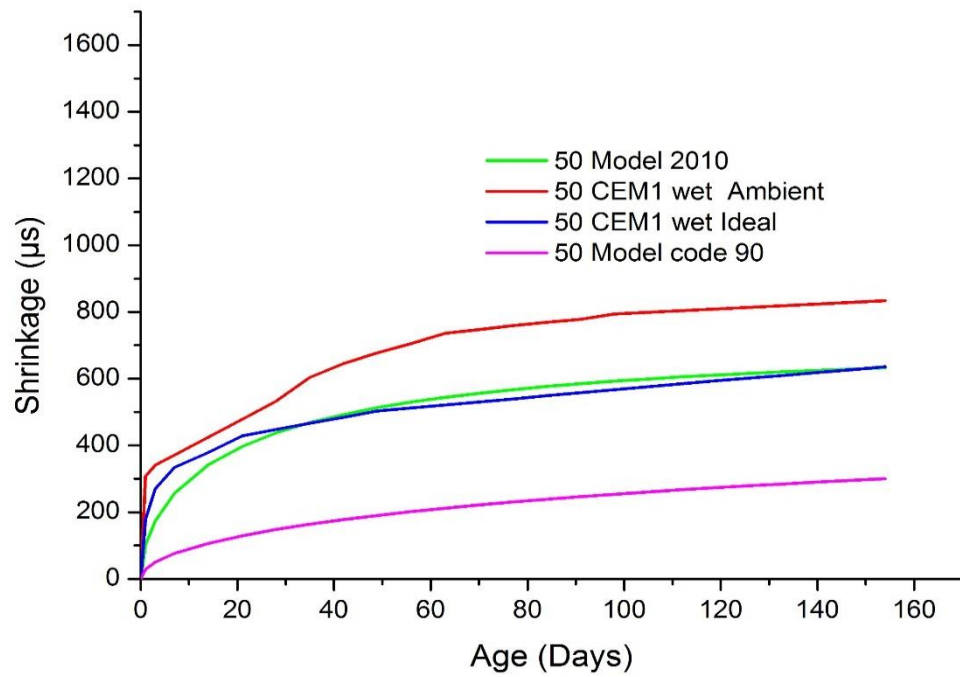


Figure A 49 Predicted shrinkage and measured ambient and ideal shrinkage for 50MPa CEM1 wet mix

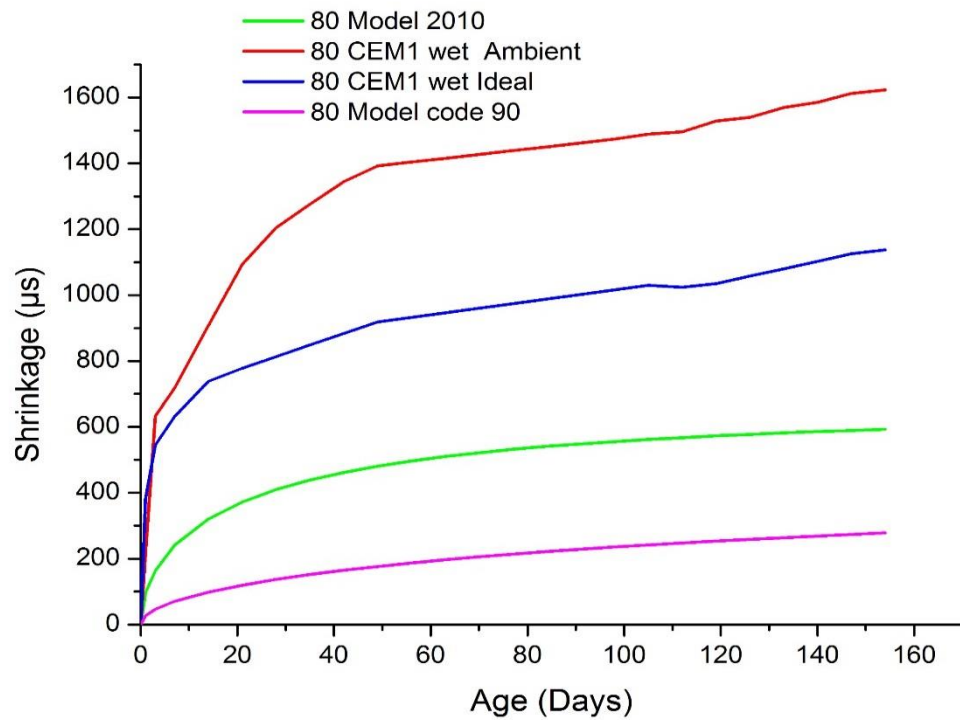


Figure A 50 Predicted shrinkage and measured ambient and ideal shrinkage for 80MPa CEM1 wet mix

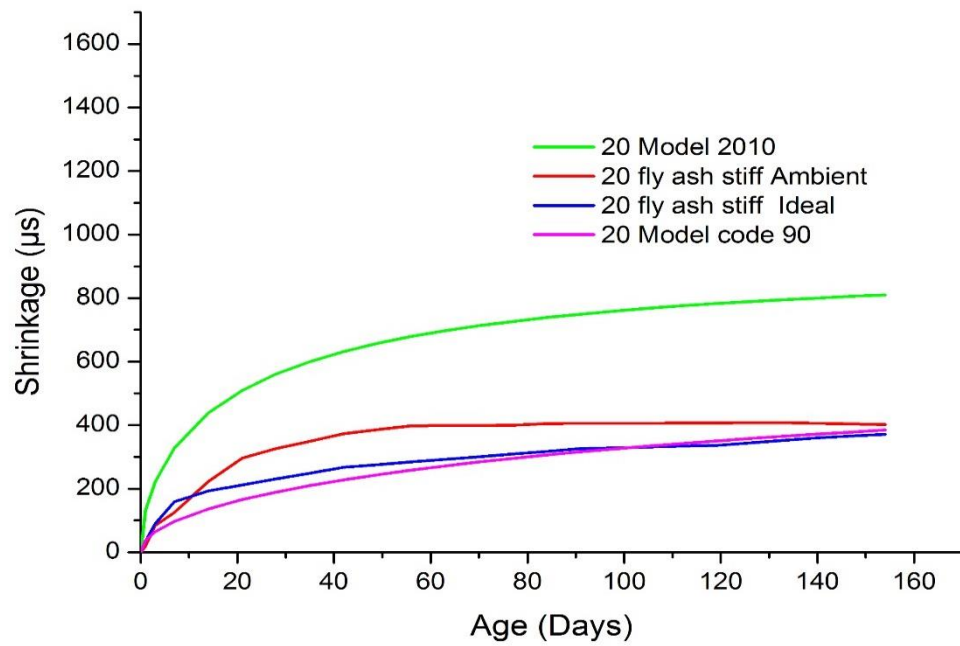


Figure A 51 Predicted shrinkage and measured ambient and ideal shrinkage for 20MPa fly ash stiff mix

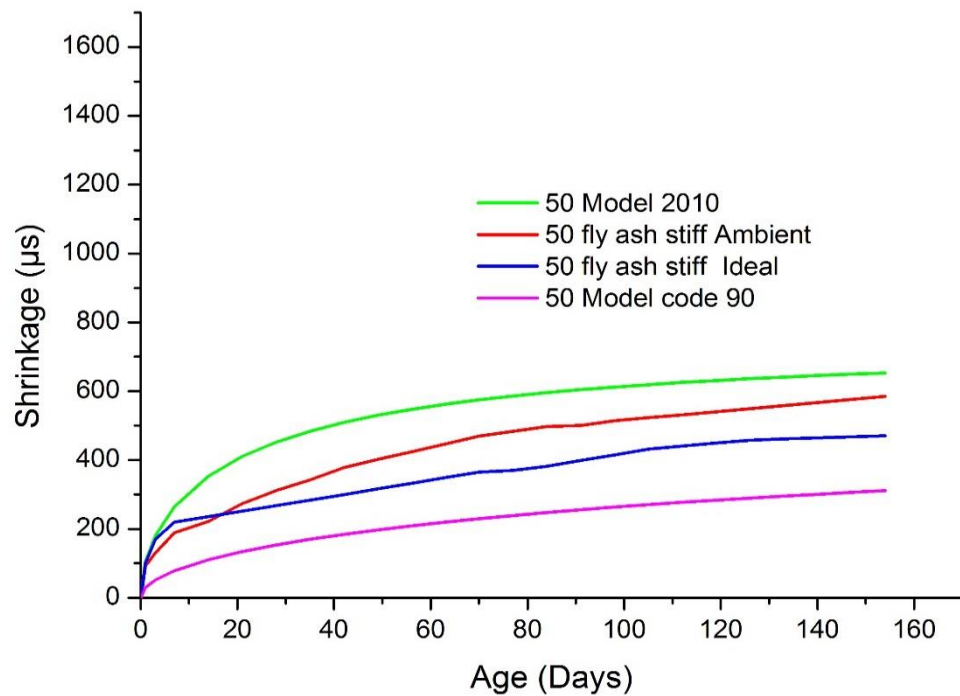


Figure A 52 Predicted shrinkage and measured ambient and ideal shrinkage for 50MPa fly ash stiff mix

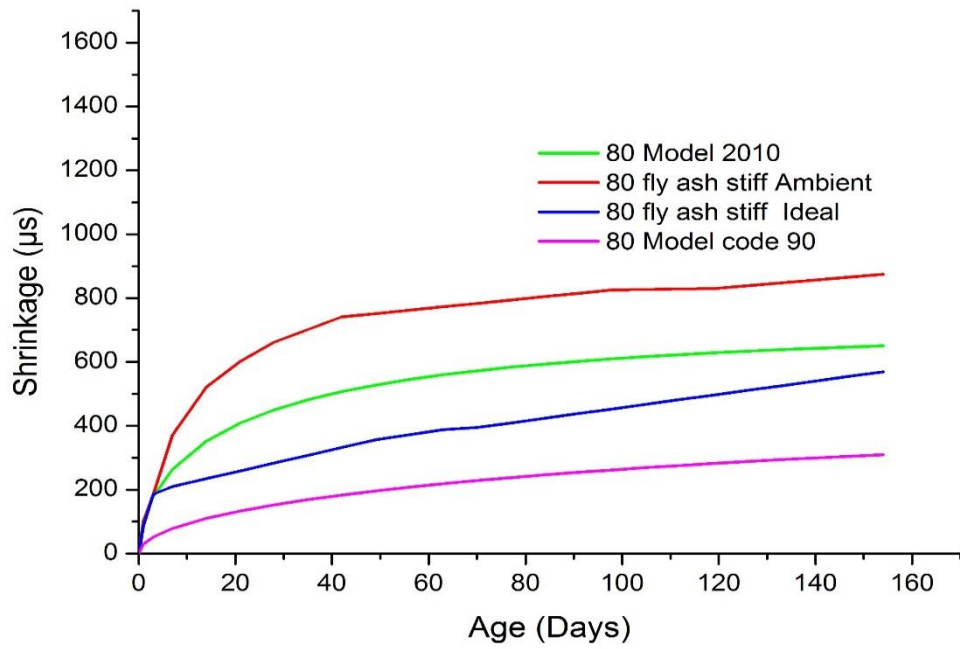


Figure A 53 Predicted shrinkage and measured ambient and ideal shrinkage for 80MPa fly ash stiff mix

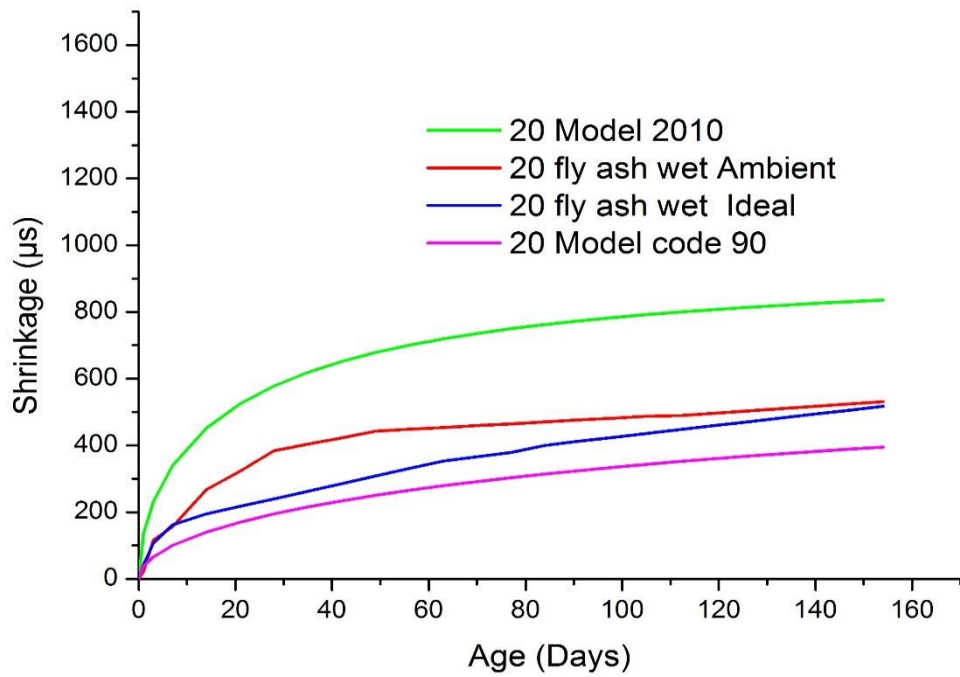


Figure A 54 Predicted shrinkage and measured ambient and ideal shrinkage for 20MPa fly ash wet mix

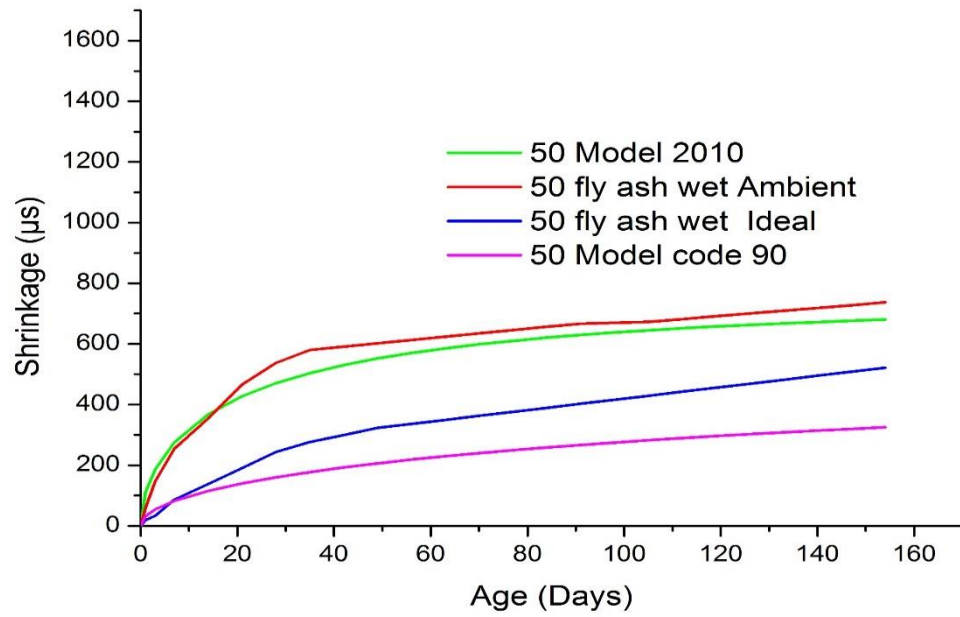


Figure A 55 Predicted shrinkage and measured ambient and ideal shrinkage for 50MPa fly ash wet mix

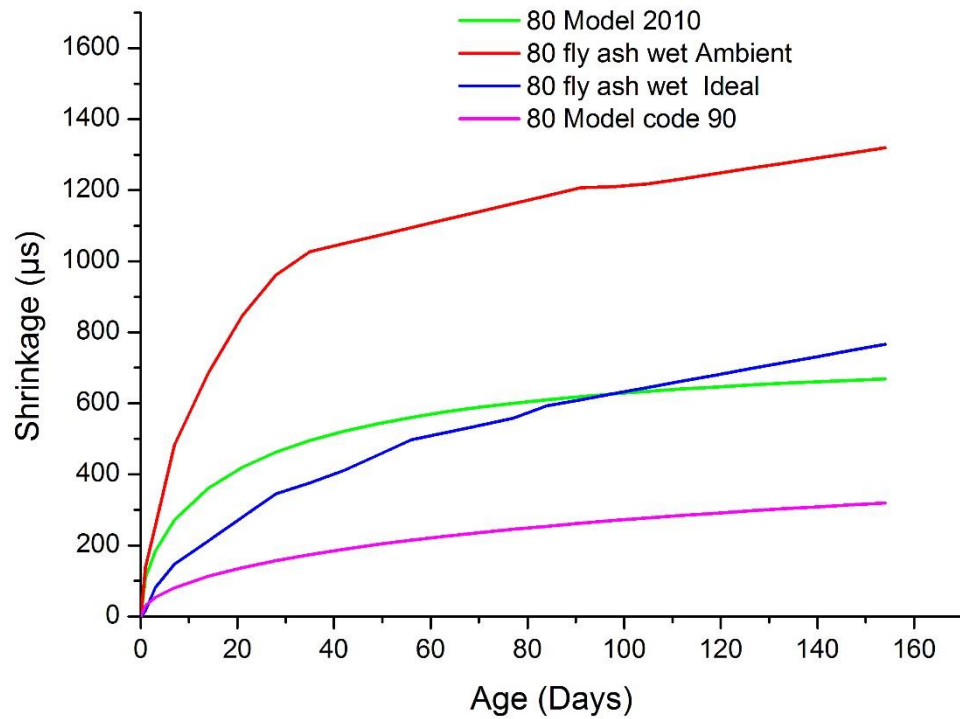


Figure A 56 Predicted shrinkage and measured ambient and ideal shrinkage for 80MPa fly ash wet mix

Normalised

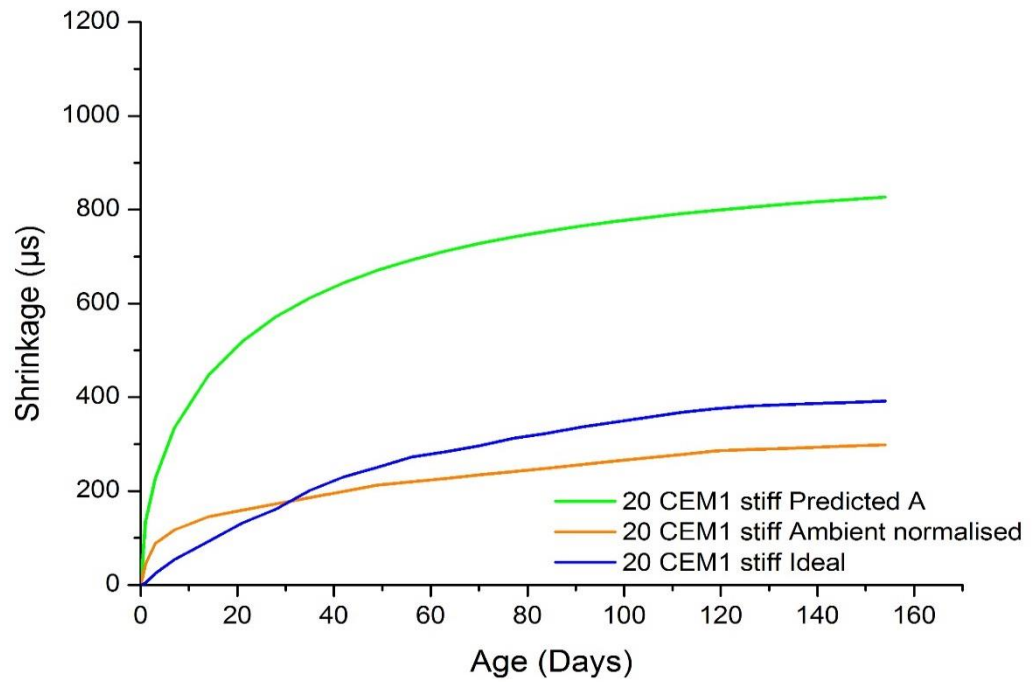


Figure A 57 Normalised shrinkage with Model code 2010 for 20MPa CEM1 stiff mix

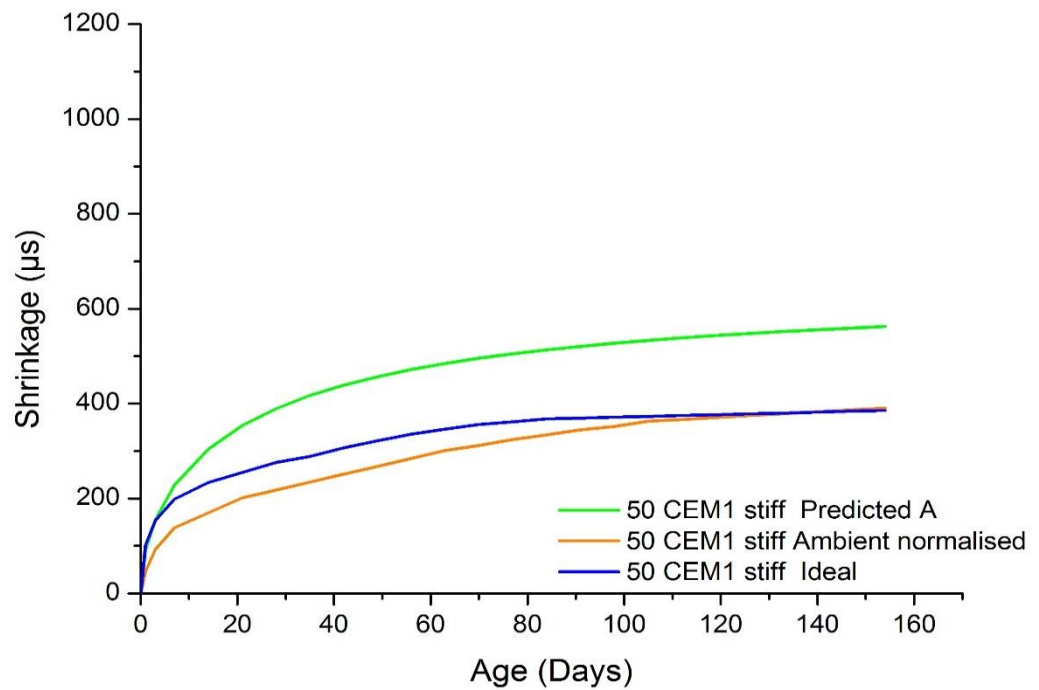


Figure A 58 Normalised shrinkage with Model code 2010 for 50MPa CEM1 stiff mix

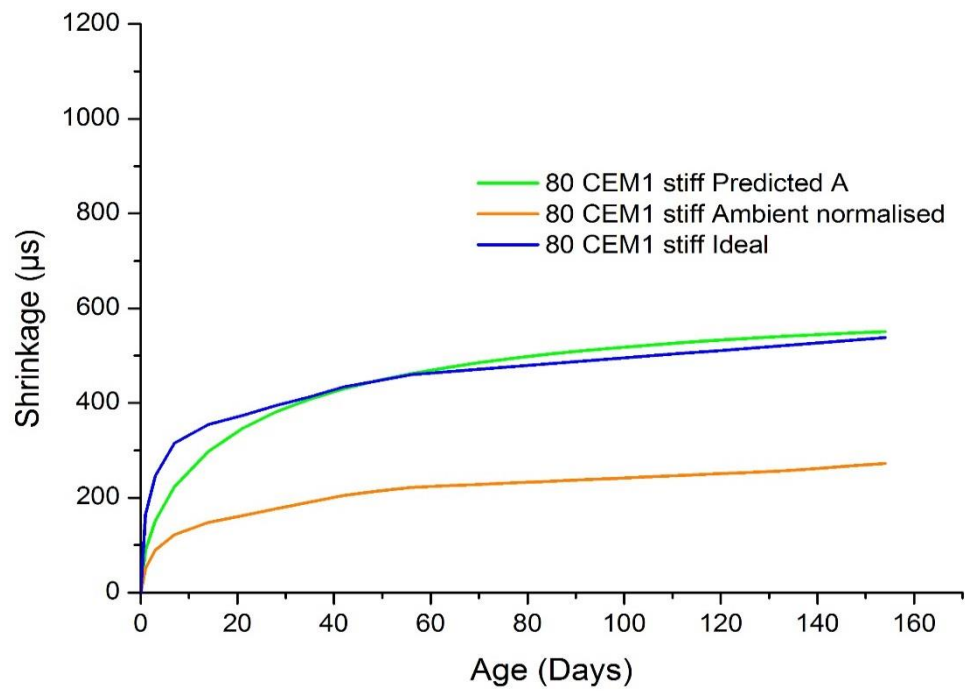


Figure A 59 Normalised shrinkage with Model code 2010 for 80MPa CEM1 stiff mix

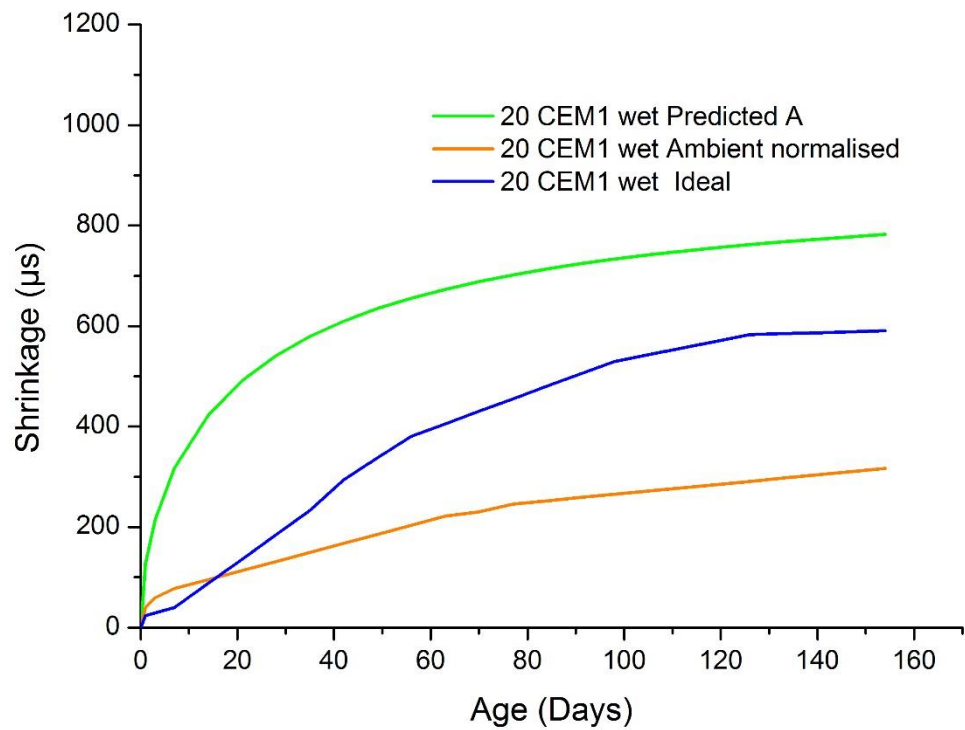


Figure A 60 Normalised shrinkage with Model code 2010 for 20MPa CEM1 wet mix

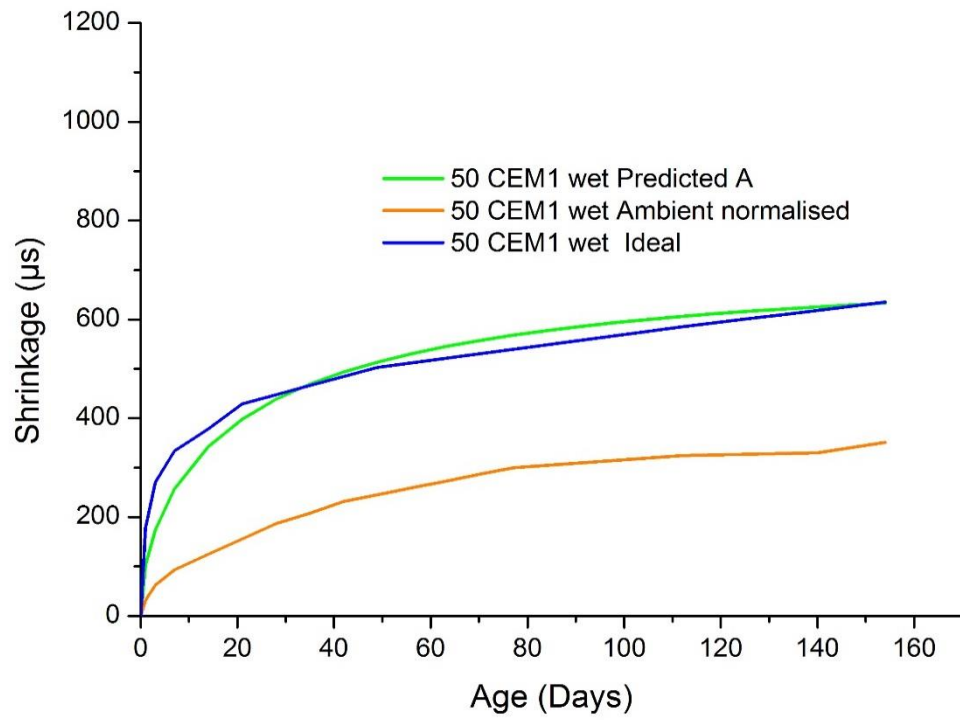


Figure A 61 Normalised shrinkage with Model code 2010 for 50MPa CEM1 wet mix

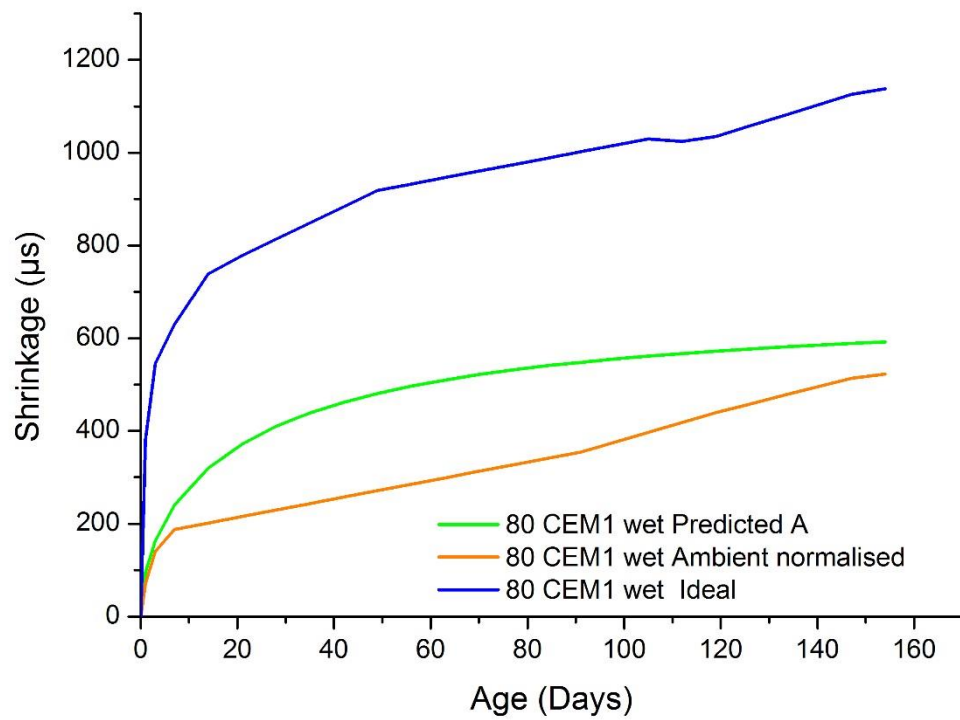


Figure A 62 Normalised shrinkage with Model code 2010 for 80MPa CEM1 wet mix

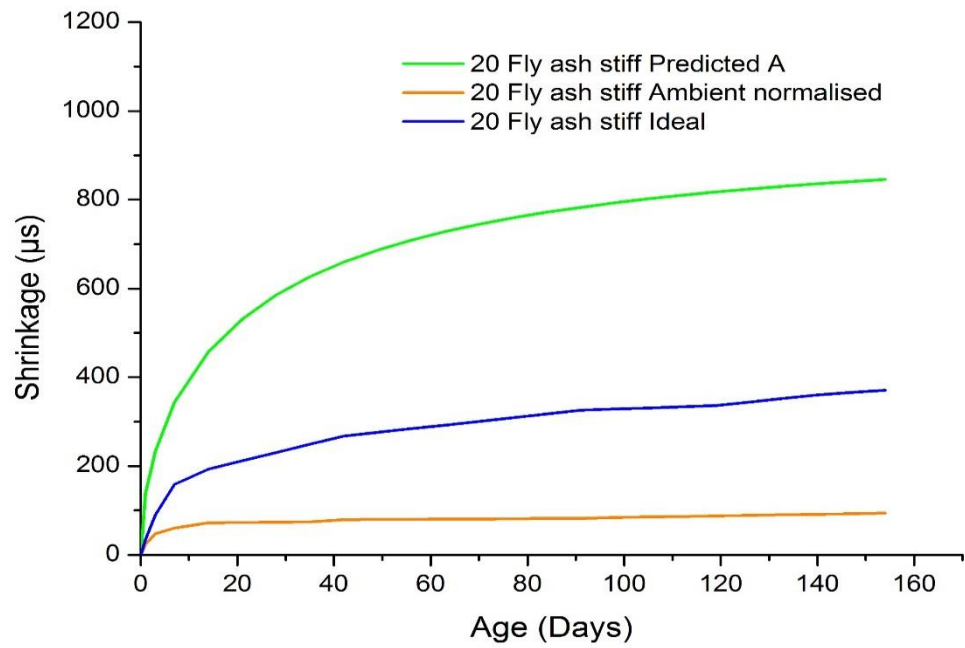


Figure A 63 Normalised shrinkage with Model code 2010 for 20MPa fly ash stiff mix

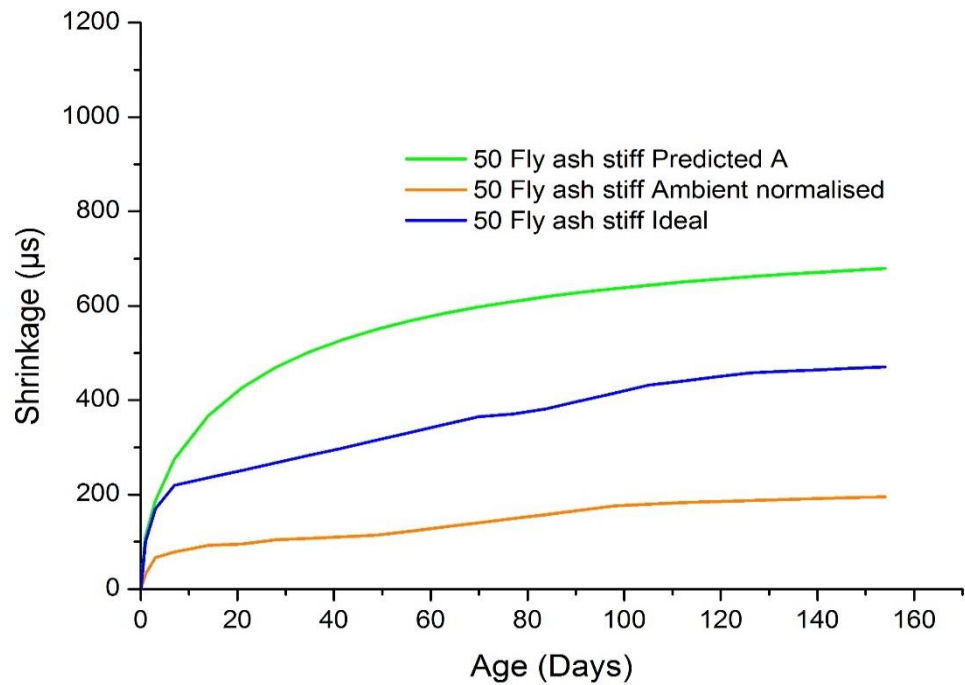


Figure A 64 Normalised shrinkage with Model code 2010 for 50MPa fly ash stiff mix

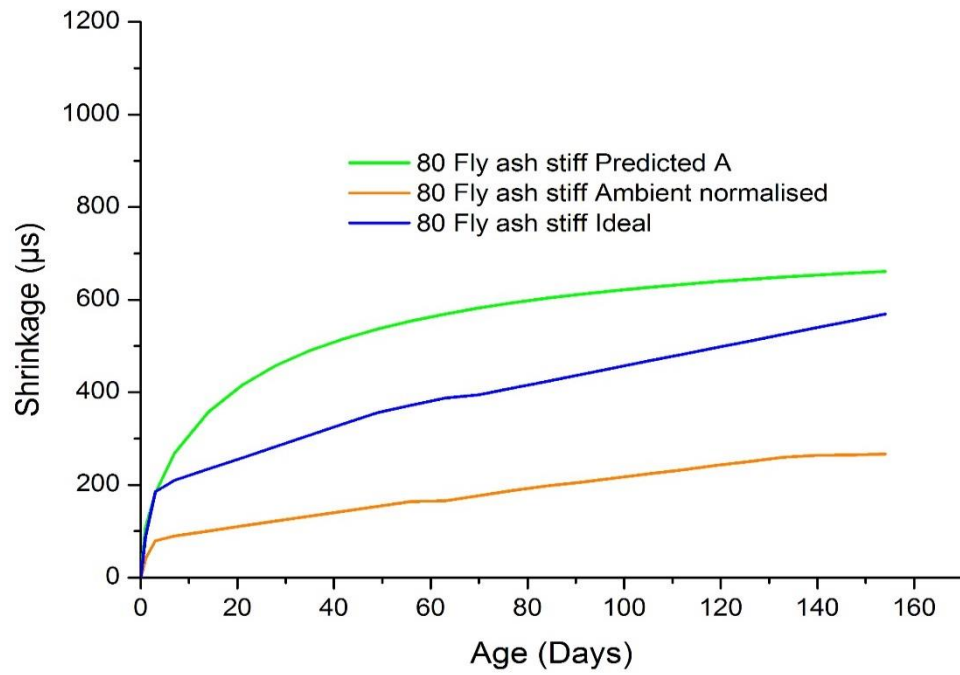


Figure A 65 Normalised shrinkage with Model code 2010 for 80MPa fly ash stiff mix

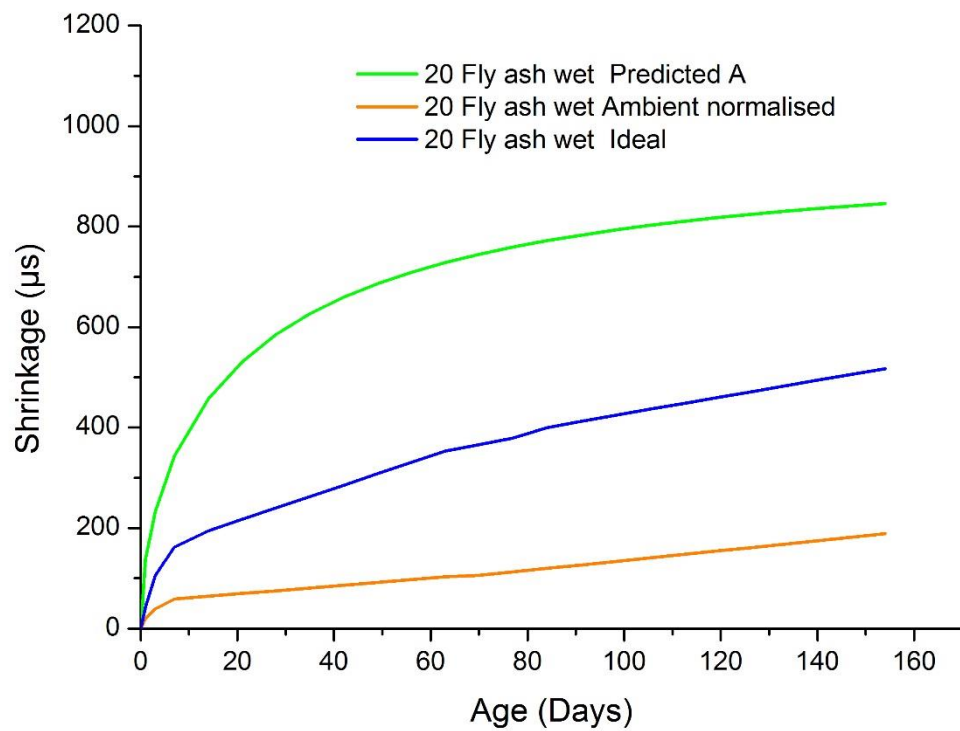


Figure A 66 Normalised shrinkage with Model code 2010 for 20MPa fly ash wet mix

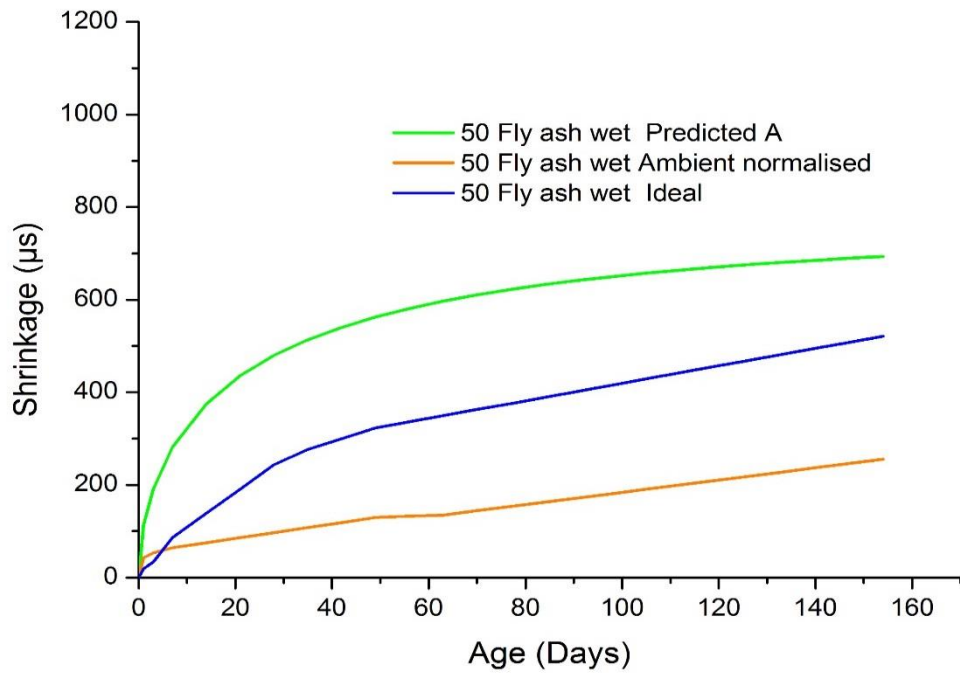


Figure A 67 Normalised shrinkage with Model code 2010 for 50MPa fly ash wet mix

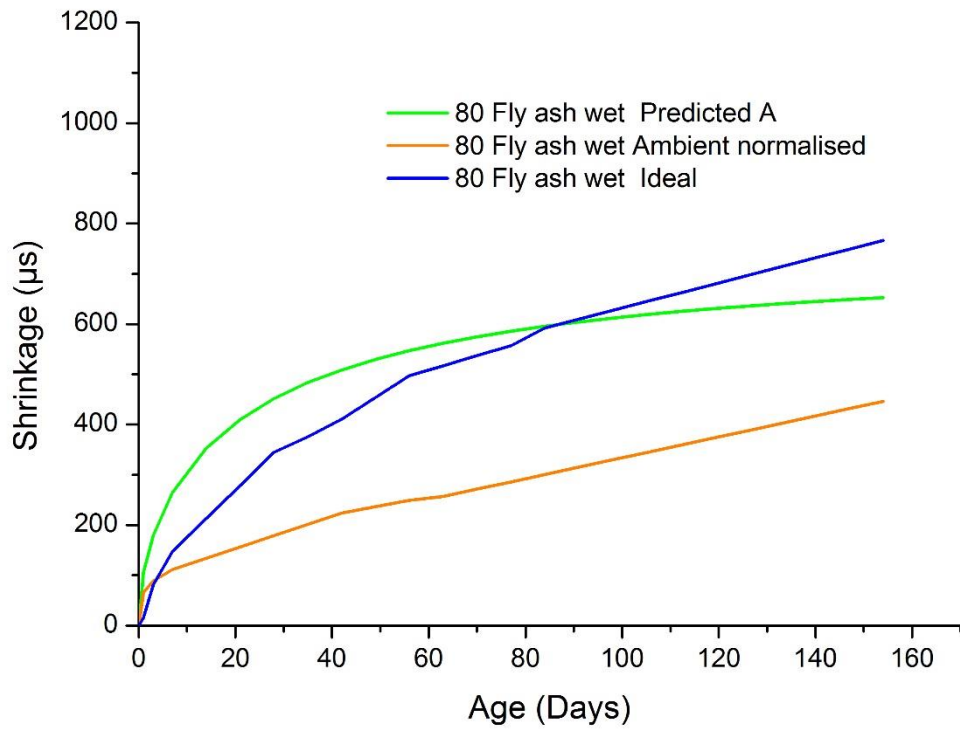


Figure A 68 Normalised shrinkage with Model code 2010 for 80MPa fly ash wet mix

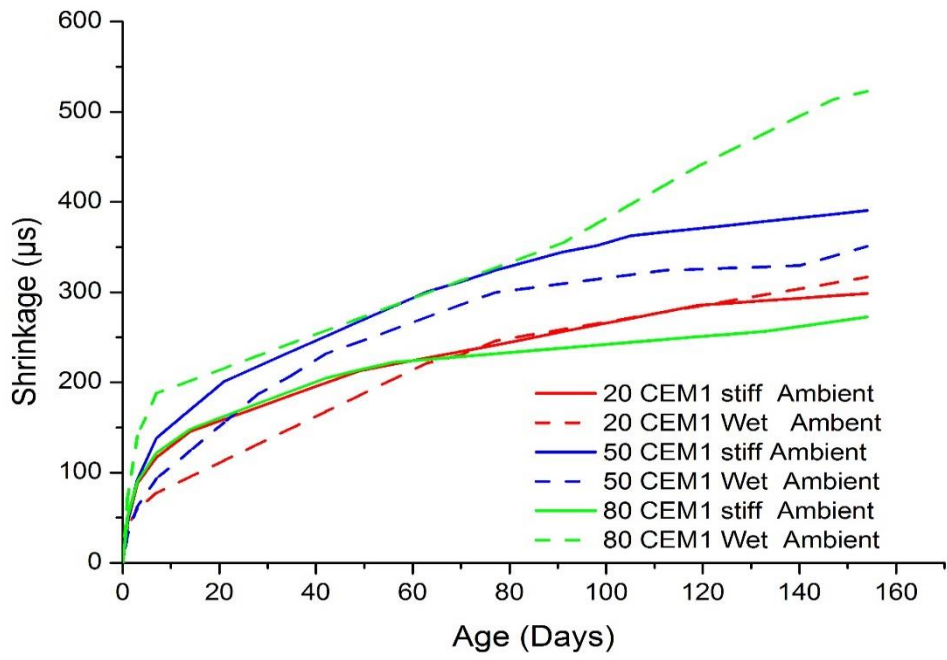


Figure A 69 Shrinkage of 20,50,80MPa CEM1 stiff and wet mix ambient cured samples

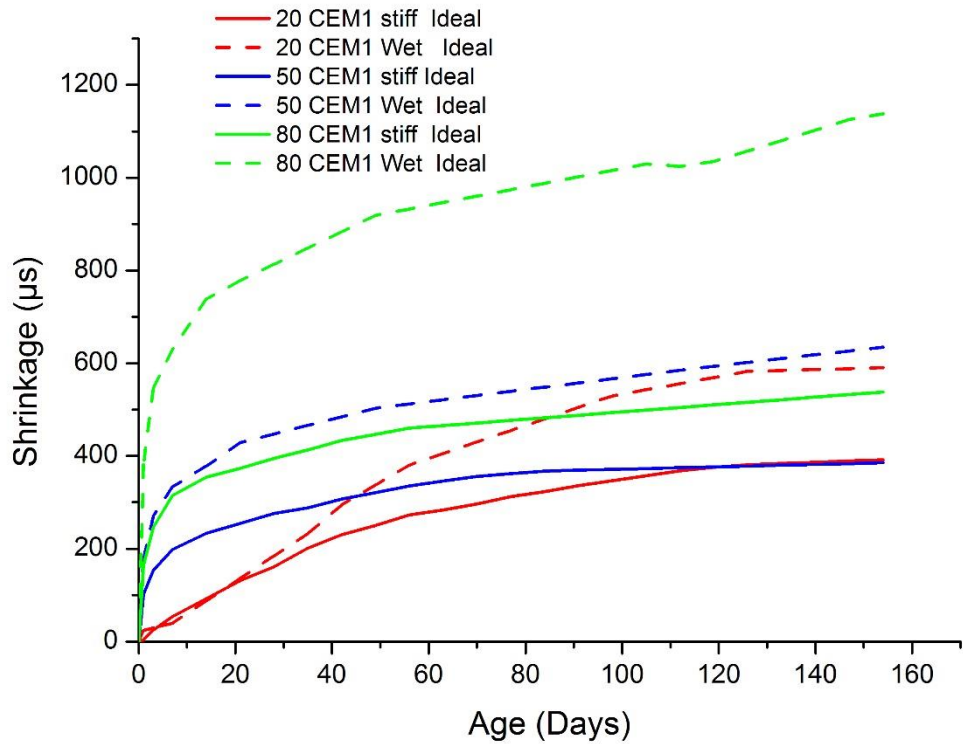


Figure A 70 Shrinkage of 20,50,80MPa CEM1 stiff and wet mix ideal cured samples

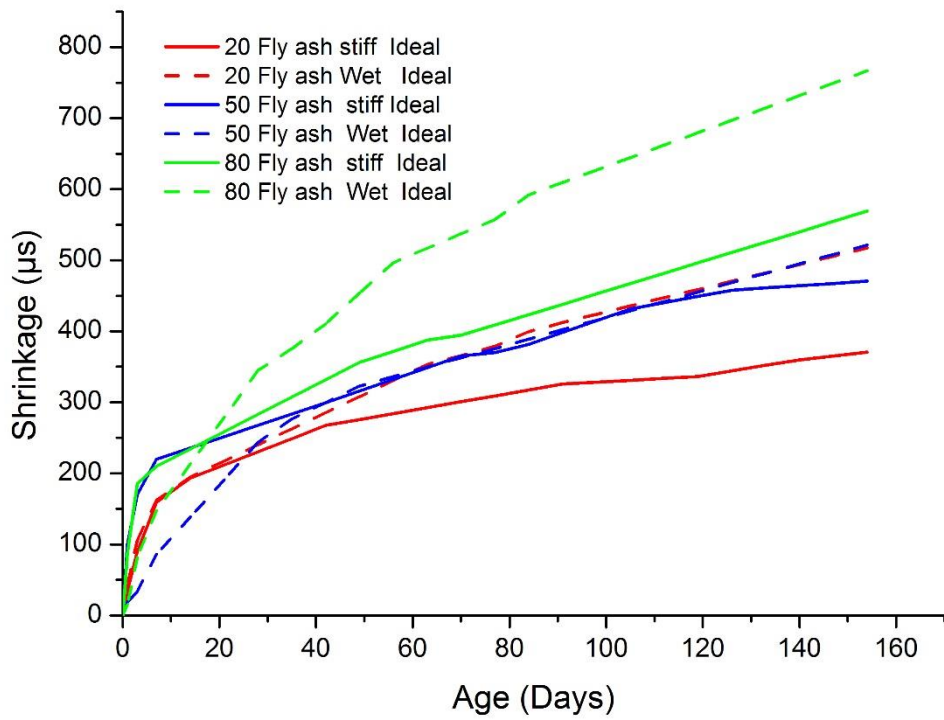


Figure A 71 Shrinkage of 20,50,80MPa fly ash stiff and wet mix ambient cured samples

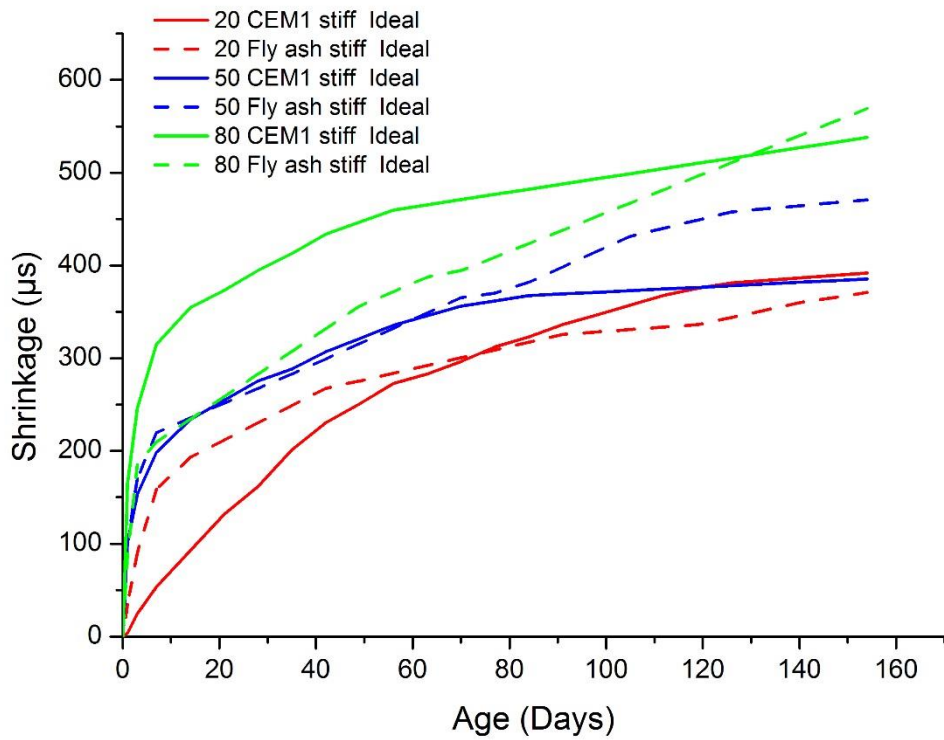


Figure A 72 Shrinkage of 20,50,80MPa fly ash stiff and wet mix ideal cured samples

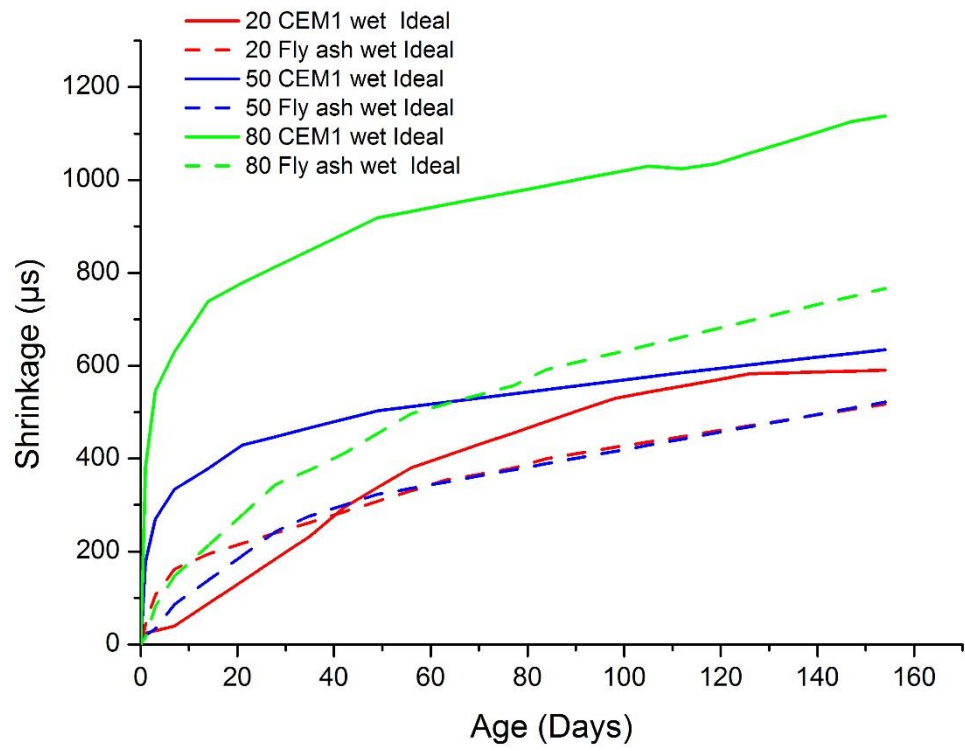


Figure A 73 Shrinkage of CEM1 and Fly ash wet mix ideal cured concretes

Appendix E Transport properties

Carbonation at 90 days

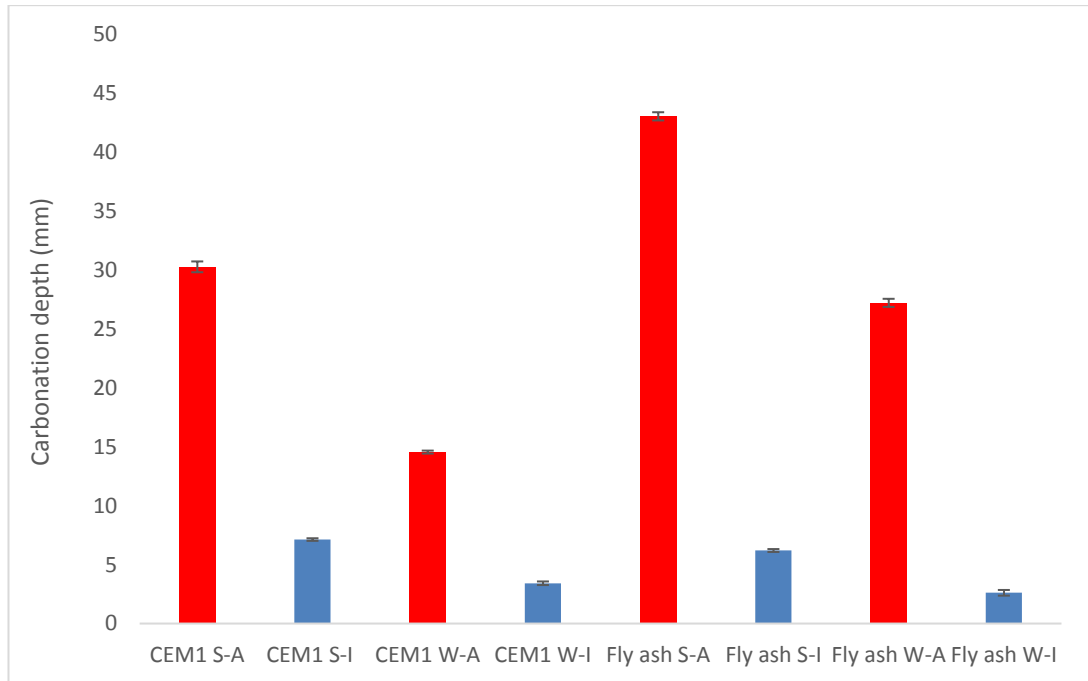


Figure A 74 Carbonation depth of ambient and ideal cured samples at 90 days

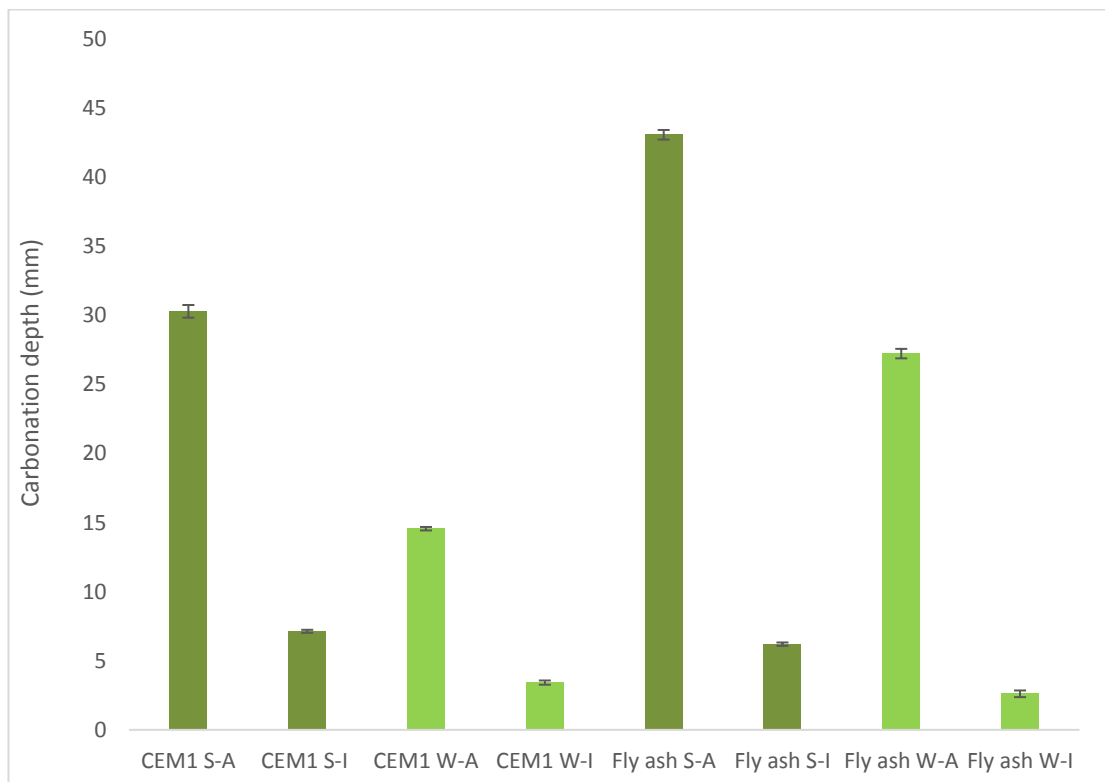


Figure A 75 Carbonation depth of stiff and wet mix samples at 90 days

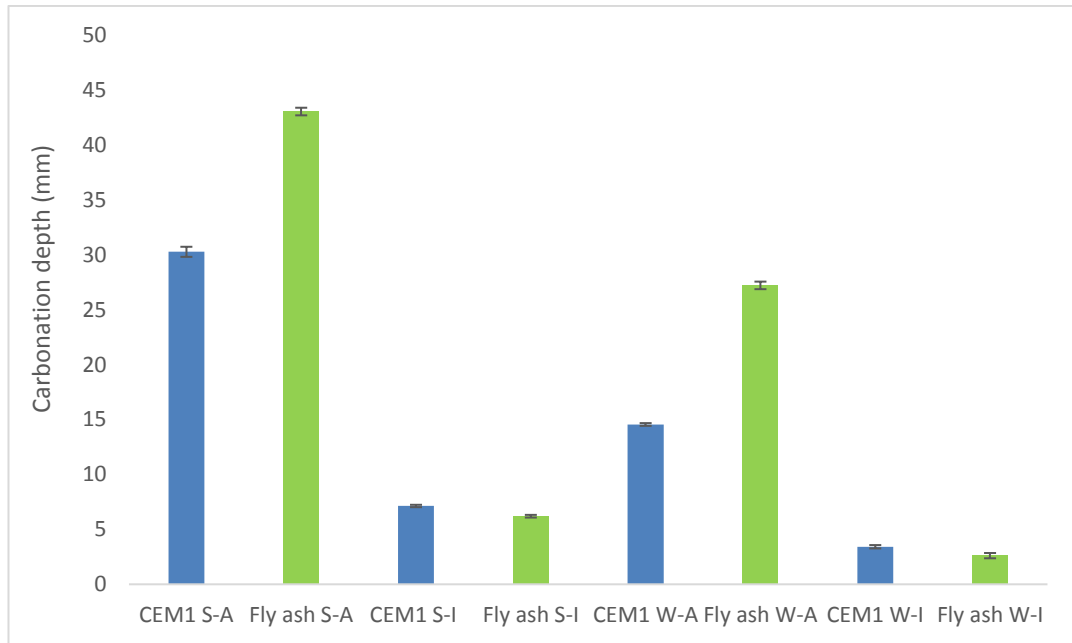


Figure A 76 Carbonation depth of CEM1 and Fly ash concretes at 90 days



Figure A 77 Carbonated samples of 20MPa CEM 1 stiff mix Ambient cured at 90days



Figure A 78 Carbonated samples of 20MPa CEM 1 stiff mix ideal cured at 90days



Figure A 79 Carbonated samples of 20MPa fly ash stiff mix ambient cured at 90 days

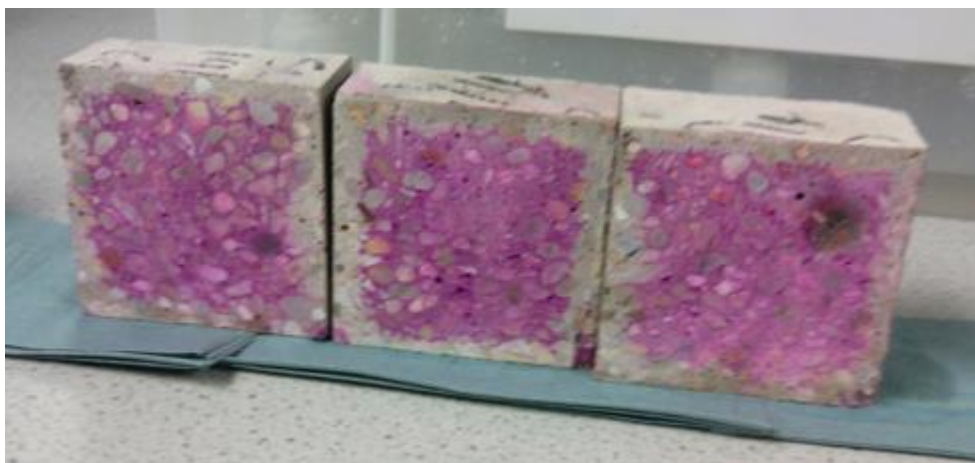


Figure A 80 Carbonated samples of 20MPa fly ash stiff mix ideal cured at 90 days

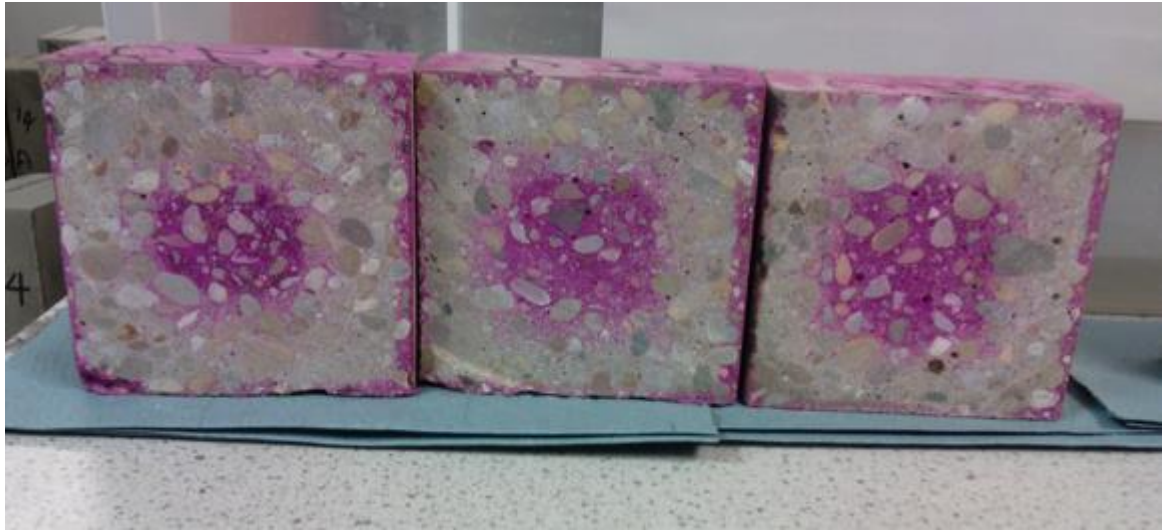


Figure A 81 Carbonated samples of 20MPa fly ash wet mix ambient cured at 90 days



Figure A 82 Carbonated samples of 20MPa fly ash wet mix ideal cured at 90 days

Permeability

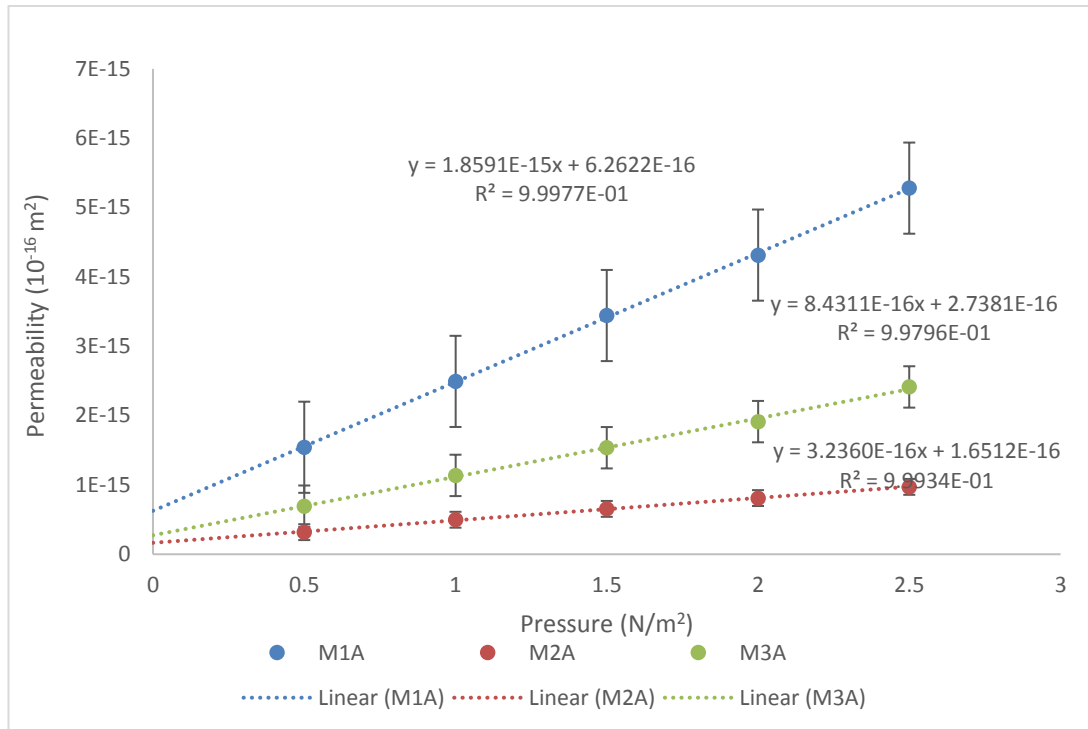


Figure A 83 Permeability of 20,50,80MPa CEM1 stiff mix ambient cured samples

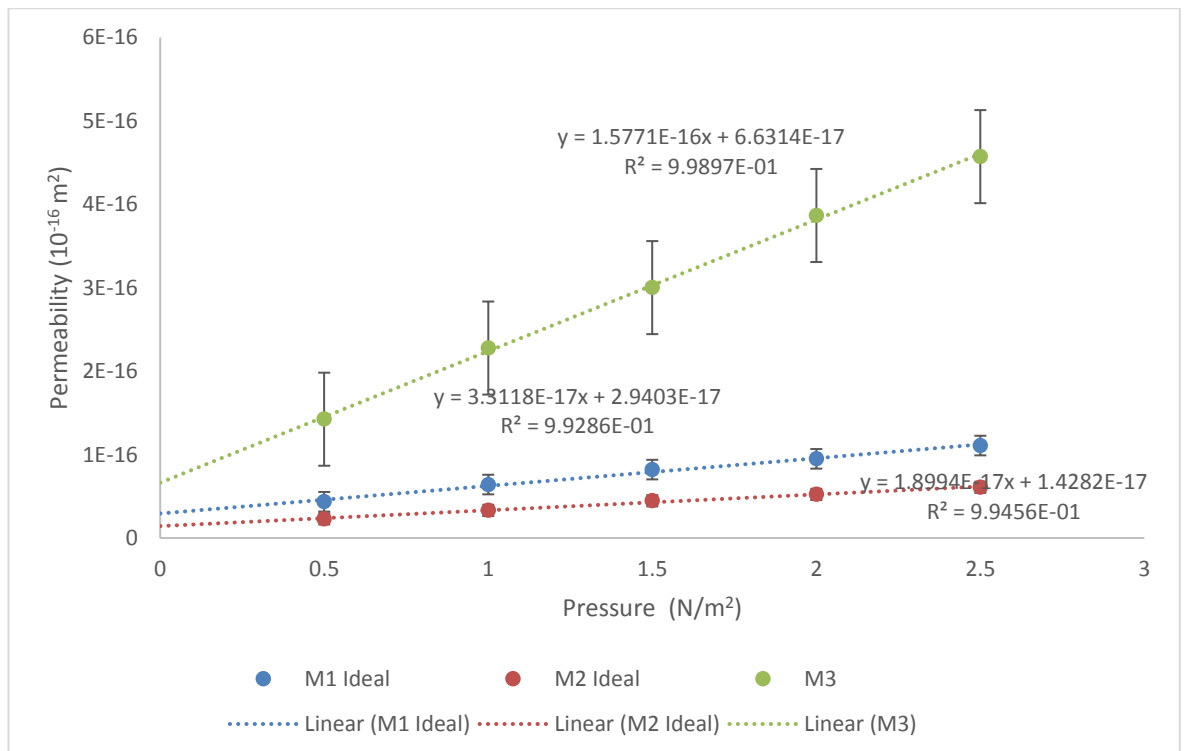


Figure A 84 Permeability of 20,50,80MPa CEM1 stiff mix ideal cured samples

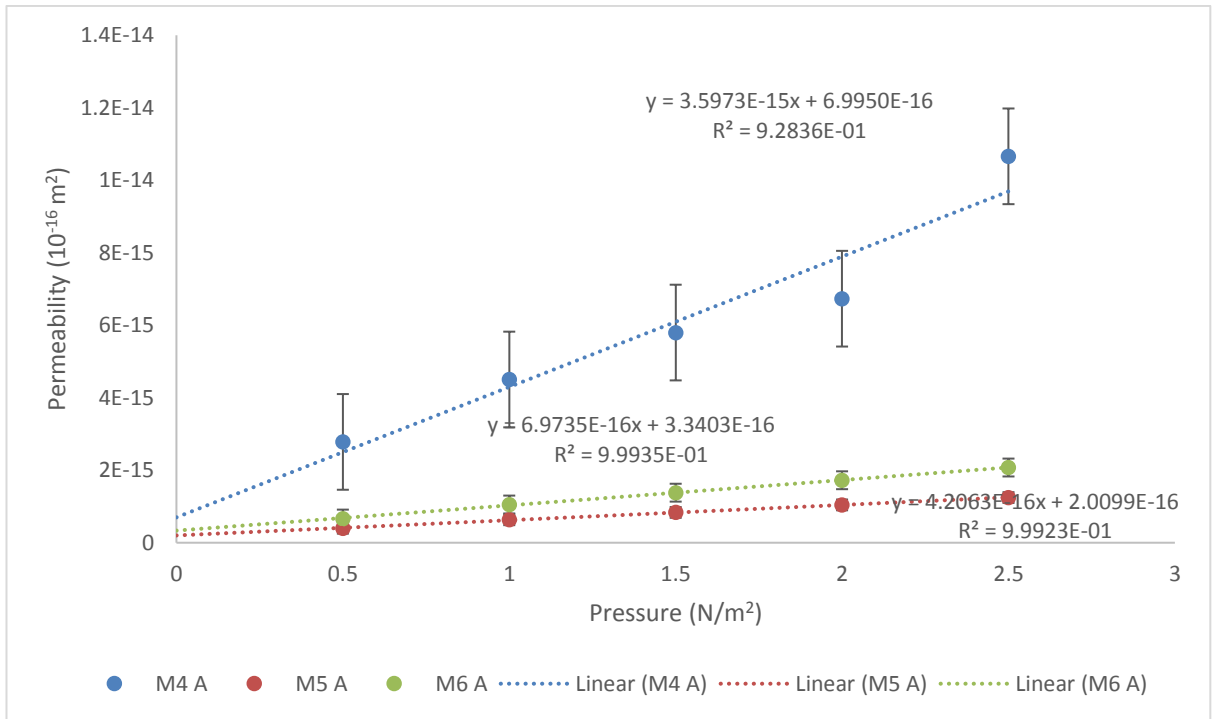


Figure A 85 Permeability of 20,50,80MPa CEM1 wet mix ambient cured samples

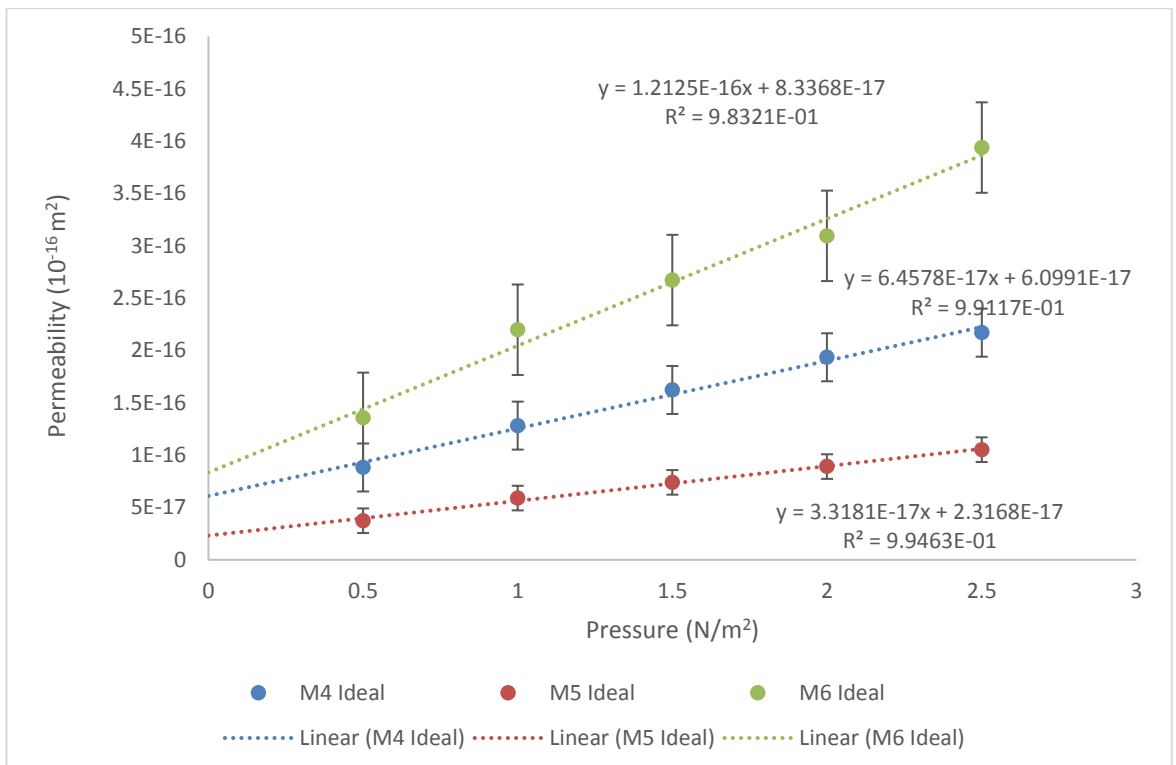


Figure A 86 Permeability of 20,50,80MPa CEM1 wet mix ideal cured samples

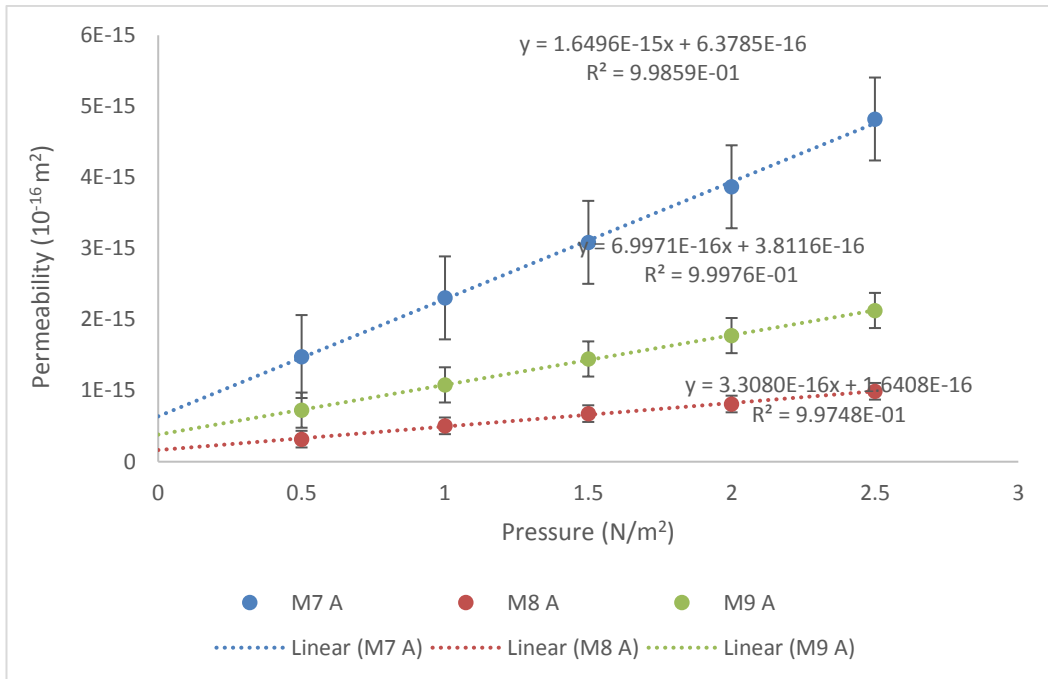


Figure A 87 Permeability of 20,50,80MPa fly ash stiff mix ambient cured samples

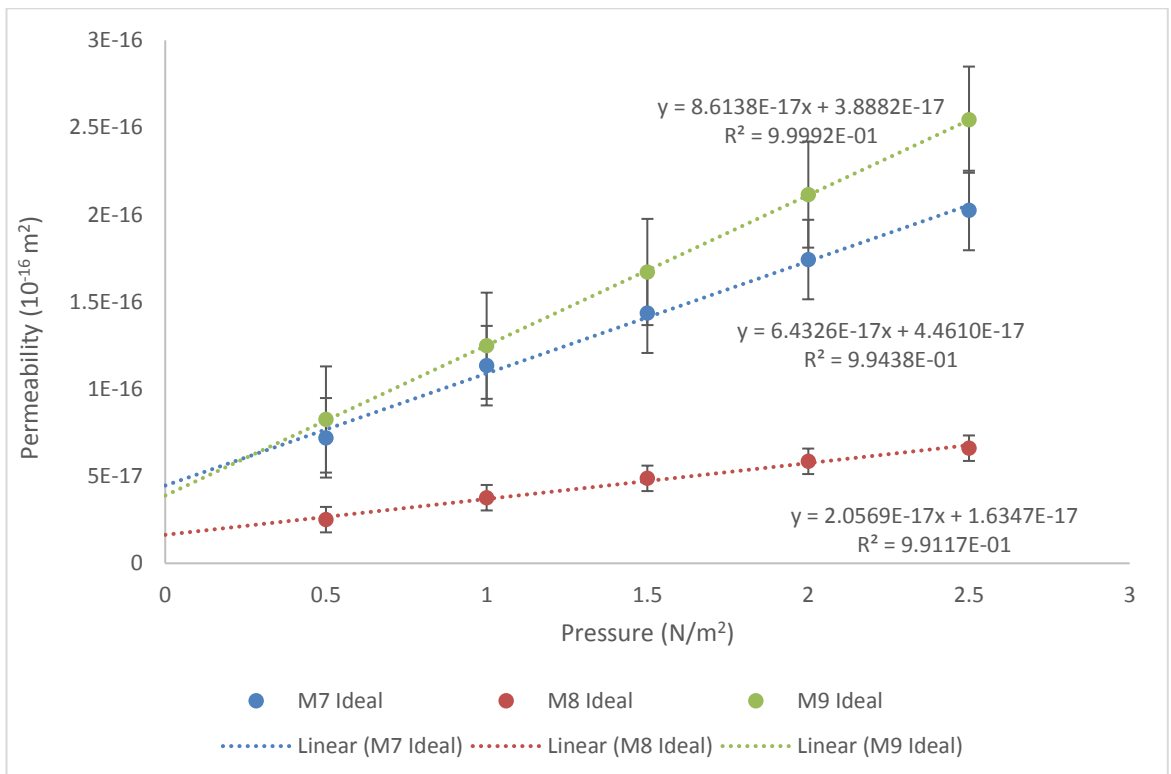


Figure A 88 Permeability of 20,50,80MPa Fly ash stiff mix ideal cured samples

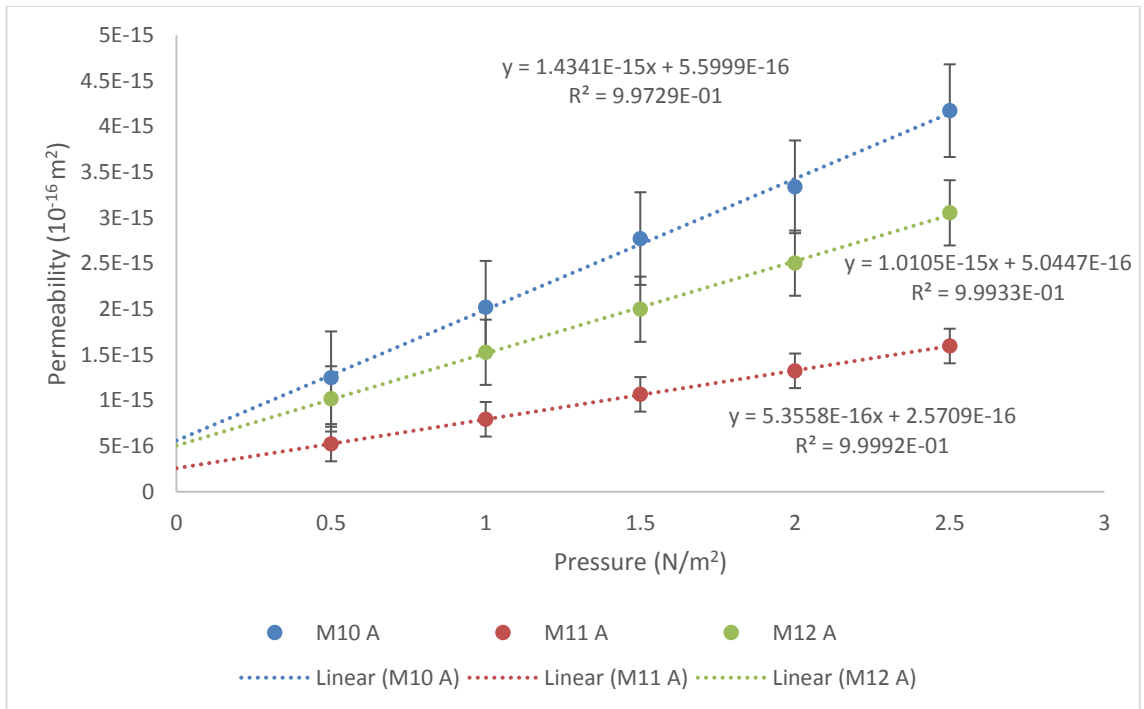


Figure A 89 Permeability of 20,50,80MPa fly ash wet mix ambient cured samples

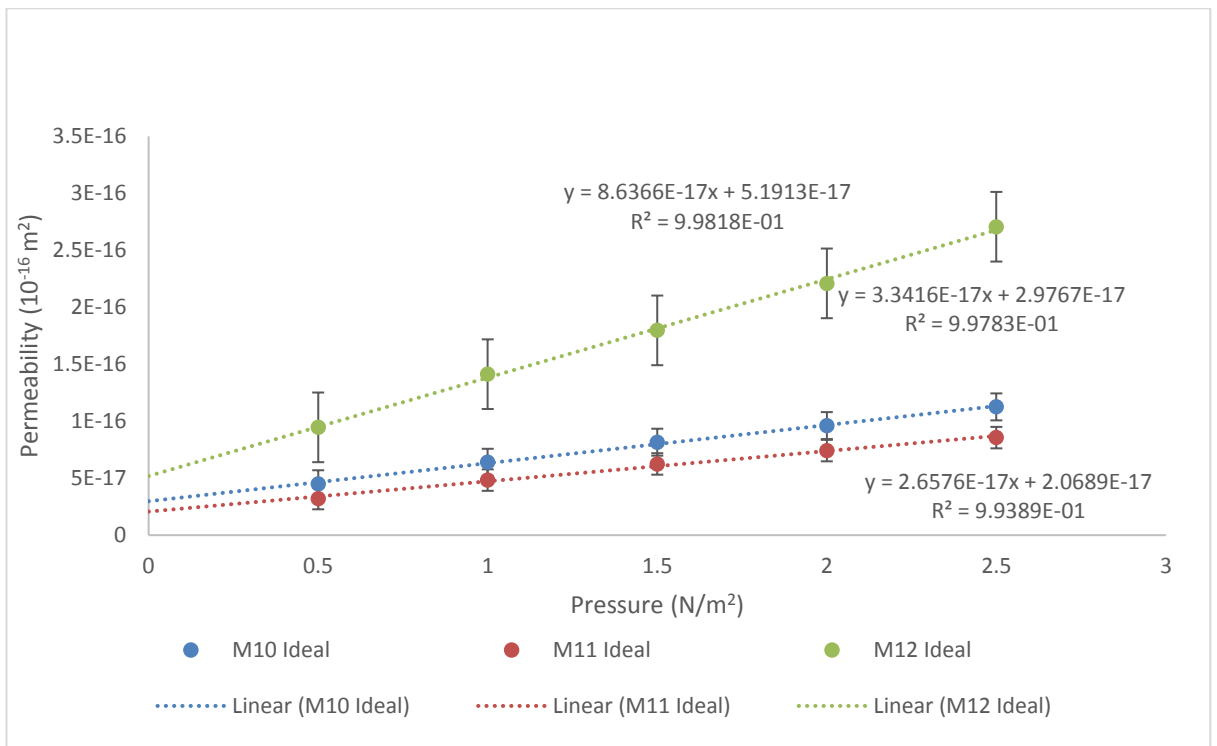


Figure A 90 Permeability of 20,50,80MPa fly ash wet mix ideal cured samples

Appendix F The SEM, TG and XRD results

The number of mixes, curing age and curing conditions with the abbreviation was presented in Table A.2. All the SEM samples were cured for 28 days but TG and XRD samples were cured for 1, 7 and 28 days for ambient and ideal conditions. Thus each mix has five results which make all the TG and XRD to have 60 results each.

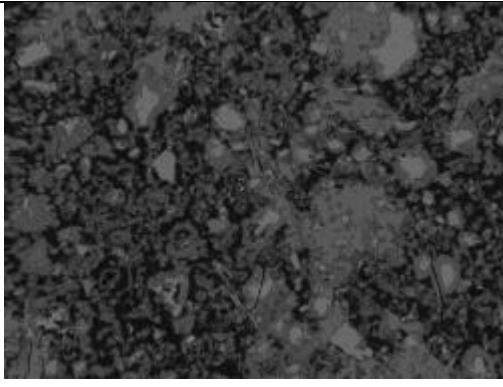
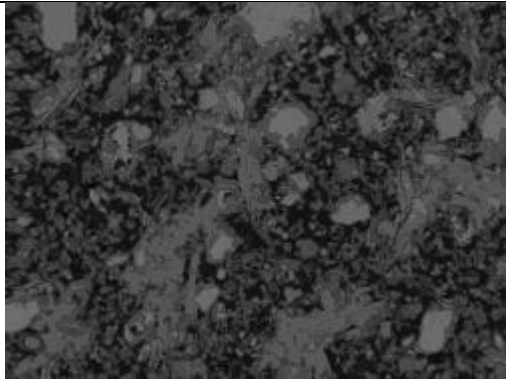
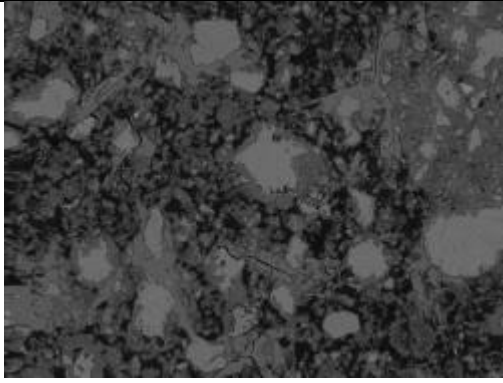
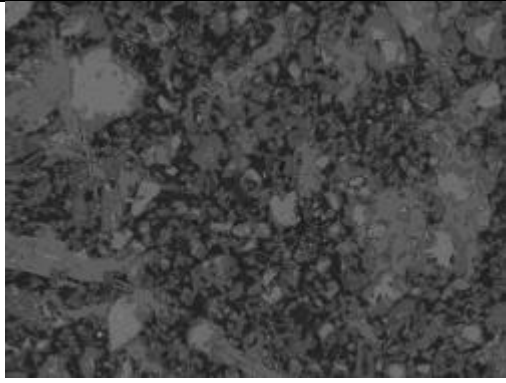
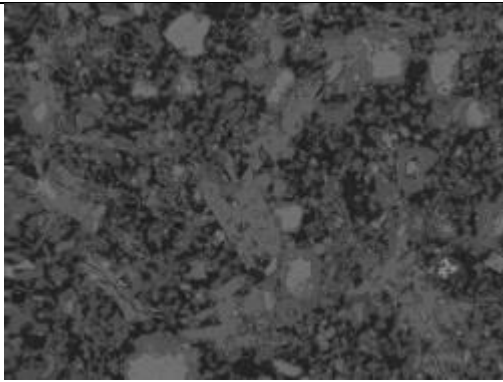
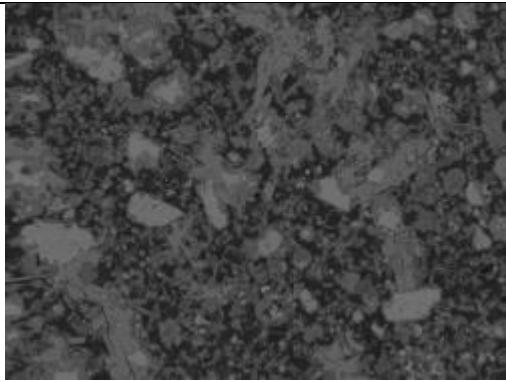
Table A 2 Mix number, curing age and curing conditions of SEM,TG and XRD

Mix Number		TG Curing age	XRD curing age	SEM curing age	Curing conditions
M1	20 MPa CEM1 stiff mix	1,7 and 28 days	1, 7 and 28 days	28 days	Ambient and Ideal
M2	50 MPa CEM1 stiff mix	1,7 and 28 days	1, 7 and 28 days	28 days	Ambient and Ideal
M3	80 MPa CEM1 stiff mix	1,7 and 28 days	1, 7 and 28 days	28 days	Ambient and Ideal
M4	20 MPa CEM1 wet mix	1,7 and 28 days	1, 7 and 28 days	28 days	Ambient and Ideal
M5	50 MPa CEM1 wet mix	1,7 and 28 days	1, 7 and 28 days	28 days	Ambient and Ideal
M6	80 MPa CEM1 wet mix	1,7 and 28 days	1, 7 and 28 days	28 days	Ambient and Ideal
M7	20 MPa fly ash stiff mix	1,7 and 28 days	1, 7 and 28 days	28 days	Ambient and Ideal
M8	50 MPa fly ash stiff mix	1,7 and 28 days	1, 7 and 28 days	28 days	Ambient and Ideal
M9	80 MPa fly ash stiff mix	1,7 and 28 days	1, 7 and 28 days	28 days	Ambient and Ideal
M10	20 MPa fly ash wet mix	1,7 and 28 days	1, 7 and 28 days	28 days	Ambient and Ideal
M11	50 MPa fly ash wet mix	1,7 and 28 days	1, 7 and 28 days	28 days	Ambient and Ideal
M12	80 MPa fly ash wet mix	1,7 and 28 days	1, 7 and 28 days	28 days	Ambient and Ideal

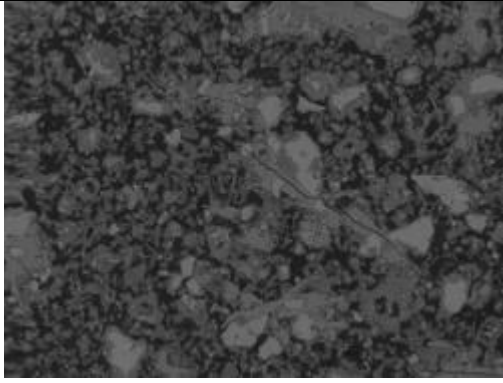
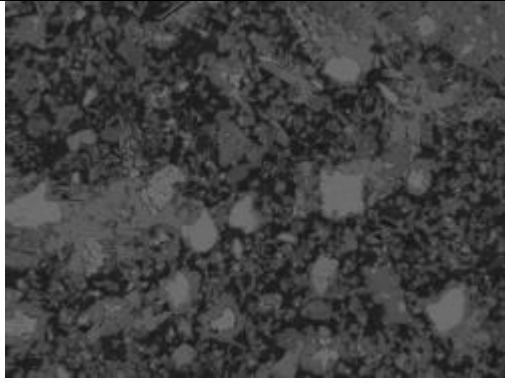
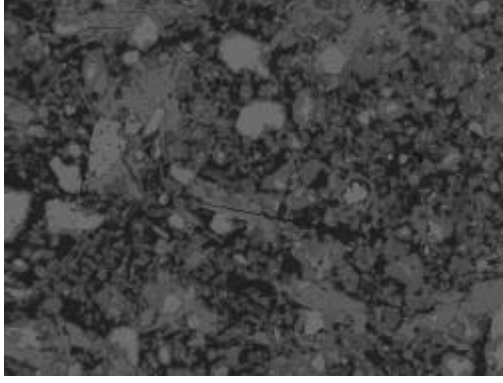
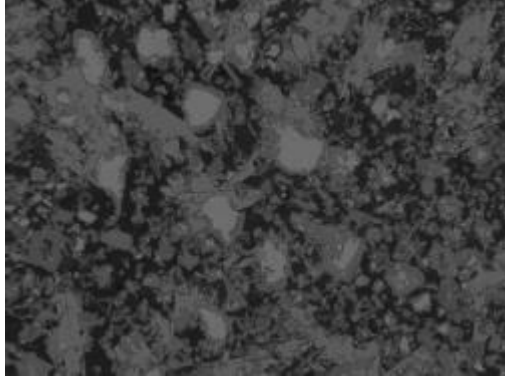
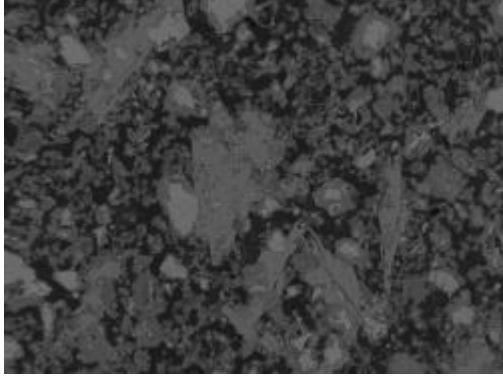
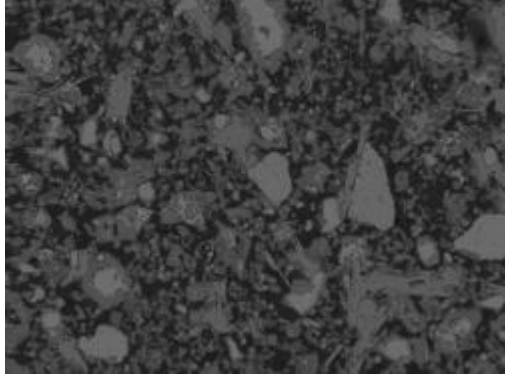
SEM appendix

Each image were obtained at 400X magnification having the scale of 100 μ m and the field of view in each image is 326 x 244 μ m. Letter A stands for ambient and W stands for ideal curing.

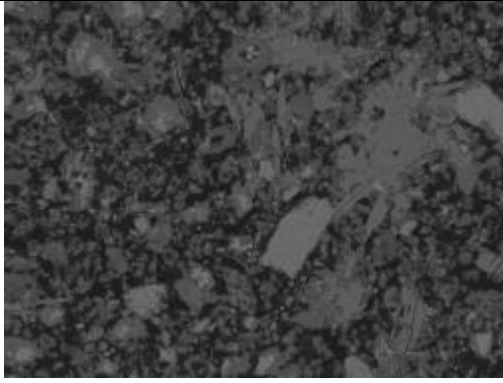
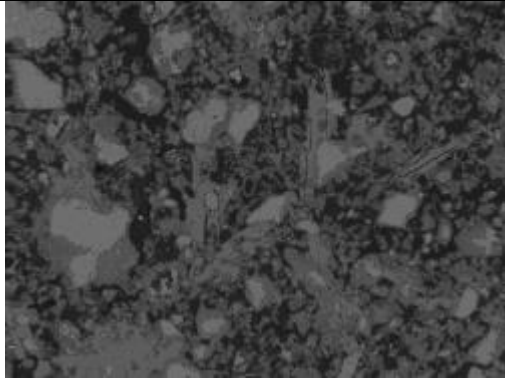
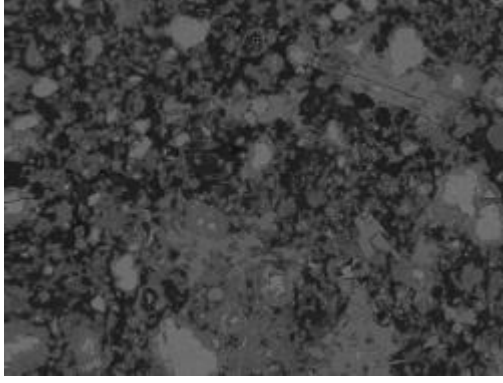
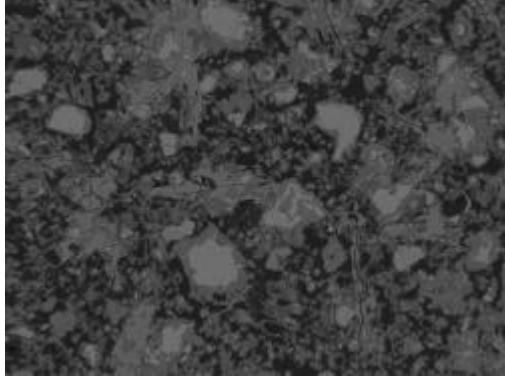
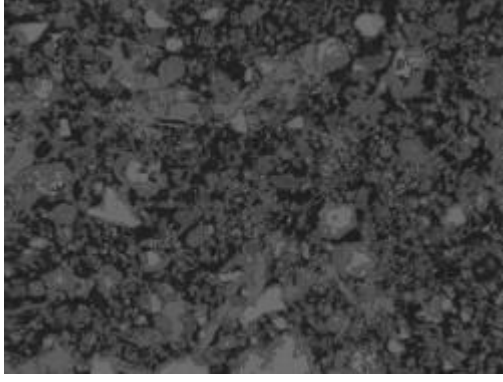
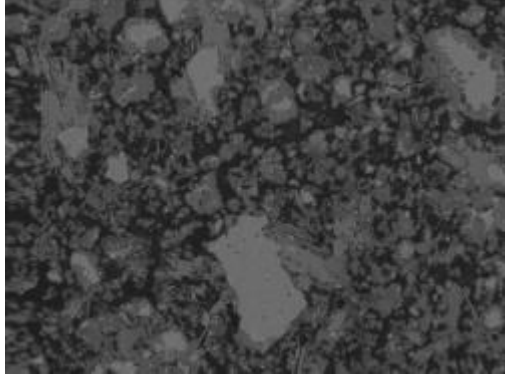
M1A

	
Image 001	Image 003
	
Image 005	Image 007
	
Image 013	Image 015

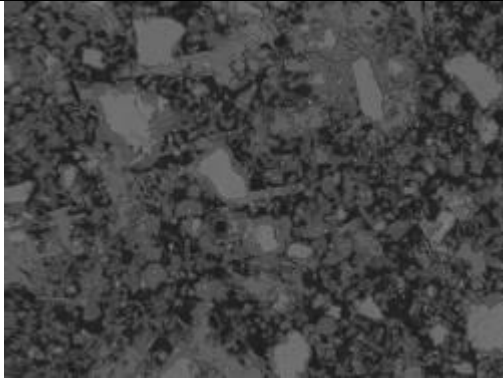
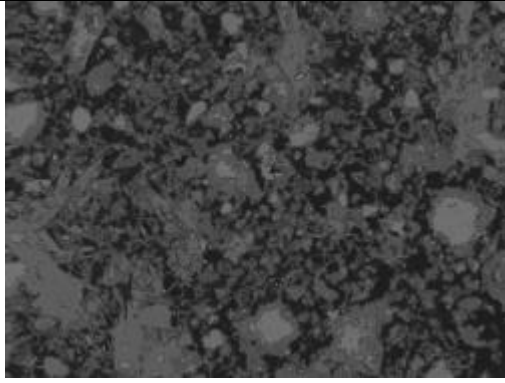
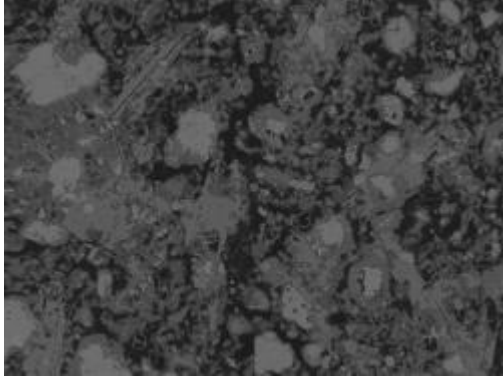
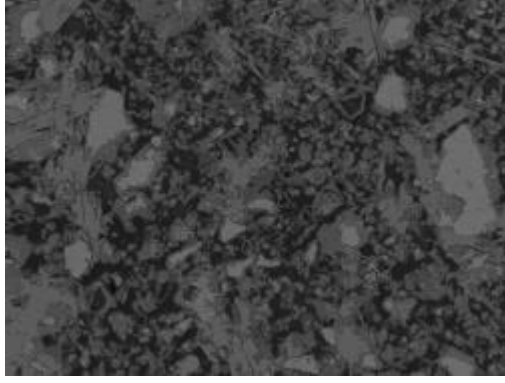
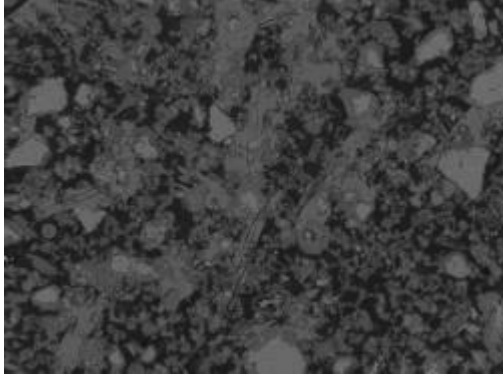
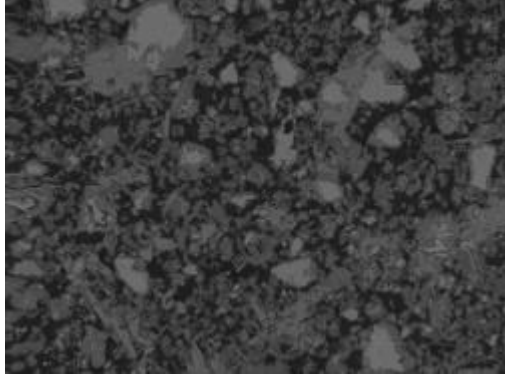
20MPa CEM1 stiff mix ambient cured

	
Image 017	Image 019
	
Image 021	Image 025
	
Image 027	Image 029

20MPa CEM1 stiff mix ambient cured

	
Image 031	Image 033
	
Image 035	Image 037
	
Image 039	Image 043

20MPa CEM1 stiff mix ambient cured

	
Image 045	Image 047
	
Image 050	Image 051
	
Image 052	Image 054

20MPa CEM1 stiff mix ambient cured

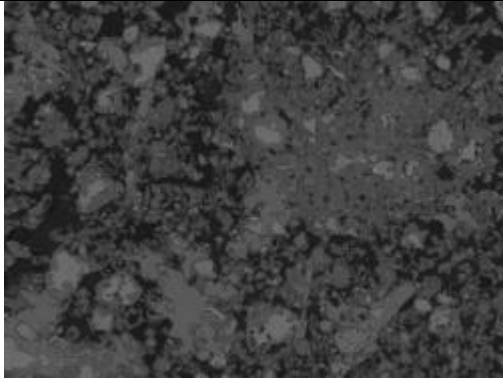
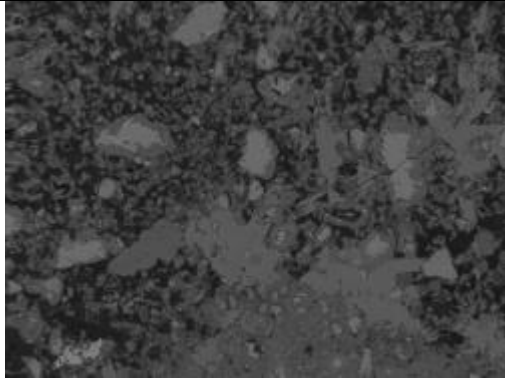
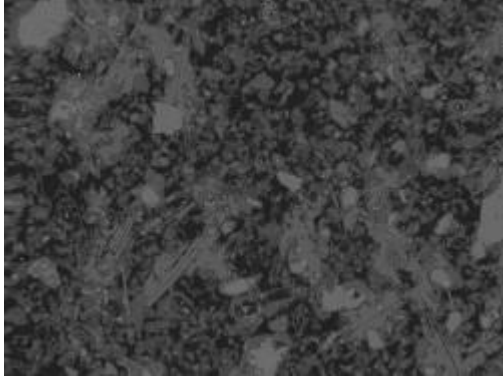
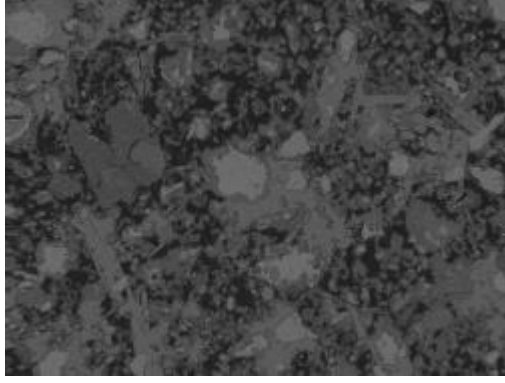
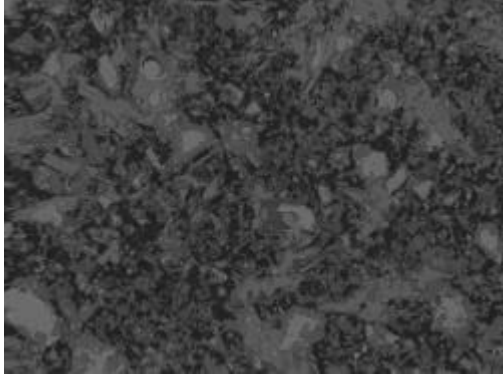
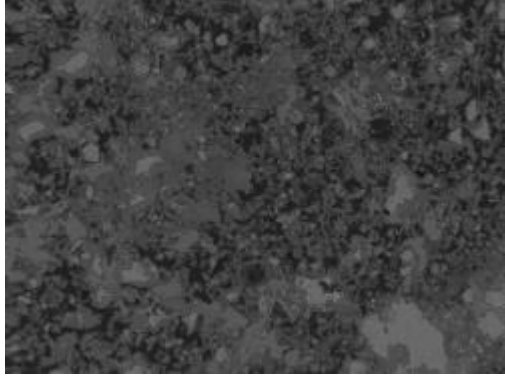
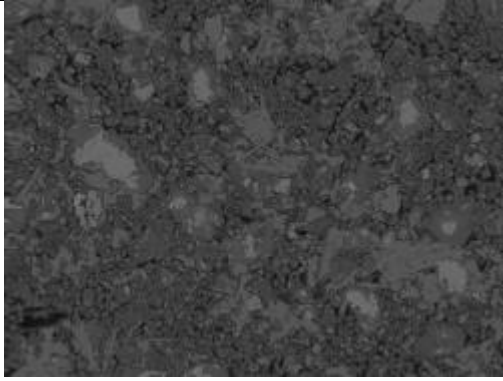
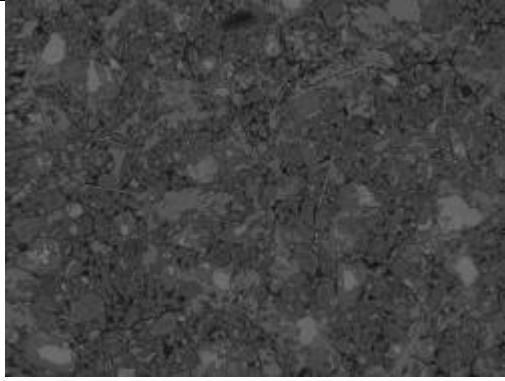
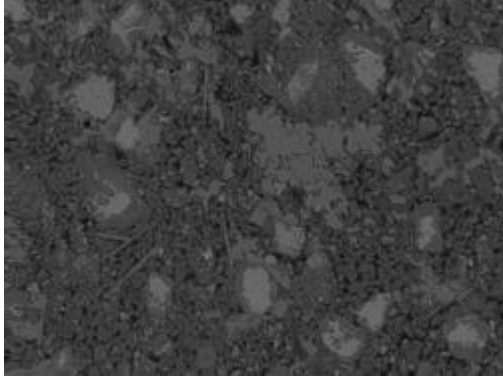
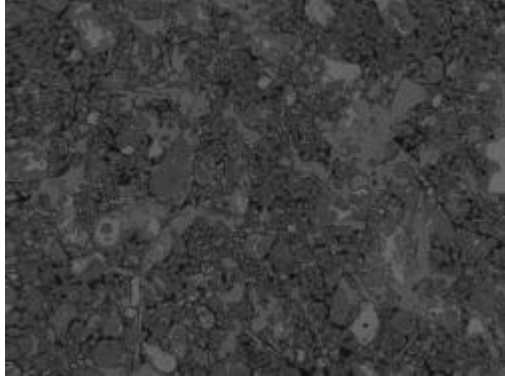
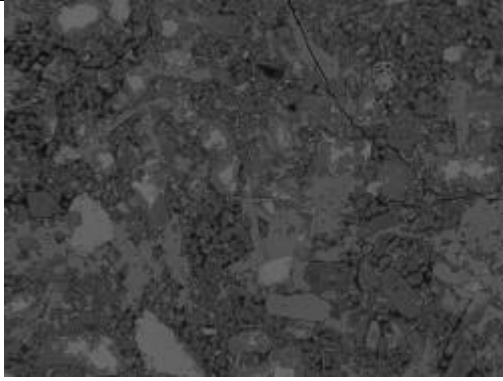
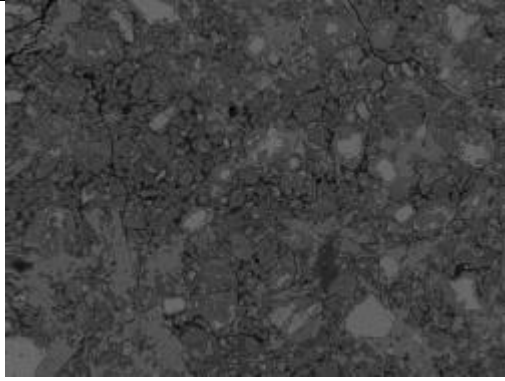
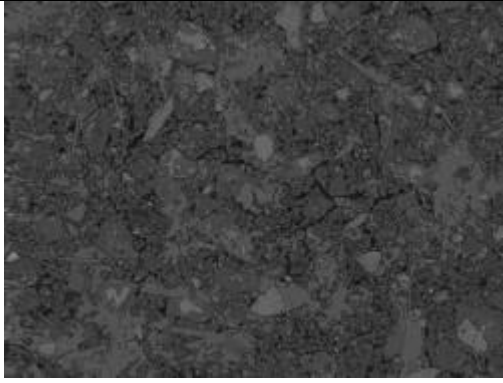
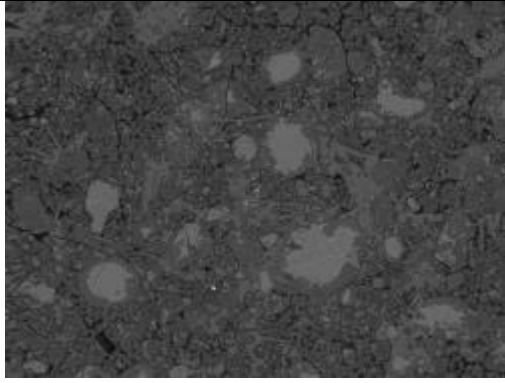
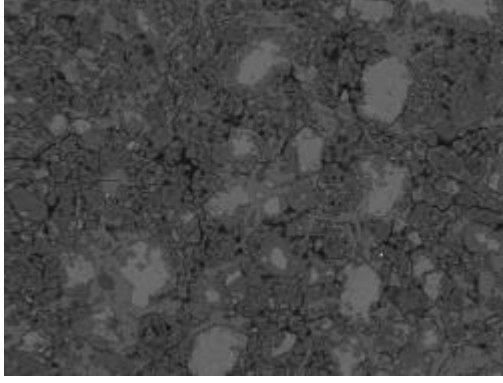
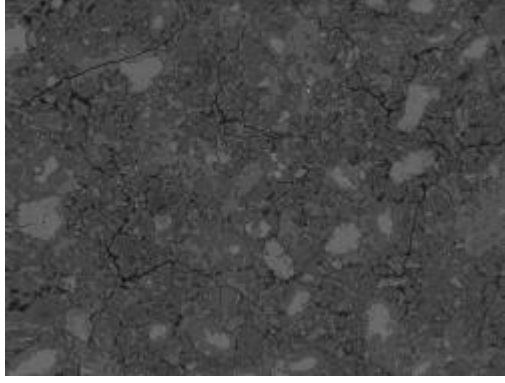
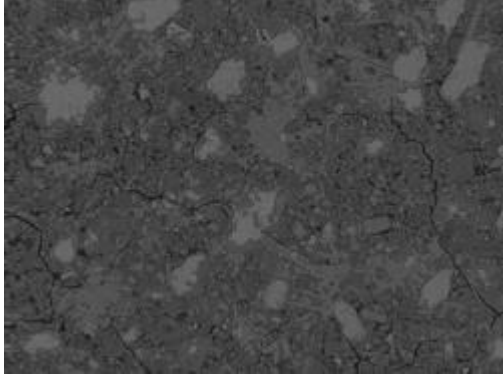
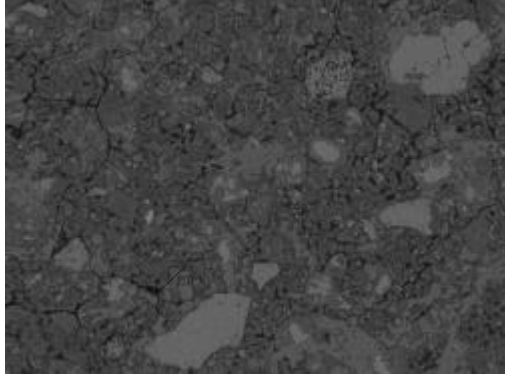
	
Image 056	Image 057
	
Image 059	Image 060
	
Image 061	Image 065

Figure A 91 Images of 20MPa CEM1 stiff mix ambient cured

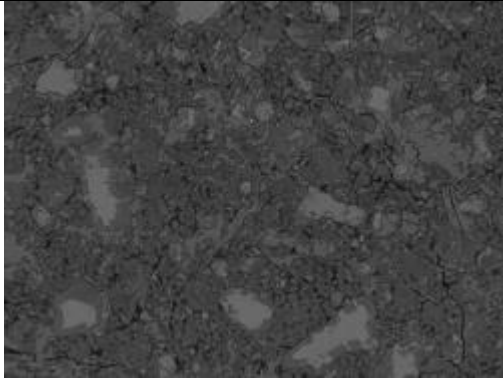
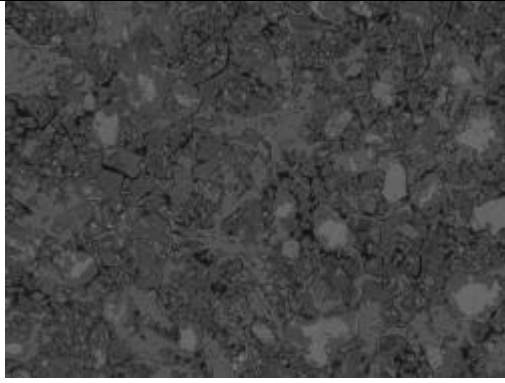
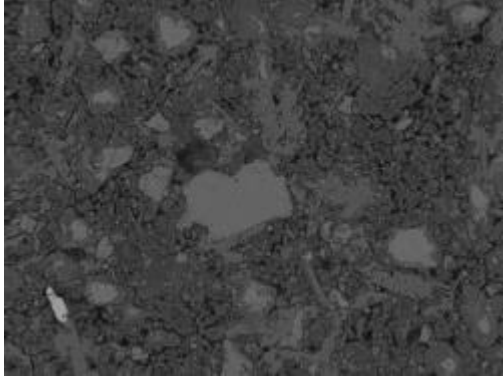
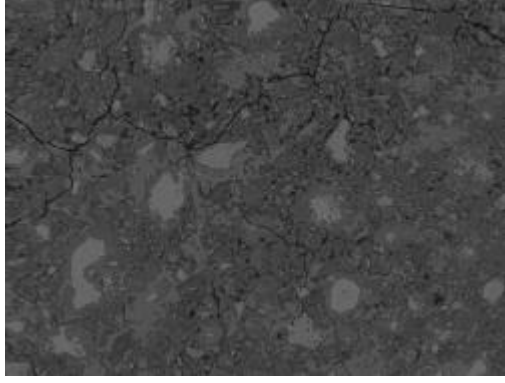
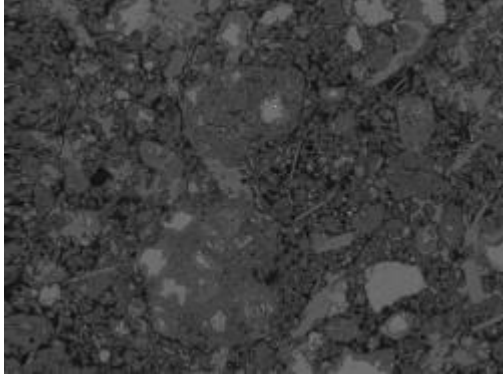
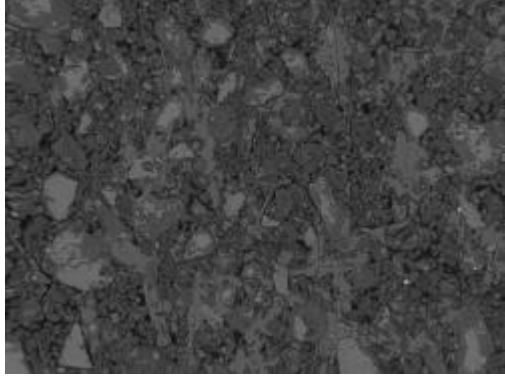
M1W

	
Image 001	Image 002
	
Image 005	Image 006
	
Image 007	Image 008

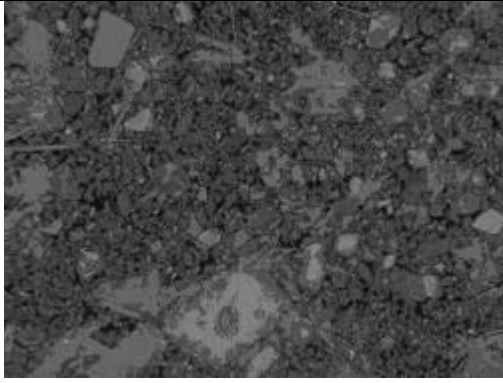
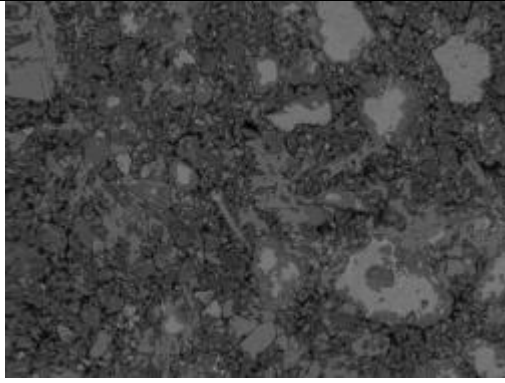
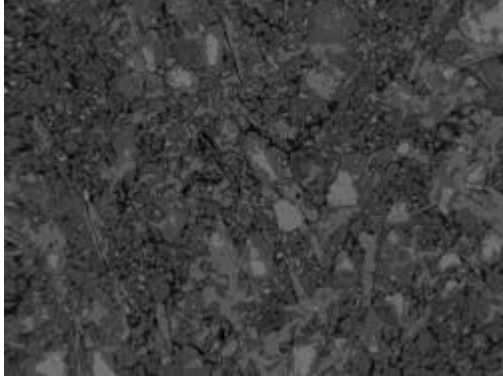
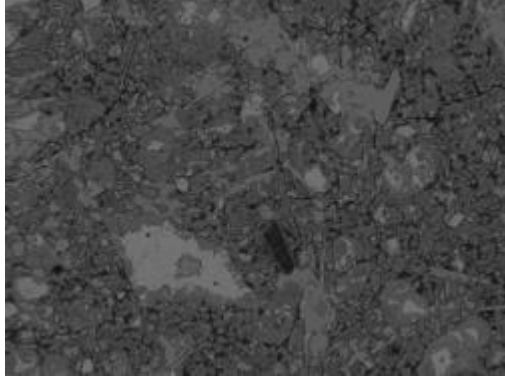
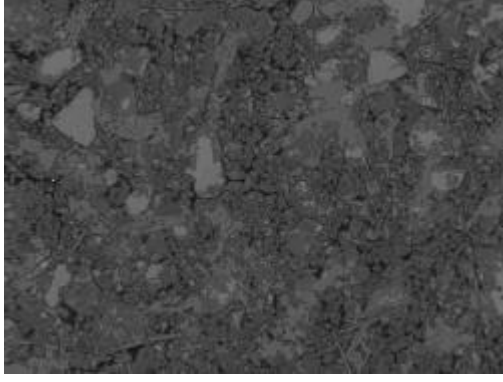
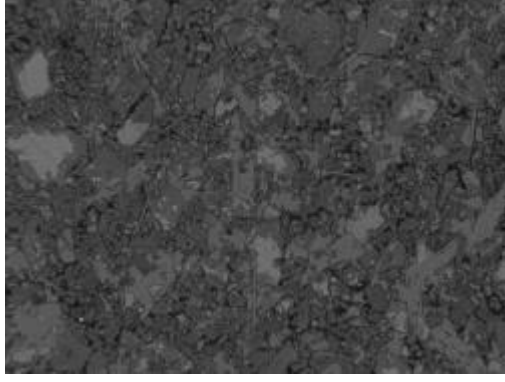
20MPa CEM1 stiff mix ideal cured

	
Image 009	Image 010
	
Image 011	Image 012
	
Image 013	Image 014

20MPa CEM1 stiff mix ideal cured

	
Image 015	Image 016
	
Image 017	Image 018
	
Image 020	Image 021

20MPa CEM1 stiff mix ideal cured

	
Image 022	Image 023
	
Image 024	Image 026
	
Image 027	Image 028

20MPa CEM1 stiff mix ideal cured

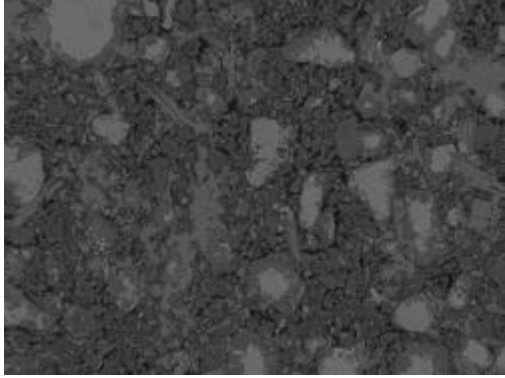
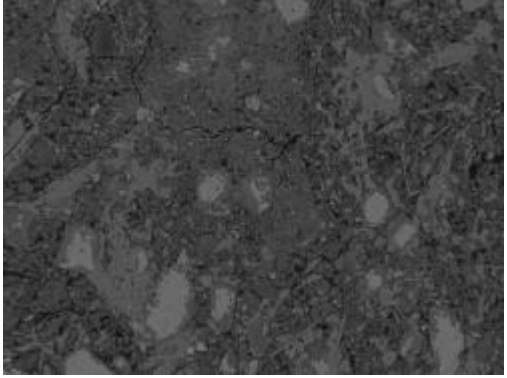
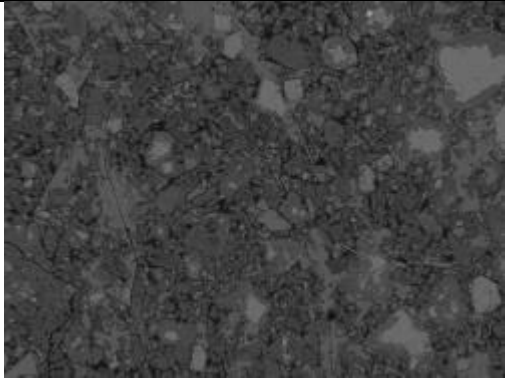
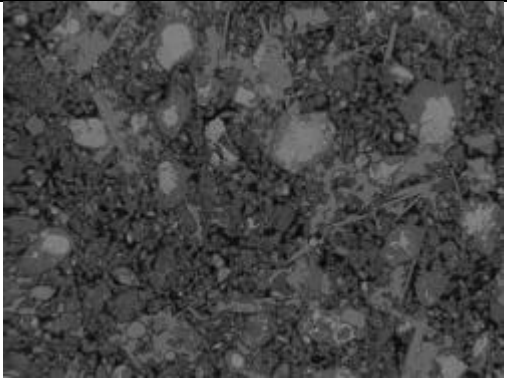
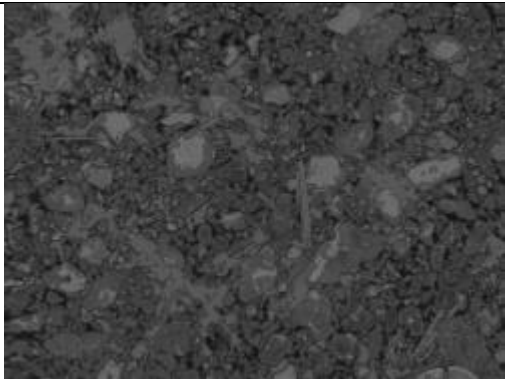
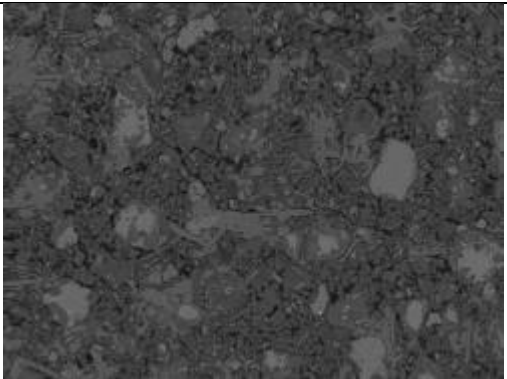
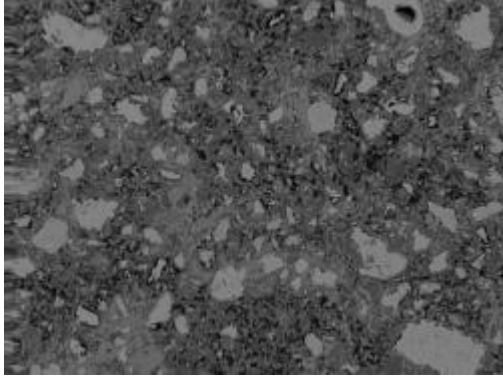
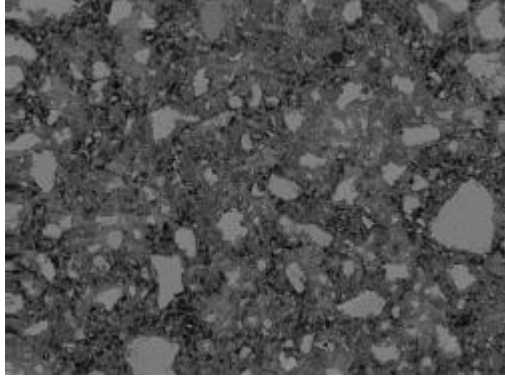
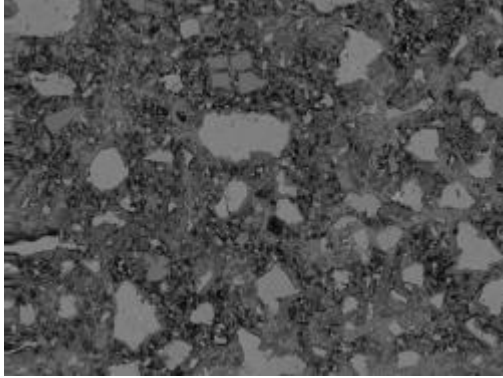
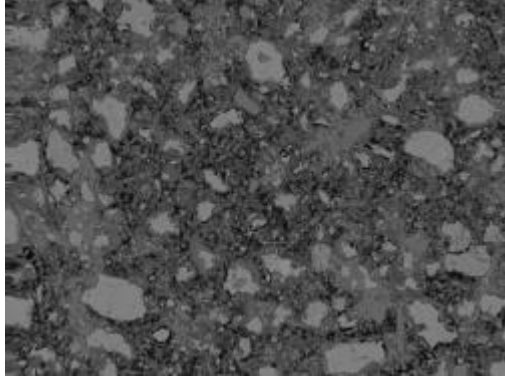
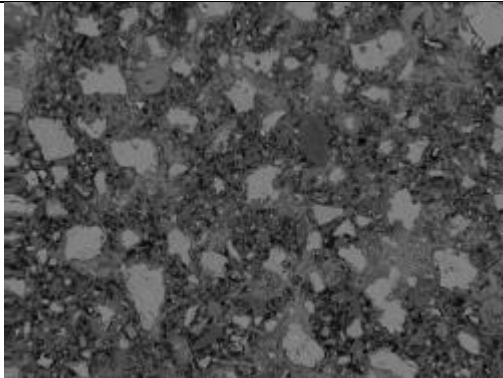
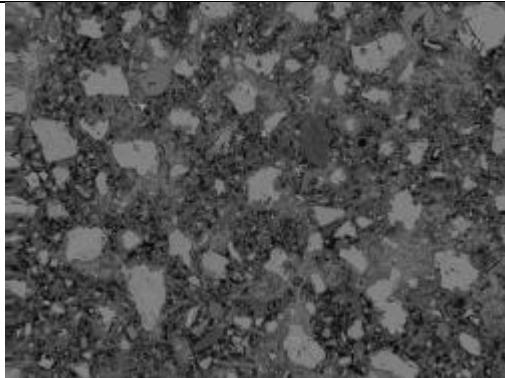
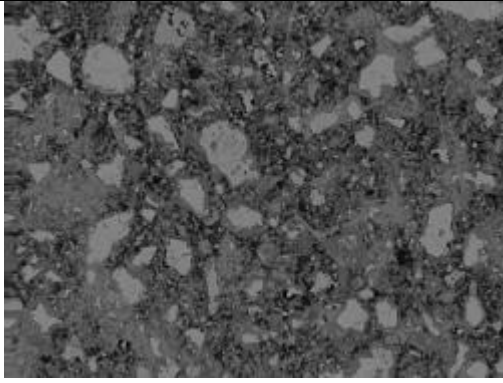
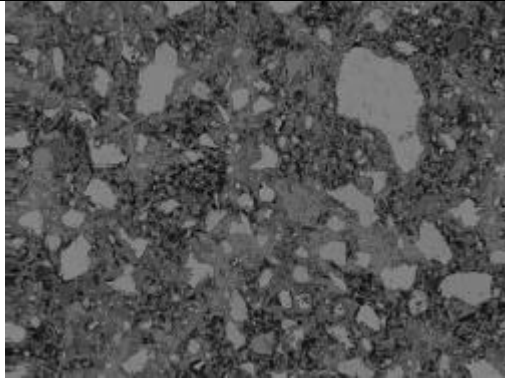
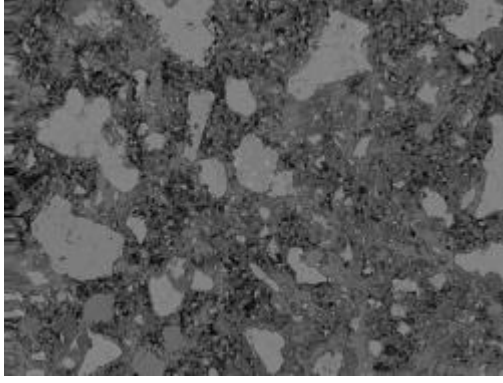
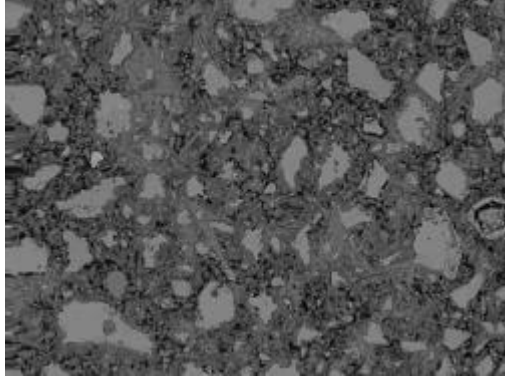
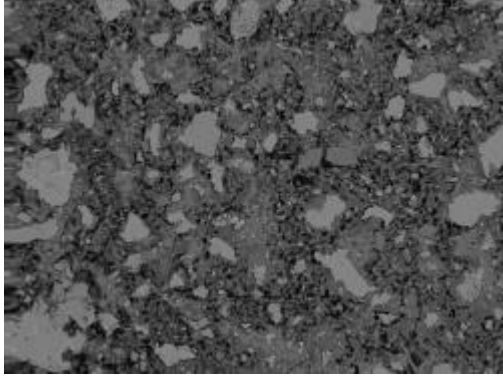
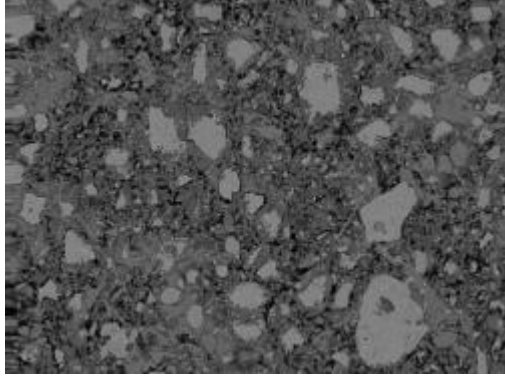
	
Image 029	Image 030
	
Image 031	Image 033
	
Image 035	Image 038

Figure A 92 Images of 20MPa CEM1 stiff mix ideal cured

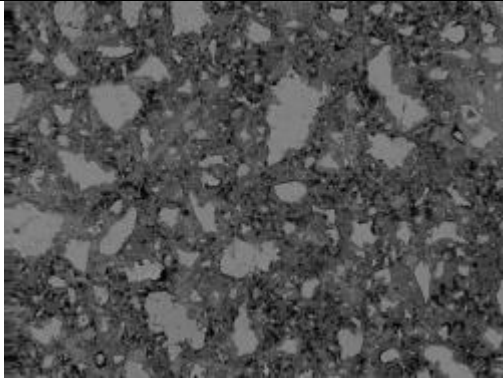
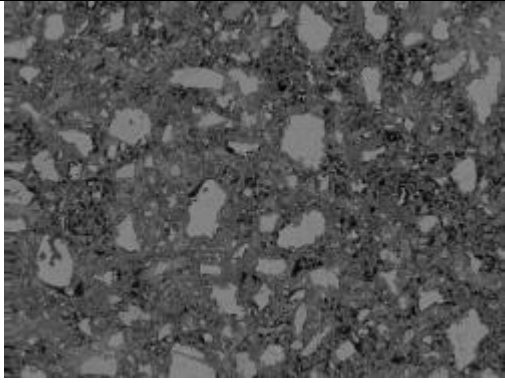
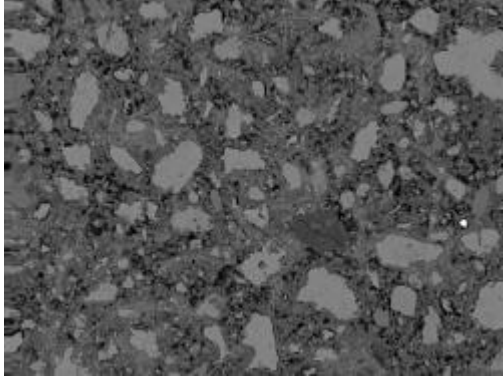
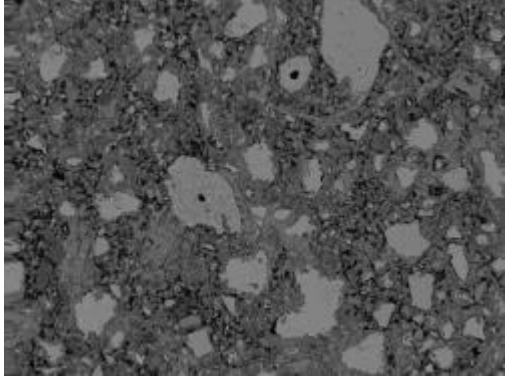
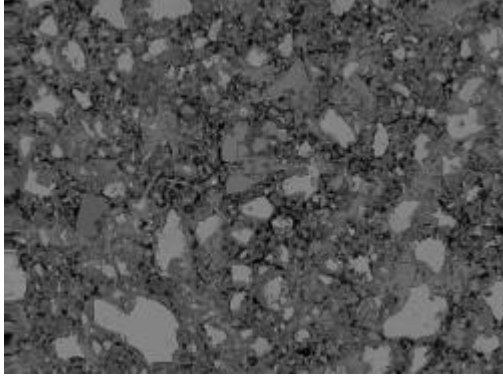
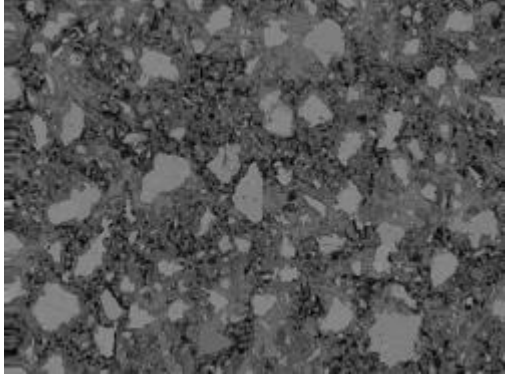
M2A

	
Image 005	Image 006
	
Image 007	Image 008
	
Image 009	Image 010

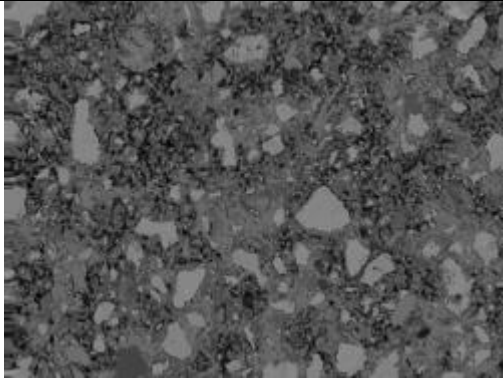
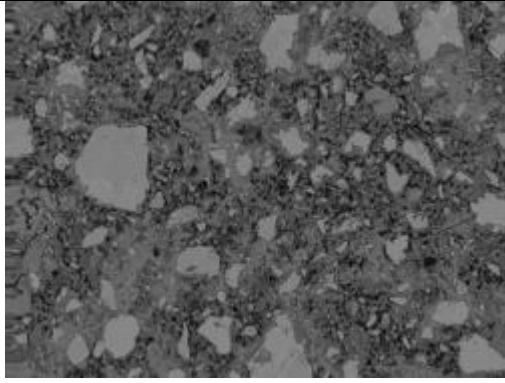
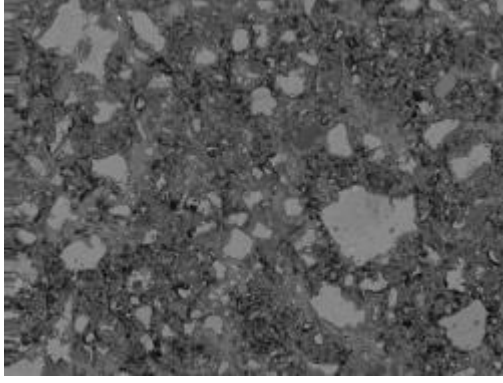
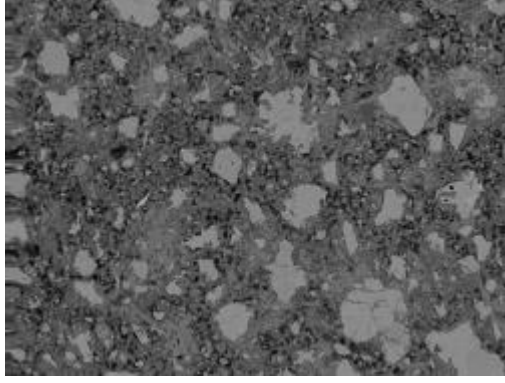
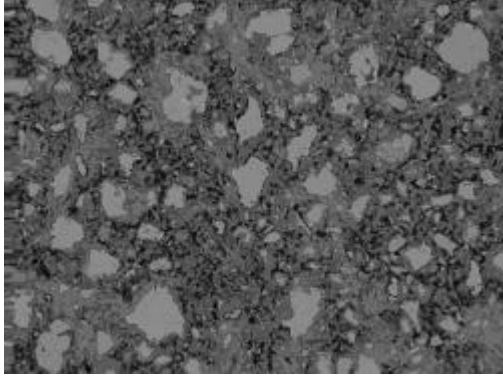
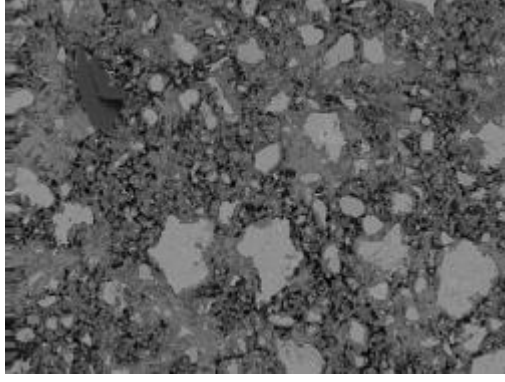
50MPa CEM1 stiff mix ambient cured

	
Image 012	Image 014
	
Image 015	Image 016
	
Image 017	Image 018

50MPa CEM1 stiff mix ambient cured

	
Image 019	Image 020
	
Image 021	Image 022
	
Image 023	Image 024

50MPa CEM1 stiff mix ambient cured

	
Image 025	Image 026
	
Image 027	Image 029
	
Image 030	Image 031

50MPa CEM1 stiff mix ambient cured

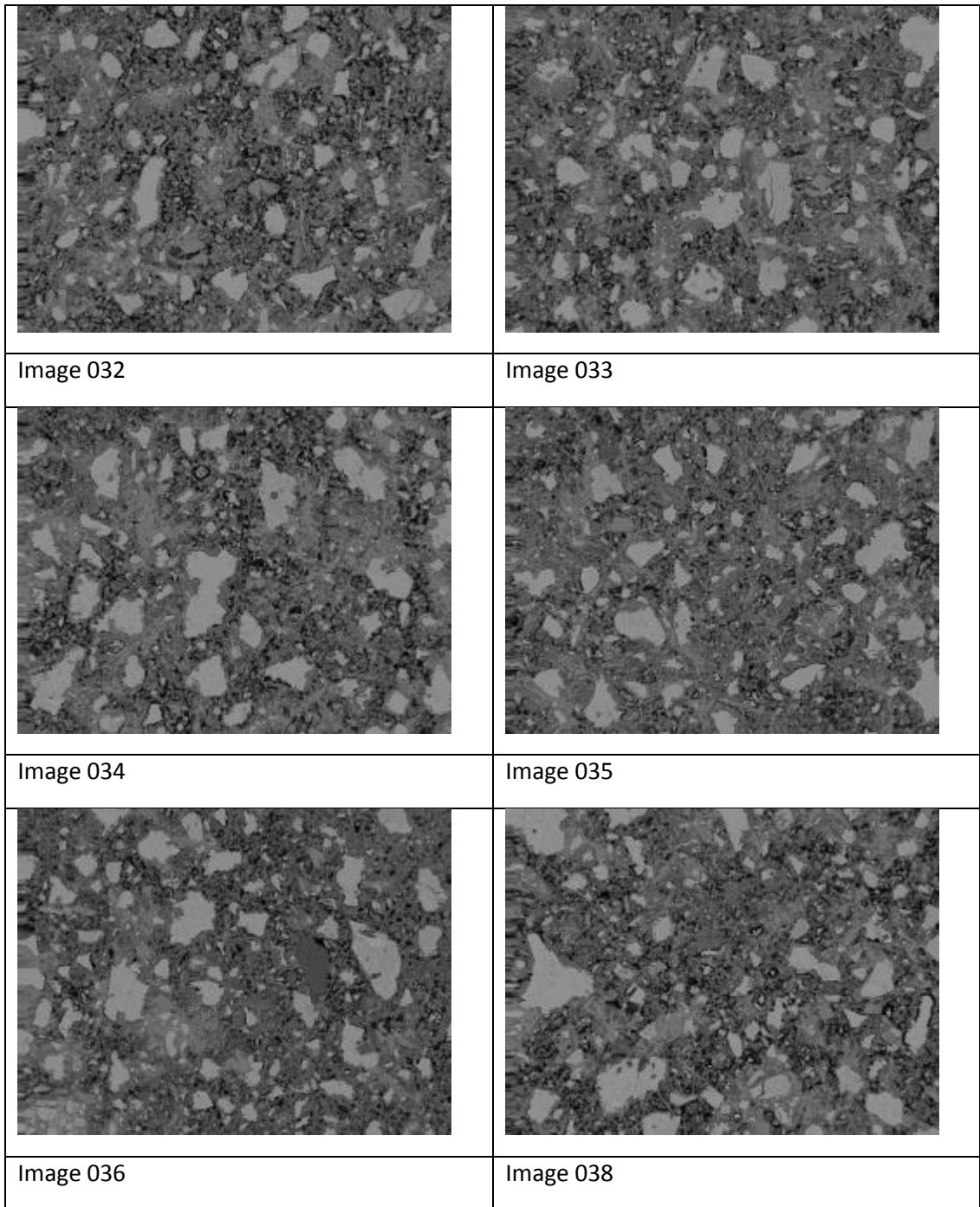
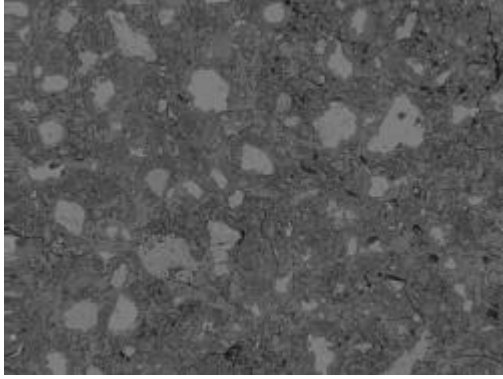
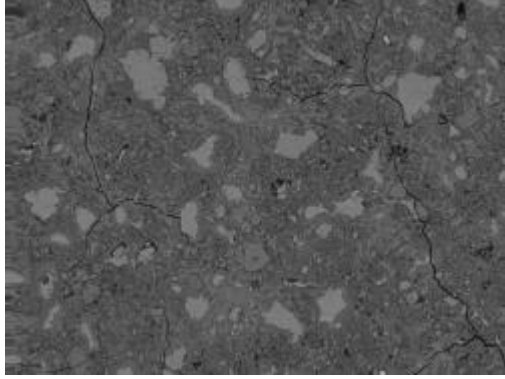
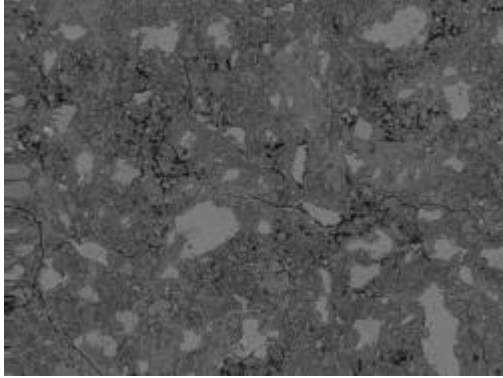
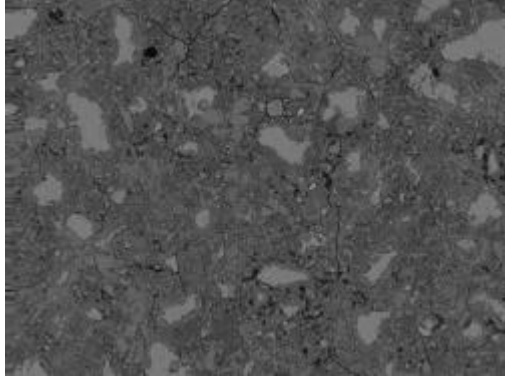
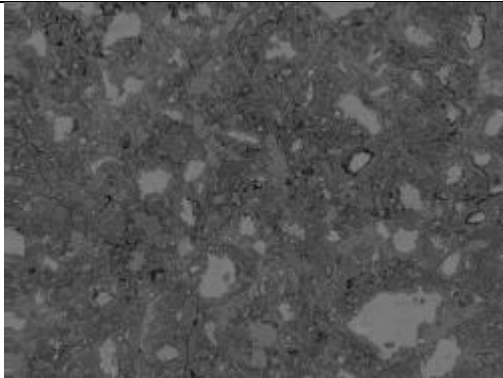
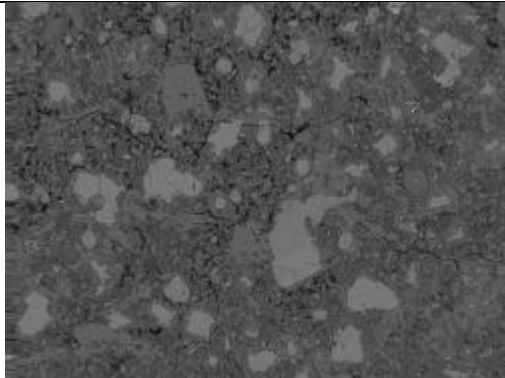
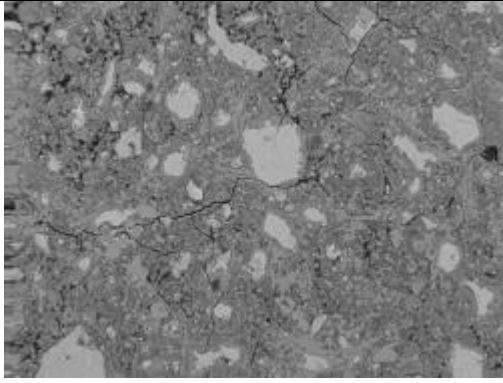
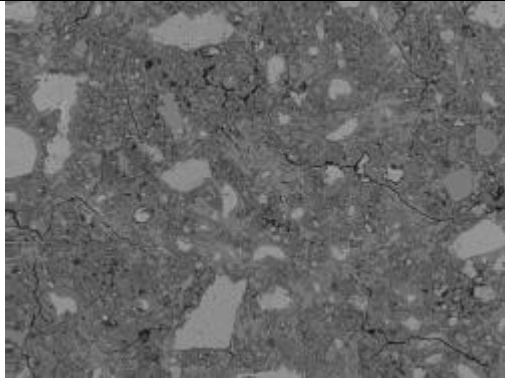
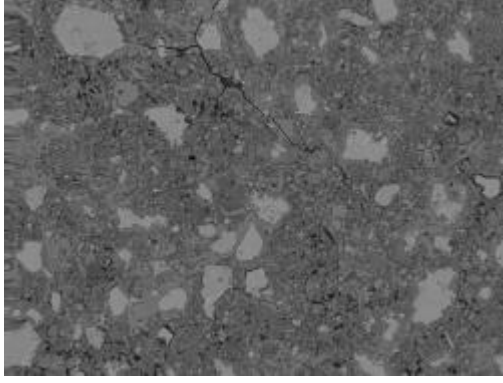
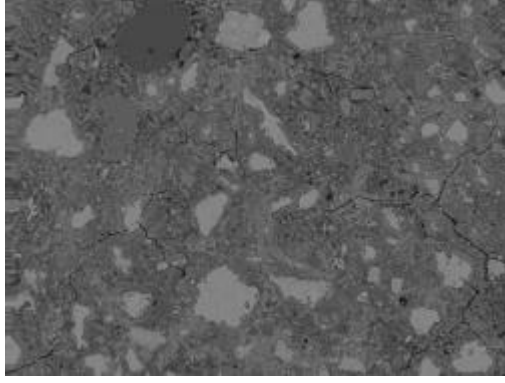
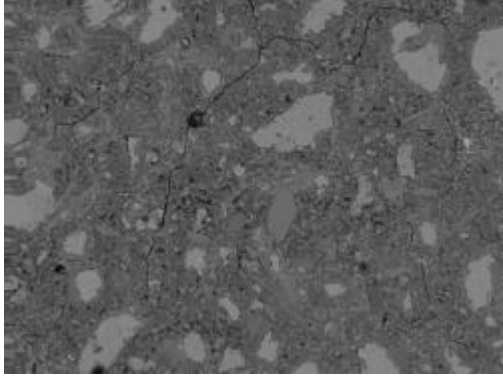
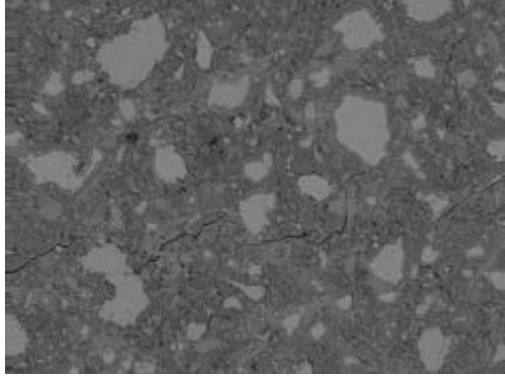


Figure A 93 Images of 50MPa CEM1 stiff mix ambient cured

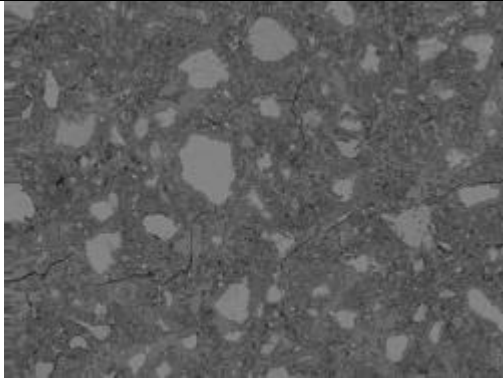
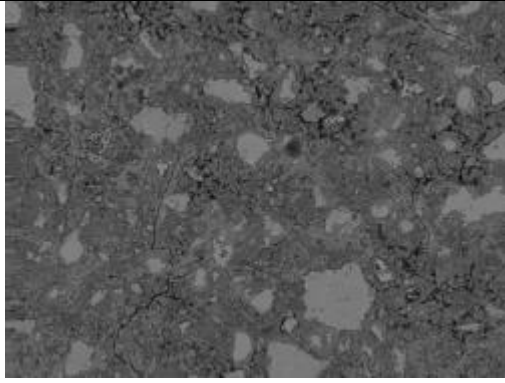
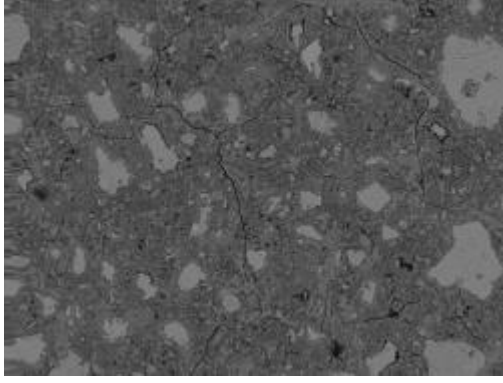
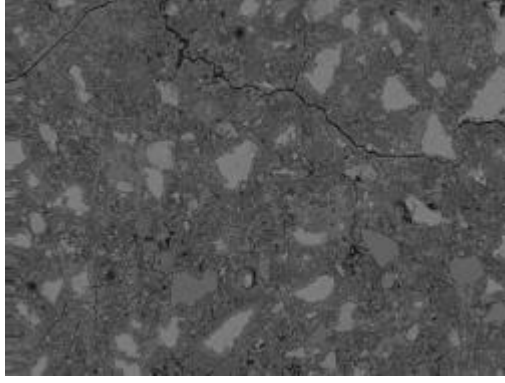
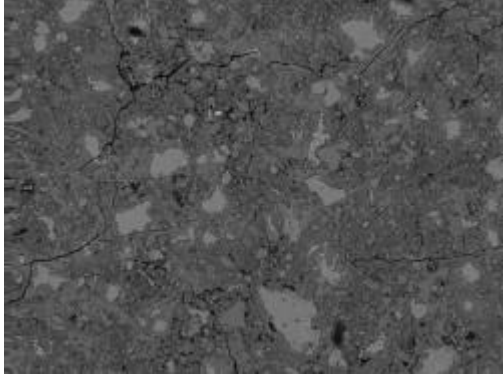
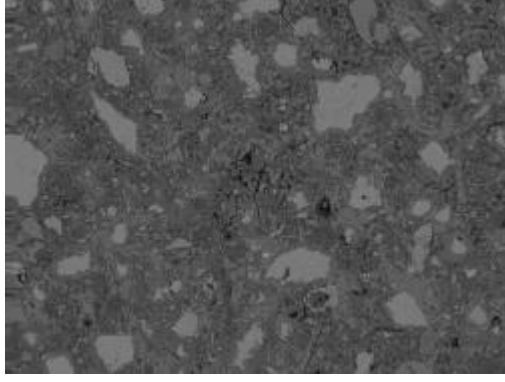
M2W

	
Image 001	Image 002
	
Image 003	Image 004
	
Image 005	Image 006

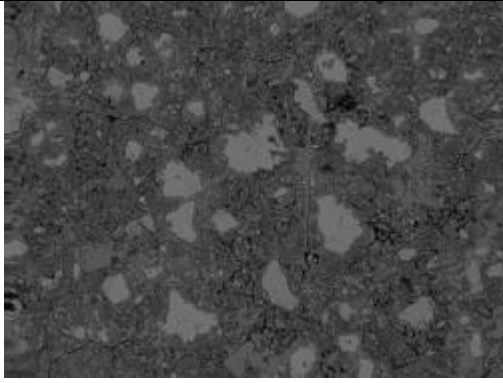
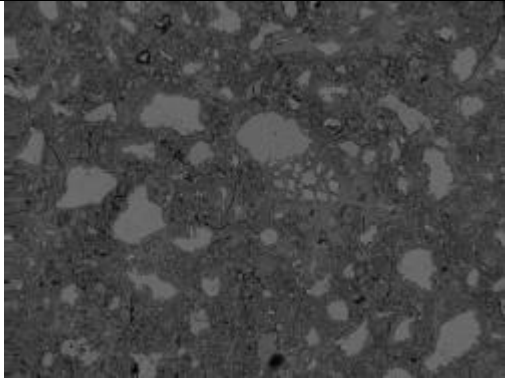
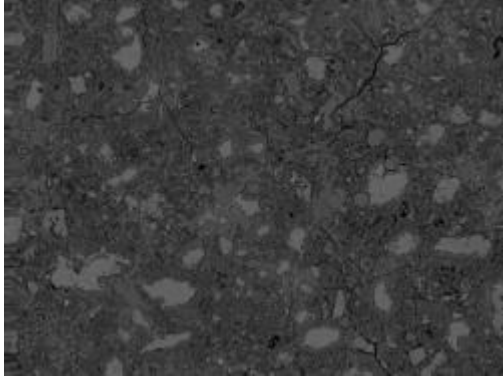
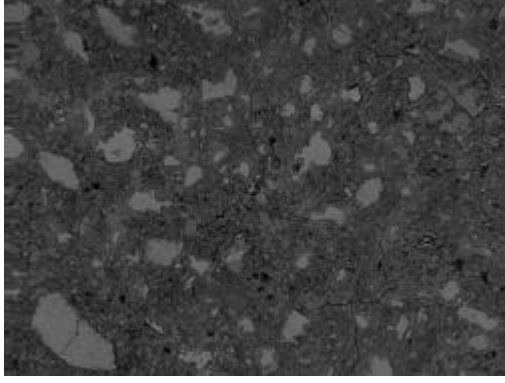
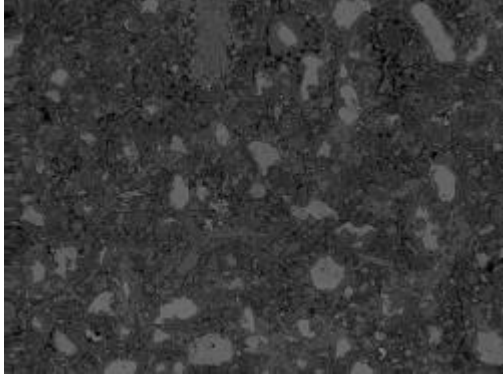
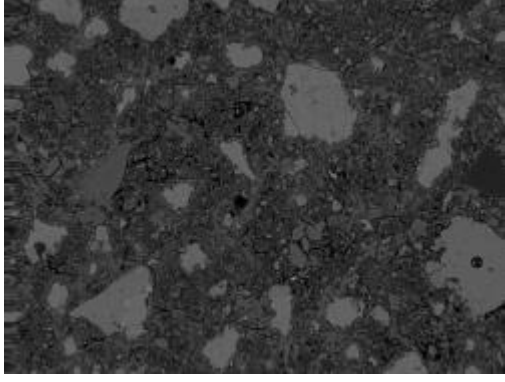
50MPa CEM1 stiff mix ideal cured

	
Image 007	Image 008
	
Image 009	Image 010
	
Image 011	Image 012

50MPa CEM1 stiff mix ideal cured

	
Image 013	Image 014
	
Image 015	Image 016
	
Image 017	Image 018

50MPa CEM1 stiff mix ideal cured

	
Image 019	Image 020
	
Image 022	Image 023
	
Image 024	Image 026

50MPa CEM1 stiff mix ideal cured

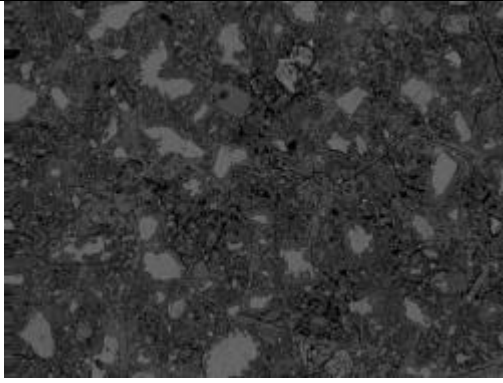
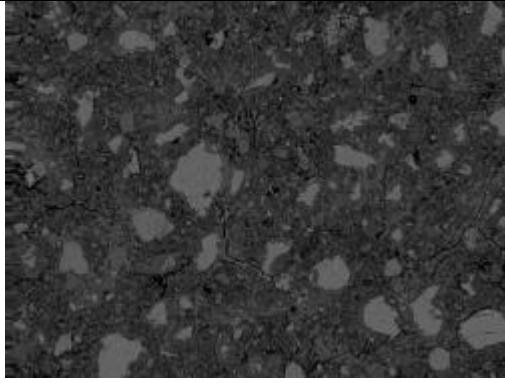
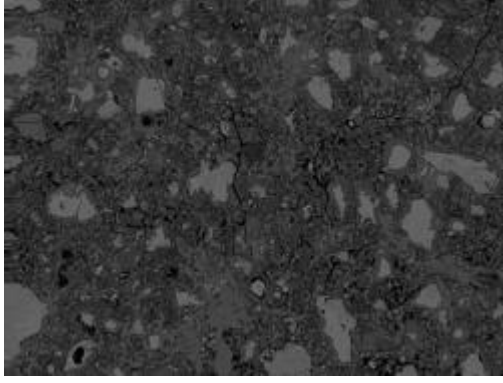
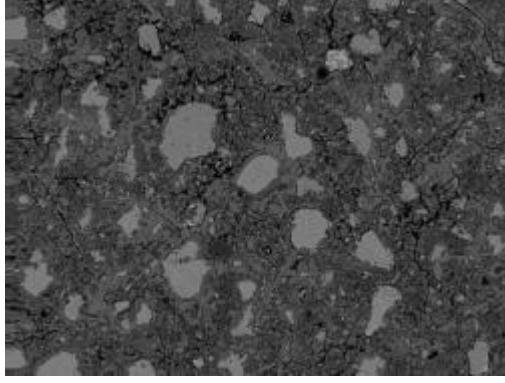
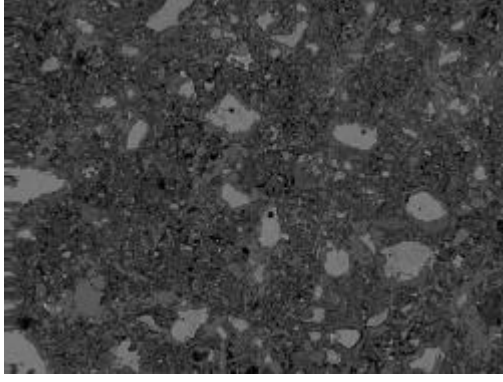
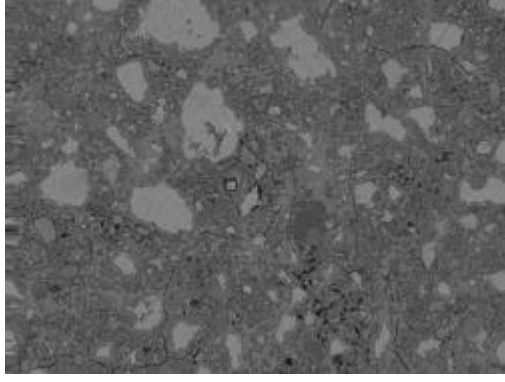
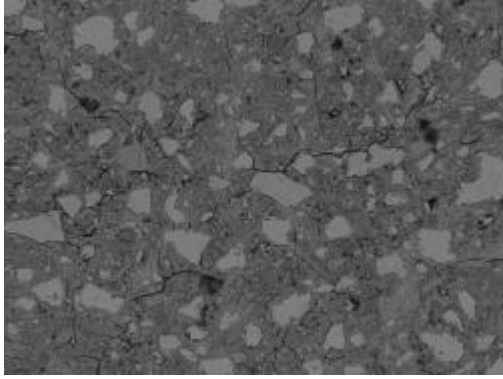
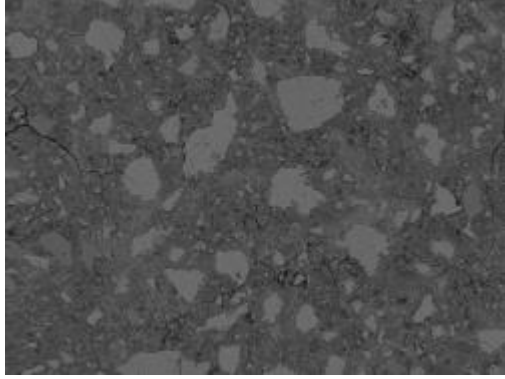
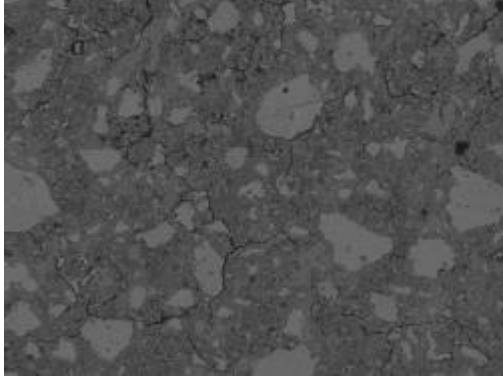
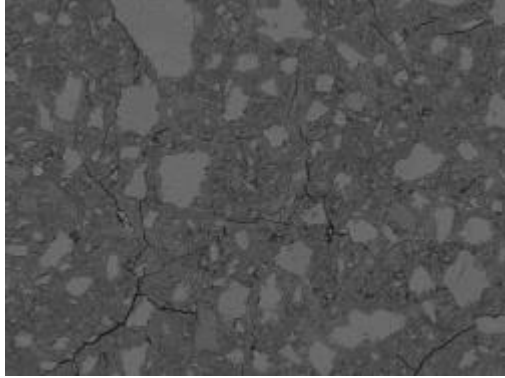
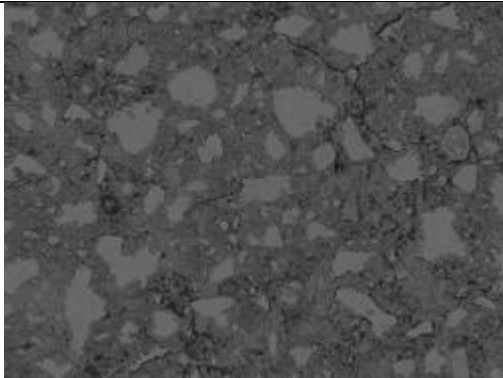
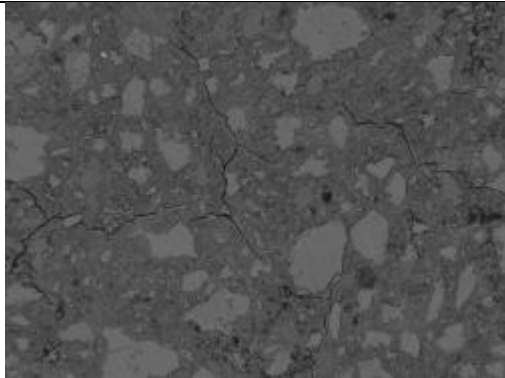
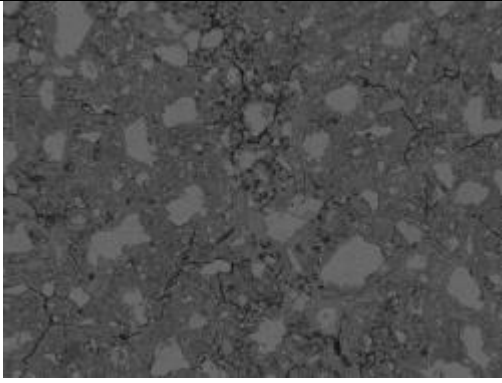
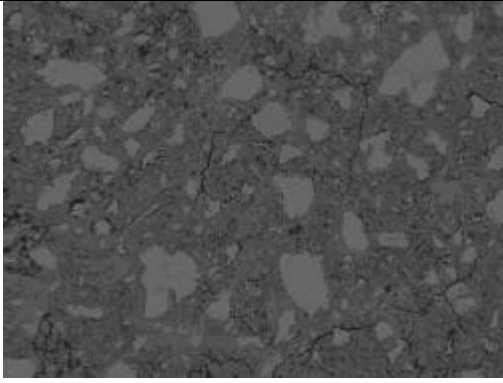
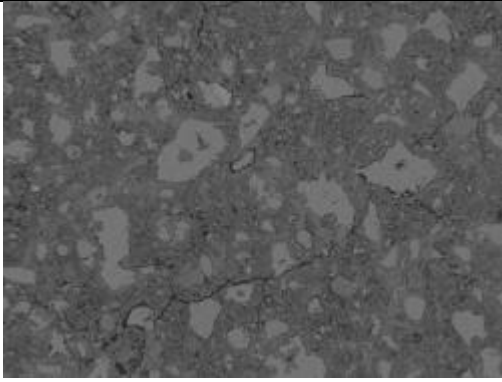
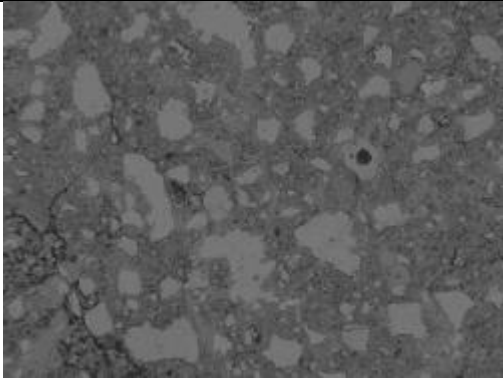
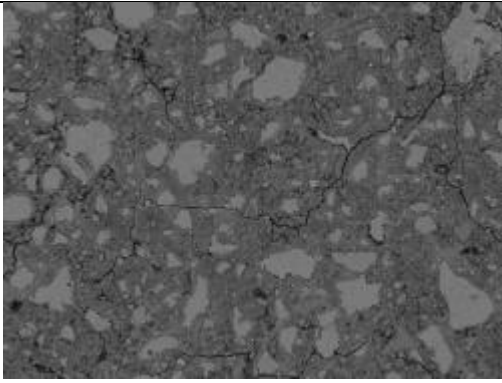
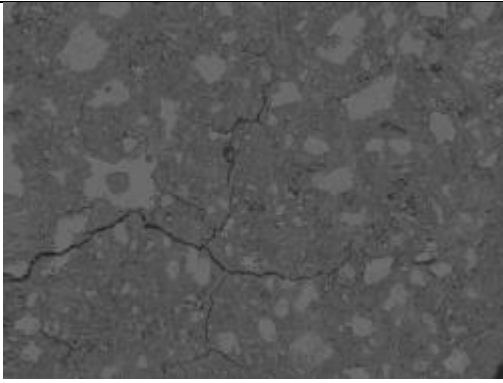
	
Image 027	Image 028
	
Image 029	Image 031
	
Image 034	Image 039

Figure A 94 Images of 50MPa CEM1 stiff mix ideal cured

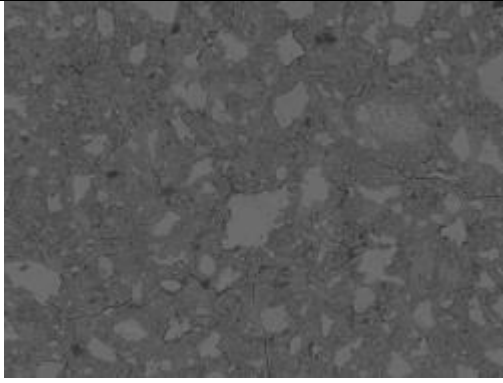
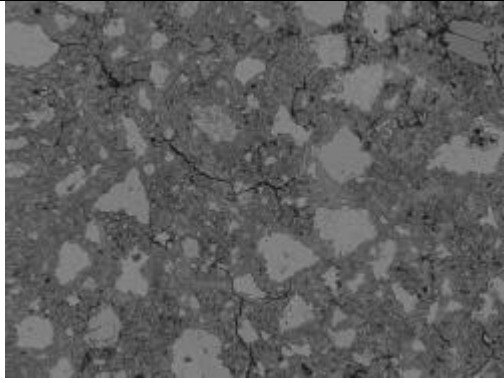
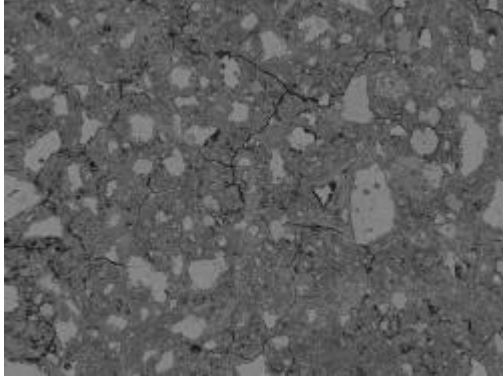
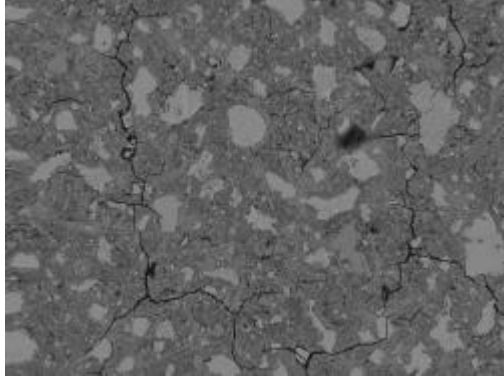
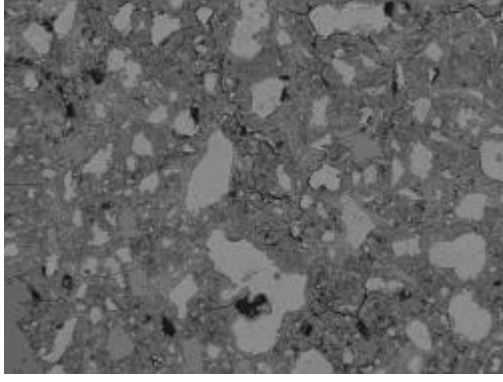
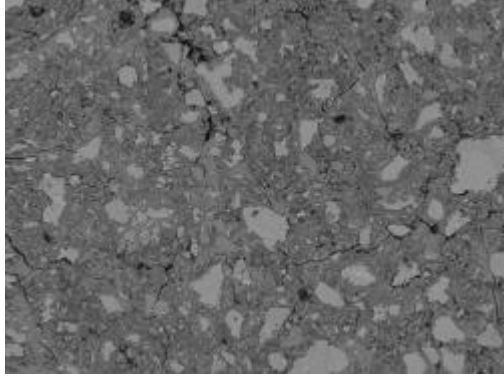
M3A

	
Image 001	Image 002
	
Image 003	Image 004
	
Image 005	Image 006

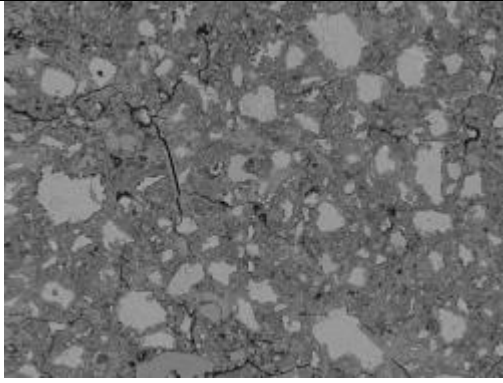
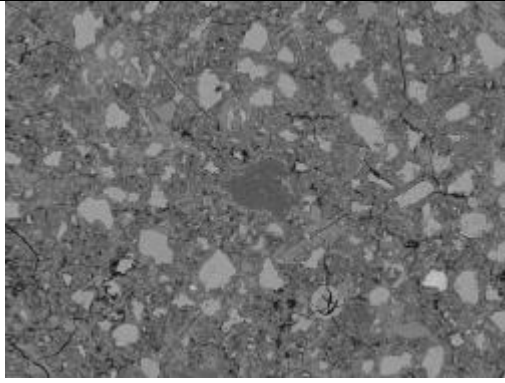
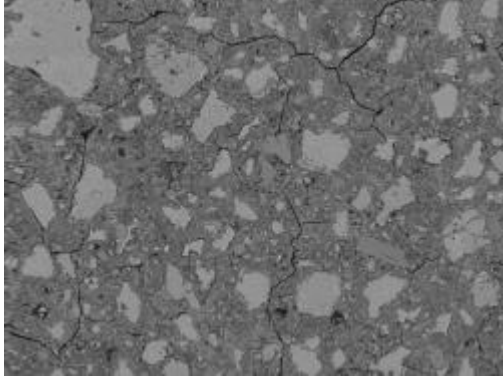
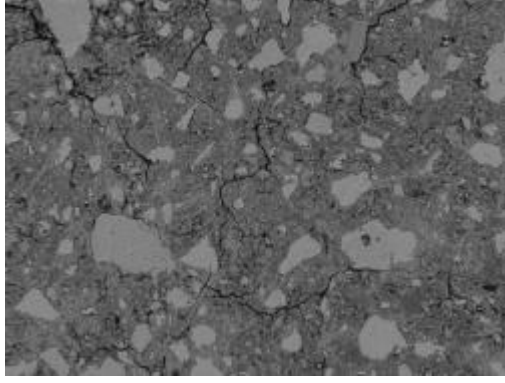
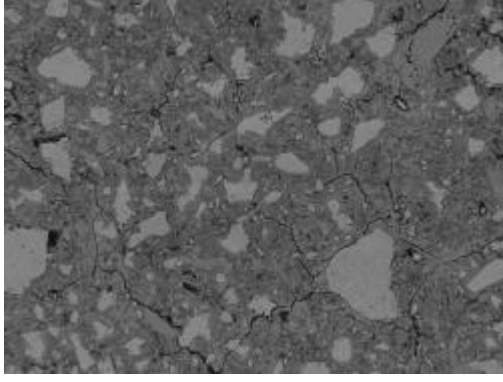
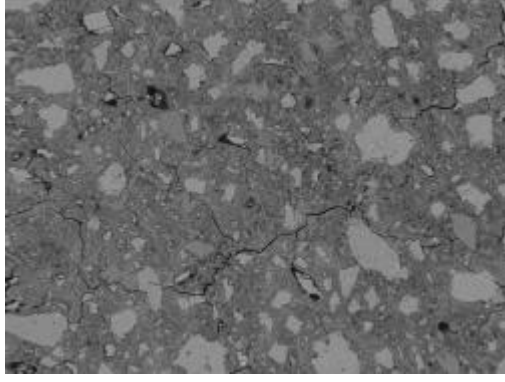
80MPa CEM1 stiff mix ambient cured

	
Image 007	Image 008
	
Image 009	Image 010
	
Image 012	Image 013

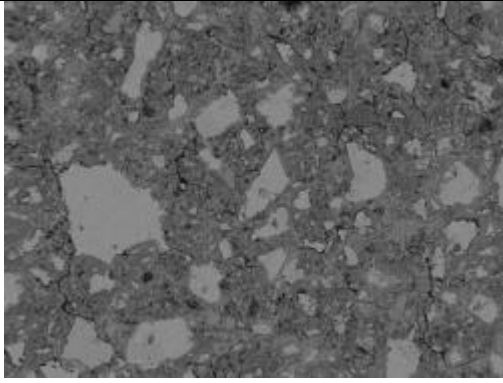
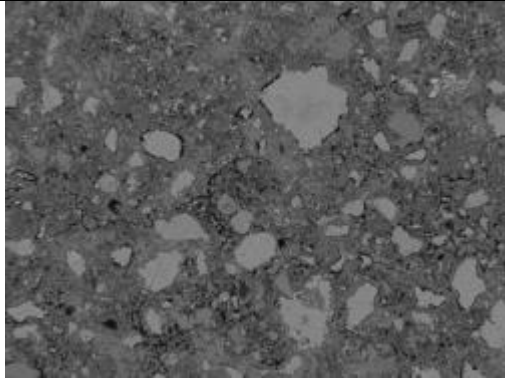
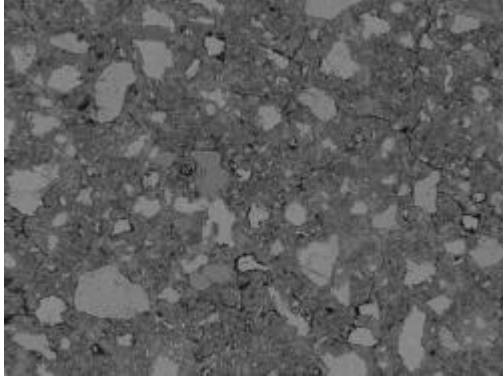
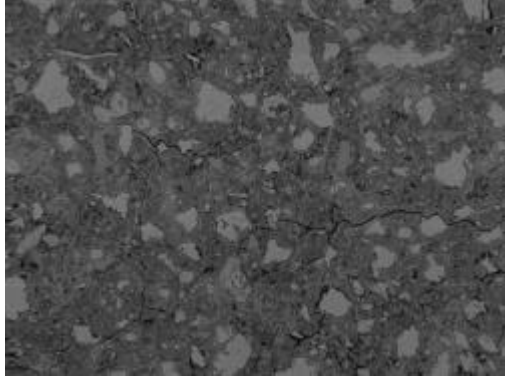
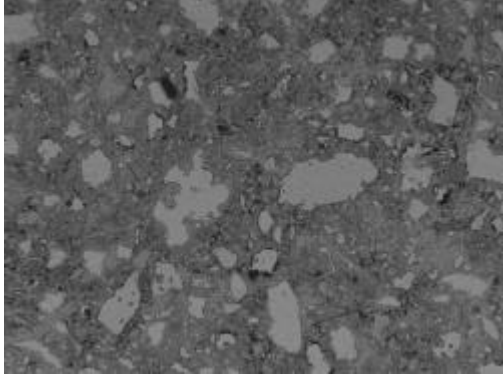
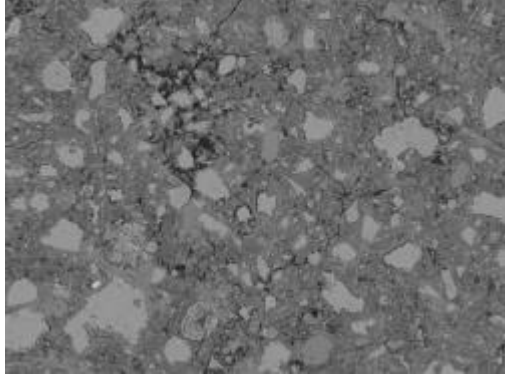
80MPa CEM1 stiff mix ambient cured

	
Image 014	Image 015
	
Image 016	Image 017
	
Image 018	Image 019

80MPa CEM1 stiff mix ambient cured

	
Image 020	Image 021
	
Image 022	Image 024
	
Image 025	Image 027

80MPa CEM1 stiff mix ambient cured

	
Image 028	Image 029
	
Image 030	Image 031
	
Image 032	Image 033

80MPa CEM1 stiff mix ambient cured

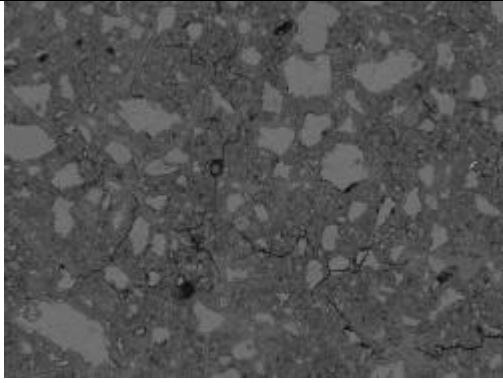
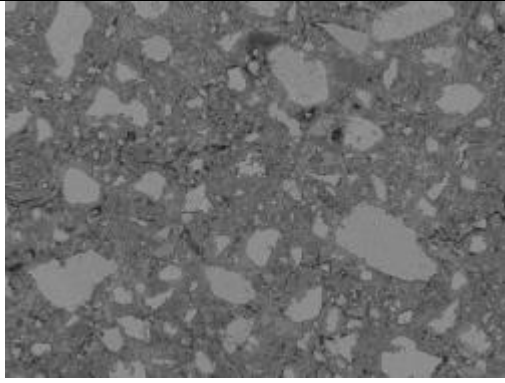
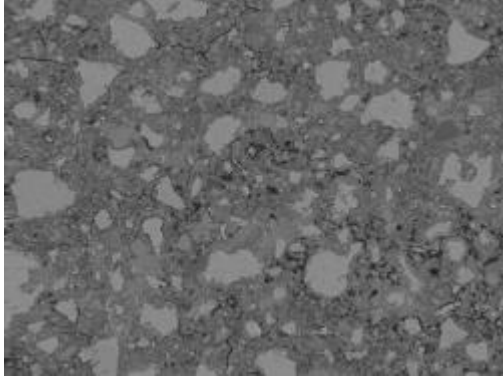
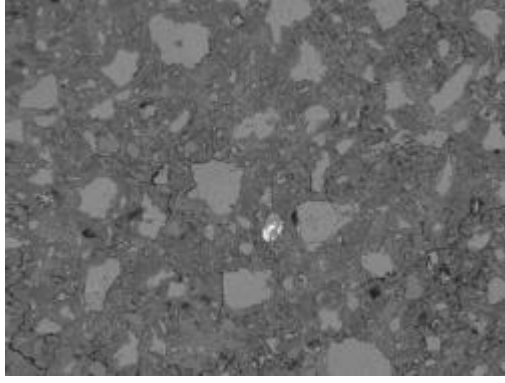
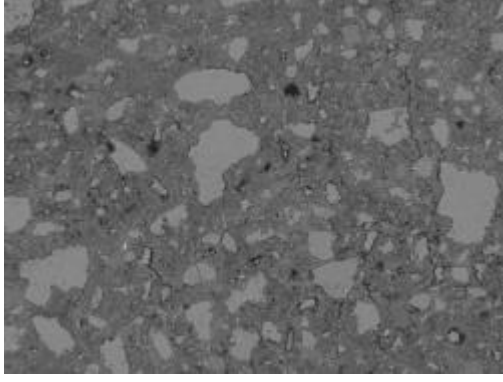
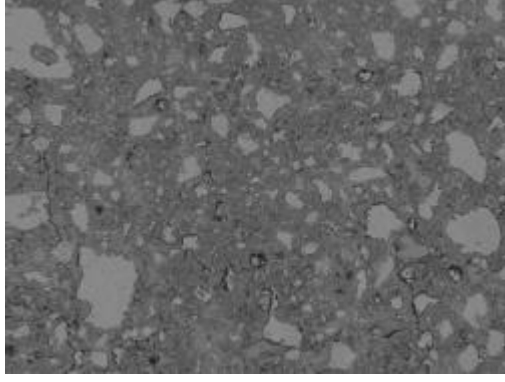
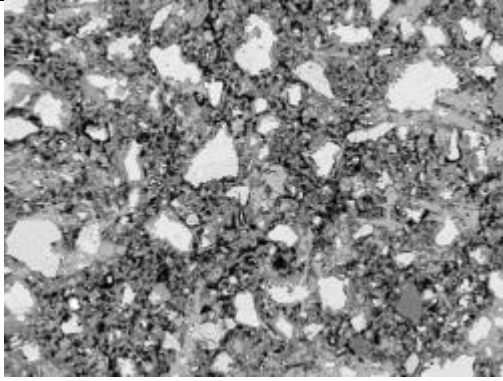
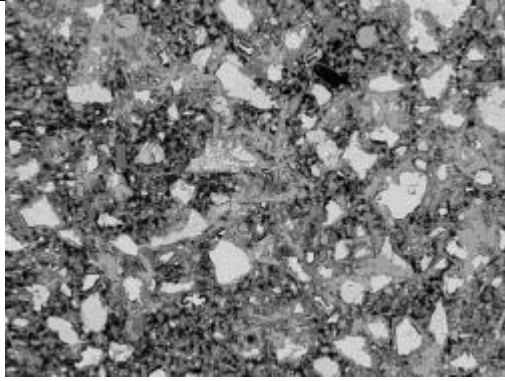
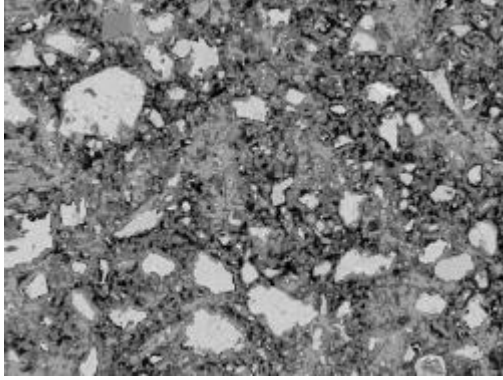
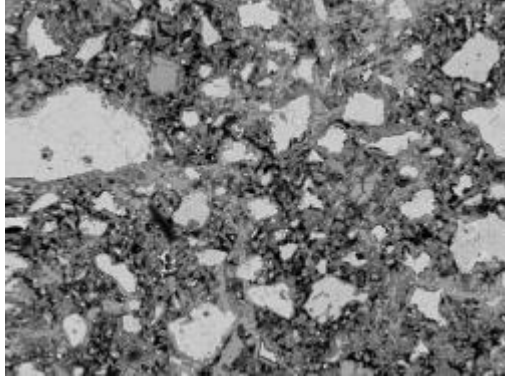
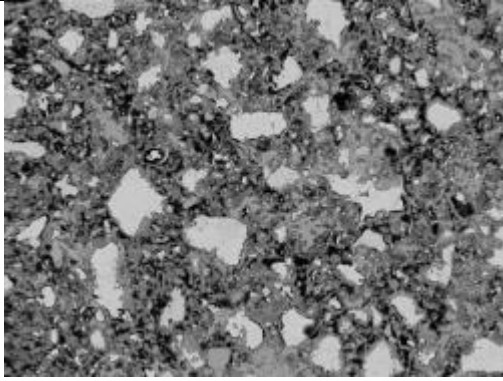
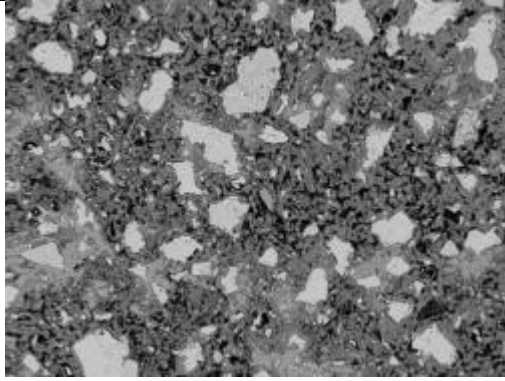
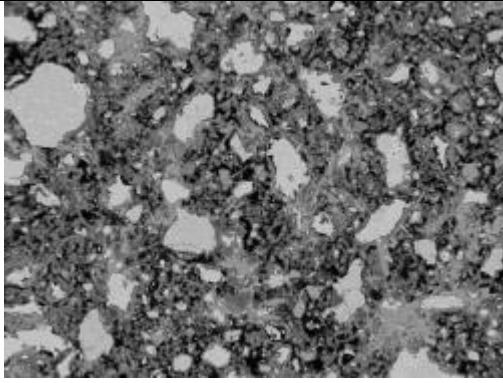
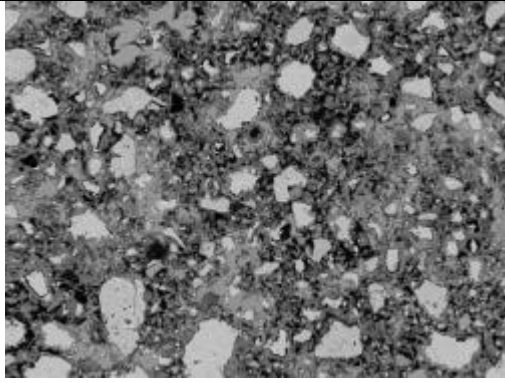
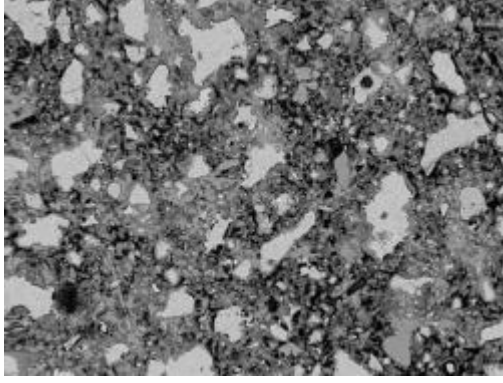
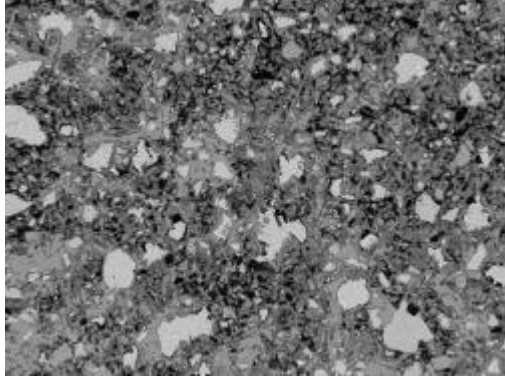
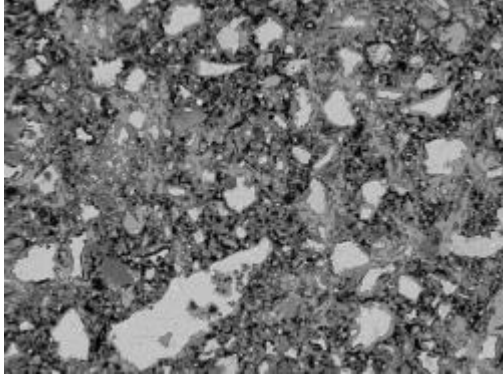
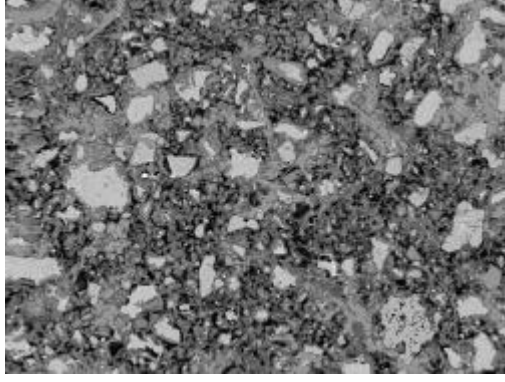
	
Image 034	Image 035
	
Image 036	Image 037
	
Image 038	Image 039

Figure A 95 Images of 80MPa CEM1 stiff mix ambient cured

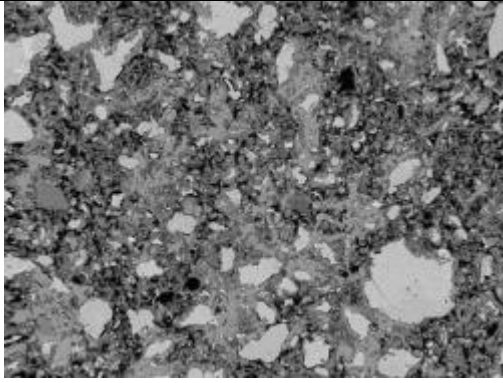
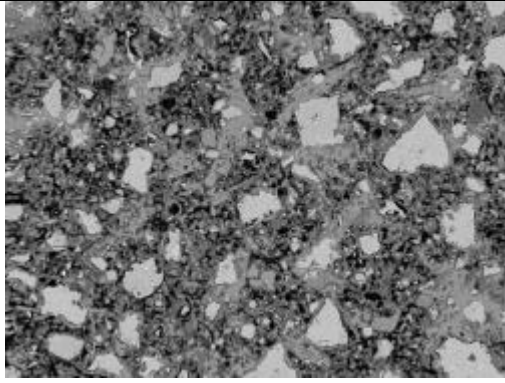
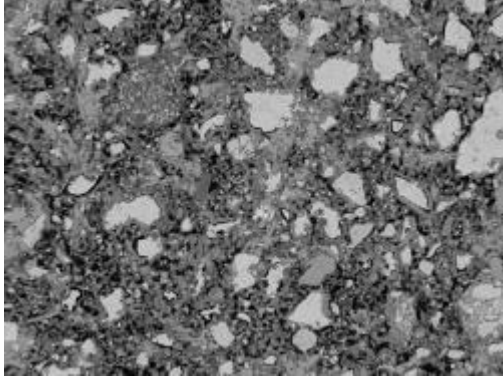
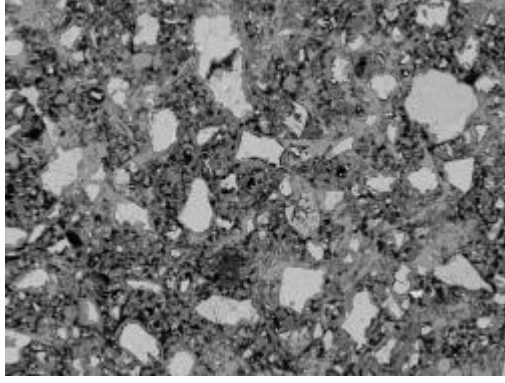
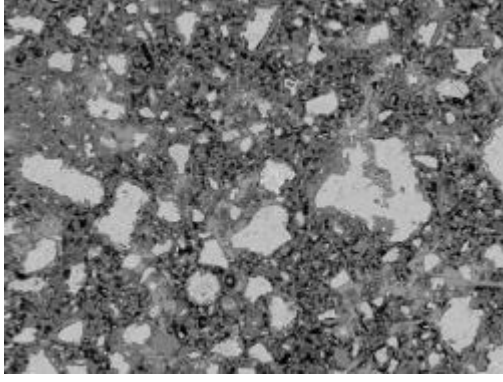
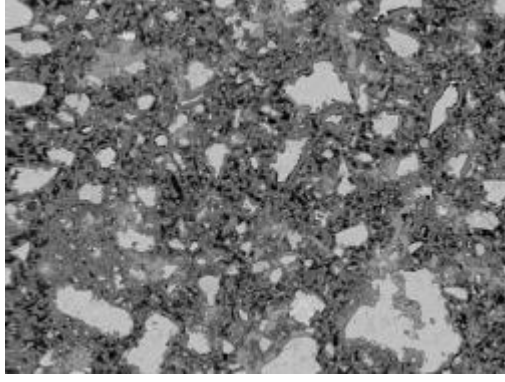
M3W

	
Image 001	Image 003
	
Image 005	Image 006
	
Image 007	Image 009

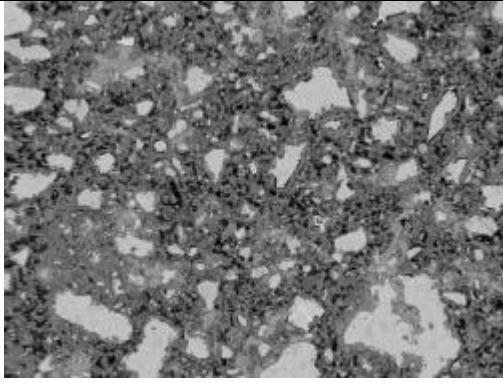
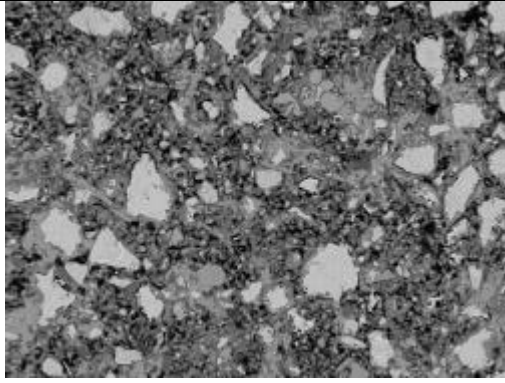
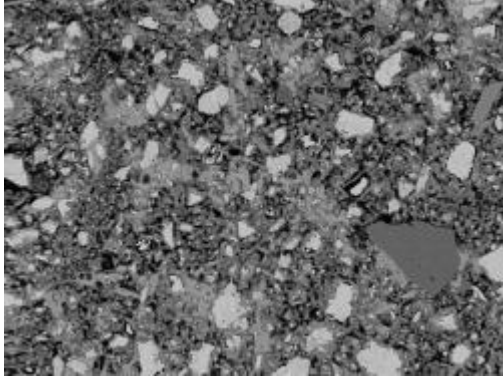
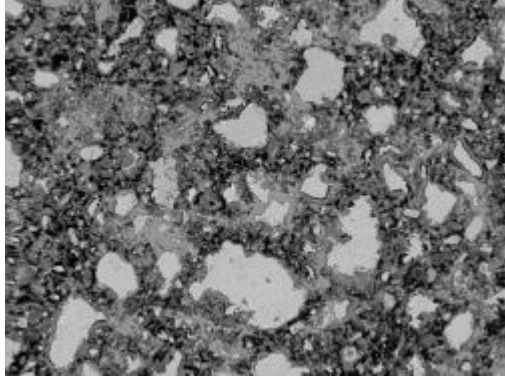
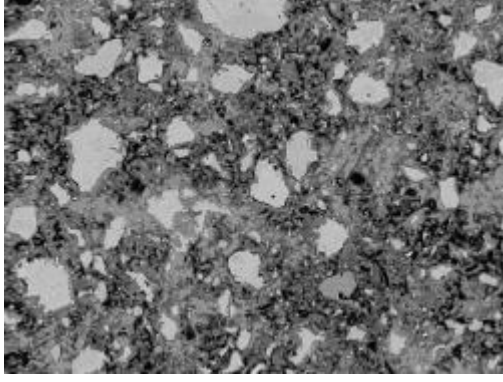
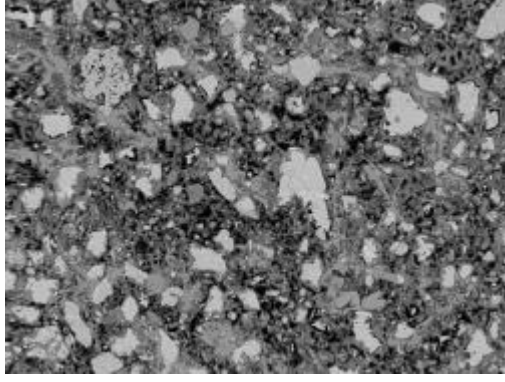
80MPa CEM1 stiff mix ideal cured

	
Image 011	Image 012
	
Image 013	Image 014
	
Image 015	Image 017

80MPa CEM1 stiff mix ideal cured

	
Image 018	Image 019
	
Image 020	Image 021
	
Image 023	Image 024

80MPa CEM1 stiff mix ideal cured

	
Image 025	Image 026
	
Image 027	Image 028
	
Image 029	Image 030

80MPa CEM1 stiff mix ideal cured

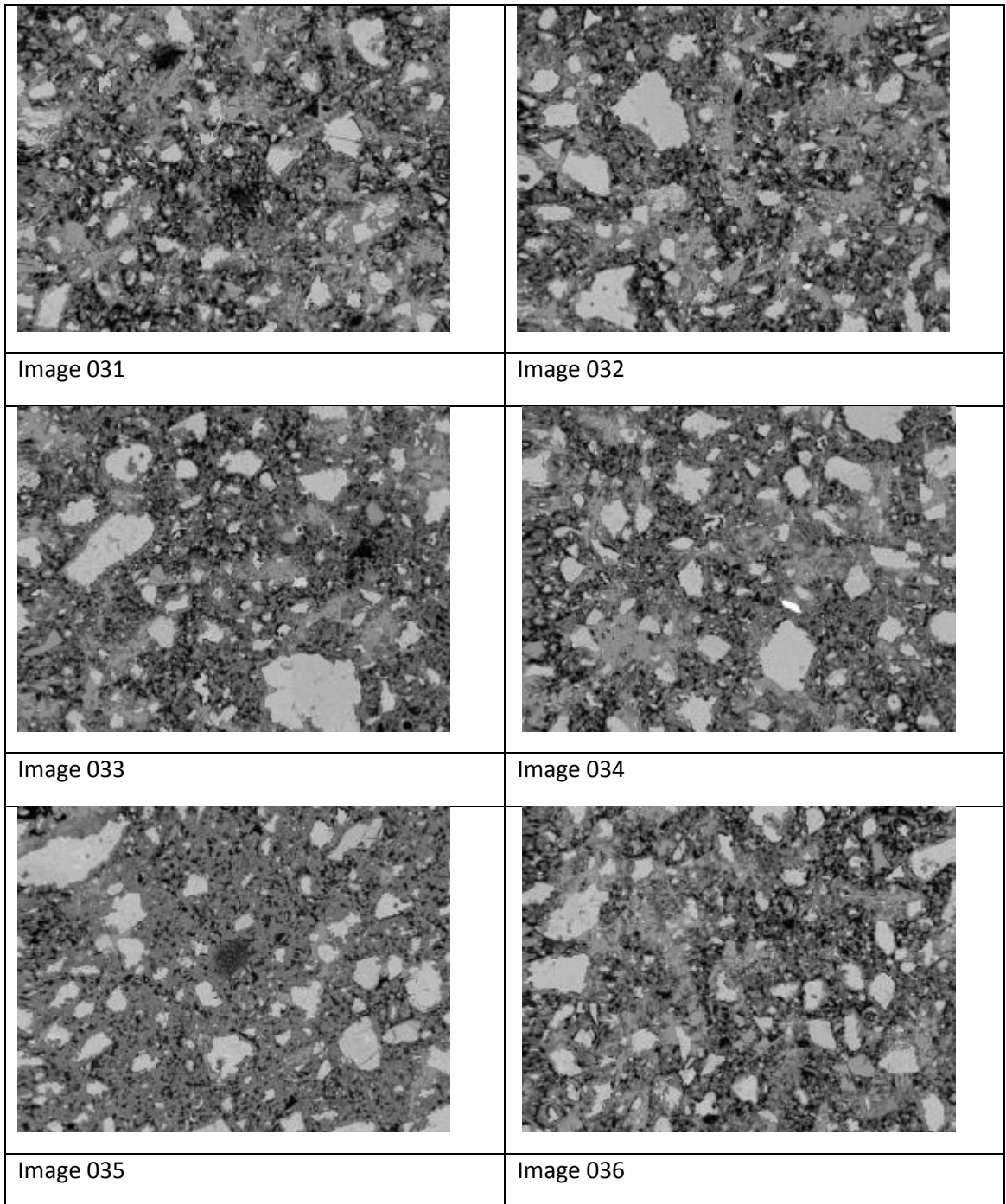
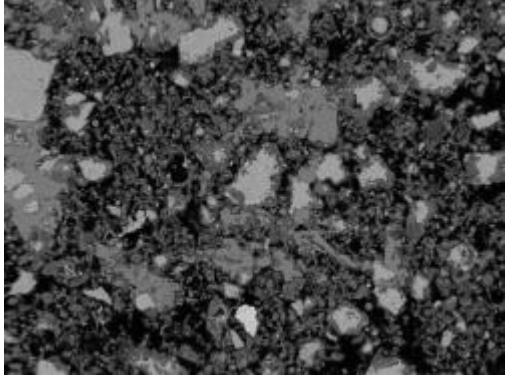
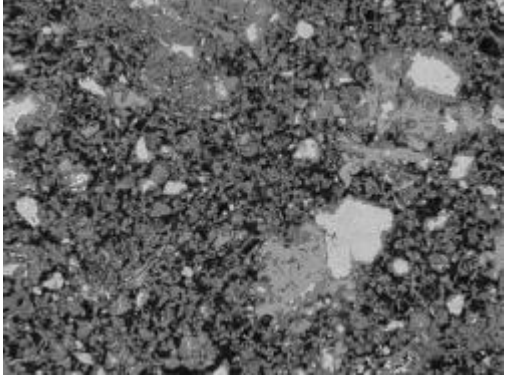
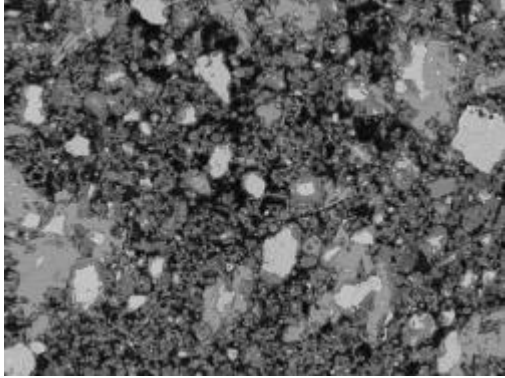
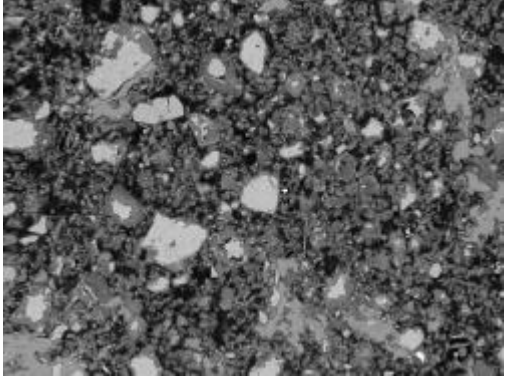
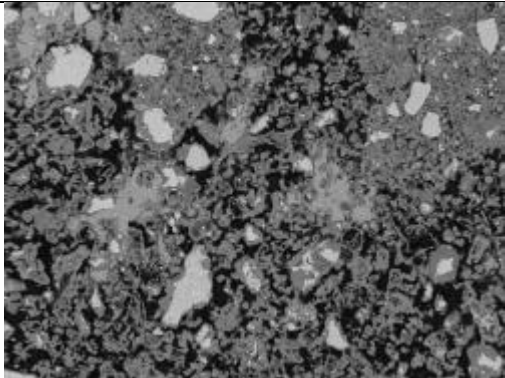
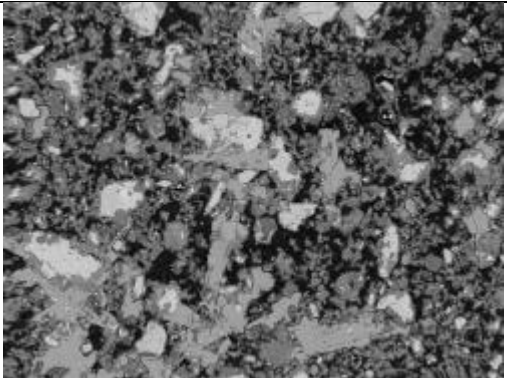
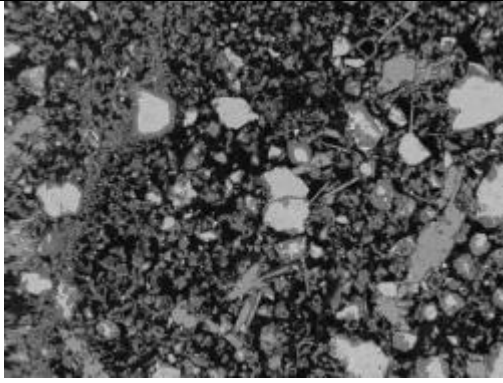
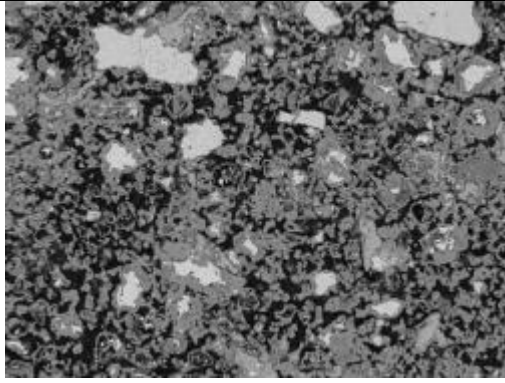
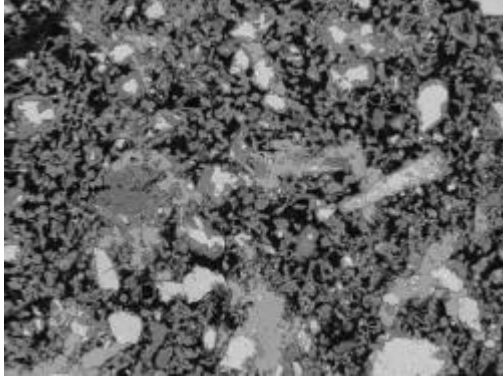
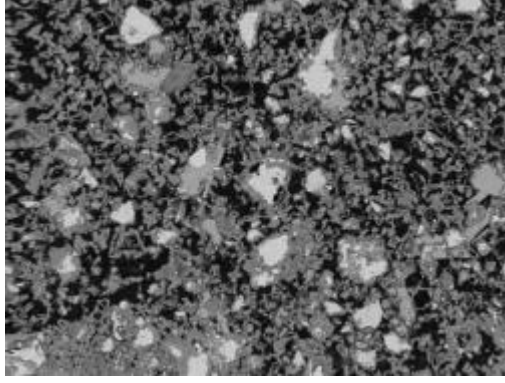
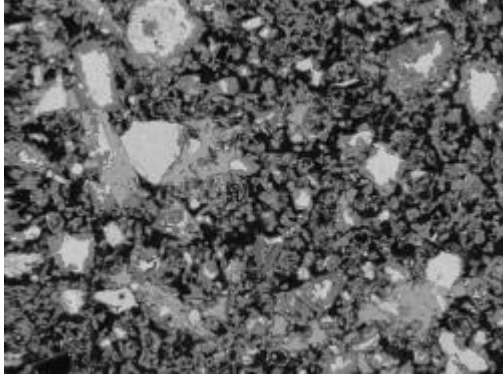
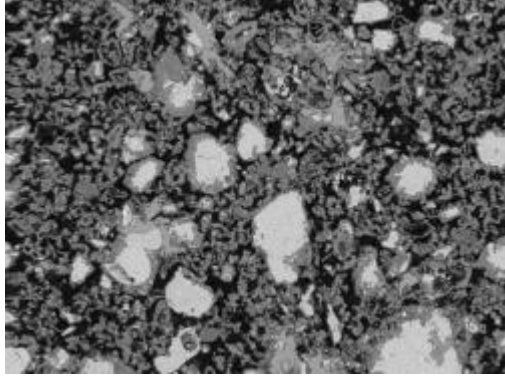


Figure A 96 Images of 80MPa CEM1 stiff mix ideal cured

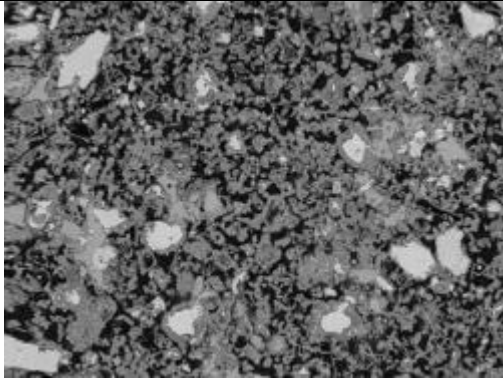
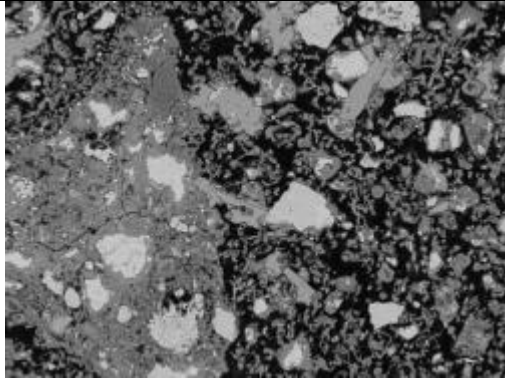
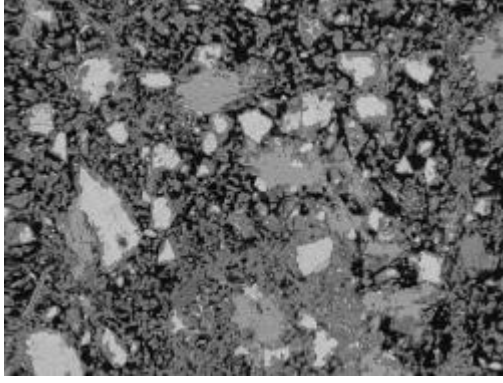
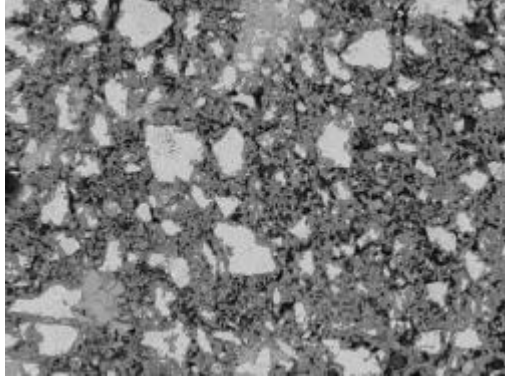
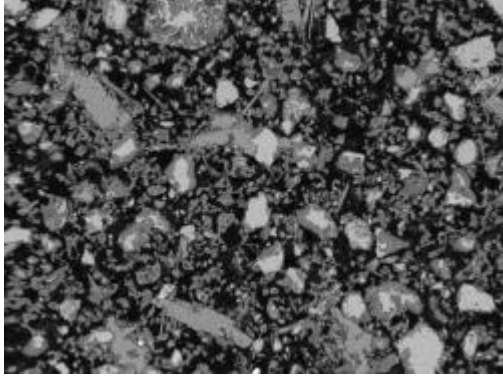
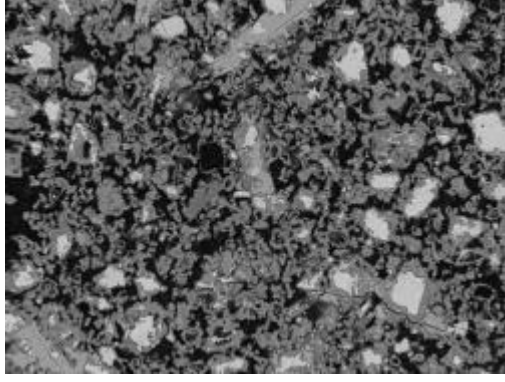
M4A

	
Image 001	Image 002
	
Image 003	Image 004
	
Image 005	Image 009

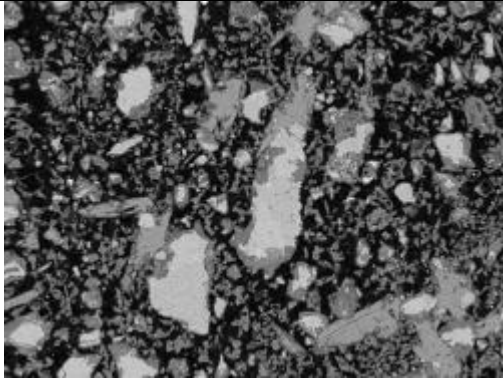
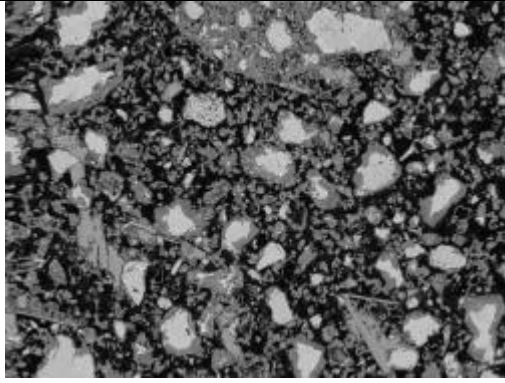
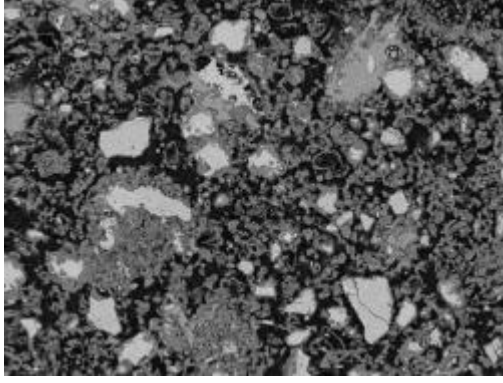
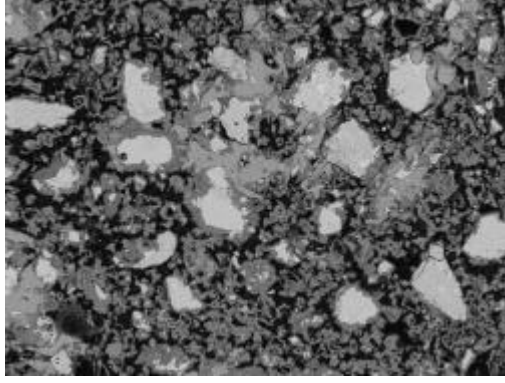
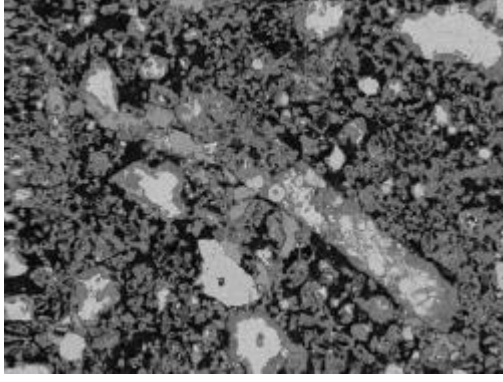
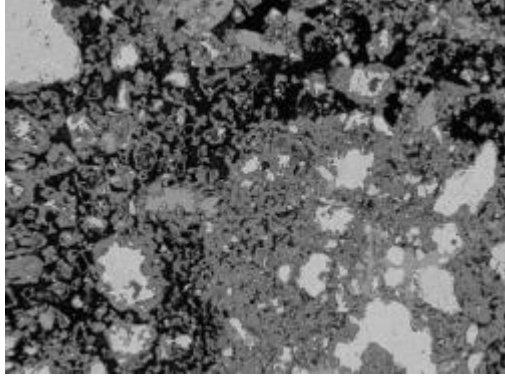
20MPa CEM1 wet mix ambient cured

	
Image 012	Image 013
	
Image 014	Image 015
	
Image 016	Image 017

20MPa CEM1 wet mix ambient cured

	
Image 018	Image 019
	
Image 020	Image 022
	
Image 023	Image 026

20MPa CEM1 wet mix ambient cured

	
Image 027	Image 028
	
Image 029	Image 030
	
Image 031	Image 033

20MPa CEM1 wet mix ambient cured

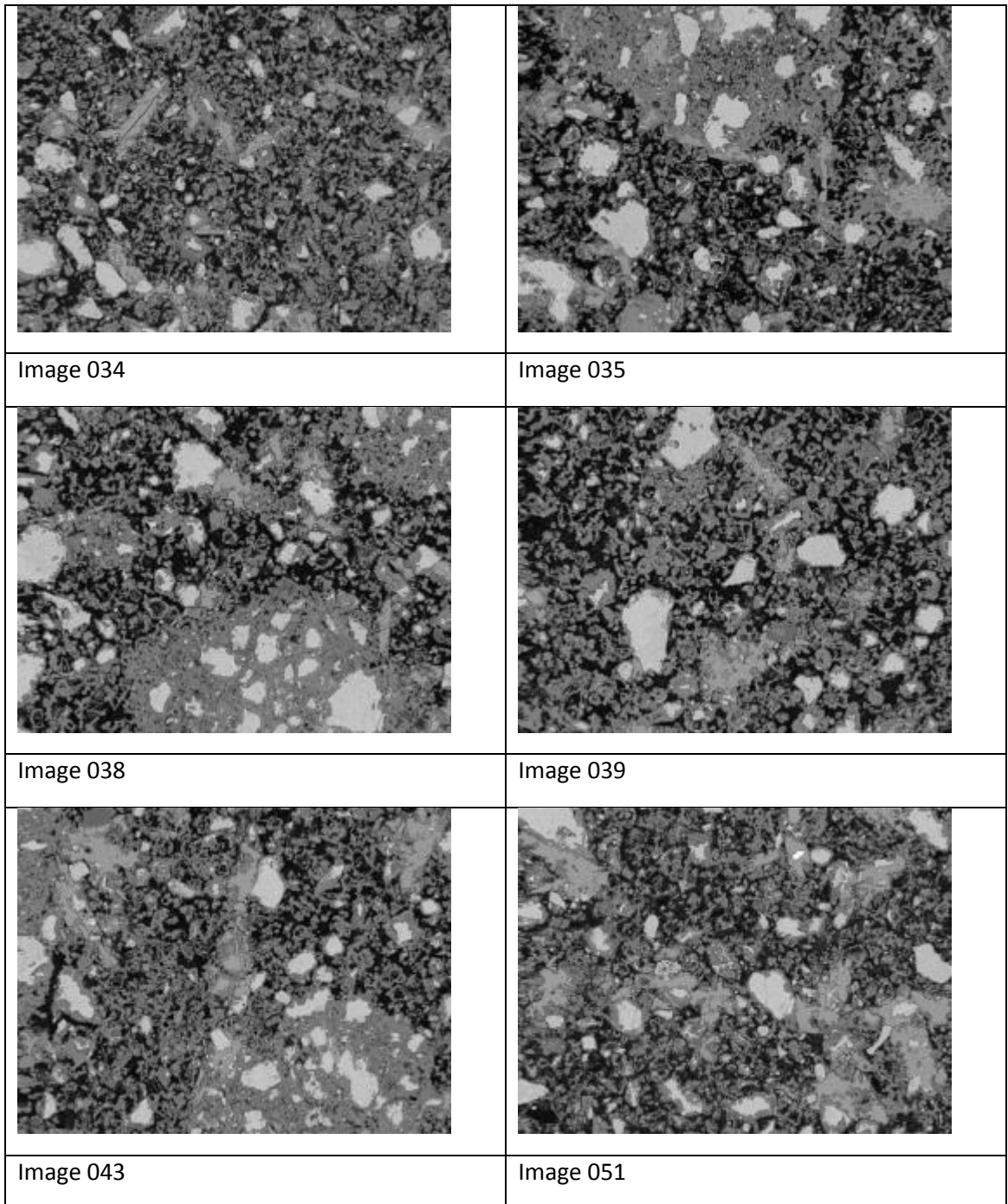
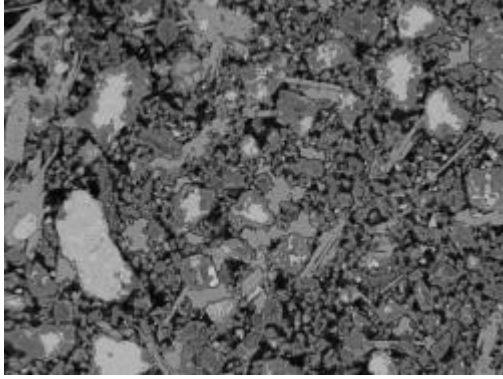
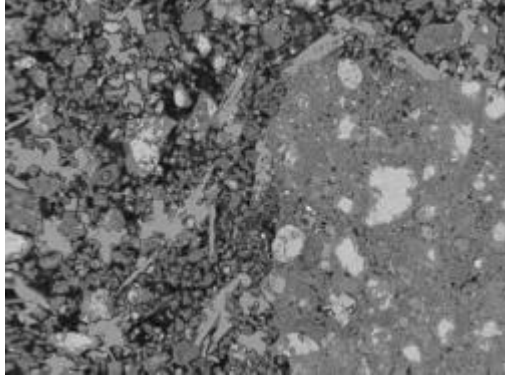
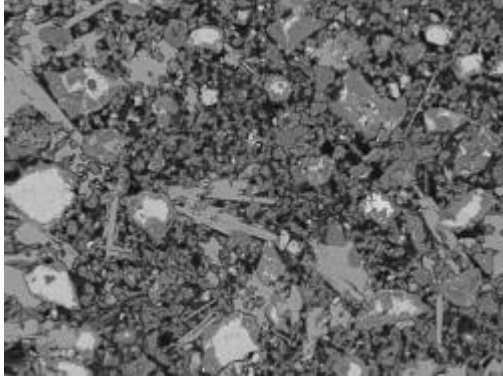
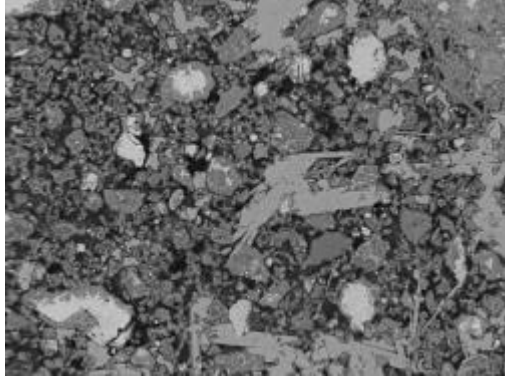
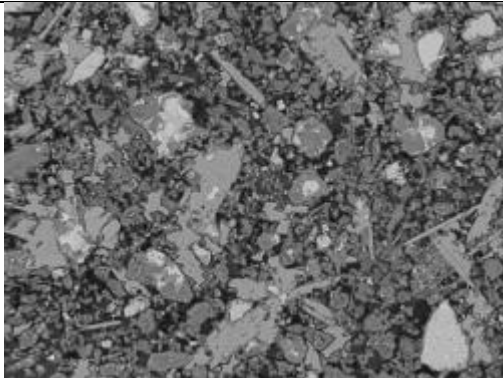
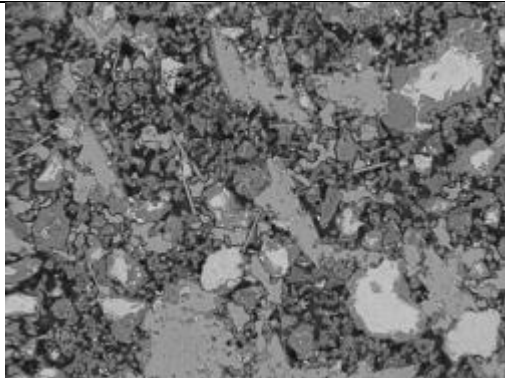
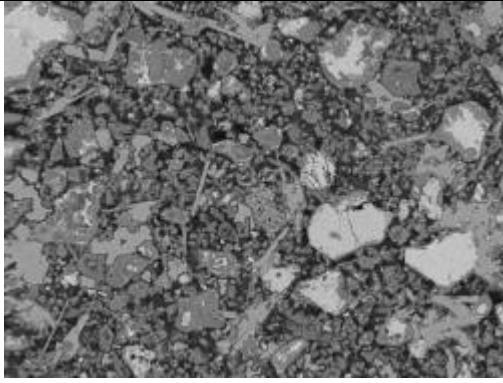
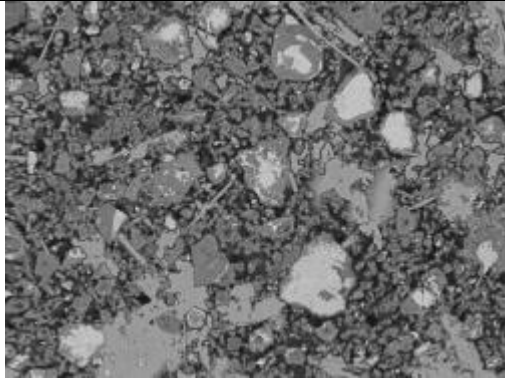
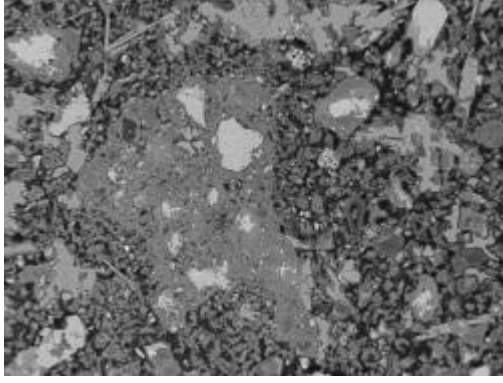
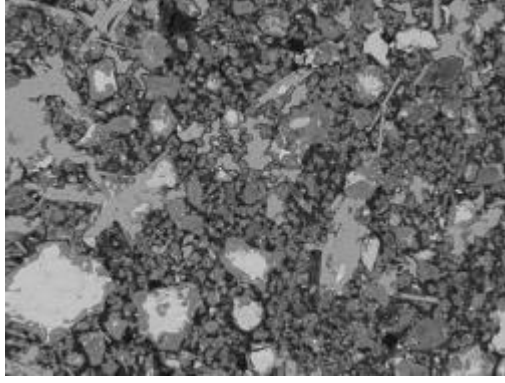
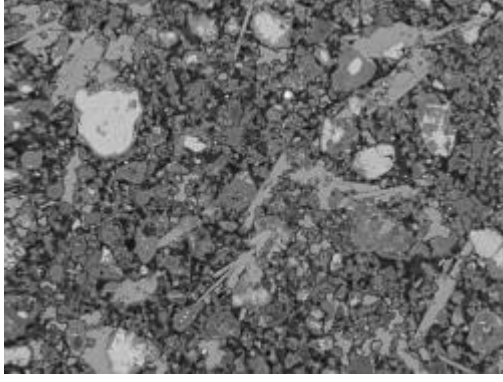
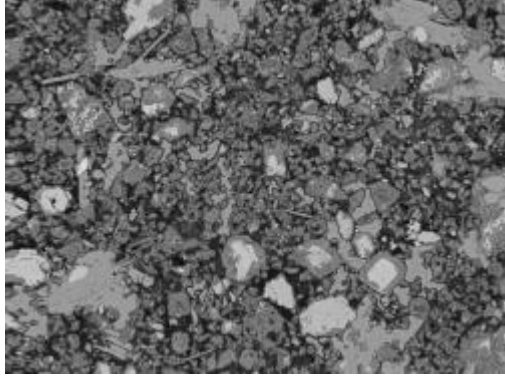


Figure A 97 Images of 20MPa CEM1 wet mix ambient cured

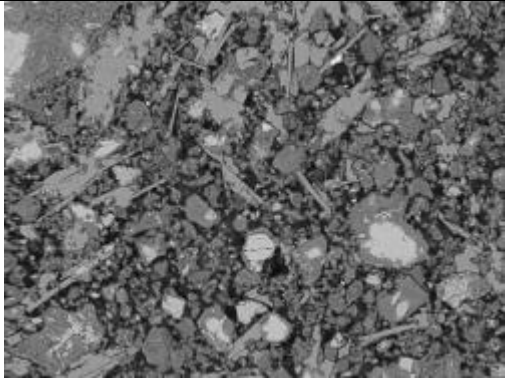
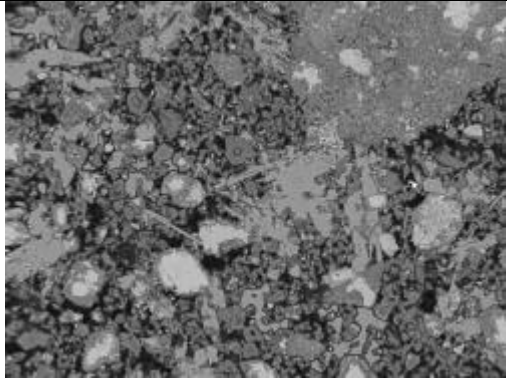
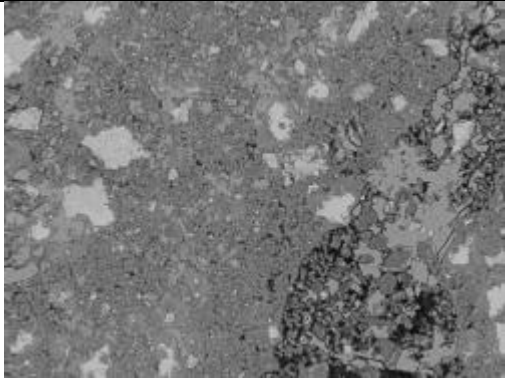
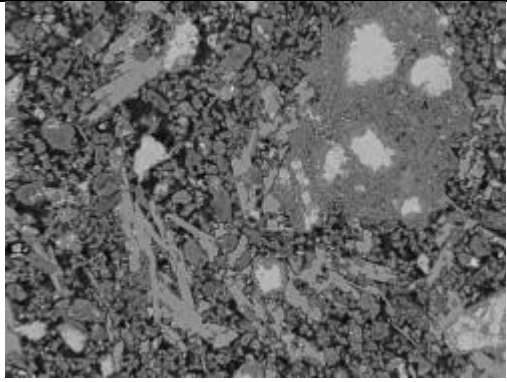
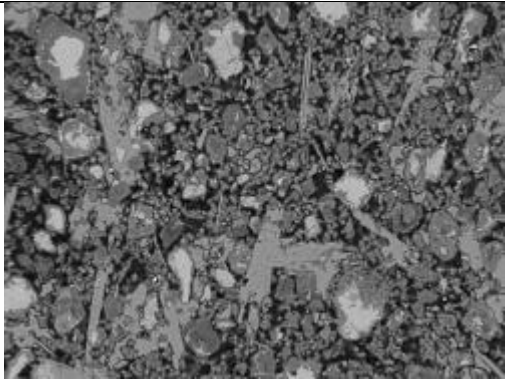
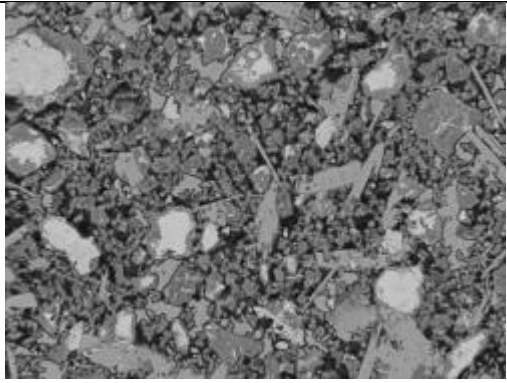
M4W

	
Image 001	Image 004
	
Image 005	Image 006
	
Image 007	Image 008

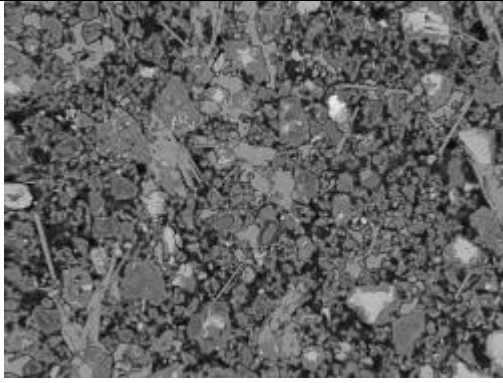
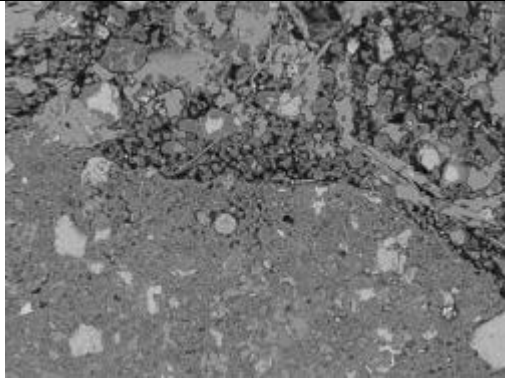
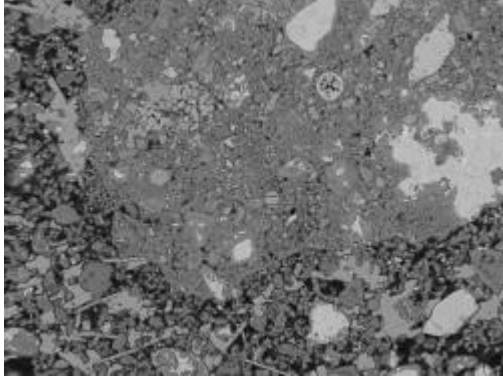
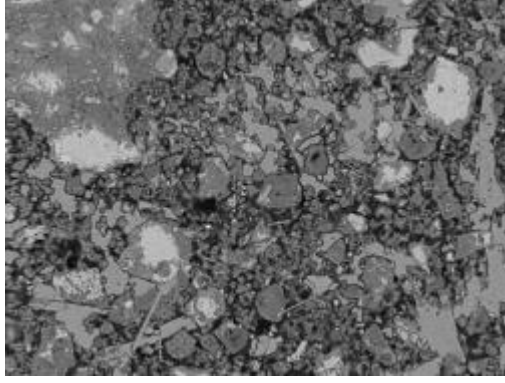
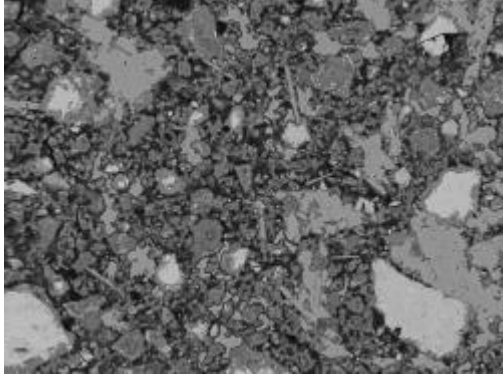
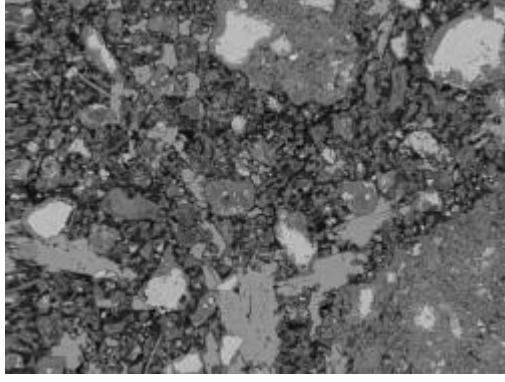
20MPa CEM1 wet mix ideal cured

	
Image 009	Image010
	
Image011	Image 013
	
Image 014	Image 015

20MPa CEM1 wet mix ideal cured

	
Image 016	Image 017
	
Image 018	Image 020
	
Image 022	Image 023

20MPa CEM1 wet mix ideal cured

	
Image 024	Image 026
	
Image 027	Image 030
	
Image 031	Image 032

20MPa CEM1 wet mix ideal cured

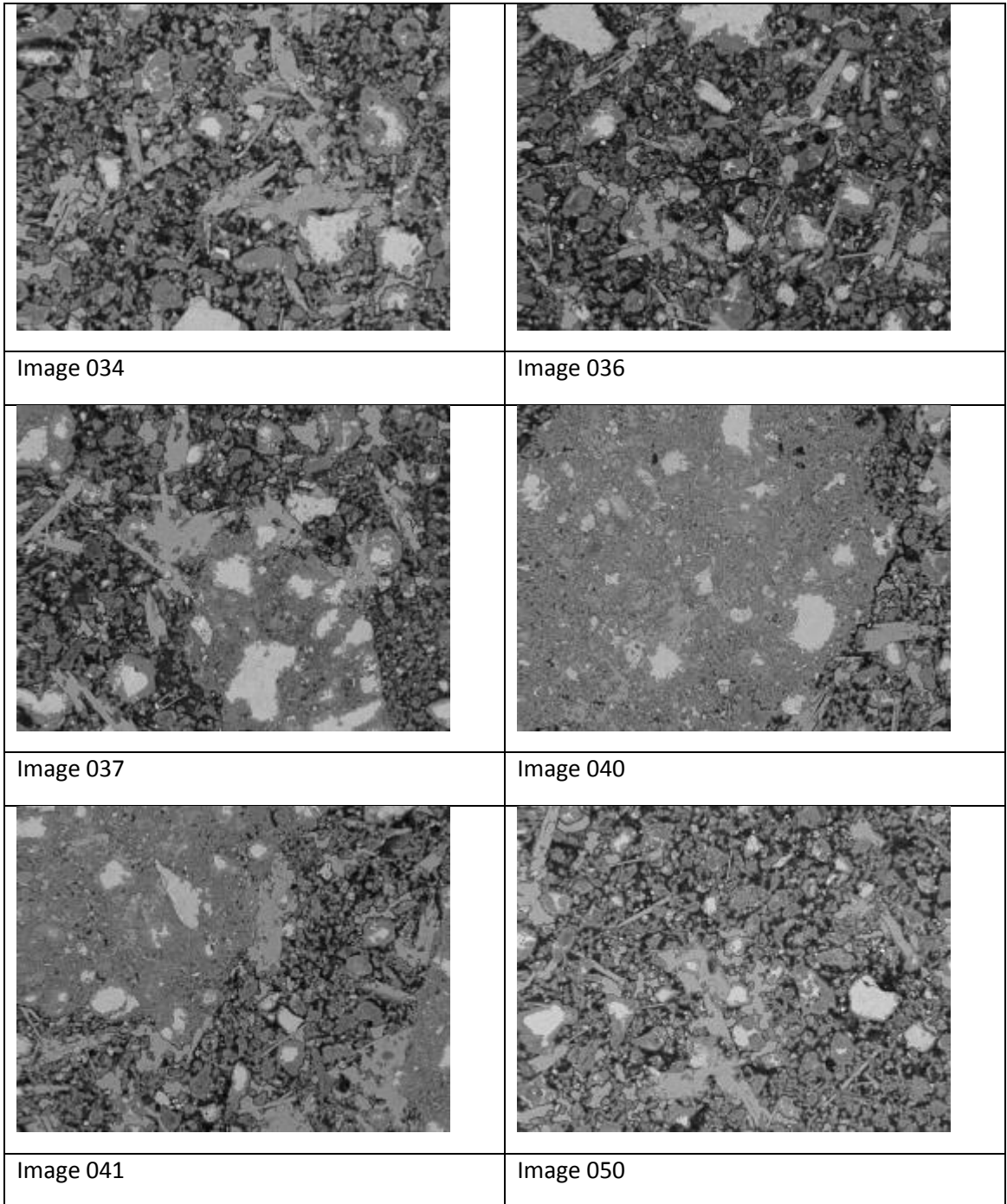
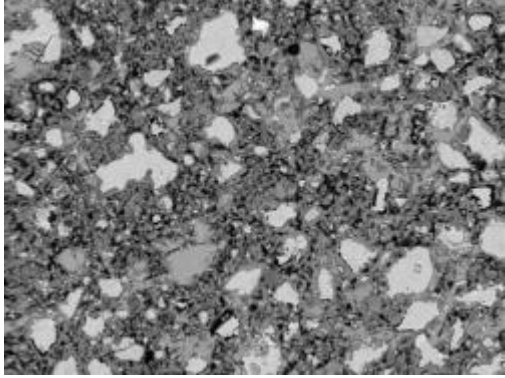
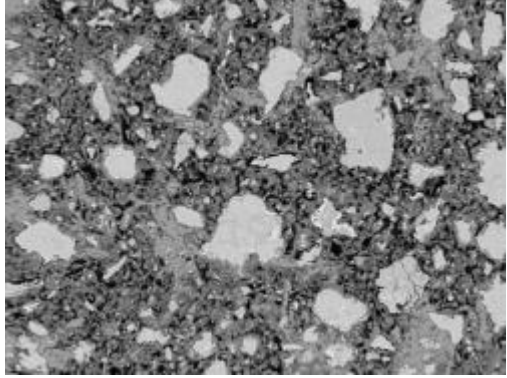
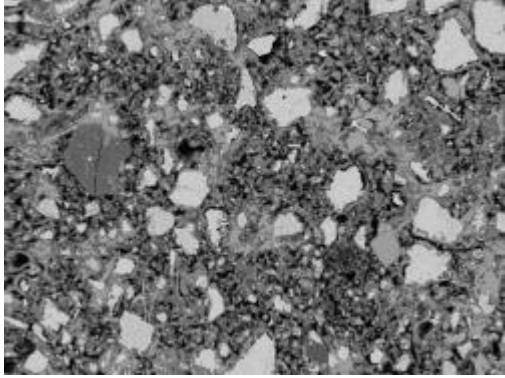
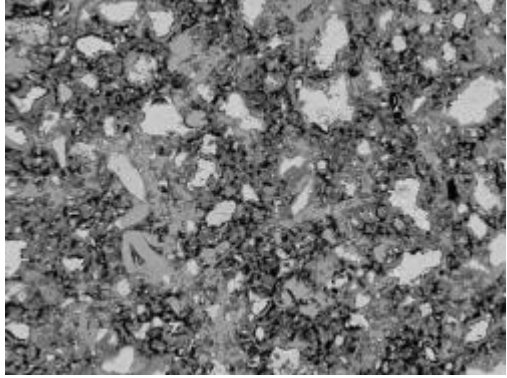
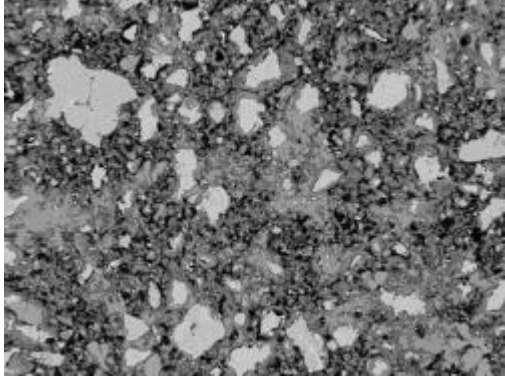
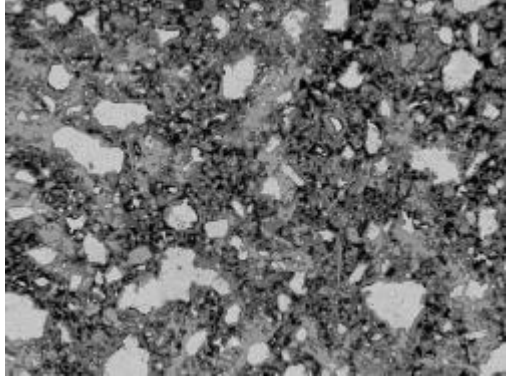
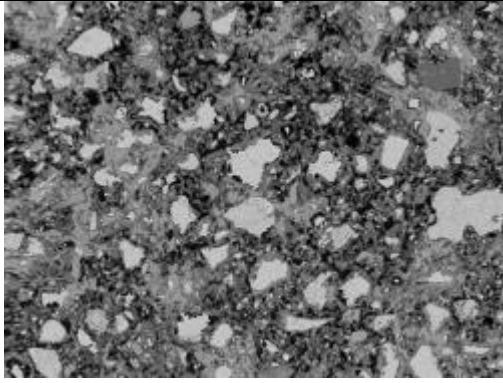
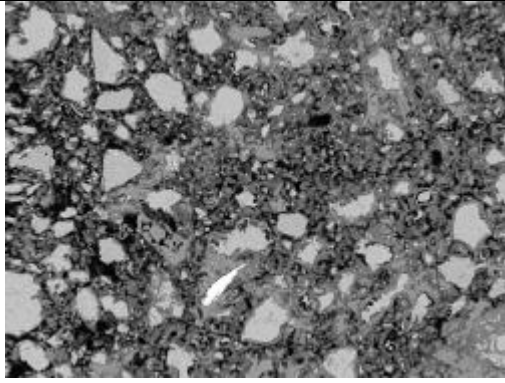
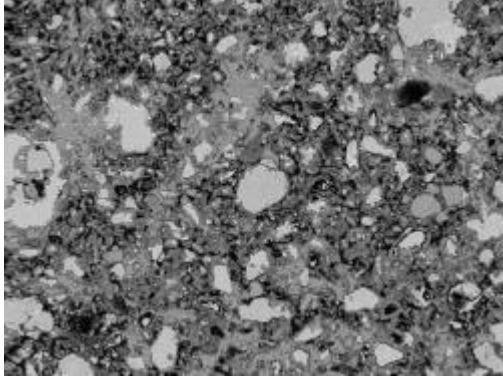
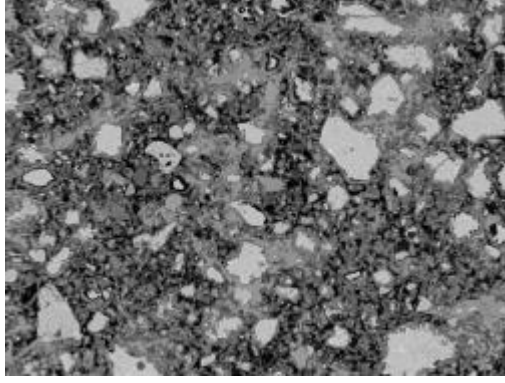
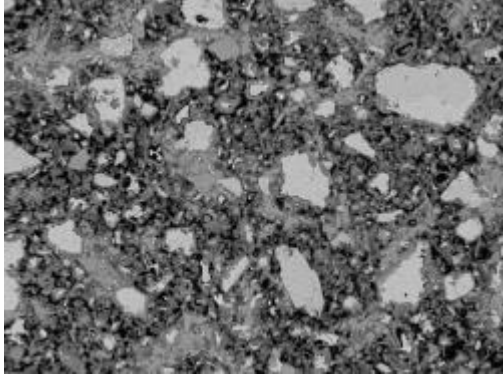
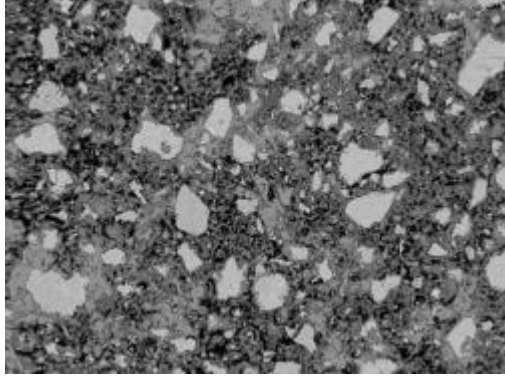


Figure A 98 Images of 20MPa CEM1 wet mix ideal cured

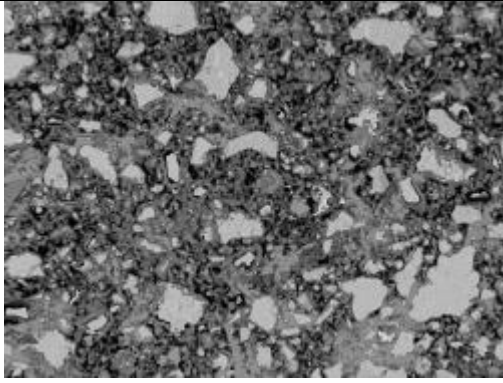
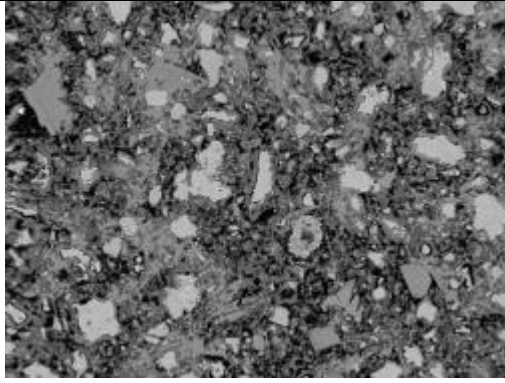
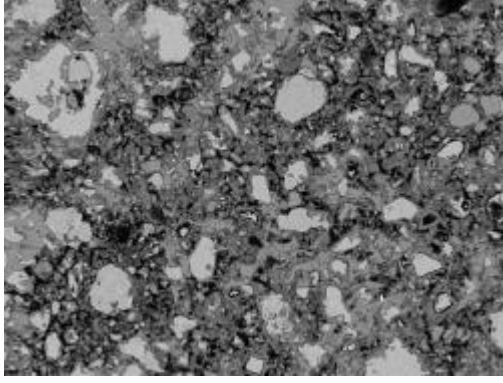
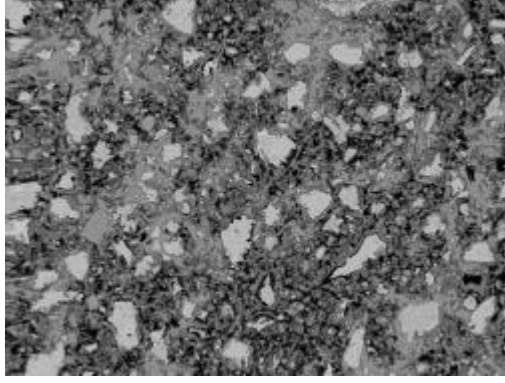
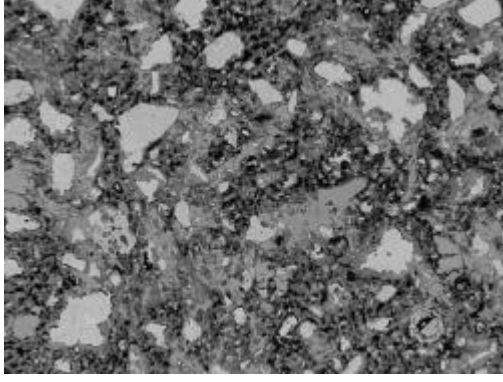
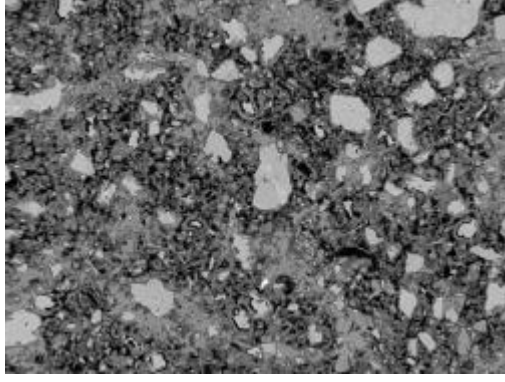
M5A

	
Image 002	Image 003
	
Image 004	Image 005
	
Image 006	Image 007

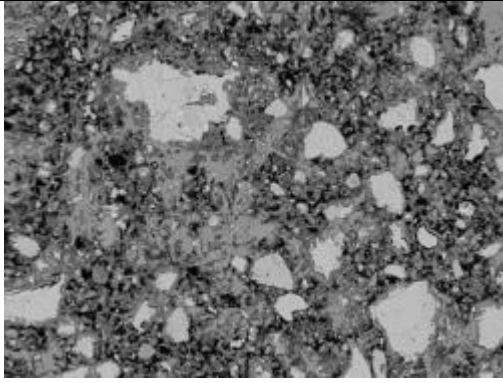
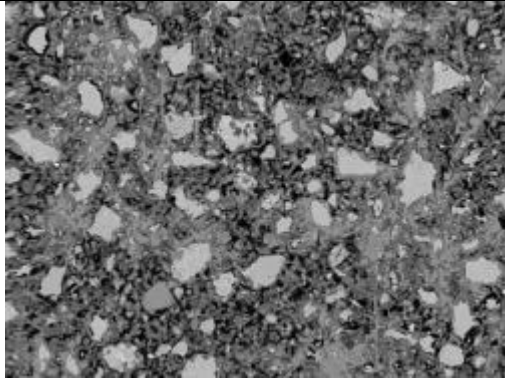
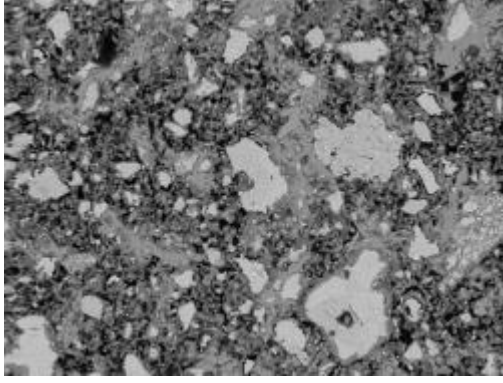
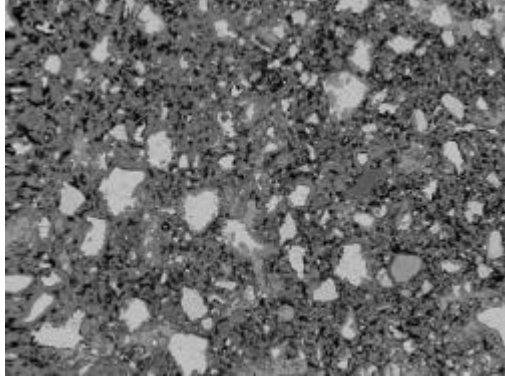
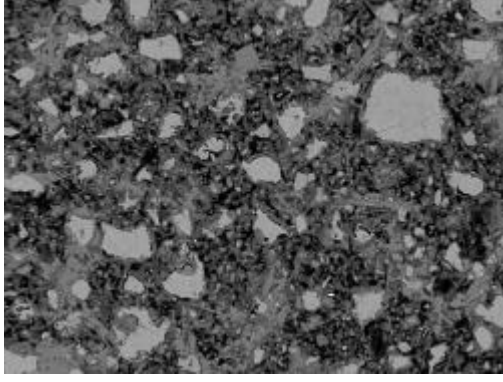
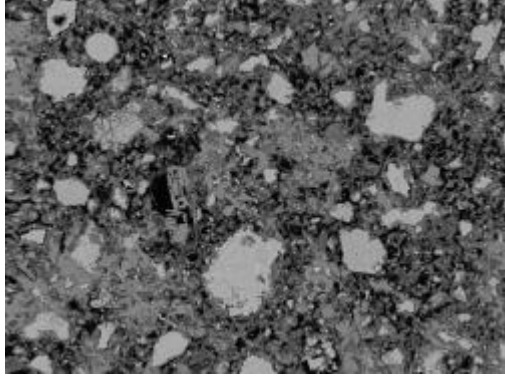
50MPa CEM1 wet mix ambient cured

	
Image 008	Image 009
	
Image 010	Image 011
	
Image 012	Image 013

50MPa CEM1 wet mix ambient cured

	
Image 014	Image 015
	
Image 016	Image 017
	
Image 018	Image 019

50MPa CEM1 wet mix ambient cured

	
Image 020	Image 021
	
Image 022	Image 023
	
Image 025	Image 026

50MPa CEM1 wet mix ambient cured

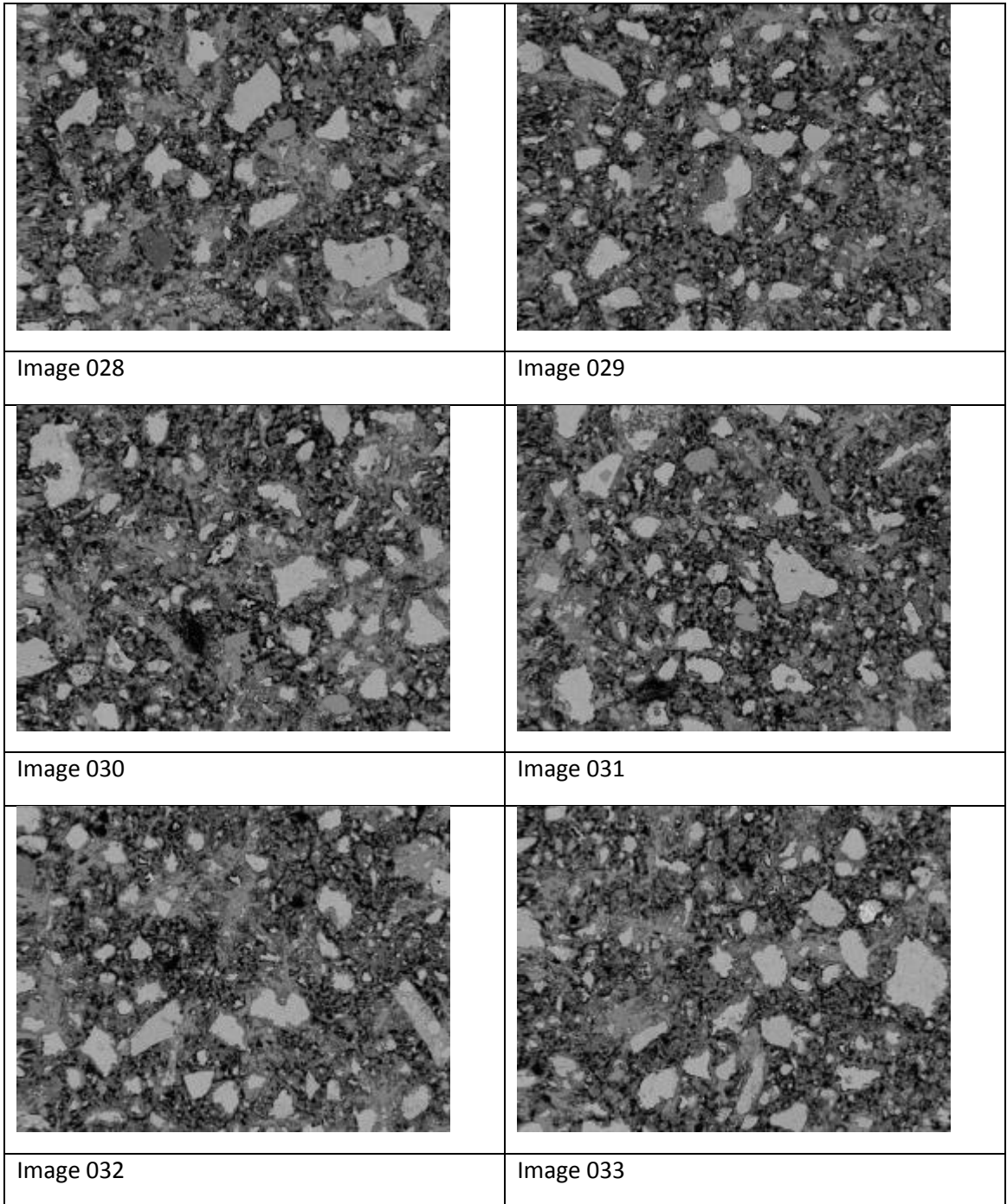
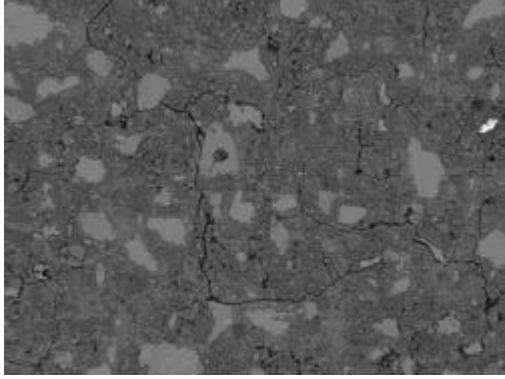
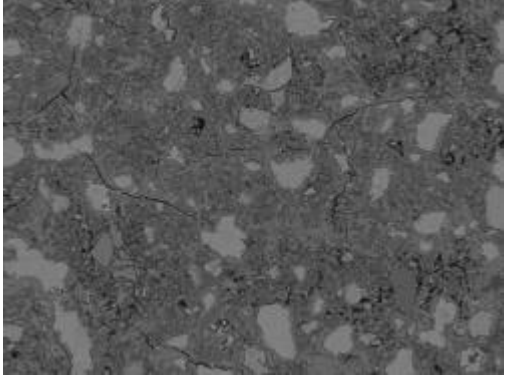
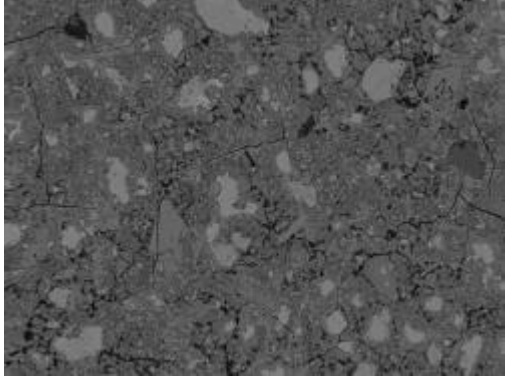
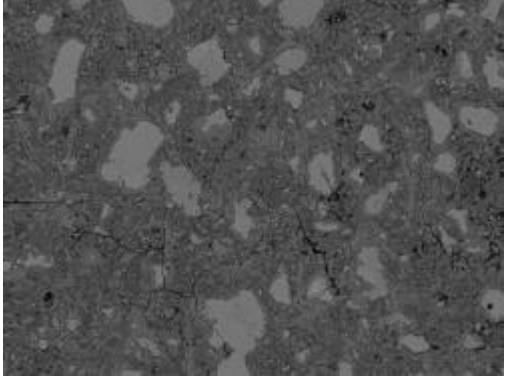
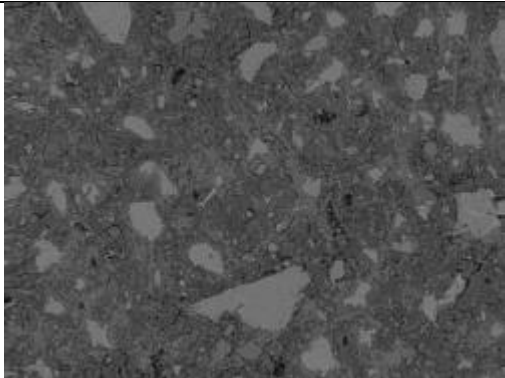
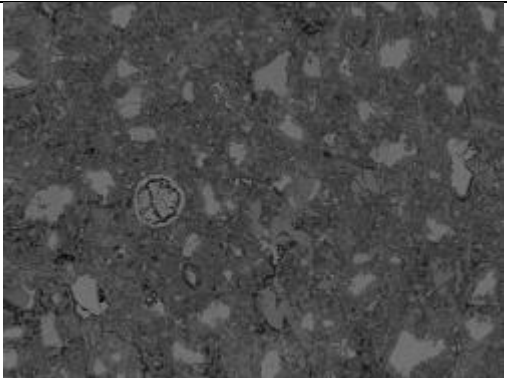
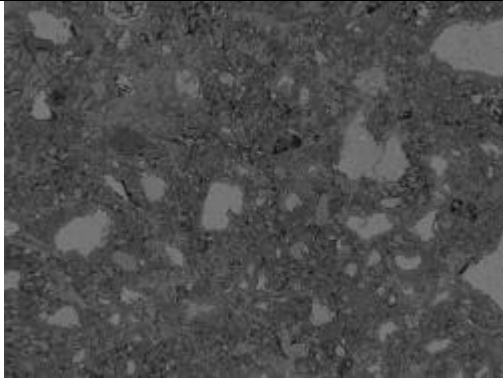
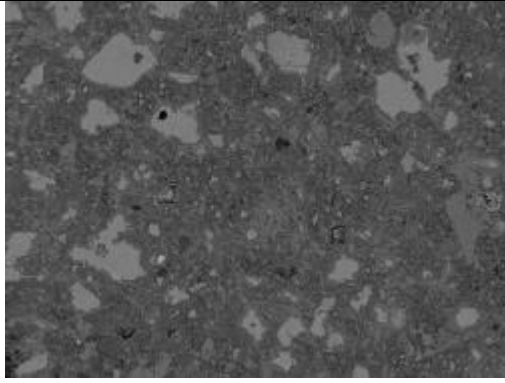
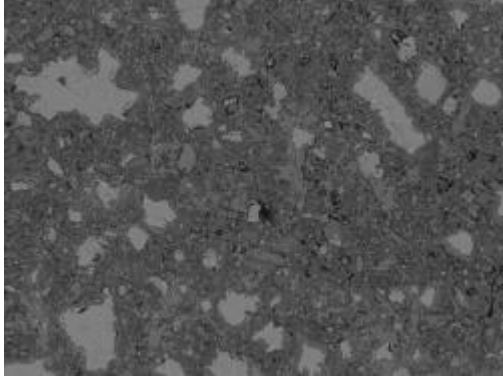
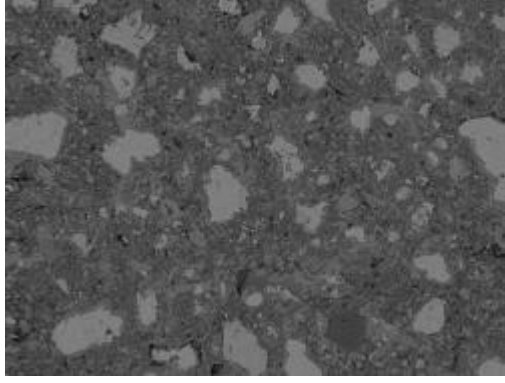
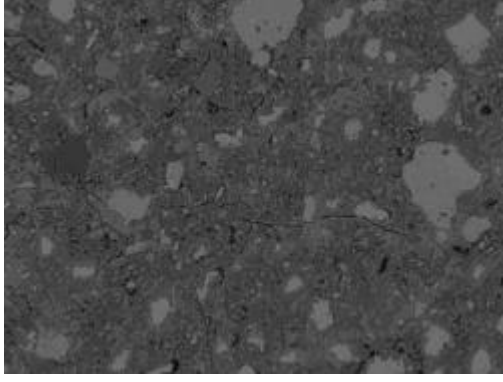
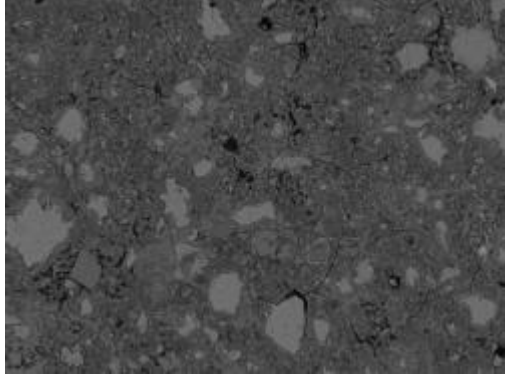


Figure A 99 Images of 50MPa CEM1 wet mix ambient cured

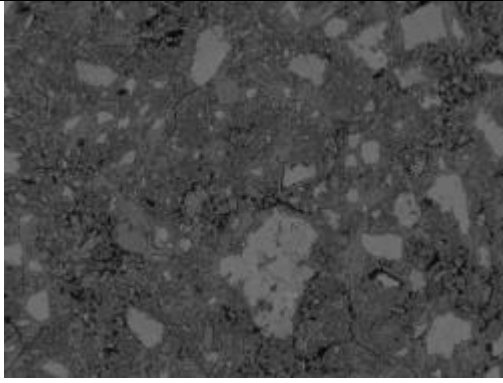
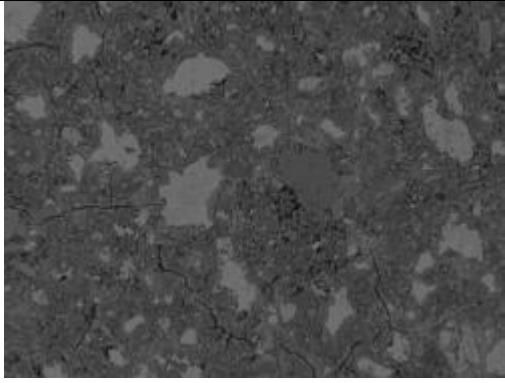
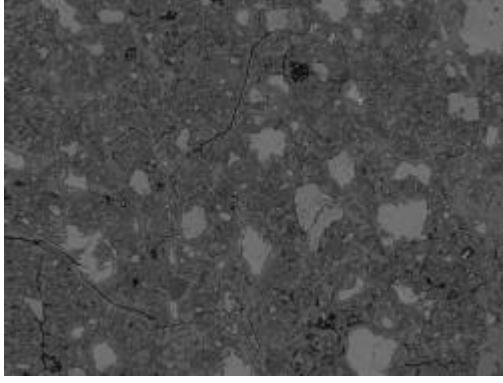
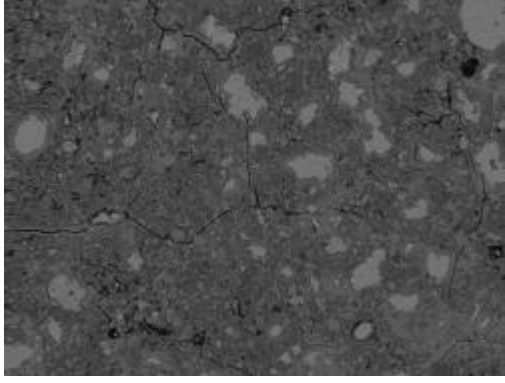
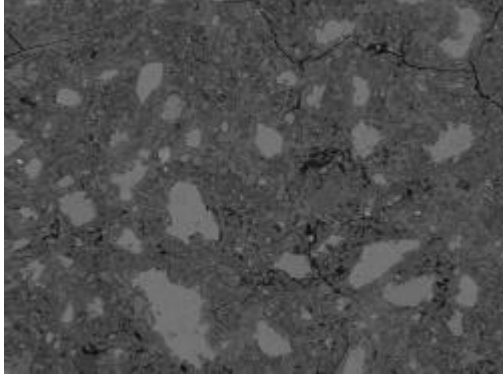
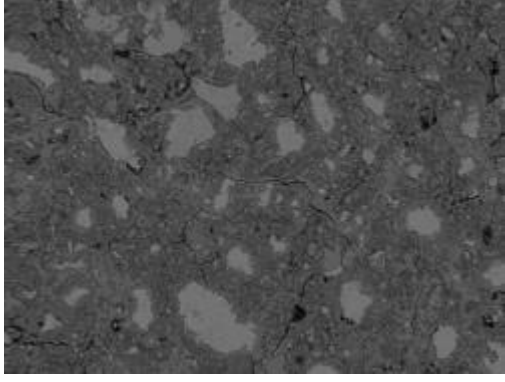
M5W

	
Image 001	Image 002
	
Image 004	Image 005
	
Image 006	Image 007

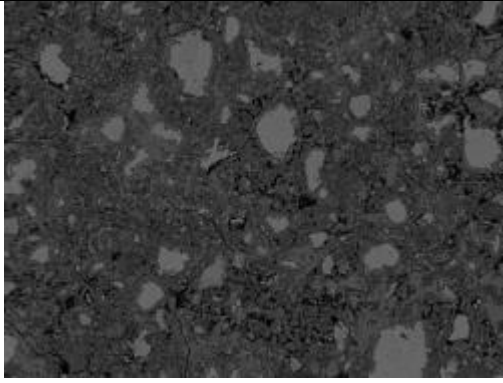
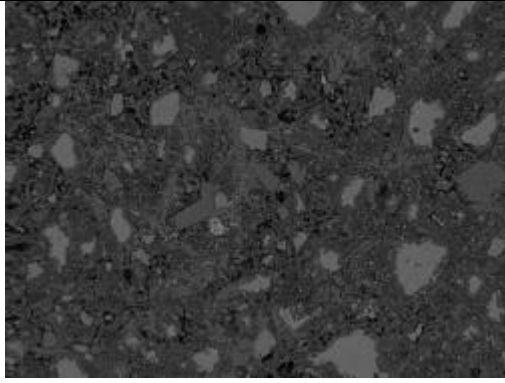
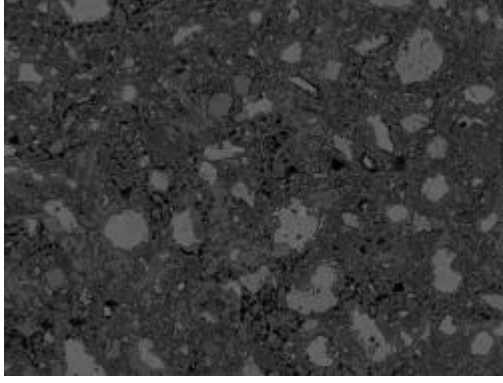
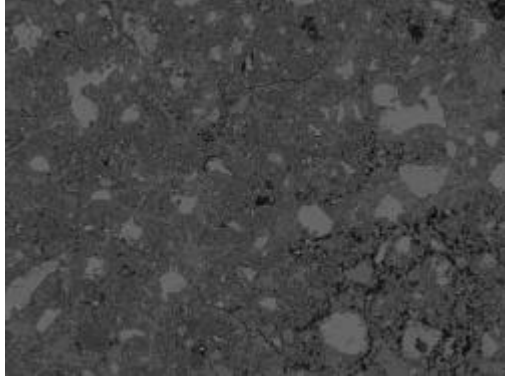
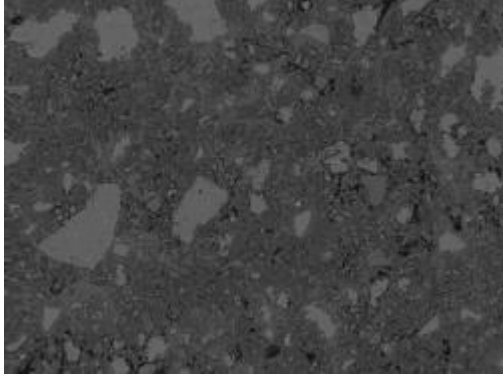
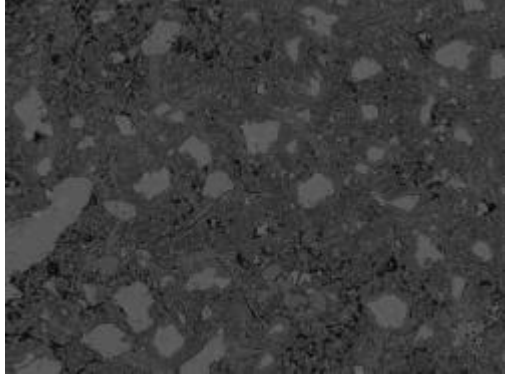
50MPa CEM1 wet mix ideal cured

	
Image 008	Image 009
	
Image 010	Image 011
	
Image 013	Image 014

50MPa CEM1 wet mix ideal cured

	
Image 015	Image 016
	
Image 017	Image 019
	
Image 020	Image 021

50MPa CEM1 wet mix ideal cured

	
Image 023	Image 024
	
Image 025	Image 026
	
Image 028	Image 029

50MPa CEM1 wet mix ideal cured

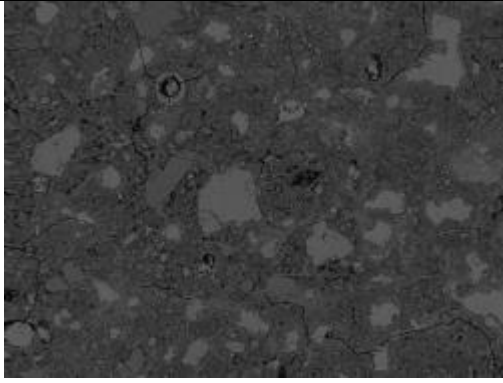
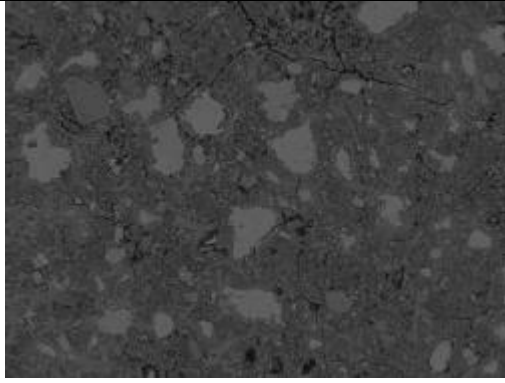
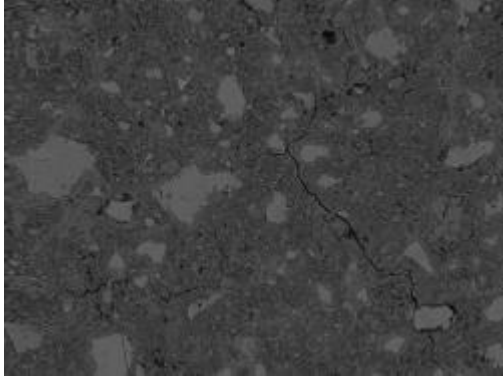
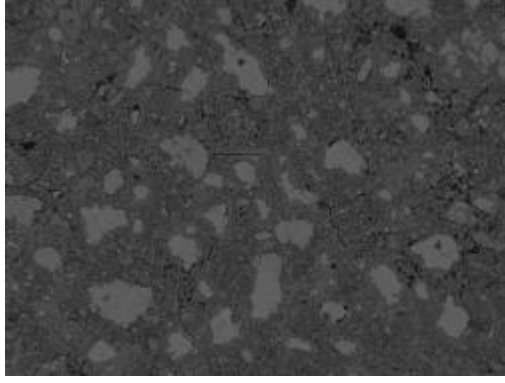
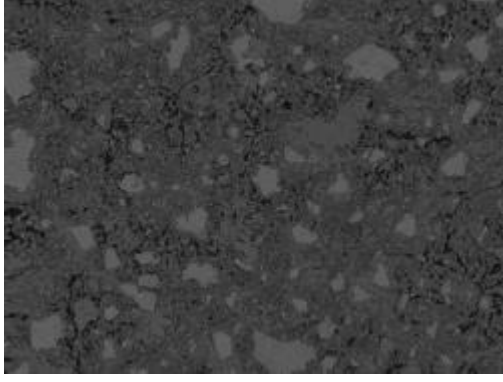
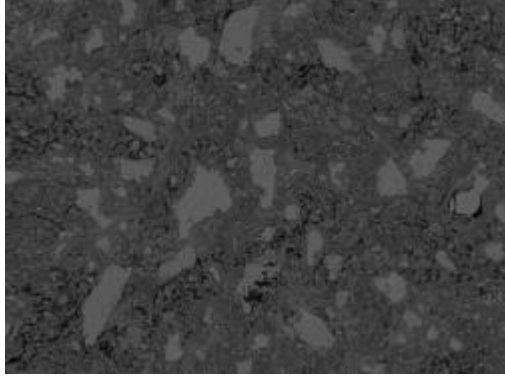
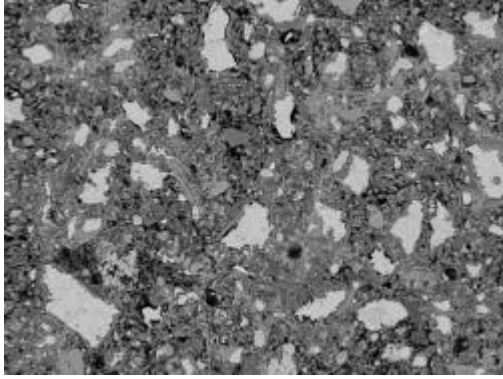
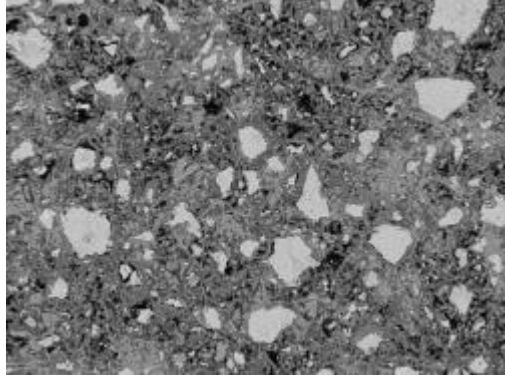
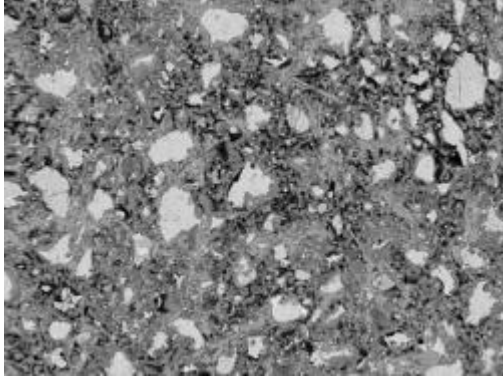
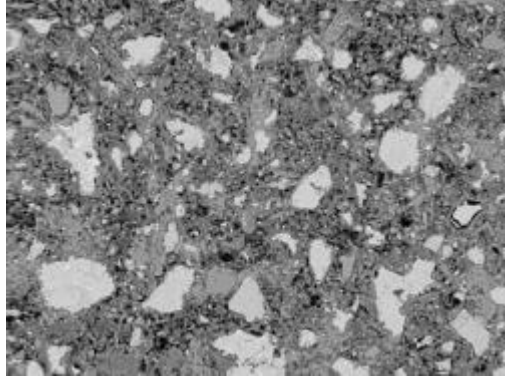
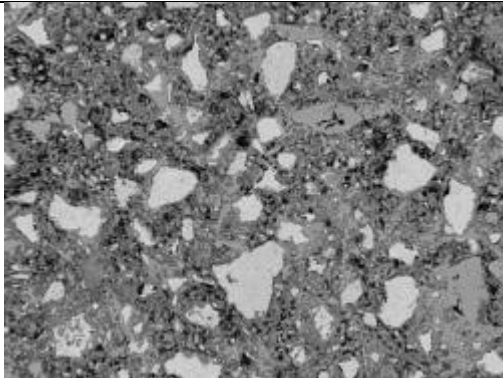
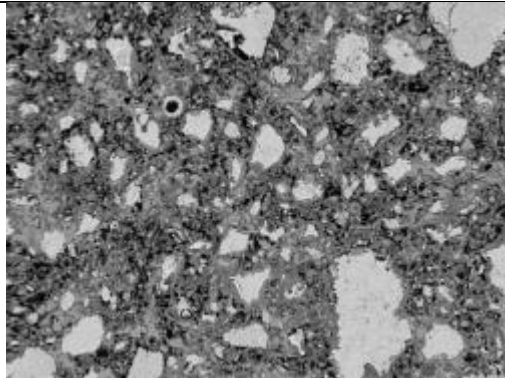
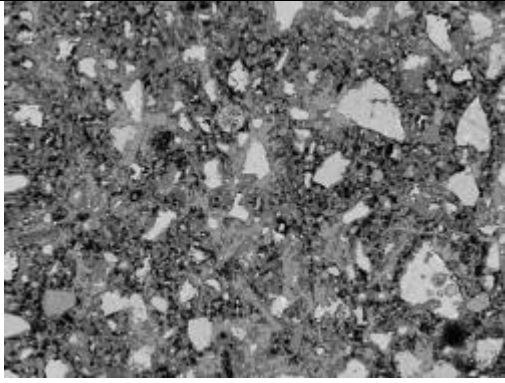
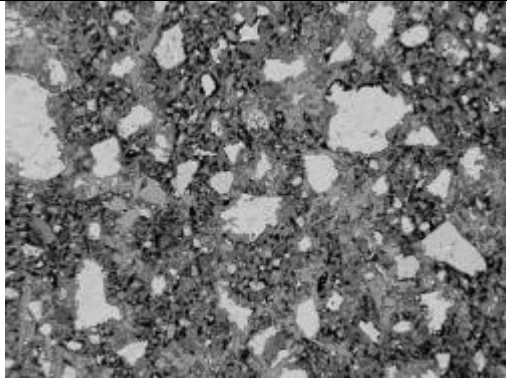
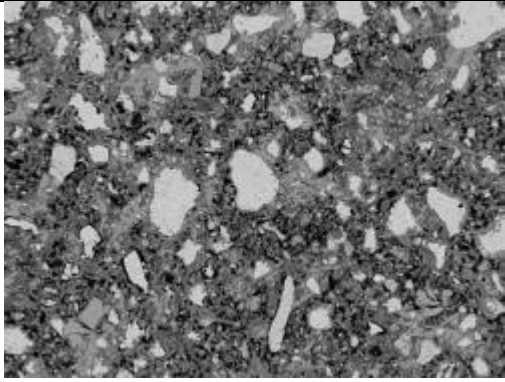
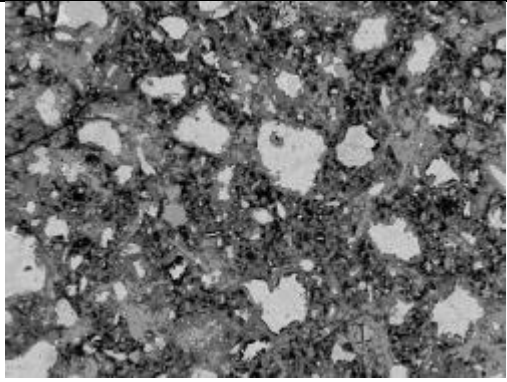
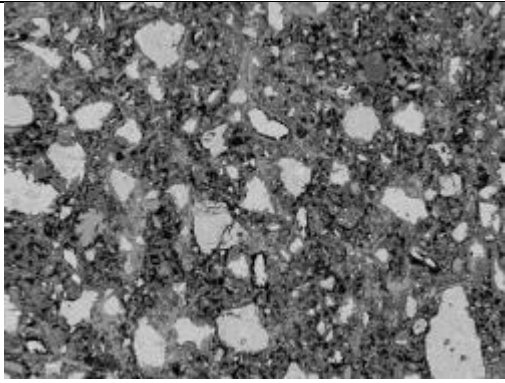
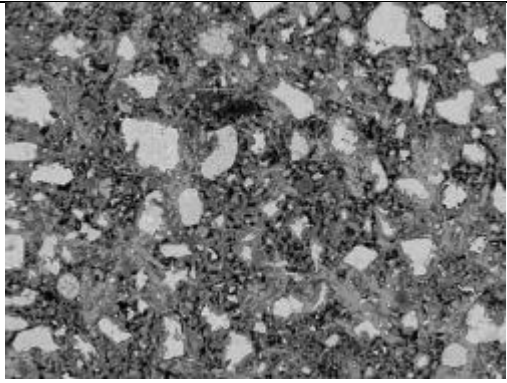
	
Image 030	Image 031
	
Image 032	Image 033
	
Image 035	Image 036

Figure A 100 Images of 50MPa CEM1 wet mix ideal cured

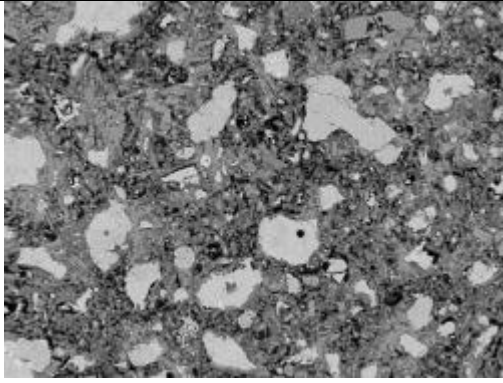
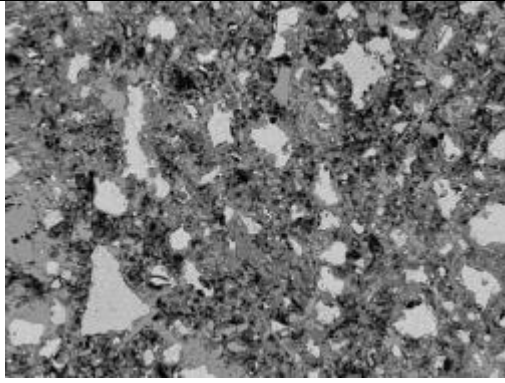
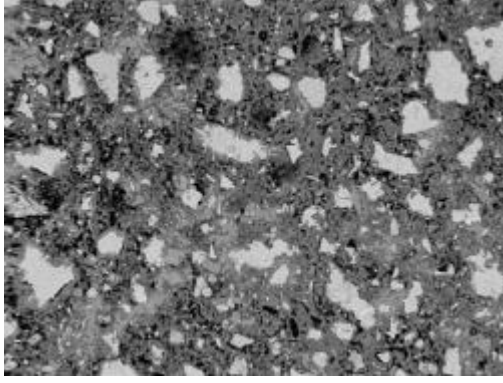
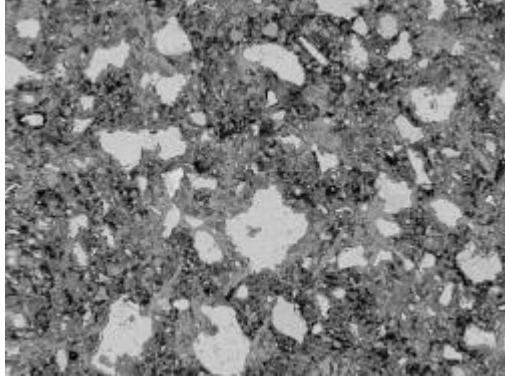
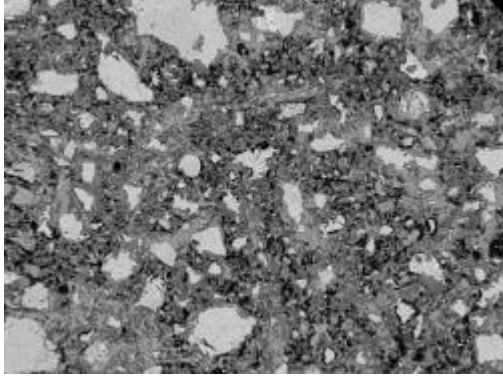
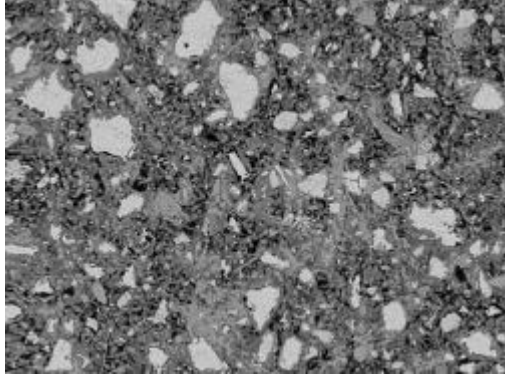
M6 A

	
Image 002	Image 003
	
Image 004	Image 005
	
Image 006	Image 007

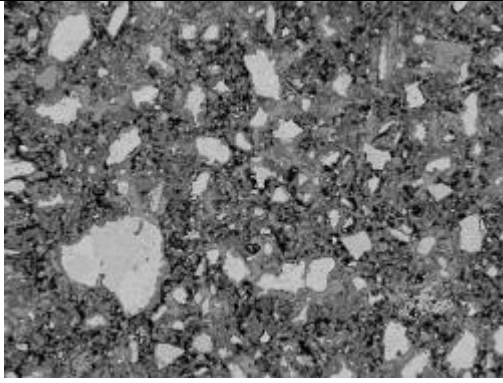
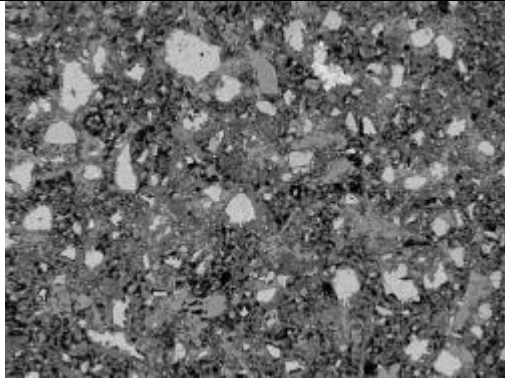
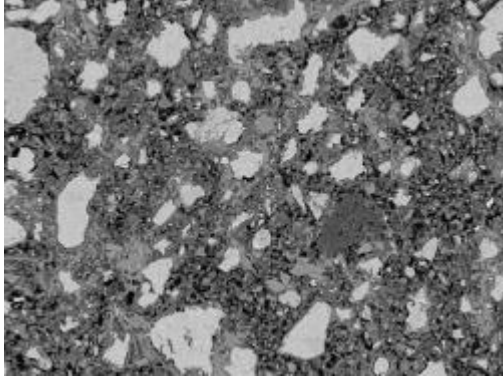
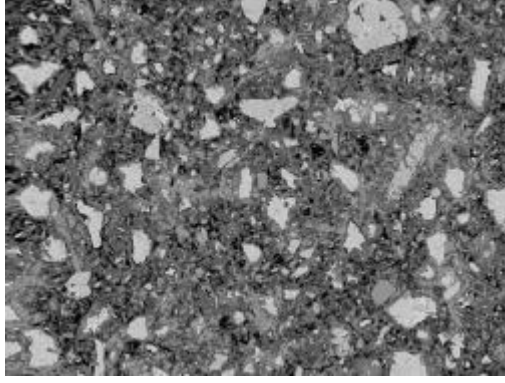
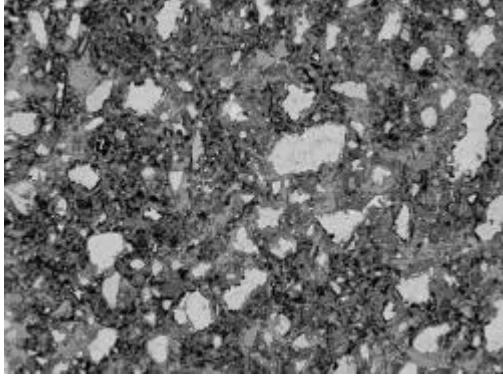
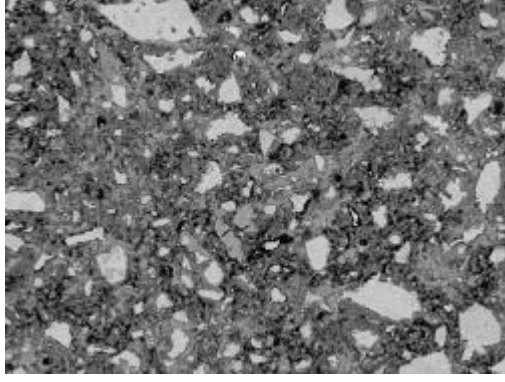
80MPa CEM1 wet mix ambient cured

	
Image 008	Image 009
	
Image 010	Image 011
	
Image 012	Image 013

80MPa CEM1 wet mix ambient cured

	
Image 015	Image 016
	
Image 018	Image 020
	
Image 021	Image 022

80MPa CEM1 wet mix ambient cured

	
Image 023	Image 024
	
Image 025	Image 026
	
Image 027	Image 028

80MPa CEM1 wet mix ambient cured

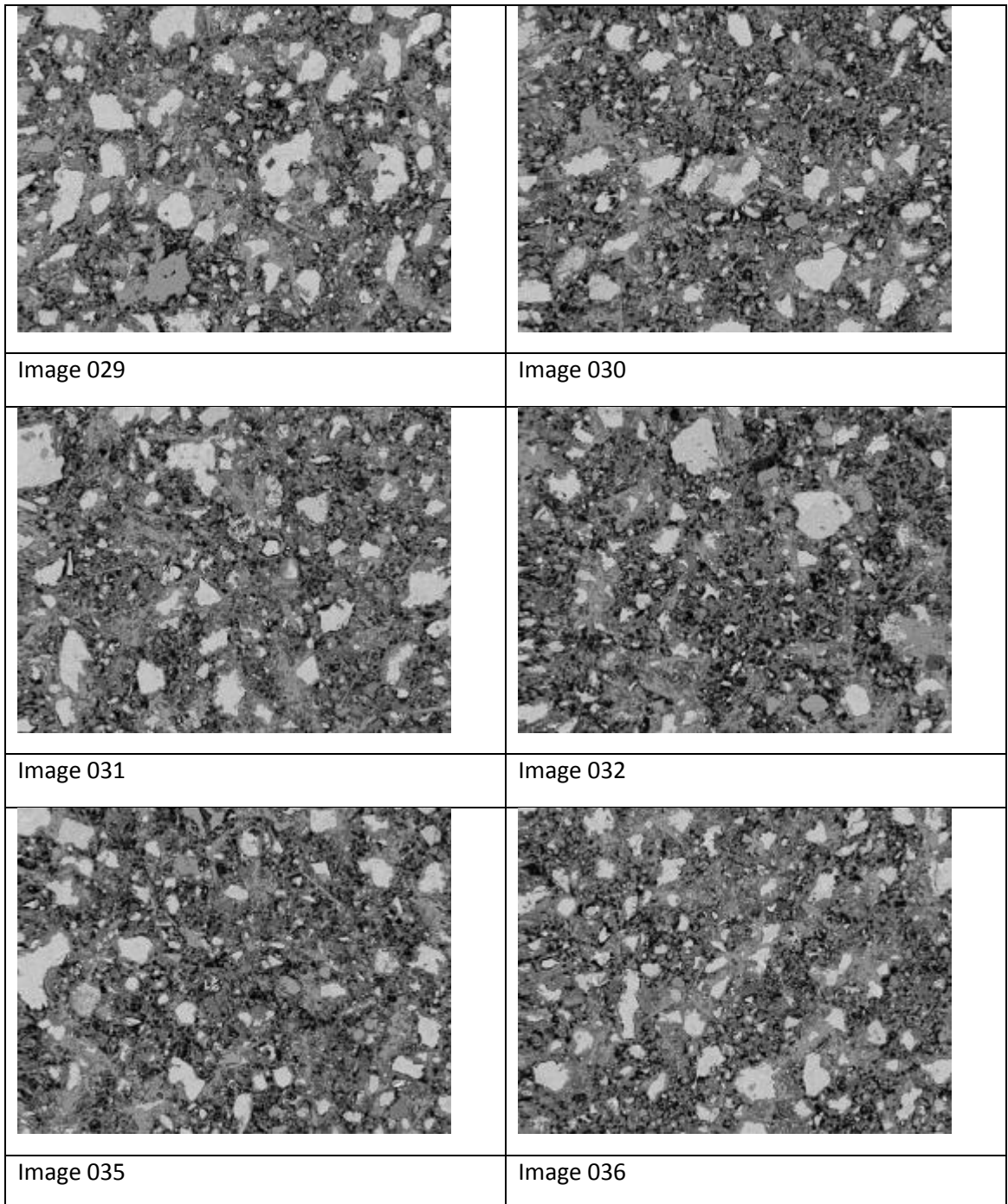
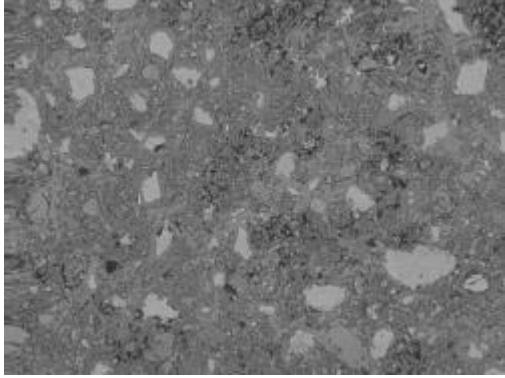
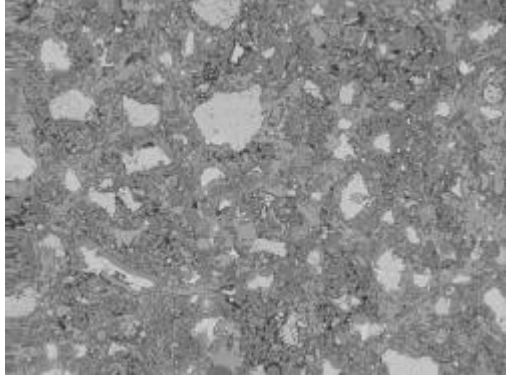
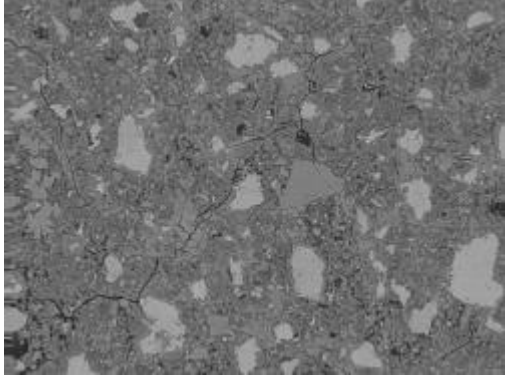
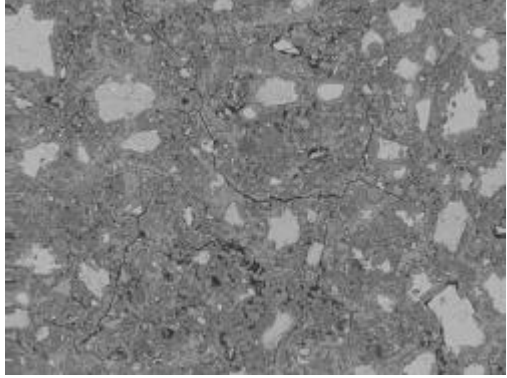
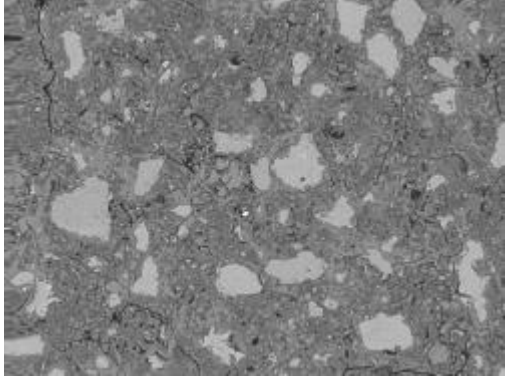
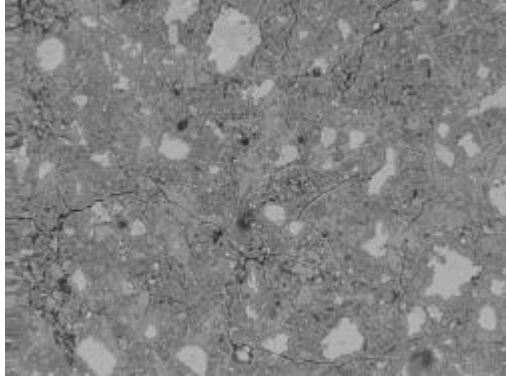
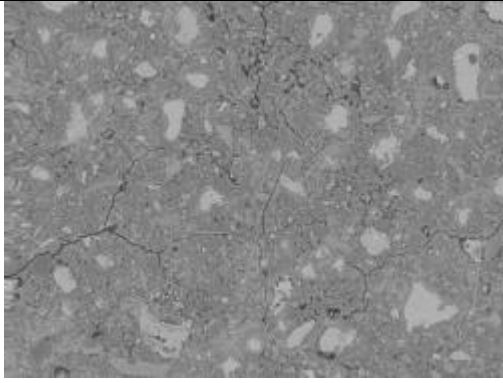
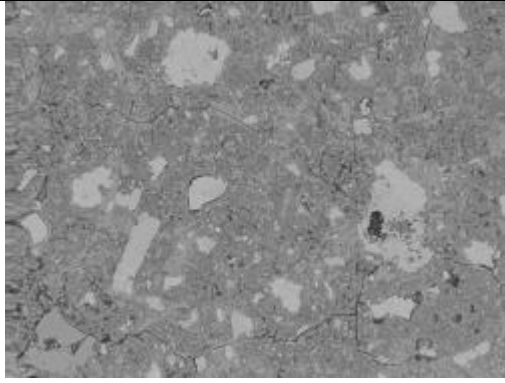
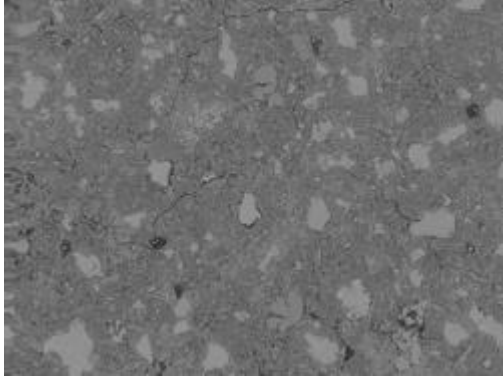
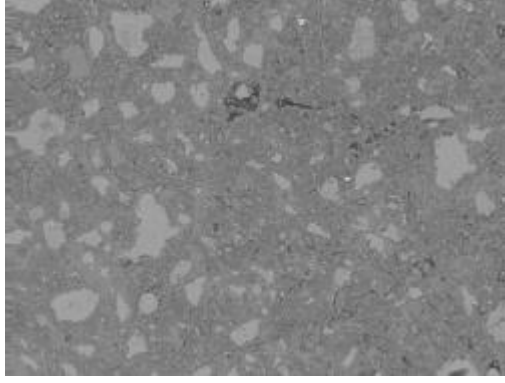
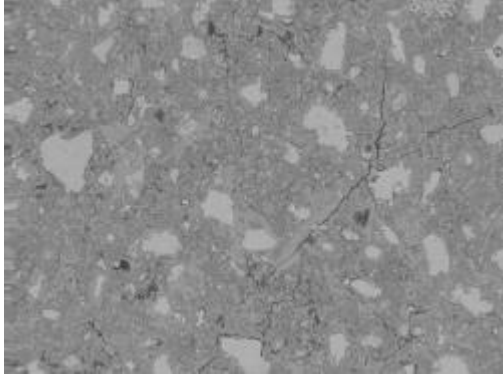
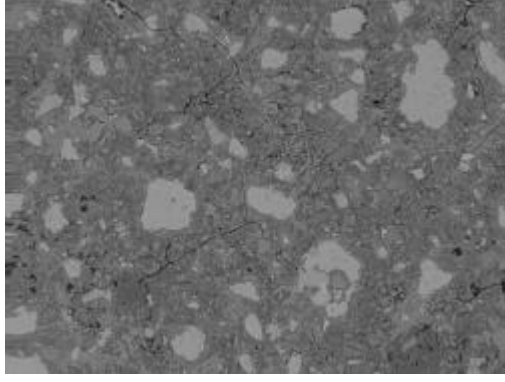


Figure A 101 Images of 80MPa CEM1 wet mix ambient cured

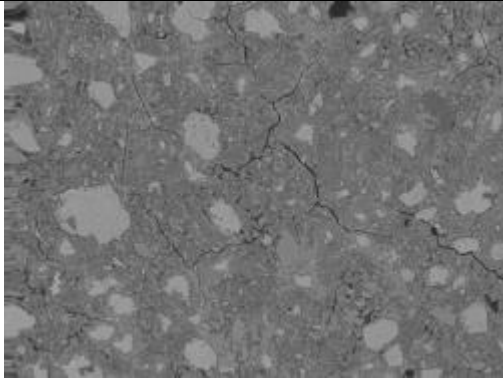
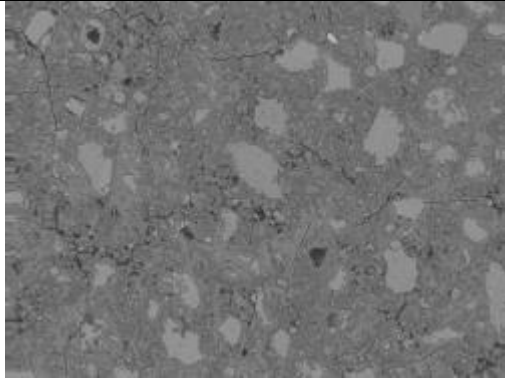
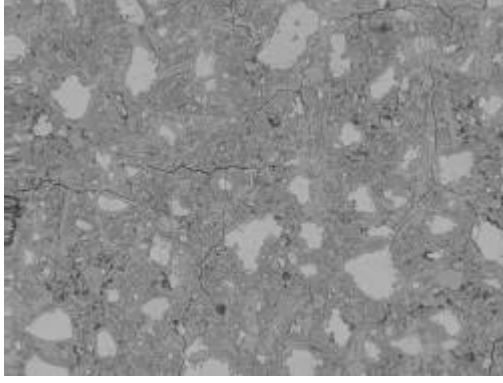
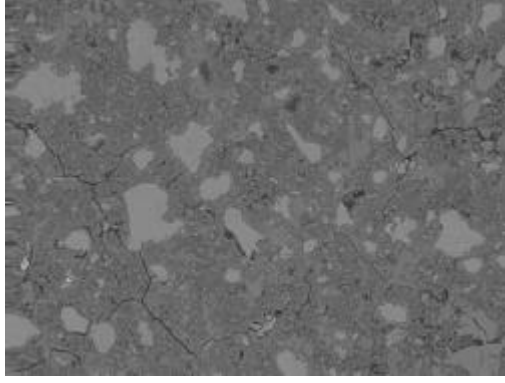
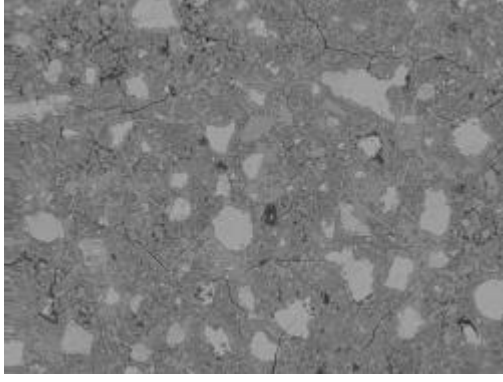
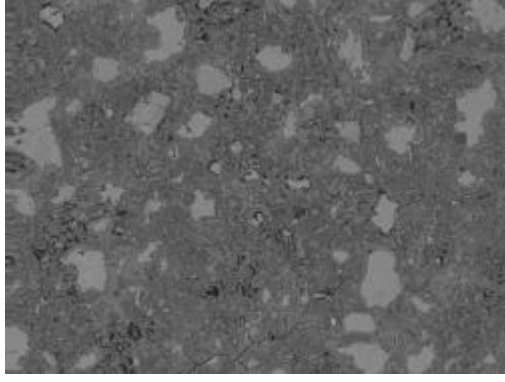
M6W

	
Image 002	Image 003
	
Image 004	Image 005
	
Image 006	Image 007

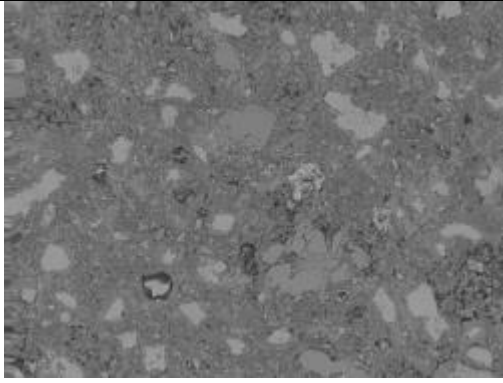
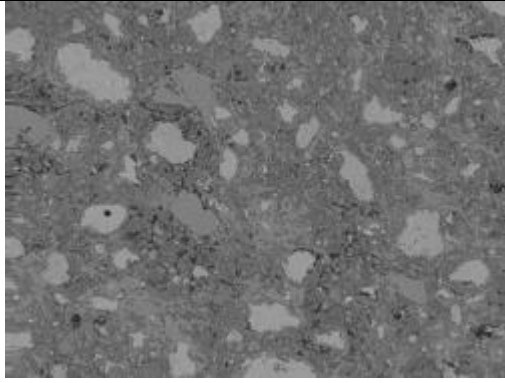
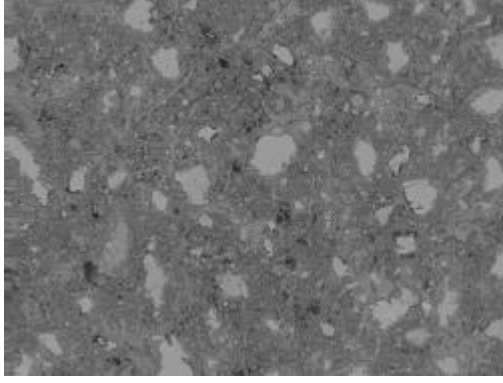
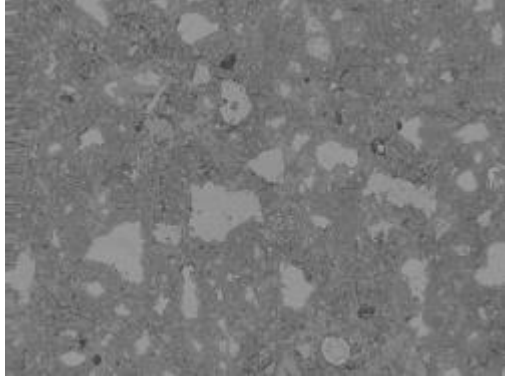
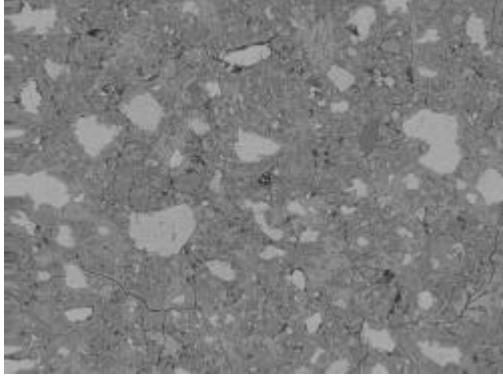
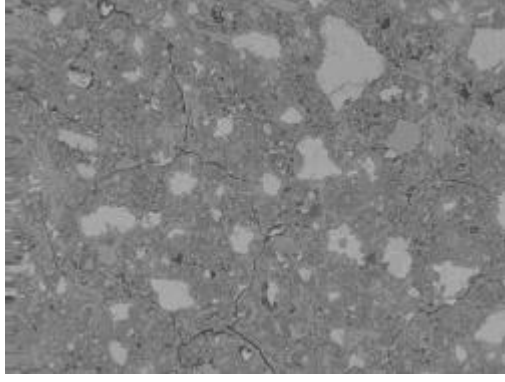
80MPa CEM1 wet mix ideal cured

	
Image 008	Image 009
	
Image 010	Image 011
	
Image 013	Image 014

80MPa CEM1 wet mix ideal cured

	
Image 015	Image 016
	
Image 017	Image 018
	
Image 019	Image 020

80MPa CEM1 wet mix ideal cured

	
Image 021	Image 022
	
Image 024	Image 025
	
Image 026	Image 027

80MPa CEM1 wet mix ideal cured

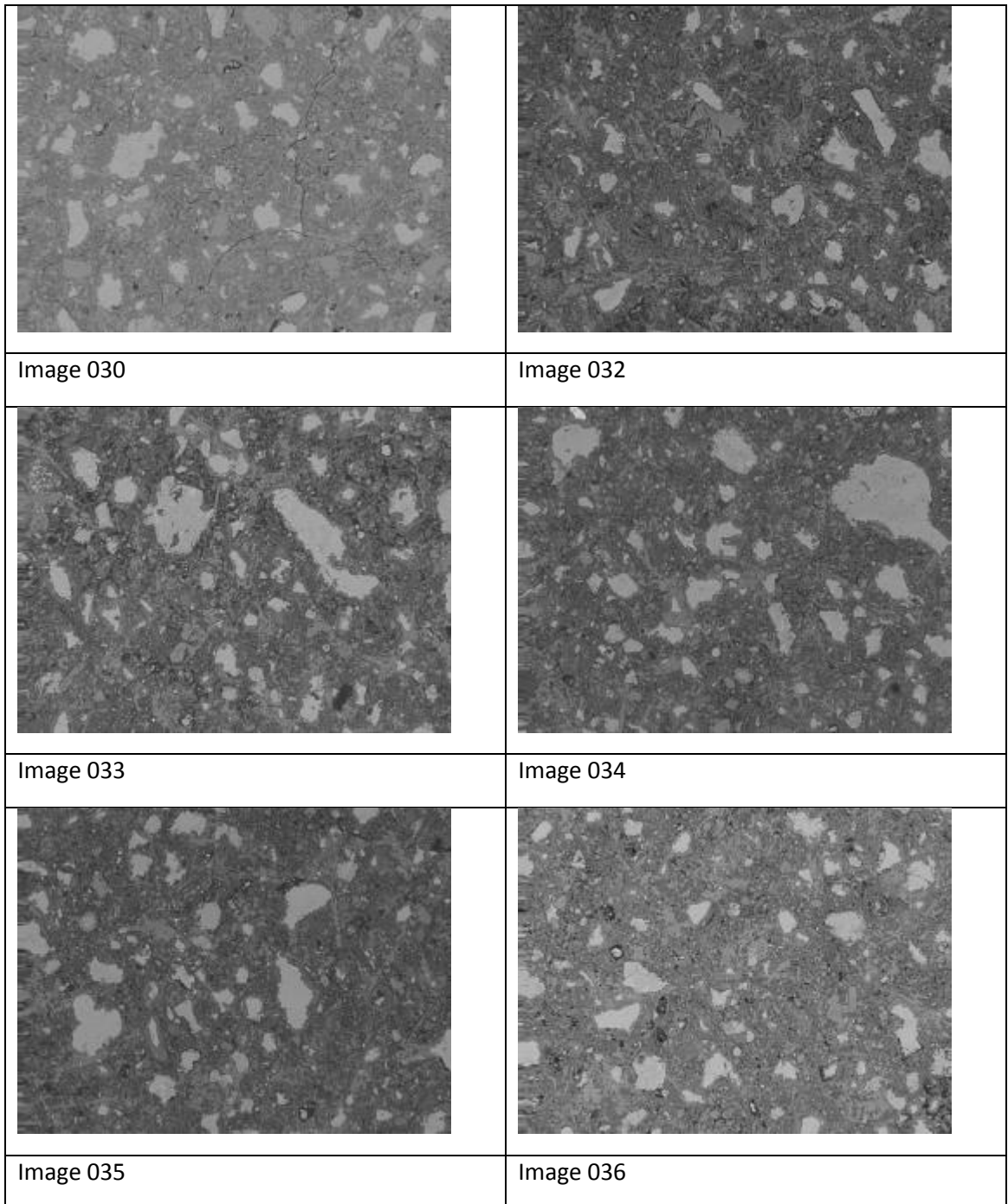
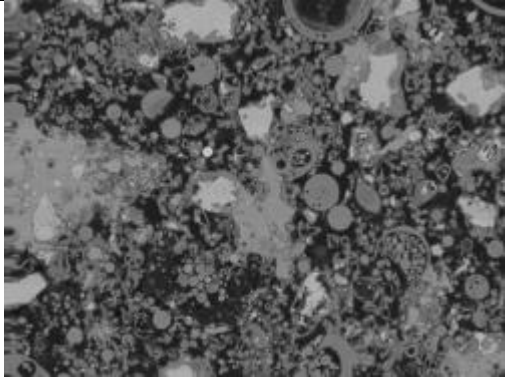
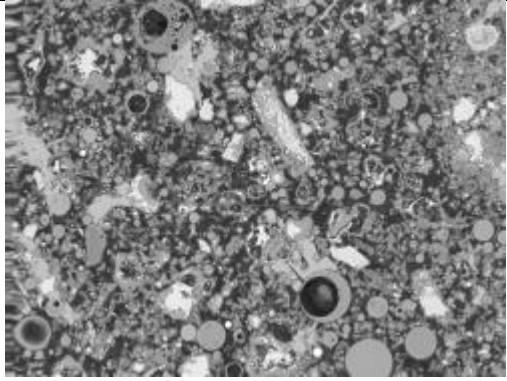
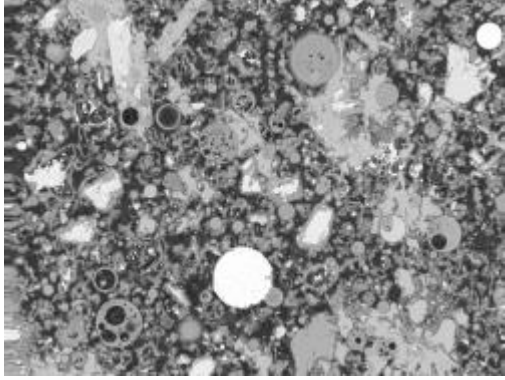
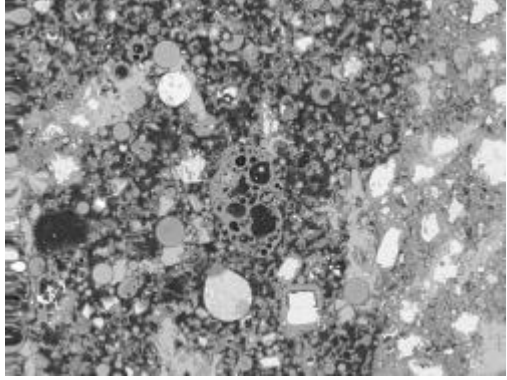
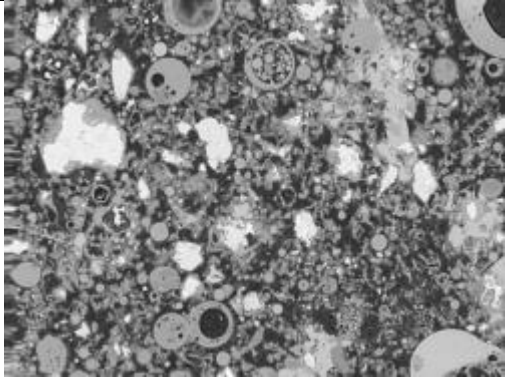
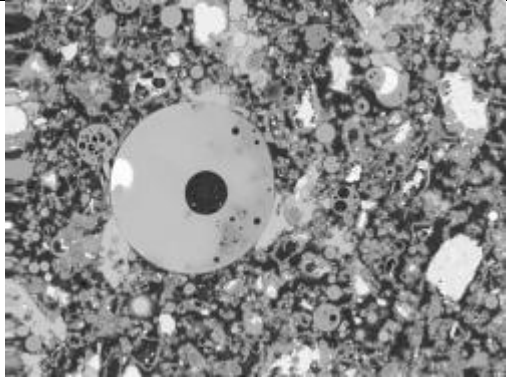
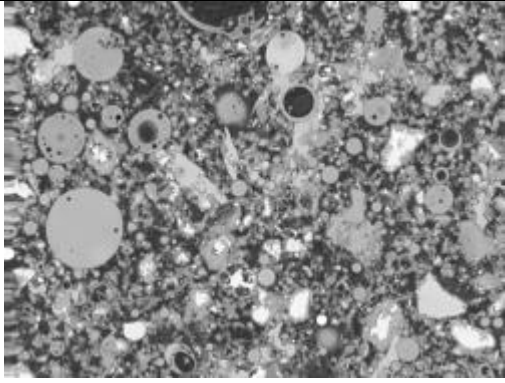
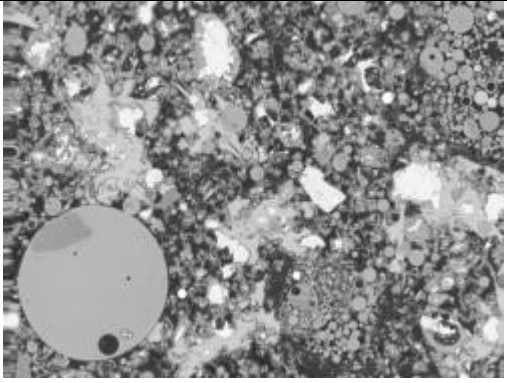
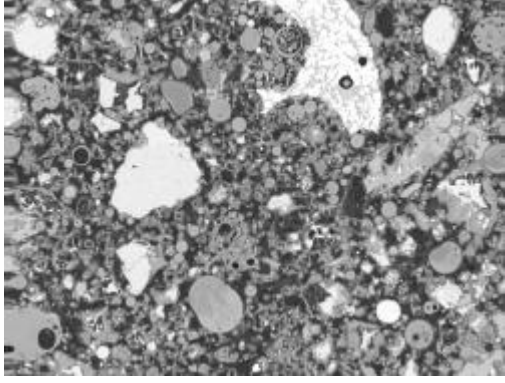
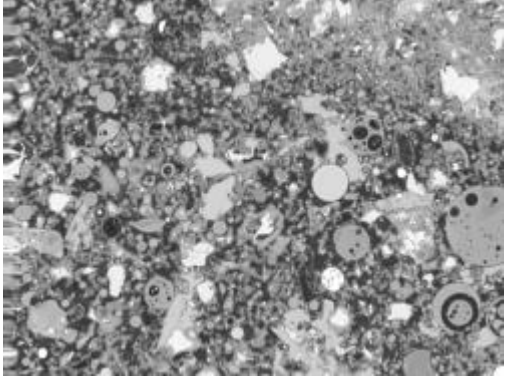
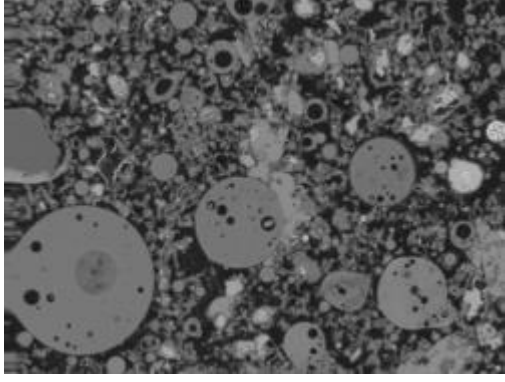
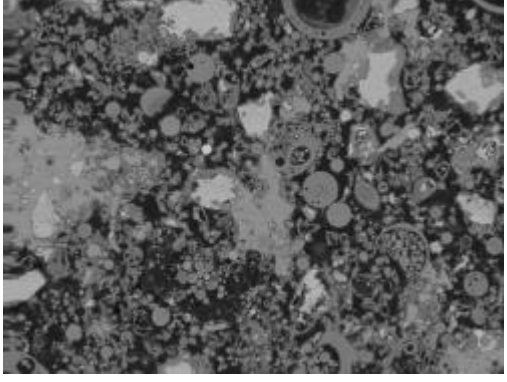


Figure A 102 Images of 80MPa CEM1 wet mix ideal cured

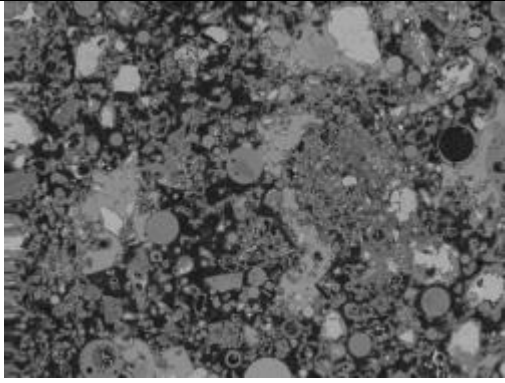
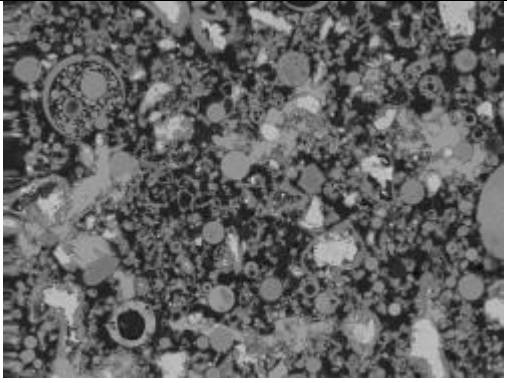
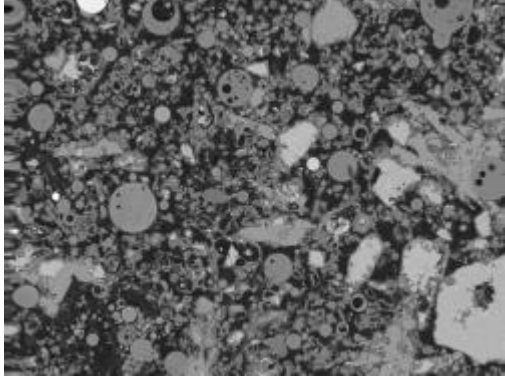
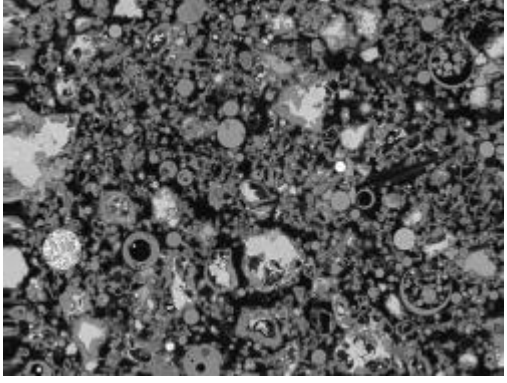
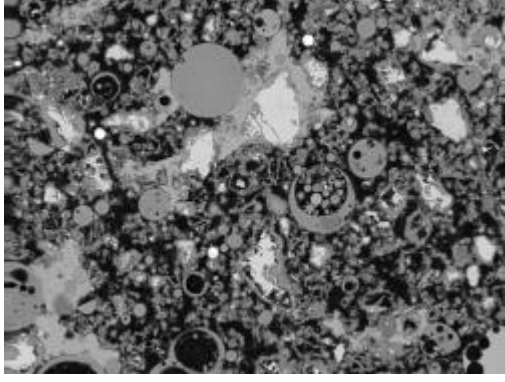
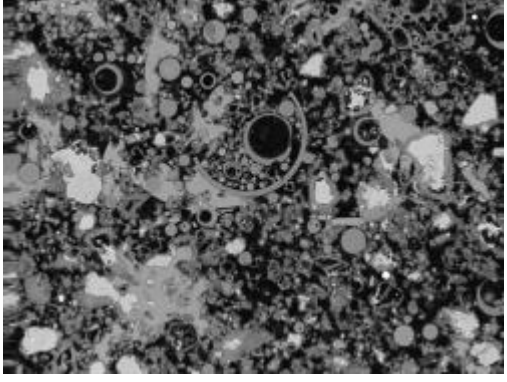
M7A

	
Image 001	Image 003
	
Image 005	Image 006
	
Image 007	Image 008

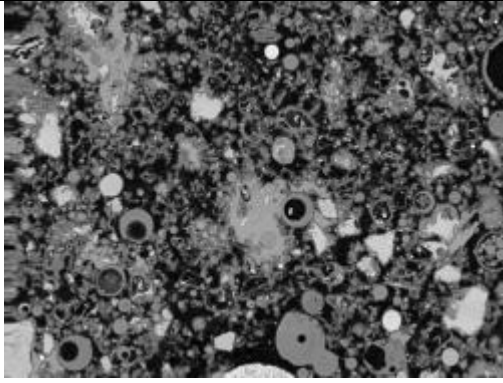
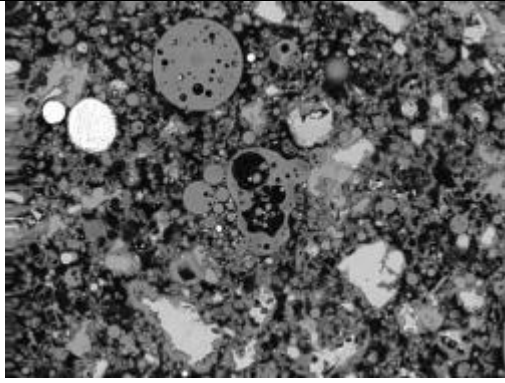
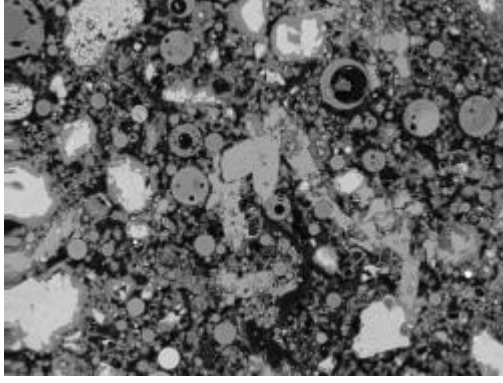
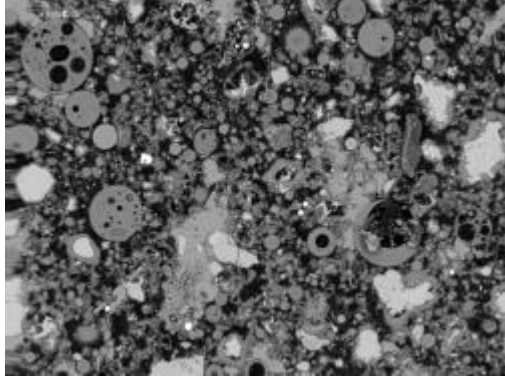
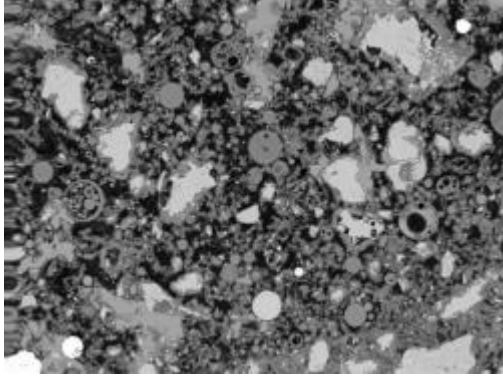
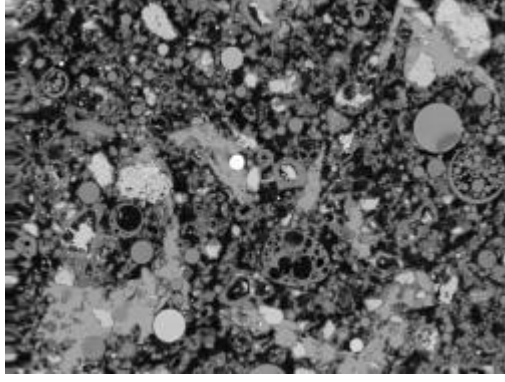
20MPa Fly ash stiff mix ambient cured

	
Image 010	Image 011
	
Image 012	Image 013
	
Image 016	Image 018

20MPa Fly ash stiff mix ambient cured

	
Image 019	Image 023
	
Image 024	Image 025
	
Image 026	Image 027

20MPa Fly ash stiff mix ambient cured

	
Image 028	Image 029
	
Image 030	Image 031
	
Image 032	Image 033

20MPa Fly ash stiff mix ambient cured

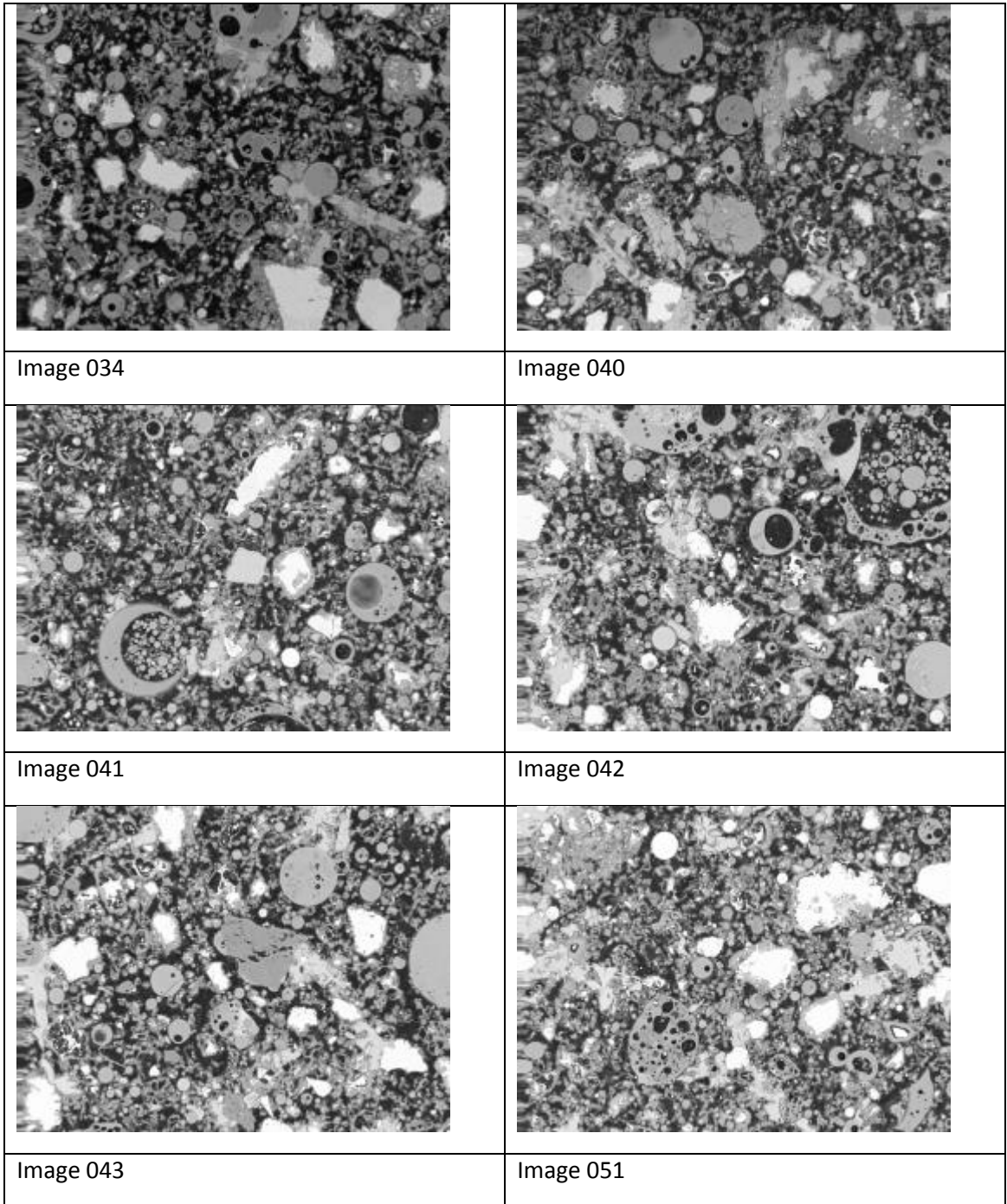
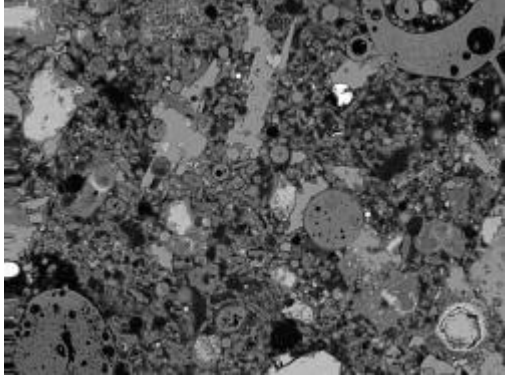
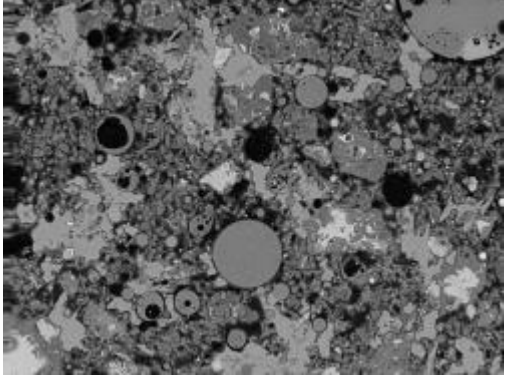
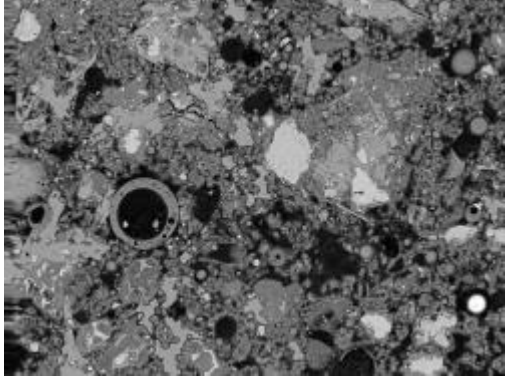
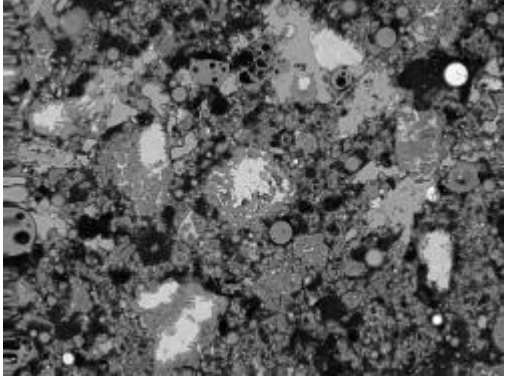
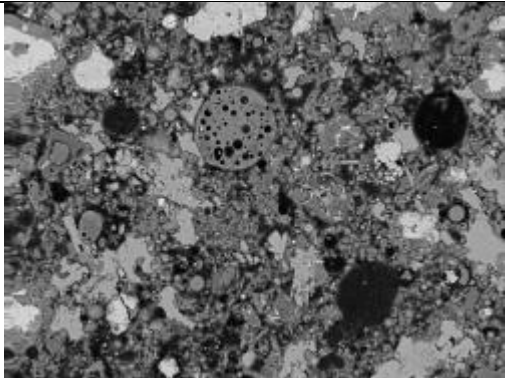
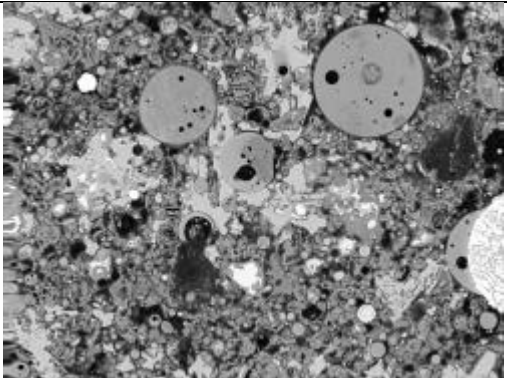


Figure A 103 Images of 20MPa Fly ash stiff mix ambient cured

M7W

	
Image 006	Image 007
	
Image 008	Image
	
Image 010	Image 013

20MPa Fly ash stiff mix ideal cured

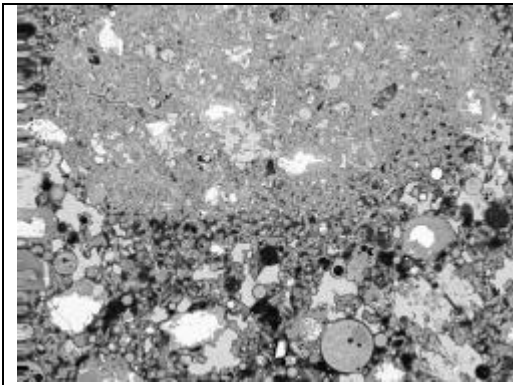


Image 014

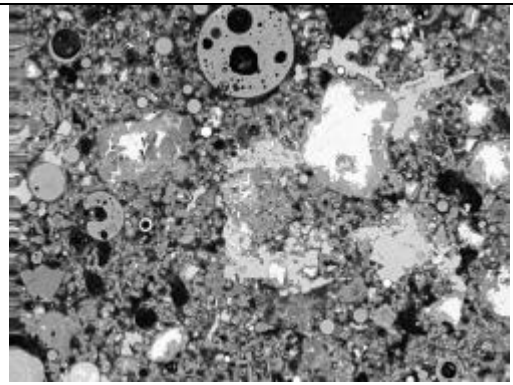


Image 016

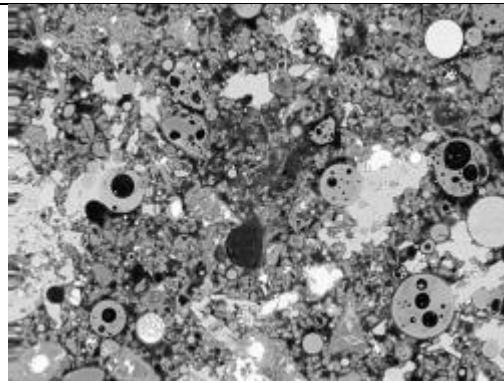


Image 017

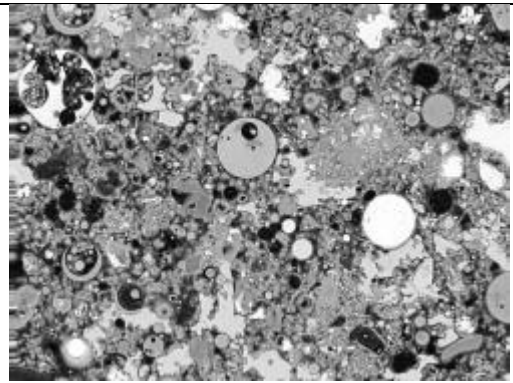


Image 018

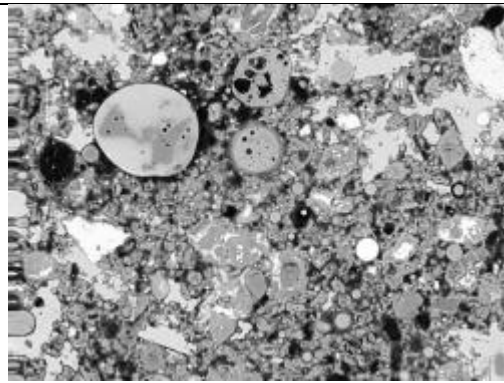


Image 019

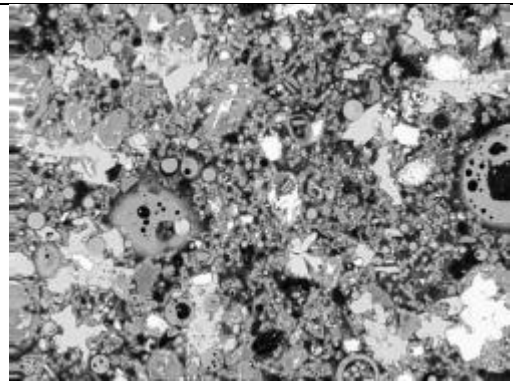
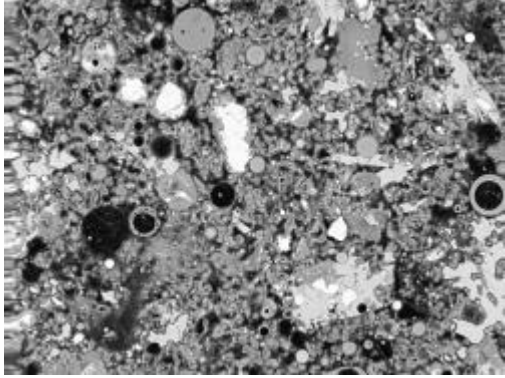
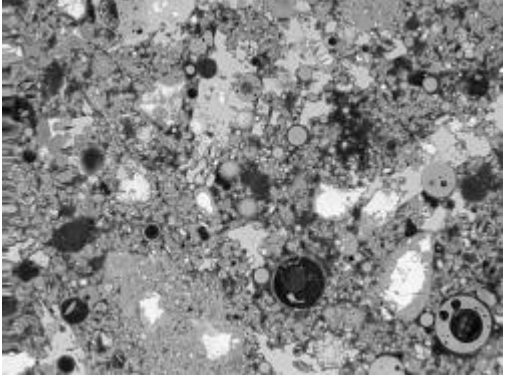
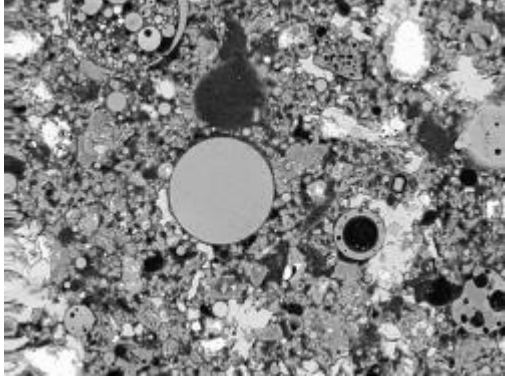
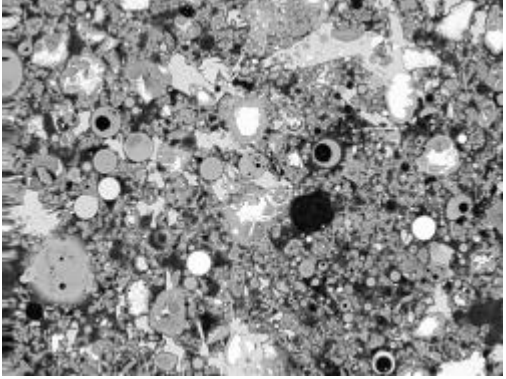
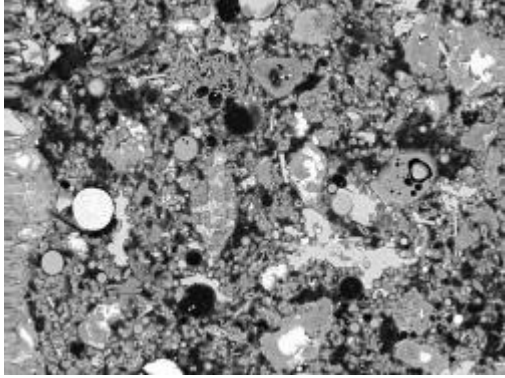
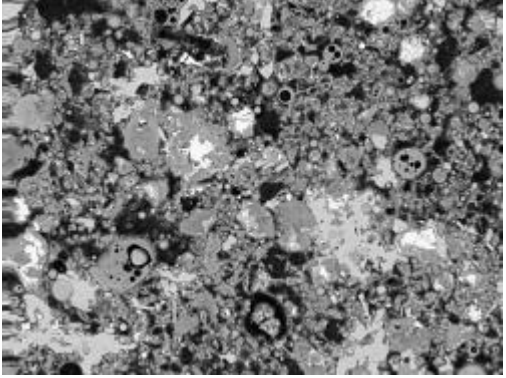
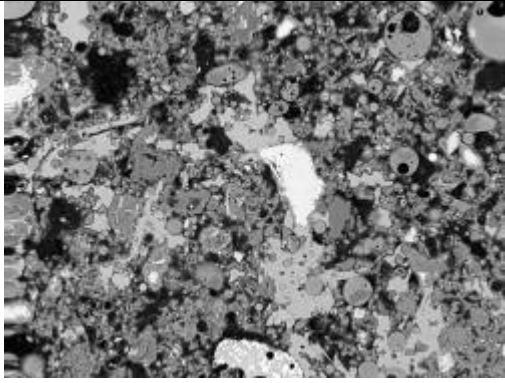
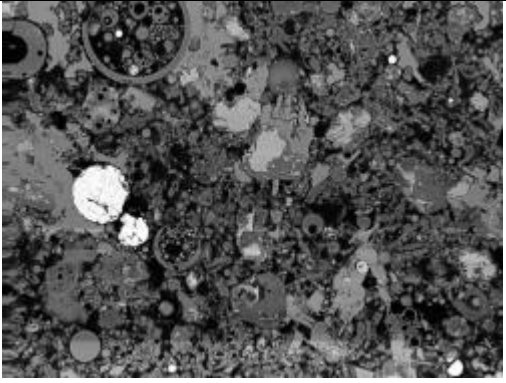
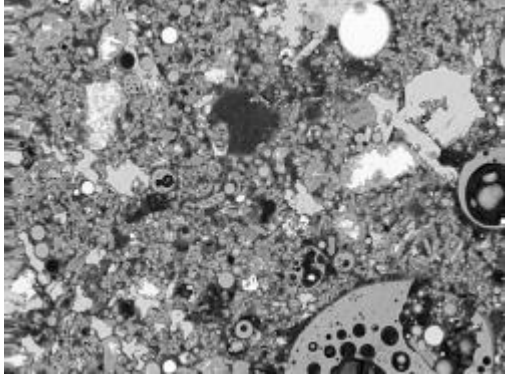
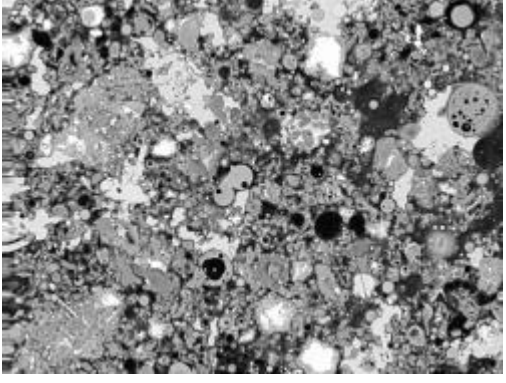
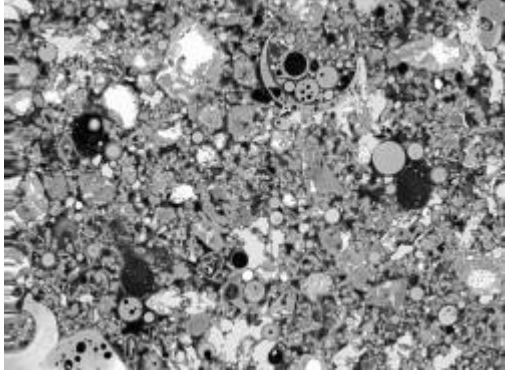
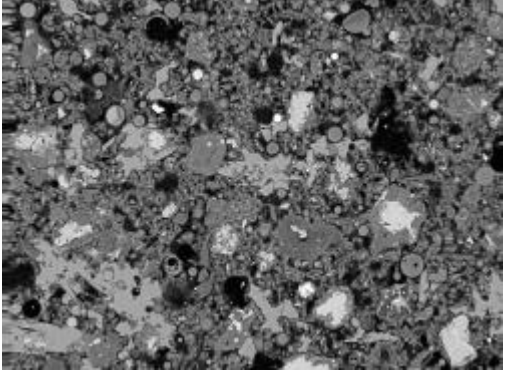


Image 020

20MPa Fly ash stiff mix ideal cured

	
Image 021	Image 022
	
Image 027	Image 028
	
Image 029	Image 030

20MPa Fly ash stiff mix ideal cured

	
Image 031	Image 032
	
Image 033	Image 035
	
Image 038	Image 040

20MPa Fly ash stiff mix ideal cured

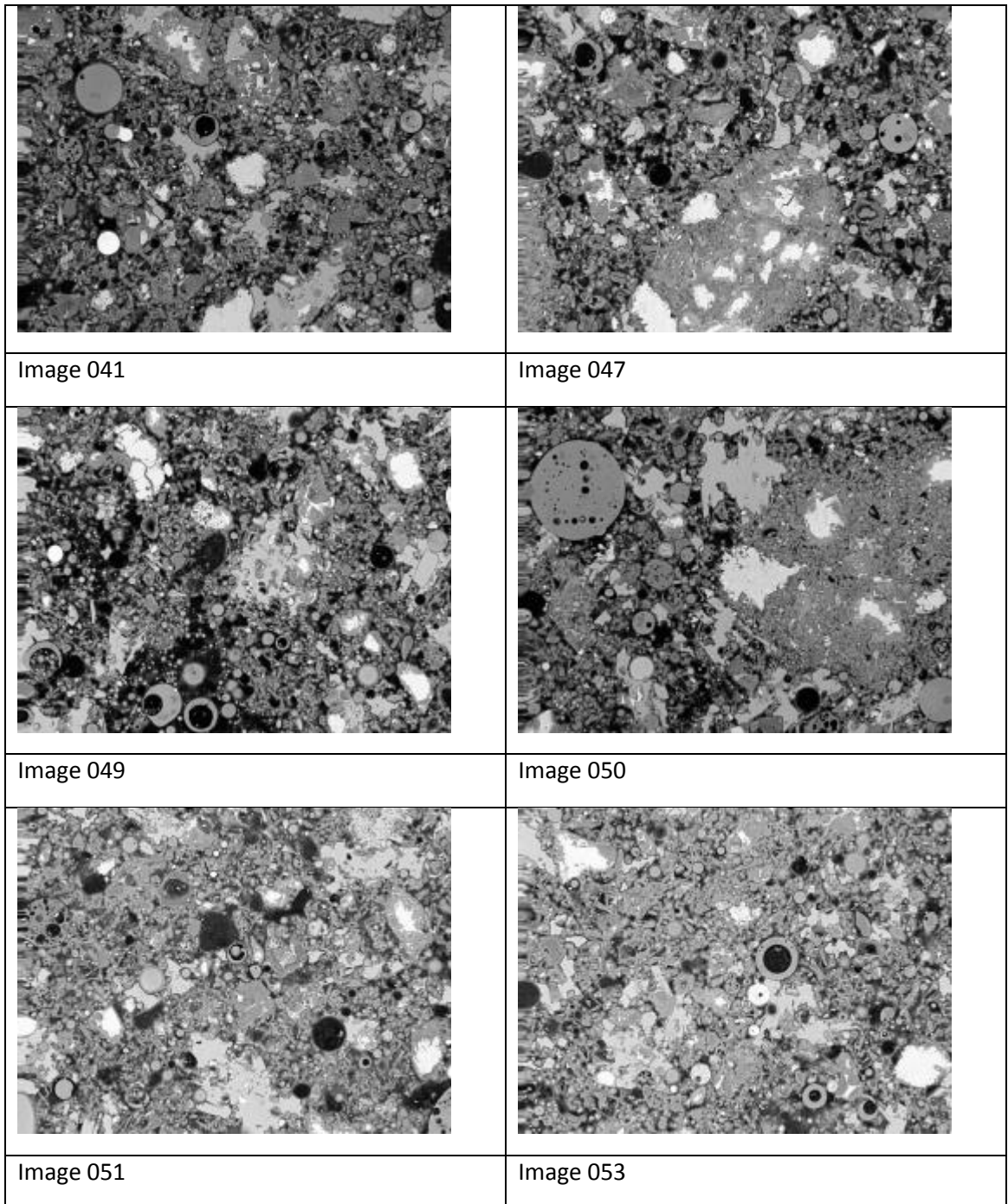
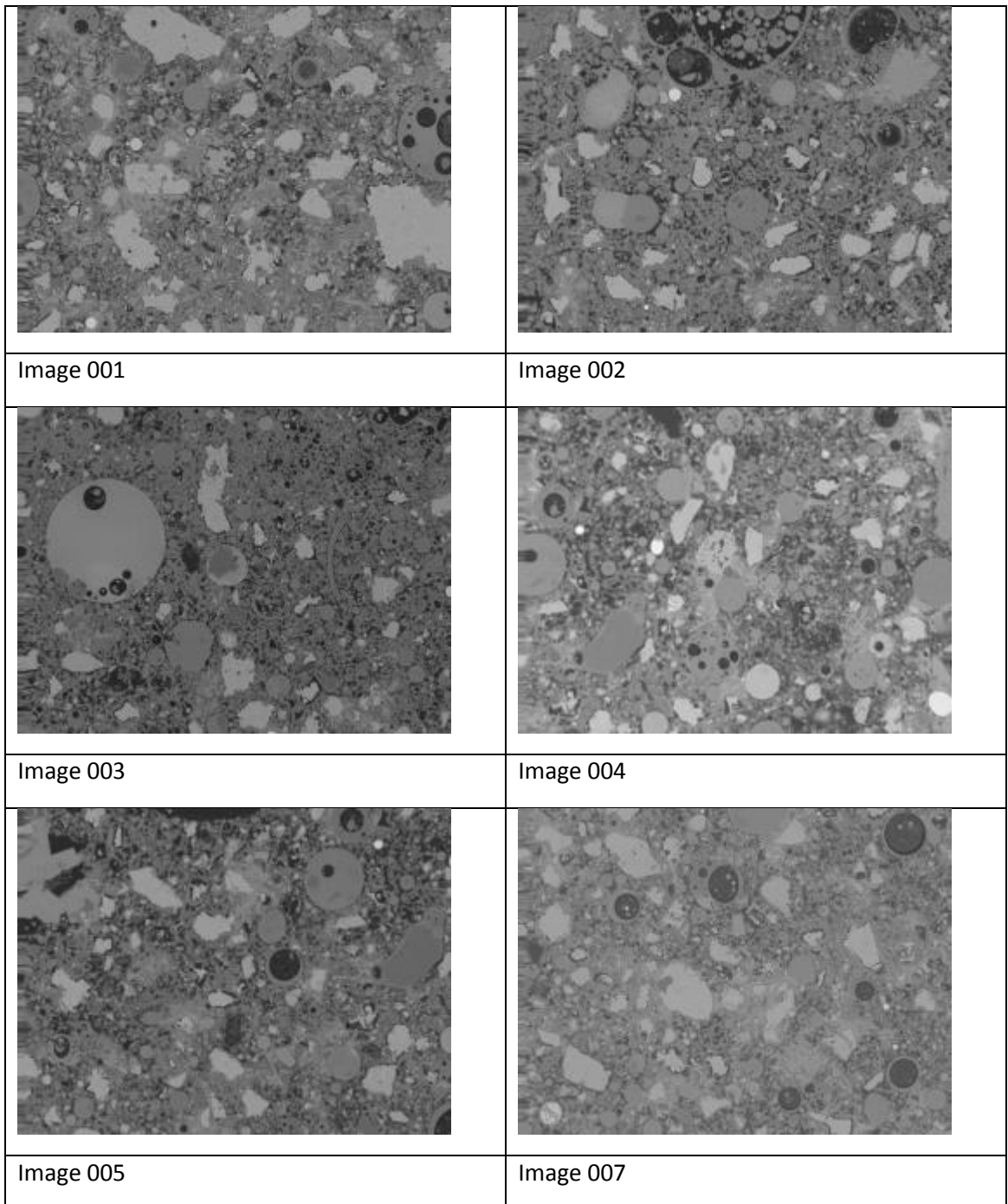
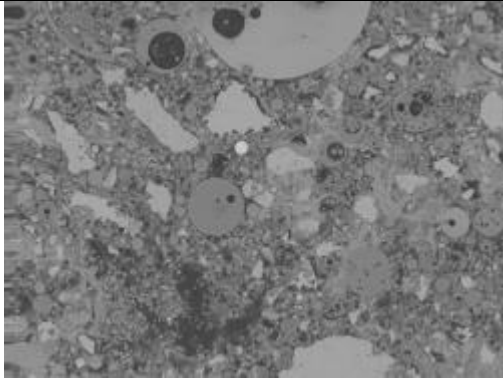
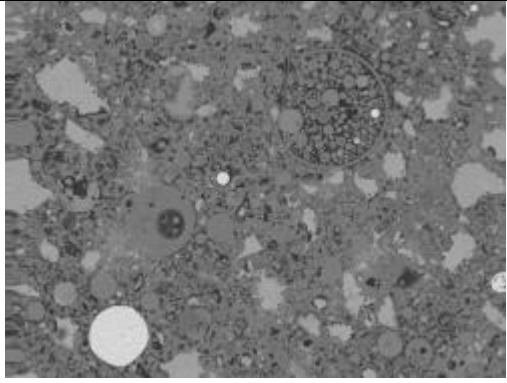
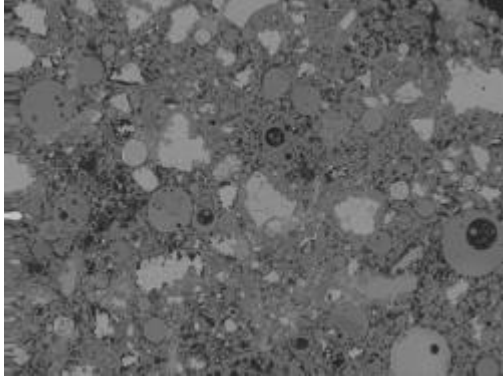
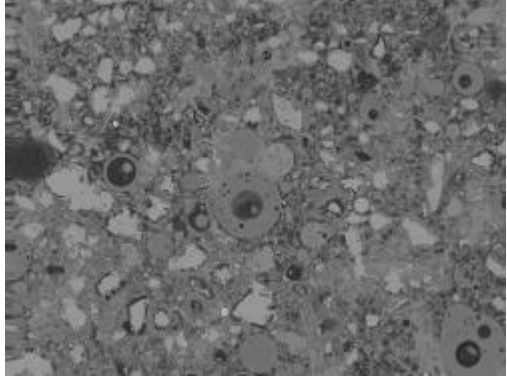
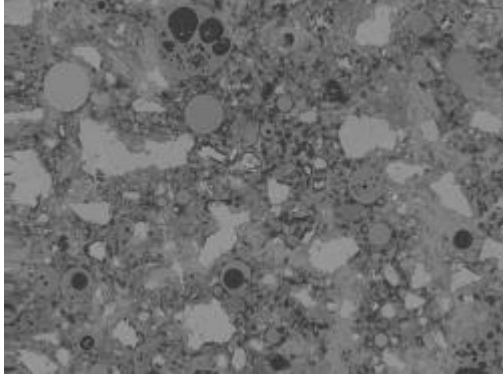
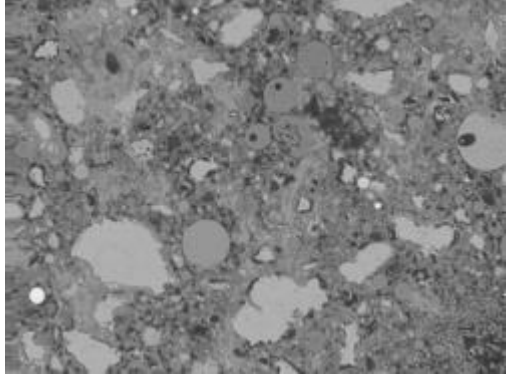


Figure A 104 Images of 20MPa Fly ash stiff mix ideal cured

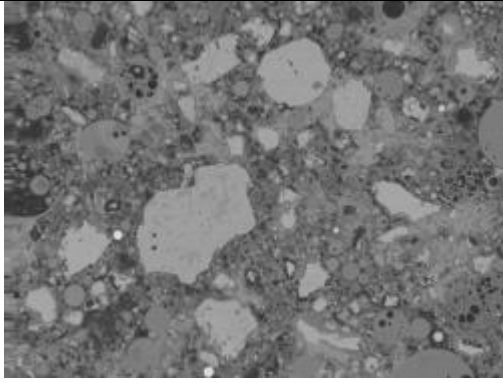
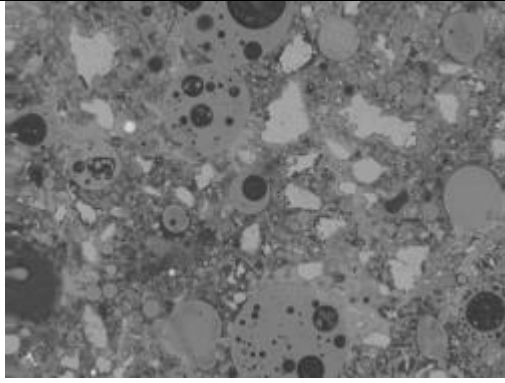
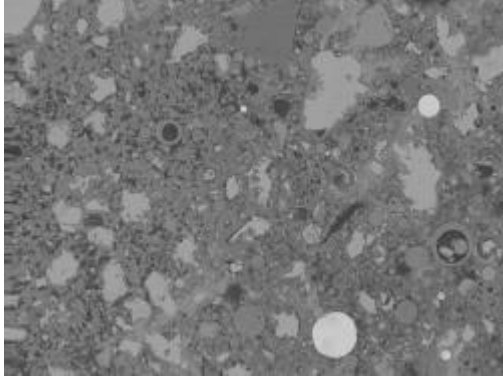
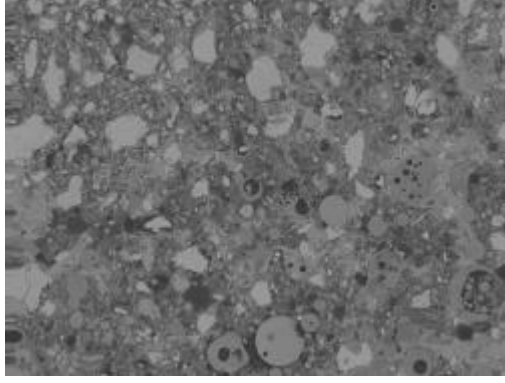
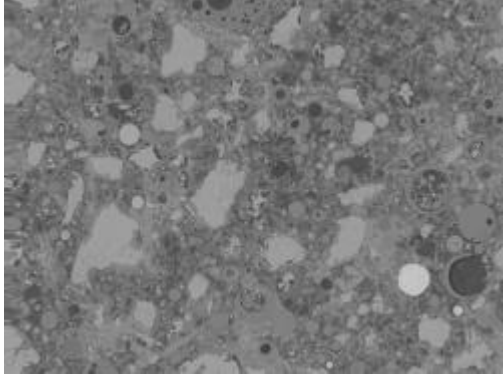
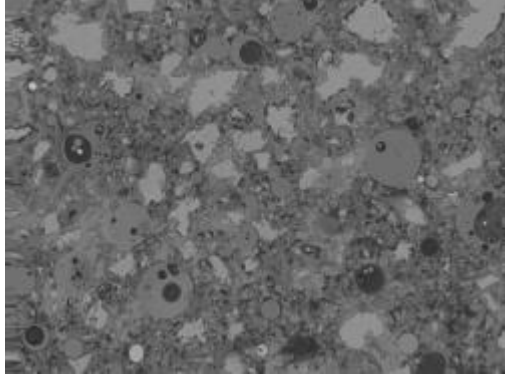
M8A



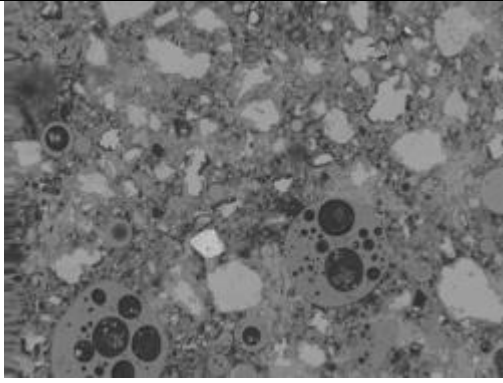
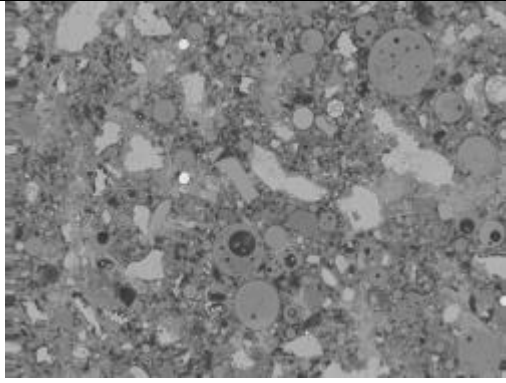
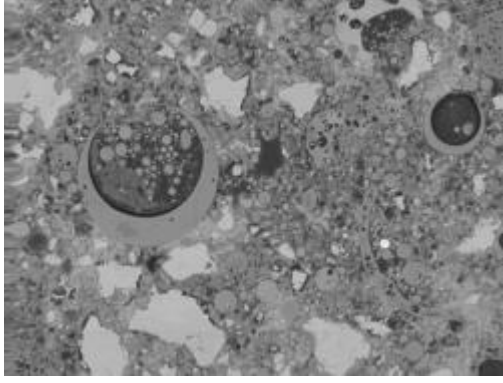
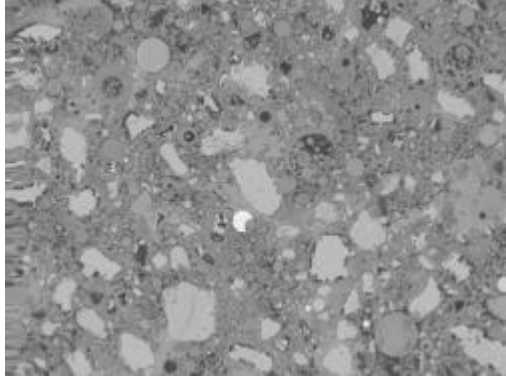
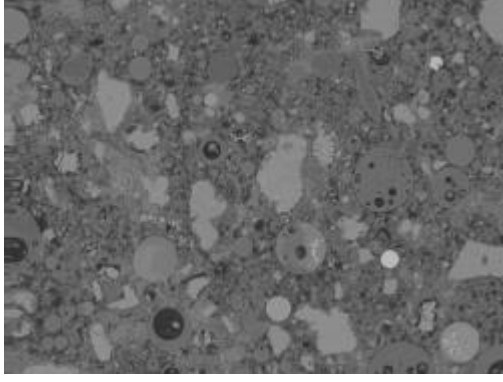
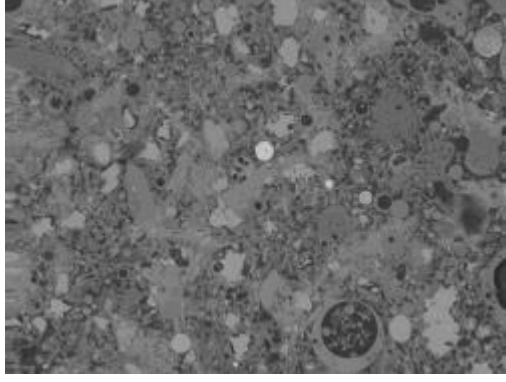
50MPa Fly ash stiff mix ambient cured

	
Image 008	Image 009
	
Image 010	Image 011
	
Image 012	Image 014

50MPa Fly ash stiff mix ambient cured

	
Image 015	Image 016
	
Image 017	Image 018
	
Image 019	Image 020

50MPa Fly ash stiff mix ambient cured

	
Image 021	Image 022
	
Image 024	Image 025
	
Image 026	Image 028

50MPa Fly ash stiff mix ambient cured

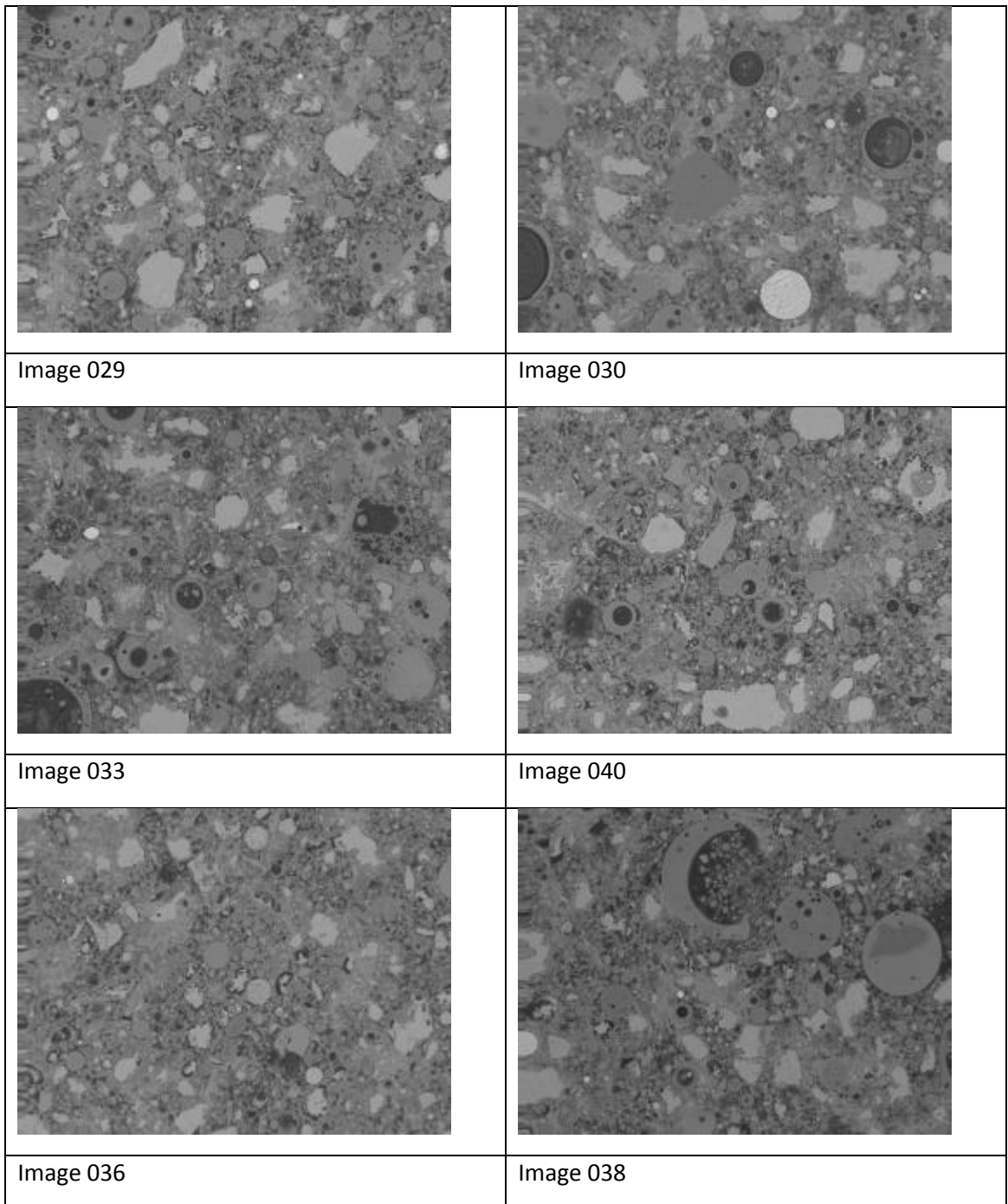
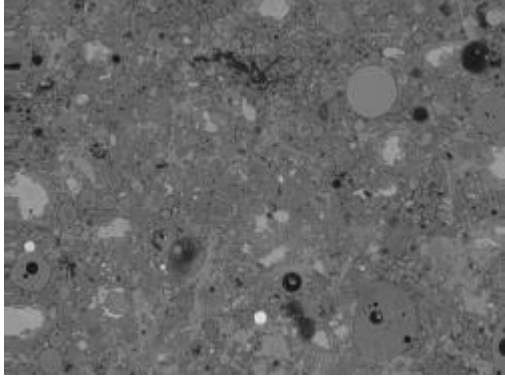
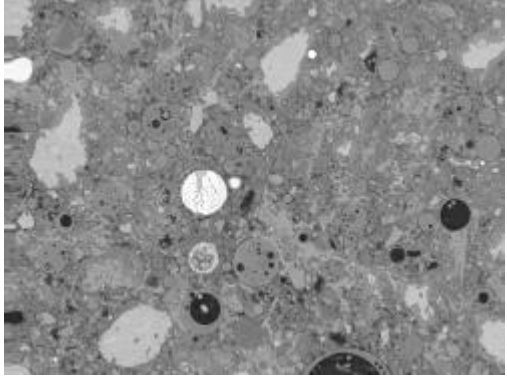
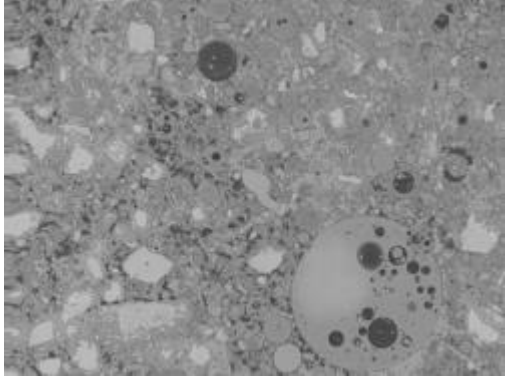
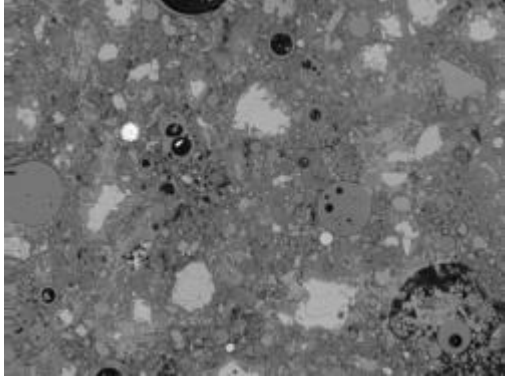
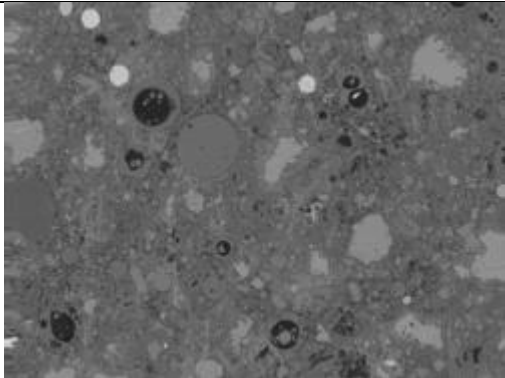
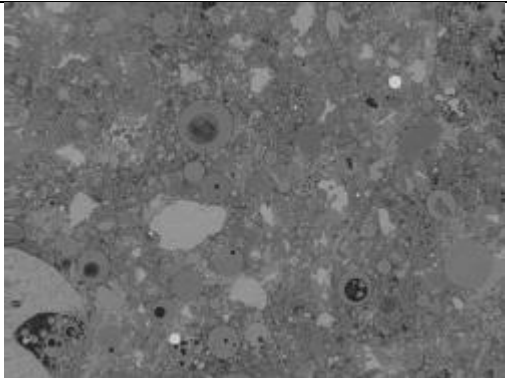
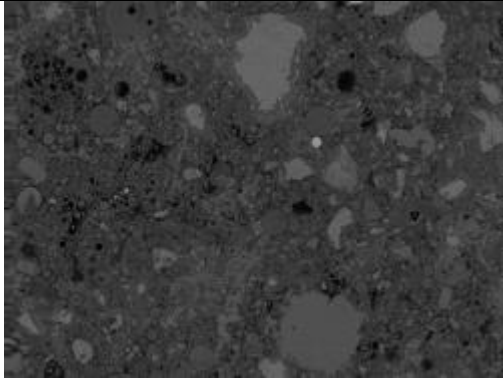
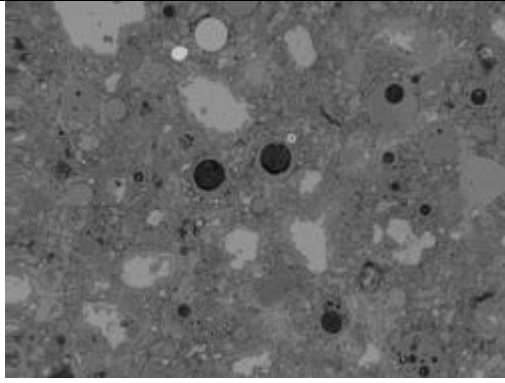
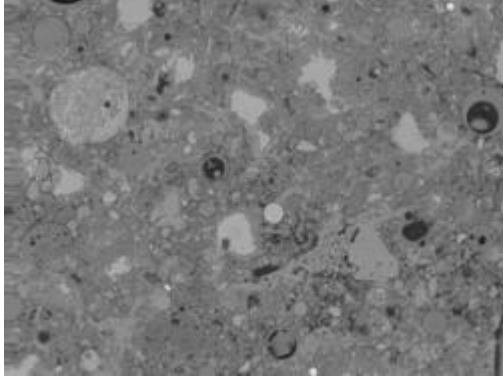
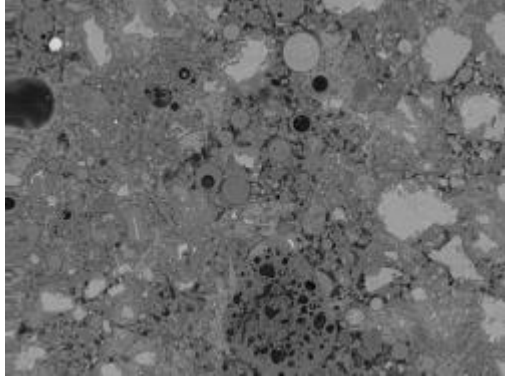
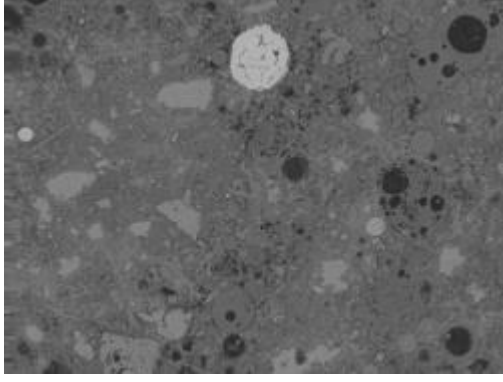
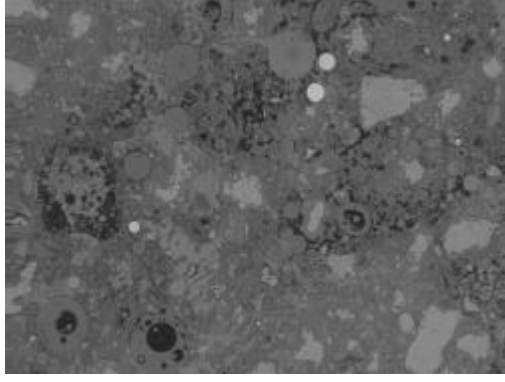


Figure A 105 Images of 50MPa Fly ash stiff mix ambient cured

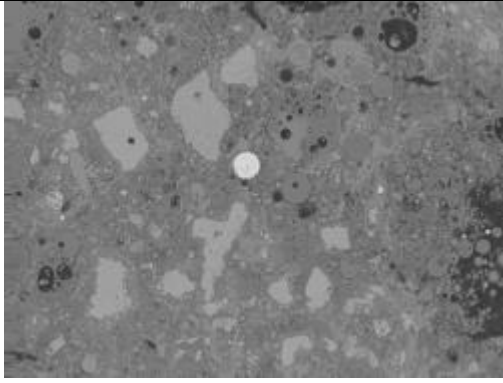
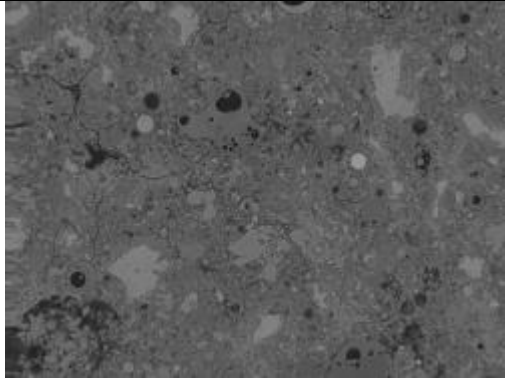
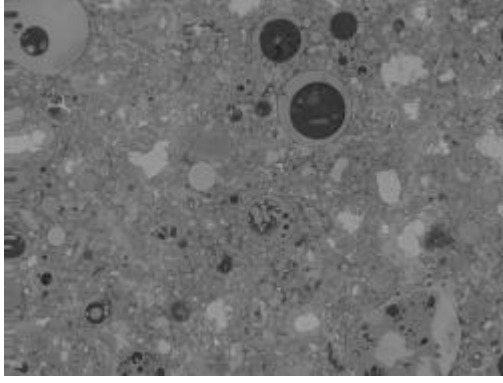
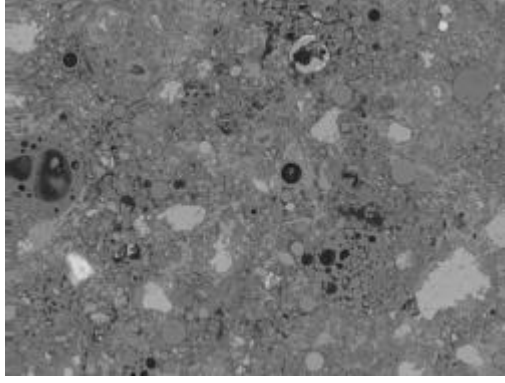
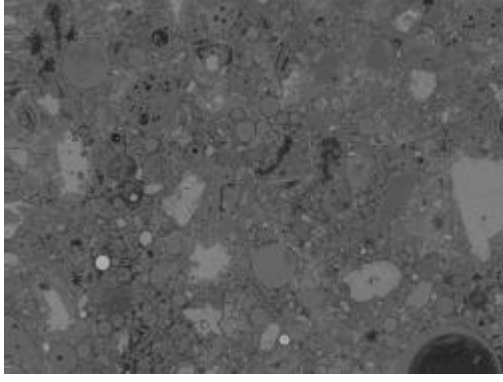
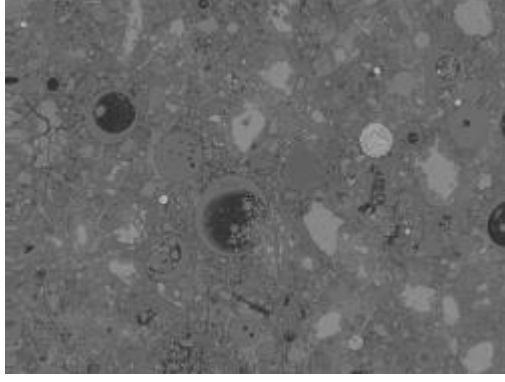
M8W

	
Image 007	Image 009
	
Image 010	Image 011
	
Image 013	Image 014

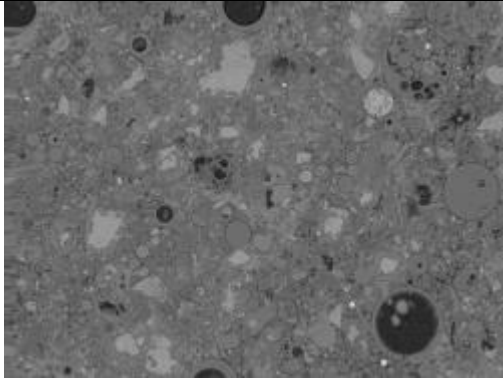
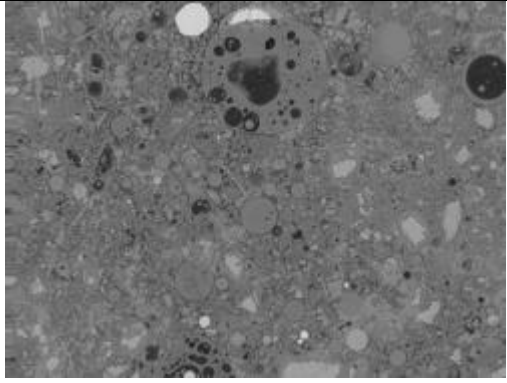
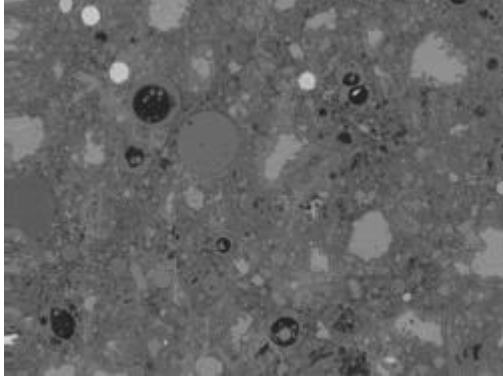
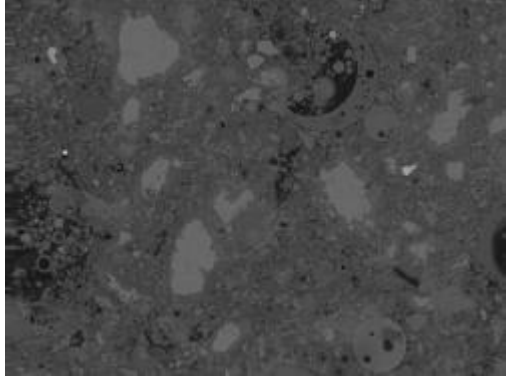
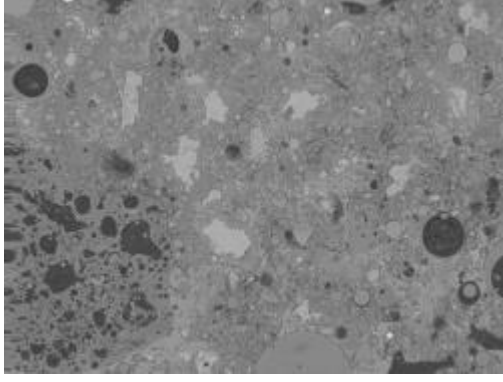
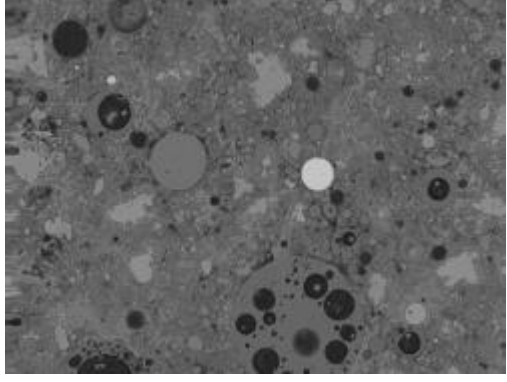
50MPa Fly ash stiff mix ideal cured

	
Image 016	Image 017
	
Image 018	Image 019
	
Image 020	Image 021

50MPa Fly ash stiff mix ideal cured

	
Image 022	Image 024
	
Image 025	Image 026
	
Image 029	Image 030

50MPa Fly ash stiff mix ideal cured

	
Image 032	Image 033
	
Image 048	Image 035
	
Image 037	Image 038

50MPa Fly ash stiff mix ideal cured

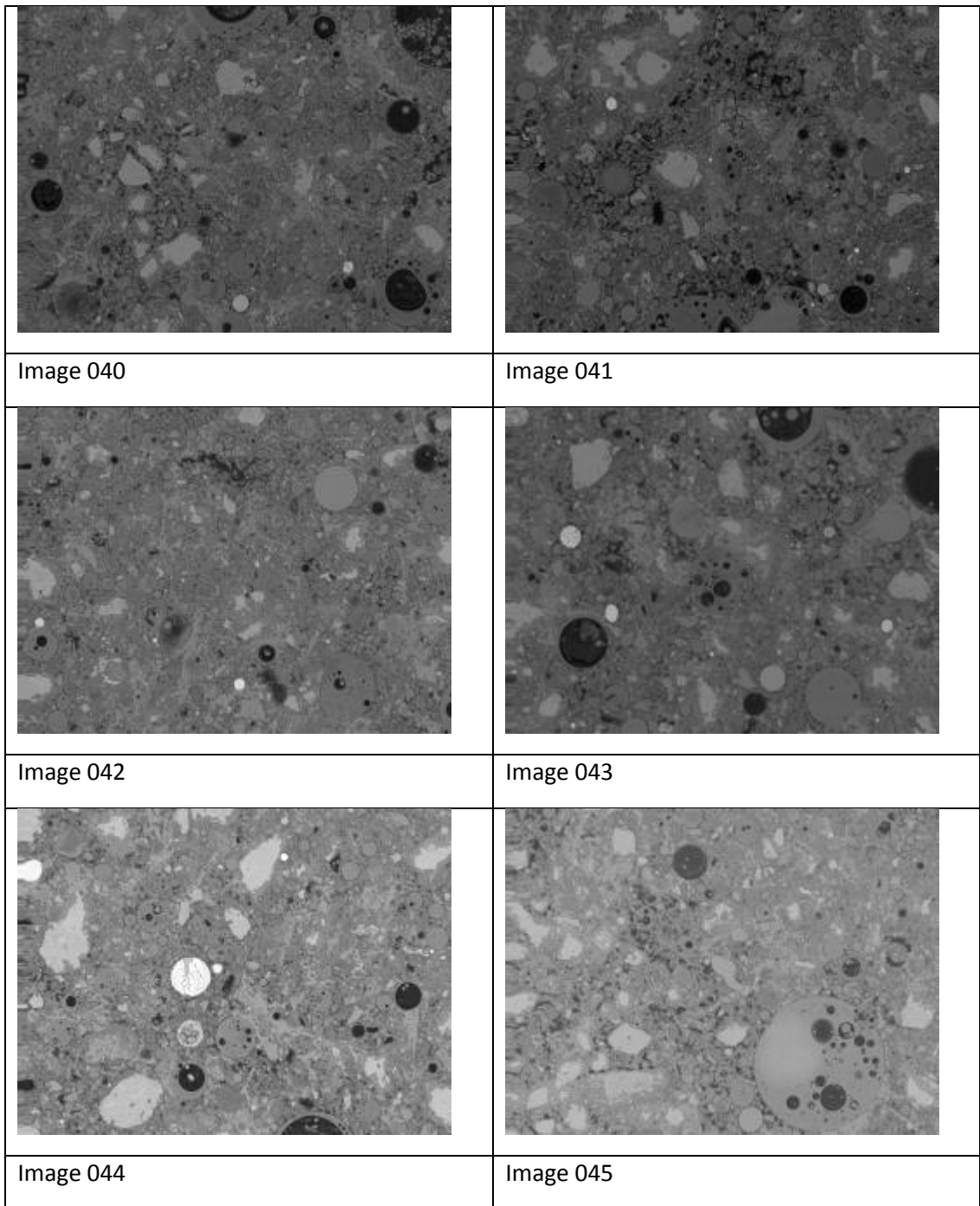
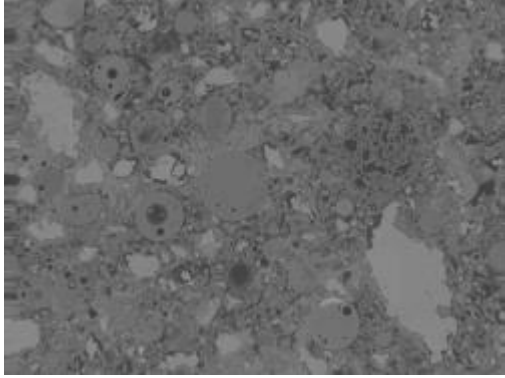
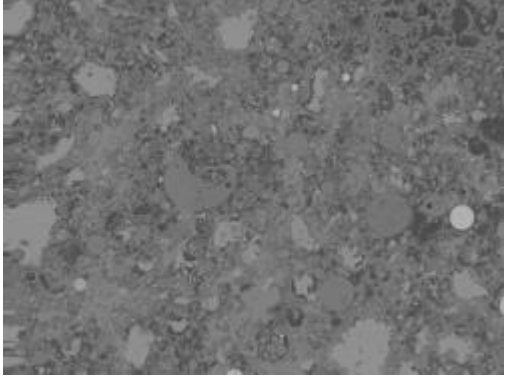
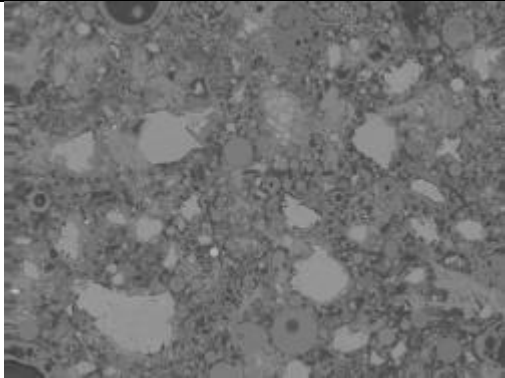
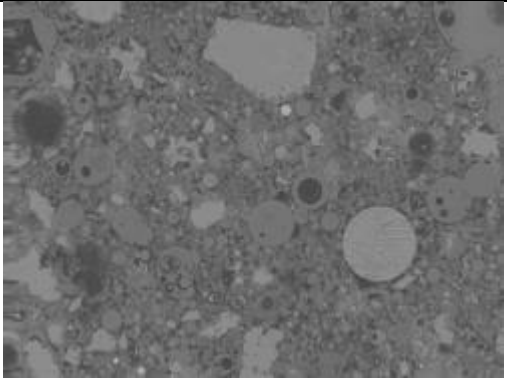
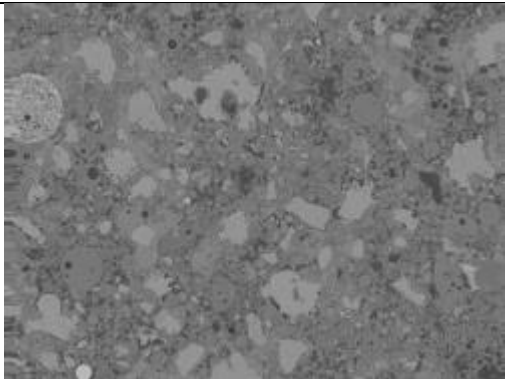
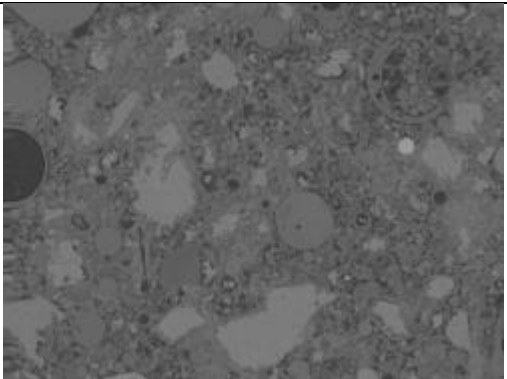
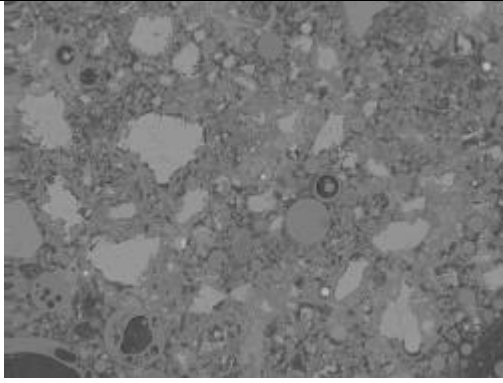
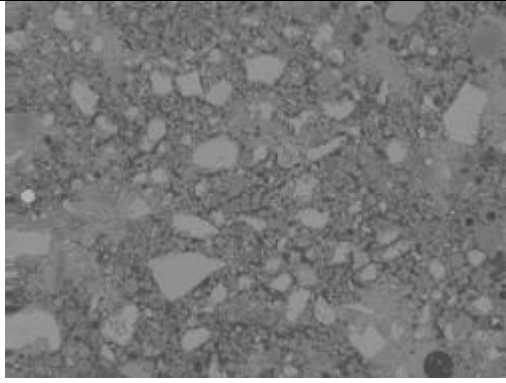
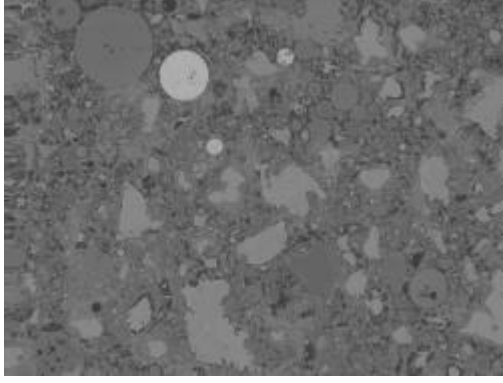
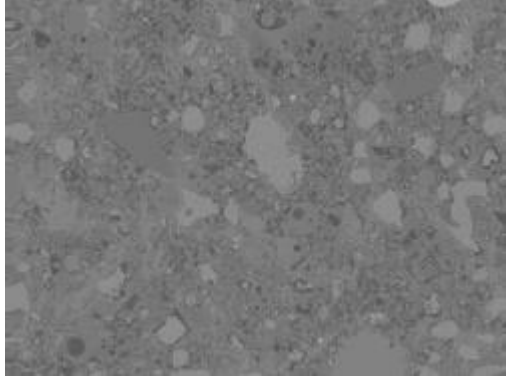
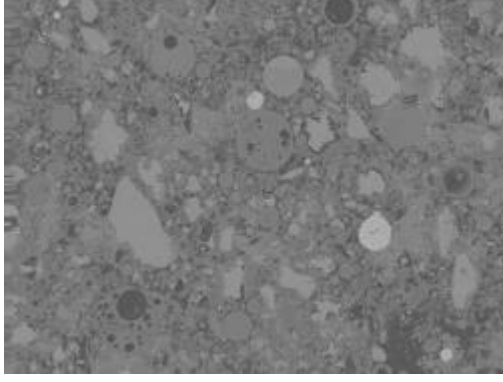
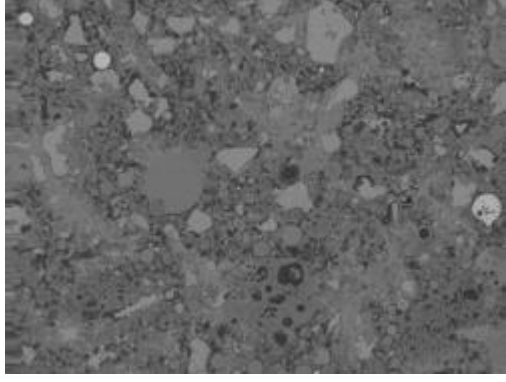


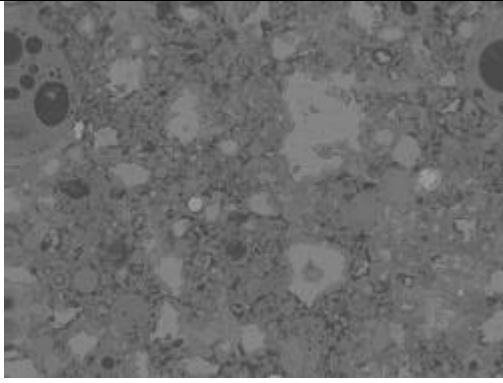
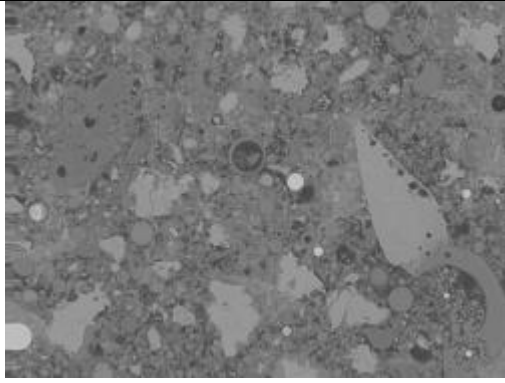
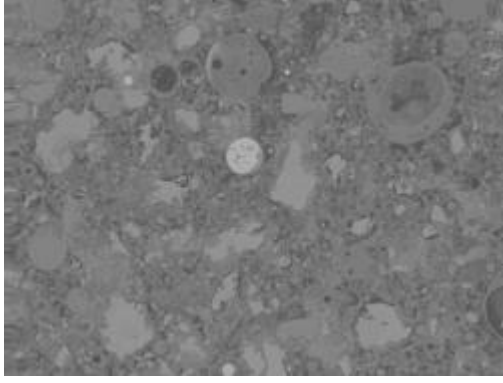
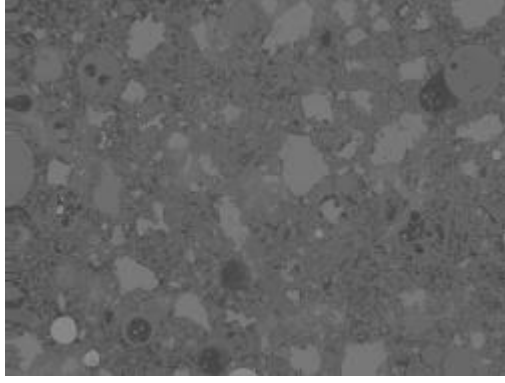
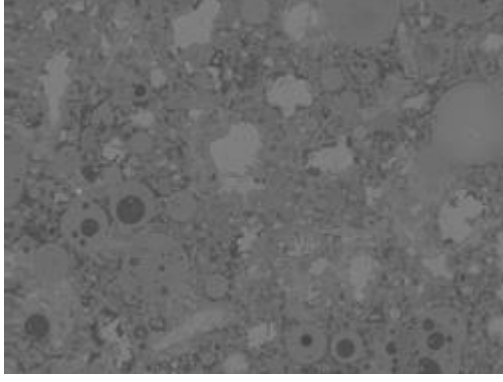
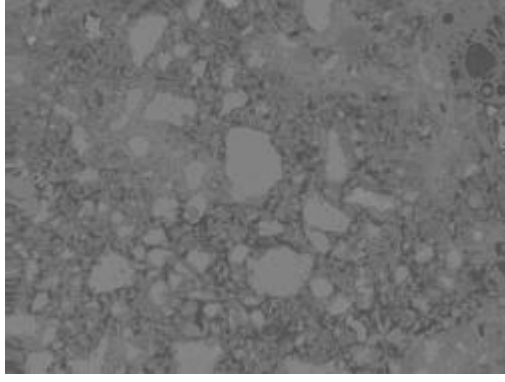
Figure A 106 Images of 50MPa Fly ash stiff mix ideal cured

	
Image 047	Image 048
	
Image 049	Image 004
	
Image 045	Image 006

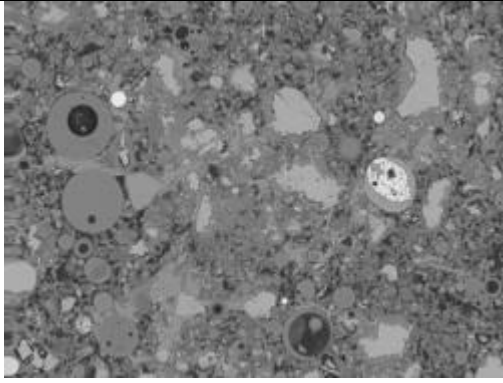
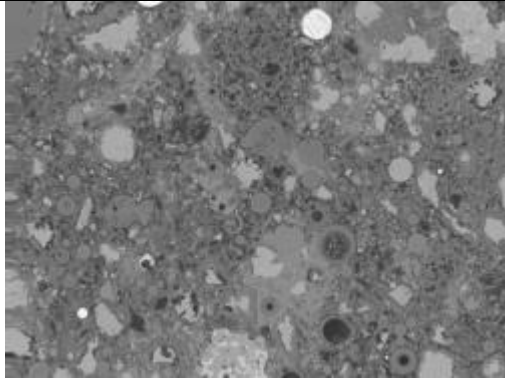
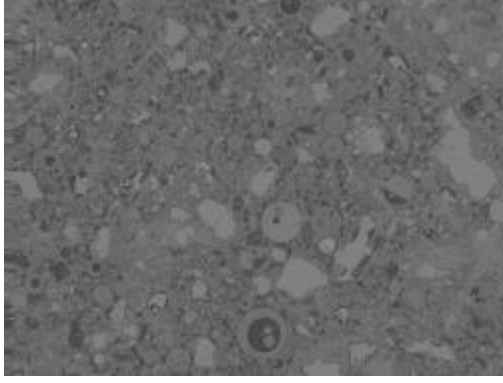
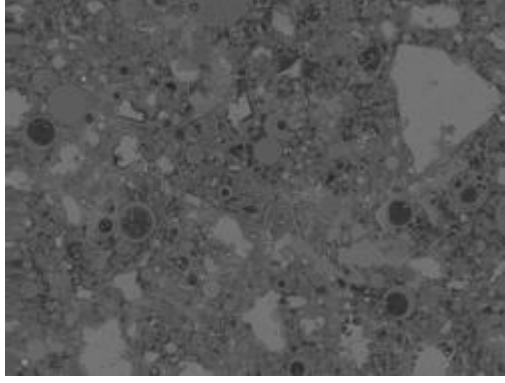
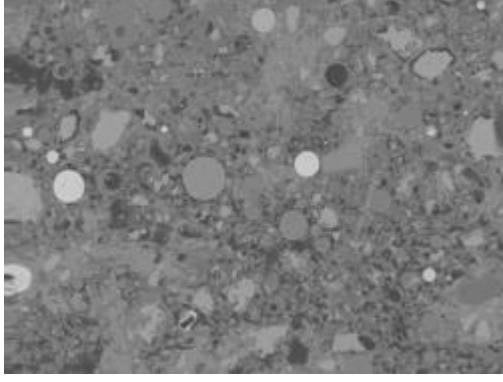
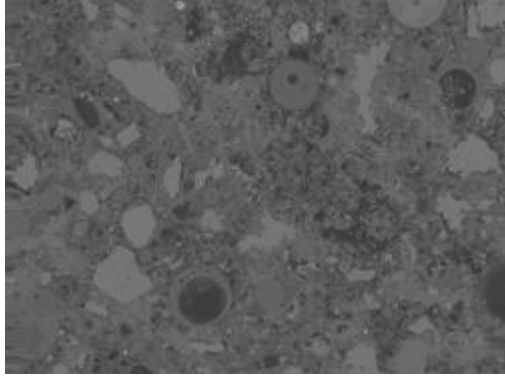
80MPa Fly ash stiff mix ambient cured

	
Image 007	Image 008
	
Image 009	Image 011
	
Image 012	Image 013

80MPa Fly ash stiff mix ambient cured

	
Image 014	Image 015
	
Image 016	Image 018
	
Image 020	Image 021

80MPa Fly ash stiff mix ambient cured

	
Image 022	Image 023
	
Image 025	Image 026
	
Image 027	Image 030

80MPa Fly ash stiff mix ambient cured

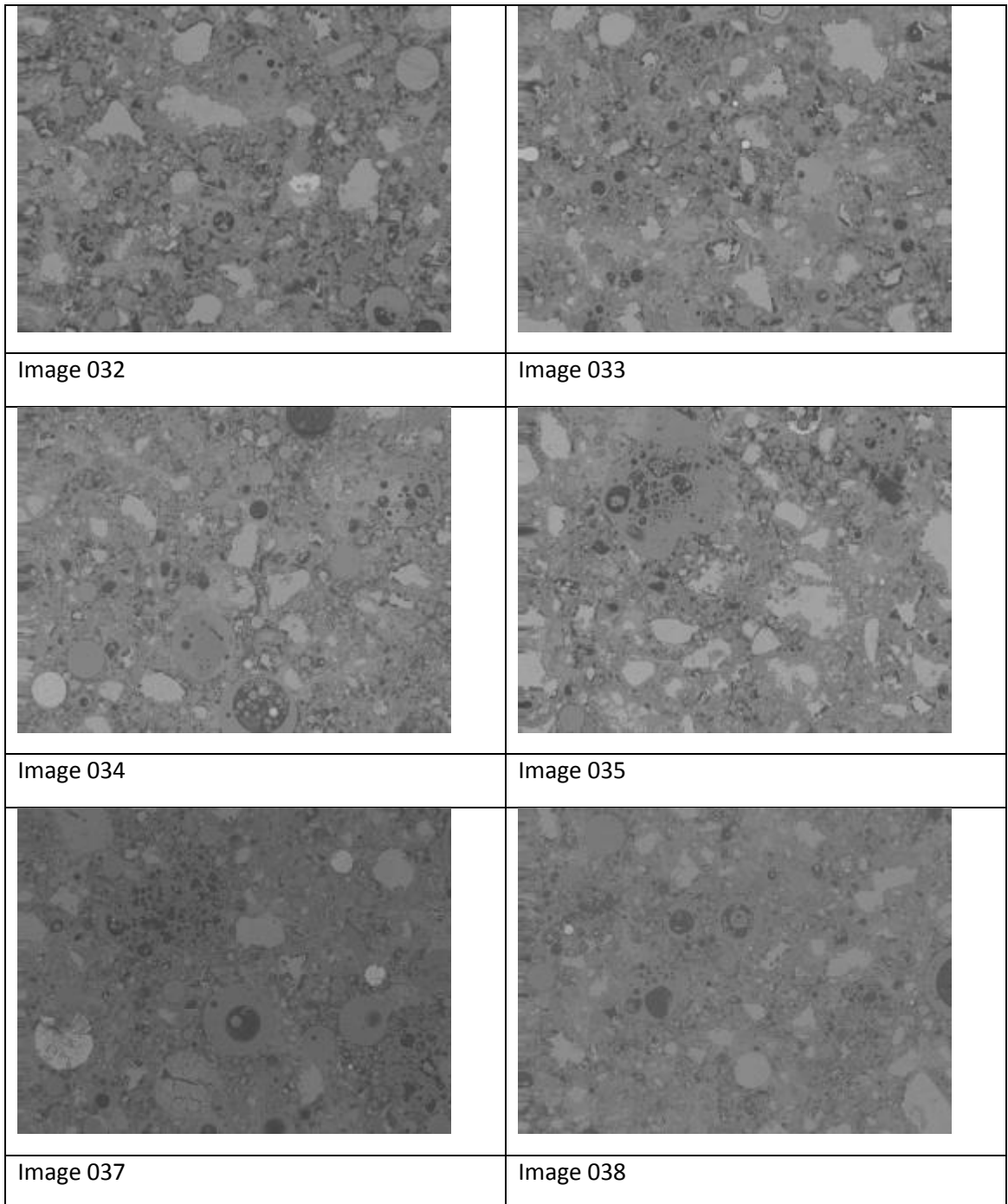
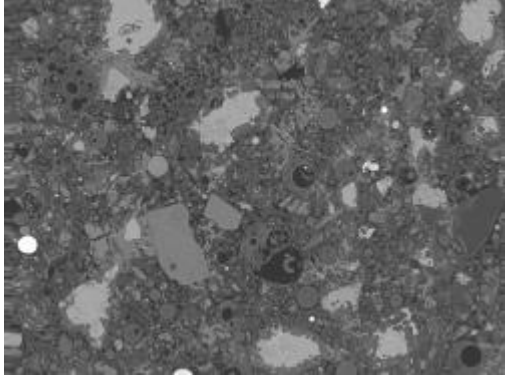
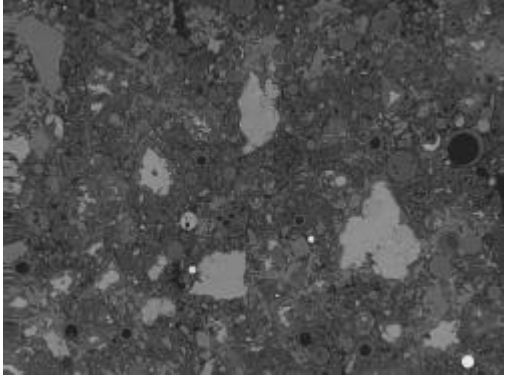
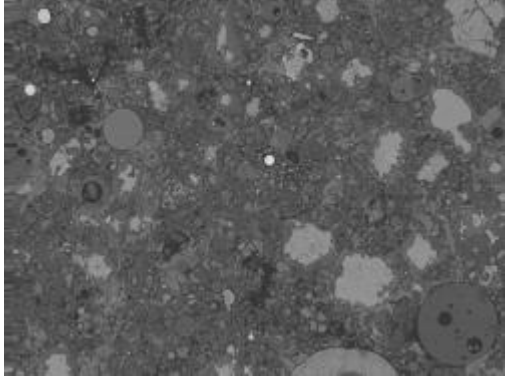
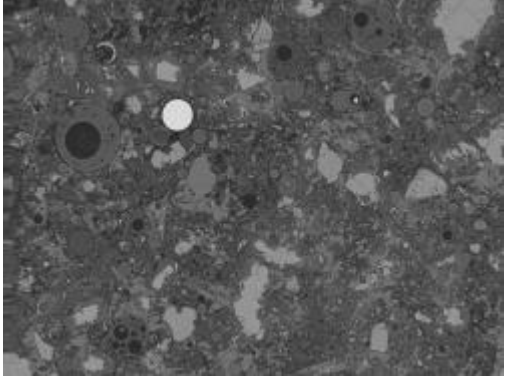
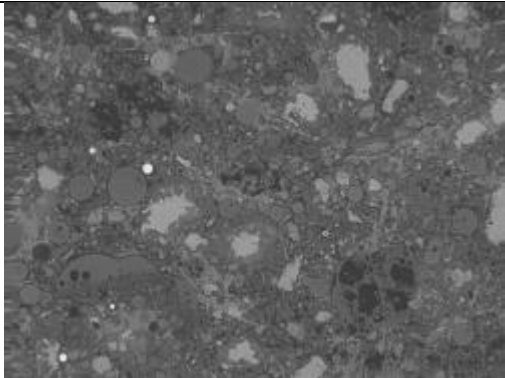
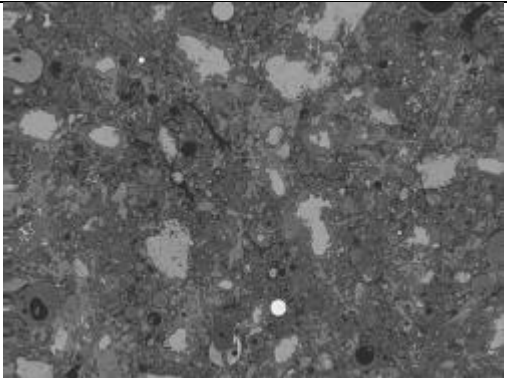
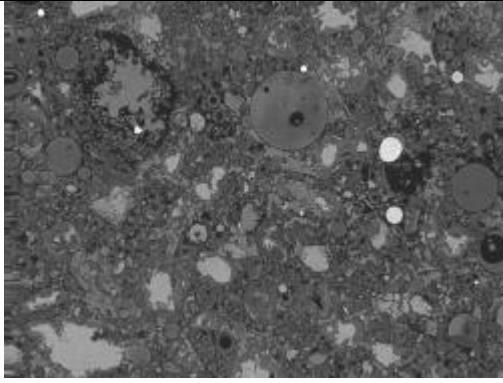
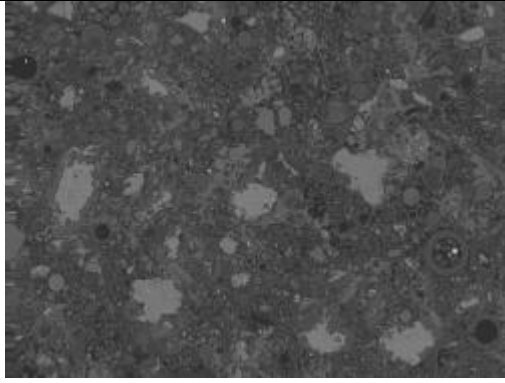
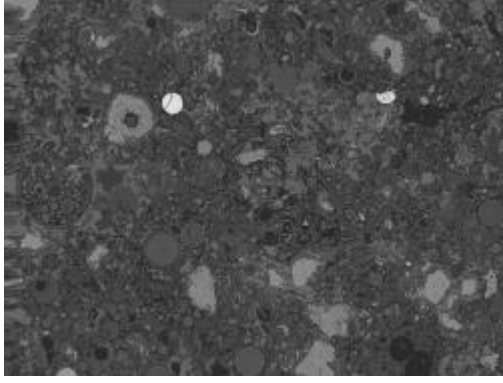
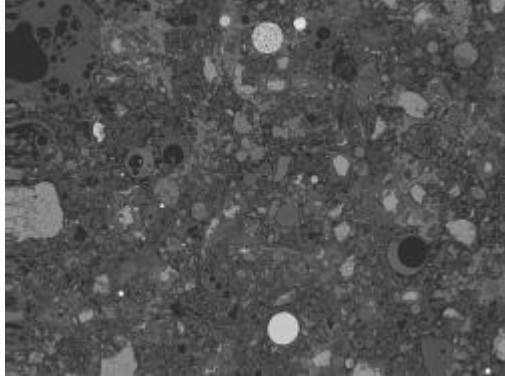
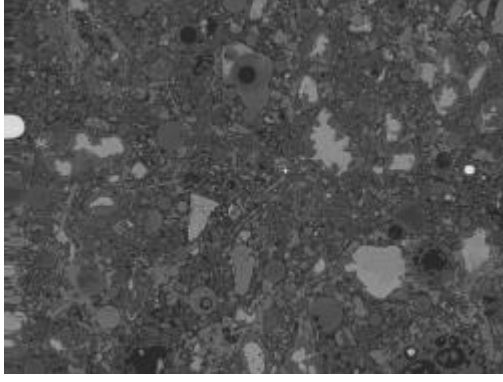
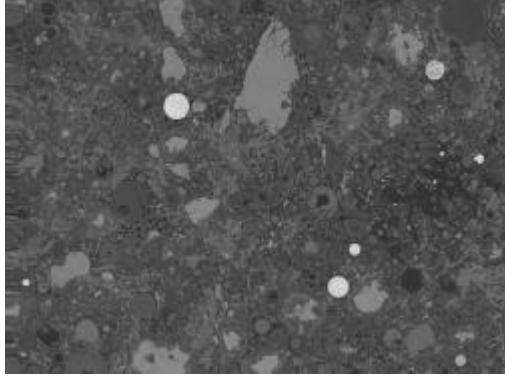


Figure A 107 Images of 80MPa Fly ash stiff mix ambient cured

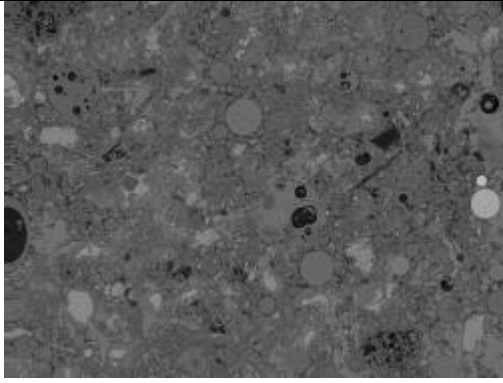
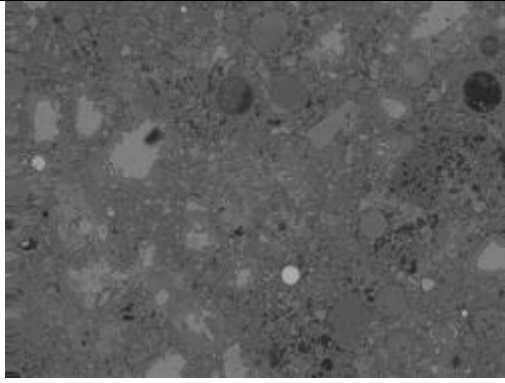
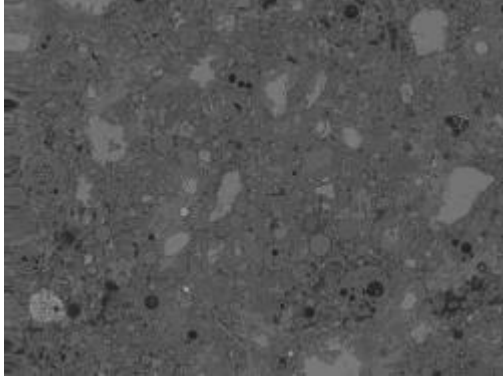
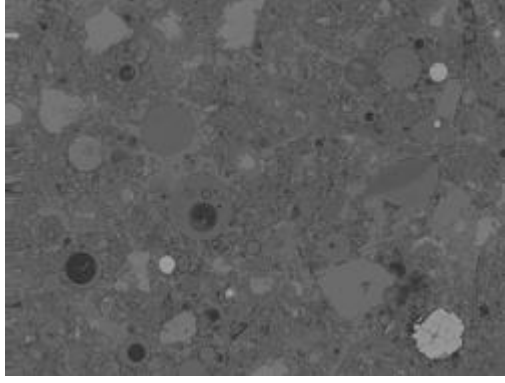
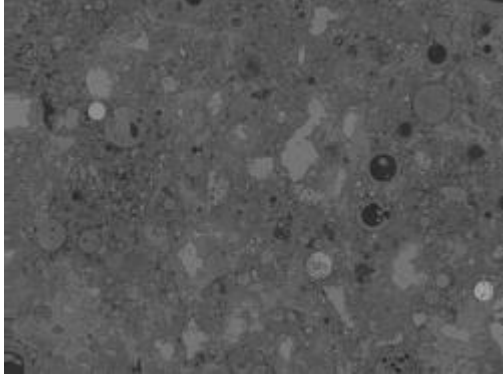
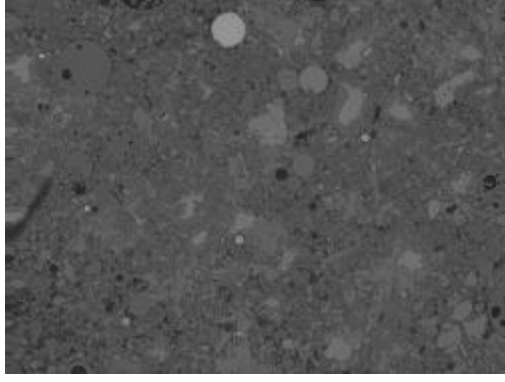
M9W

	
Image 002	Image 003
	
Image 004	Image 005
	
Image 006	Image 007

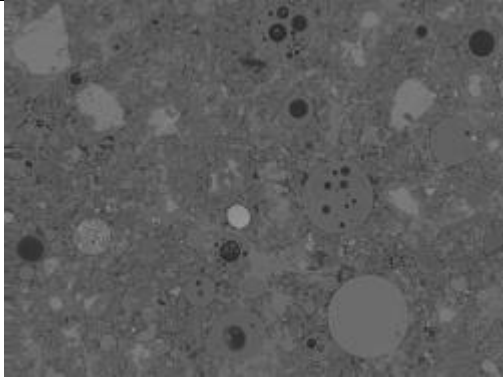
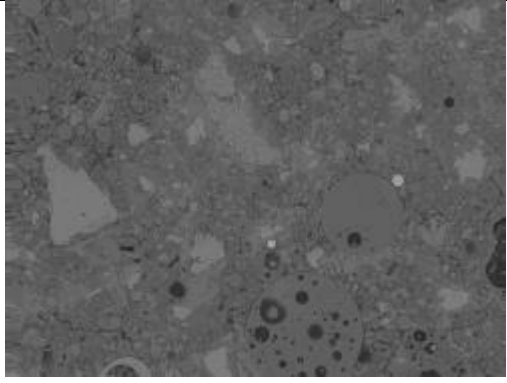
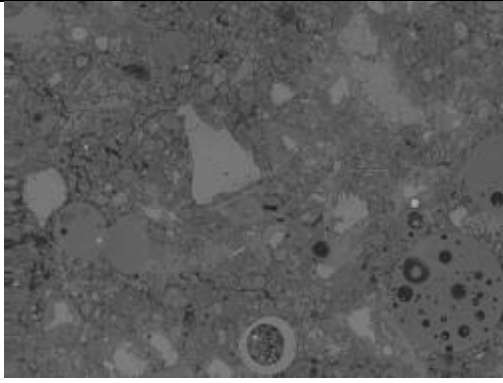
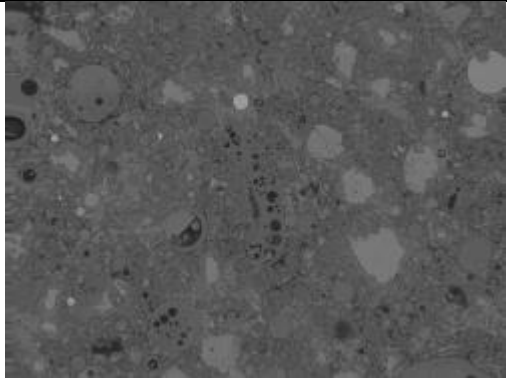
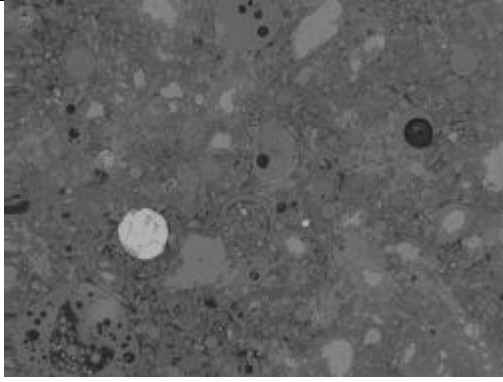
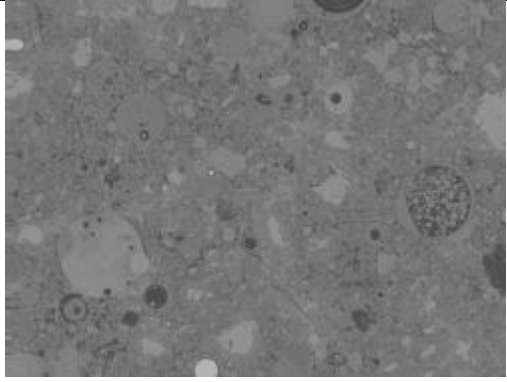
80MPa Fly ash stiff mix ideal cured

	
Image 008	Image 009
	
Image 011	Image 013
	
Image 014	Image 015

80MPa Fly ash stiff mix ideal cured

	
Image 018	Image 019
	
Image 020	Image 021
	
Image 022	Image 024

80MPa Fly ash stiff mix ideal cured

	
Image 026	Image 027
	
Image 028	Image 029
	
Image 030	Image 033

80MPa Fly ash stiff mix ideal cured

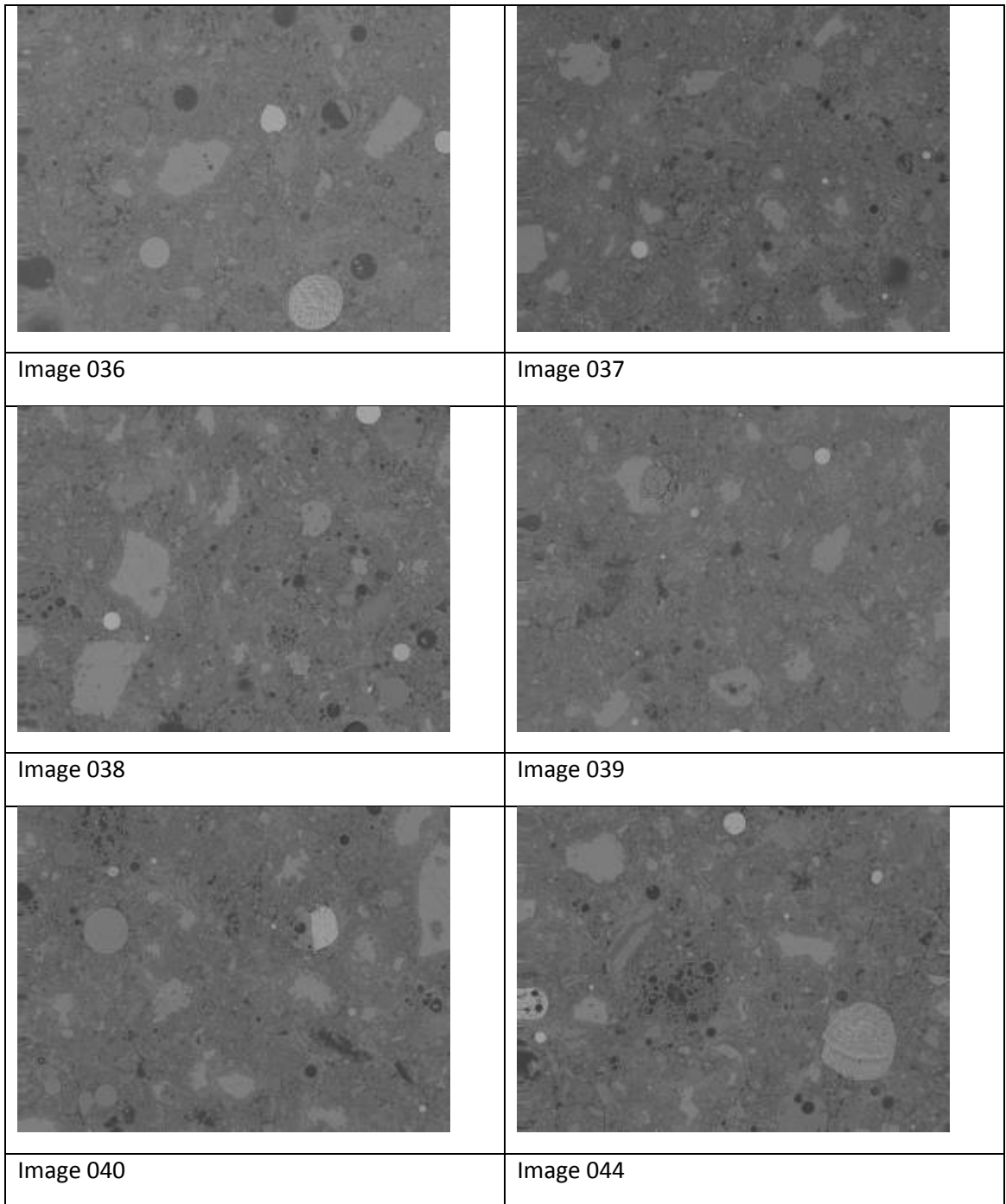
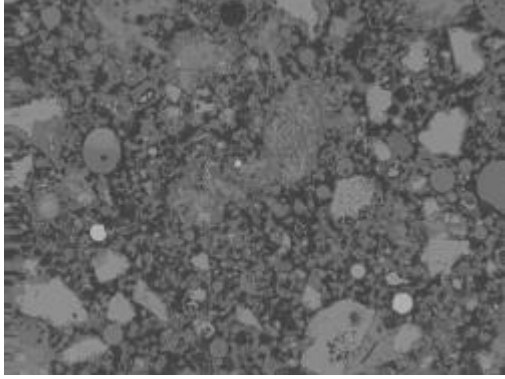
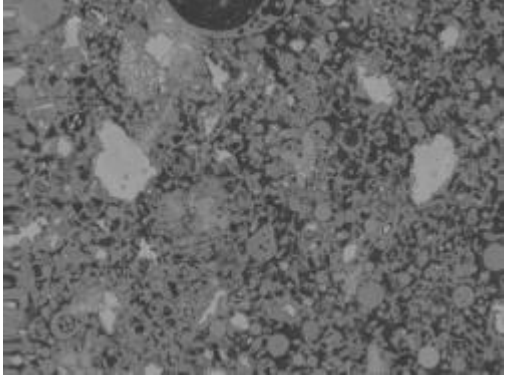
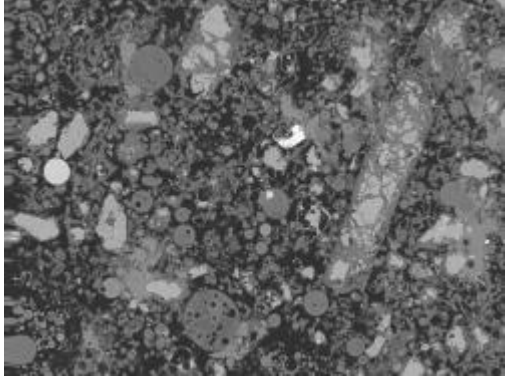
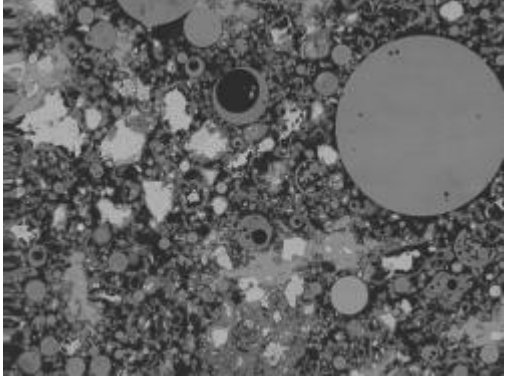
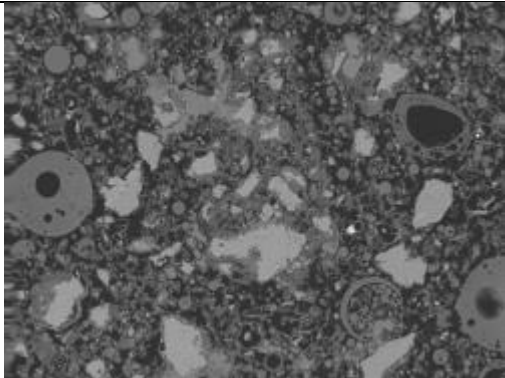
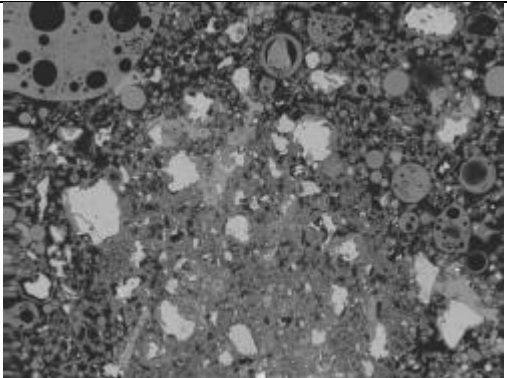
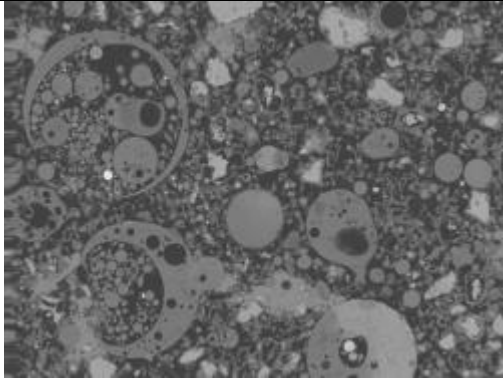
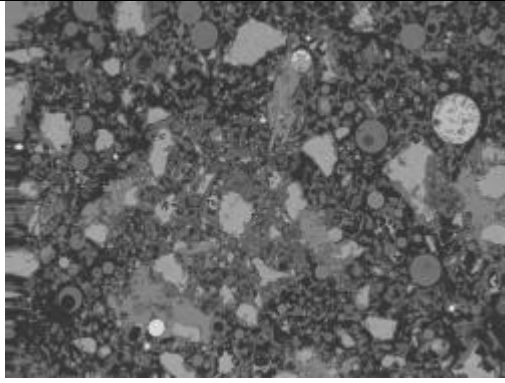
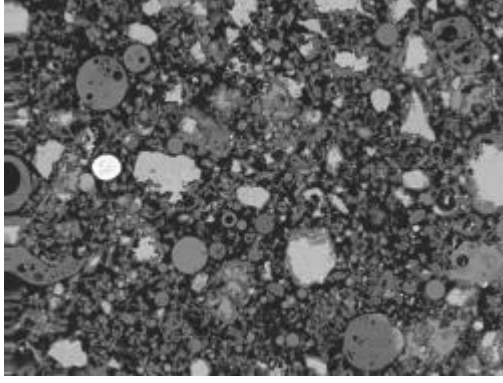
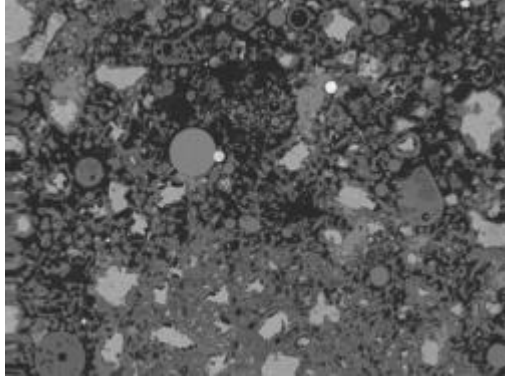
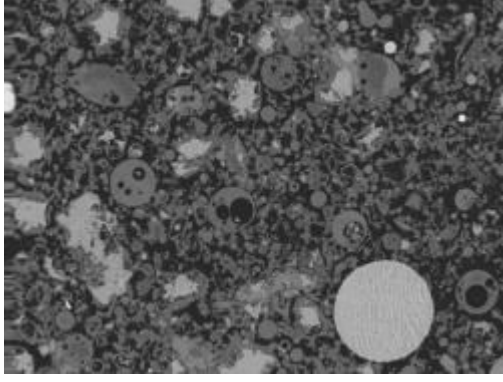
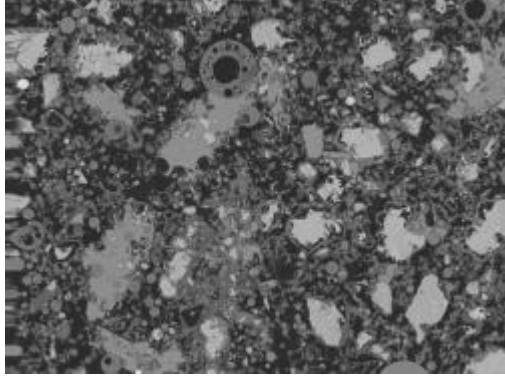


Figure A 108 Images of 80MPa Fly ash stiff mix ideal cured

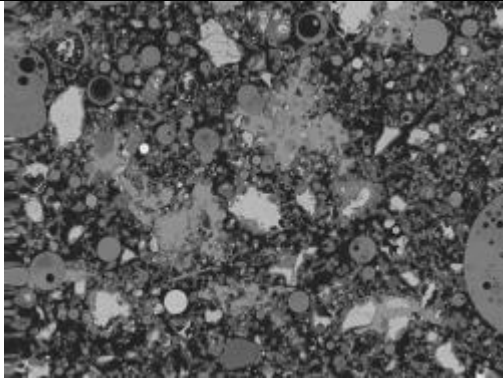
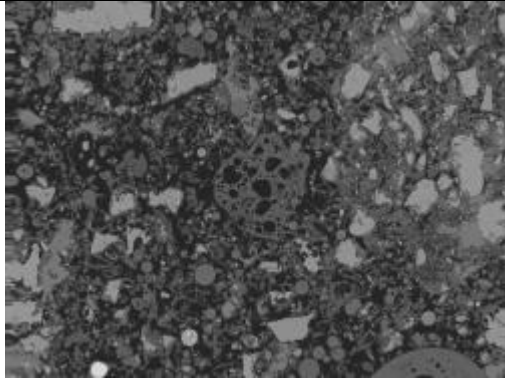
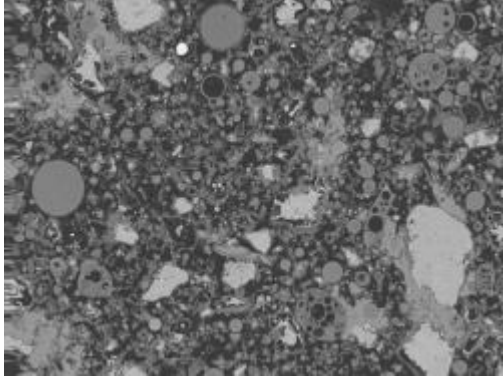
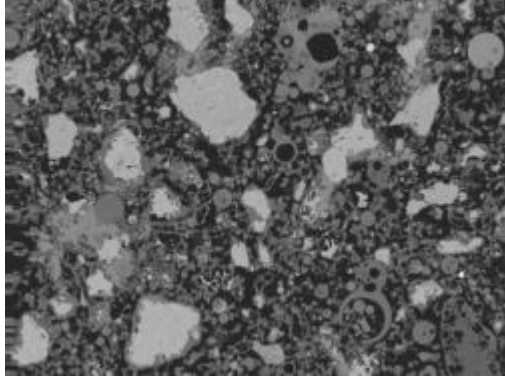
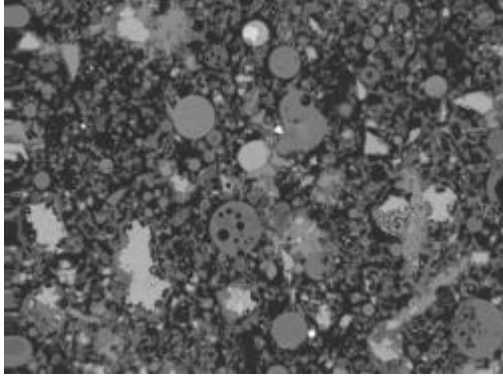
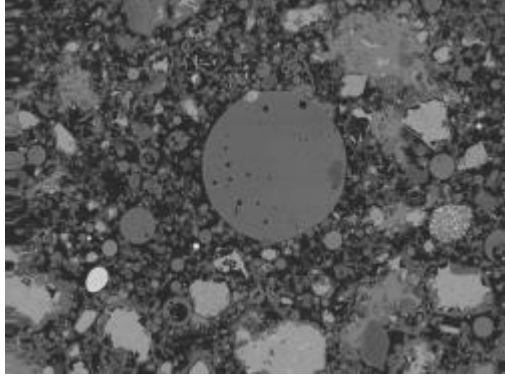
M10A

	
Image 041	Image 049
	
Image 003	Image 004
	
Image 005	Image 006

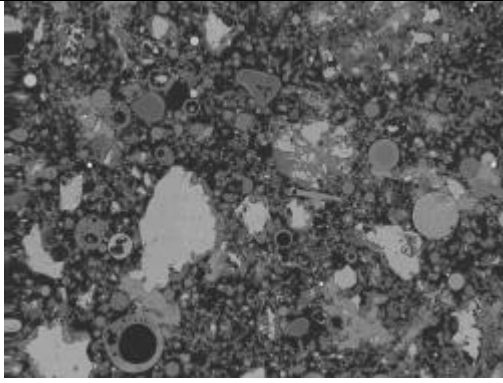
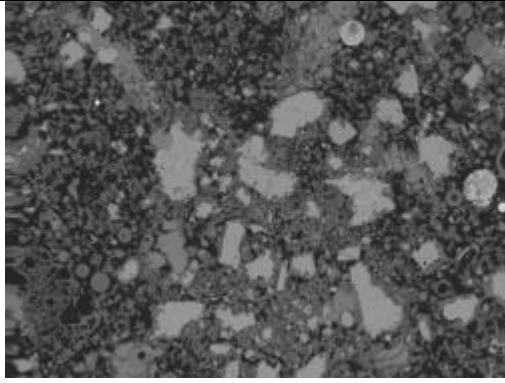
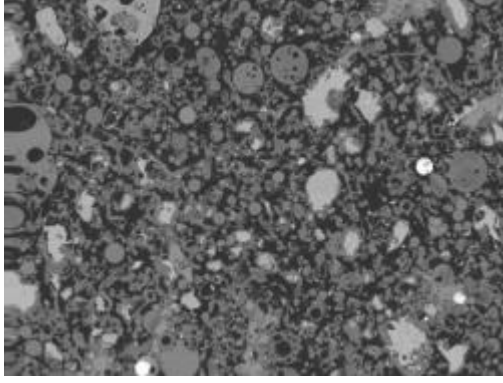
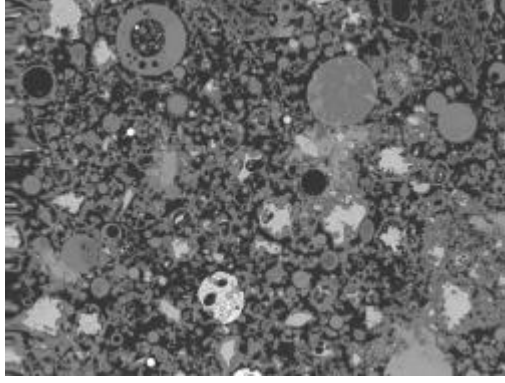
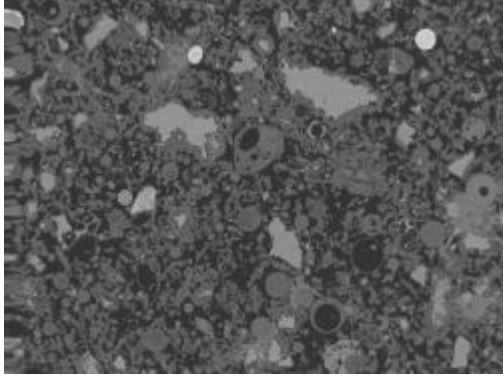
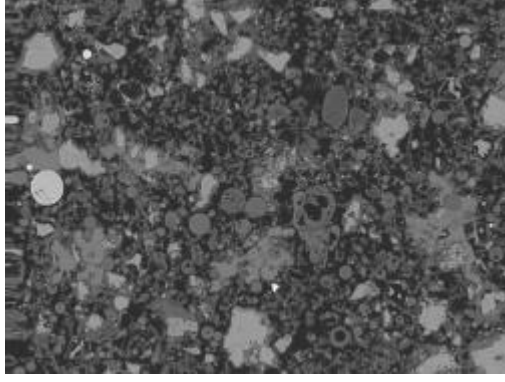
20MPa Fly ash wet mix ambient cured

	
Image 007	Image 008
	
Image 009	Image 010
	
Image 011	Image 012

20MPa Fly ash wet mix ambient cured

	
Image 013	Image 014
	
Image 016	Image 019
	
Image 020	Image 022

20MPa Fly ash wet mix ambient cured

	
Image 024	Image 026
	
Image 027	Image 028
	
Image 030	Image 032

20MPa Fly ash wet mix ambient cured

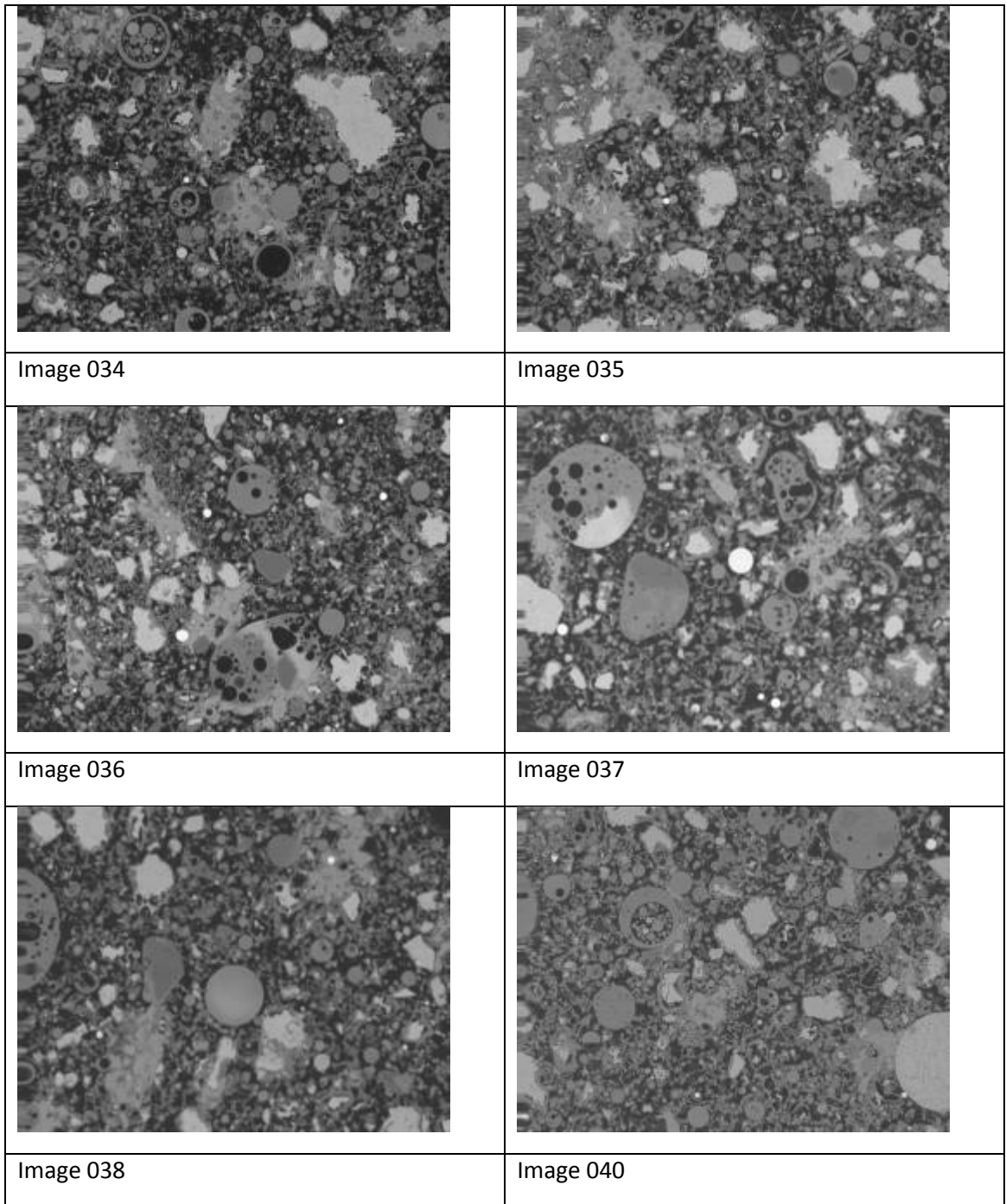
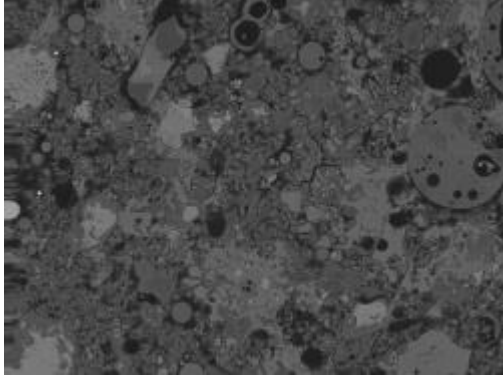
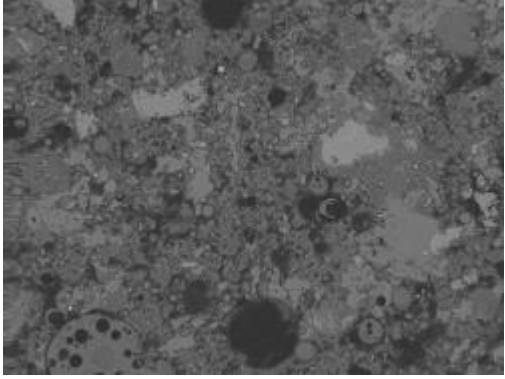
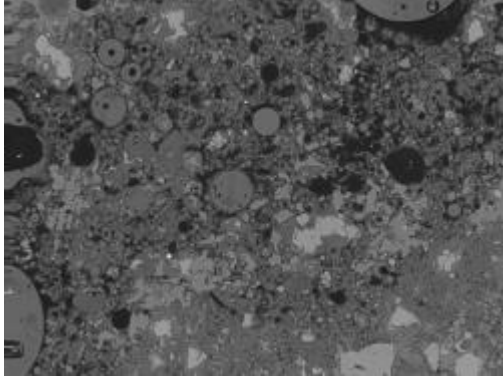
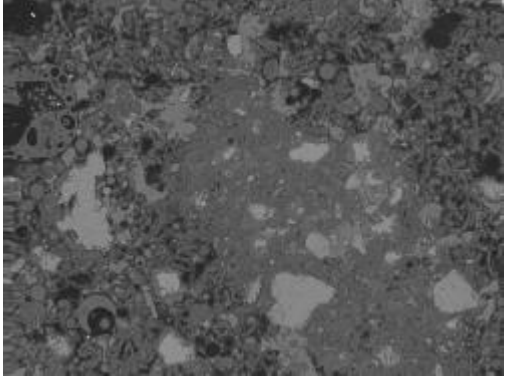
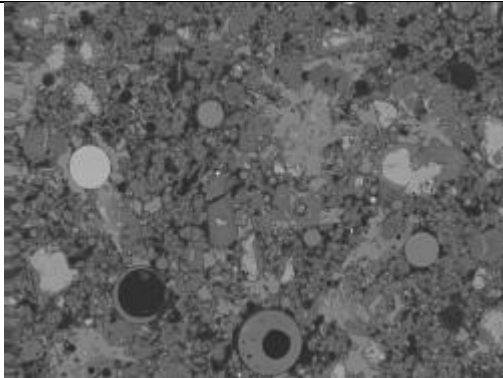
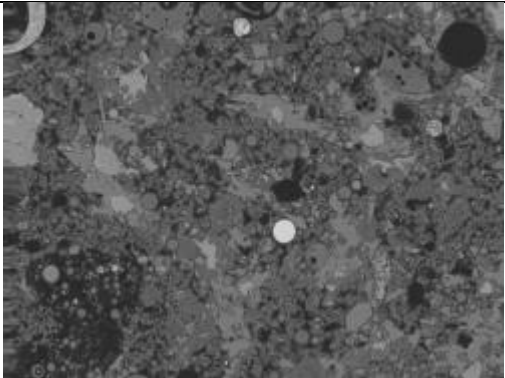
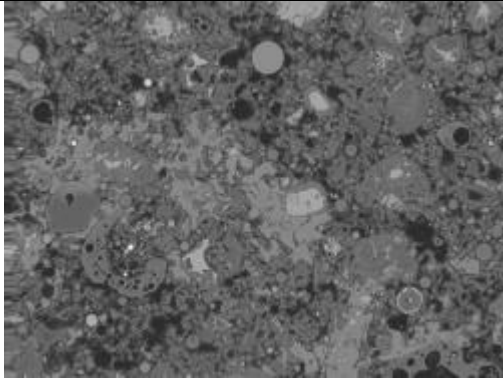
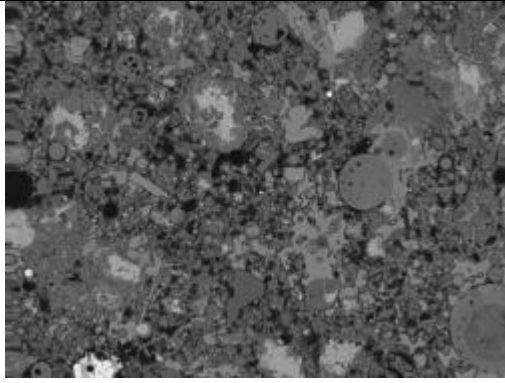
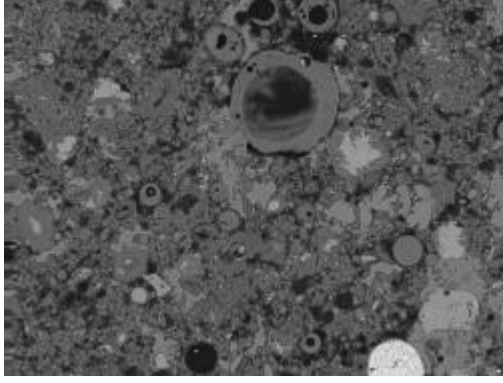
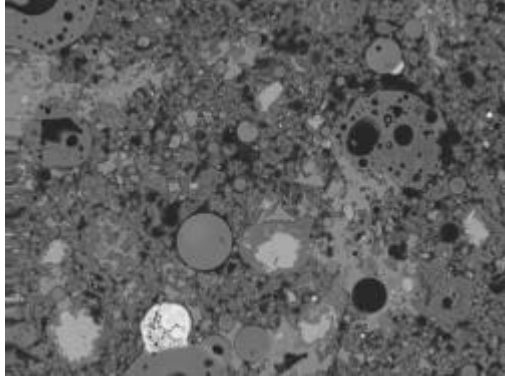
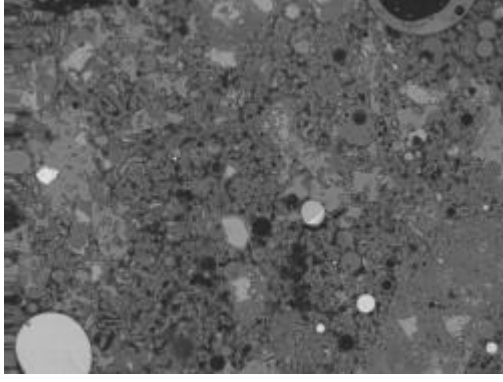
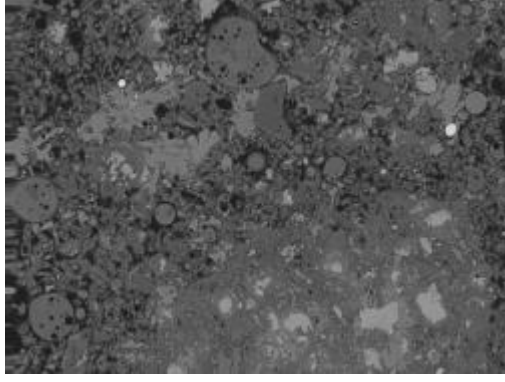


Figure A 109 Images of 20MPa Fly ash wet mix ambient cured

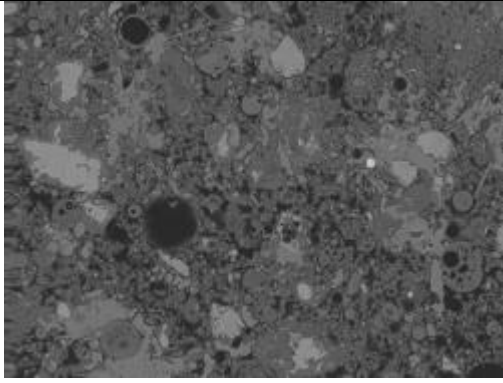
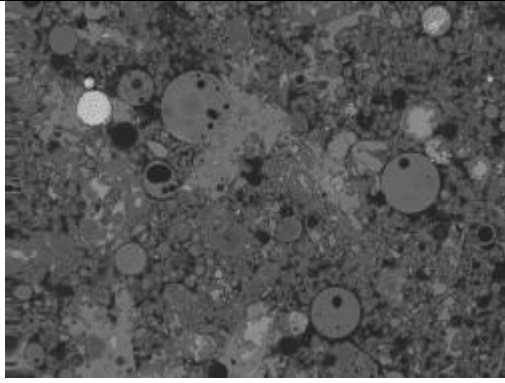
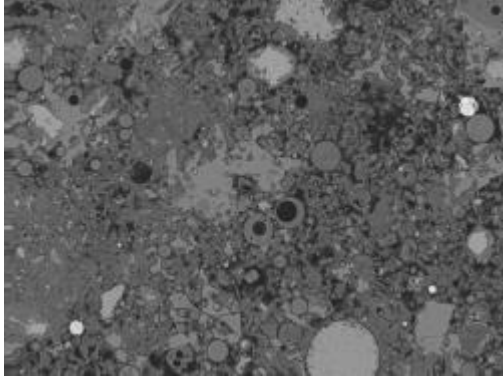
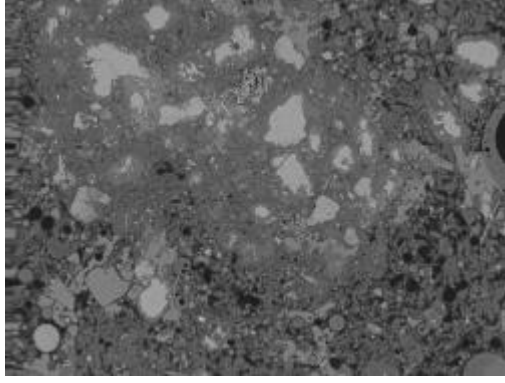
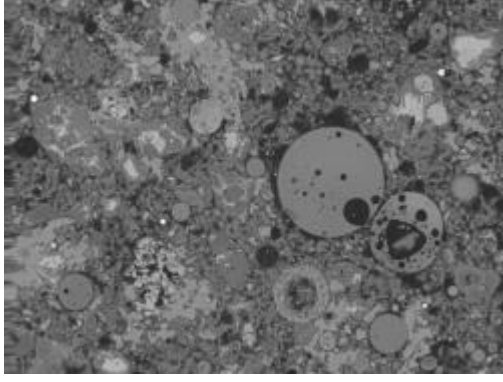
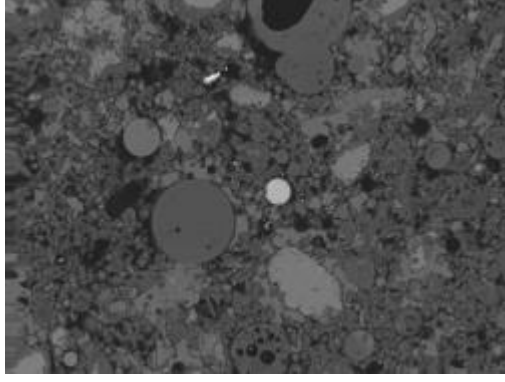
M10 W

	
Image 001	Image 002
	
Image 006	Image 007
	
Image 008	Image 009

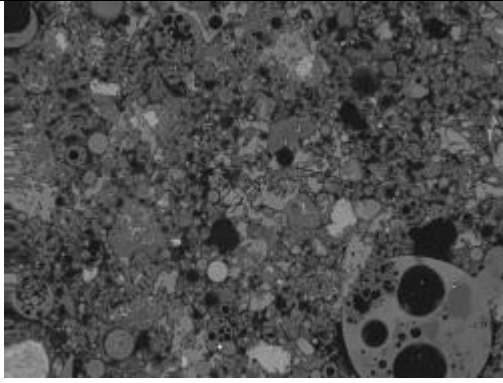
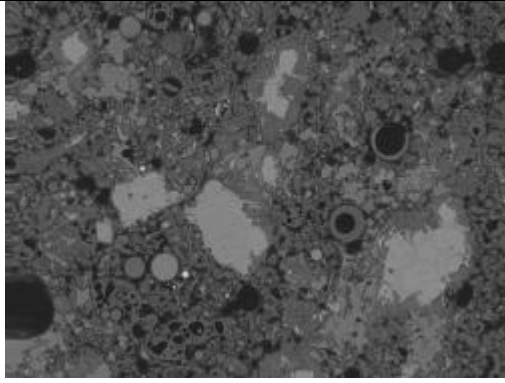
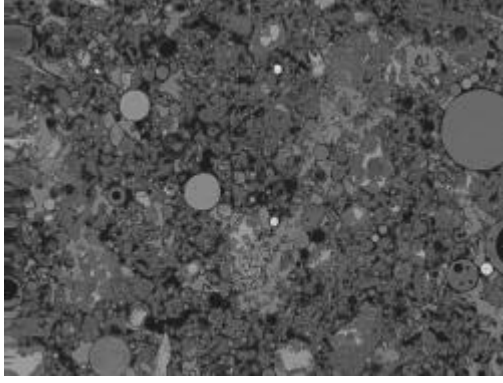
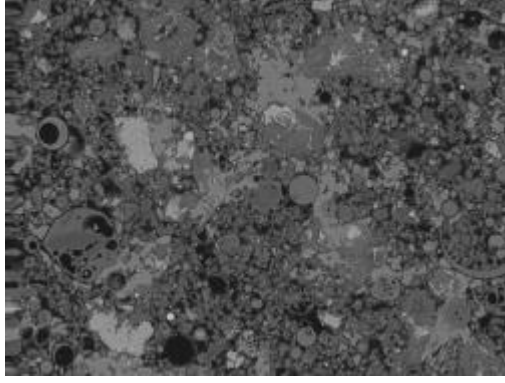
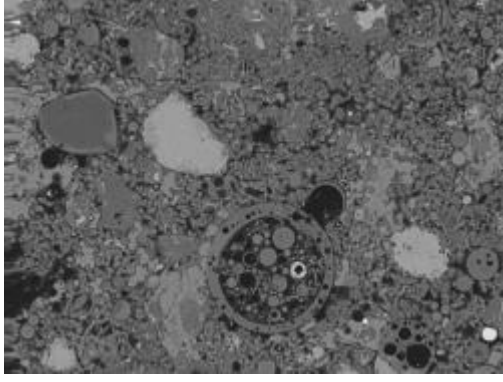
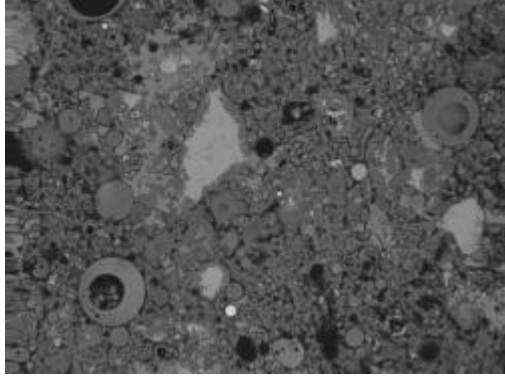
20MPa Fly ash wet mix ideal cured

	
Image 010	Image 011
	
Image 012	Image 014
	
Image 015	Image 017

20MPa Fly ash wet mix ideal cured

	
Image 018	Image 019
	
Image 020	Image 021
	
Image 022	Image 024

20MPa Fly ash wet mix ideal cured

	
Image 028	Image 029
	
Image 031	Image 032
	
Image 036	Image 037

20MPa Fly ash wet mix ideal cured

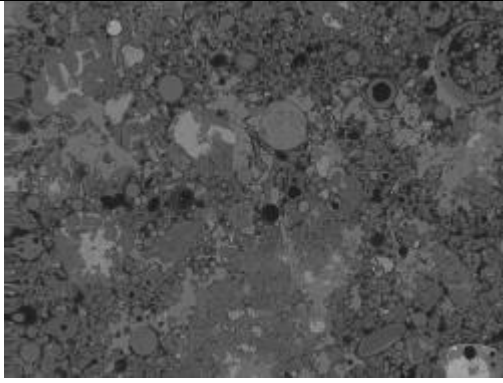
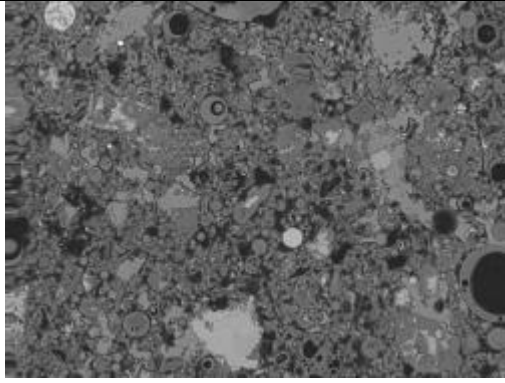
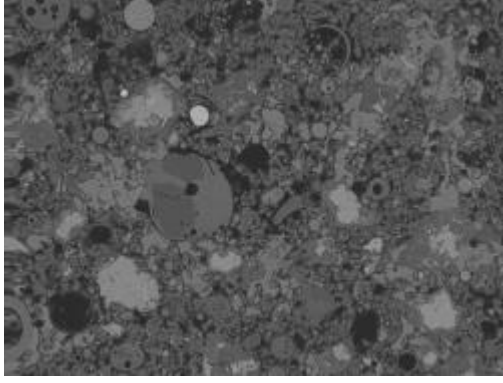
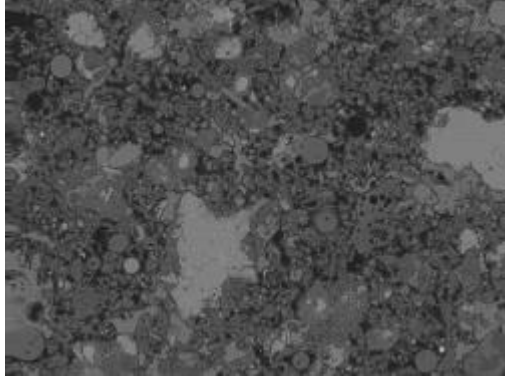
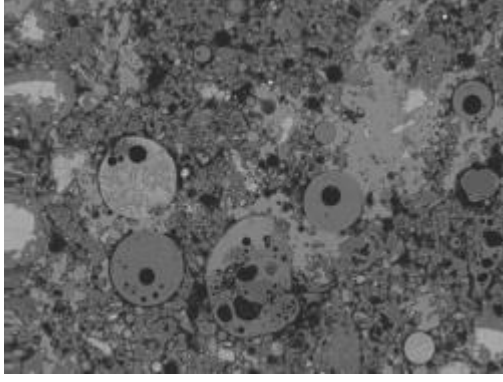
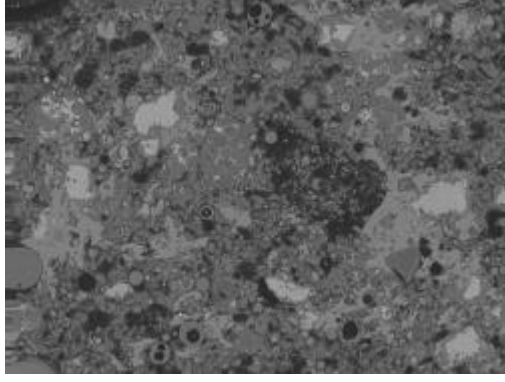
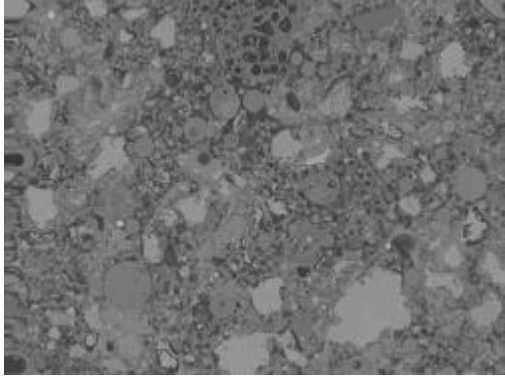
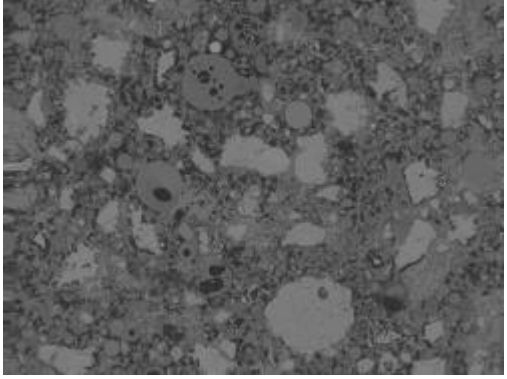
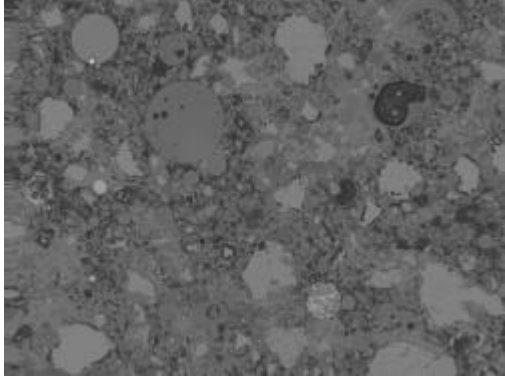
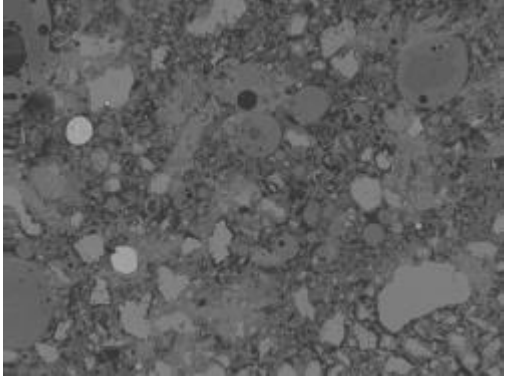
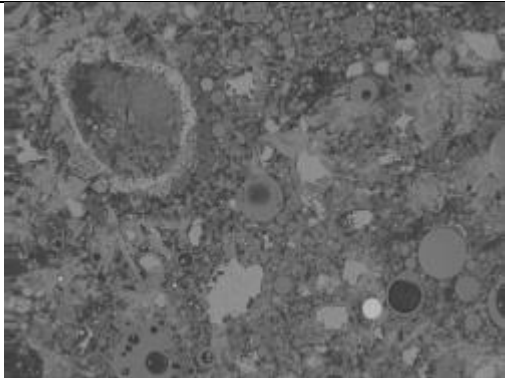
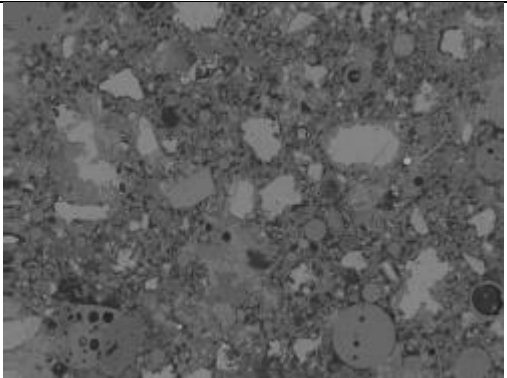
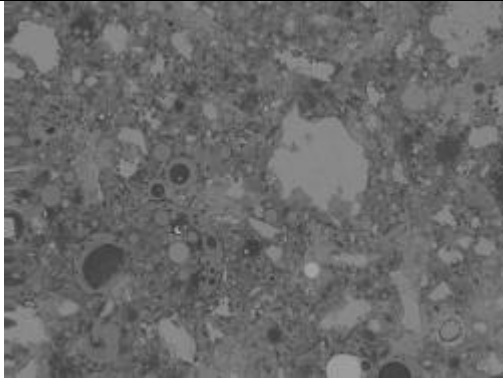
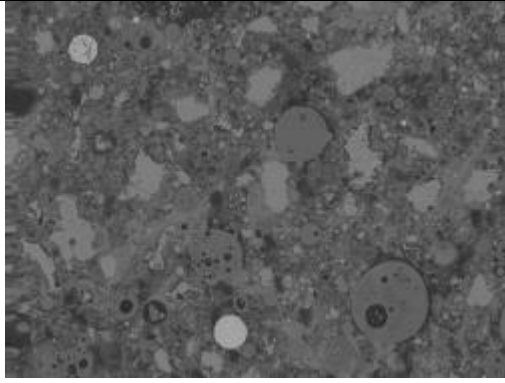
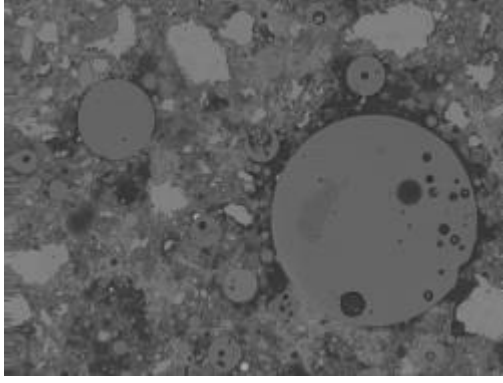
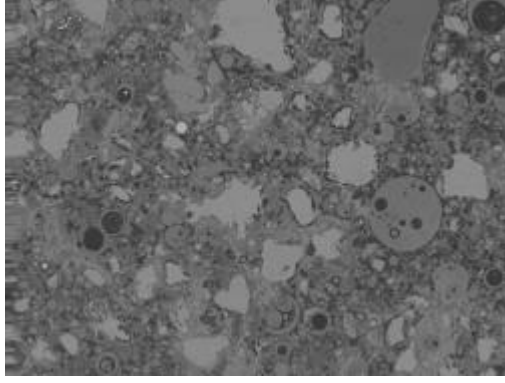
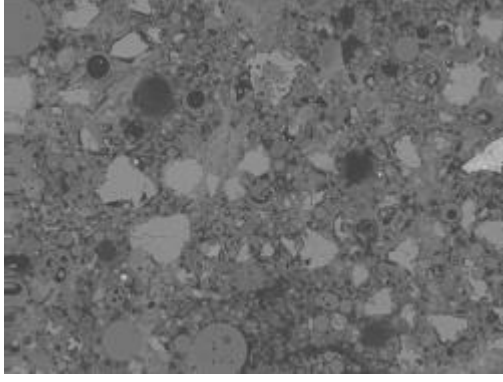
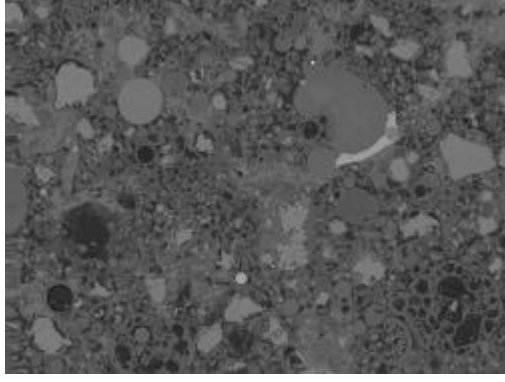
	
Image 038	Image 039
	
Image 040	Image 041
	
Image 044	Image 049

Figure A 110 Images of 20MPa Fly ash wet mix ideal cured

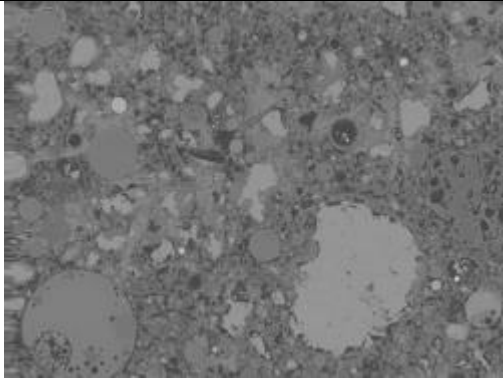
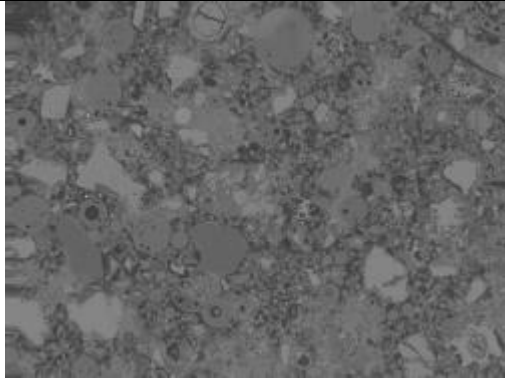
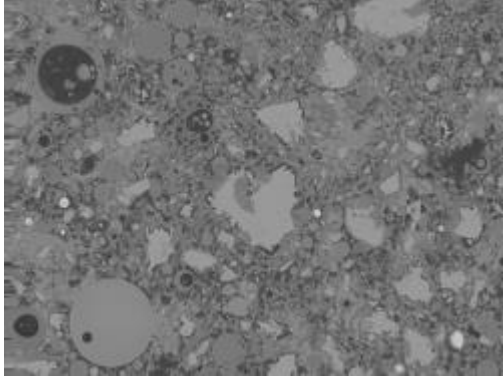
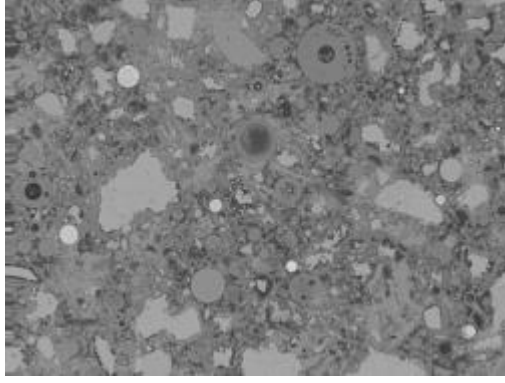
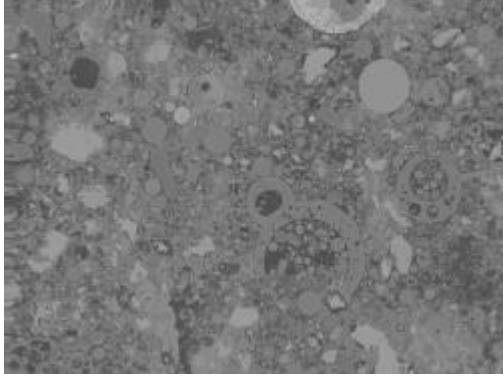
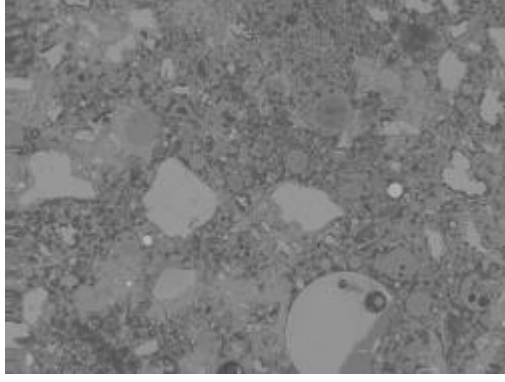
M11A

	
Image 003	Image 004
	
Image 005	Image 007
	
Image 008	Image009

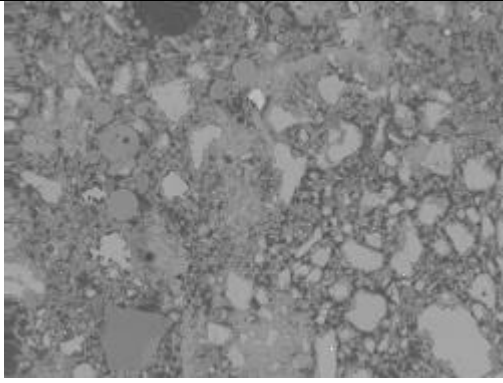
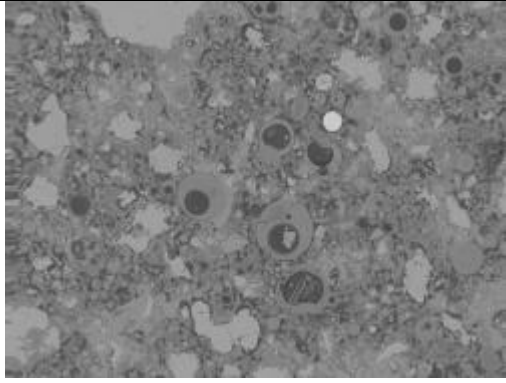
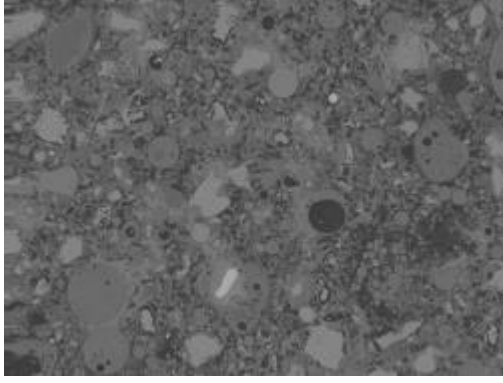
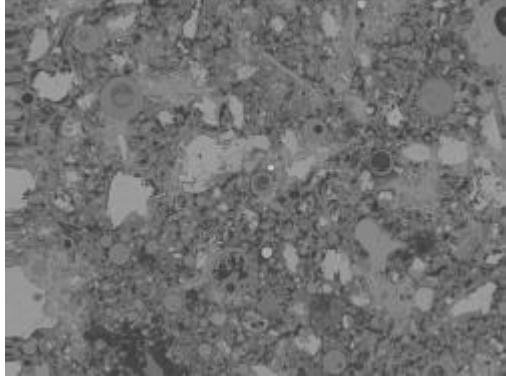
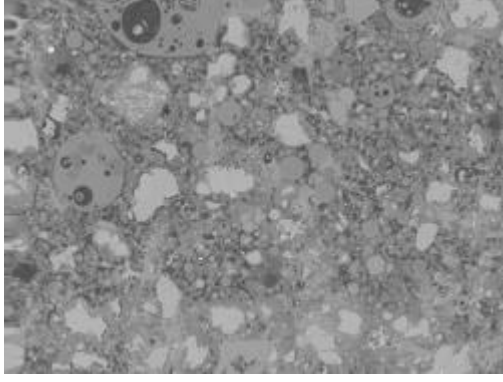
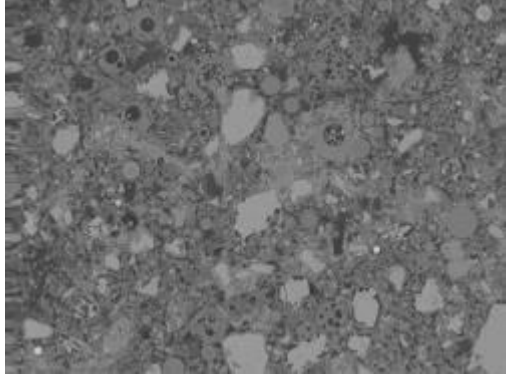
50MPa Fly ash wet mix ambient cured

	
Image 010	Image 011
	
Image 012	Image 013
	
Image 014	Image 015

50MPa Fly ash wet mix ambient cured

	
Image 016	Image 017
	
Image 018	Image 019
	
Image 020	Image 021

50MPa Fly ash wet mix ambient cured

	
Image 022	Image 023
	
Image 024	Image 025
	
Image 026	Image 027

50MPa Fly ash wet mix ambient cured

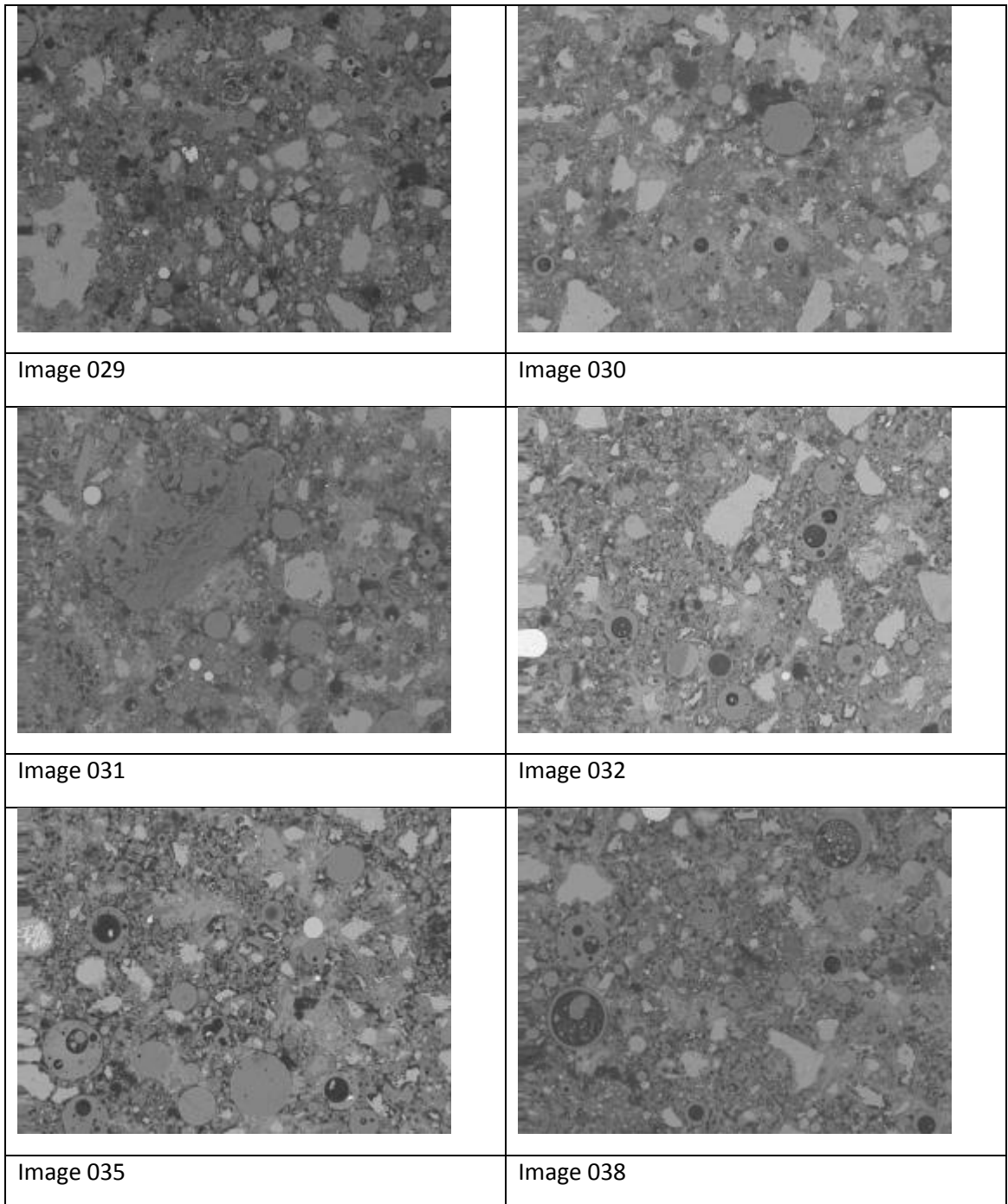
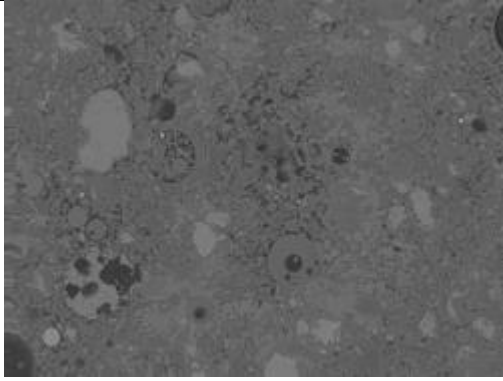
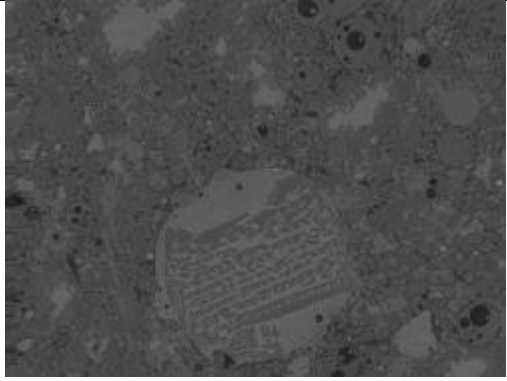
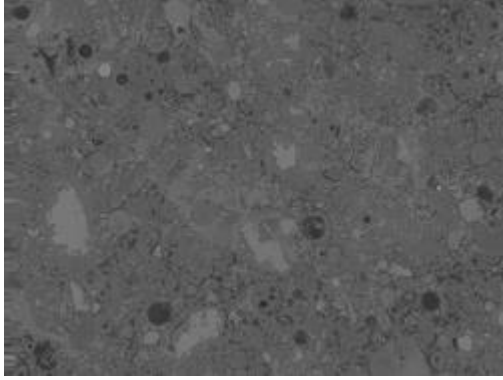
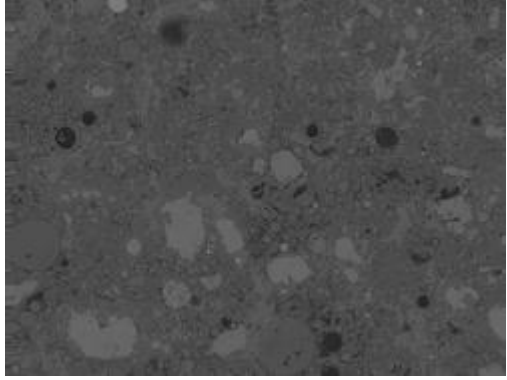
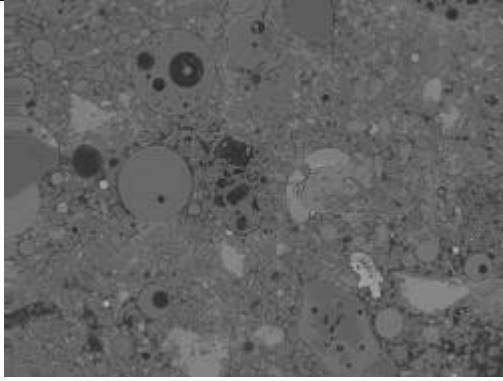
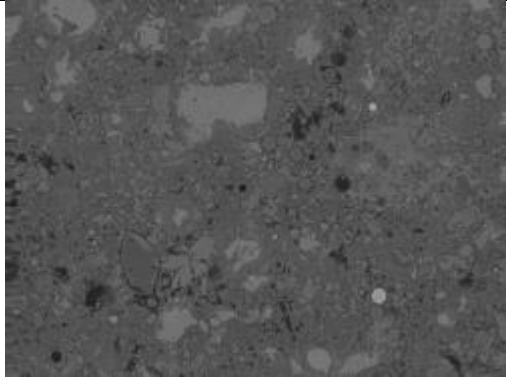
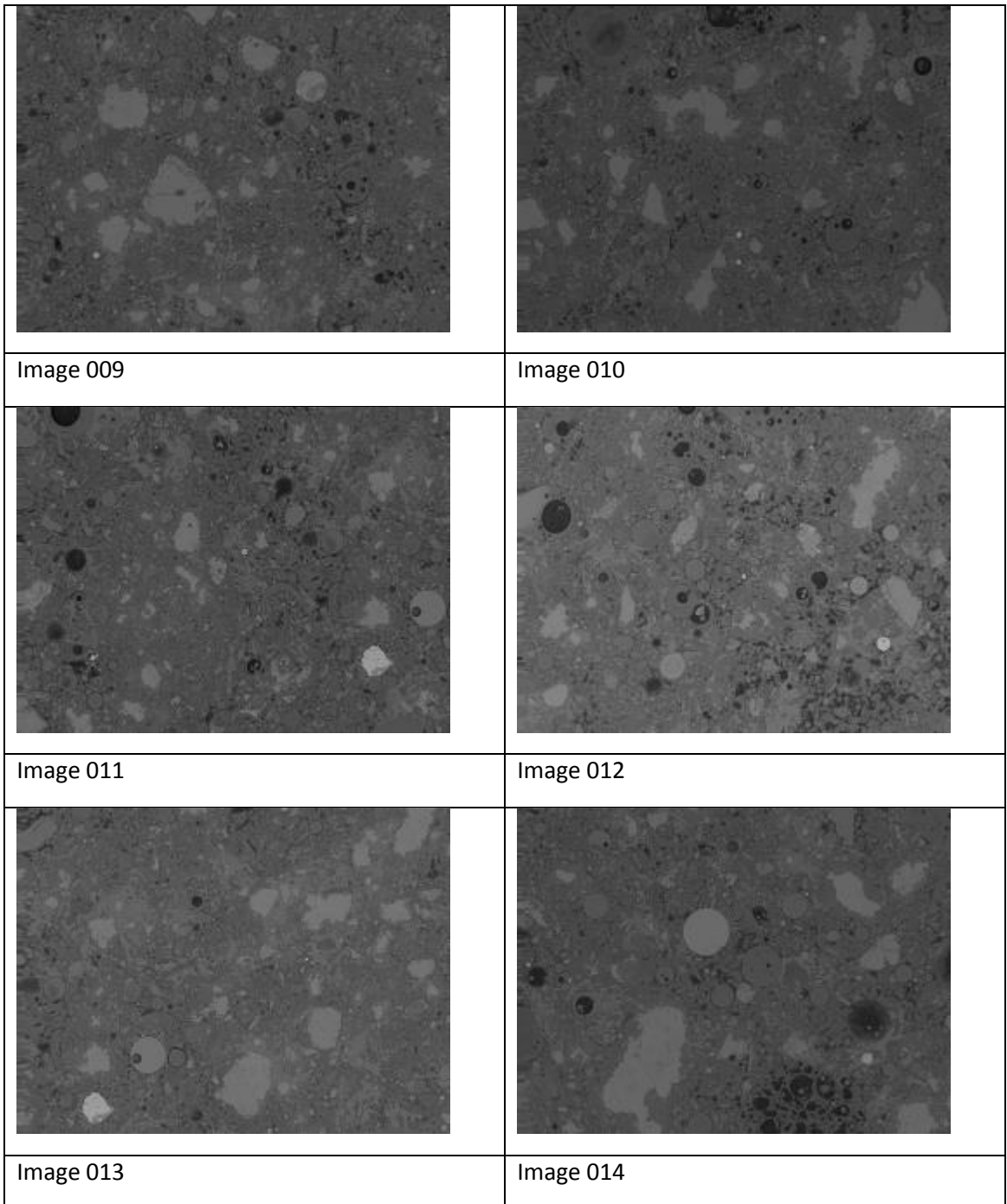


Figure A 111 Images of 50MPa Fly ash wet mix ambient cured

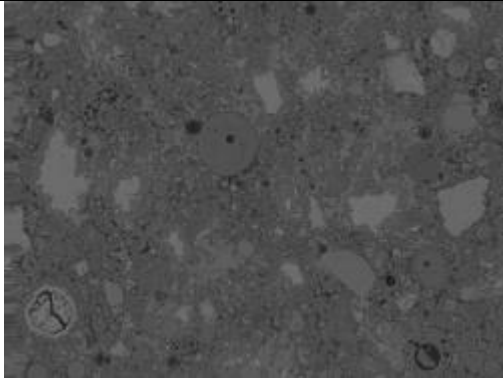
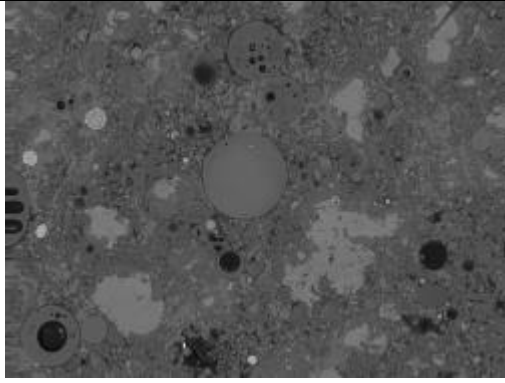
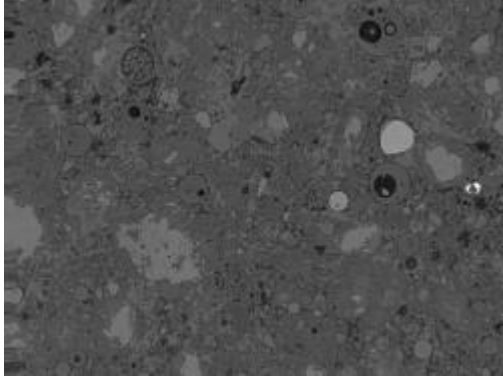
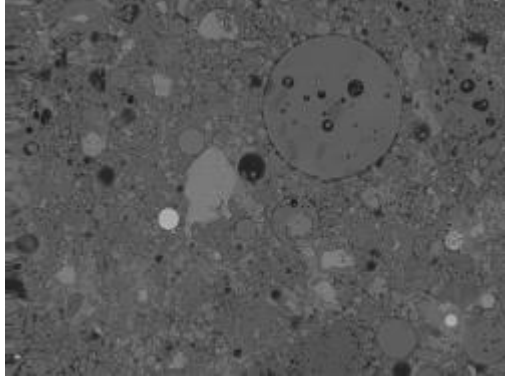
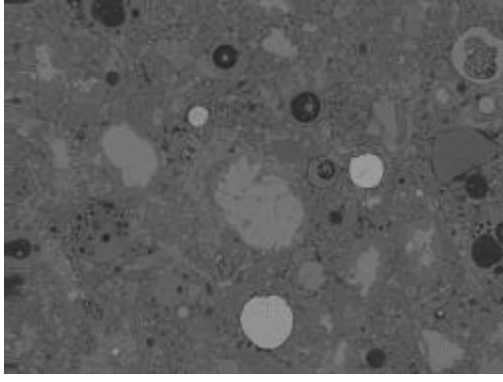
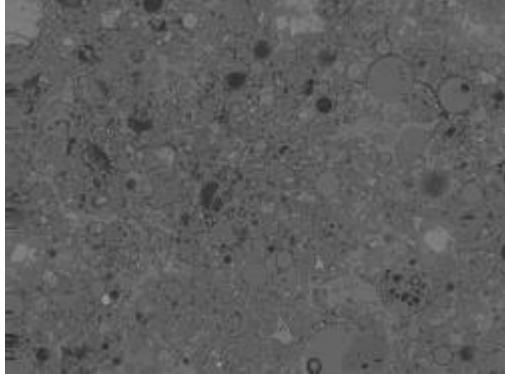
M11W

	
Image 002	Image 004
	
Image 005	Image 006
	
Image 007	Image 008

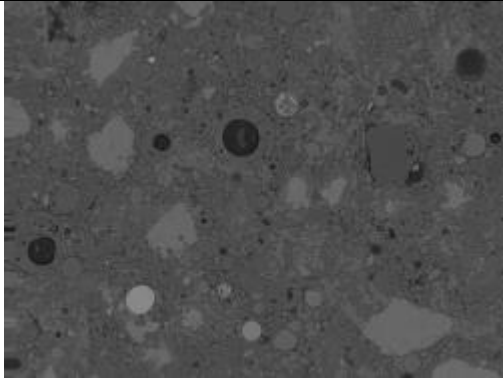
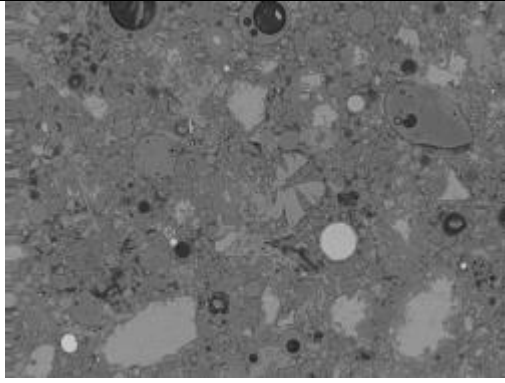
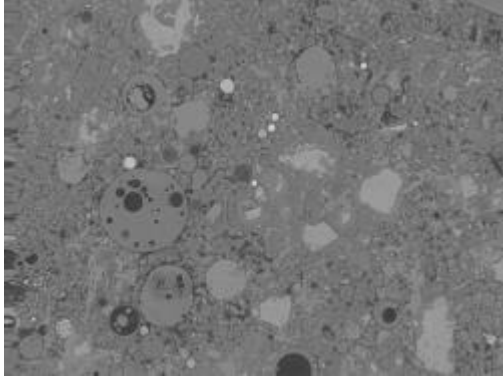
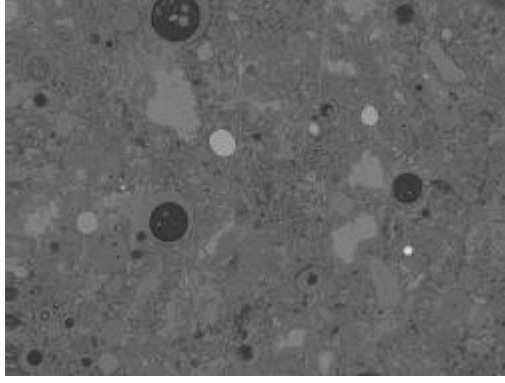
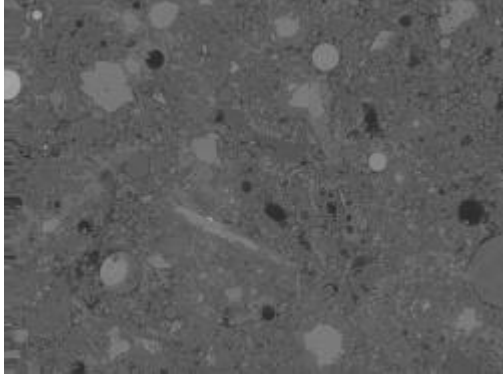
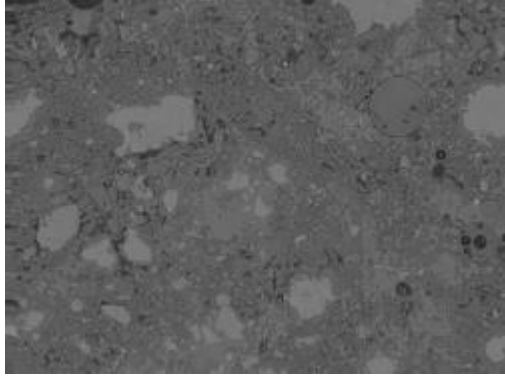
50MPa Fly ash wet mix ideal cured



50MPa Fly ash wet mix ideal cured

	
Image 015	Image 016
	
Image 019	Image 020
	
Image 021	Image 022

50MPa Fly ash wet mix ideal cured

	
Image 023	Image 024
	
Image 025	Image 026
	
Image 027	Image 028

50MPa Fly ash wet mix ideal cured

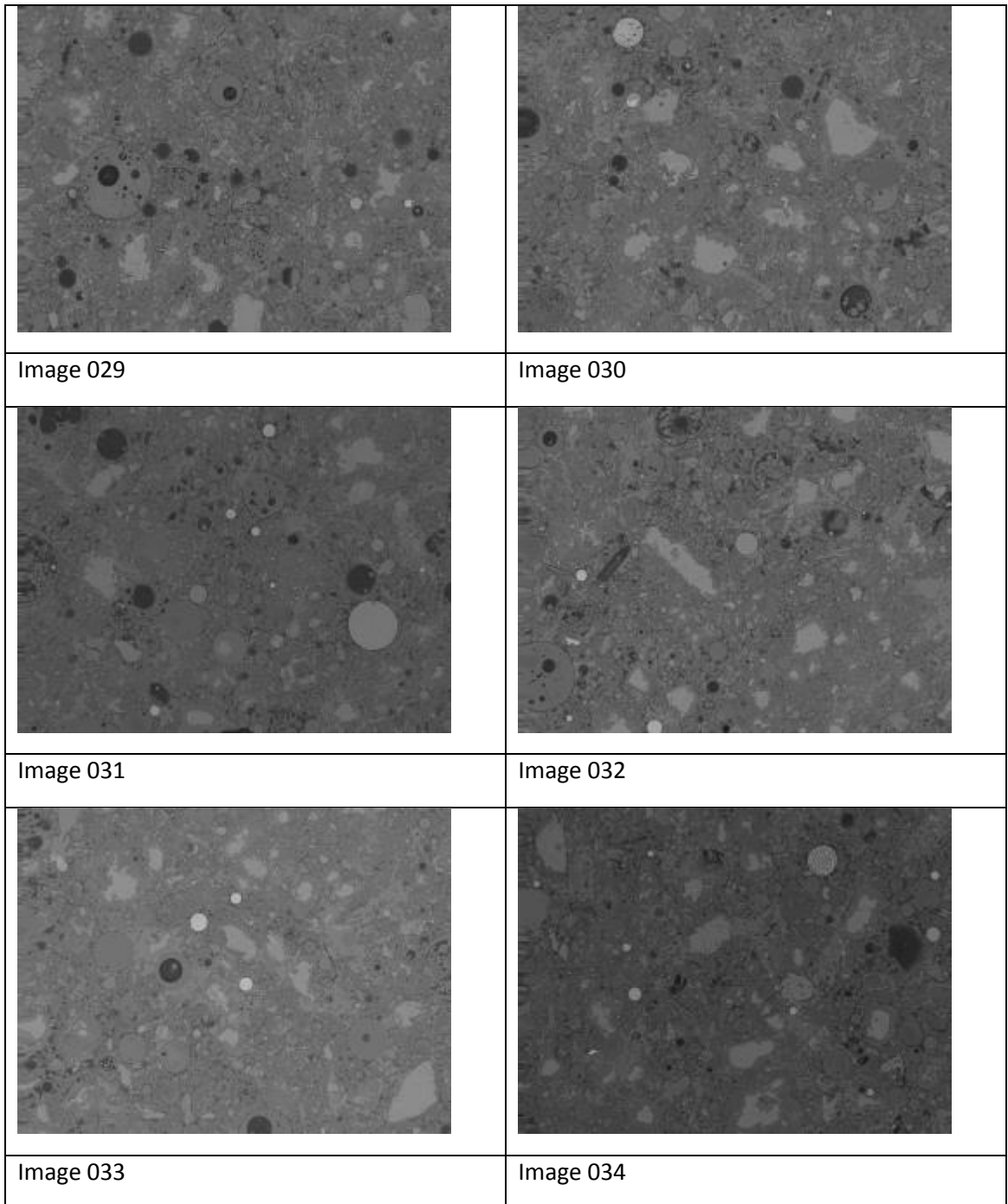
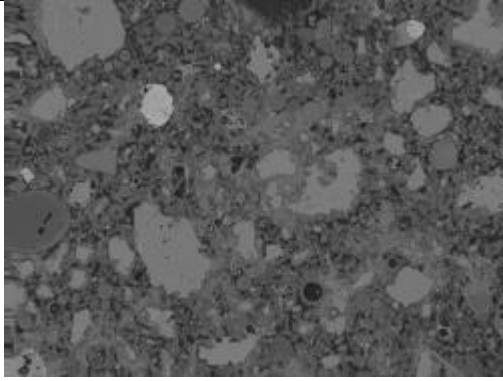
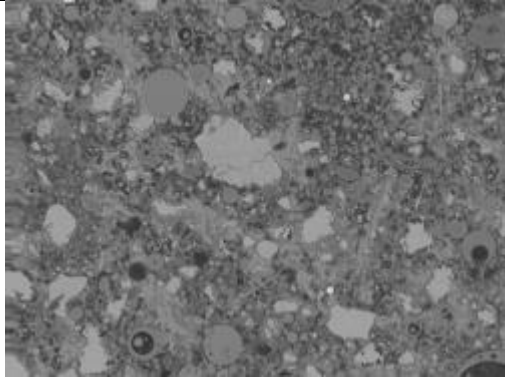
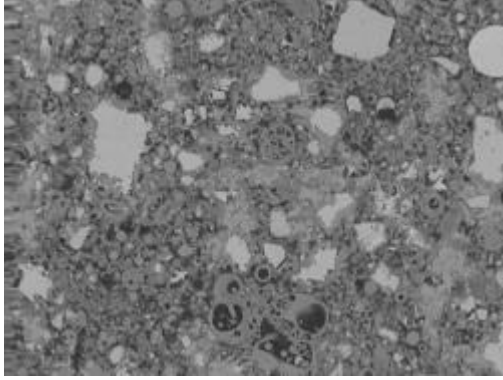
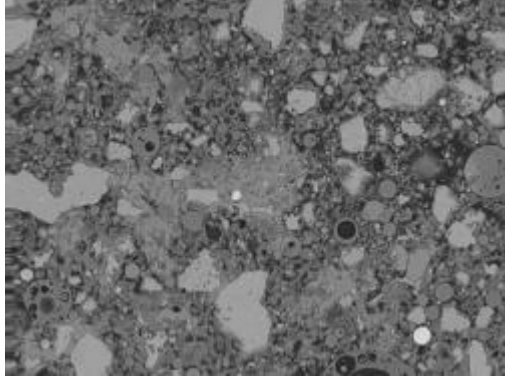
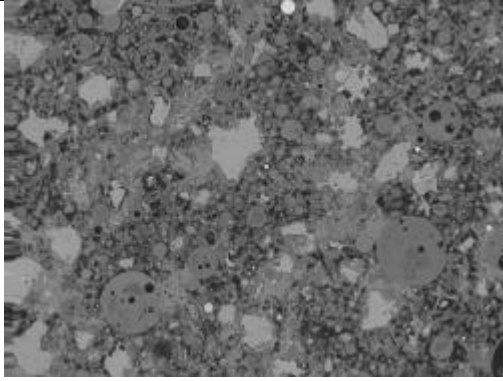
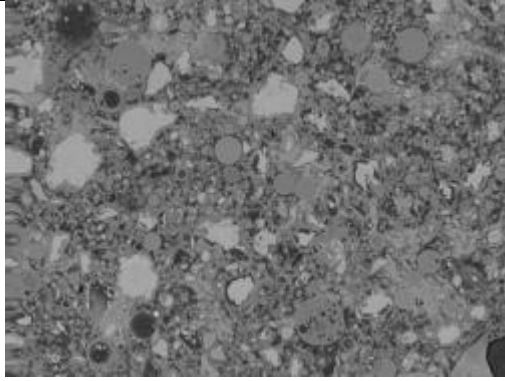
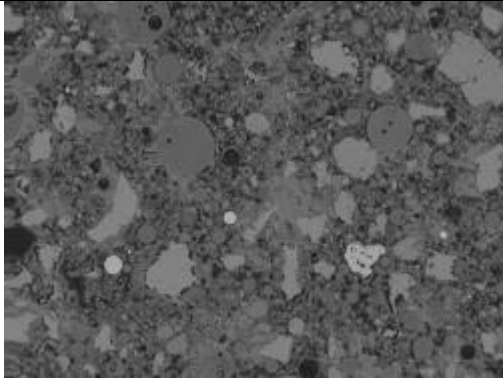
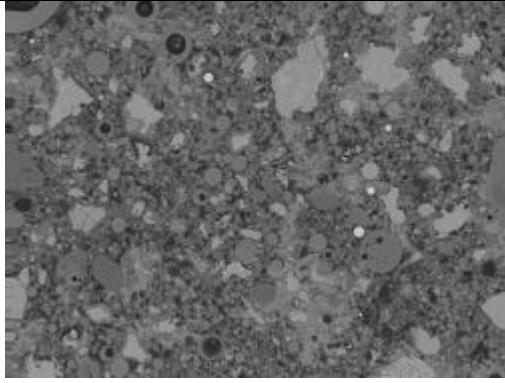
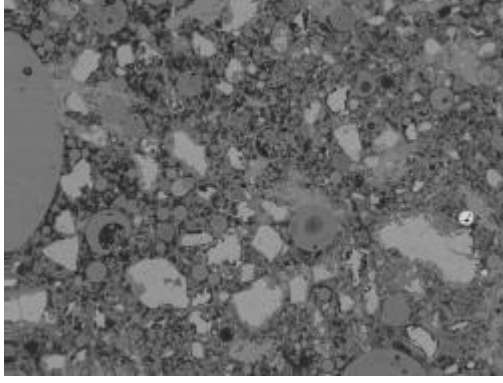
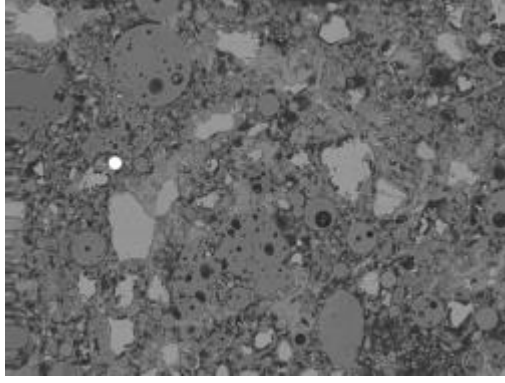
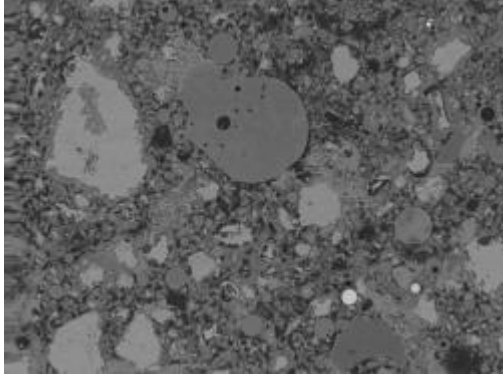
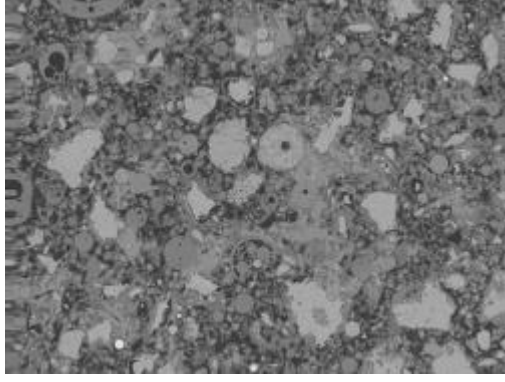


Figure A 112 Images of 50MPa Fly ash wet mix ideal cured

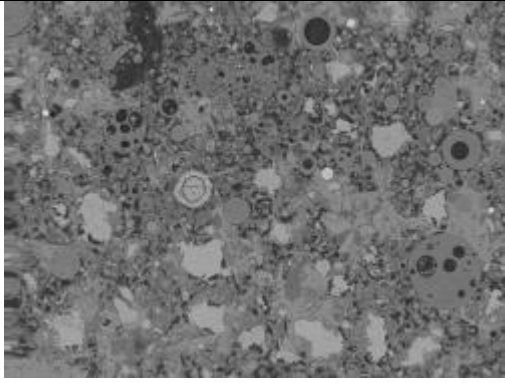
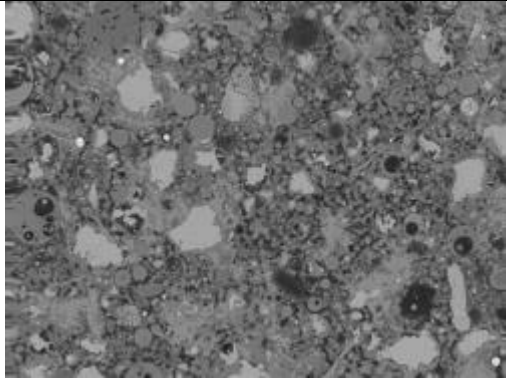
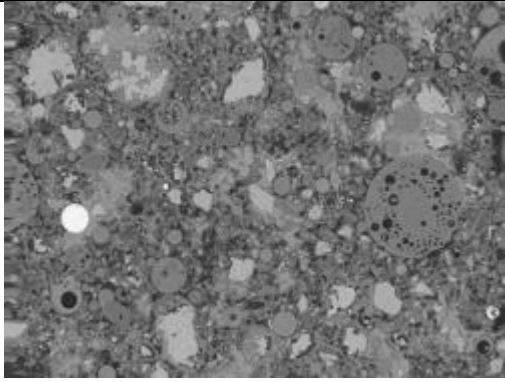
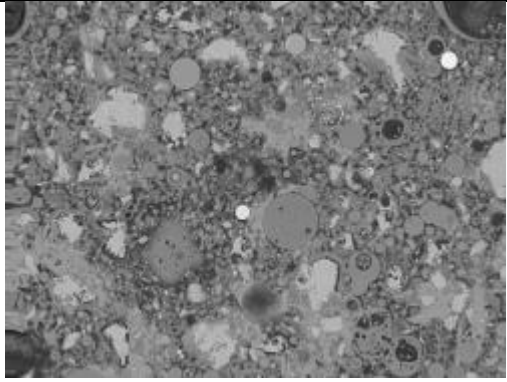
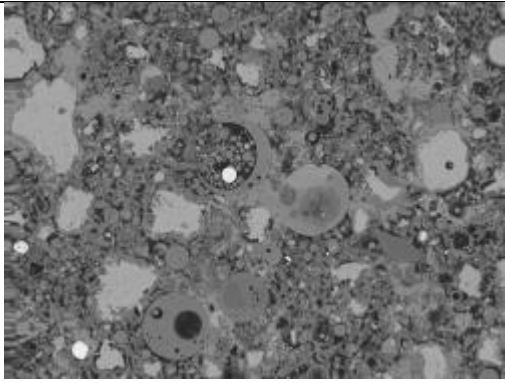
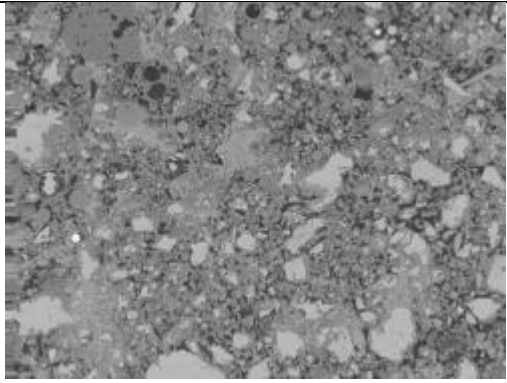
M12A

	
Image 001	Image 002
	
Image 004	Image 006
	
Image 007	Image 008

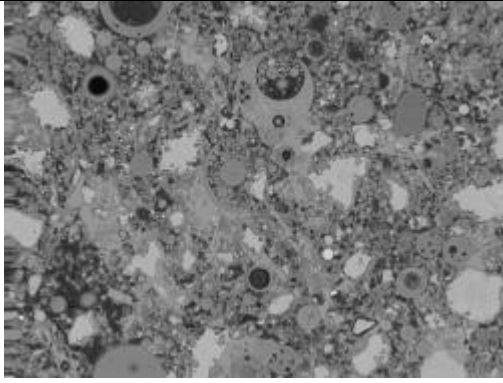
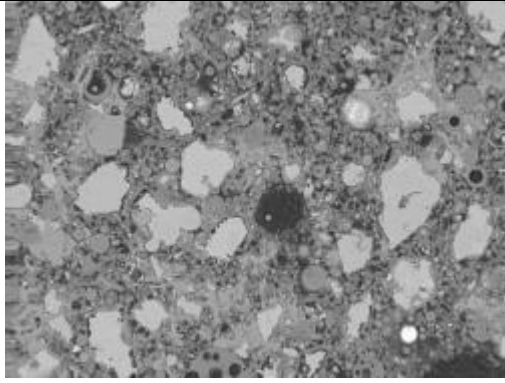
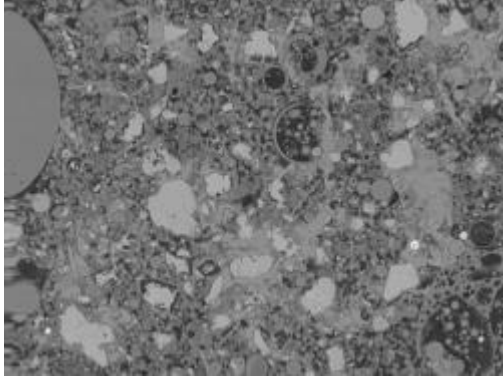
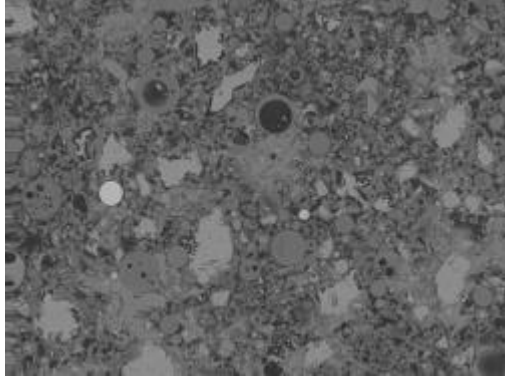
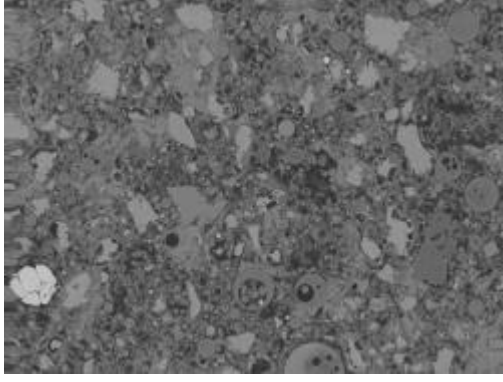
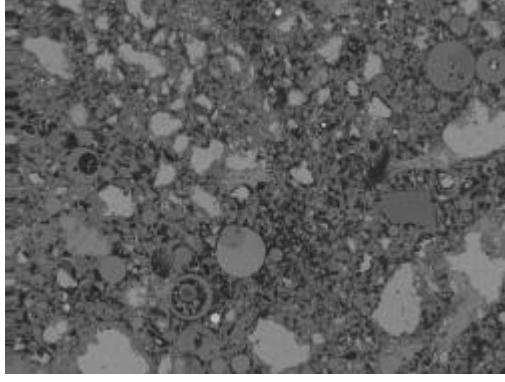
80MPa Fly ash wet mix ambient cured

	
Image 009	Image 010
	
Image 011	Image 012
	
Image 013	Image 014

80MPa Fly ash wet mix ambient cured

	
Image 016	Image 017
	
Image 018	Image 020
	
Image 021	Image 022

80MPa Fly ash wet mix ambient cured

	
Image 025	Image 026
	
Image 027	Image 029
	
Image 030	Image 031

80MPa Fly ash wet mix ambient cured

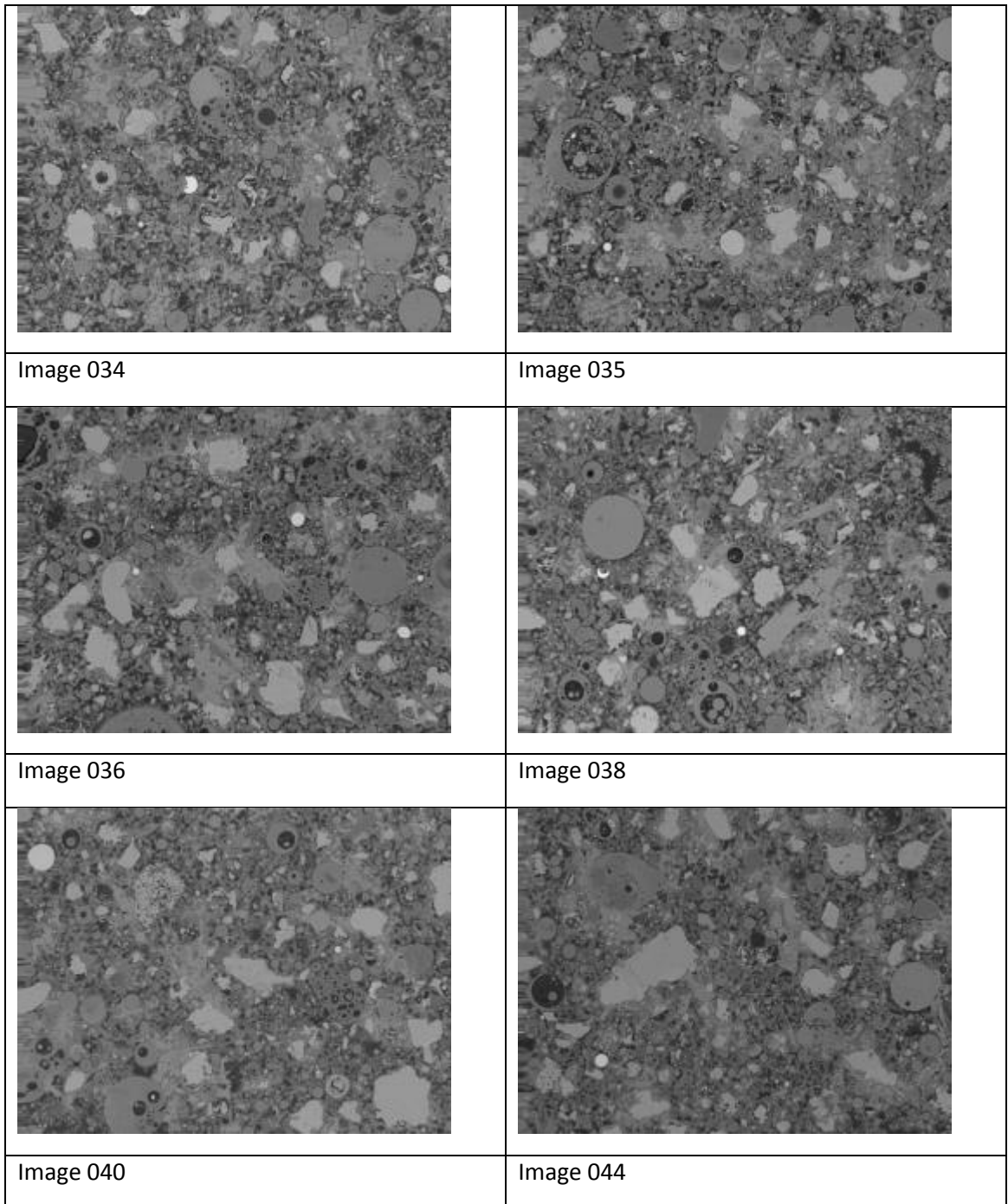
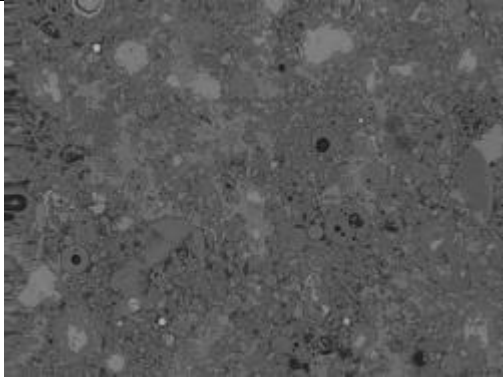
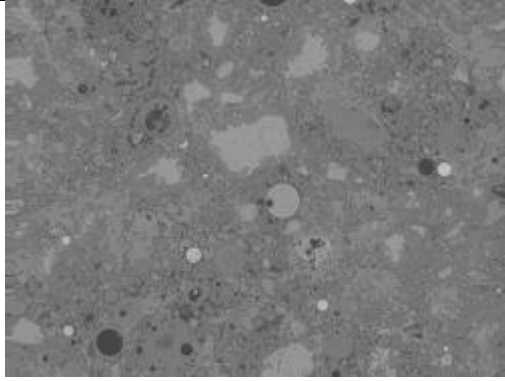
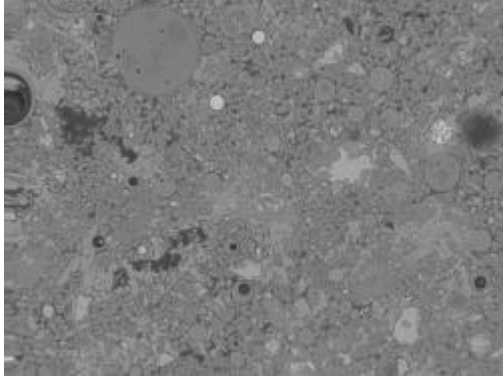
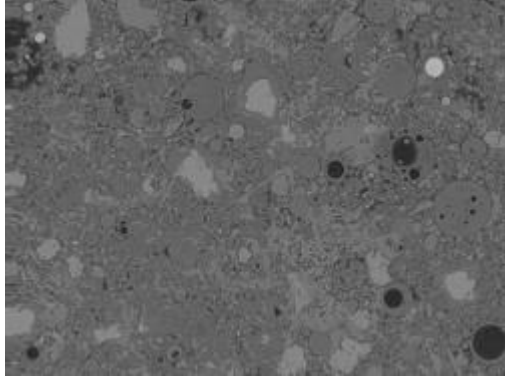
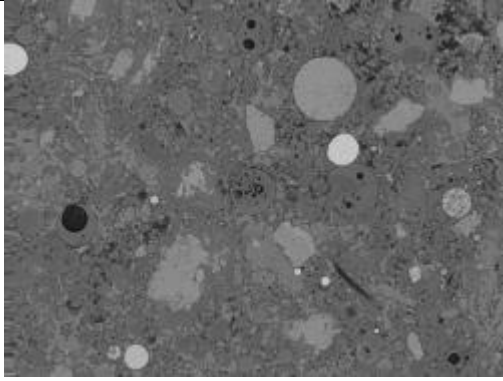
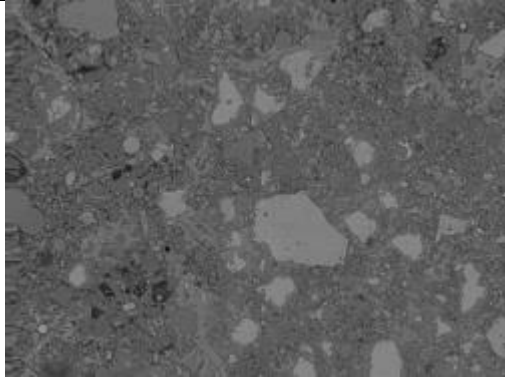
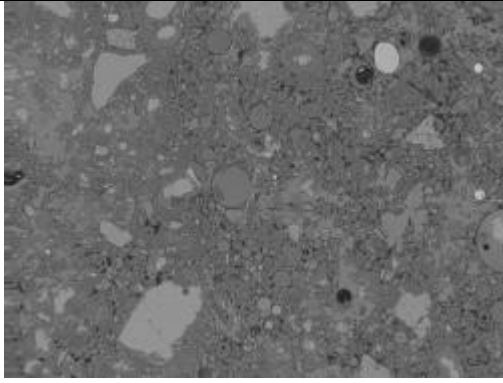
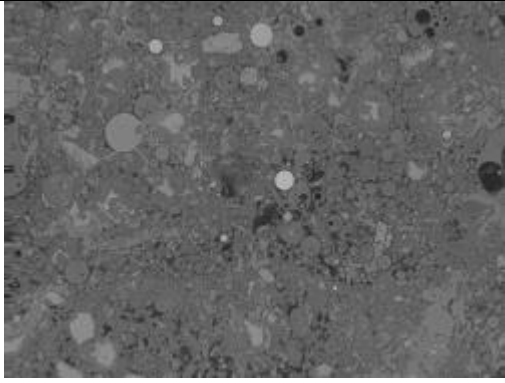
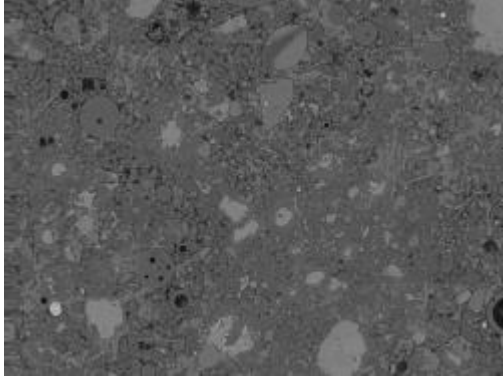
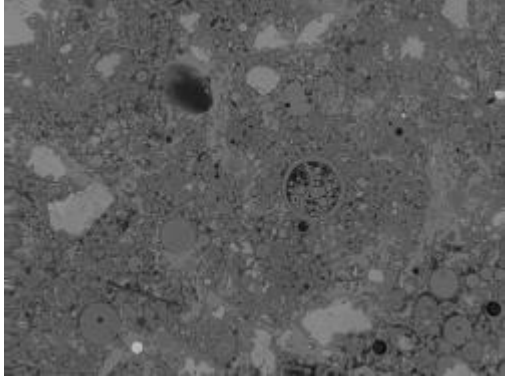
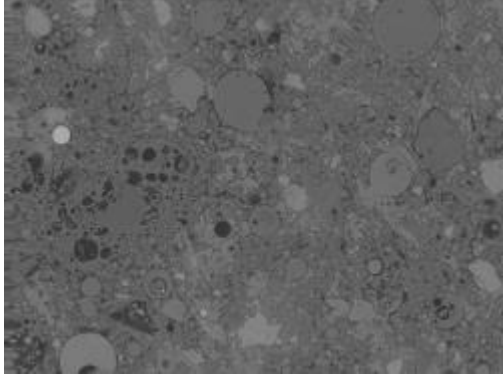
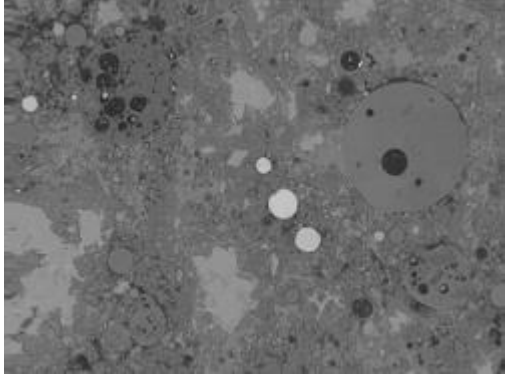


Figure A 113 Images of 80MPa Fly ash wet mix ambient cured

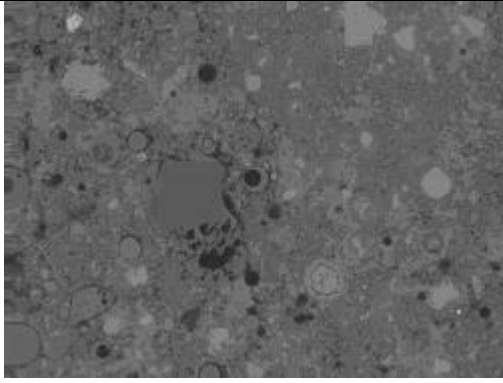
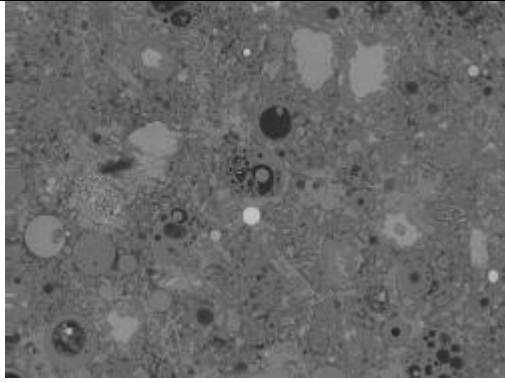
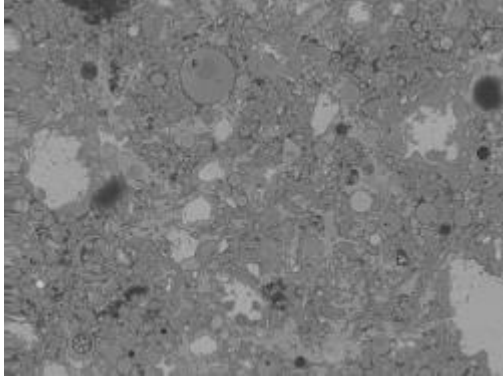
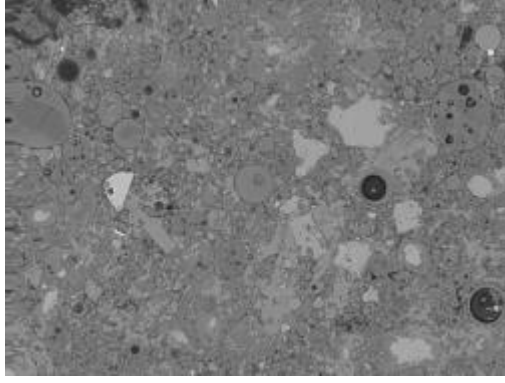
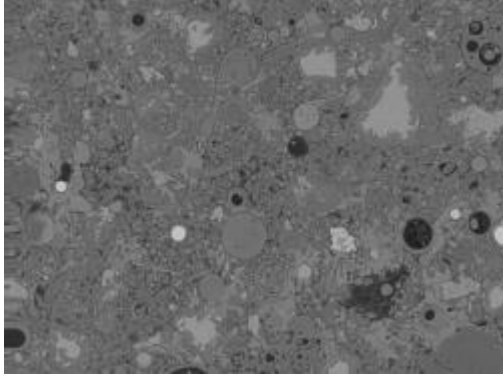
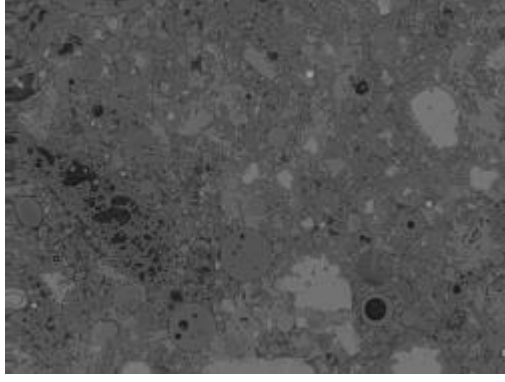
M12W

	
Image 001	Image 002
	
Image 003	Image 004
	
Image 005	Image 006

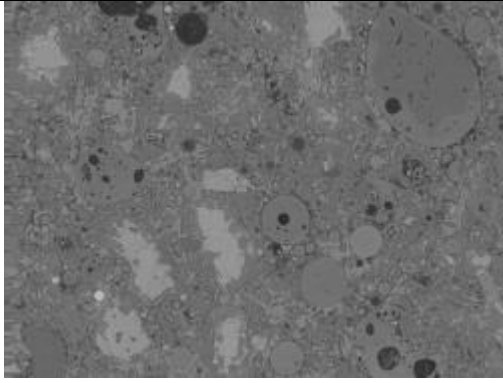
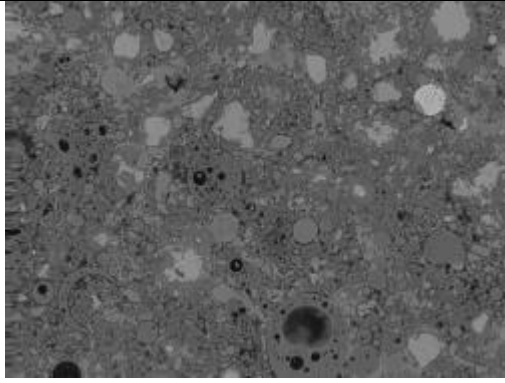
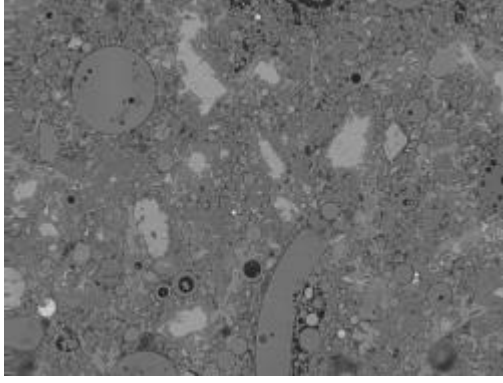
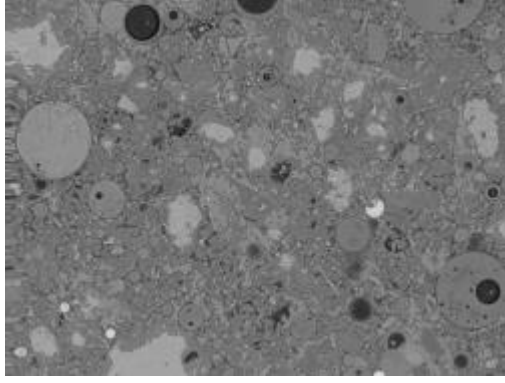
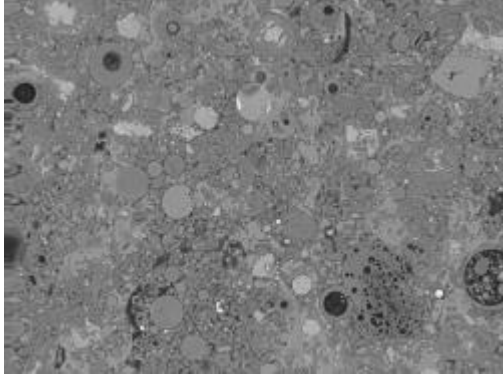
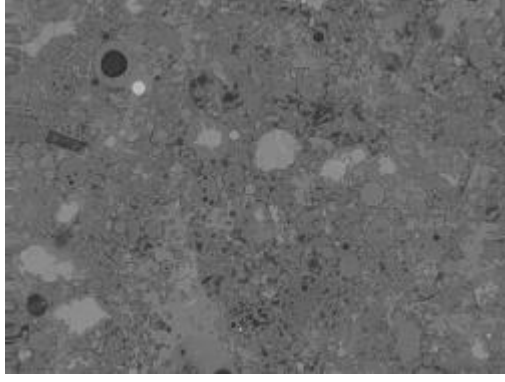
80MPa Fly ash wet mix ideal cured

	
Image 007	Image 008
	
Image 009	Image 011
	
Image 012	Image015

80MPa Fly ash wet mix ideal cured

	
Image 016	Image 017
	
Image 018	Image 019
	
Image 020	Image 021

80MPa Fly ash wet mix ideal cured

	
Image 023	Image 024
	
Image 026	Image 027
	
Image 028	Image 029

80MPa Fly ash wet mix ideal cured

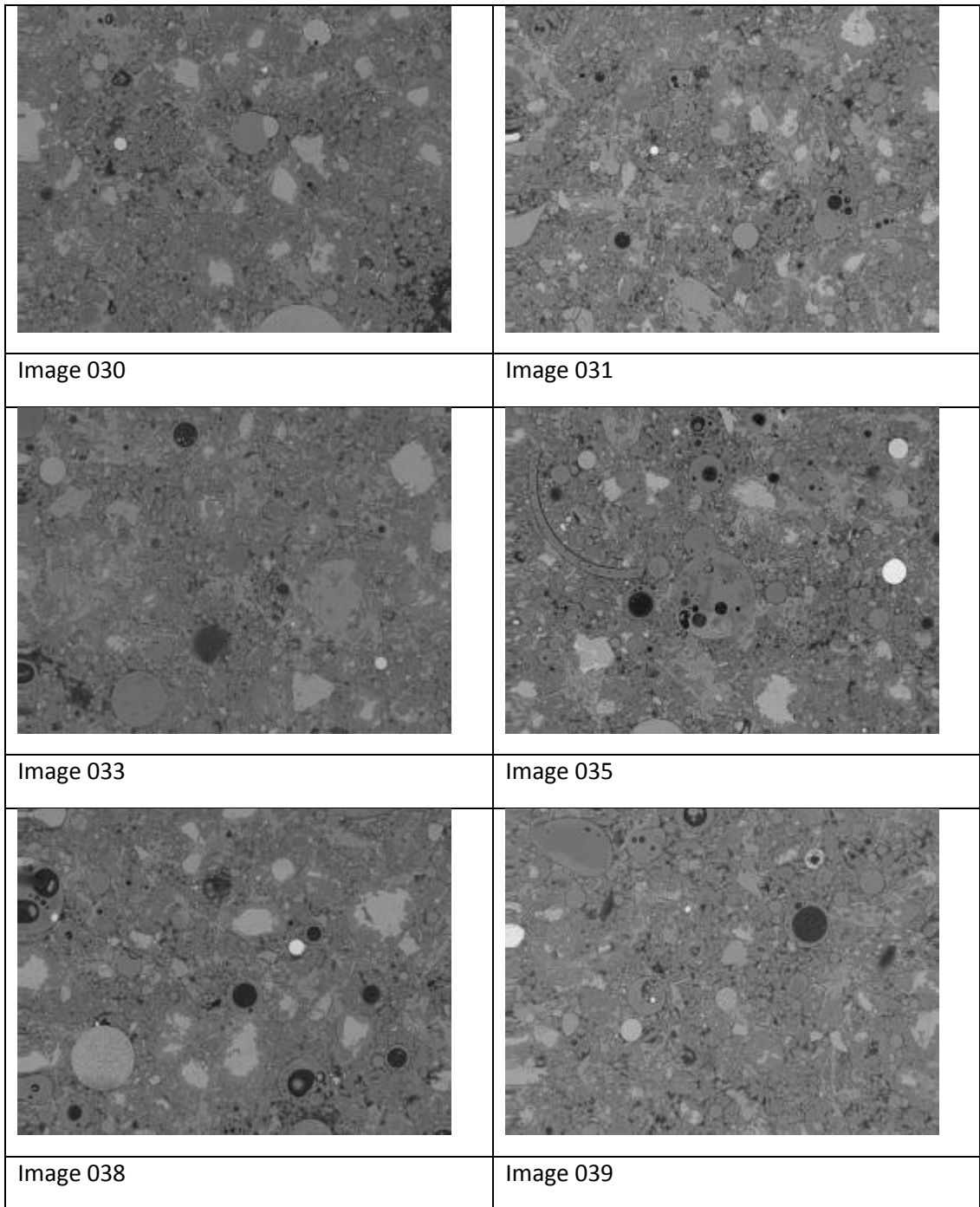


Figure A 114 Images of 80MPa Fly ash wet mix ideal cured

The TG results

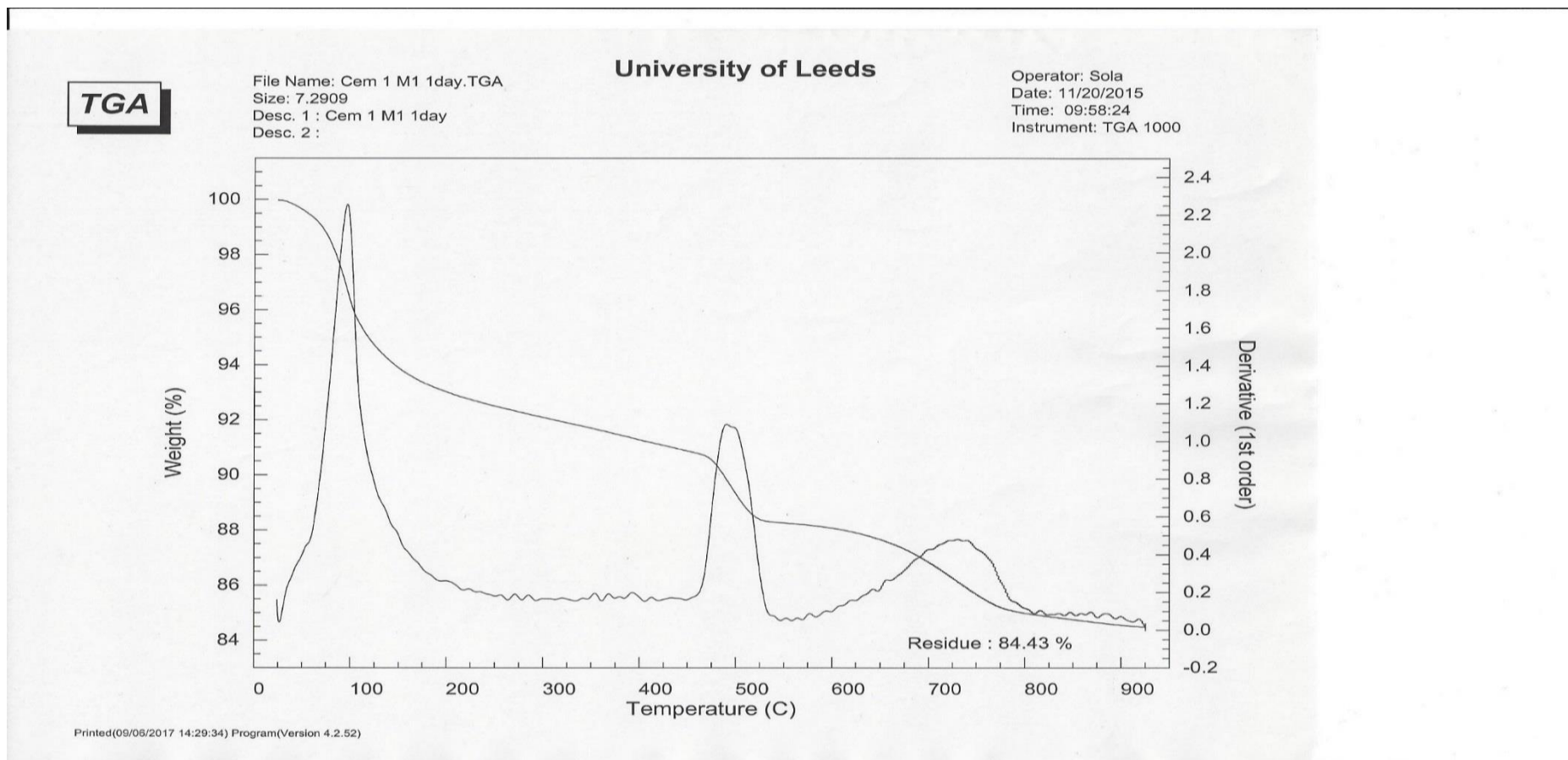


Figure A 115 TG result of 20MPa CEM1 stiff mix ambient cured 1 day

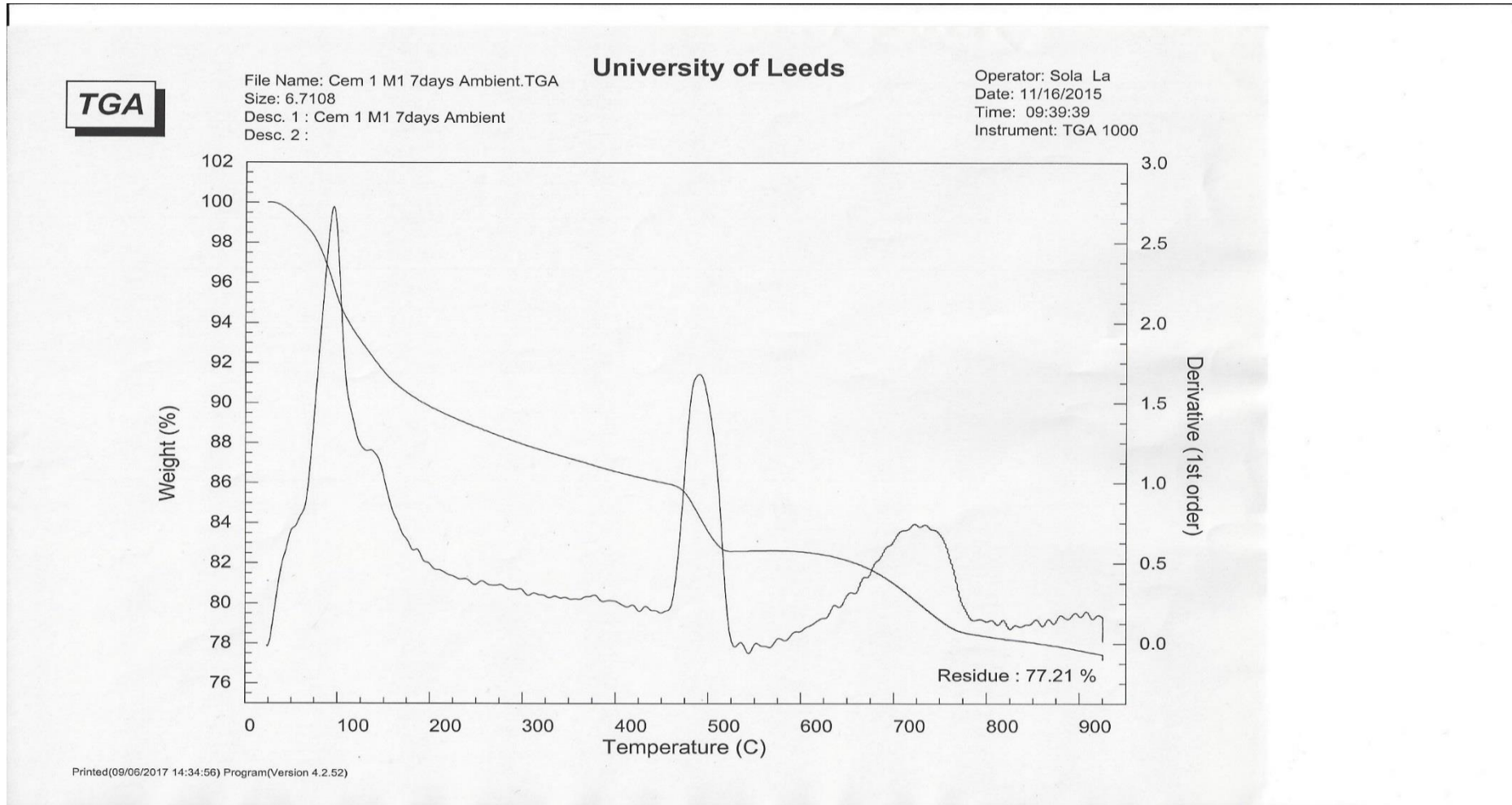


Figure A 116 TG result of 20MPa CEM1 stiff mix ambient cured 7 days

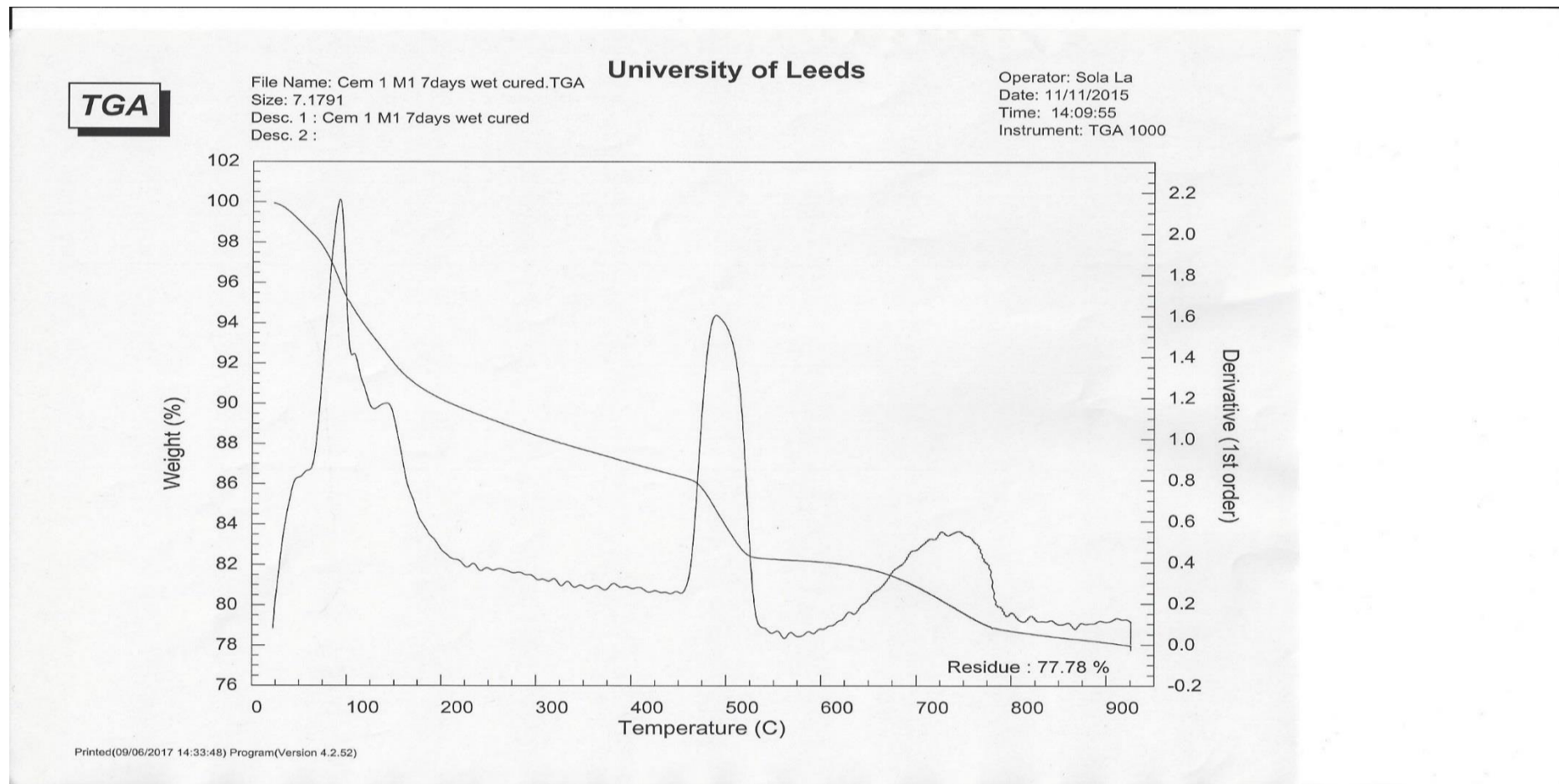


Figure A 117 TG result of 20MPa CEM1 stiff mix ideal cured 7 days

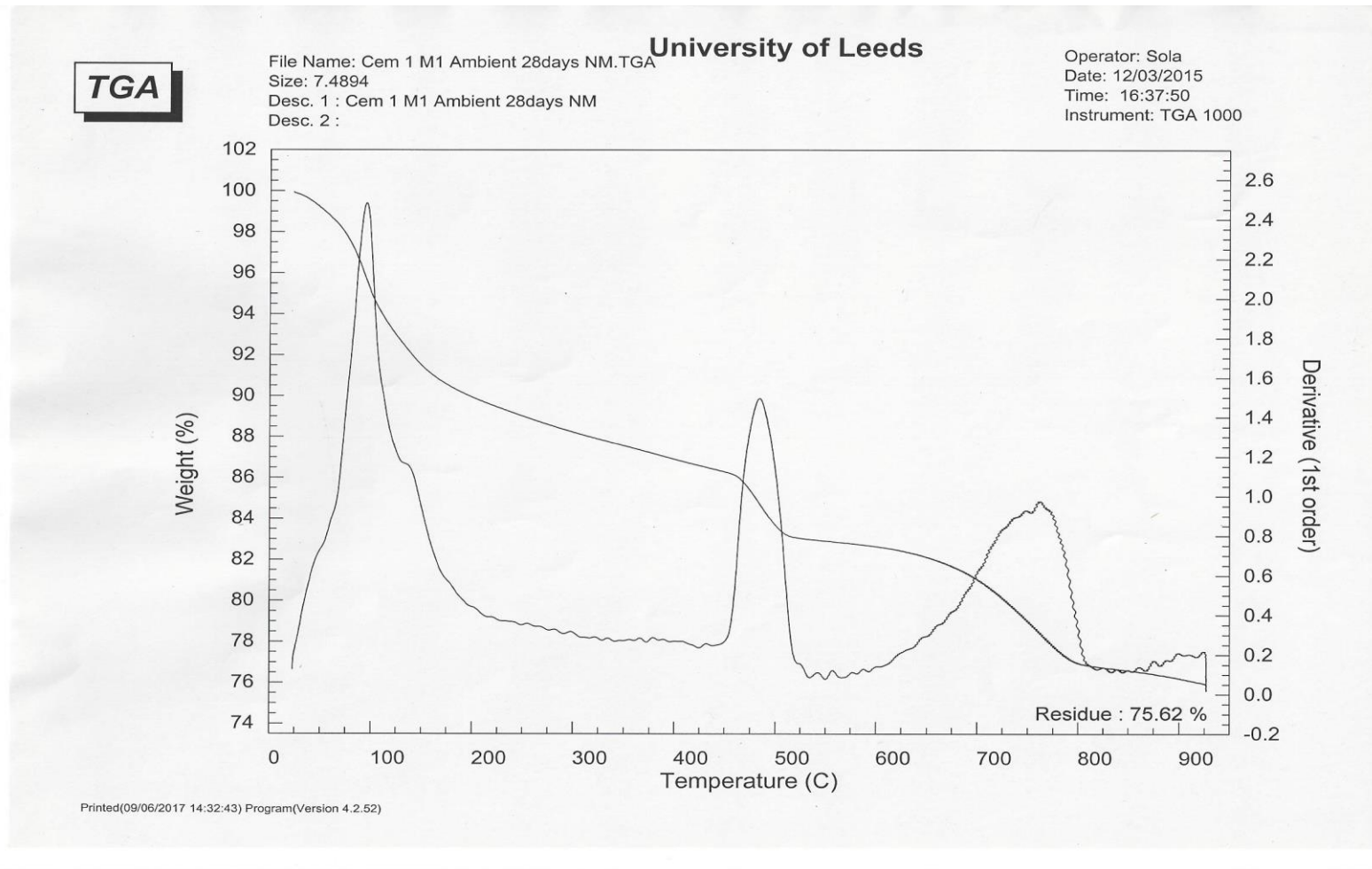


Figure A 118 TG result of 20MPa CEM1 stiff mix ambient cured 28 days

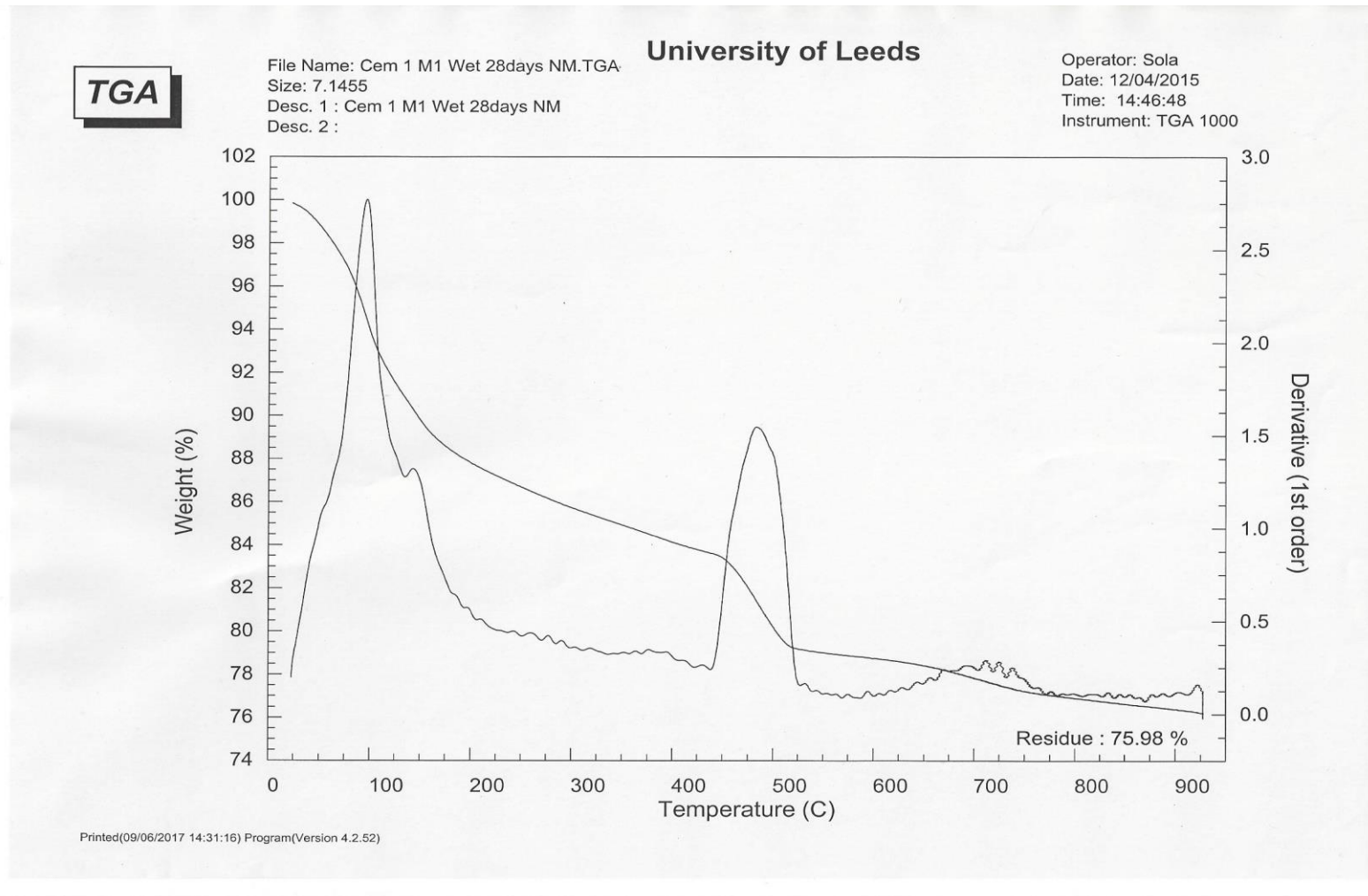


Figure A 119 TG result of 20MPa CEM1 stiff mix ideal cured 28 days

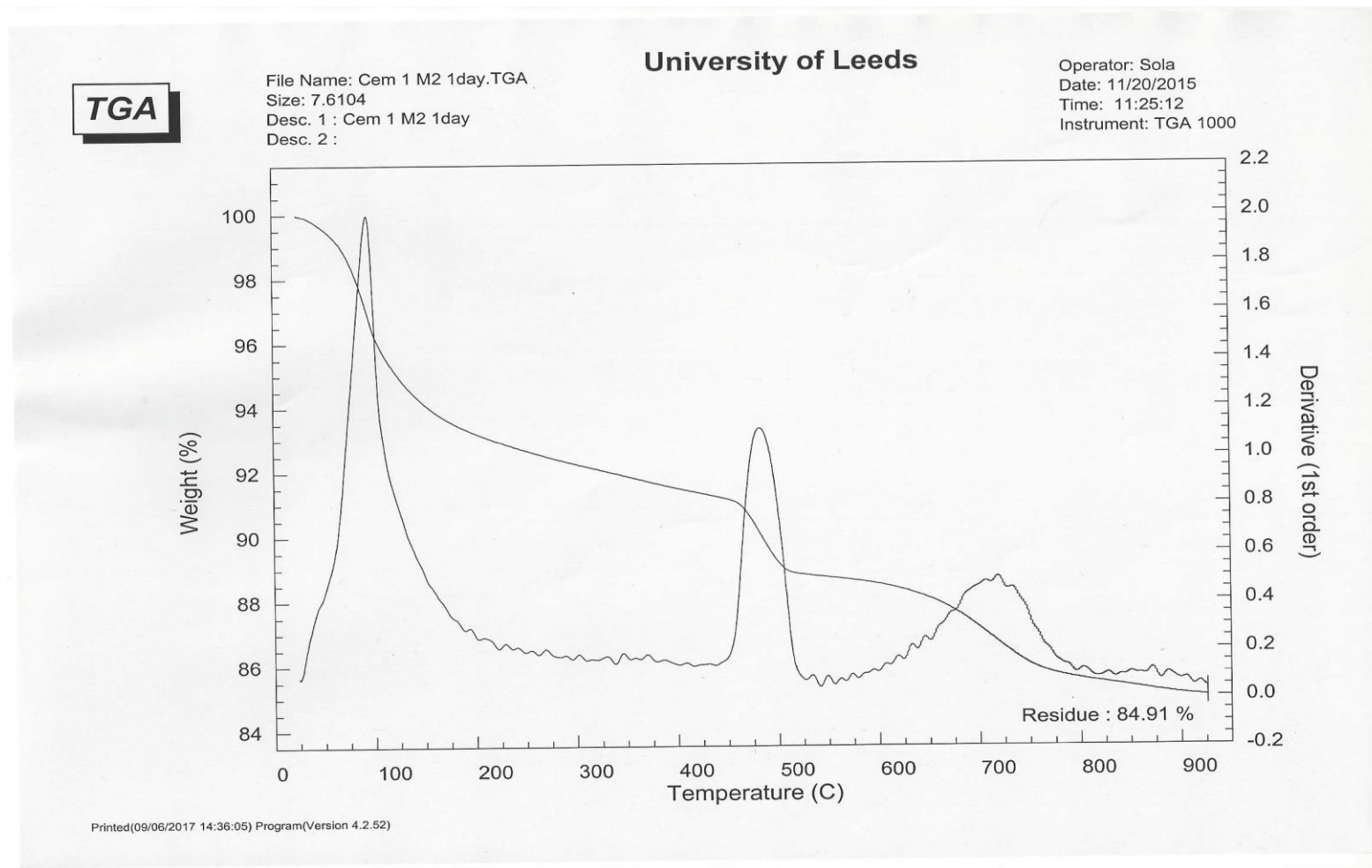


Figure A 120 TG result of 50MPa CEM1 stiff mix ambient cured 1 day

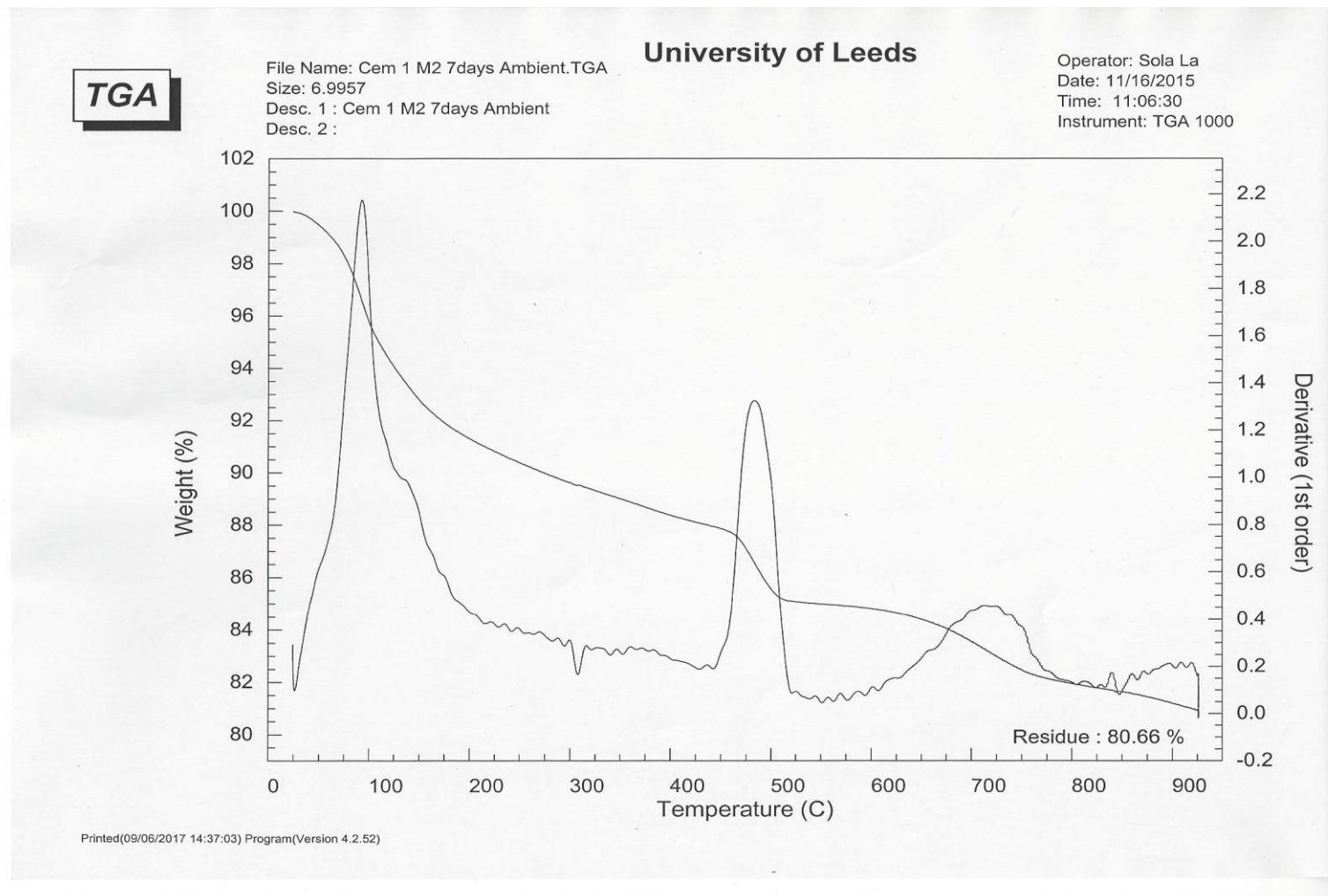


Figure A 121 TG result of 50MPa CEM1 stiff mix ambient cured 7 day

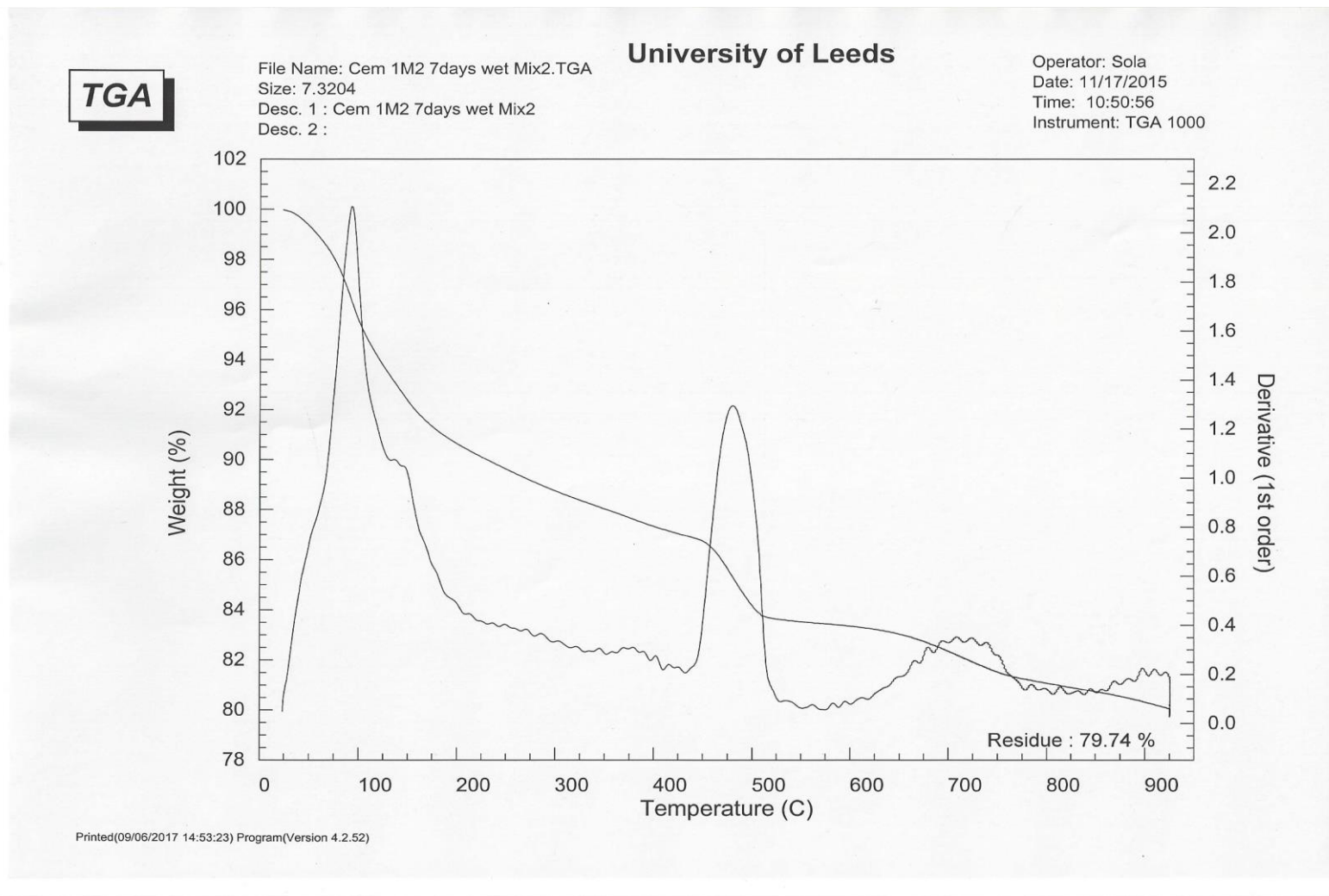


Figure A 122 TG result of 50MPa CEM1 stiff mix ideal cured 7 day

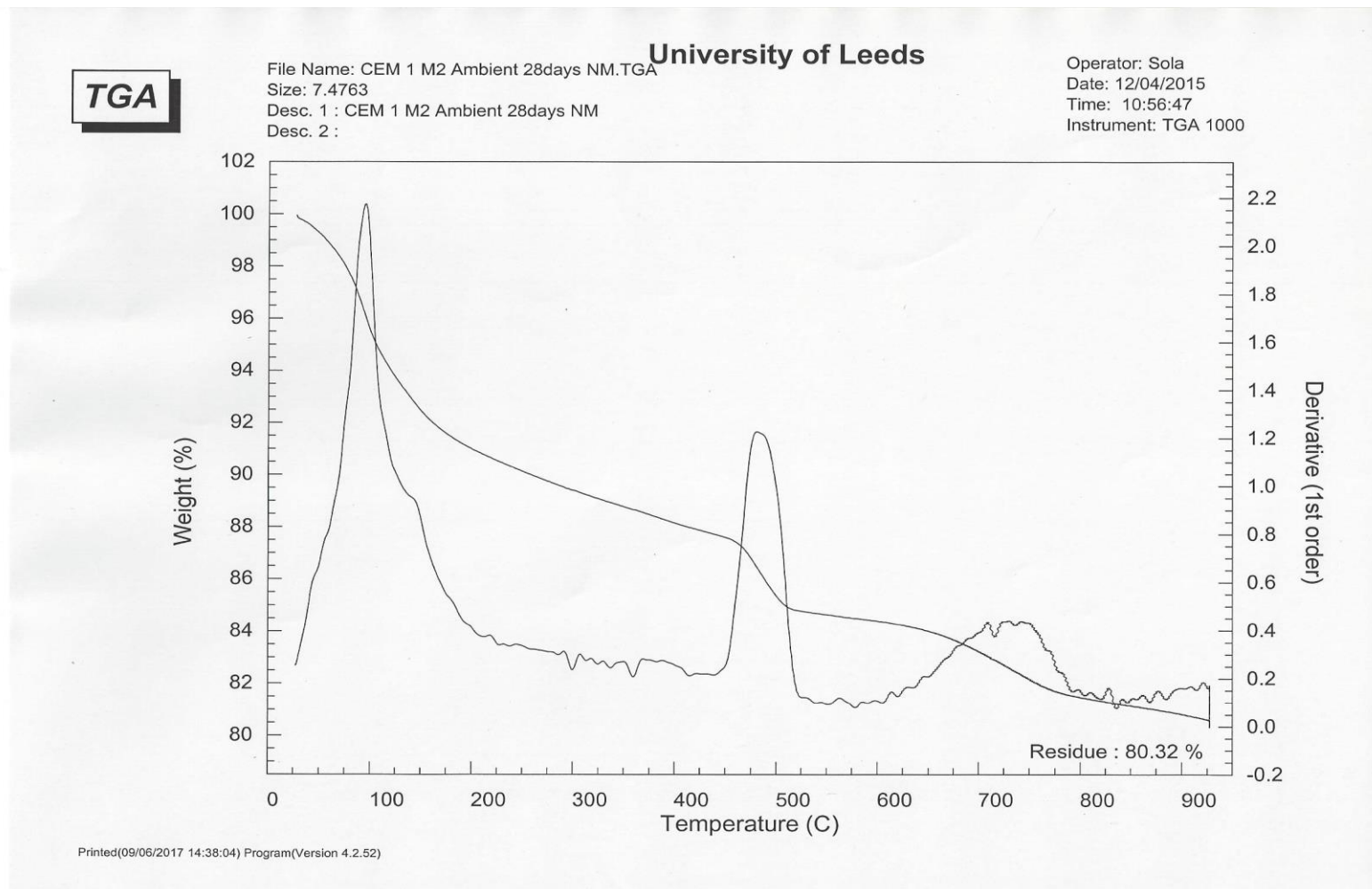


Figure A 123 TG result of 50MPa CEM1 stiff mix ambient cured 28 day

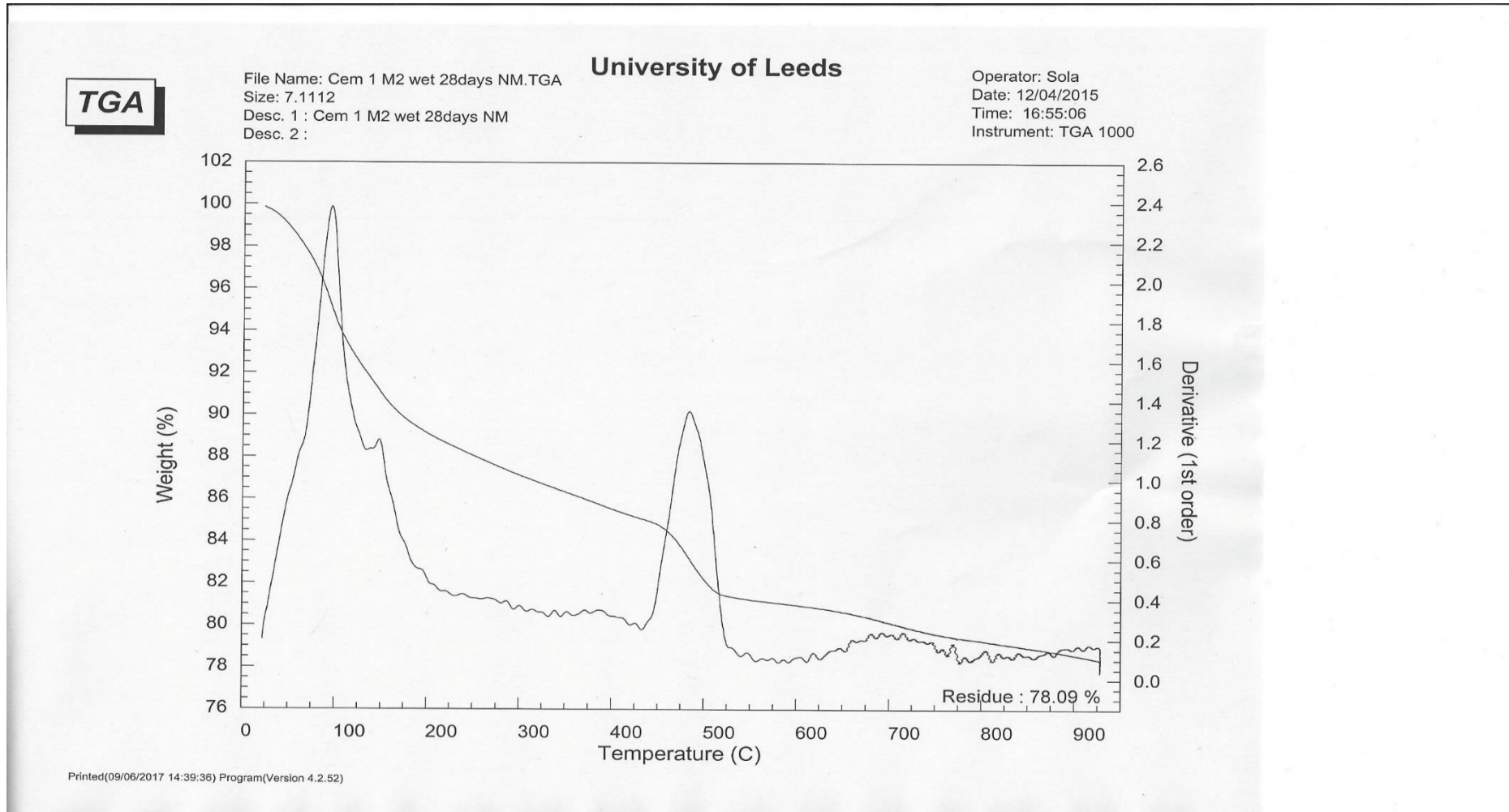


Figure A 124 TG result of 50MPa CEM1 stiff mix ideal cured 28 days

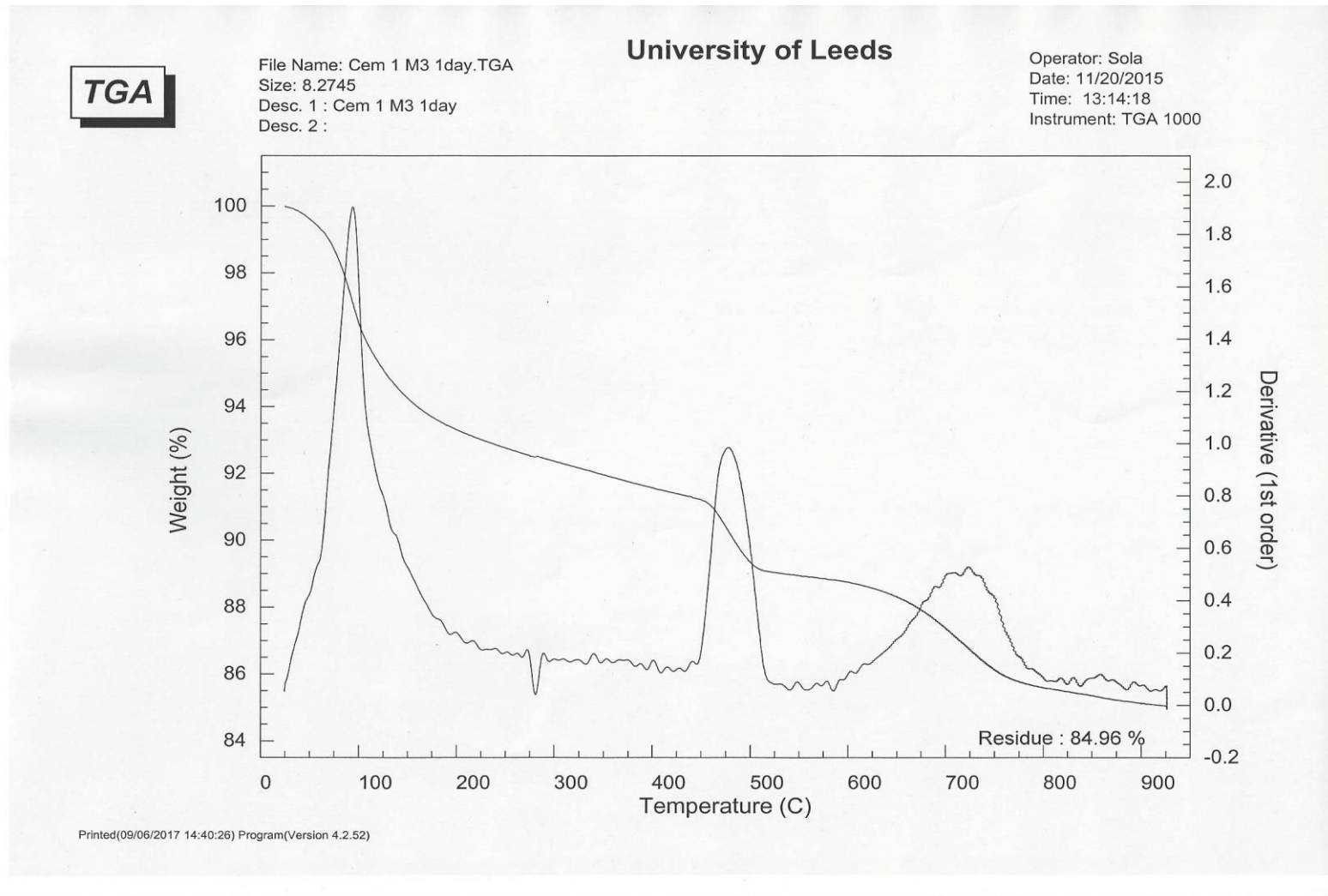


Figure A 125 TG result of 80MPa CEM1 stiff mix ambient cured 1 day

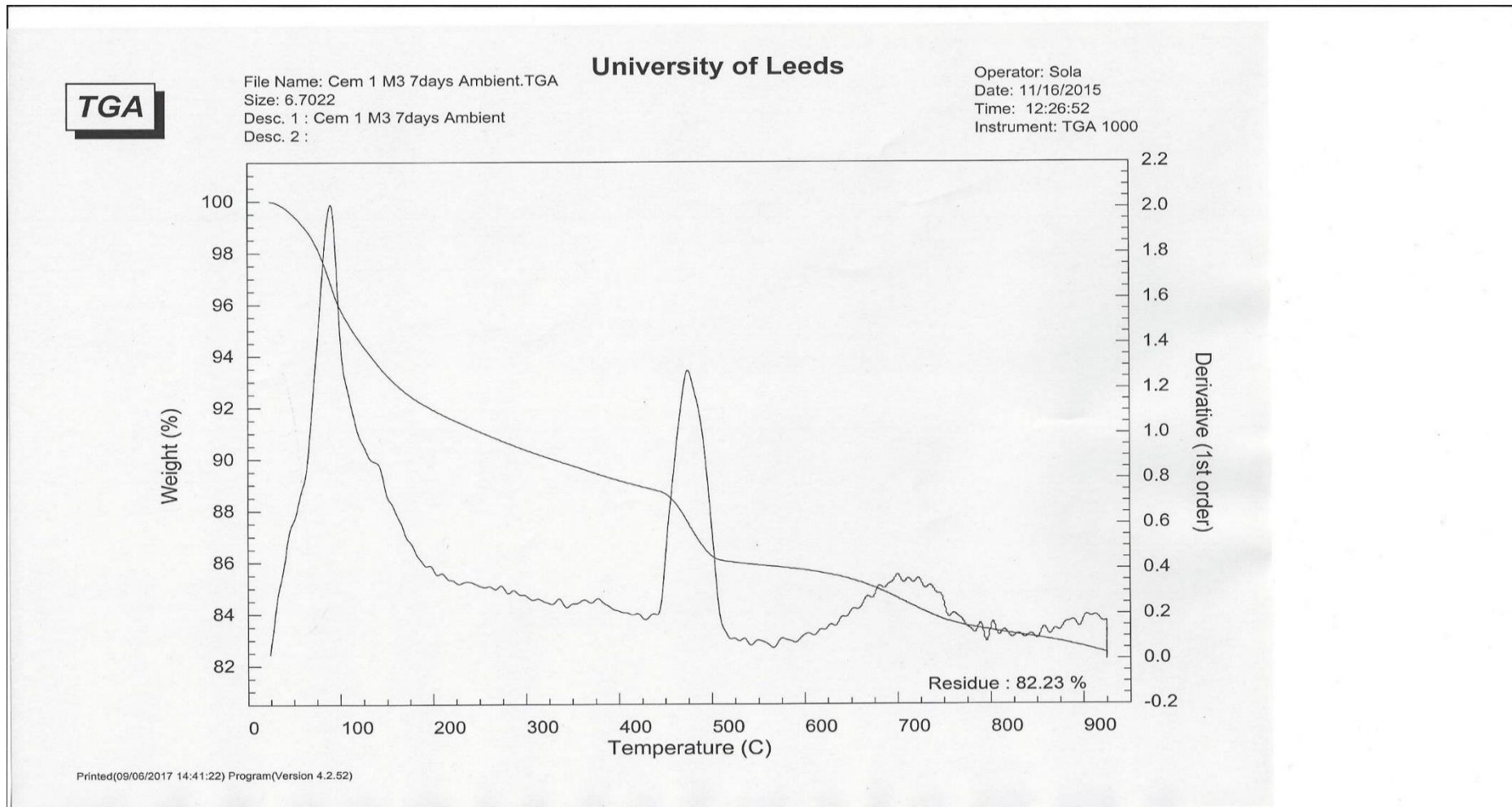


Figure A 126TG result of 80MPa CEM1 stiff mix ambient cured 7 days

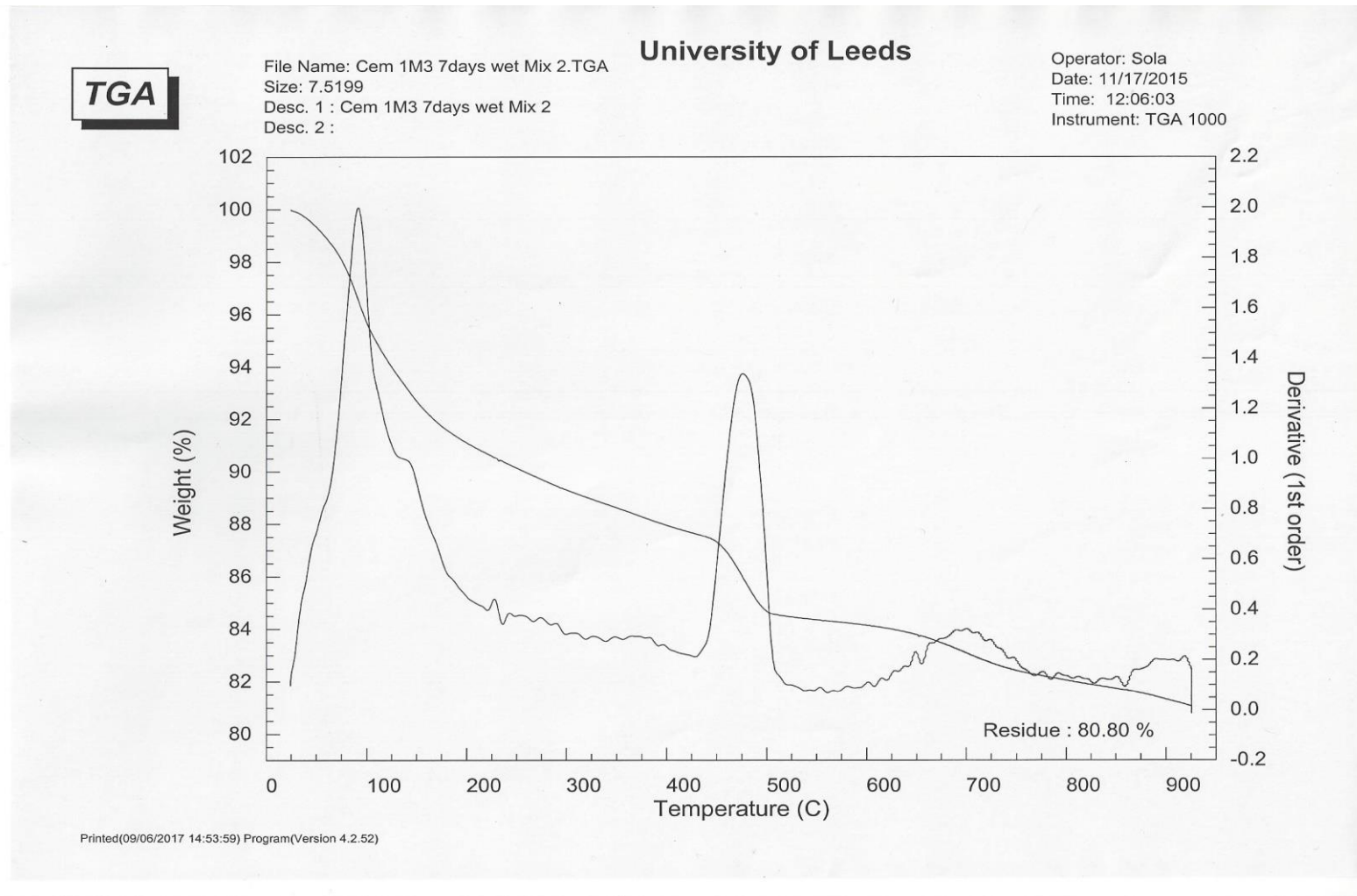


Figure A 127 TG result of 80MPa CEM1 stiff mix ideal cured 7 days

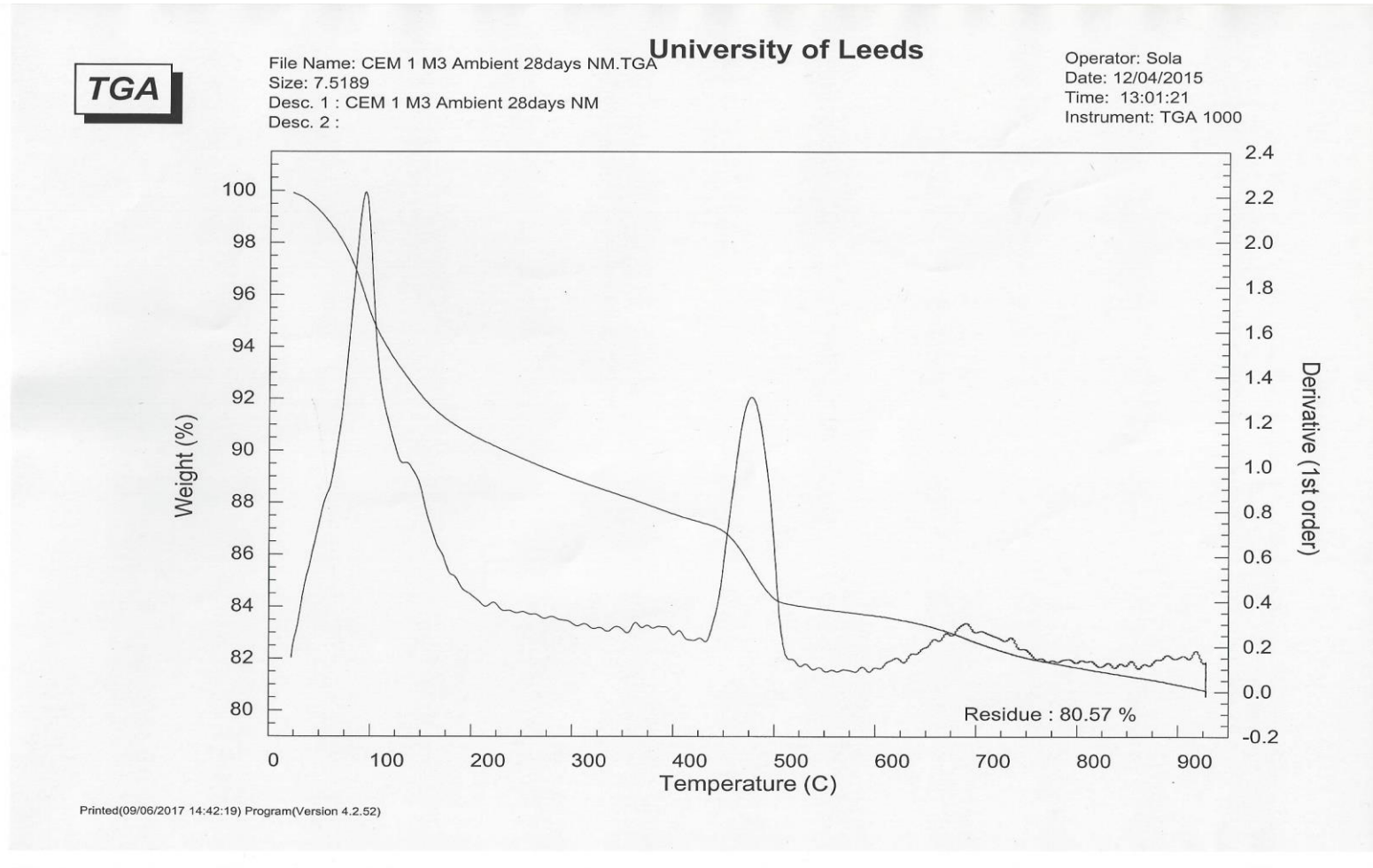


Figure A 128 TG result of 80MPa CEM1 stiff mix ambient cured 28 days

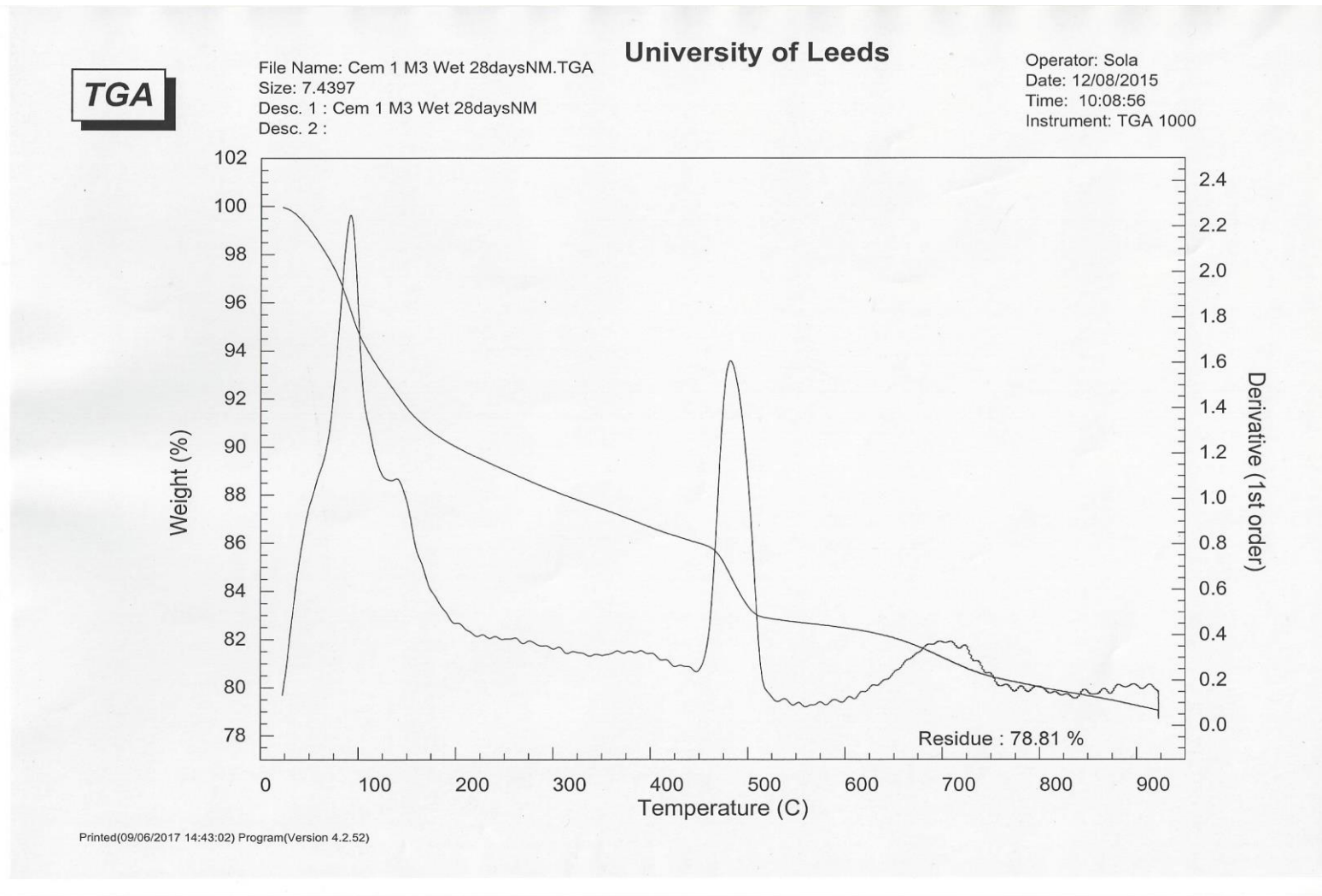


Figure A 129 TG result of 80MPa CEM1 stiff mix ideal cured 28 days

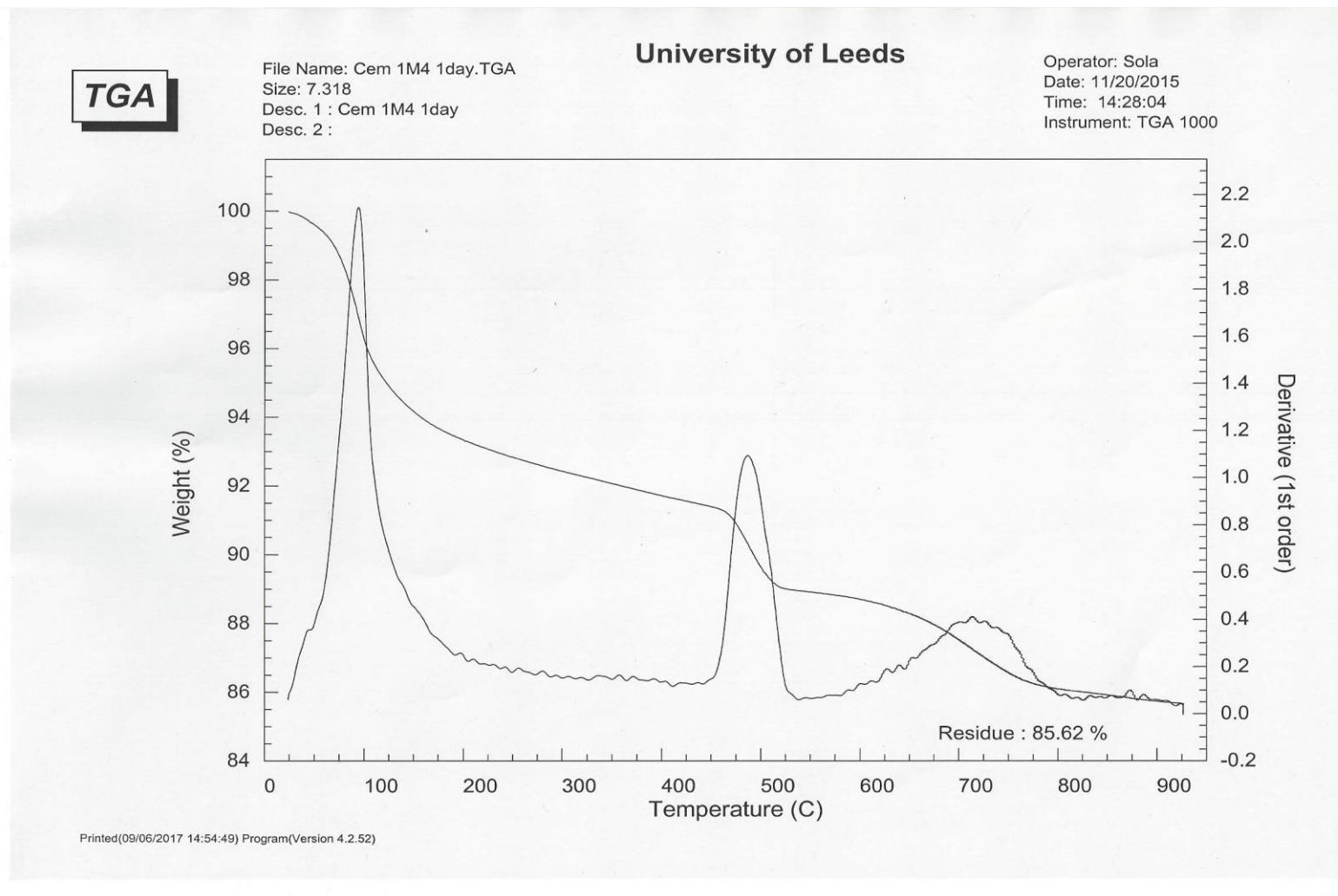


Figure A 130 TG result of 20MPa CEM1 wet mix ambient cured 1 day

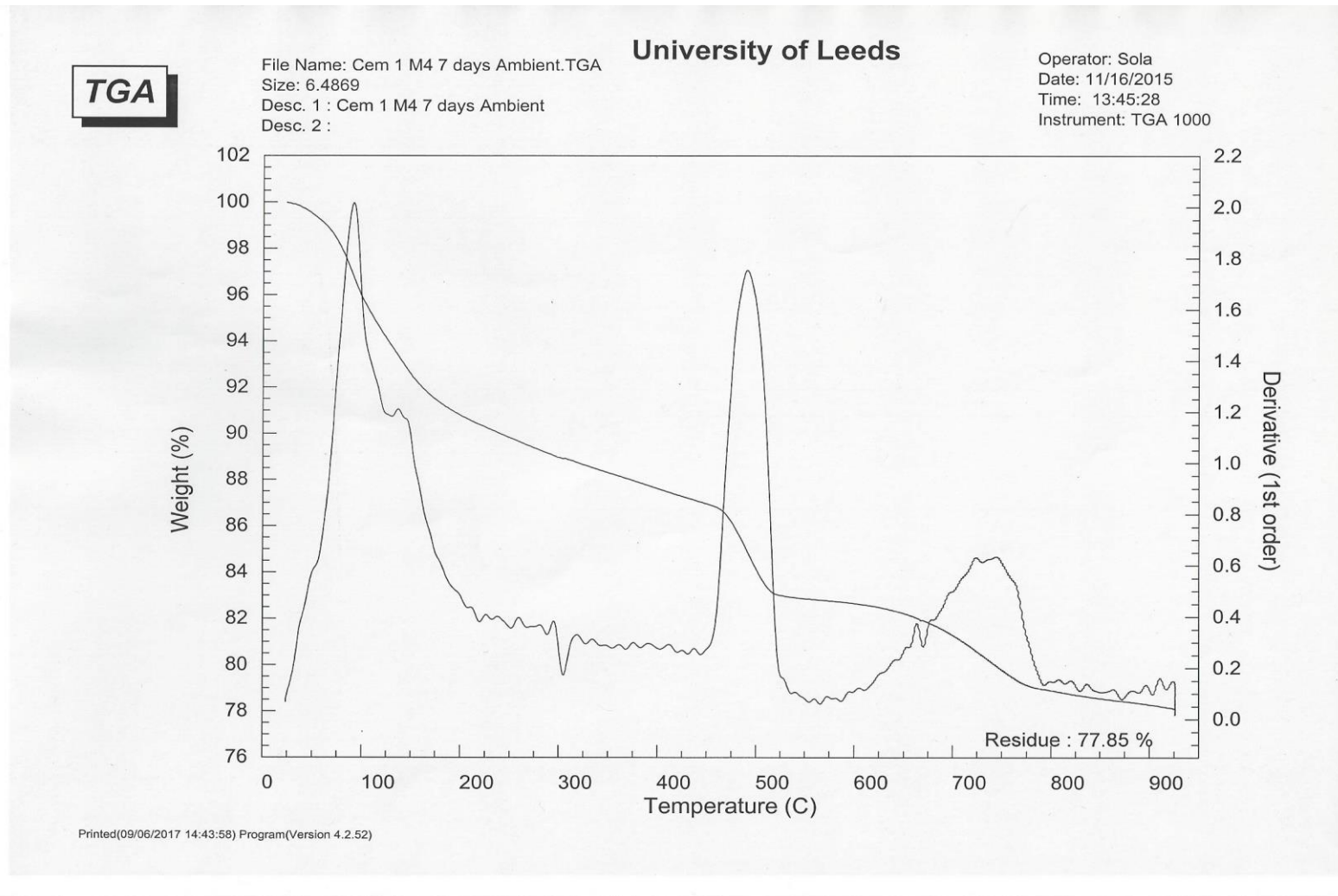


Figure A 131 TG result of 20MPa CEM1 wet mix ambient cured 7 days

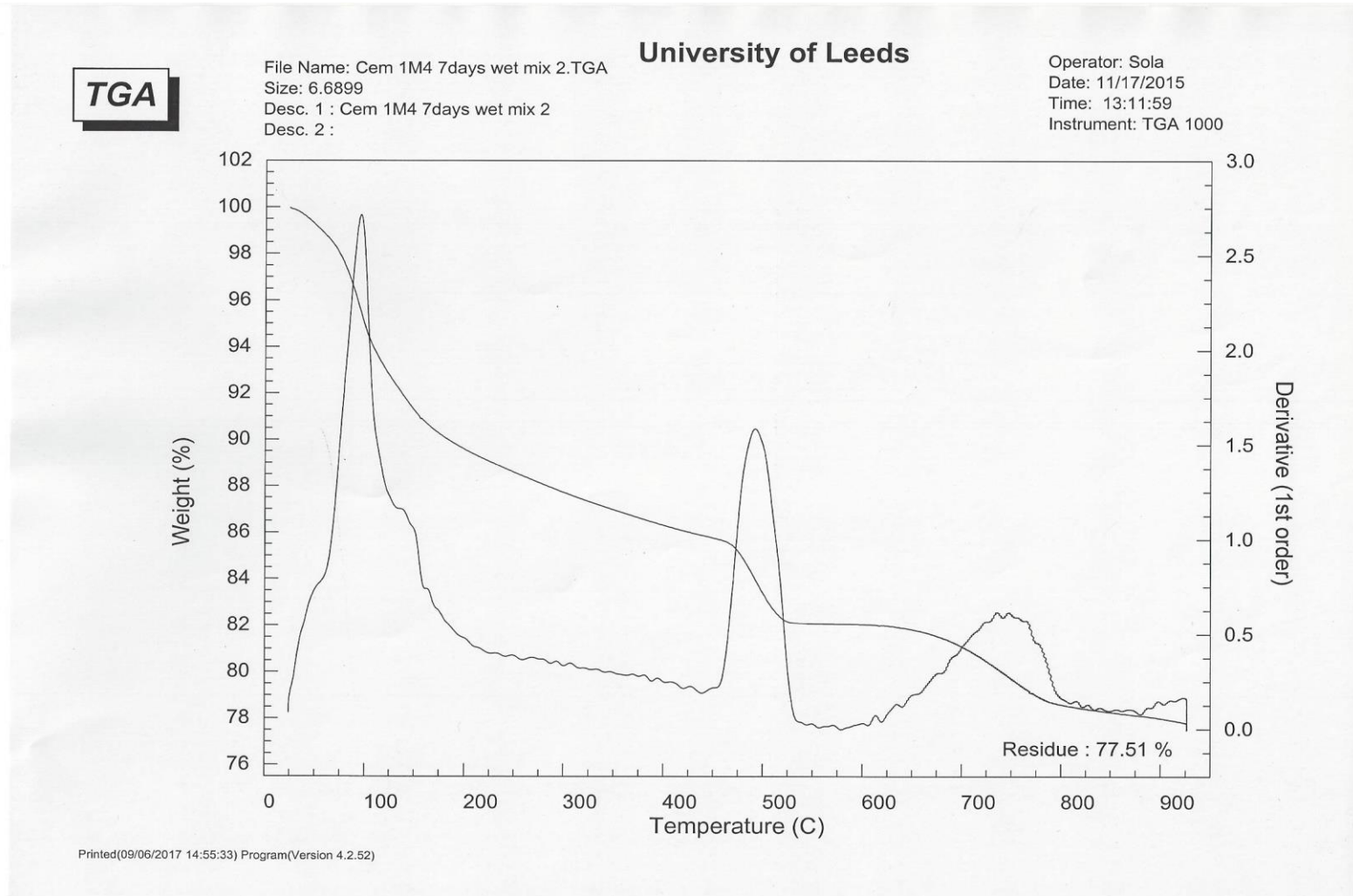


Figure A 132 TG result of 20MPa CEM1 wet mix ideal cured 7 days

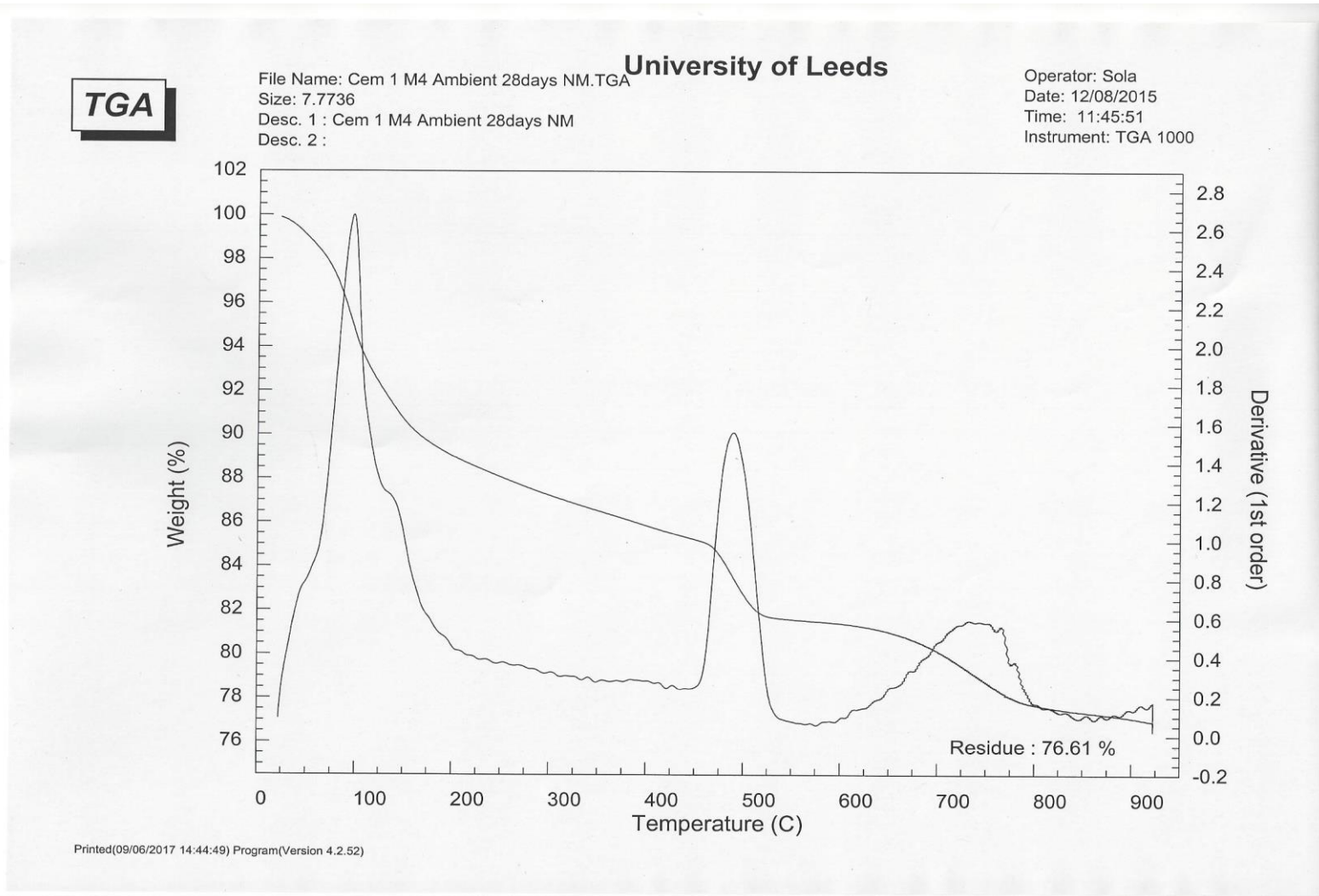


Figure A 133 TG result of 20MPa CEM1 wet mix ambient cured 28 days

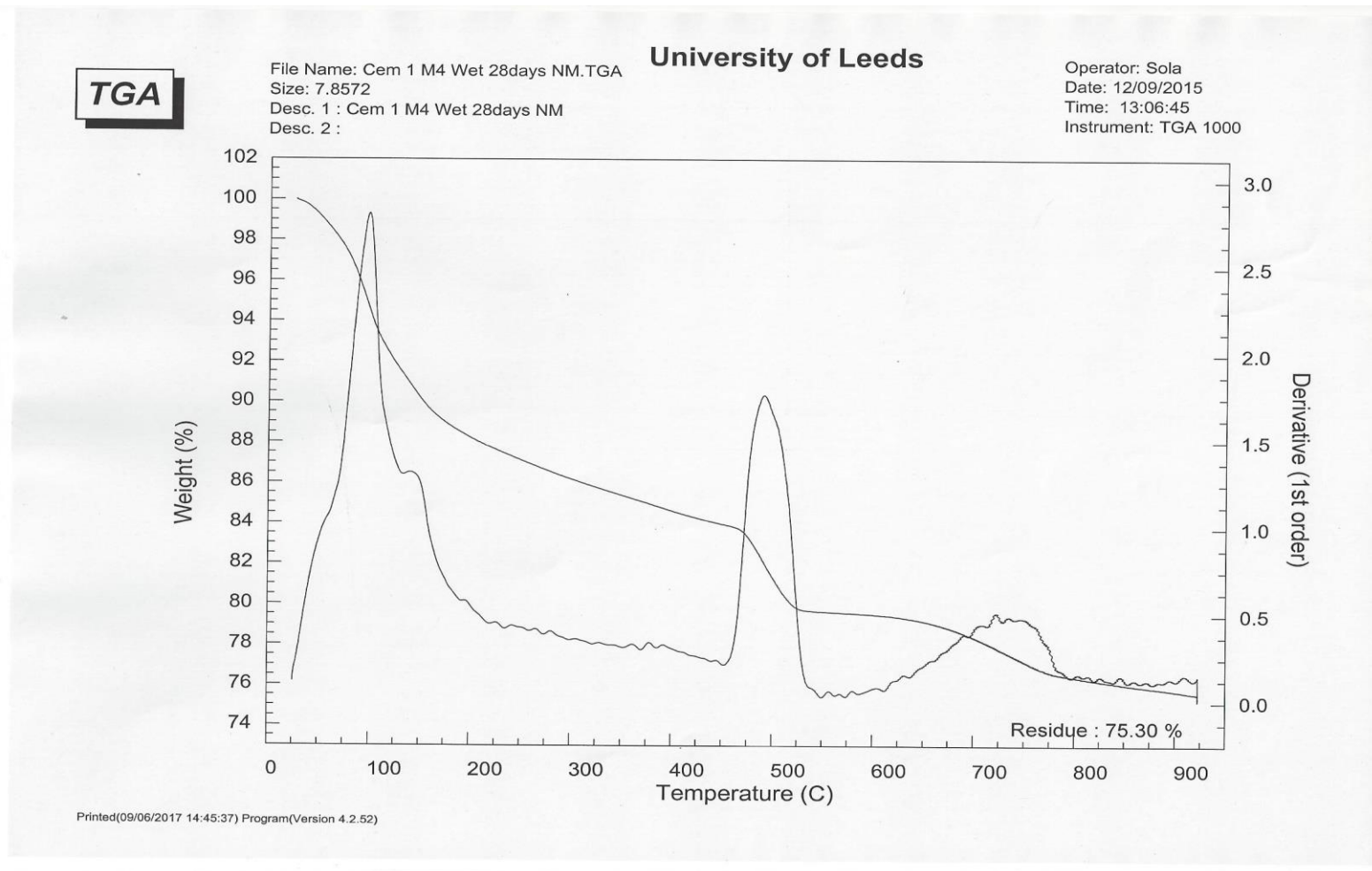


Figure A 134 TG result of 20MPa CEM1 wet mix ideal cured 28 days

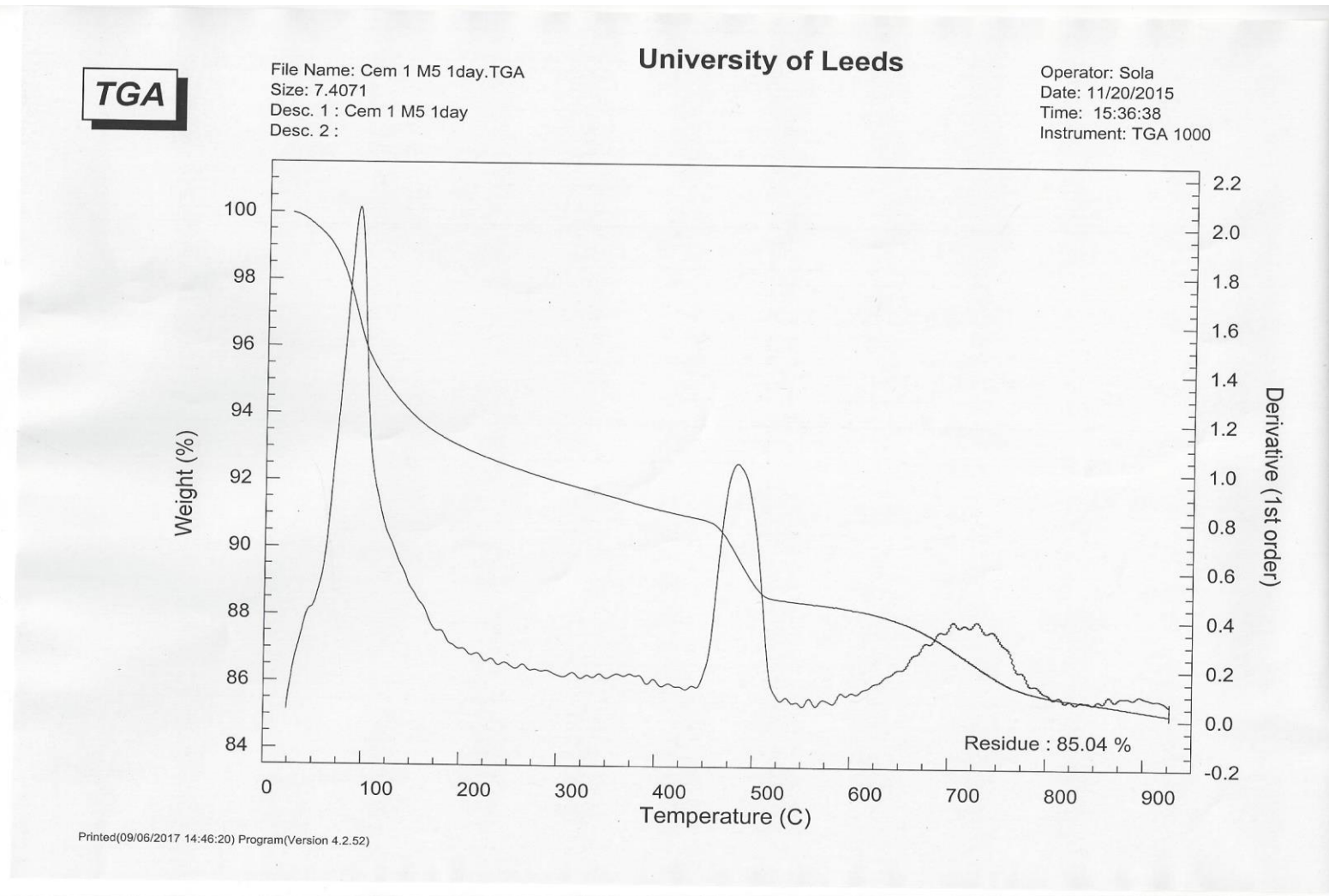


Figure A 135 TG result of 50MPa CEM1 wet mix ambient cured 1 day

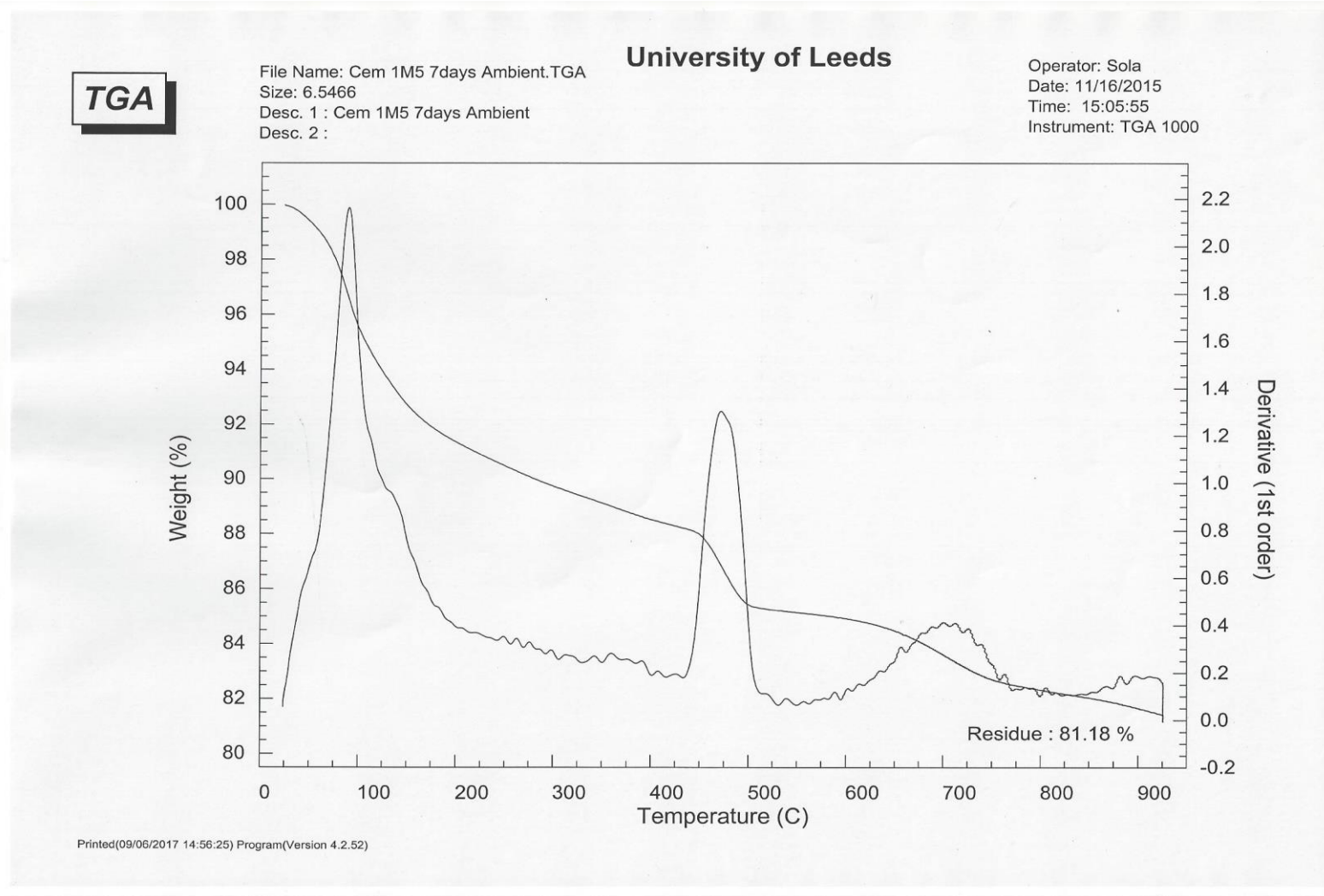


Figure A 136 TG result of 50MPa CEM1 wet mix ambient cured 7days

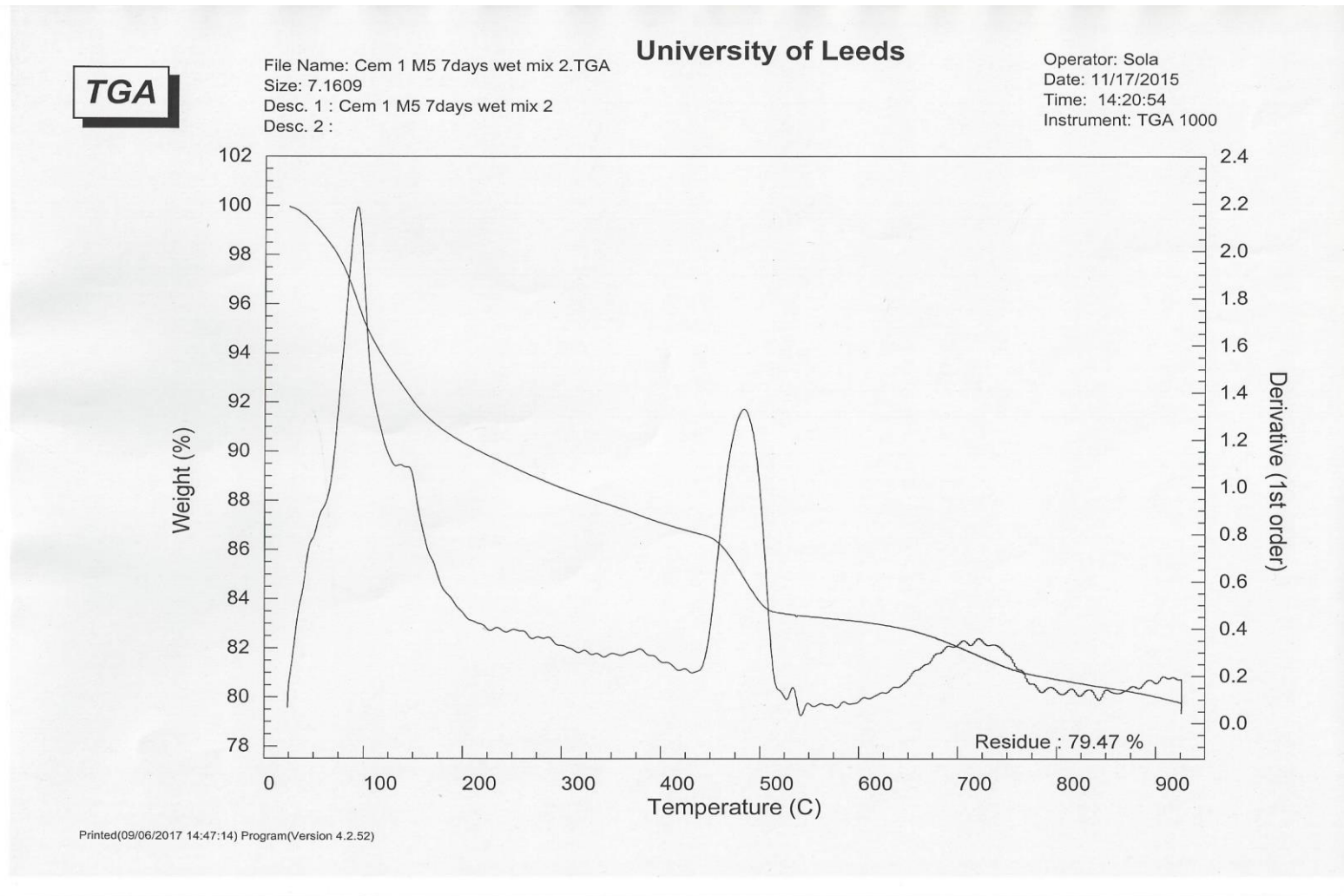


Figure A 137 TG result of 50MPa CEM1 wet mix ideal cured 7 days

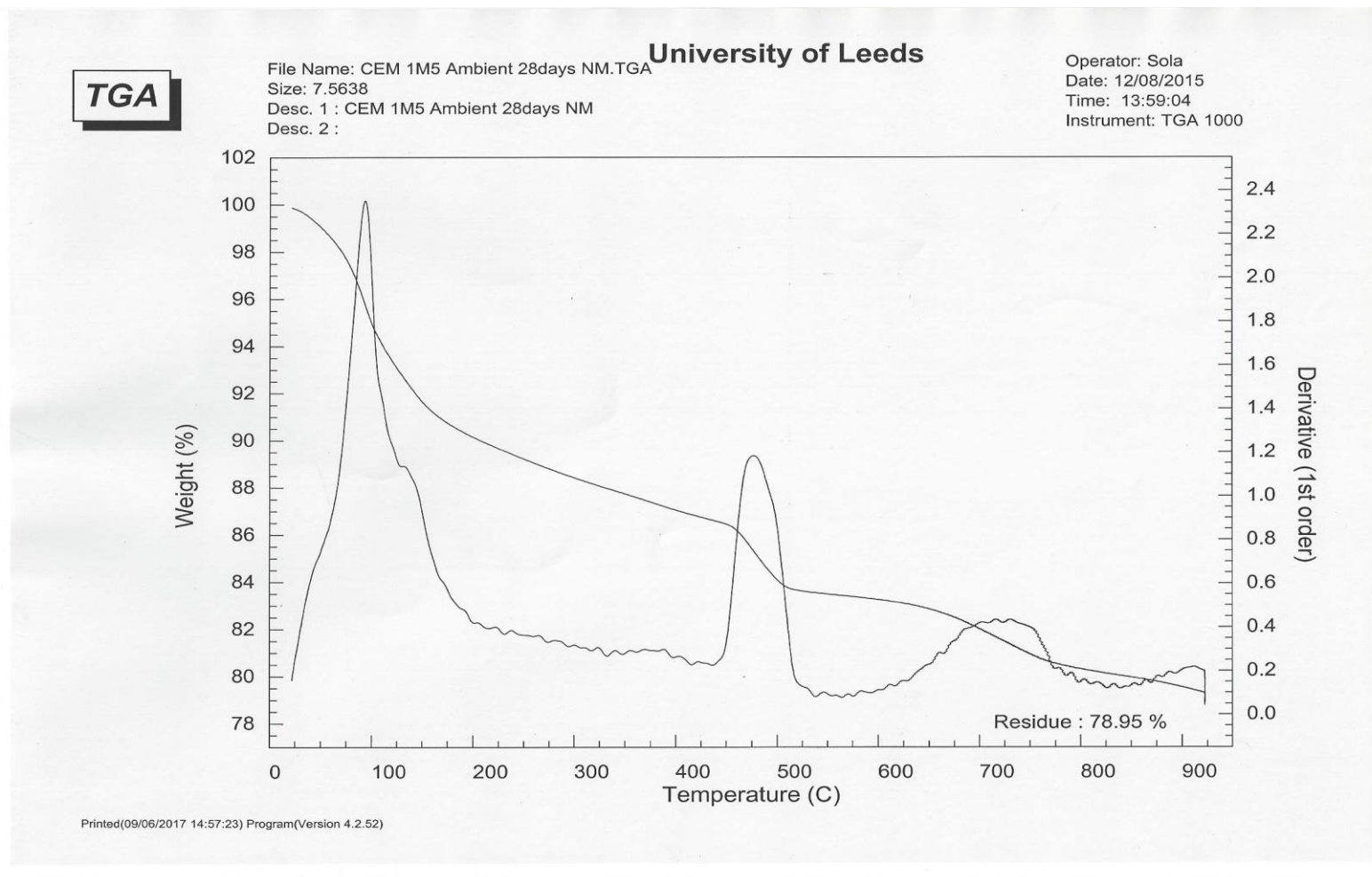


Figure A 138 TG result of 50MPa CEM1 wet mix ambient cured 28 days

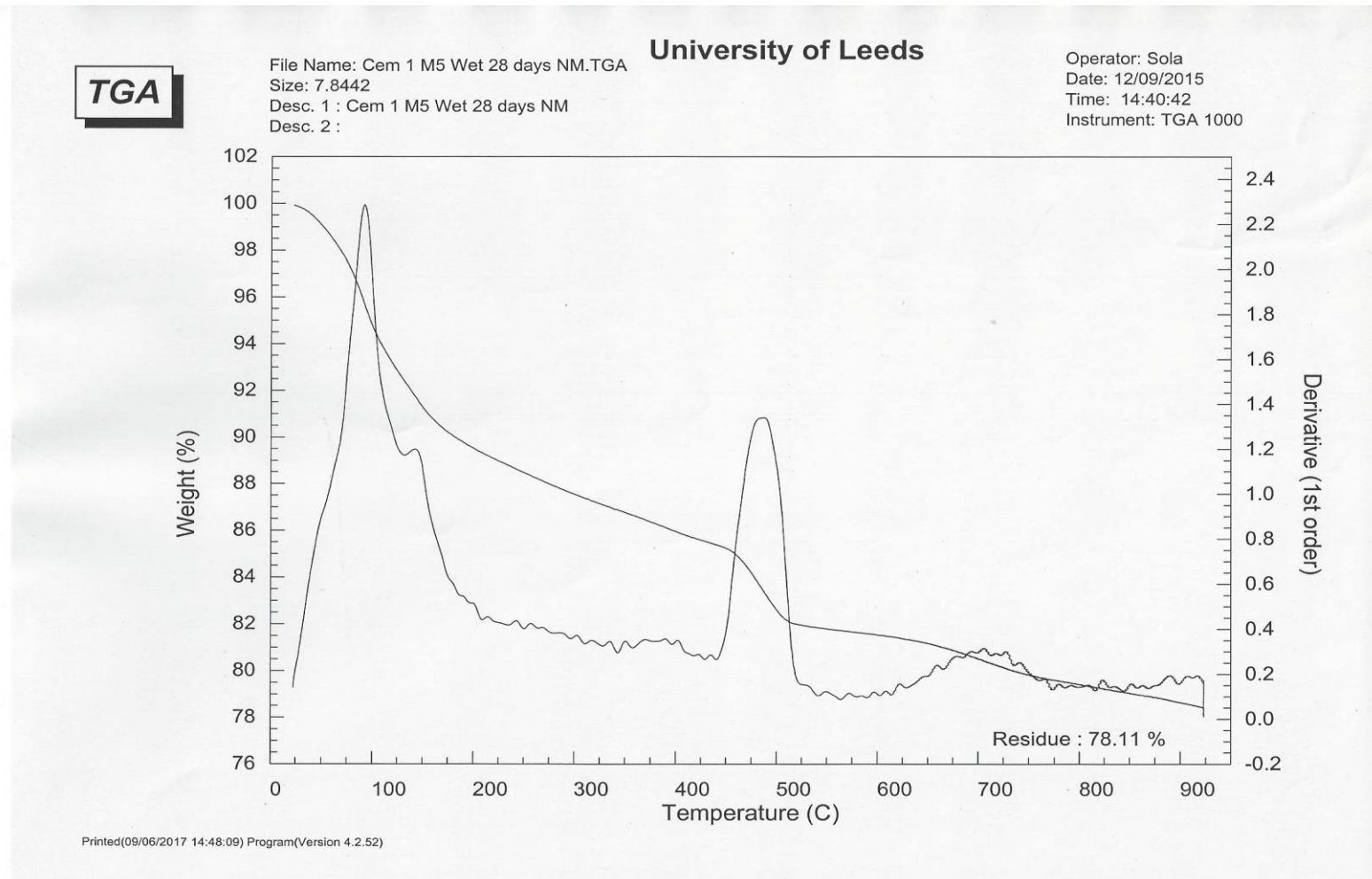


Figure A 139 TG result of 50MPa CEM1 wet mix ideal cured 28 days

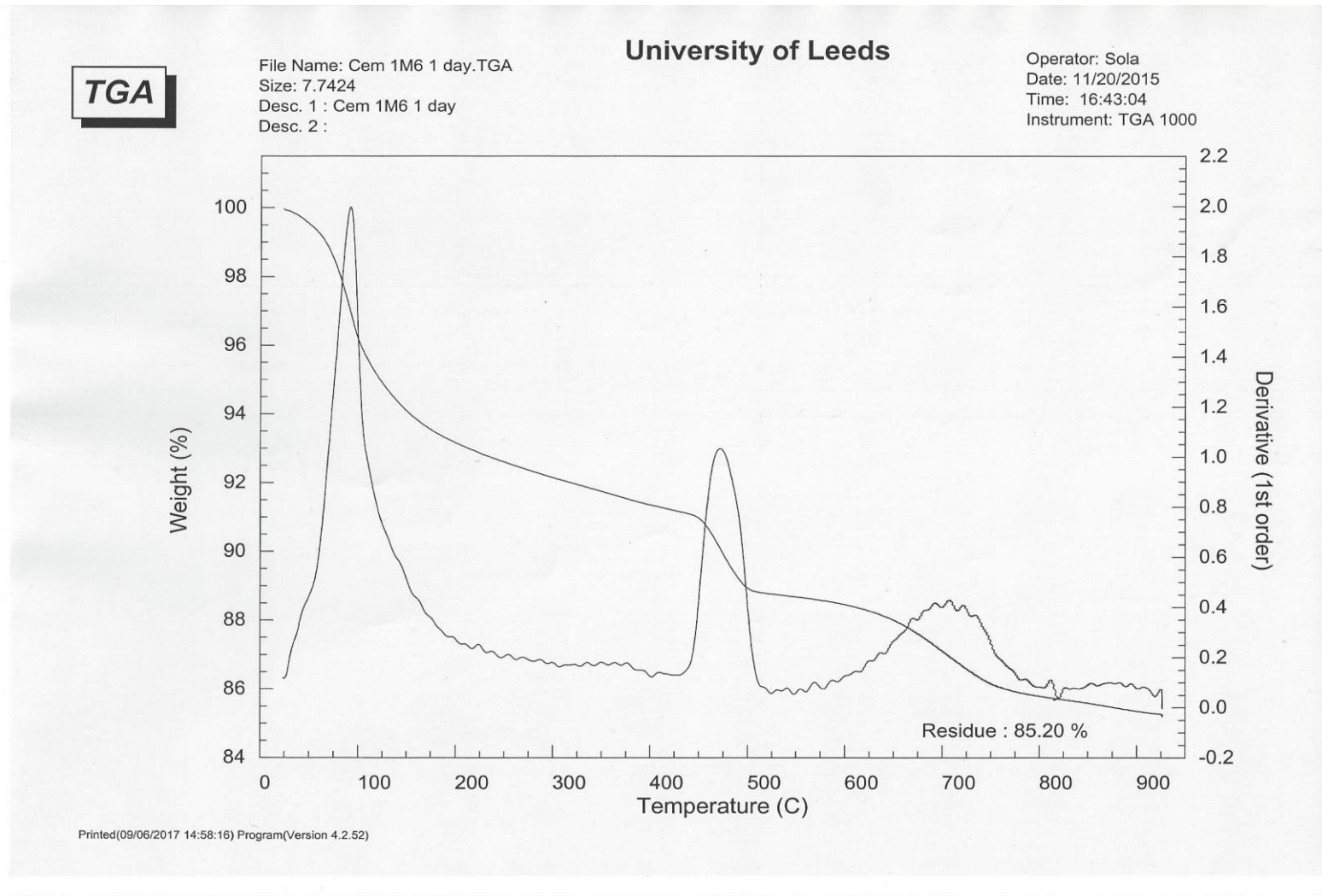


Figure A 140 TG result of 80MPa CEM1 wet mix ambient cured 1 day

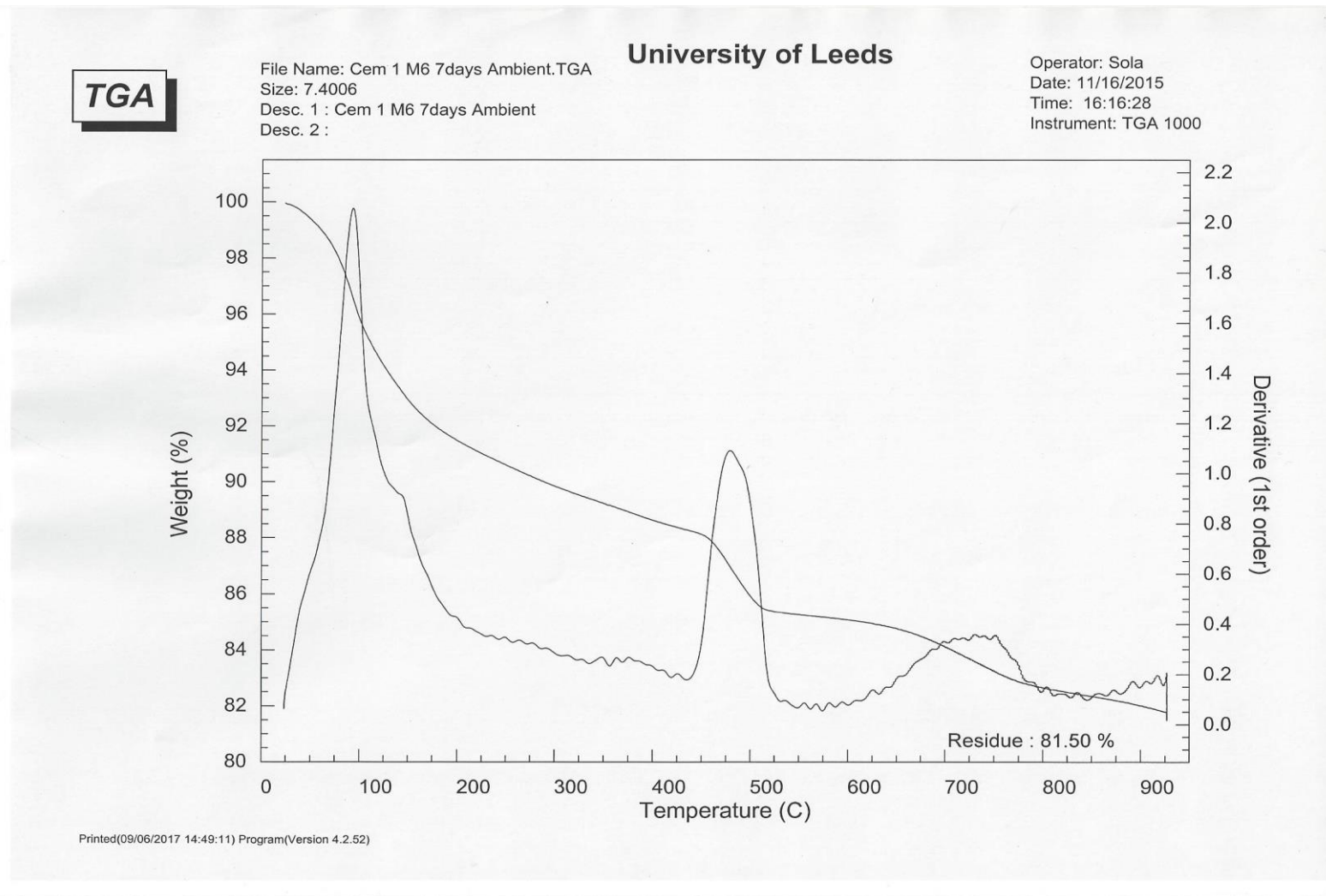


Figure A 141 TG result of 80MPa CEM1 wet mix ambient cured 7 days

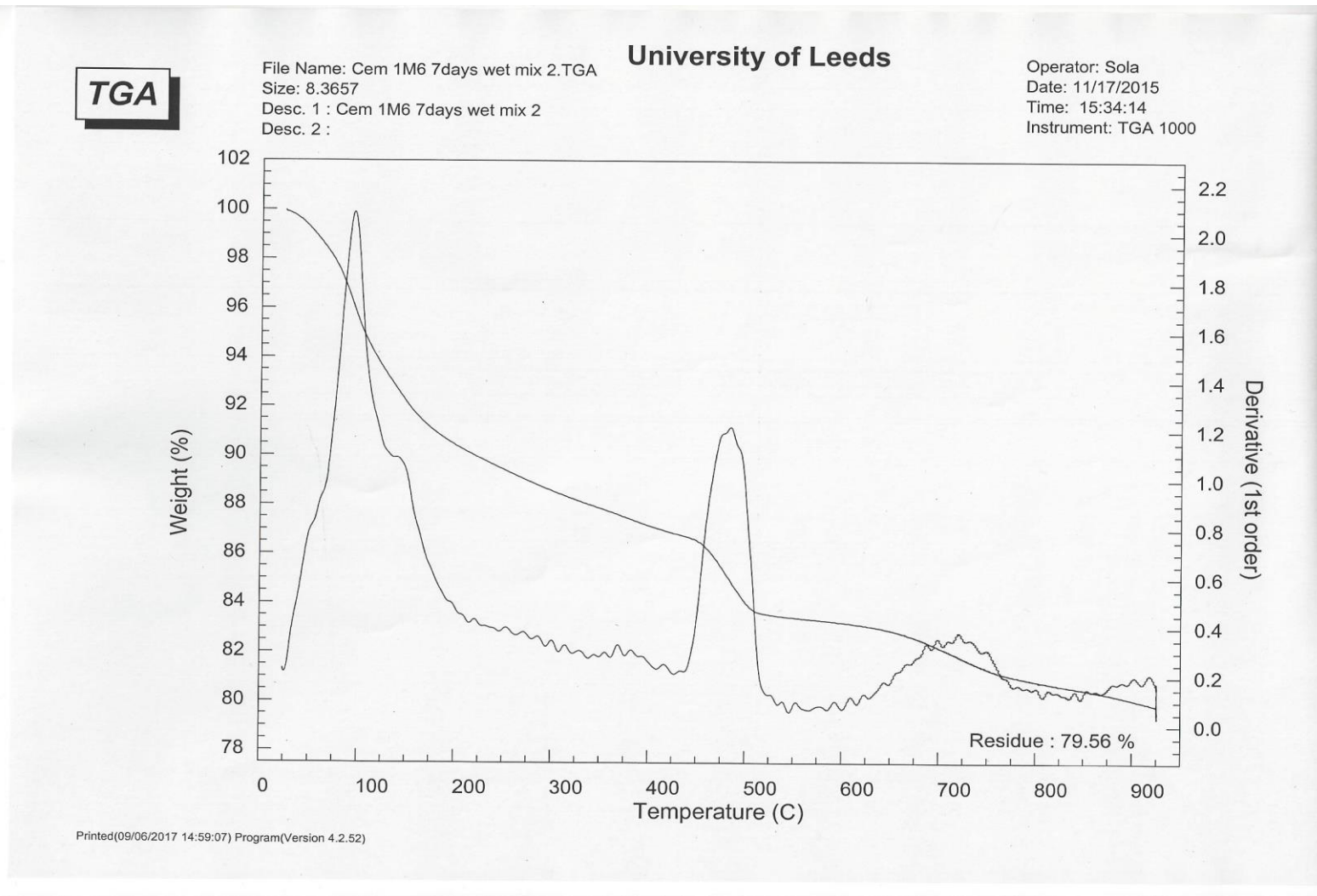


Figure A 142 TG result of 80MPa CEM1 wet mix ideal cured 7 days

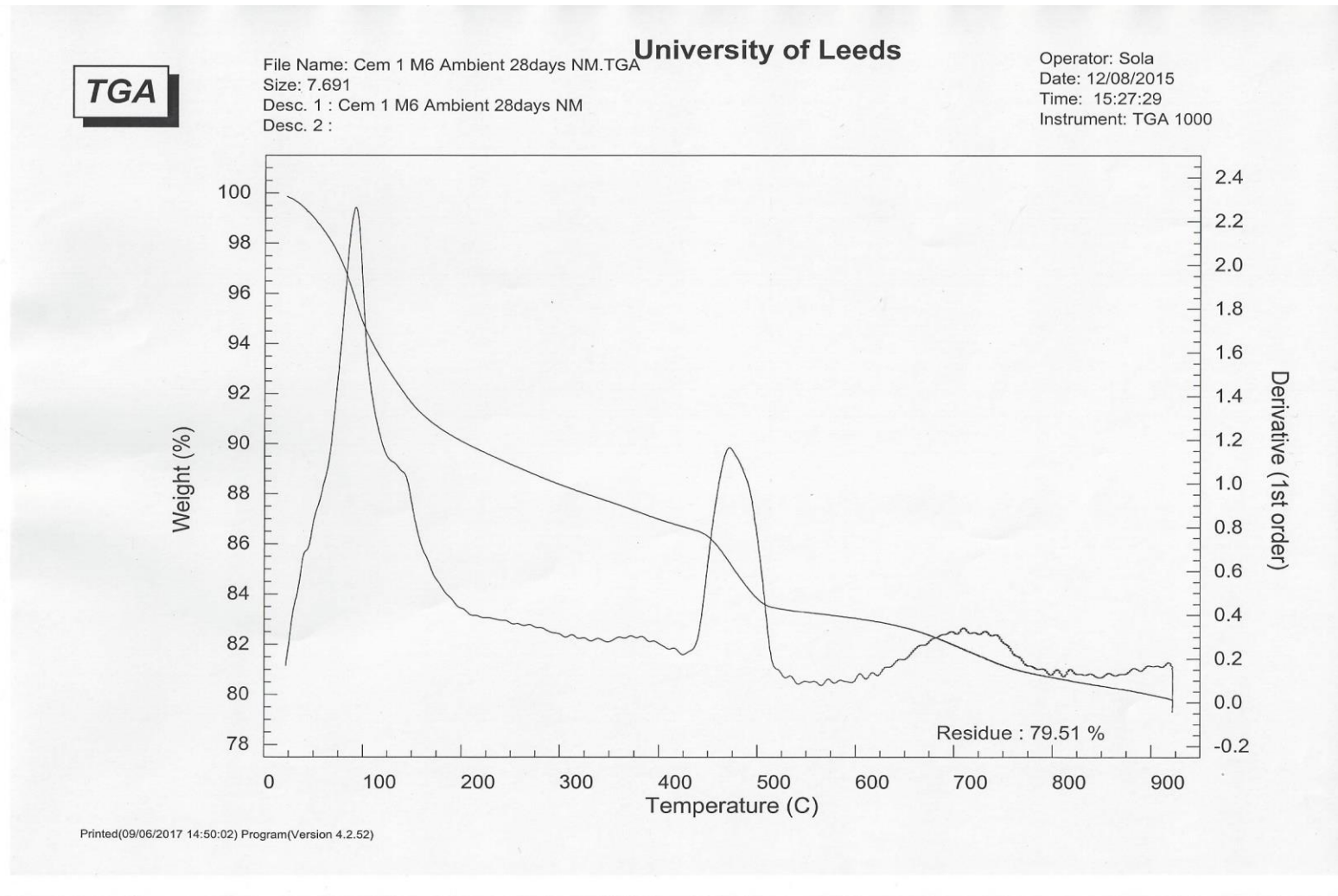


Figure A 143 80MPa CEM1 wet mix ambient cured 28 days

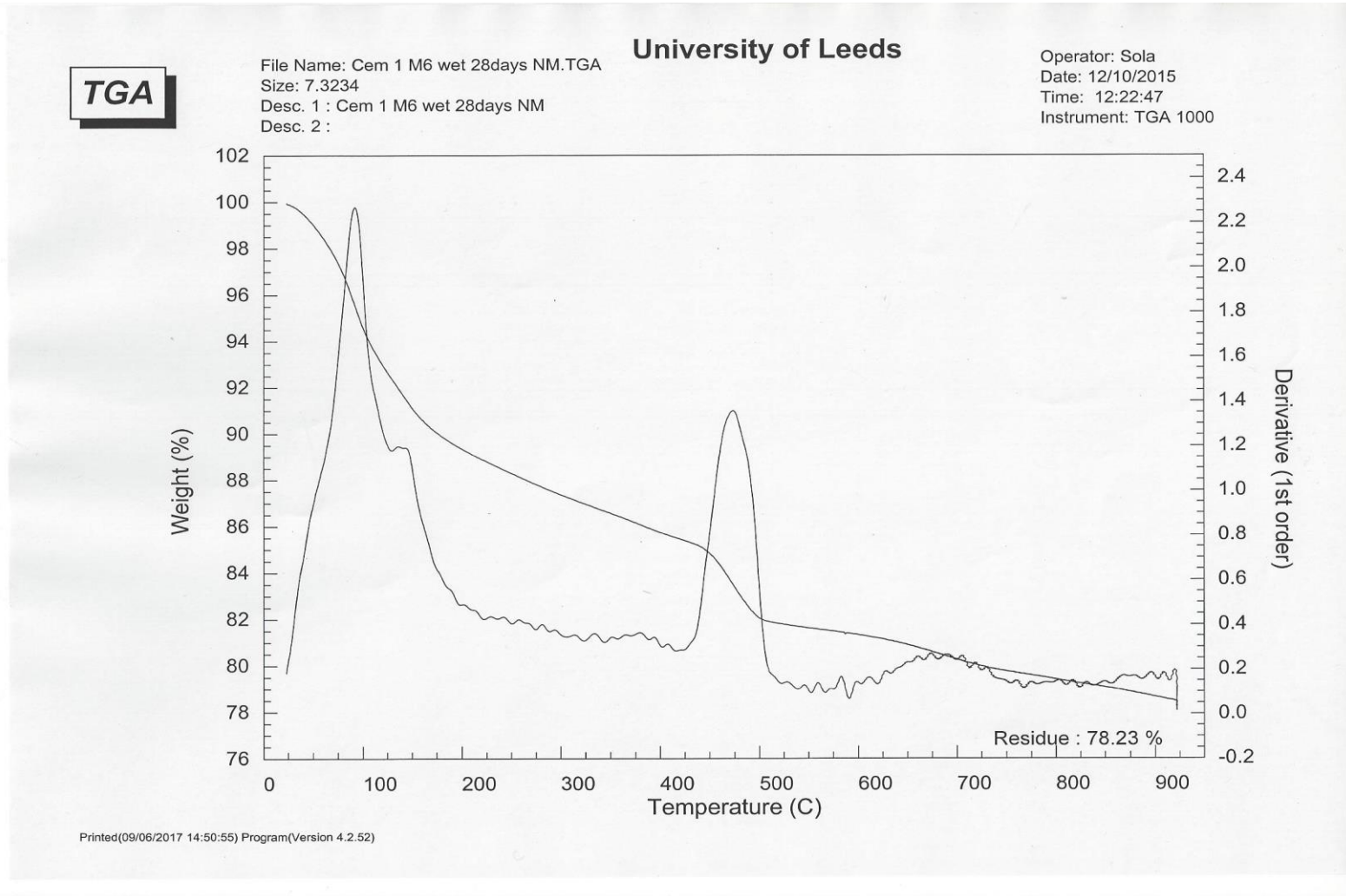


Figure A 144 TG result of 80MPa CEM1 wet mix ideal cured 28 days

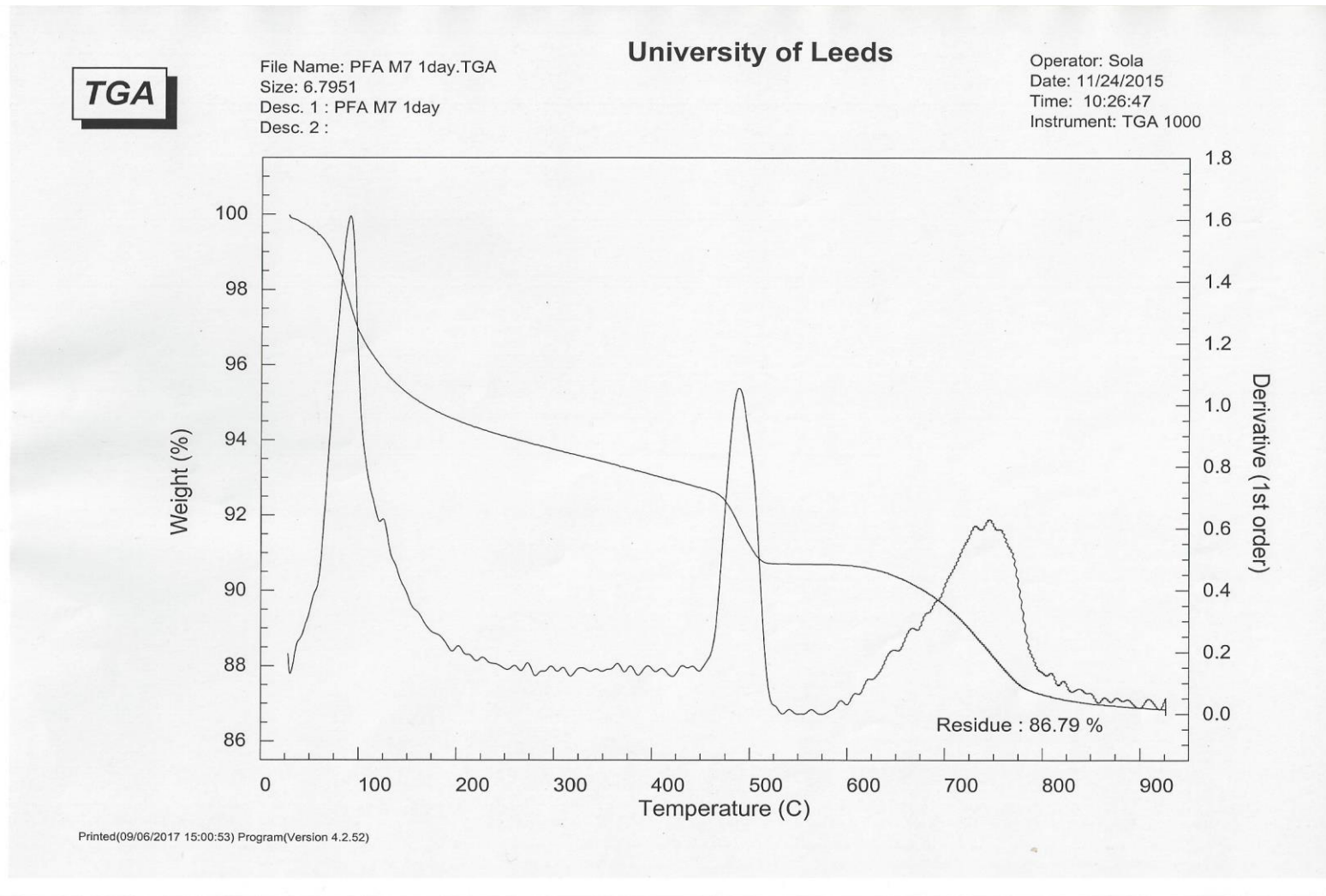


Figure A 145 20MPa Fly ash stiff mix ambient cured 1 day

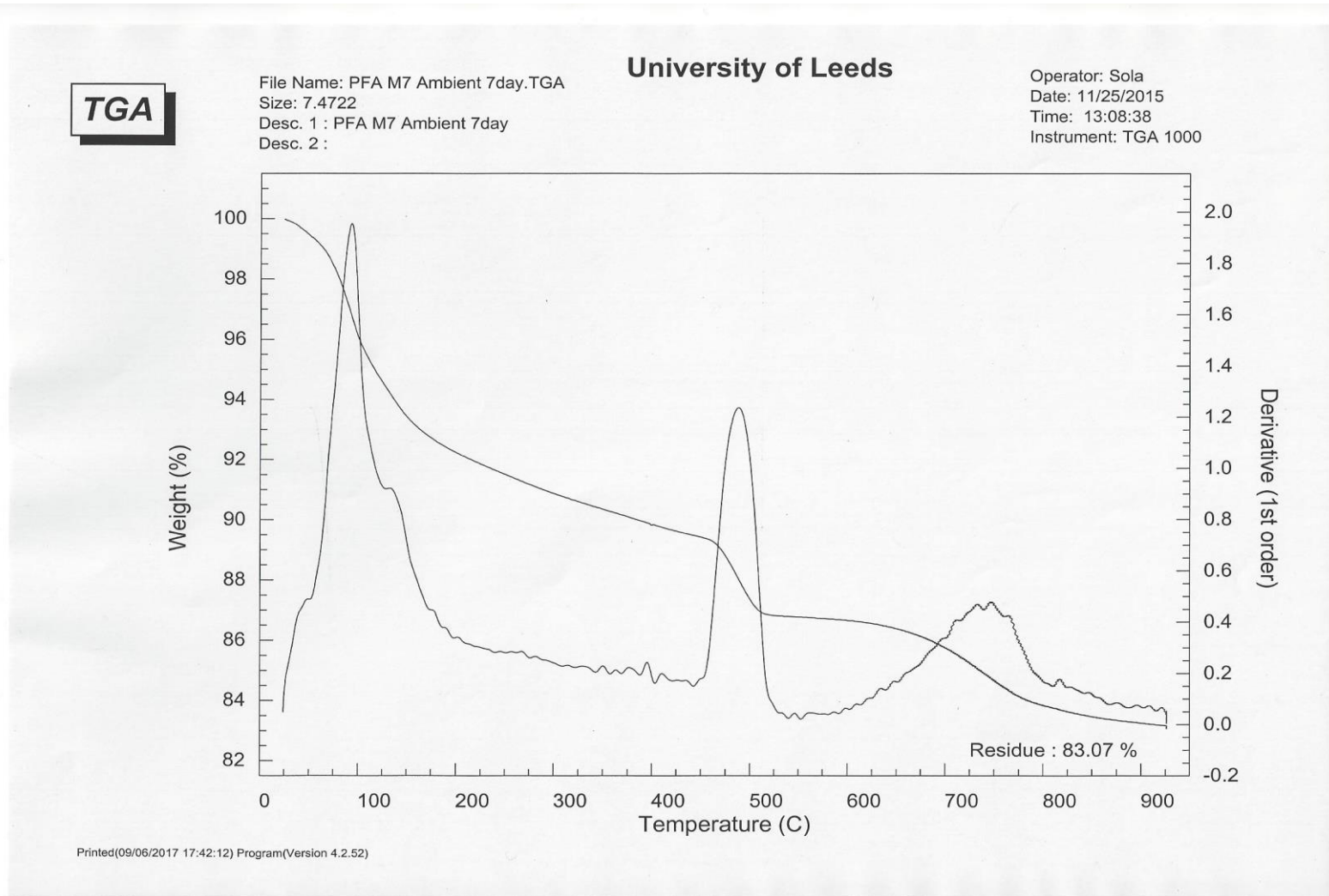


Figure A 146 TG result of 20MPa Fly ash stiff mix ambient cured 7 days

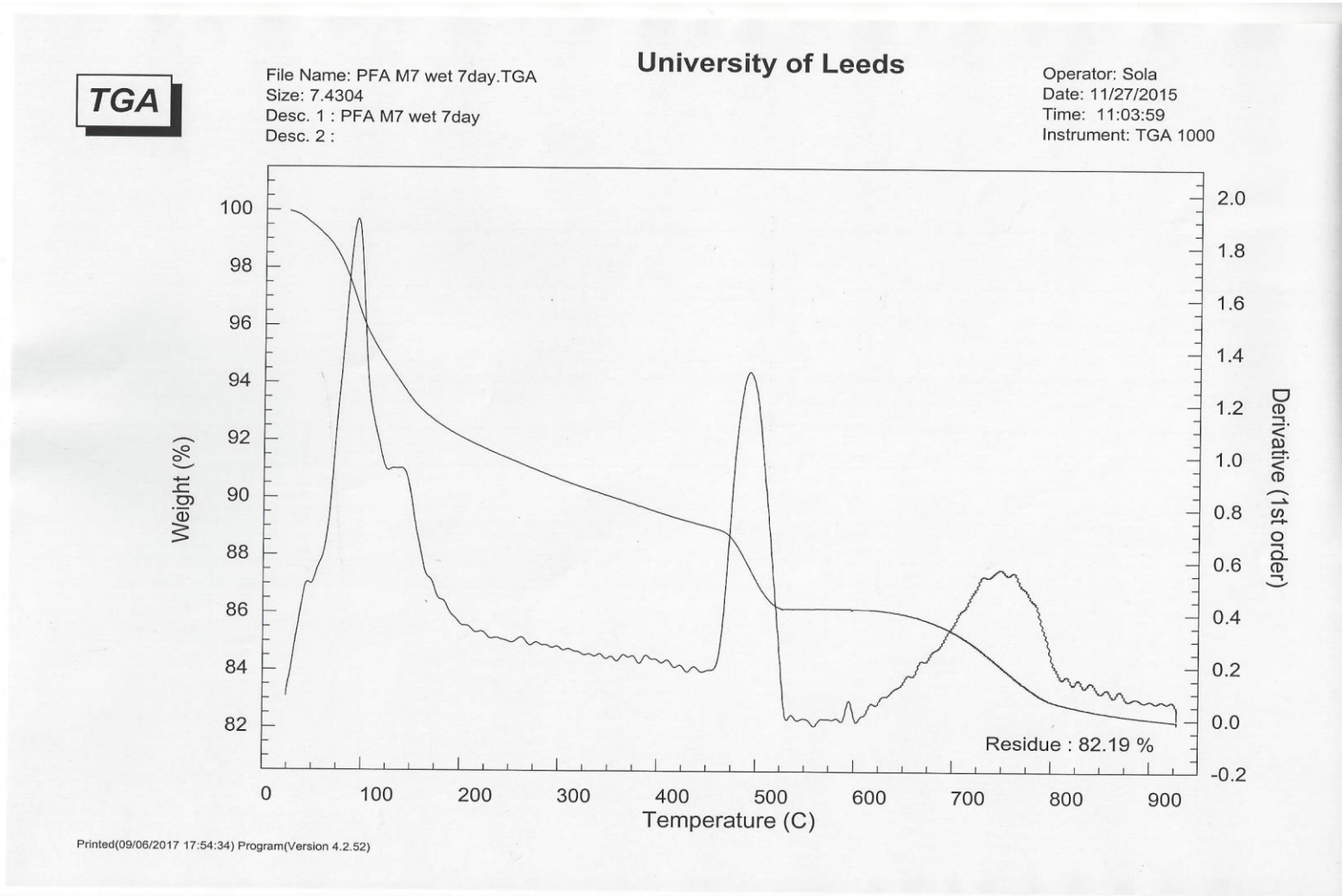


Figure A 147 TG result of 20MPa Fly ash stiff mix ideal cured 7 days

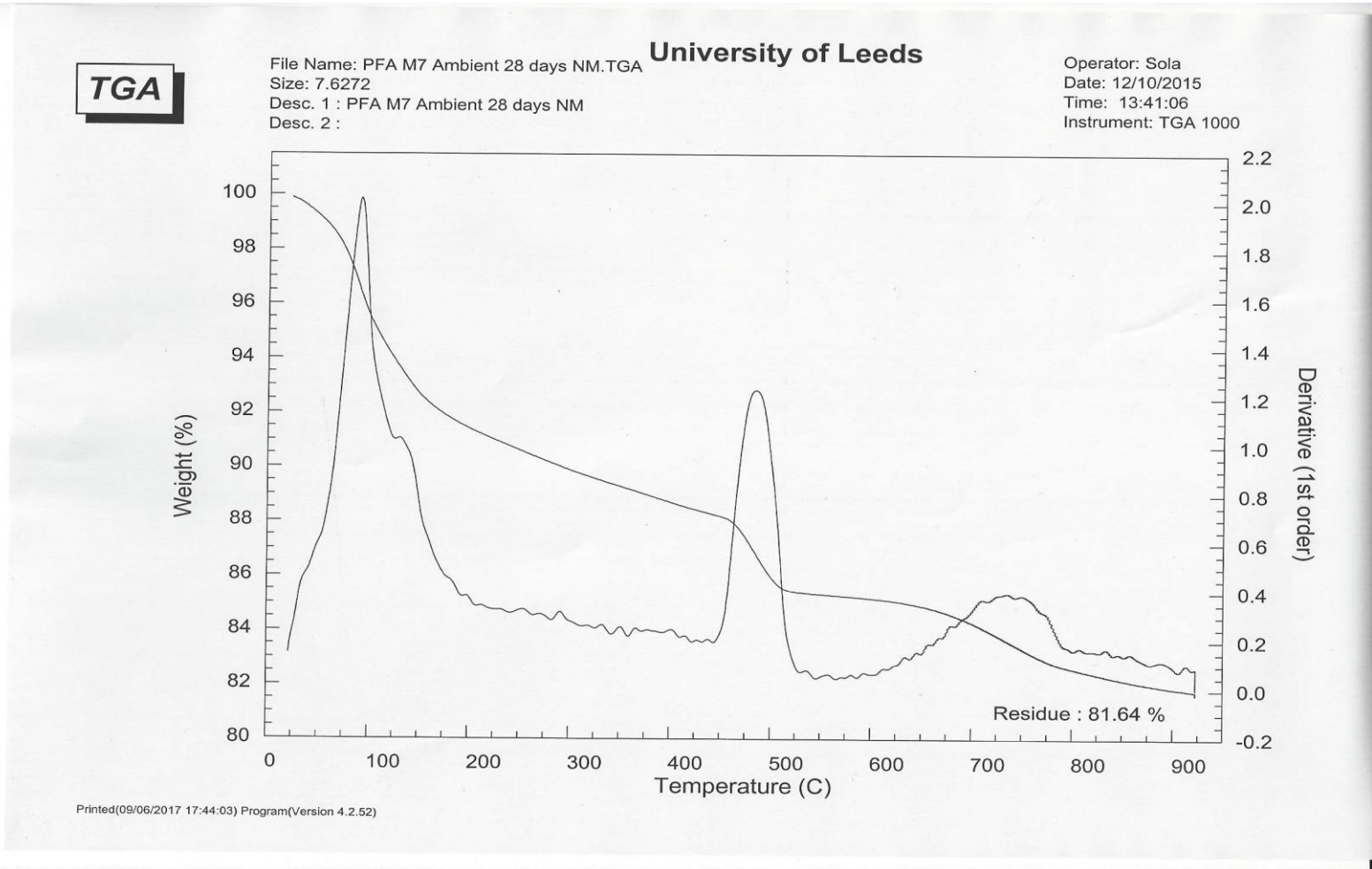


Figure A 148 TG result of 20MPa Fly ash stiff mix ambient cured 28 days

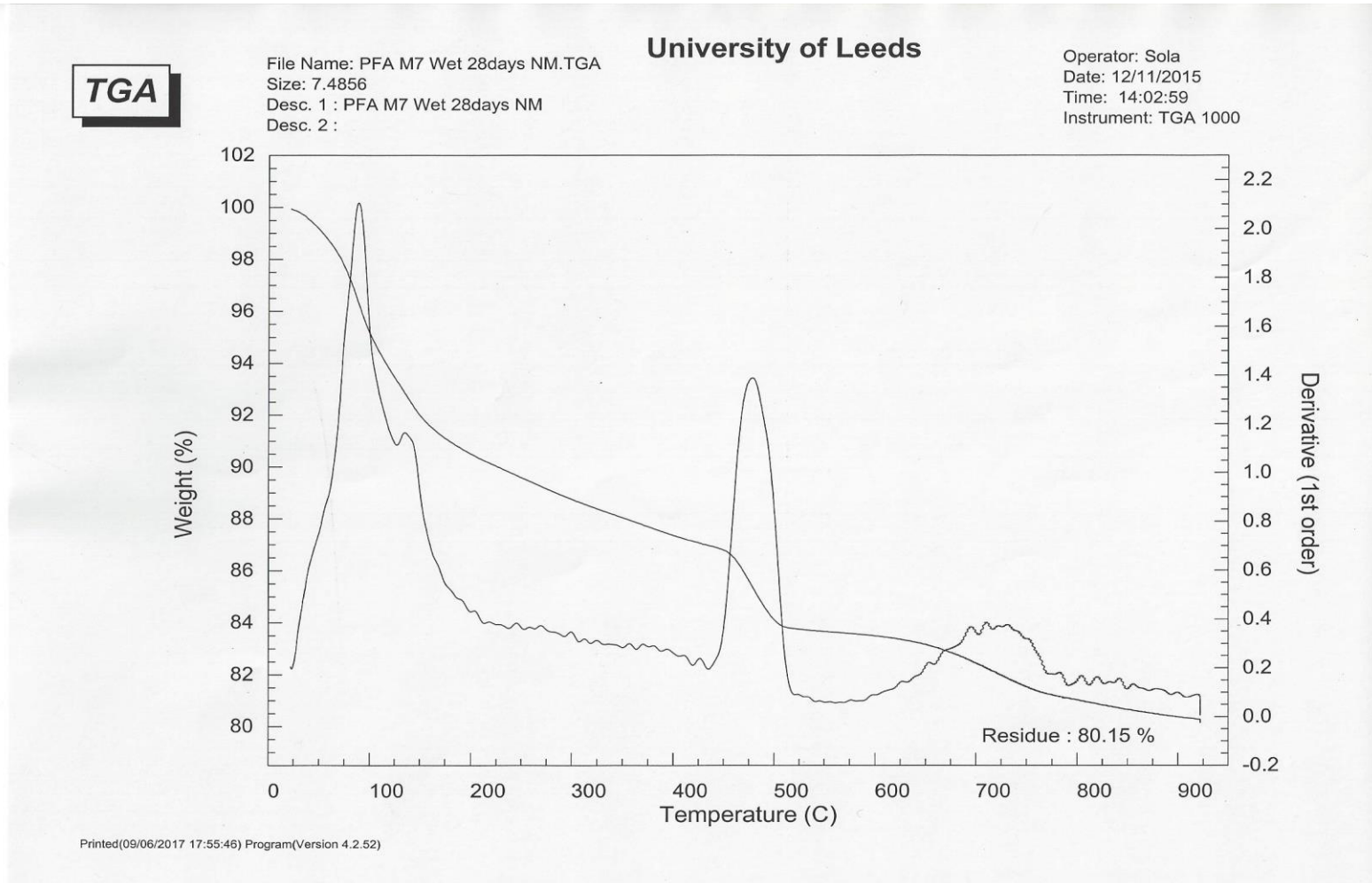


Figure A 149 TG result of 20MPa Fly ash stiff mix ideal cured 28 days

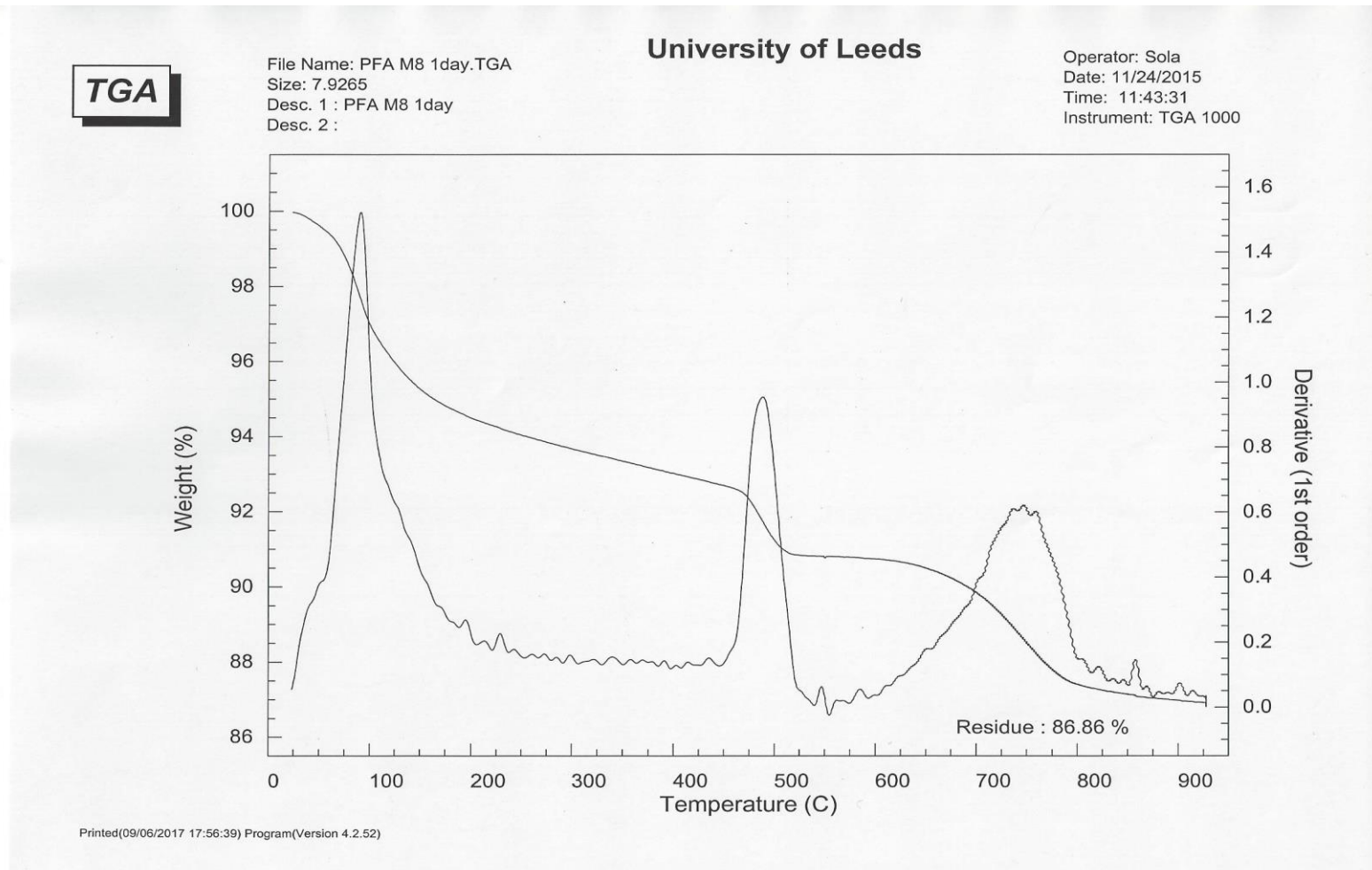


Figure A 150 TG result of 50MPa Fly ash stiff mix ambient cured 1 day

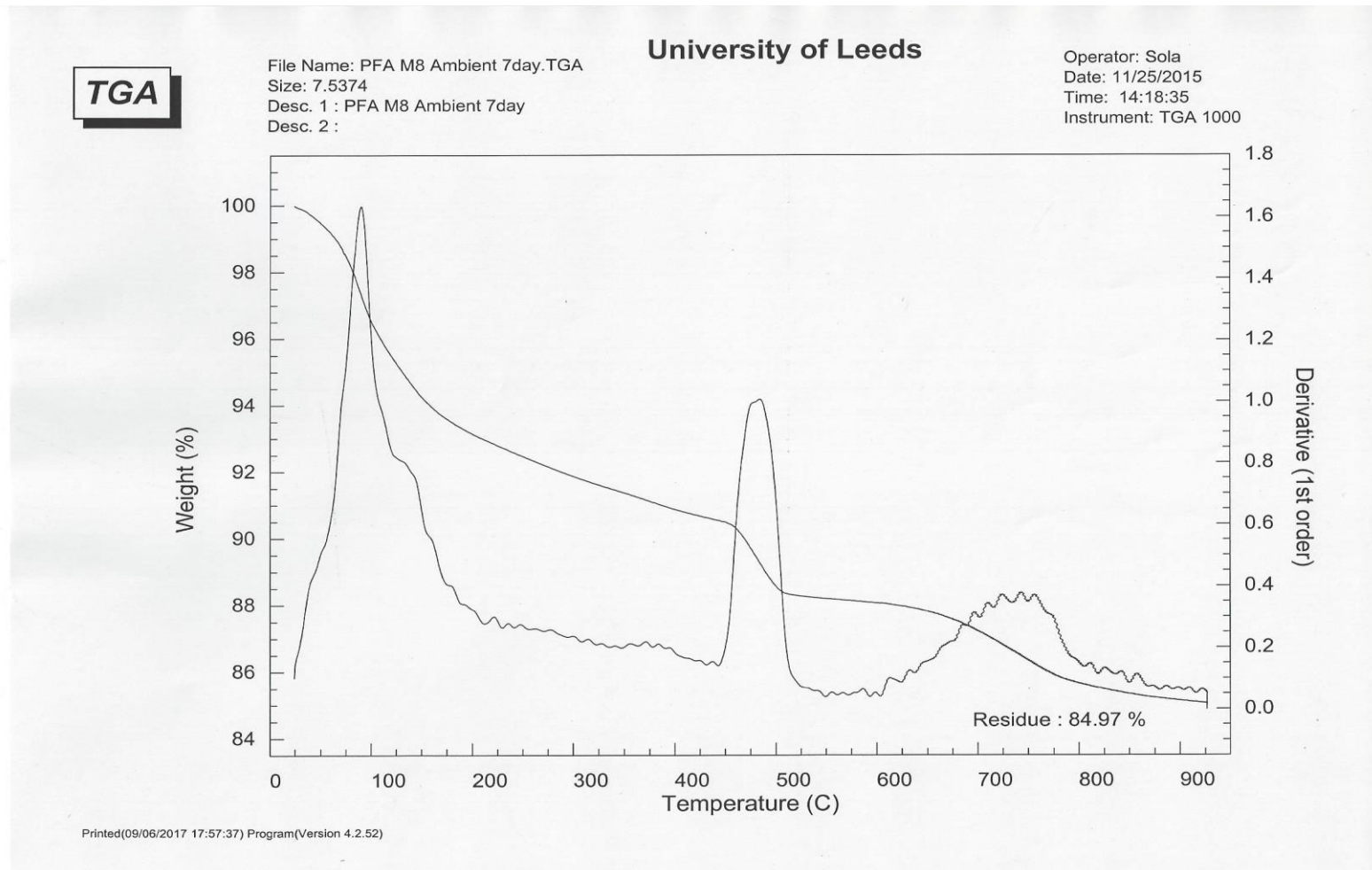


Figure A 151 TG result of 50MPa Fly ash stiff mix ambient cured 7 days

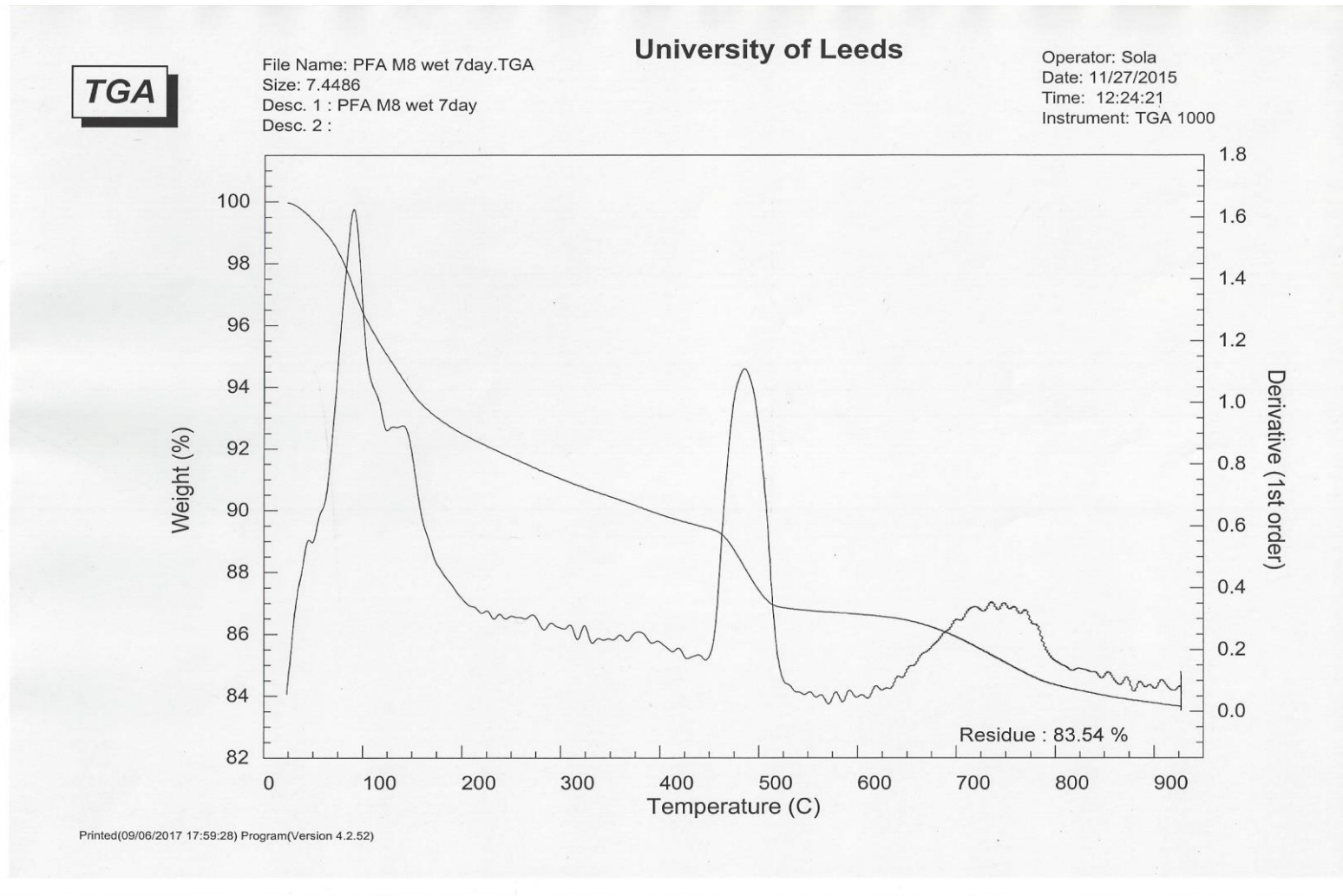


Figure A 152 TG result of 50MPa Fly ash stiff mix ideal cured 7 days

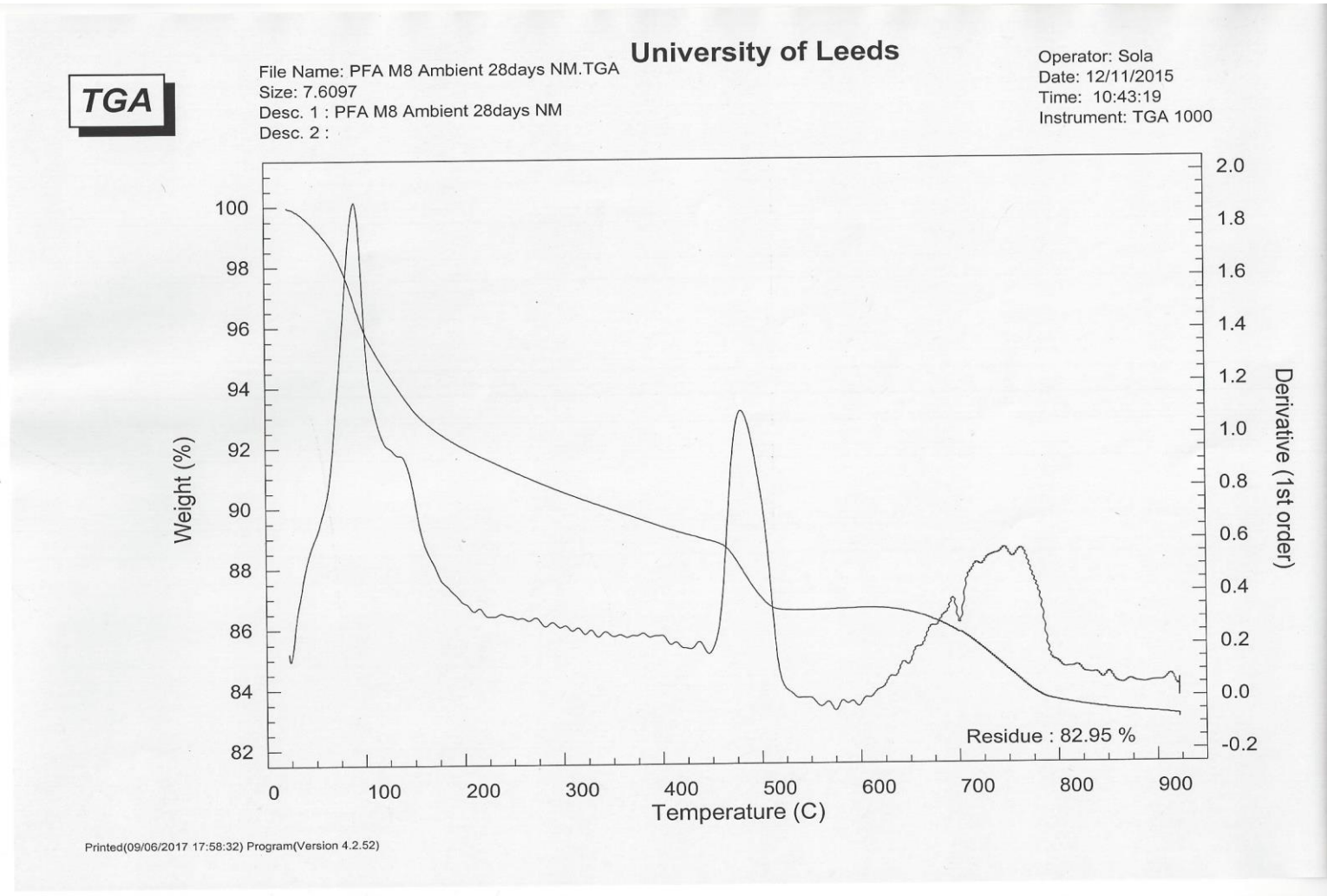


Figure A 153 TG result of 50MPa Fly ash stiff mix ambient cured 28 days

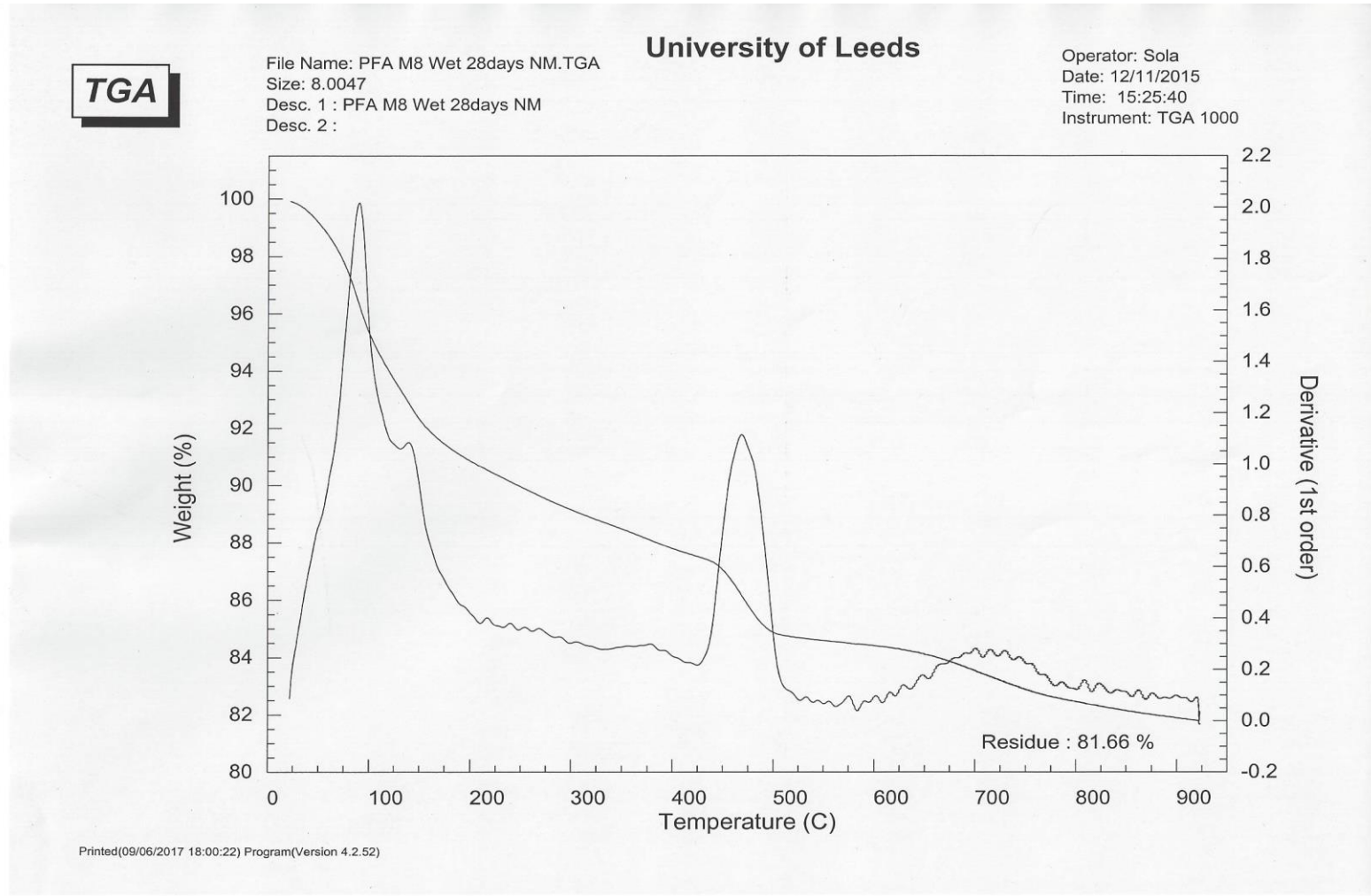


Figure A 154 TG result of 50MPa Fly ash stiff mix ideal cured 28 days

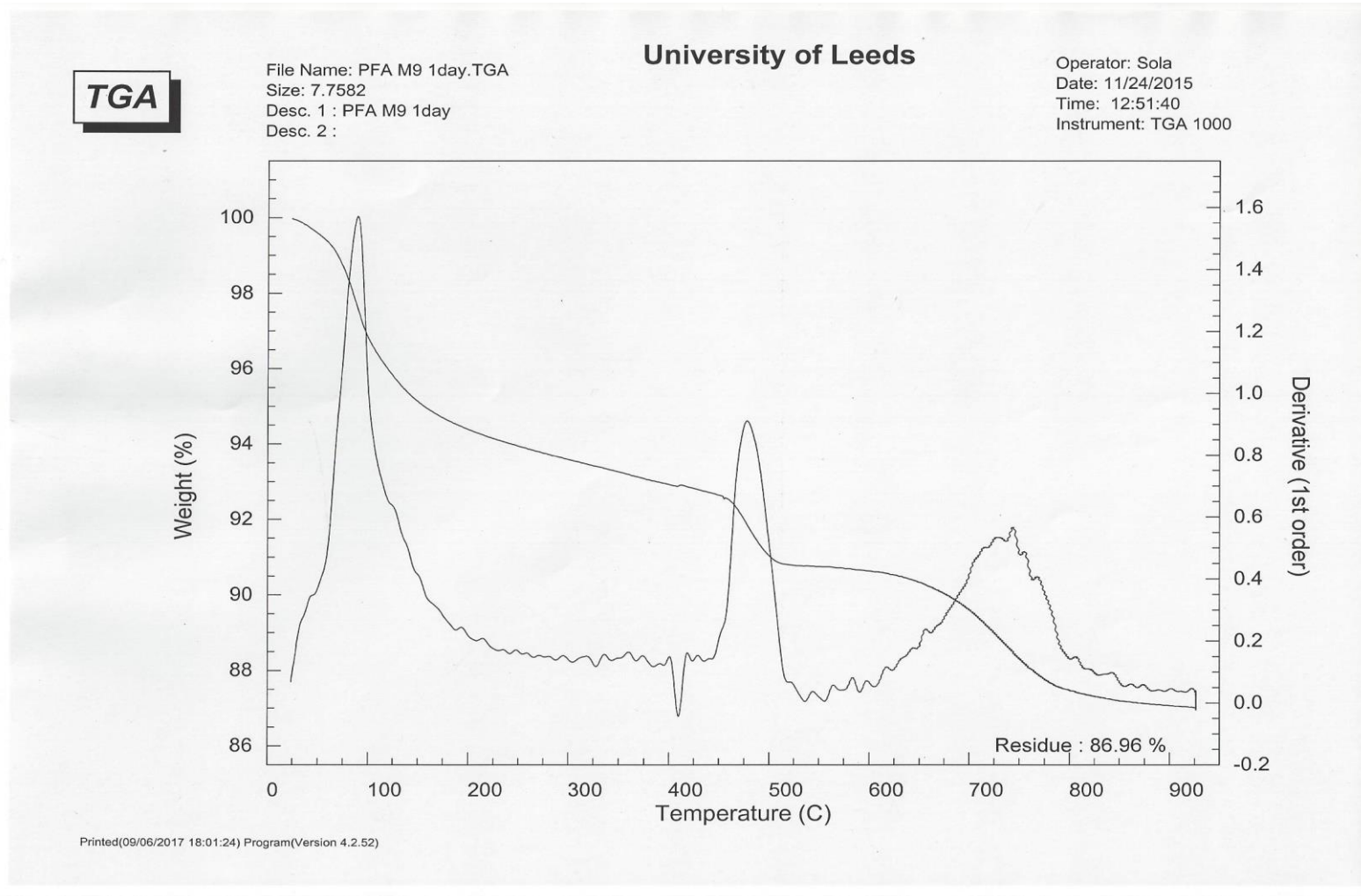


Figure A 155 TG result of 80MPa Fly ash stiff mix ambient cured 1 day

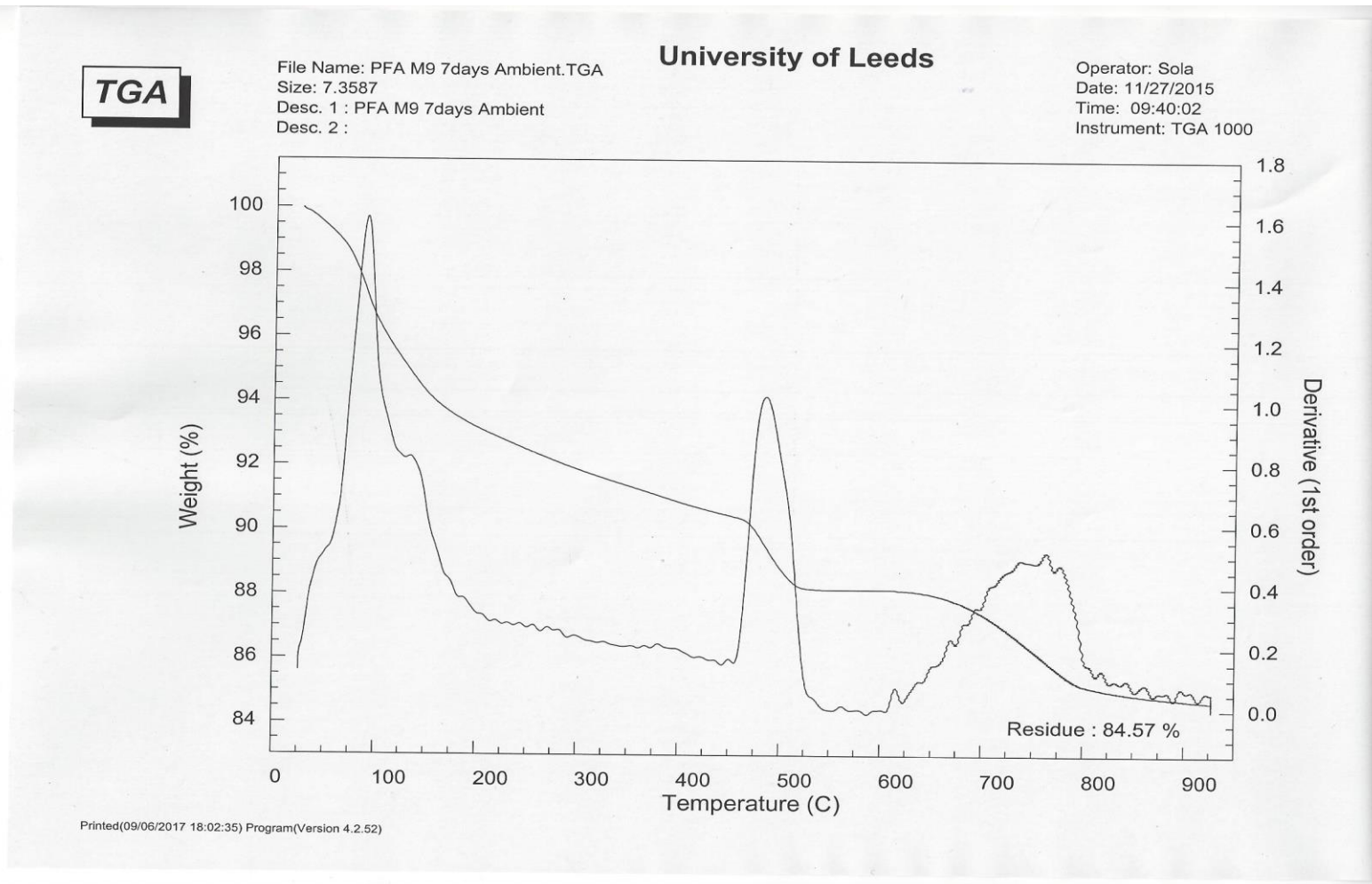


Figure A 156 TG result of 80MPa Fly ash stiff mix ambient cured 7 days

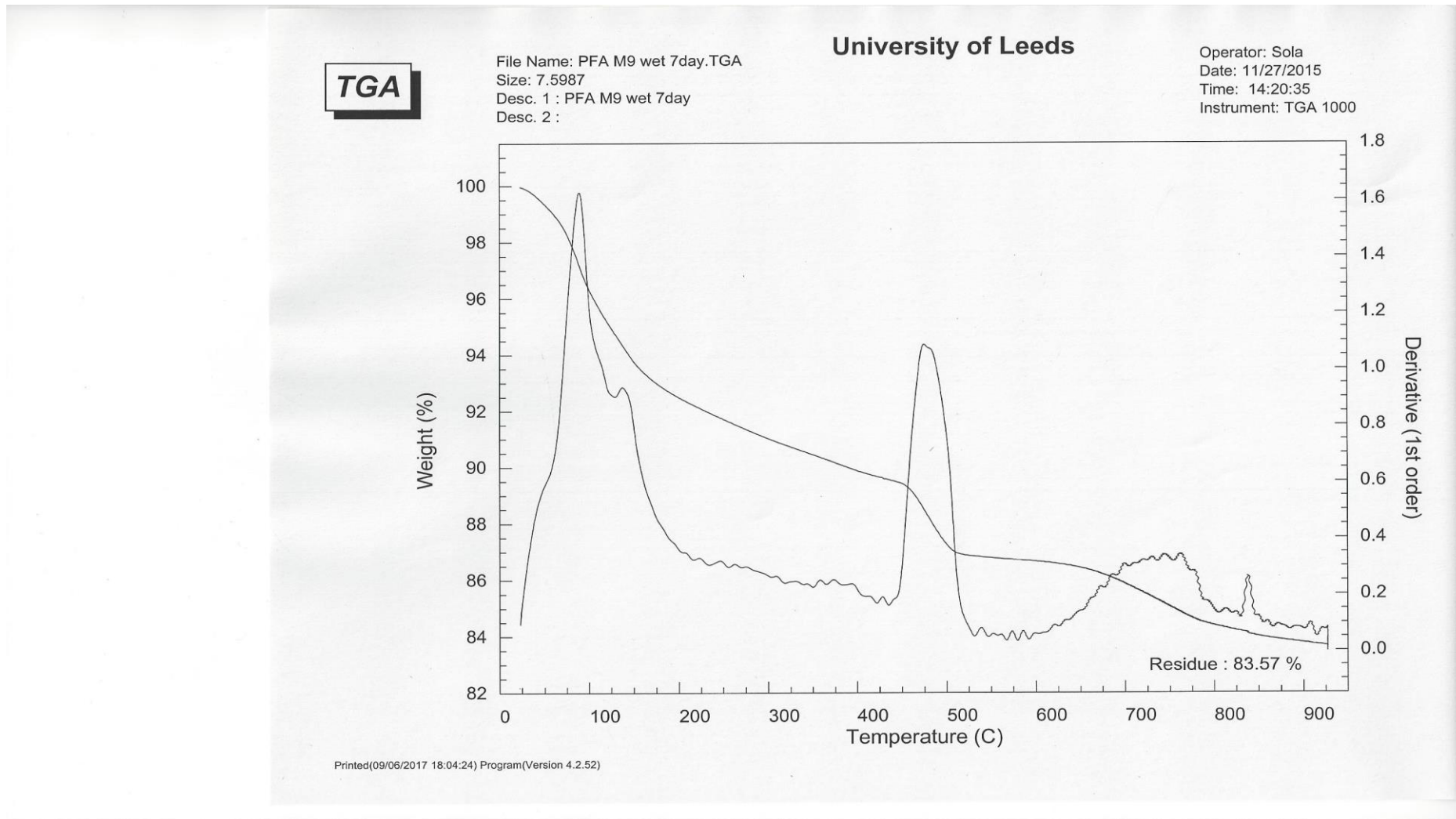


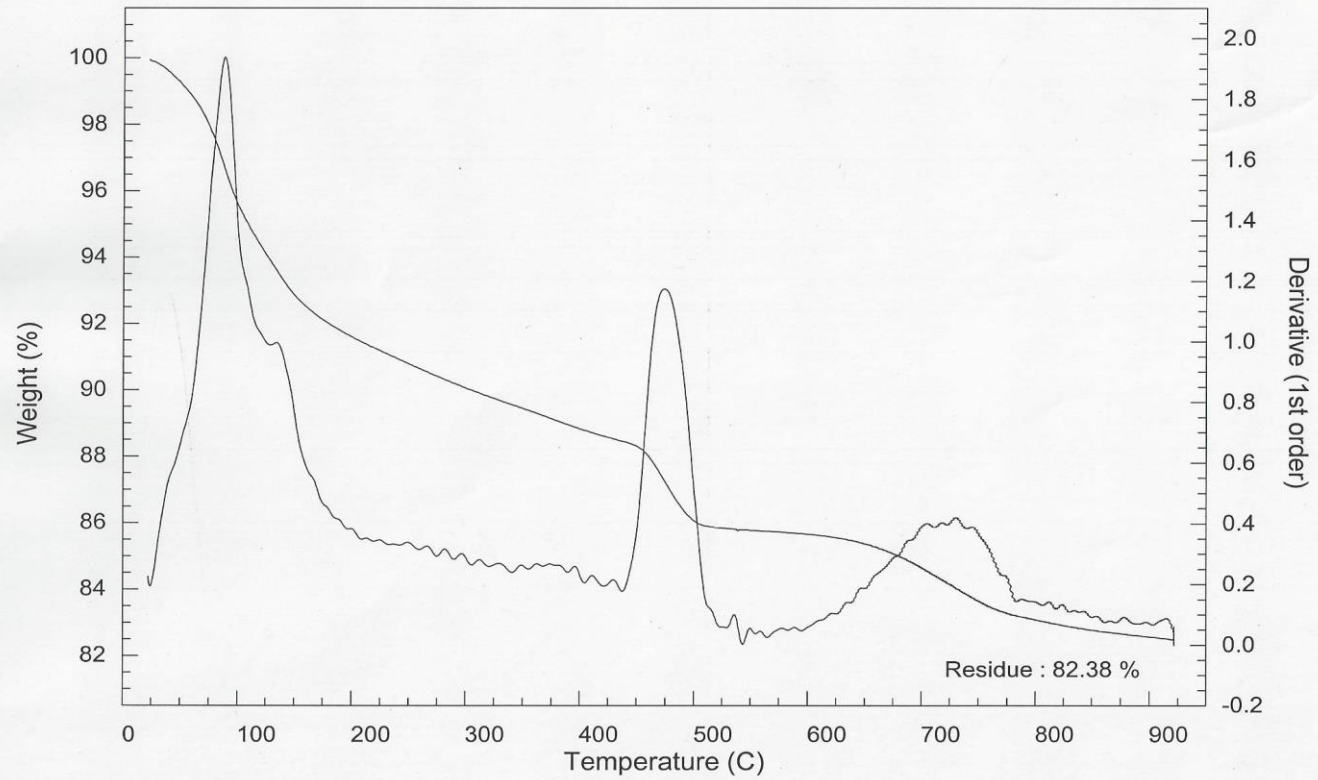
Figure A 157 TG result of 80MPa Fly ash stiff mix ideal cured 7 days

TGA

File Name: PFA M9 Ambient 28days NM.TGA
Size: 7.3793
Desc. 1 : PFA M9 Ambient 28days NM
Desc. 2 :

University of Leeds

Operator: Sola
Date: 12/11/2015
Time: 12:18:54
Instrument: TGA 1000



Printed(09/06/2017 18:03:31) Program(Versio 4.2.52)

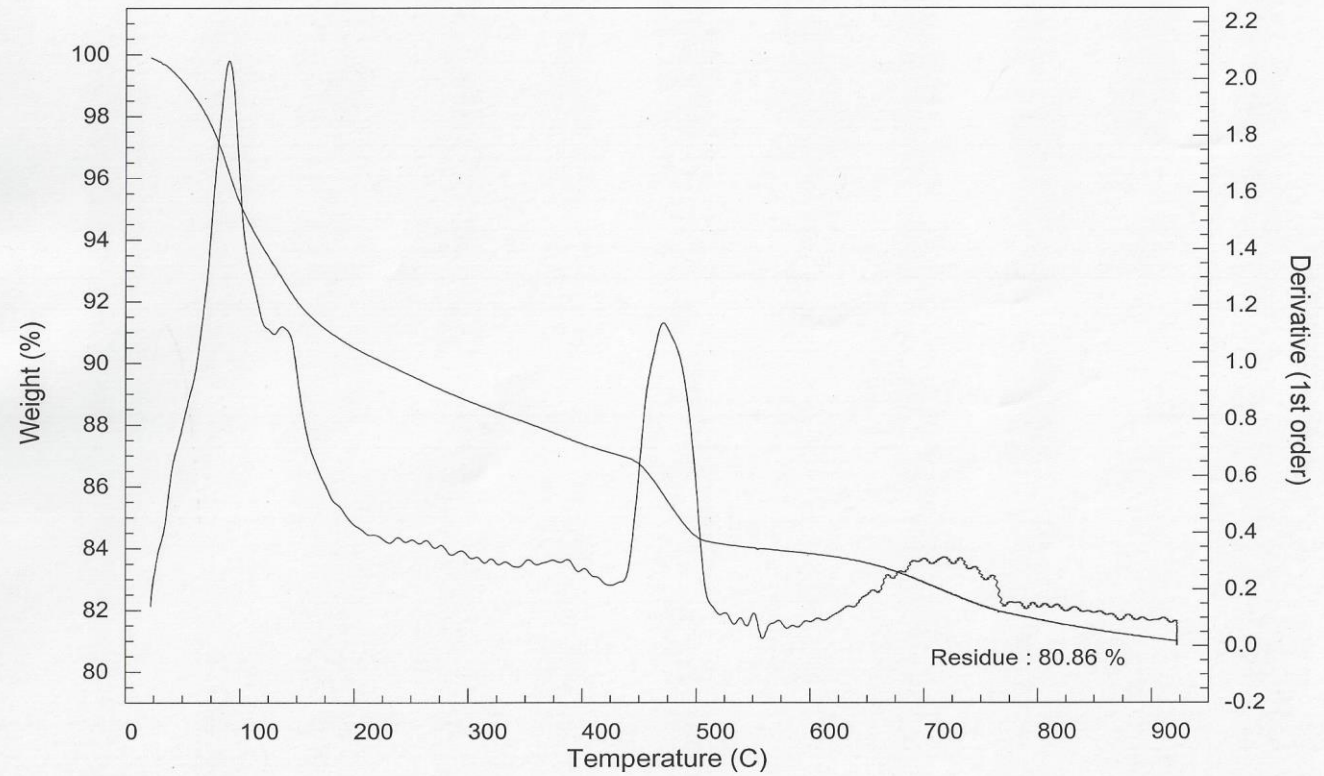
Figure A 158 TG result of 80MPa Fly ash stiff mix ambient cured 28 days

TGA

File Name: PFA M9 Wet 28days NM.TGA
Size: 7.8528
Desc. 1 : PFA M9 Wet 28days NM
Desc. 2 :

University of Leeds

Operator: Sola
Date: 12/11/2015
Time: 16:35:16
Instrument: TGA 1000



Printed(09/06/2017 18:05:15) Program(Versio 4.2.52)

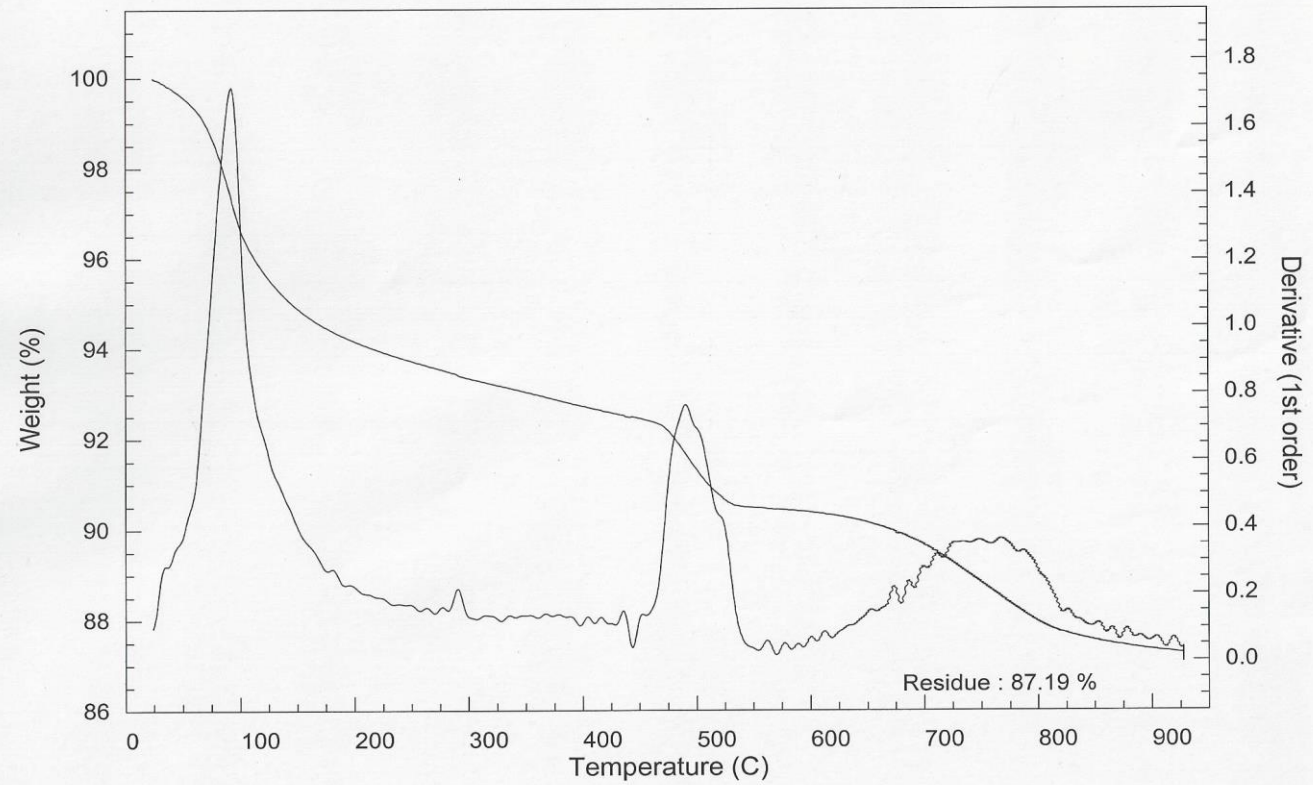
Figure A 159 TG result of 80MPa Fly ash stiff mix ideal cured 28 days

TGA

File Name: PFA M10 1 day.TGA
Size: 8.2676
Desc. 1 : PFA M10 1 day
Desc. 2 :

University of Leeds

Operator: Sola
Date: 11/24/2015
Time: 14:39:53
Instrument: TGA 1000



Printed(09/06/2017 18:06:16) Program(Versio 4.2.52)

Figure A 160 TG result of 20MPa Fly ash wet mix ambient cured 1 day

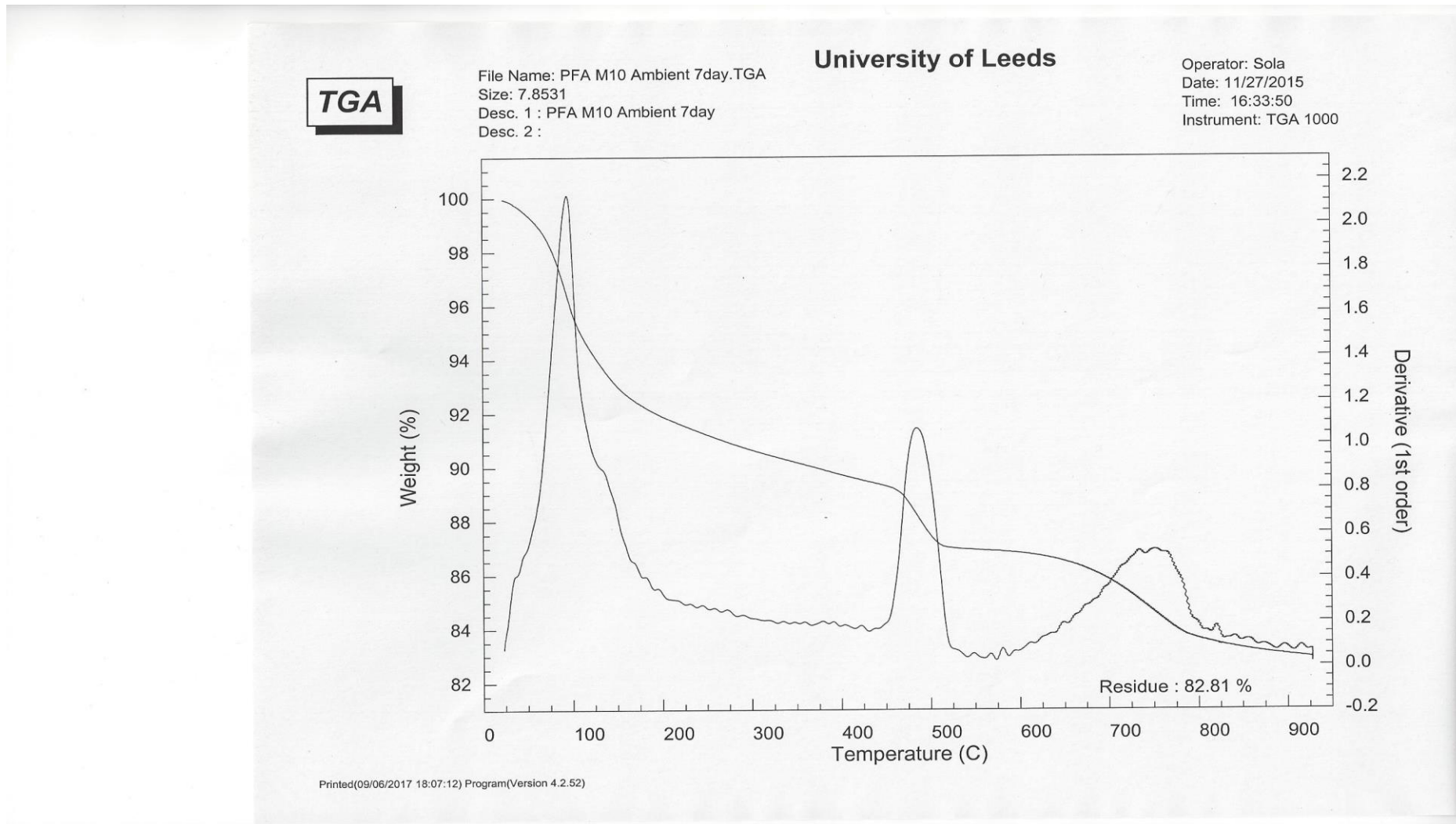


Figure A 161 TG result of 20MPa Fly ash wet mix ambient cured 7 days

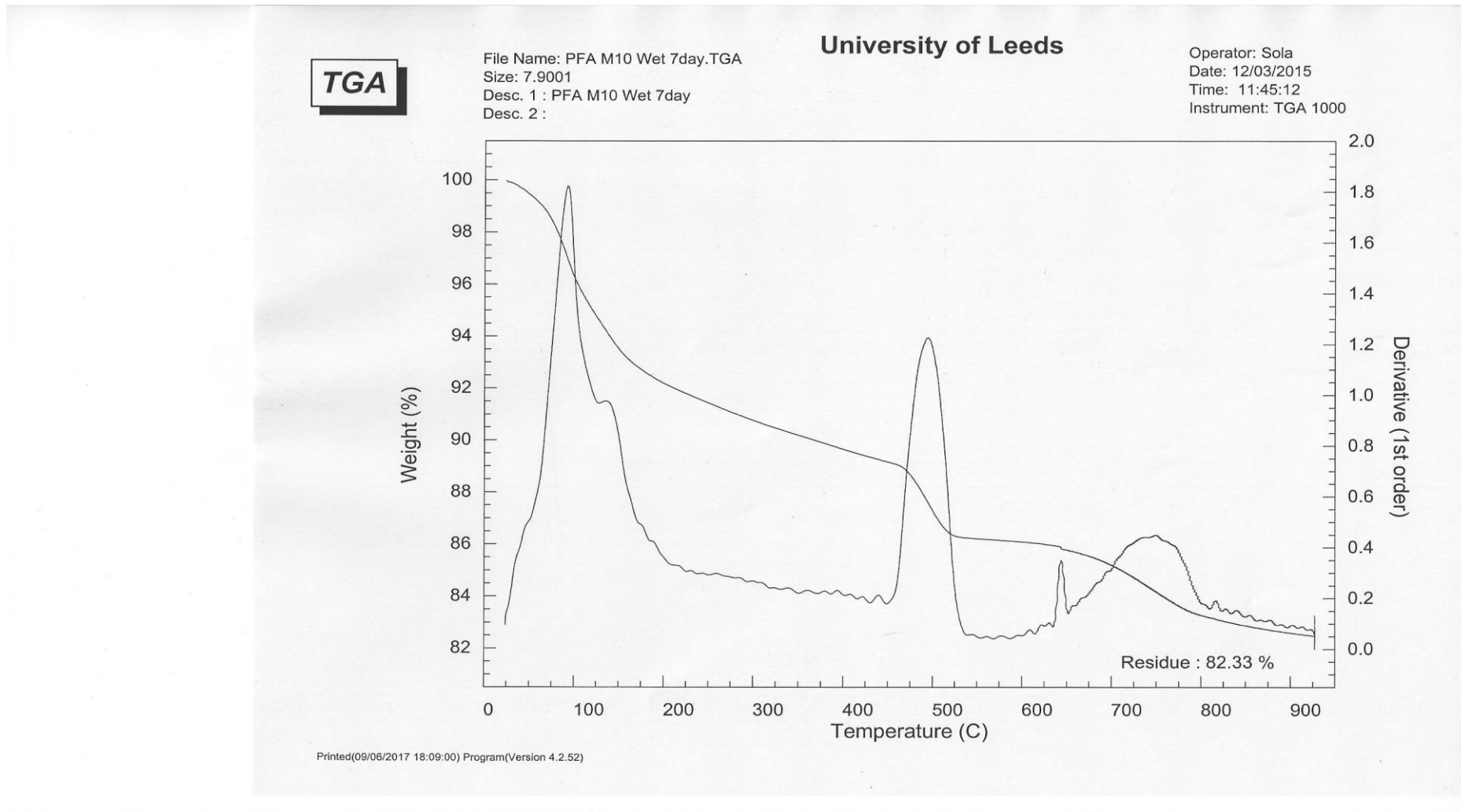


Figure A 162 TG result of 20MPa Fly ash wet mix ideal cured 7 days

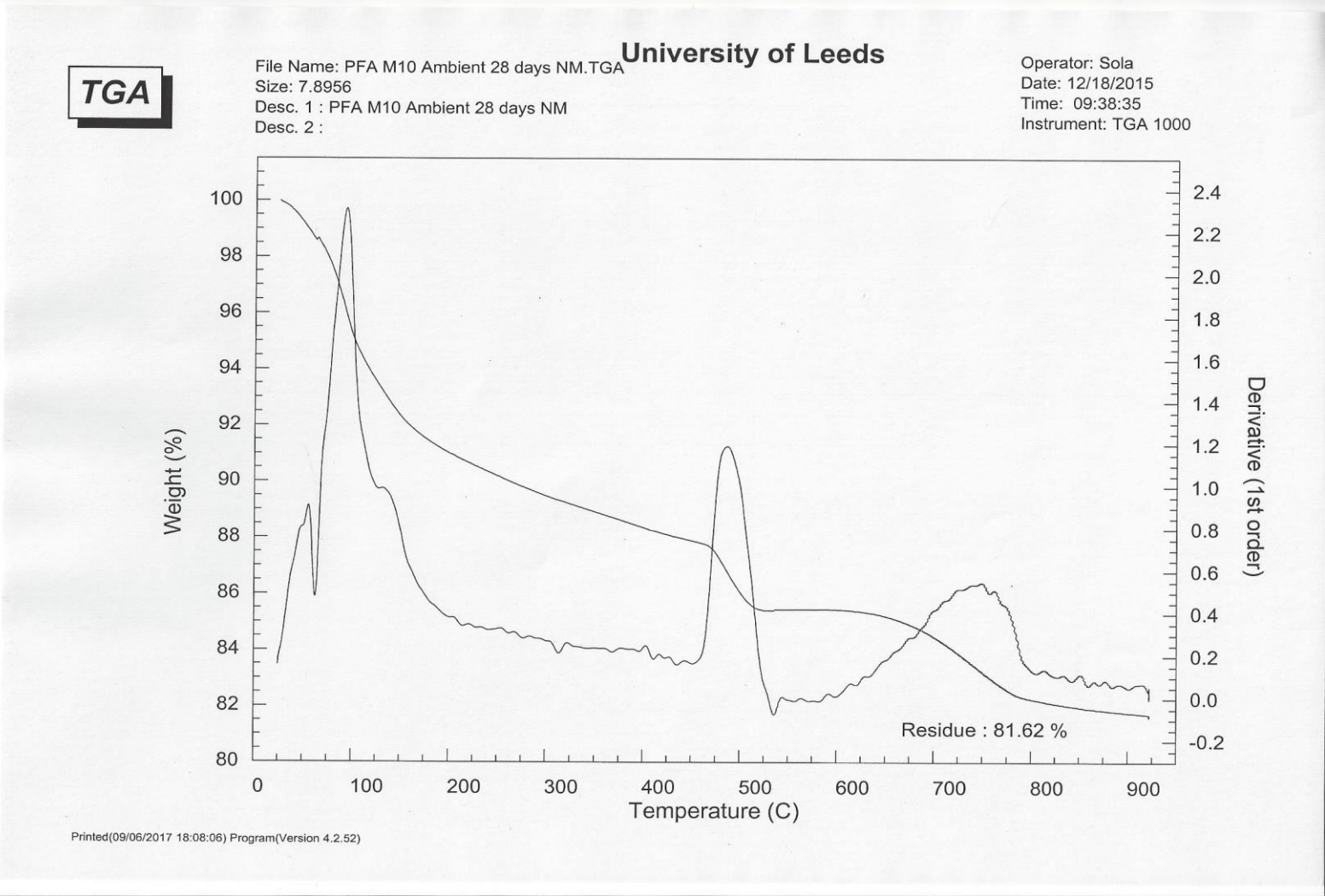


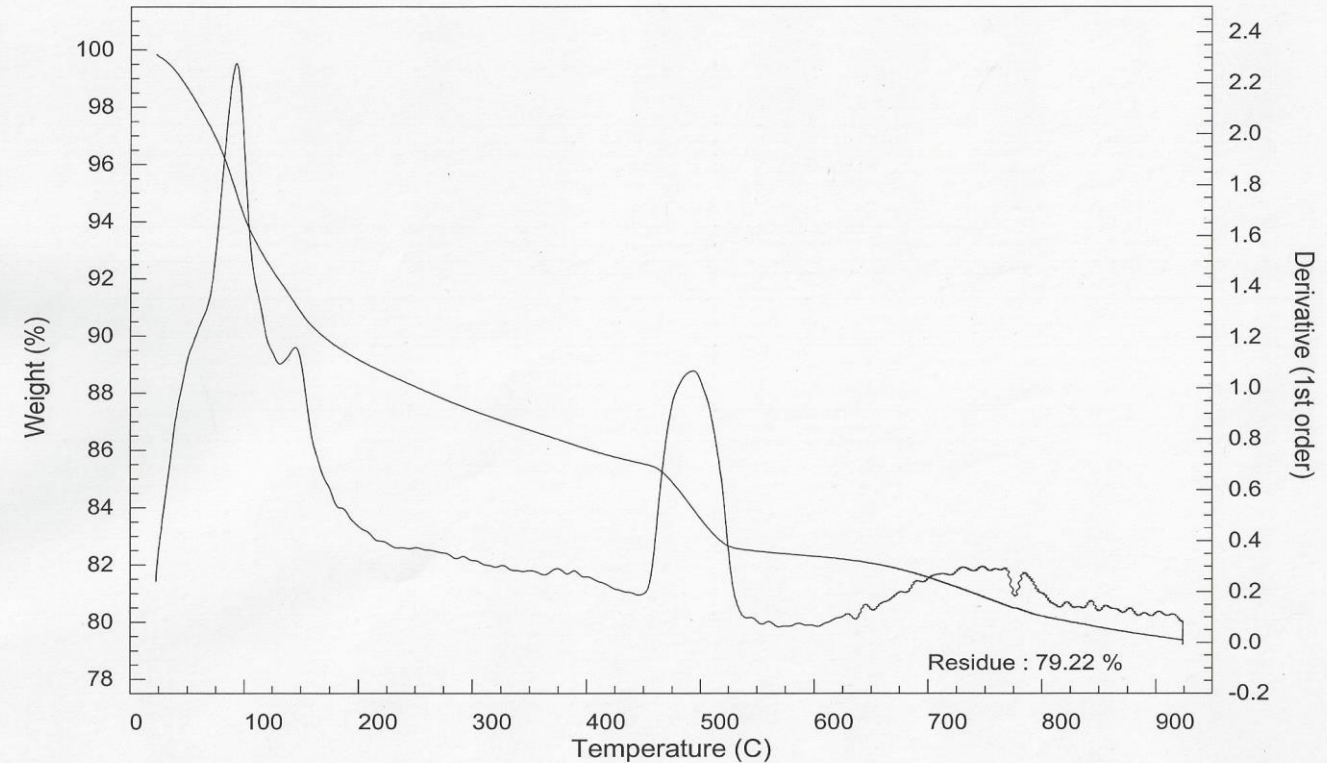
Figure A 163 TG result of 20MPa Fly ash wet mix ambient cured 28 days

TGA

File Name: PFA M10 wet 28 days NM 2.TGA
Size: 7.6598
Desc. 1 : PFA M10 wet 28 days NM 2
Desc. 2 :

University of Leeds

Operator: Sola
Date: 12/18/2015
Time: 14:43:28
Instrument: TGA 1000



Printed(09/06/2017 18:09:59) Program(Versio 4.2.52)

Figure A 164 TG result of 20MPa Fly ash wet mix ideal cured 28 days

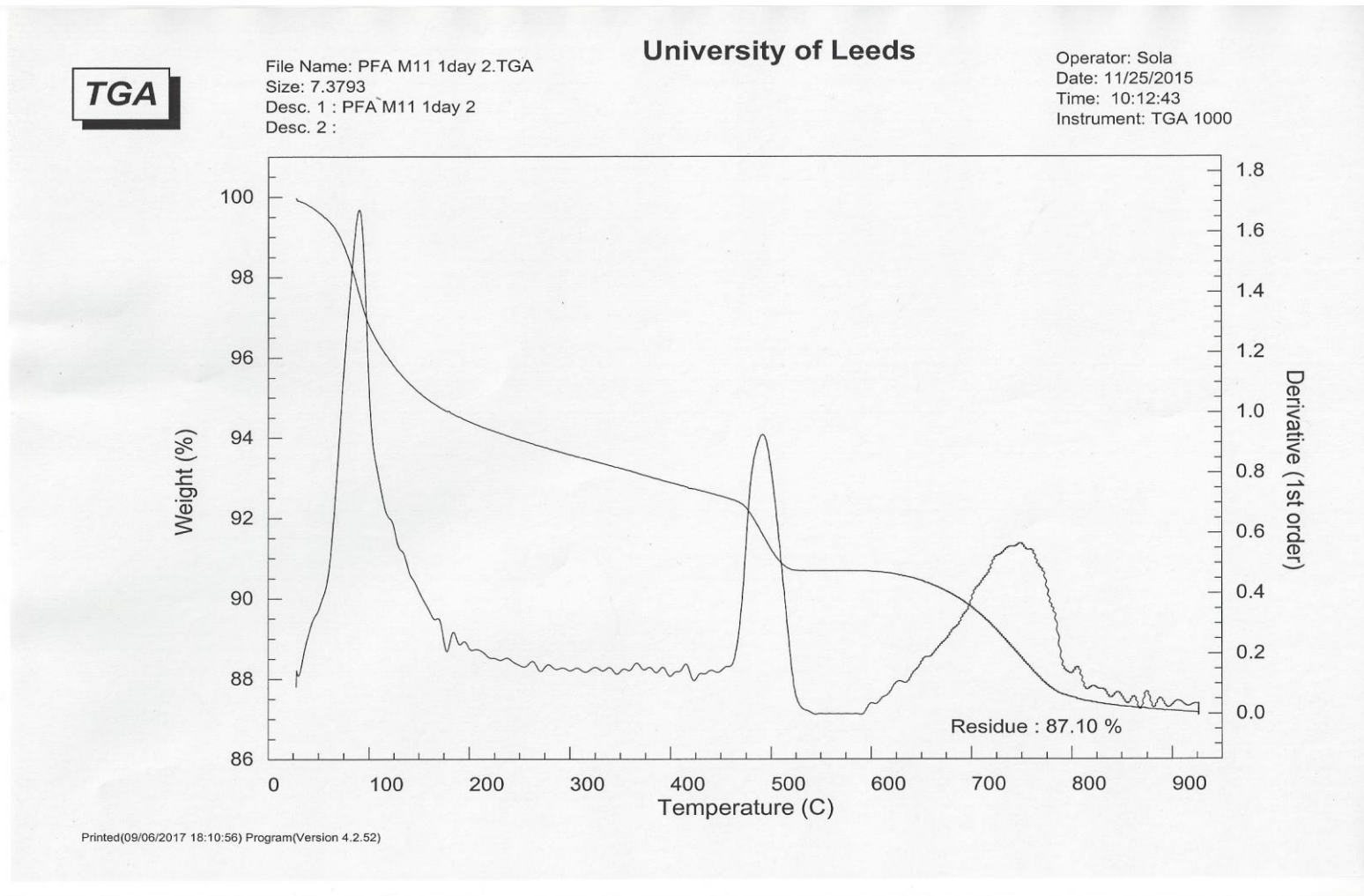


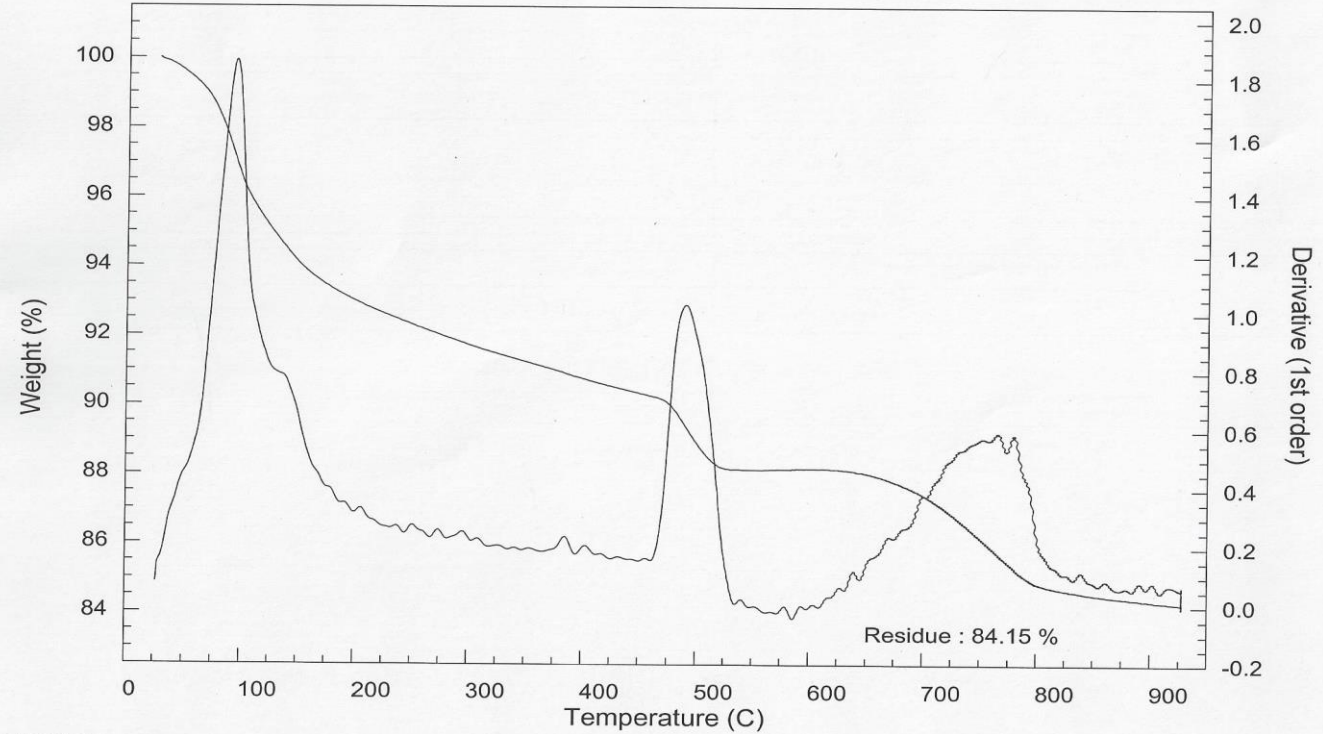
Figure A 165 TG result of 50MPa Fly ash wet mix ambient cured 1 day

TGA

File Name: PFA M11 Ambient 7 days.TGA
Size: 7.4949
Desc. 1 : PFA M11 Ambient 7 days
Desc. 2 :

University of Leeds

Operator: Sola
Date: 11/30/2015
Time: 11:00:42
Instrument: TGA 1000



Printed(09/06/2017 18:11:45) Program(Versio 4.2.52)

Figure A 166 TG result of 50MPa Fly ash wet mix ambient cured 7 days

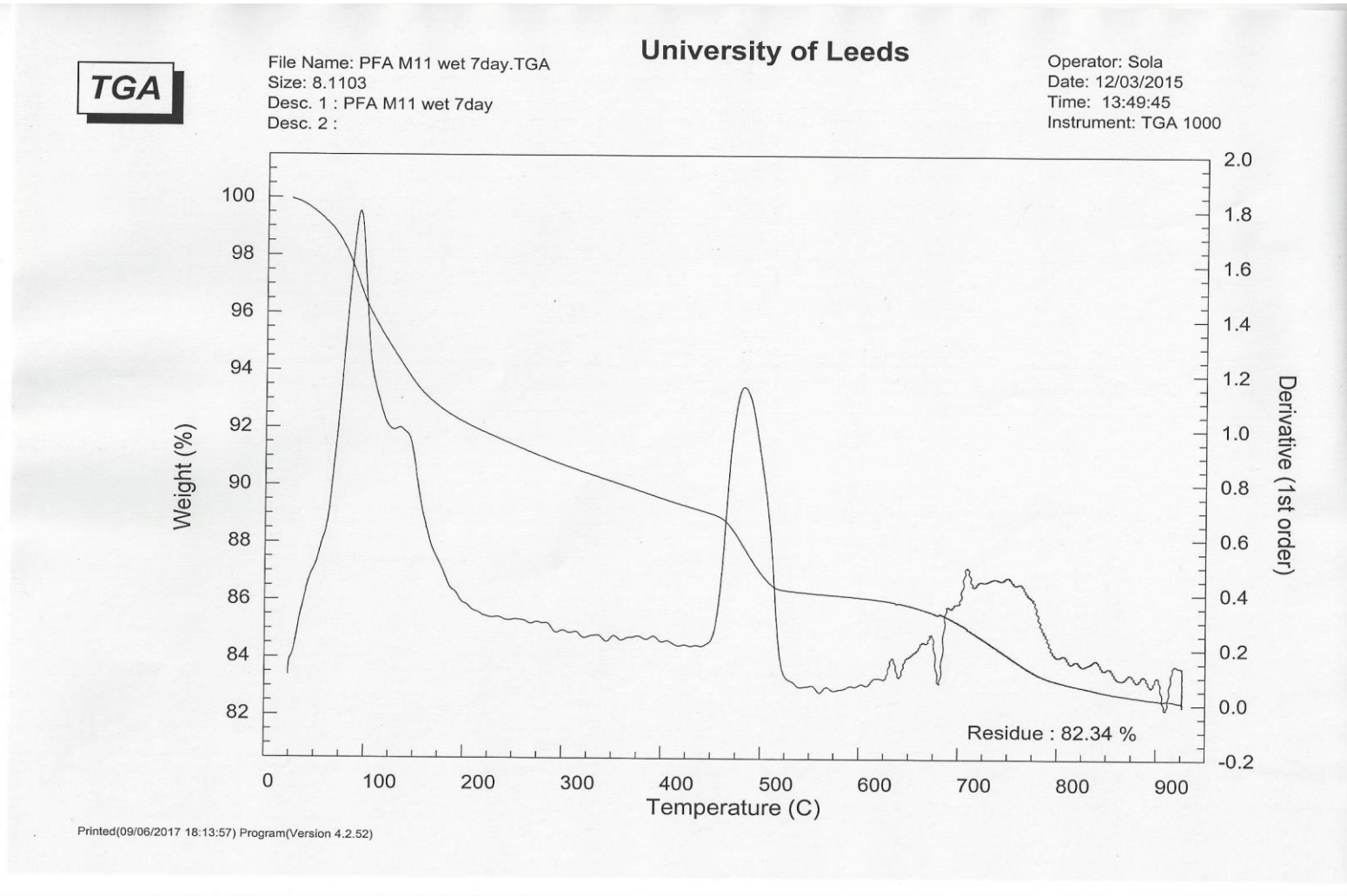


Figure A 167 TG result of 50MPa Fly ash wet mix ideal cured 7 days

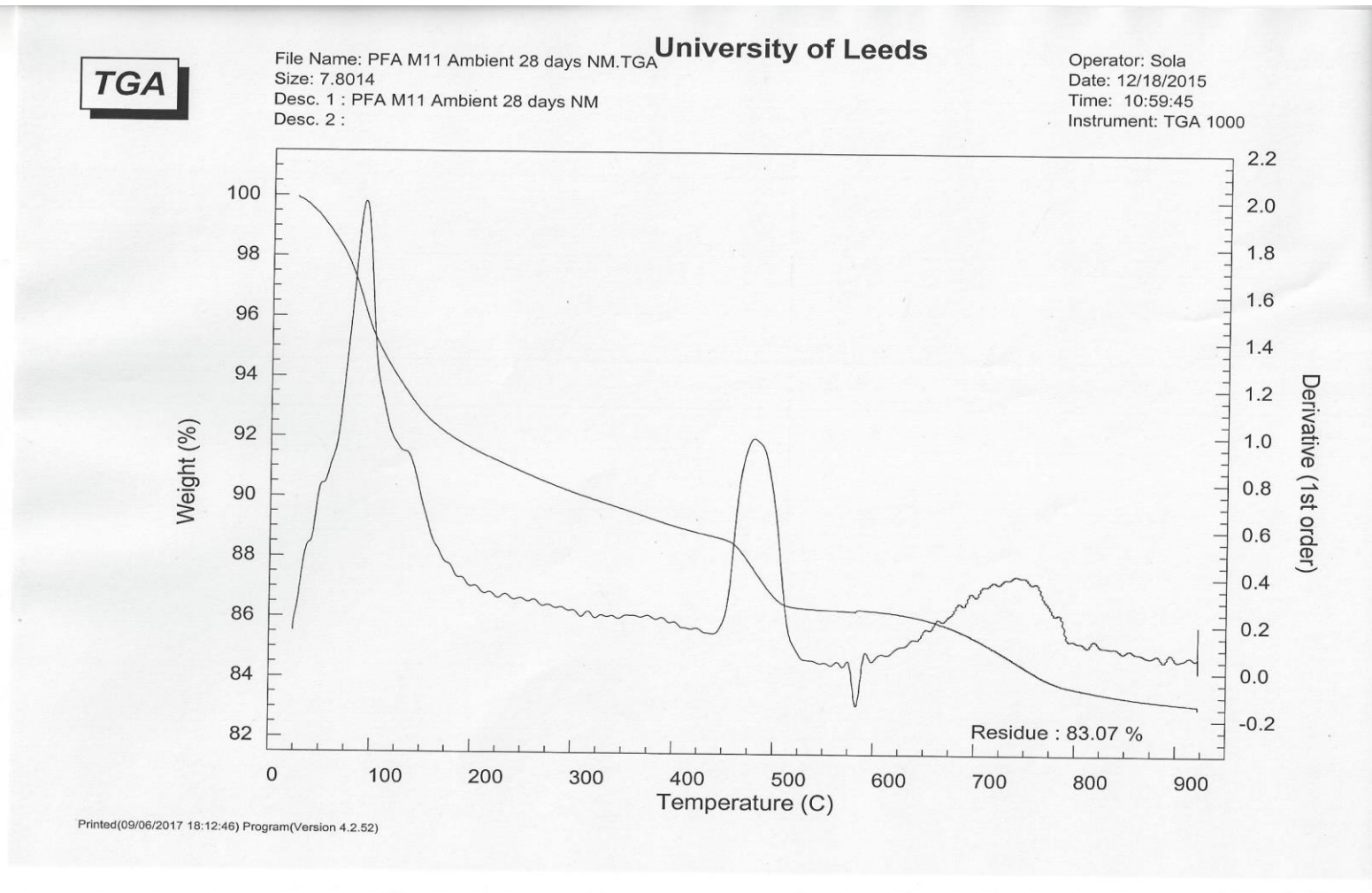


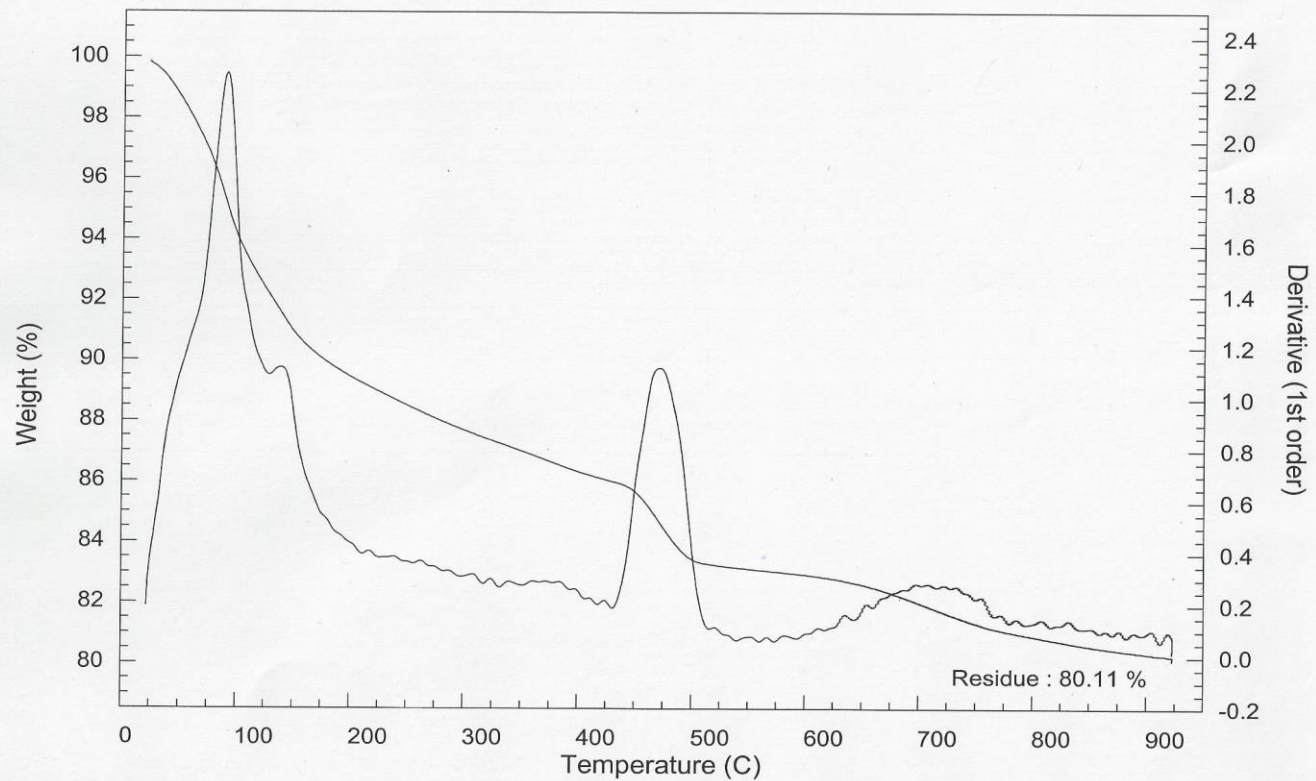
Figure A 168 TG result of 50MPa Fly ash wet mix ambient cured 28 days



File Name: PFA M11 wet 28 days NM.TGA
Size: 7.2981
Desc. 1 : PFA M11 wet 28 days NM
Desc. 2 :

University of Leeds

Operator: Sola
Date: 12/18/2015
Time: 16:03:04
Instrument: TGA 1000



Printed(09/06/2017 18:14:49) Program(Versioin 4.2.52)

Figure A 169 TG result of 50MPa Fly ash wet mix ideal cured 28days

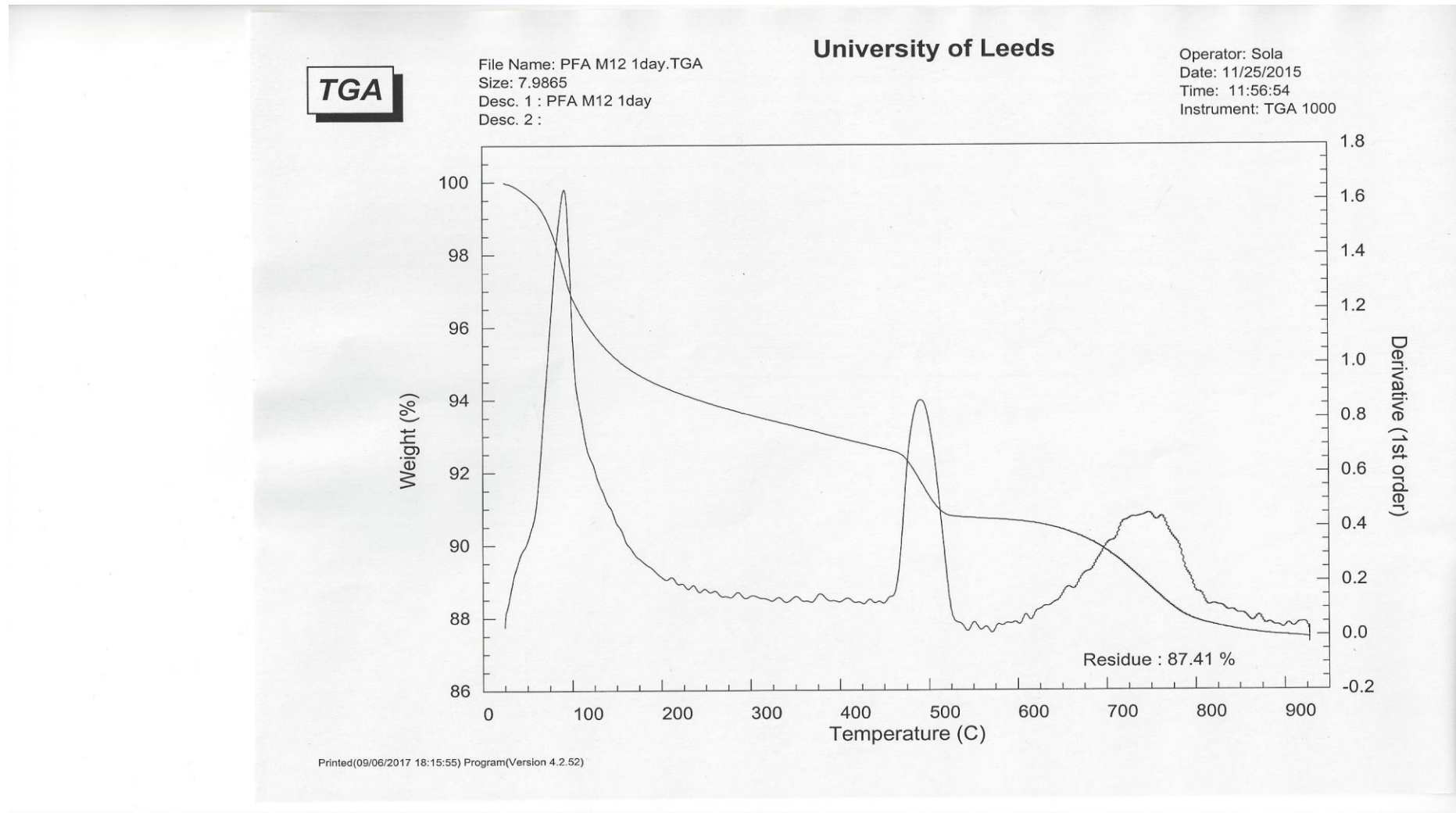


Figure A 170 TG result of 80MPa Fly ash wet mix ambient cured 1 day

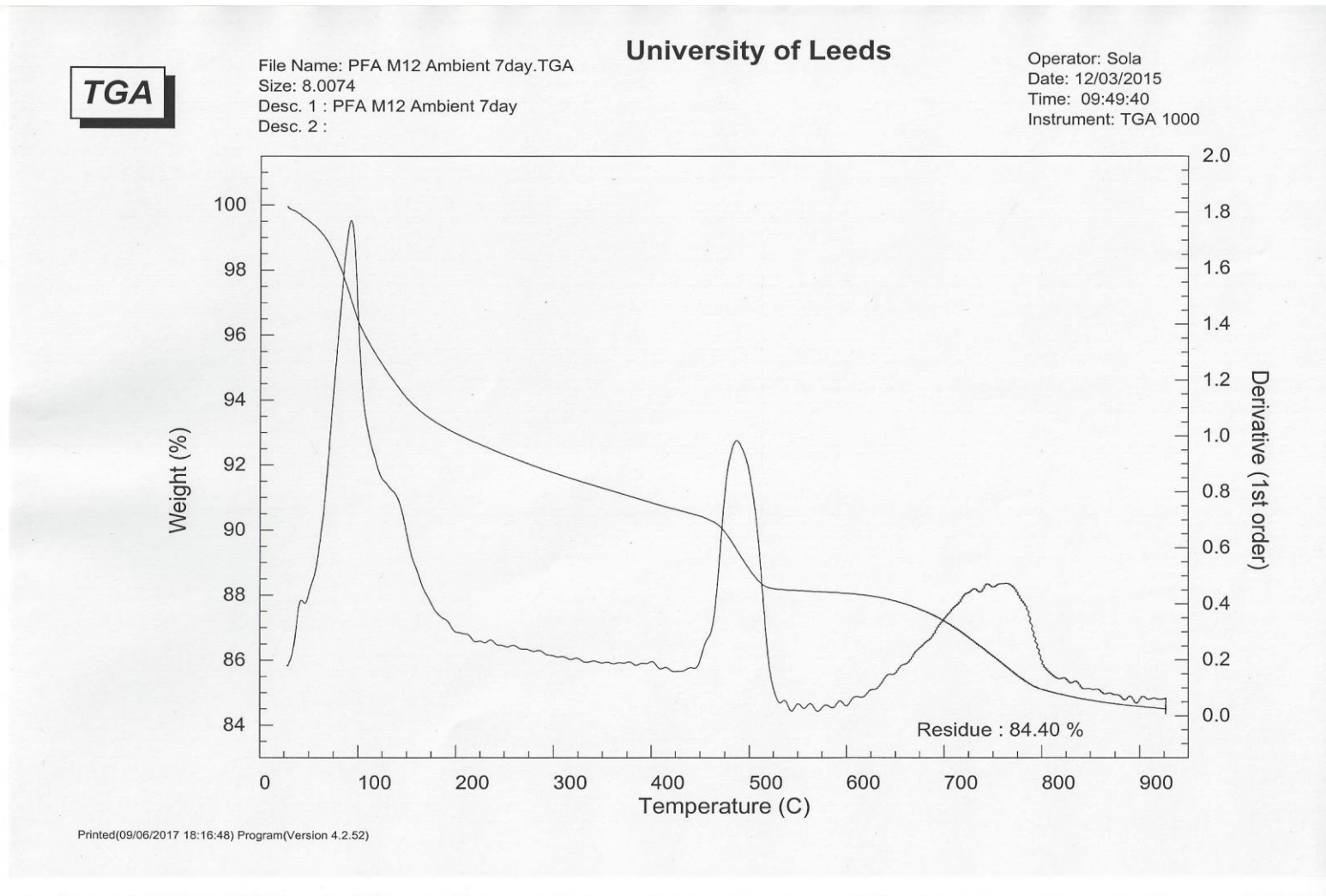


Figure A 171 TG result of 80MPa Fly ash wet mix ambient cured 7 days

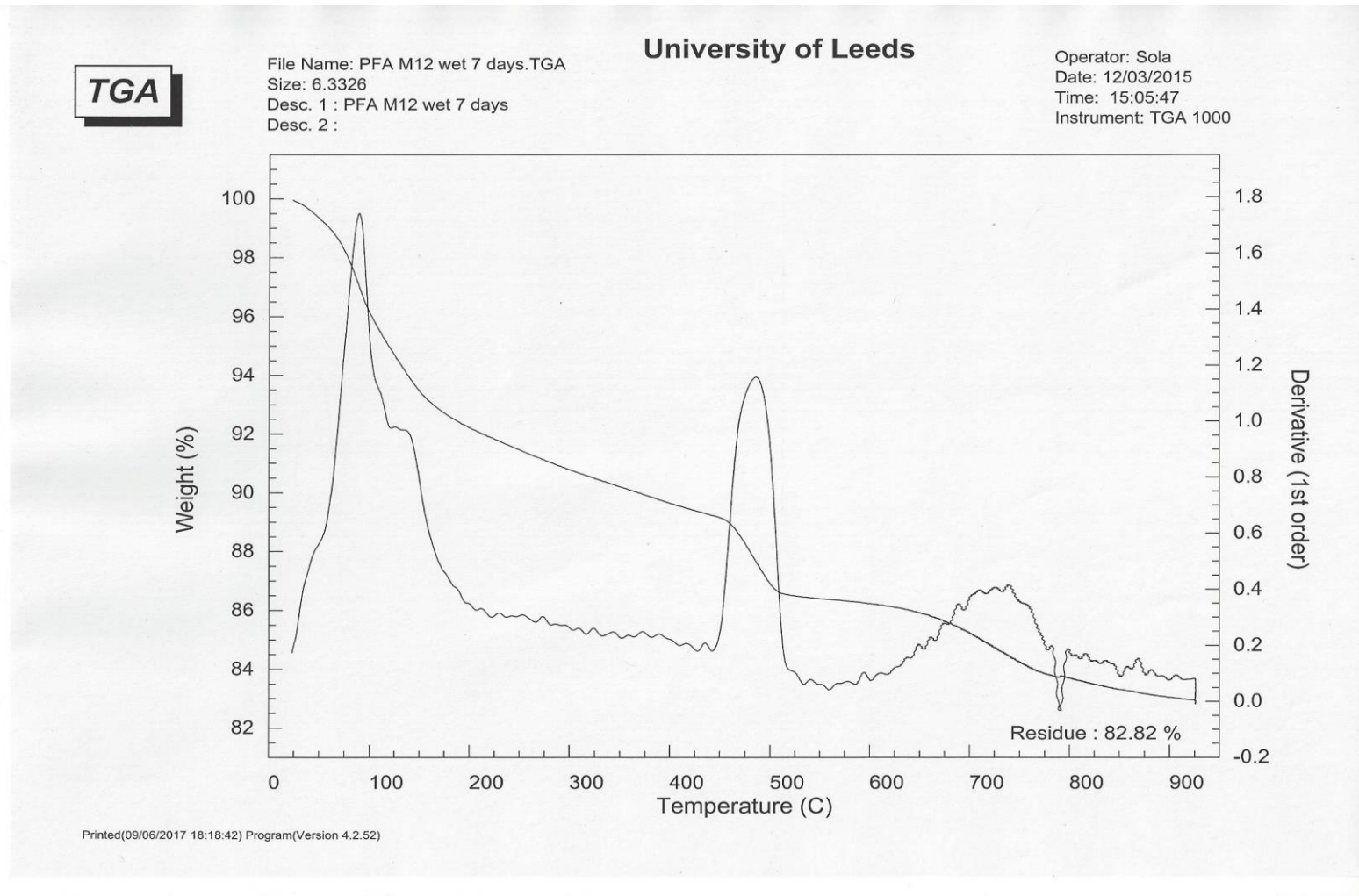


Figure A 172 TG result of 80MPa Fly ash wet mix ideal cured 7 days

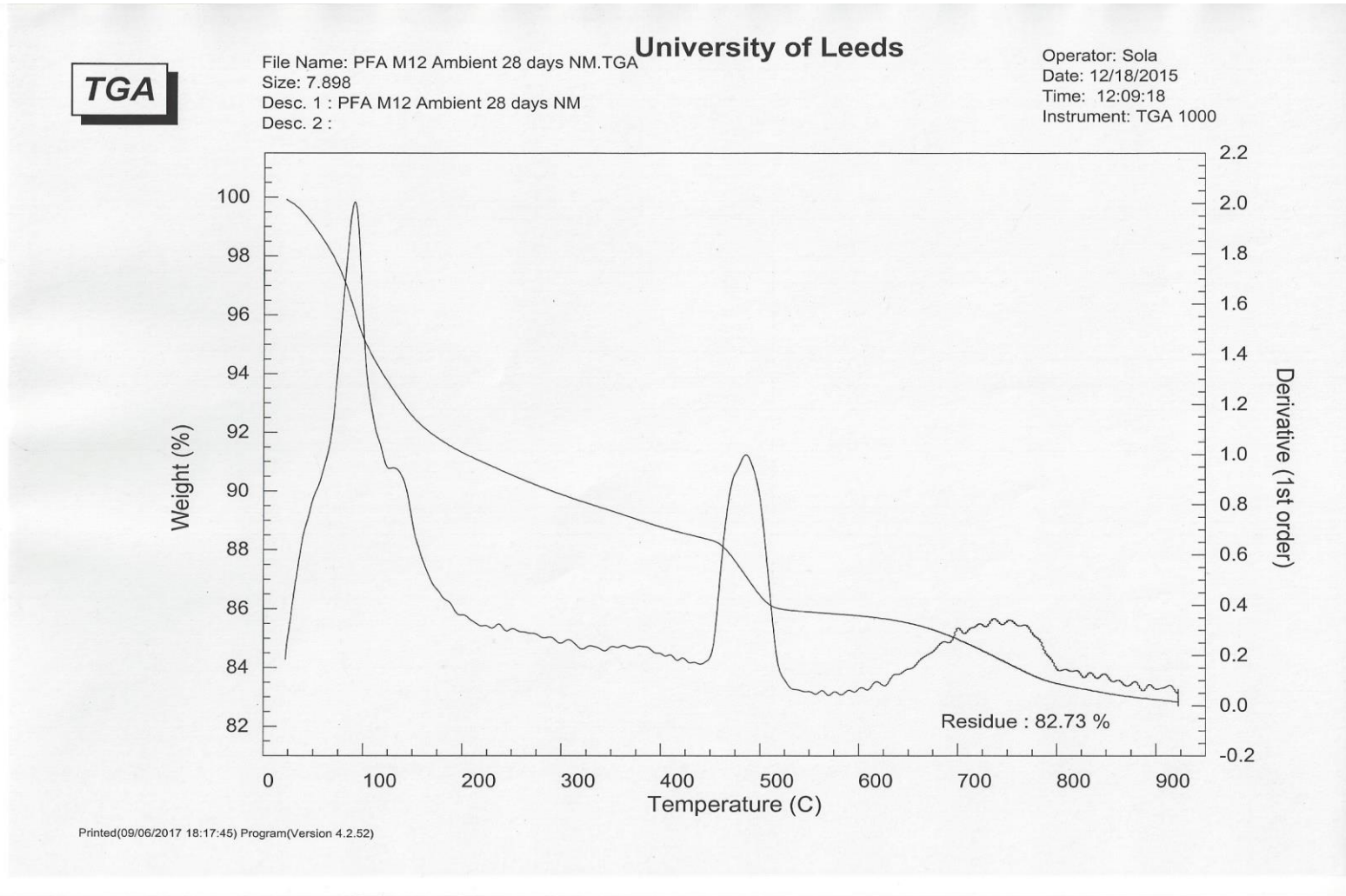


Figure A 173 TG result of 80MPa Fly ash wet mix ambient cured 28 days

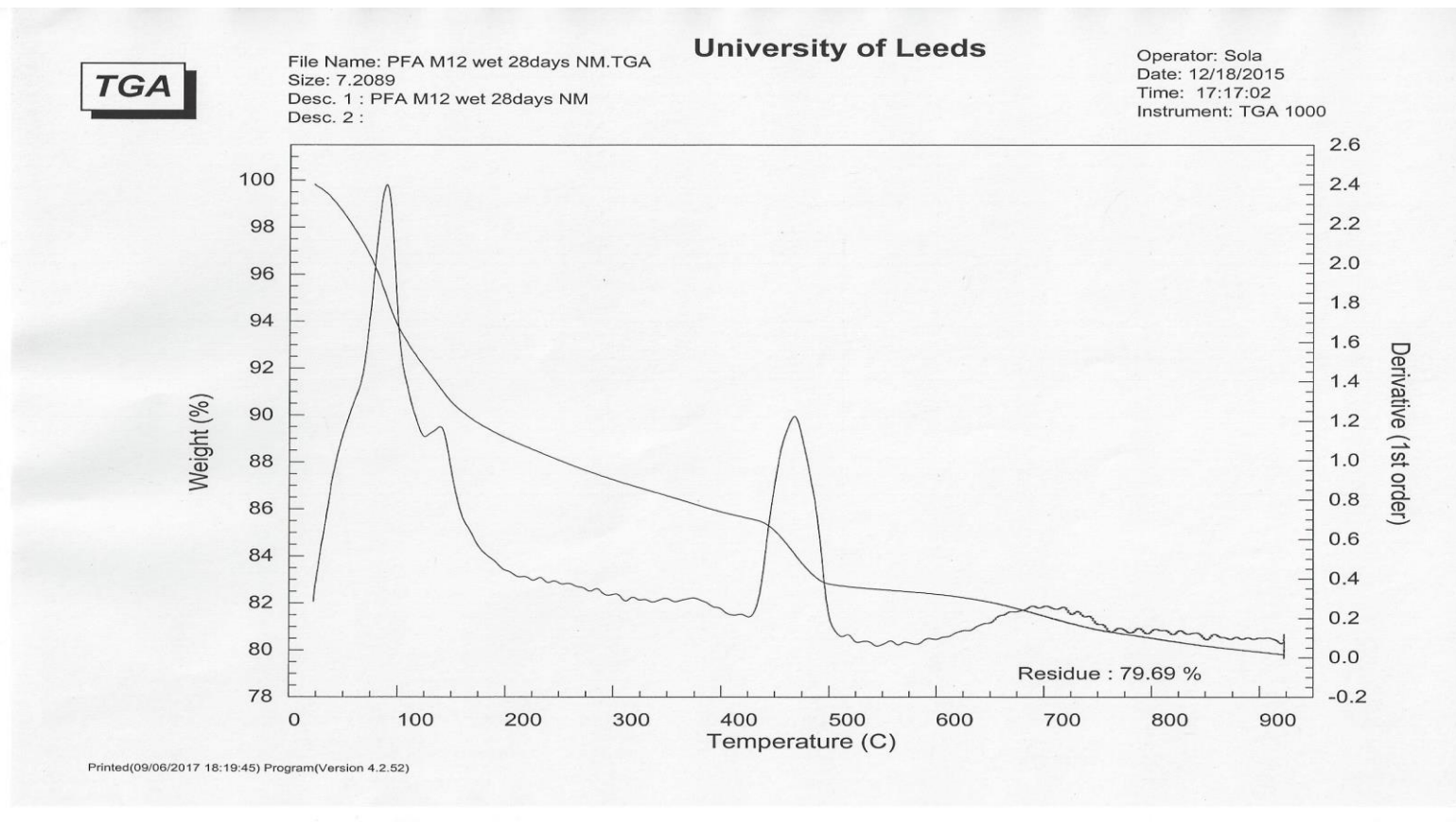


Figure A 174 TG result of 80MPa Fly ash wet mix ideal cured 28 days

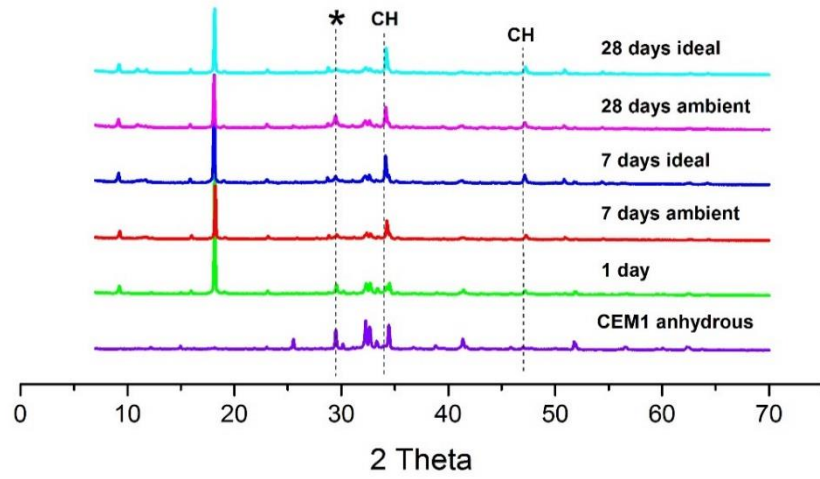


Figure A 175 XRD of 20MPa CEM1 stiff mix from 1 day to 28days of curing with CEM1 anhydrous

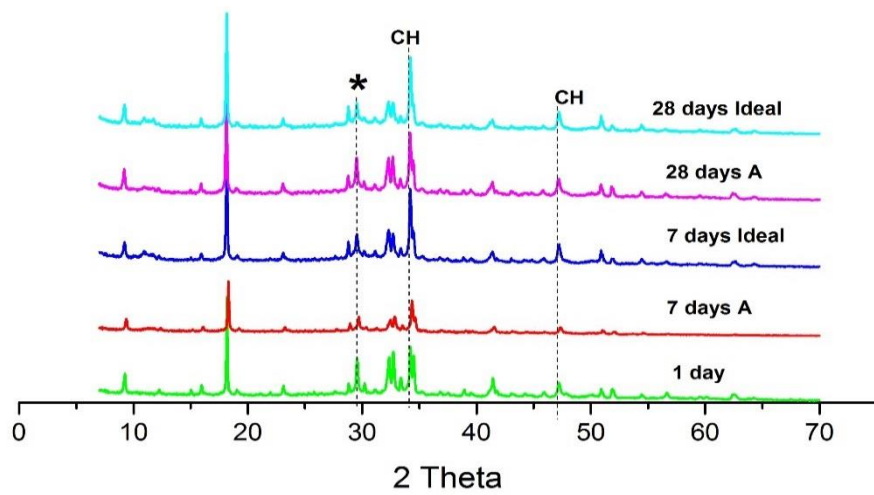


Figure A 176 XRD of 50MPa CEM1 stiff mix from 1 day to 28 days of curing

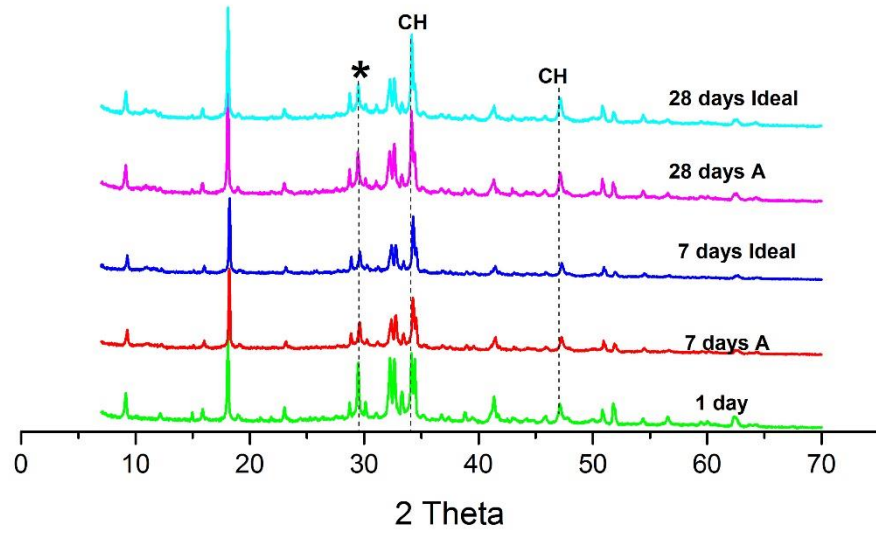


Figure A 177 XRD of 80MPa CEM1 stiff from 1 day to 28days of curing

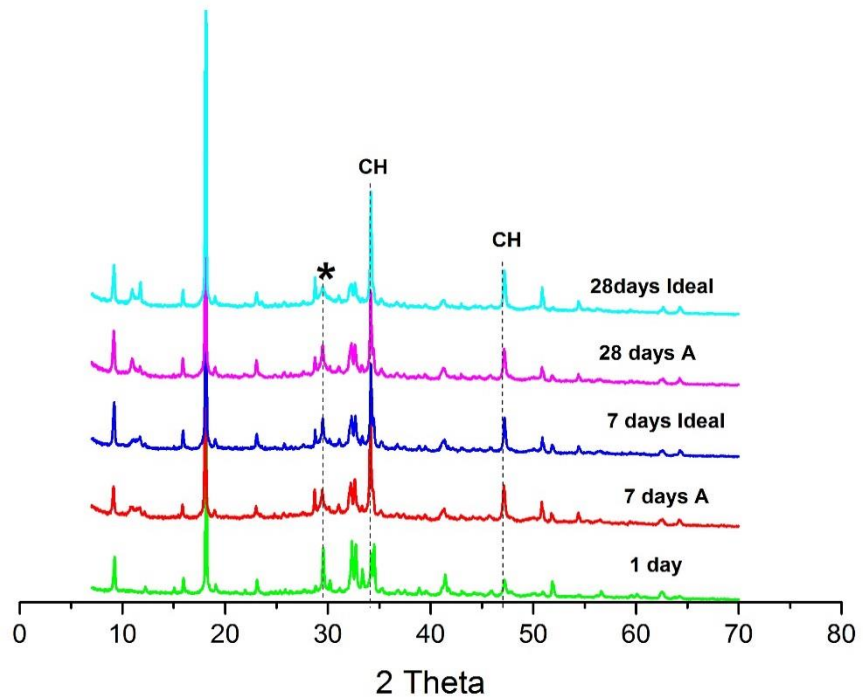


Figure A 178 XRD of 20MPa CEM1 wet mix from 1 day to 28days of curing

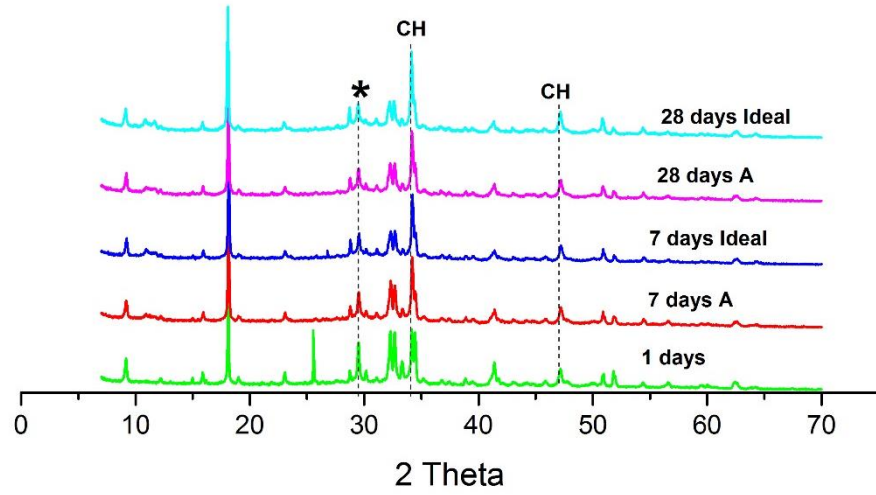


Figure A 179 XRD of 50MPa CEM1 wet mix from 1 day to 28days of curing

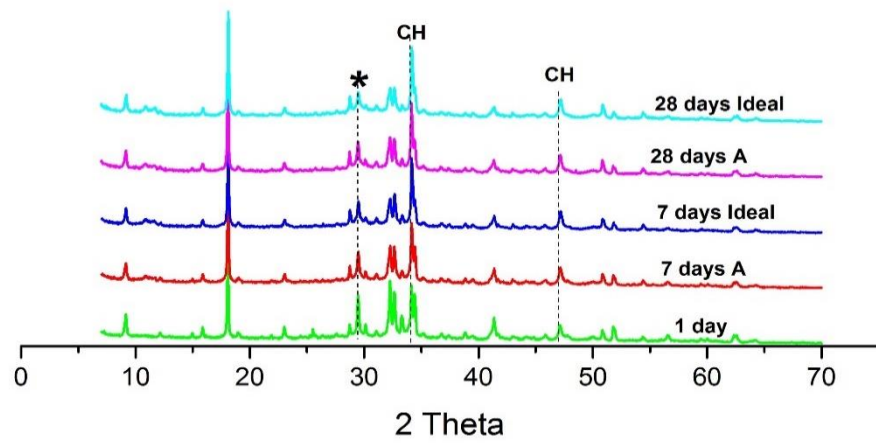


Figure A 180 XRD of 80MPa CEM1 wet mix from 1 day to 28days of curing

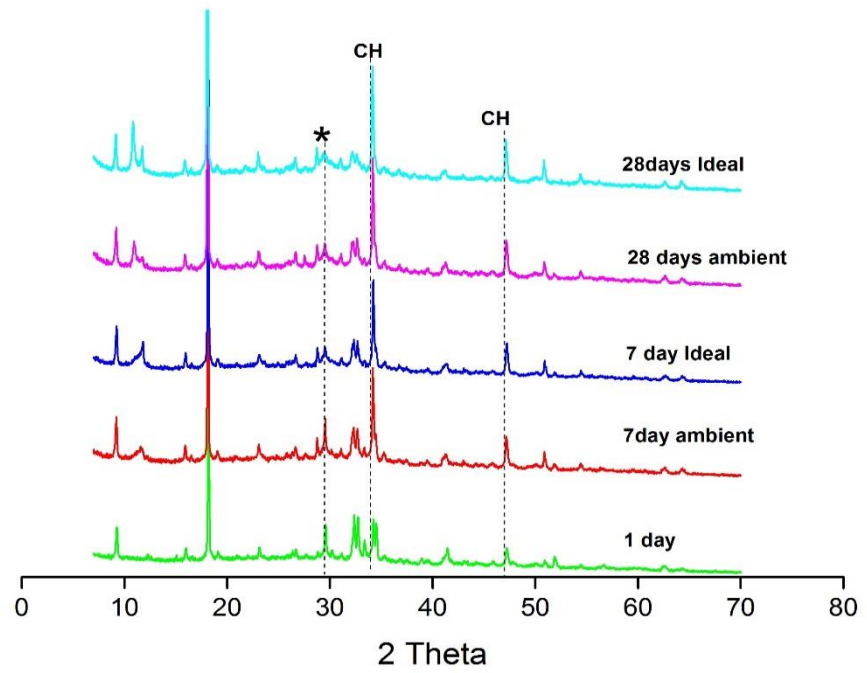


Figure A 181 XRD of 20MPa fly ash stiff mix from 1 day to 28days of curing

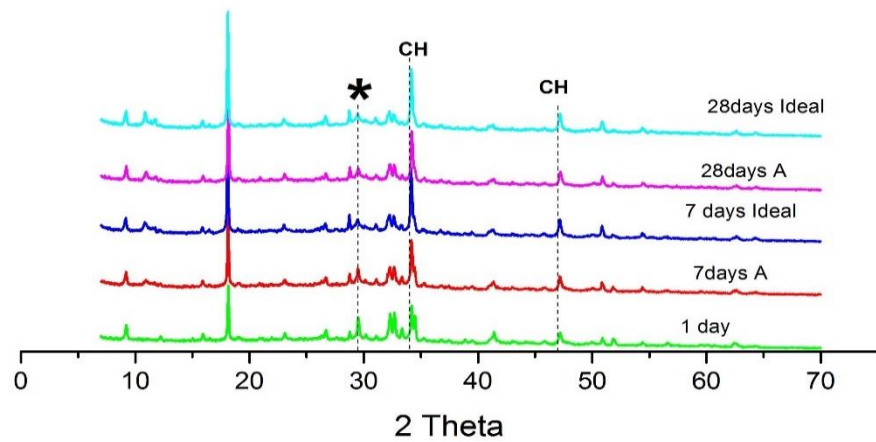


Figure A 182 XRD of 50MPa Fly ash stiff mix from 1 day to 28days of curing

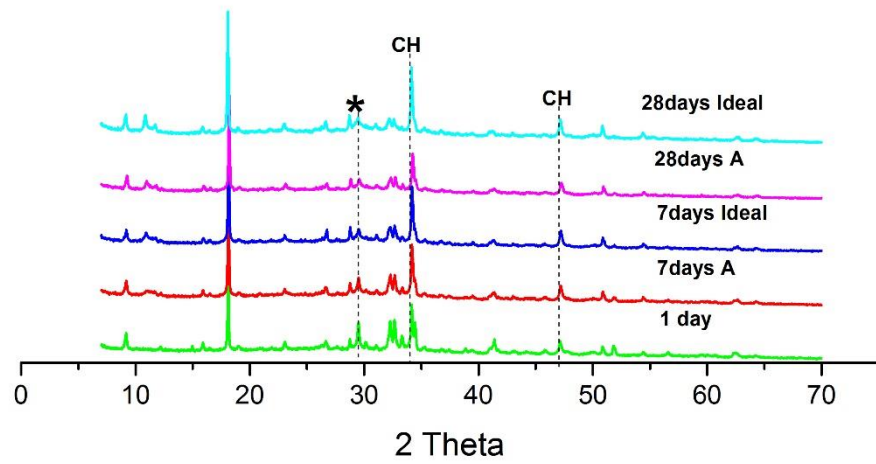


Figure A 183 XRD of 80MPa Fly ash stiff mix from 1 day to 28days of curing

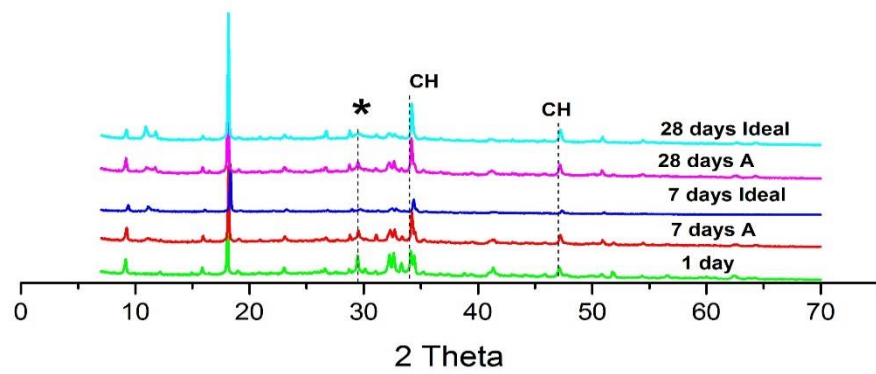


Figure A 184 XRD of 20MPa Fly ash wet mix from 1 day to 28days of curing

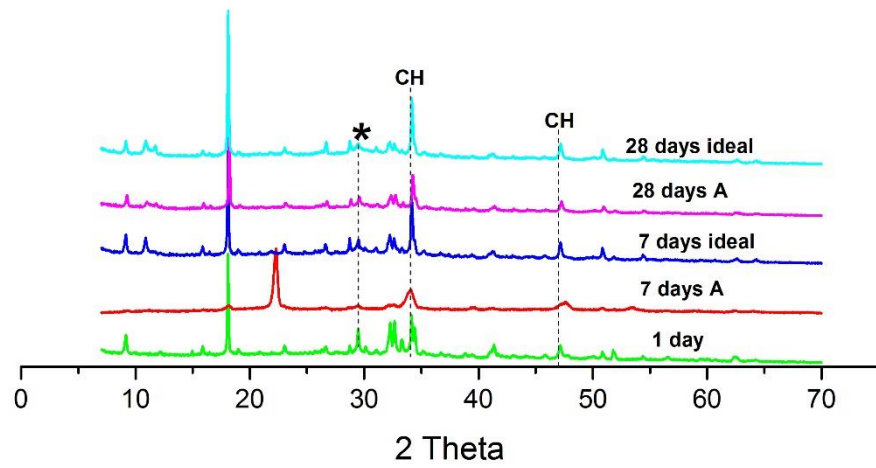


Figure A 185 XRD of 50MPa Fly ash wet mix from 1 day to 28days of curing

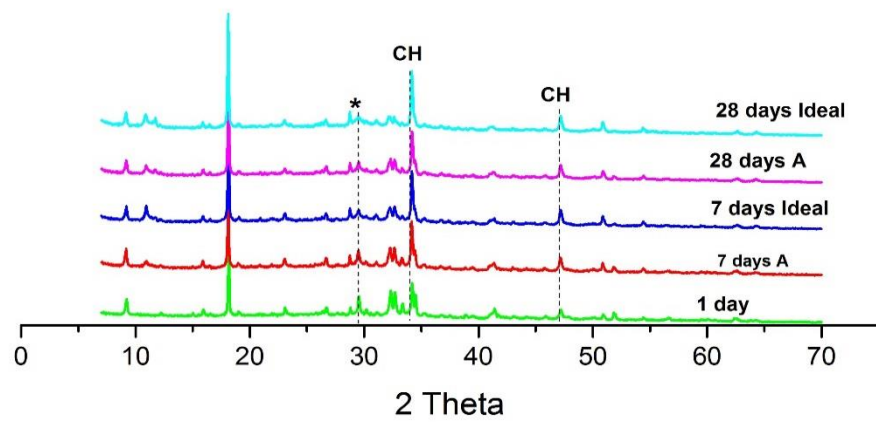


Figure A 186 XRD of 80MPa Fly ash wet mix from 1 day to 28days of curing

Appendix G Image J procedure with figures

Detailed Procedures of Image J analysis with the image for each steps involved to the summary result for unreacted cement calculations and the porosity from SEM images.

1 Open image J programme

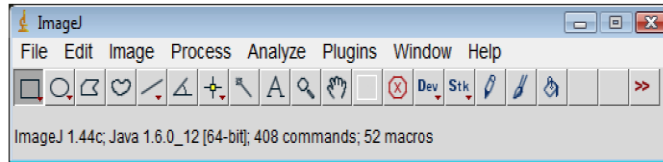


Figure A 187 Image j menu bar

2 On Menu bar click File, then click Open and select the picture file of the image to open on the screen

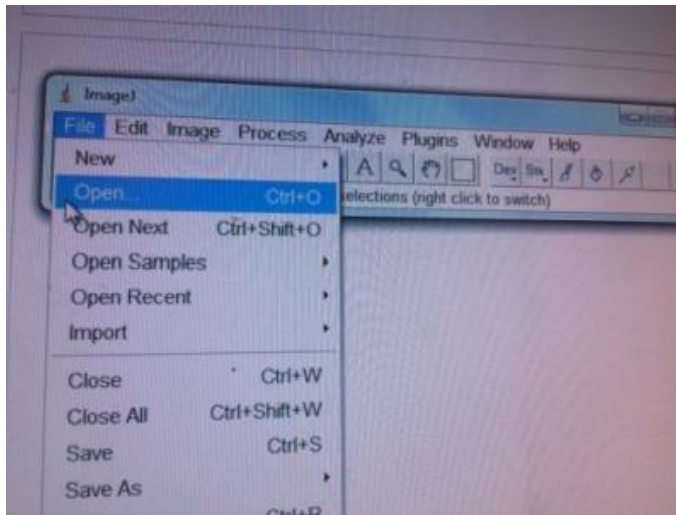


Figure A 188 Open file from menu bar

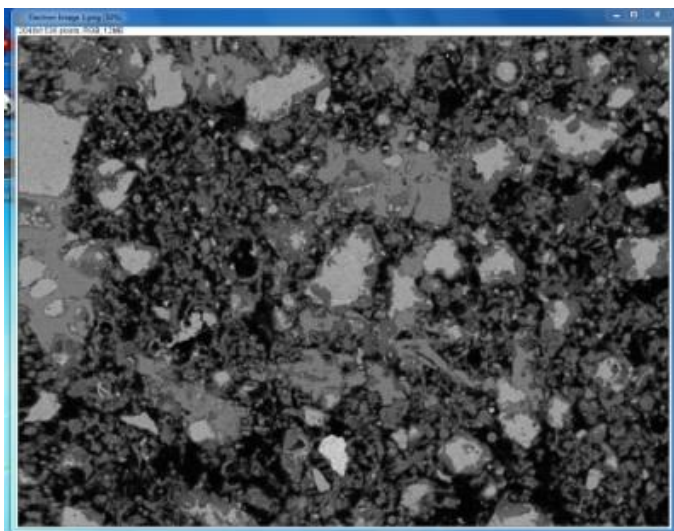


Figure A 189 Image opened from file

- 2 On the Menu bar click Image, then Type, then select 8-bit to change the colour image into the greyscale image if not already in that format;

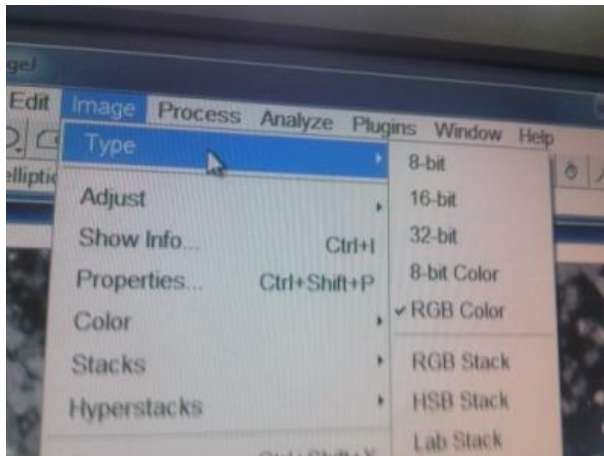


Figure A 190 Image Type showing RGB colour before selecting the type

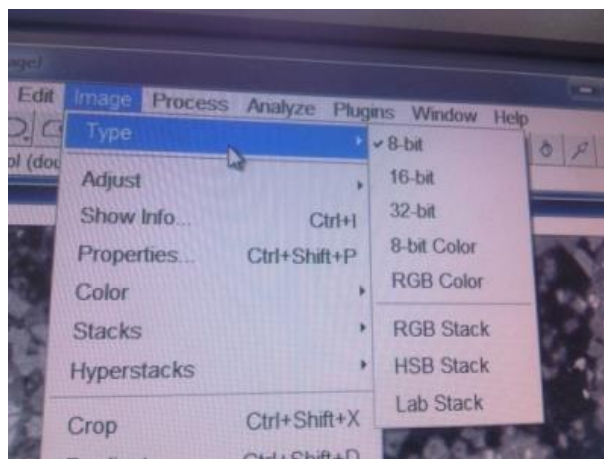


Figure A 191 Image type changing the colour image into the greyscale image

- 3 On the Menu bar click Image, then Adjust, then select Brightness/contrast. Then select Auto and Apply

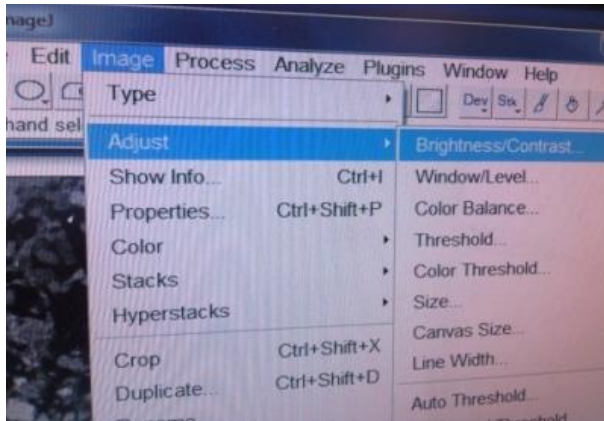


Figure A 192 Brightness/contrast control screen from image j menu bar

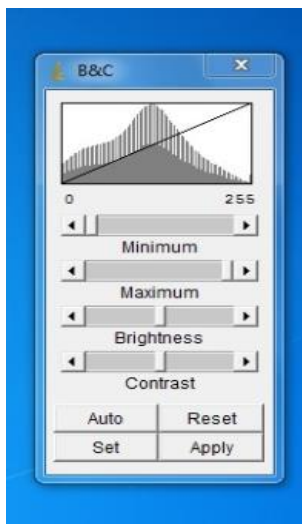


Figure A 193 The Auto and Apply to select the Brightness/Contrast

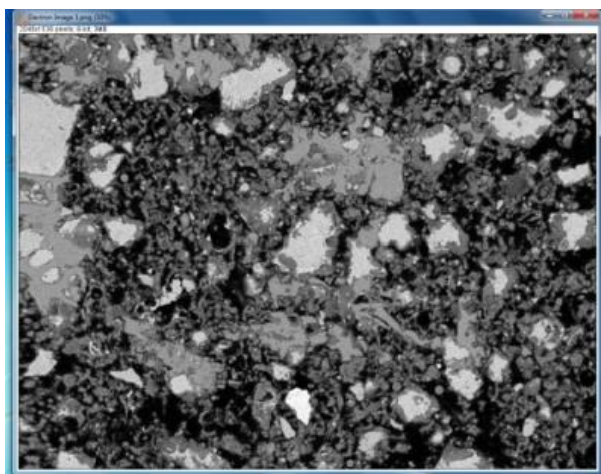


Figure A 194 Image showing the corrected brightness/contrast

- 4 On the menu bar click Process select smooth

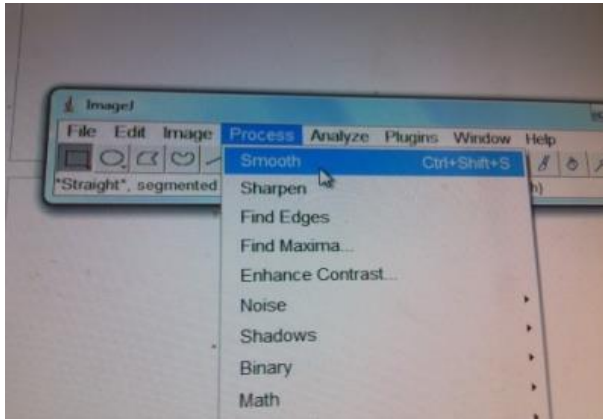


Figure A 195 Menu bar showing process to smooth

- 5 On the menu bar Click Process then select Filters then median

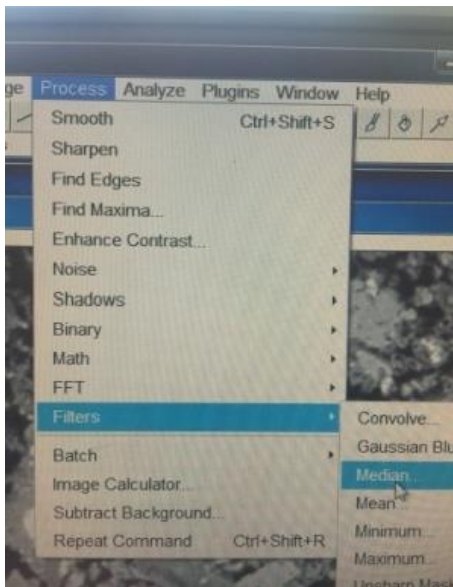


Figure A 196 Menu bar showing process-Filters then median

When the median is clicked radius of 2 will be ok

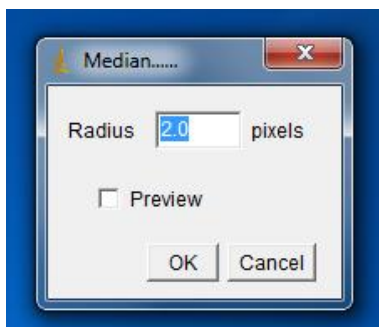


Figure A 197 Figure showing the median and the radius

6 On the Menu bar click Image then select Adjust then Threshold

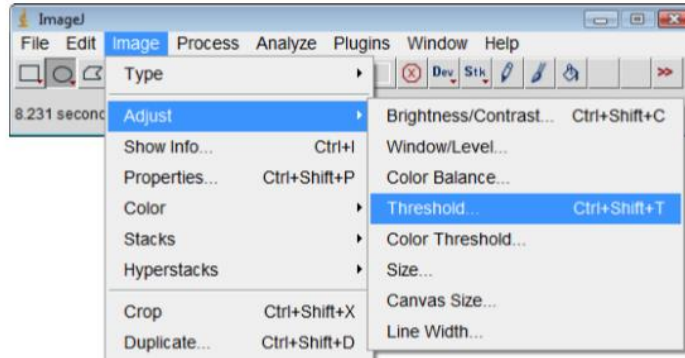


Figure A 198 Adjust/Threshold control screen

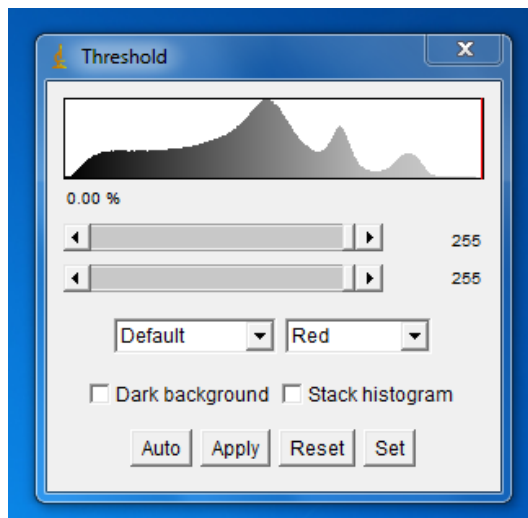


Figure A 199 Grey level histogram

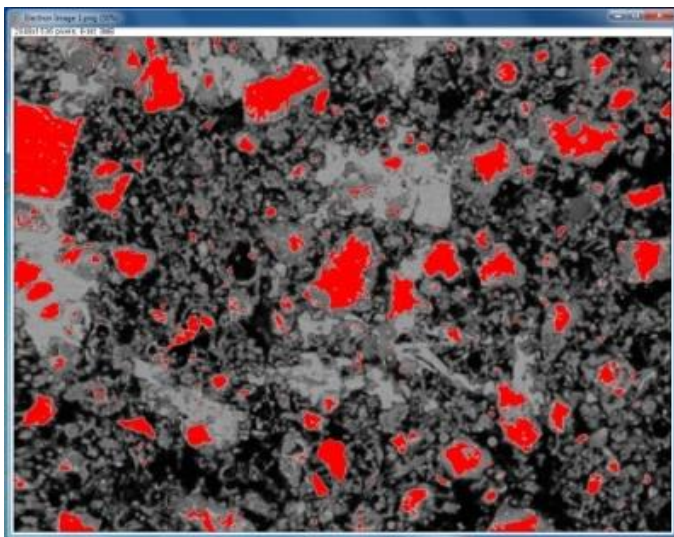


Figure A 200 Image showing unreacted cement in red colour

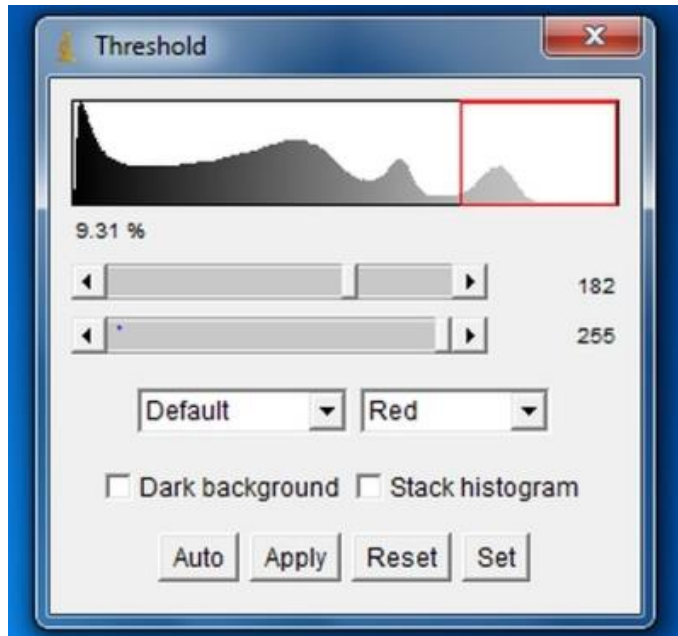


Figure A 201 Figure showing unreacted clinker selected

7 On the menu bar click Analyze then select Analyze particles

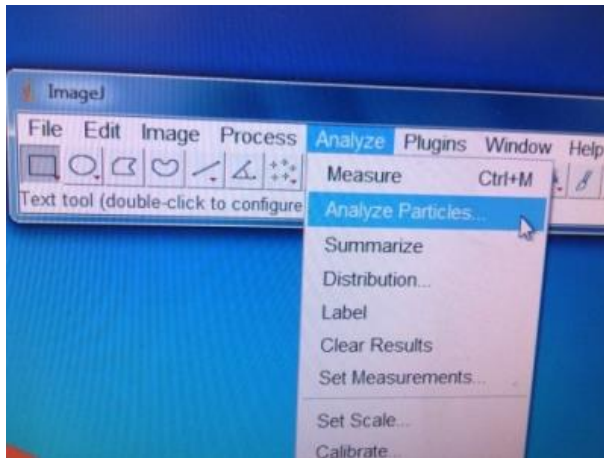


Figure A 202 Menu bar showing analyse particle selected

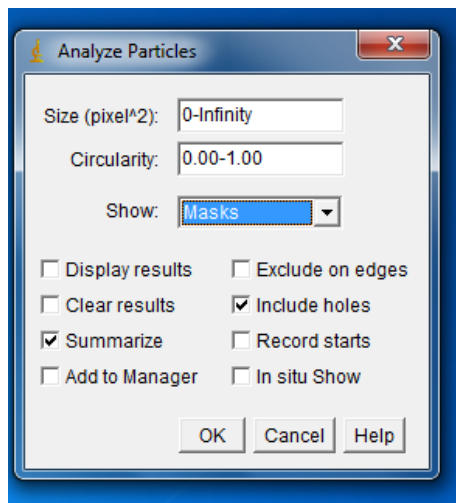


Figure A 203 Analyze particle showing various option to be picked

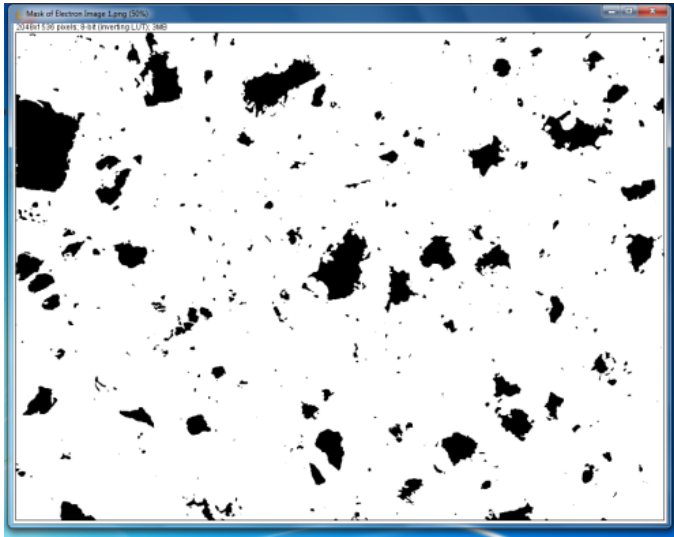


Figure A 204 Image showing the masks of unreacted cement

Table A 3 Result summary for unreacted clinker to calculate the degree of hydration

Slice	Count	Total Area	Average Size	%Area	Mean
Electron Image 1.png	462	227310	492.013	7.226	198.958
Electron Image 2.png	501	232129	463.331	7.379	198.470
Electron Image 3.png	506	235076	464.577	7.473	201.971
Electron Image 4.png	593	167753	282.889	5.333	201.385
Electron Image 5.png	442	265274	600.167	8.433	205.907
Electron Image 6.png	368	157347	427.573	5.002	204.911
Electron Image 7.png	418	224690	537.536	7.143	202.565
Electron Image 8.png	493	187918	381.172	5.974	202.818
Electron Image 9.png	584	126649	216.865	4.026	208.382
Electron Image 10.png	316	224442	710.259	7.135	203.486

Porosity

The above process will be repeated for each image to calculate the porosity. The porosity will be selected as shown in Figure below

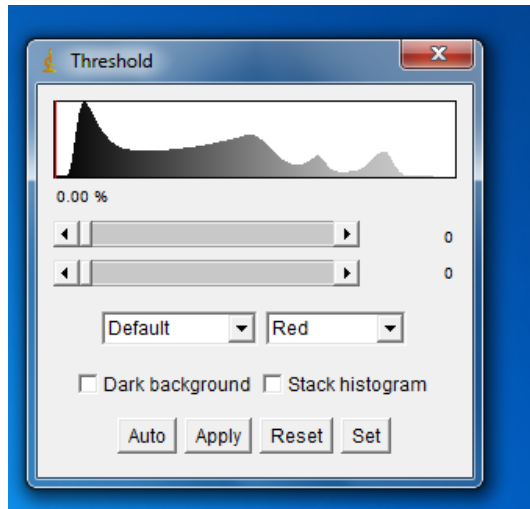


Figure A 205 Grey level histogram to select porosity

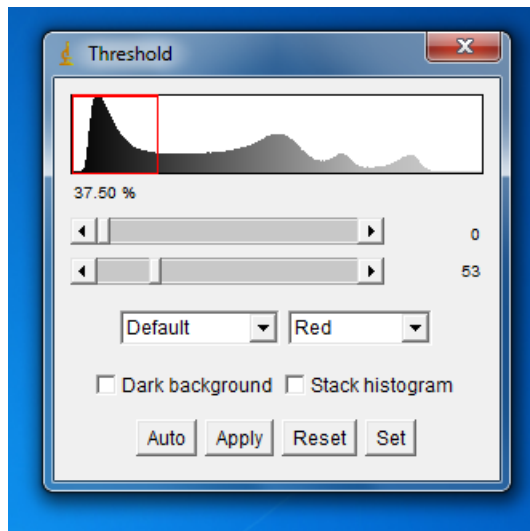


Figure A 206 Porosity of the selected image

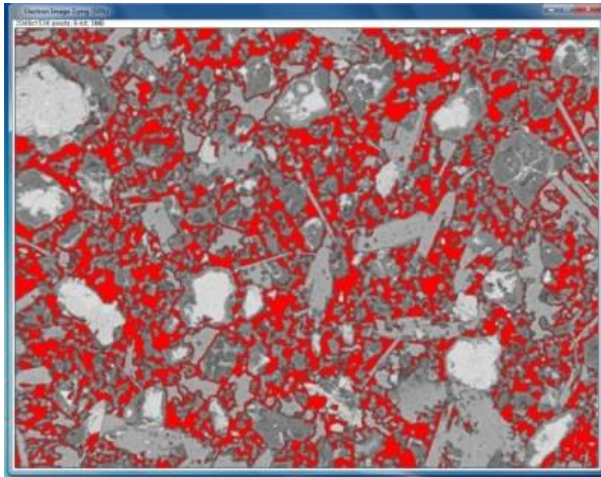


Figure A 207 Image showing the porosity in red colour

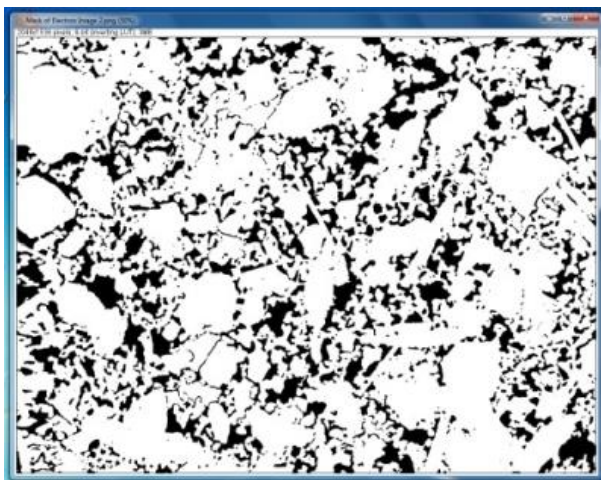


Figure A 208 Image showing the porosity masks

Table A 4 Porosity summary result

Slice	Count	Total Area	Average Size	%Area	Mean
Electron Image 1.png	842	1185498	1407.955	37.686	49.040
Electron Image 2.png	897	1014343	1130.817	32.245	36.568
Electron Image 3.png	529	1358801	2568.622	43.195	41.320
Electron Image 4.png	1260	967331	767.723	30.751	58.433
Electron Image 5.png	855	1027184	1201.385	32.653	46.098
Electron Image 6.png	1065	791546	743.236	25.163	66.351
Electron Image 7.png	1017	1065701	1047.887	33.878	53.056
Electron Image 8.png	1238	1066459	861.437	33.902	58.858
Electron Image 9.png	959	1284732	1339.658	40.841	68.485
Electron Image 10.png	1619	1010865	624.376	32.135	68.854